HYPOXIA-ACTIVATED DELIVERY OF CHEMICAL PROBES AND IMAGING AGENTS





CANCER RESEARCH UK



CANCER IMAGING CENTRE

A thesis submitted for the degree of
Doctor of Philosophy in Organic Chemistry

Charles N. G. Evans
University College, University of Oxford

Supervisors:
Prof. Stuart J. Conway and Prof. Ester M. Hammond

The studies detailed in this thesis were performed at the Chemistry Research Laboratory, University of Oxford and the Cancer Research UK/MRC Oxford Institute for Radiation Oncology, University of Oxford. This work was funded by the Cancer Research UK/EPSRC Cancer Imaging Centre in Oxford (OCIC2).

Trinity Term 2018
University of Oxford

SCHOOL OF CHEMISTRY

DECLARATION OF AUTHORSHIP

Name: CHARLES EVANS **Candidate number:** 463721

College: UNIVERSITY COLLEGE **Supervisors:** Prof. Stuart J. Conway and Prof. Ester M. Hammond

Title of Thesis: Hypoxia-activated Delivery of Chemical Probes and Imaging Agents

Word count: 72856

Please tick to confirm the following:

I have read and understood the University's disciplinary regulations concerning conduct in examinations and, in particular, the regulations on plagiarism. ☐

I have read and understood the Education Committee's information and guidance on academic good practice and plagiarism. ☐

The dissertation I am submitting is entirely my own work except where otherwise indicated. ☐

It has not been submitted, either partially or in full, either for this Honour School or qualification or for another Honour School or qualification of this University (except where the Special Regulations for the subject permit this), or for a qualification at any other institution. ☐

I have clearly indicated the presence of all material I have quoted from other sources, including any diagrams, charts, tables or graphs. ☐

I have clearly indicated the presence of all paraphrased material with appropriate references. ☐

I have acknowledged appropriately any assistance I have received in addition to that provided by my supervisors. ☐

I have not copied from the work of any other candidate. ☐

I have not used the services of any agency providing specimen, model or ghostwritten work in the preparation of this dissertation. ☐

I agree to retain an electronic copy of this work until the publication of my final examination result, except where submission in hand-written format is permitted. ☐

I agree to make any such electronic copy available to the examiners should it be necessary to confirm my word count or to check for plagiarism. ☐

Candidate's signature: Date: ……..

……..

Abstract

Regions of hypoxia are a common feature of solid tumours and are associated with an aggressive phenotype and resistance to chemotherapy and radiotherapy. The differences in redox environment between normoxic and hypoxic tissue can be exploited by hypoxia-activated prodrugs (HAPs), which enable targeted delivery of drugs and imaging agents. Several HAPs have been developed but have had limited success in the clinic, partly resulting from a lack of understanding of their distribution and activation *in vivo*. We therefore wished to develop hypoxia-activated prodrugs, and fluorophores for use in drug-fluorophore conjugates. These conjugates would be activated in hypoxic tissue, releasing both a 'switch-on' fluorophore and a biologically active cargo molecule. We proposed that these molecules could be used to study HAP behaviour in tissue.

We began by building upon our earlier work around a hypoxia-activated prodrug of a clinical candidate Chk1 inhibitor, SAR020106. The original prodrug lacked efficacy in clonogenic survival assays, which we attributed to slow fragmentation kinetics. We attempted to synthesise analogues which, we hypothesised, would have more rapid fragmentation kinetics than the original prodrug and therefore greater efficacy. This synthesis proved challenging, and no new prodrug forms could be produced.

We then developed three near-infrared fluorophore scaffolds as potential hypoxia-activated bioreductive imaging probes. The first, a very small fluorophore with an unusual mechanism of activation was synthesised in a potential hypoxia-activated form, and whilst it underwent metabolism and fragmentation in hypoxia, the modified fluorophore exhibited greatly reduced fluorescence and was deemed unsuitable for imaging applications. The second scaffold was based on an arylazide-containing hydrogen sulfide probe with the uncommon benzopyrylium core. The nitroaryl analogue was synthesised and evaluated *in vitro*. The molecule proved to be susceptible to biologically-relevant nucleophiles including NADPH and L-GSH, although we demonstrated that the molecule could be used to selectively image hypoxic cancer cells. Due to this molecule's instability in a biological environment, we moved onto a third scaffold which had been explored previously in our group. Synthesis of analogues of this fluorophore with a biologically active cargo proved challenging, and we thus investigated a related fluorophore with visible-wavelength emission properties. We synthesised the nitroaryl and azidoaryl analogues an evaluated them *in vitro*. Biochemical reduction assays were unsuccessful, and cellular imaging experiments showed that whilst both molecules could be used as imaging agents, neither were effective as hypoxia sensors. We also synthesised an analogue of the nitro compound to which we attached a bromodomain ligand. This molecule proved to be highly unstable and could not be adequately evaluated.

Finally, we wished to incorporate ^{18}F-PET as a second imaging modality to our drug-fluorophore conjugates. We modified the synthesis of our bromodomain ligands to enable the use of fluorination chemistry which is applicable to radiolabelling. The fluorination was demonstrated cold using ^{19}F NMR, and a deprotection reaction compatible with radiosynthesis was also identified. This chemistry will be useful in the radiolabelling of our bromodomain ligands for use in dual-modal imaging agents.

Table of Contents

Abstract ii
Acknowledgements vi
List of Abbreviations viii
Chapter 1 Introduction 1
1.1 Cancer 1
1.2 Hypoxia 3
1.2.1 Treatment of hypoxic tumours 5
1.3 Hypoxia-Activated Prodrugs (HAPs) 5
1.3.1 Activation of HAPs 6
1.3.2 Classes of HAPs 8
1.3.2.1 Quinone HAPs 8
1.3.2.2 Nitroaromatic HAPs 10
1.3.2.3 N-Oxide HAPs 14
1.3.2.4 Transition metal complex HAPs 15
1.4 Cancer imaging 16
1.4.1 Contrast-enhanced imaging modalities 17
1.4.1.1 Magnetic Resonance Imaging (MRI) 17
1.4.1.2 Single-photon emission computed tomography (SPECT) 20
1.4.1.3 Positron emission tomography (PET) 21
1.4.1.4 Fluorescence imaging 24
1.4.2 Hypoxia imaging 28
1.5 Theranostic agents 30
1.6 Aims 31
Chapter 2 Towards Hypoxia-Activated Prodrug Forms of the Clinical Candidate Chk1 Inhibitor SAR020106 33
2.1 Checkpoint 1 Kinase (Chk1) 33
2.1.1 Structure and function 33
2.1.2 Inhibition of Chk1 as a therapeutic strategy 35
2.1.3 Targeted delivery of Chk1 inhibitors 36
2.2 Aims of the study 40
2.3 Synthesis 41
2.3.1 Synthesis of a model substrate 41
2.3.2 Synthesis of *N*-alkyl-linked prodrugs 44
2.3.2.1 2-Nitrofuranyl prodrugs 44
2.3.2.2 2-Nitrothiopheneyl prodrugs 45
2.3.2.3 6-Nitroquinoline prodrugs 47

2.3.3 Synthesis of carbamate-linked bioreductives 48
2.3.4 Synthesis of trimethyl lock-based prodrug forms 55
2.4 Testing of the ‘trimethyl lock’ platform 63
2.4.1 Chemical reduction of **122** 64
2.5 Conclusions and Outlook 66
Chapter 3 A minimal, hypoxia-activated bioreductive fluorophore 69
3.1 Introduction 69
3.2 Design of target molecules 71
3.3 Synthesis 73
3.4 Characterisation 81
3.4.1 UV-Vis absorbance and fluorescence spectra 81
3.4.2 Chemical reduction of **136** 84
3.4.3 Enzymatic reduction of **136** 85
3.5 Conclusions and Outlook 87
Chapter 4 A new bioreductive near-infrared fluorophore for hypoxia imaging 89
4.1 Choice of scaffold 89
4.2 Synthesis of analogues 91
4.3 Characterisation 96
4.3.1 UV-Vis absorbance and fluorescence spectra 96
4.3.2 Chemical reduction assay 97
4.3.3 Enzymatic reduction assay 98
4.3.4 Identification of new species 99
4.3.5 Susceptibility to biological nucleophiles 102
4.3.6 Chemical reduction by hydride ions 106
4.3.7 Cellular permeability assay 109
4.3.8 Cellular imaging of hypoxia 110
4.4 Concluding remarks and future direction 115
Chapter 5 Towards bioreductive, hypoxia-activated theranostic agents 117
5.1 Theranostic agents 117
5.2 Design of compounds 117
5.2.1 Near-infrared (NIR) scaffolds 117
5.2.2 Visible-wavelength scaffold 119
5.2.3 Target compounds 120
5.3 Synthesis 122
5.3.1 Synthesis of near-infrared fluorophores 122
5.3.2 Synthesis of visible-wavelength fluorophores 127
5.4 Photophysical characterisation 129

5.5 Enzymatic reduction studies of chromenone-based compounds 133
5.6 Chromenone photoisomerisation 136
5.7 Cellular imaging 138
5.7.1 Imaging of amine **182** in cells 138
5.7.2 Imaging of cellular hypoxia 139
5.8 Fluorescence-activated cell sorting (FACS) analysis 144
5.9 Synthesis of theranostic fluorophore-drug conjugates 145
5.10 Photophysical characterisation of drug-fluorophore conjugate 155
5.11 Enzymatic reduction studies of drug-fluorophore conjugate **231** 156
5.12 Concluding remarks and future work 157
Chapter 6 Towards an ^{18}F-PET imaging probe for BET proteins 160
6.1 Introduction 160
6.1.1 Dual-modal imaging 160
6.1.2 Positron Emission Tomography (PET) imaging 160
6.1.3 The BET family of bromodomain-containing proteins 161
6.2 Compound design 162
6.3 Synthesis 166
6.3.1 Ir-catalysed C-H borylation 166
6.3.2 Direct Grignard reaction with pendant boronate species 167
6.3.3 Miyaura borylation 168
6.3.4 Synthesis of fluorination precursor 169
6.3.4 Radiolabelling-compatible fluorination studies 170
6.3.5 Radiosynthesis-compatible removal of Boc protecting groups 171
6.4 Concluding remarks 176
Chapter 7 Conclusions and Outlook 177
7.1 Conclusions 177
7.2 Future Outlook 181
Chemistry Experimental 183
General experimental 183
Synthetic procedures 190
Biological Materials and Methods 263
Bibliography 271
APPENDICES 282

Acknowledgements

First and foremost, I would like to thank my supervisors Professor Stuart Conway and Professor Ester Hammond, who generously gave me this incredible opportunity to work in two fantastic institutions, in two diverse and stimulating environments, on a truly collaborative and ambitious project. My experience and development as a scientist has been deeply shaped by their influence.

I am indebted to the help, support and companionship of friends and colleagues past and present from both the Conway and Hammond groups: Dr Anthony Chan, for your enthusiasm and positivity; Dr Lingbing Kong, for your intellect, friendship and truly unique outlook on life; Dr Ewen Calder, for your support and generosity with your time; Dr James Clayton, your humour, support and enormous personality are an impossible act to follow; Dr Ishna Mistry, for all the biology you taught me and the sanity you brought to my time in Oncology; Dr Matthias Schiedel, a more patient and selfless friend one could not ask for; Drs Shaliny Ramachandran, Greg Dobrynin and Kasia Leszczynska, your patience, watchful eyes and kind support helped me find my feet in a new discipline, and for that I am truly thankful.

DPhils come and DPhils go, and I have worked with some of the sharpest and most talented of them during my time in Oxford: Amélie, thanks for teaching me how to run; Sam Grayer, you helped me keep things in perspective; Angie, I owe you more than I can ever repay (although my Sigh Jar will make a good start!); Michelle, thanks for tolerating the newbie in your midst; Brian, Friday afternoons aren't the same without you. Michael, you let me vent my frustrations more often than I can count – thanks for always knowing the answer (and all the Lincoln dinners!); Saunders, I hope you're keeping the top chat going; Mus, your relentless positivity and humour is an inspiration. Delaforce, I wish I had even half your talents in the lab – you're a true one-man band! Thanks also to GG, Coco, Larissa, Amy, Natalie, Sam Bader, Joe and Klem – it's been great sharing a lab with you guys! Lastly, but most importantly, thanks to Dr Liam O'Connor, to whom I am eternally grateful. You paved the way for my project, gave me endless advice that was always invaluable, and set the benchmark to which I aspired. Thank you so much for everything.

The visiting students, Masters' students and Part IIs I've worked with have put my own abilities to shame and have been great companions both in and out of the lab. Jay, Sophie and Candise, without you guys the start of my DPhil wouldn't have been half as fun! Katie, Jessie, Fern and Jesse, thanks for the limitless supplies of top chat banter. Bea, Elliot, Leila and Ed, it was a pleasure to share the lab with you all. Thanh, Angelika, Eva-Maria, Alex Axer, Ray and John Ient – thanks for everything!

Much of the data contained in this thesis could not have been produced without the help and support of so many talented staff from Chemistry, Biochemistry and Oncology. Thanks to Barbra, Tina and Maria for the NMR support. Thanks to Dr James Wickens and Dr Victor Mikhailov for low- and high-resolution mass spectrometry. Tanks to Dr David Staunton for fluorimetry assistance. Thanks to Dr Graham Brown and Rhodri Wilson for microscopy support. Extra special thanks to Dr Lisa Folkes, Alix Hampson and Dr Mike Stratford for HPLC-MS support (and a **lot** of patience). Thanks to Ron, Debbie and Alan for keeping the CRL, and G11, running so smoothly for so many years.

Thank you to University College for the support over the years. Particularly, thank you to Rev. Dr Andrew Gregory, Prof. Peter Jezzard, Lady Jill and Sir Ivor Crewe for their generosity and help. Thank you to the members of the University College Weir Common Room, and a particular thank-you to the men and women of University College Boat Club. It has been a pleasure to row with them, and without it my DPhil could easily have driven me to distraction. Thank you for keeping me sane.

Thank you to my family for endlessly supporting me and having the belief in me that I usually lacked – my mother Beth, my father Crispin, my grandparents Bill and Joan, my sister Joscelyn and her family, and Gillian, Gareth, Megan and Hannah.

Finally, thank you so much to my wonderful girlfriend Rosie. You were always there to help and support me, cheer me up when I was feeling down (which was a **lot**), take my mind off my work when it was consuming me, and keep me focussed on my goals. I honestly couldn't have made it to the end without your love, support, and unwavering faith in me. Thank you.

List of Abbreviations

ADP	Adenosine diphosphate
AIBN	Azobisisobutyronitrile
AML	Acute myeloid leukaemia
APCI	Atmospheric-Pressure Chemical Ionisation
ATP	Adenosine triphosphate
ATR	Ataxia telangiectasia and Rad3-related protein, a kinase
AU	Absorbance Units
BBB	Blood-Brain Barrier
BET	Bromodomain and Extra-Terminal
BINAP	2,2'-Bis(diphenylphosphino)-1,1'-binaphthyl
BIPY	2,2'-Bipyridine
Boc	*Tert*-butyloxycarbonyl
BOLD-MRI	Blood Oxygen Level-Dependent MRI
Bq	Becquerel, a unit of radioactivity
BRD3	The gene encoding the protein BRD3
BRD4	The gene encoding the protein BRD4
BRD3	A member of the BET family of proteins
BRD4	A member of the BET family of proteins
BTFFH	Fluoro-*N*,*N*,*N*′,*N*′-bis(tetramethylene)formamidinium hexafluorophosphate
CAIX	Carbonic anhydrase IX
CDC25	Cell Division Cycle 25, a phosphatase
CDI	1,1'-Carbonyldiimidazole
CDK	Cyclin-Dependent Kinase
Chk1	Checkpoint 1 kinase
Chk2	Checkpoint 2 kinase
c-Met	Tyrosine-protein kinase Met
COD	1,5-Cyclooctadiene
CPR	Cytochrome p450 reductase (also known as cytochrome *c*)
CT	Computed Tomography
CYP/P450	Cytochrome p450, a large family of metabolic enzymes
Da	Dalton, a unit of mass for subatomic particles and atoms
DAPI	4',6-Amidino-2-phenylindole, fluorescent stain for (live) cell nuclei
DAST	Diethylaminosulfur trifluoride
dba	Dibenzylideneacetone
DDR	DNA Damage Response
DFT	Density Functional Theory
DIBAL-H	Di*iso*butylaluminium hydride
DIPEA	*N,N*-diisopropylethylamine, or Hünig's base
DMAP	4-Dimethylaminopyridine
DME	Dimethoxyethane
DMF	*N,N*-dimethylformamide
DMSO	Dimethyl sulfoxide
DNA	Deoxyribonucleic acid
DOPA	Dihydroxyphenylalanine
dppf	1,1'-Bis(diphenylphosphino)ferrocene
DPTA	Diethylenetriaminepentaacetic acid, or Pentetic acid
DW-MRI	Diffusion-Weighted MRI

e^-	An electron
E1cB	Unimolecular elimination *via* a conjugate base
EDC	1-Ethyl-3-(3-dimethylaminopropyl)carbodiimide
EEDQ	2-Ethoxy-1-ethoxycarbonyl-1,2-dihydroquinoline
EGFR	Epithelial Growth Factor Receptor
EM	Electromagnetic (Spectrum)
eq.	Equivalents
ESI	Electrospray ionisation
eV	Electron volts
FAD	Flavin adenine dinucleotide
FACS	Fluorescence-Assisted Cell Sorting
FAZA	Fluoroazomycin arabinoside
FBS	Fetal bovine serum
FDA	Food and Drug Administration, a US Government department
FDG	Fluorodeoxyglucose (2-Deoxy-2-fluoro-D-glucose)
FMISO	Fluoromisonidazole
FMN	Flavin mononucleotide
FRET	Förster Resonance Energy Transfer
g	Acceleration due to gravity
GFP	Green Fluorescent Protein
GLUT1	Glucose transporter 1
GSH	Glutathione
GTV	Gross Tumour Volume
HAP	Hypoxia-Activated Prodrug
HATU	Hexafluorophosphate Azabenzotriazole Tetramethyl Uronium
Her2	Human epidermal growth factor receptor 2
HMBC	Heteronuclear multiple-bond correlation
HMDS	Hexamethyldisilazane (or hexamethyldisilazide when associated with a cation)
HOBt	Hydroxybenzotriazole
HOMO	Highest Occupied Molecular Orbital
HPLC	High Performance Liquid Chromatography
HSA	Human Serum Albumin
HSQC	Heteronuclear single quantum correlation
HWE	Horner-Wadsworth-Emmons reaction
Hz	Hertz
IC_{50}	Half-maximal inhibitory concentration
ICG	Indocyanine Green
ICT	Intramolecular Charge Transfer
iNOS	Nitric oxide synthase
IPA	*Iso*propyl alcohol
IR	Infrared
J	Coupling constant
K_d	Constant of dissociation
K_i	Constant of inhibition
K_{O2}	Oxygen concentration for 50% inhibition of reduction
LDA	Lithium di*iso*propylamide
LRMS	Low Resolution Mass Spectrometry
LUMO	Lowest Unoccupied Molecular Orbital
MHz	Megahertz

MR(I)	Magnetic Resonance (Imaging)
MS	Mass Spectrometry
MTBE	Methyl *tert*-butyl ether
µW	Microwave
NAD(P)$^+$	Nicotinamide adenine dinucleotide (phosphate), oxidised
NAD(P)H	Nicotinamide adenine dinucleotide (phosphate), reduced
NBS	*N*-bromosuccinimide
NCS	*N*-chlorosuccinimide
NDOR1	NADPH-dependent diflavin oxidoreductase 1
NFSI	*N*-fluorobenzenesulfonimide
NIR	Near-infrared
NMC	NUT Midline Carcinoma
NMP	*N*-Methyl-2-pyrrolidone
NMR	Nuclear Magnetic Resonance
NQO1	NADPH dehydrogenase (quinone) 1
N.R.	No Reaction
NUTM1	A gene encoding the protein NUT family member 1
OE21	An oesophageal cell line
OMs	Methanesulfonate, of mesylate
OTf	Trifluoromethanesulfonate, or triflate
p53	Tumour protein p53, a tumour suppressor protein
PA	Photoacoustic
PBS	Phosphate-buffered saline
PCC	Pyridinium chlorochromate
PD	Pharmacodynamics
PDAC	Pancreatic Ductal Adenocarcinoma
PDB	Protein Databank
PET	Positron Emission Tomography
pH	“Power of Hydrogen”, a measure of acidity or basicity
φ_{FL}	Fluorescence quantum yield
PI3K	Phosphatidylinositol-4,5-bisphosphate 3-kinase
PK	Pharmacokinetics
pK_a	Logarithm of the acid dissociation constant K_a
pO_2	Partial pressure of oxygen
ppm	Parts per million
PSMA	Prostate-Specific Membrane Antigen
***p*-TSA**	*para*-toluenesulfonic acid
py	Pyridine
RCY	Radiochemical Yield
R_f	Retention factor
RKO	A rectal carcinoma cell like
ROS	Reactive Oxygen Species
RT	Room Temperature, or Retention Time (HPLC)
SAR	Structure-Activity Relationship
SCC7	A mouse squamous cell carcinoma cell line
SET	Single Electron Transfer
SM	Starting Material
S_NAr	Nucleophilic aromatic substitution
SPECT	Single Photon Emission Computed Tomography
SPIO(N)	Super-Paramagnetic Iron Oxide (Nanoparticles)

TBAF	Tetra-*n*-butylammonium fluoride
TBD	To be determined
TBDMS	*tert*-butyldimethylsilane, or *tert*-butyldimethylsilyl
TBME	*tert*-butyl methyl ether
TFA	Trifluoroacetic acid
THF	Tetrahydrofuran
TIC	Total Ion Count
TIPS	Tri*iso*propylsilyl
TLC	Thin Layer Chromatography
TMS	Trimethylsilyl, or tetramethylsilane
TPZ	Tirapazamine
UV	Ultraviolet

Chapter 1
Introduction

1.1 Cancer

Cancer is the second most common cause of death worldwide, with an estimated 8.8 million cancer-related deaths in 2015, accounting for 1 in every 6 of all deaths globally.[1] The cancers which cause the most deaths include those of the lung (1,690,000 deaths in 2015), liver (788,000 deaths), and colorectal organs (774,000 deaths).[1] In the UK, it is estimated that 1 in every 2 people born after 1960 will be diagnosed with a cancer at some point in their lifetime.[2] There have been many advances in our understanding of cancer, resulting in improved diagnosis, treatment, and prevention. Whilst survival trends have improved for many types of cancer, including common cancers such as breast and prostate, these trends have not been seen in all types of cancer (see Figure **1**).[3,4] 10-year survival rates for prostate cancer, for example, have more than tripled, from roughly 25% in 1971-72 to greater than 75% in 2010-11. By contrast, pancreatic cancer 10-year survival rates have seen no improvement over that period and remain exceptionally low. Whilst pancreatic cancer is a relatively uncommon form of cancer, a similar lack of improvement can be seen for lung cancer, which is the most prevalent cancer in the UK.

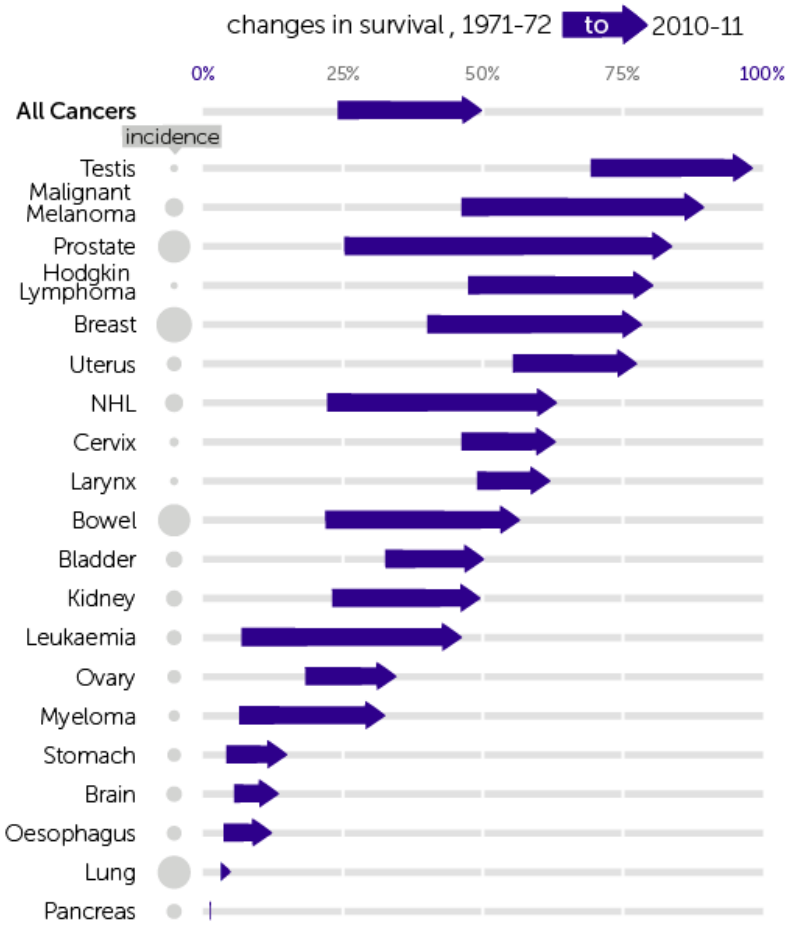


Figure 1: Age-standardised 10-year net survival trends for selected cancers in adults aged 15-99, England and Wales, from 1971-72 to 2010-11. Reproduced with permission from Cancer Research UK, https://www.cancerresearchuk.org/health-professional/cancer-statistics/survival/common-cancers-compared, accessed July 2018.[3,4]

Cancer is characterised by several distinct phenotypes, known as the "Hallmarks of Cancer" (Figure **2**), and include uncontrolled proliferation of cells, resistance to cell death, sustained angiogenesis, and increased invasive potential of cancerous cells into other tissues.[5] More recent understanding of the complex behaviours of different cancers has added to these hallmarks, including altered metabolism, genomic instability, and immune system evasion.[6] These phenotypes can result from genetic mutations, causing abnormal protein function and altered patterns of gene expression. Any tissue which divides may become cancerous, and cancers are referred to by the tissues from which they primarily arise. Cancer is, however, a highly heterogeneous disease; many different patterns of genetic mutation may result in tumourigenesis, and

no two tumours are genetically identical.[7] Moreover, a single tumour may harbour distinct populations of cells with markedly differing phenotypes, adding further complexity to diagnosis and treatment.[8]

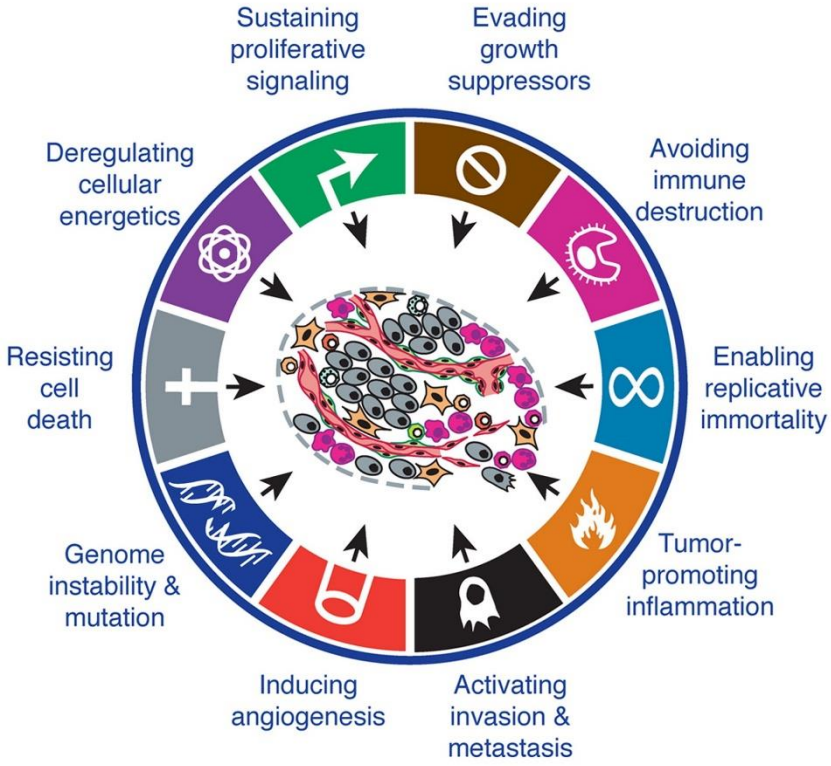


Figure 2: The "Hallmarks of Cancer", a set of characteristic phenotypes displayed by cancerous tissue. Adapted with permission from Cell *144*, Hanahan and Weinberg, "Hallmarks of Cancer: The Next Generation", 646–674, **2011** with permission from Elsevier (license number 4395861165847).

1.2 Hypoxia

One of the most significant hallmarks of cancer is the change in the constituent chemical and biological environment, giving rise to the concept of the "tumour microenvironment". Rapidly-dividing cells in a tumour consume large amounts of nutrients and oxygen, resulting in upregulated growth of supplying vasculature, a process known as angiogenesis. Rapidly-dividing solid tumours grow faster than their supplying vasculature, resulting in a chaotic local vascular network which is unable to provide adequate supplies of oxygen to all regions of the tumour (Figure **3**). This lack of oxygen is known as tumour hypoxia and is a common feature of solid tumours.

Hypoxia is associated with an increased resistance to both chemotherapy and radiotherapy, and results in a poor prognosis for patients.[9,10]

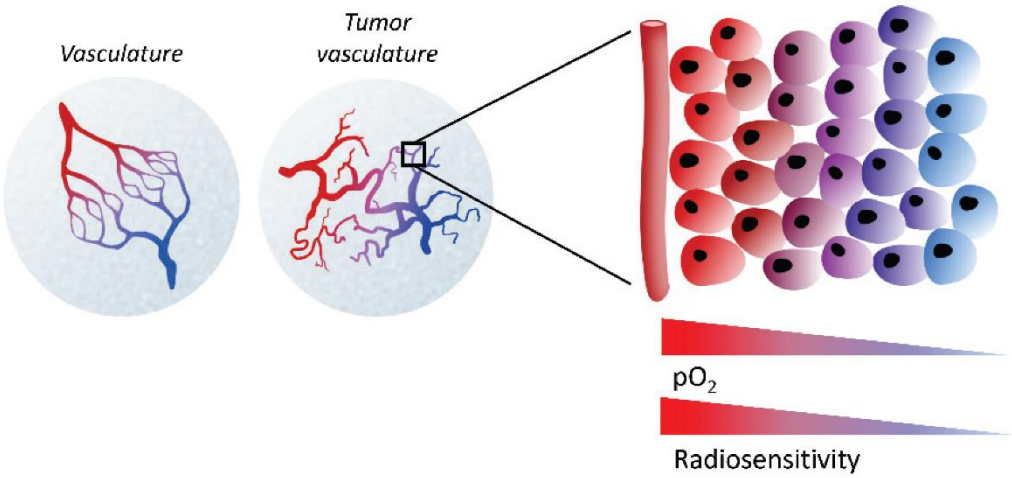


Figure 3: Tumour vasculature and hypoxia. Tumours have chaotic, leaky vasculature which does not provide an adequate oxygen supply to all regions of the tumour. Cells that are distant from blood vessels become hypoxic, which is associated with resistance to chemotherapy and radiotherapy. Figure reproduced from Ramachandran *et al.*, *Genes* 2015 under a Creative Commons Attribution License (CC-BY 4.0).[11]

The hypoxic environment is toxic to both healthy and cancerous cells, resulting in cell death.[12] However, a proportion of cancer cells may have genetic adaptations which allow them to survive in hypoxia. This surviving hypoxic tumour fraction exhibits an aggressive phenotype, characterised by promoted growth and increased metabolism, caused by upregulation of pro-growth and survival genes.[12] This enhanced metabolism is known as the Warburg effect, in which the cancerous cells start to rely primarily on glycolysis for the production of ATP *via* lactate fermentation, rather than through the oxidative phosphorylation mechanism of the TCA cycle.[13]

Two distinct types of hypoxia are found in tumours.[14] In acute, or perfusion-limited, hypoxia blood vessels become temporarily occluded, resulting in fluctuating oxygen levels, even in tissues adjacent to the vessels. In chronic, or diffusion-limited, hypoxia the limited oxygen supply is consumed rapidly by nearby tissue, and thus tissues which are too far from the nearest blood vessel to receive

adequate oxygen (typically >100 μm) become hypoxic; this hypoxia does not fluctuate and cannot be readily alleviated.[15,16]

1.2.1 Treatment of hypoxic tumours

Tumour hypoxia presents a significant obstacle to tumour treatment, and patients with hypoxic tumours respond poorly to therapy.[17,18] Normal tissue vasculature is required for delivery of chemotherapies to diseased tissue, yet blood delivery is often impraied in hypoxic tumours. Dissolved oxygen is necessary for radiotherapy to be effective, yet hypoxic tumours have little or no oxygen, rendering this treatment less effective.

One current method of tackling hypoxia in cancer therapy is the use of radiosensitising drugs.[19] These drugs act in a variety of ways, typically by forming radical species which induce DNA lesions in a similar way to radiation-induced reactive oxygen species (ROS) do in well-oxygenated tissue.

Another strategy that has been explored for treatment of hypoxia is the alleviation of hypoxia by targeting the vasculature.[20] Significant effort has gone into antiangiogenic therapies; drugs which block angiogenesis to “normalise” the disordered and chaotic vasculature of a tumour.[21,22] These efforts have been met with limited success.[23,24]

1.3 Hypoxia-Activated Prodrugs (HAPs)

Hypoxia-Activated Prodrugs (HAPs) are a class of compounds which are being explored as possible treatments for hypoxic tumours. These compounds bear chemical modifications which significantly reduce their activity, until they are metabolised by enzymes in a low-oxygen environment.[25] Upon metabolism, structural changes to these molecules convert them to an active form (Figure **4**) and they can then exert their biological effect, usually to kill cells.

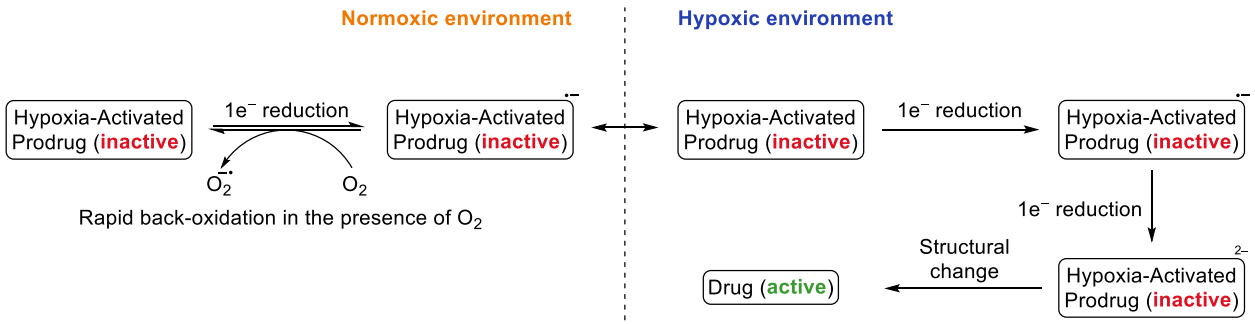


Figure 4: Concept of a hypoxia-activated prodrug (HAP). Enzymatic single-electron reductions of the inactive prodrug are reversed by oxygen but proceed unhindered in hypoxia. The resulting structural change causes the release of the active substance in the hypoxic environment.

Most conventional cancer chemotherapies are highly toxic and often have little-to-no selectivity for diseased tissue over healthy tissue or rely on differences in tissue proliferation rates. Consequently, cancer chemotherapies are often accompanied by side-effects, many of which are intolerable for patients, reducing their quality of life. It is proposed that by selectively delivering toxic drugs to hypoxic tissue, while sparing healthy tissue, significant benefits can be derived for patients, including greater efficacy and reduced side-effects.

1.3.1 Activation of HAPs

HAPs are activated by enzymatic reduction *in vivo*.[25] The oxygen-sensitive pathway for activation of HAPs relies on single-electron reductase enzymes, which perform multiple single-electron transfers (SET) to the molecule resulting in overall reduction and structural change. As detailed in Figure **4**, the intermediates formed by single-electron reduction are sensitive to the presence of molecular oxygen, which rapidly back-oxidises these intermediates and forms superoxide (O_2^{-}). This futile redox cycling prevents release of the active substance under oxygenated conditions. In the absence of molecular oxygen (*i.e.* in hypoxia) this metabolism proceeds unhindered and produces the active compound. These single-electron reductases are upregulated in hypoxia, providing a further handle for selective targeting of hypoxic tumours.[26]

A number of one-electron reductase enzymes which activate the different classes of HAPs have been identified or implicated.[27,28] These enzymes are one- or two-electron reductases; in the case of two-electron reductases, they may metabolise these prodrugs in the presence of oxygen and hence lose oxygen sensitivity.

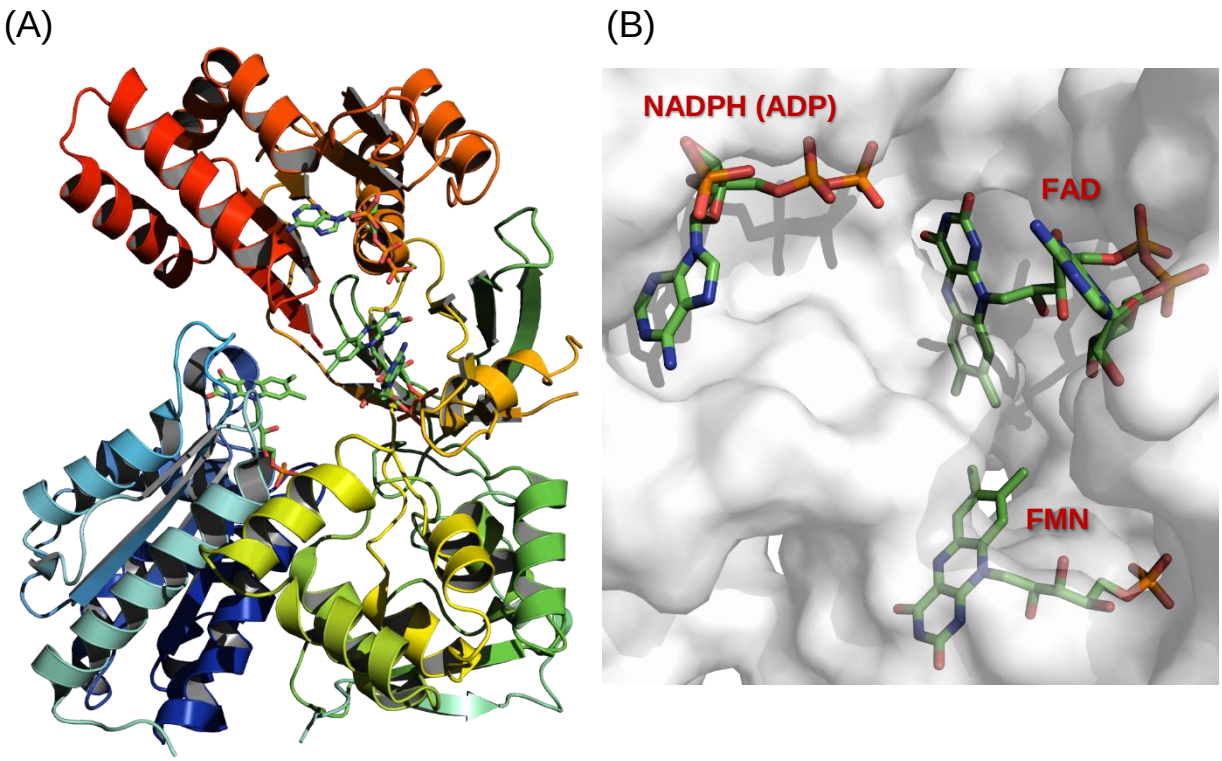


Figure 5: (A) X-Ray crystal structure of human cytochrome p450 reductase (PDB: 3QE2).[29] The cofactors are shown in stick representation. The crystal structure is homodimeric; for clarity, a single subunit of the protein is shown. (B) The cofactor binding domains of human cytochrome p450 reductase, with each cofactor labelled. NADPH is disordered in the crystal structure, and hence ADP is shown in its place.

One of the most commonly studied enzymes for the oxygen-sensitive metabolism of potential new HAPs is cytochrome p450 reductase (CPR, also known as NADPH-hemoprotein reductase, or cytochrome *c*).[30] This protein contains both flavin adenine dinucleotide (FAD) and flavin mononucleotide (FMN) cofactors, and relies on reduced nicotinamide-adenine dinucleotide (NADPH) as its terminal electron donor.[31] The primary function of cytochrome p450 reductase is to mediate electron transfer from the two-electron donor NADPH to the heme cofactors of cytochrome P450 enzymes, which are one-electron acceptors.[31] CPR is also a significant enzyme for oxygen-sensitive metabolism of many HAPs, and has broad substrate specificity for

exogenous molecules with reduction potentials close to or above the FAD and FMN cofactors.[25] The X-ray crystal structure of cytochrome p450 reductase (Figure **5a&b**) shows the FAD and FMN cofactors bound, and adenine dinucleotide phosphate (ADP) in place of NADPH. CPR is the primary metabolic enzyme used in the studies contained herein.

Alongside CPR, there are several other enzymes which have been identified as important in the one-electron and two-electron reduction of HAPs. These include nitric oxide synthase (iNOS),[32] NADPH-dependent diflavin oxidoreductase 1 (NDOR1),[33] xanthine oxidase,[34] ferrodoxin reductase (FDXR),[35] and the cytochrome P450s (CYPs), including CYPA4.[36]

1.3.2 Classes of HAPs

There are several different classes of HAPs that are distinguished by the chemical functional groups they bear, and the mechanisms by which these functionalities are reduced. These classes are quinones, nitroaromatics, aromatic or aliphatic *N*-oxides, and transition metal complexes.[26,37] These can be further classed based on their behaviour, divided into Class I and Class II HAPs.[38] Class I HAPs are reduced under mild hypoxia (K_{O_2} [O_2 concentration for 50% inhibition of reduction] ≈ 1 μM) and release a cytotoxin, damaging the cell in which the agent is released but with no effect on neighbouring cells.[39] Class II HAPs may be reduced under more severe hypoxia (K_{O_2}≈ 0.1 μM) but release more stable species which may diffuse between local cells, causing the so-called “bystander effect”.[39]

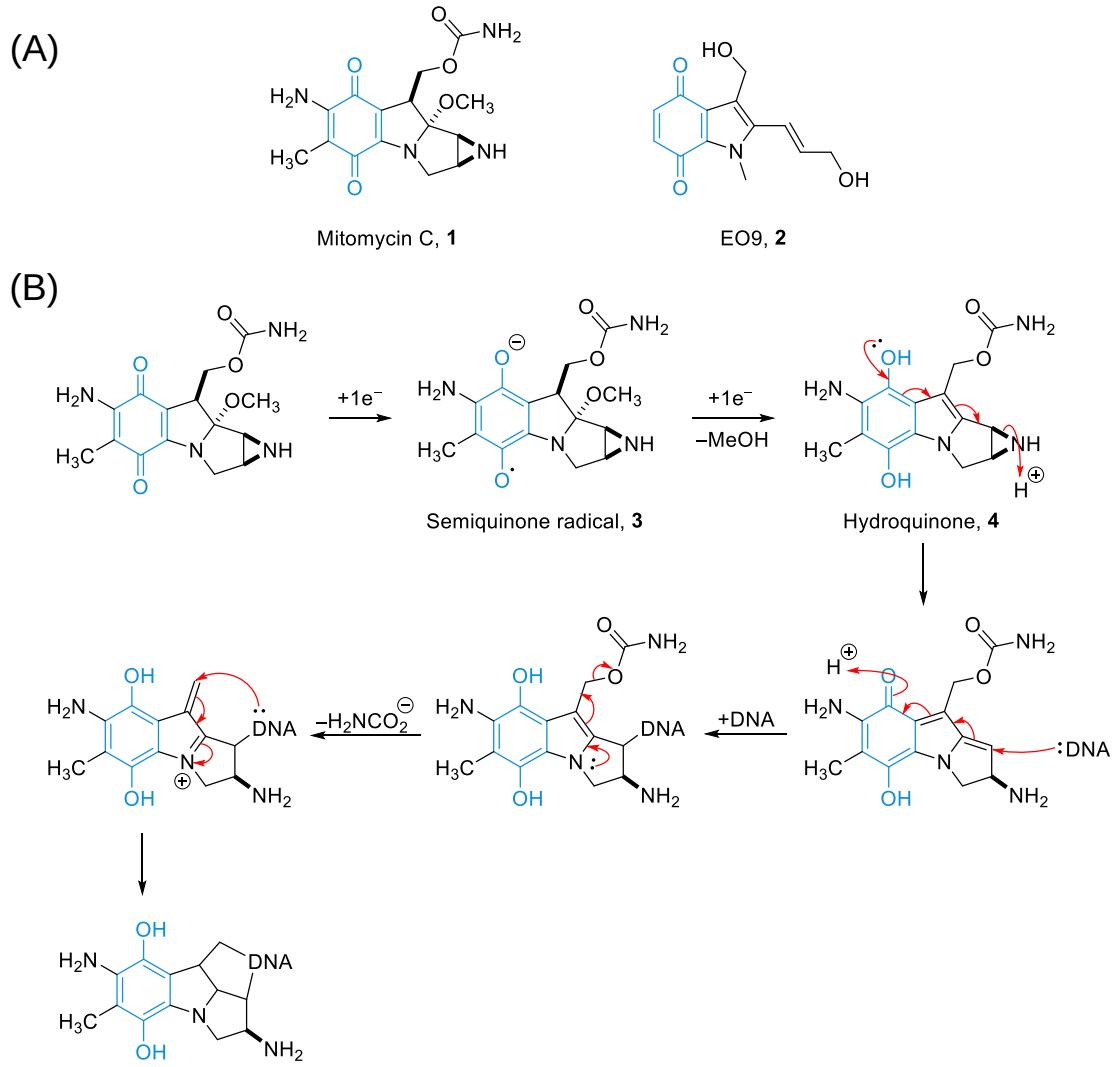
1.3.2.1 Quinone HAPs

The quinone motif is found in many naturally-occurring molecules with potential therapeutic benefit.[40] Quinones are redox-active and can be reduced by several bioreductive enzymes.[25] Quinone therapeutics typically work either *via* structural

rearrangement into an active form (usually a DNA alkylating form), or through the production of reactive oxygen species (ROS) *via* redox cycling.[41]

Two of the most well-studied quinone HAPs are Mitomycin C **1** and E09 **2** (Scheme **1a**). Both are reduced by two electrons, either *via* two-electron reduction or sequential single-electron reduction, to form the hydroquinone intermediate. These intermediates then undergo significant structural rearrangement, forming conjugate acceptors which alkylate nucleophilic residues in DNA. An illustrative mechanism for Mitomycin C **1** is given in Scheme **1b**.

Despite the potent toxicity of quinones like Mitomycin C and EO9, clinical progress in treatment of cancer has been limited.[26] These molecules have limited selectivity for hypoxic tissue over normoxic tissue, and selectivity is lost in tissues expressing NQO1.[42,43]

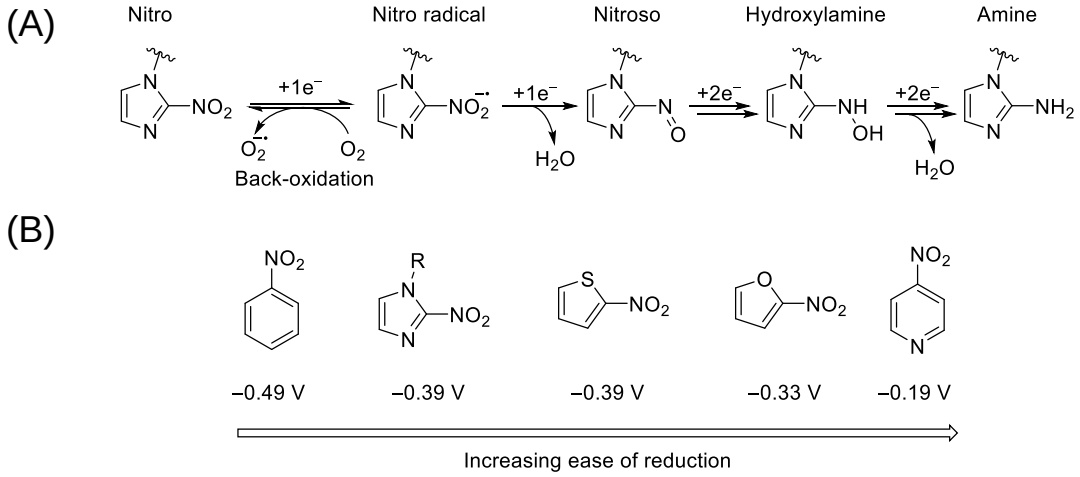


Scheme 1: (A) Chemical structures of two of the most commonly studied quinone-based bioreductive prodrugs, Mitomycin C **1** and EO9 **2**. The bioreductive motif is highlighted in blue. (B) Mechanism of action of Mitomycin C.[40] Two-electron reduction produces the hydroquinone intermediate **4** (or successive singe-electron reductions *via* the semiquinone radical **3**). Subsequent ring-opening of the aziridine produces a conjugate acceptor which alkylates nucleophilic residues of DNA. Further fragmentation with the loss of carbamate produces a second conjugate acceptor, which undergoes intramolecular cyclisation with the bound DNA to give secondary alkylation.

1.3.2.2 Nitroaromatic HAPs

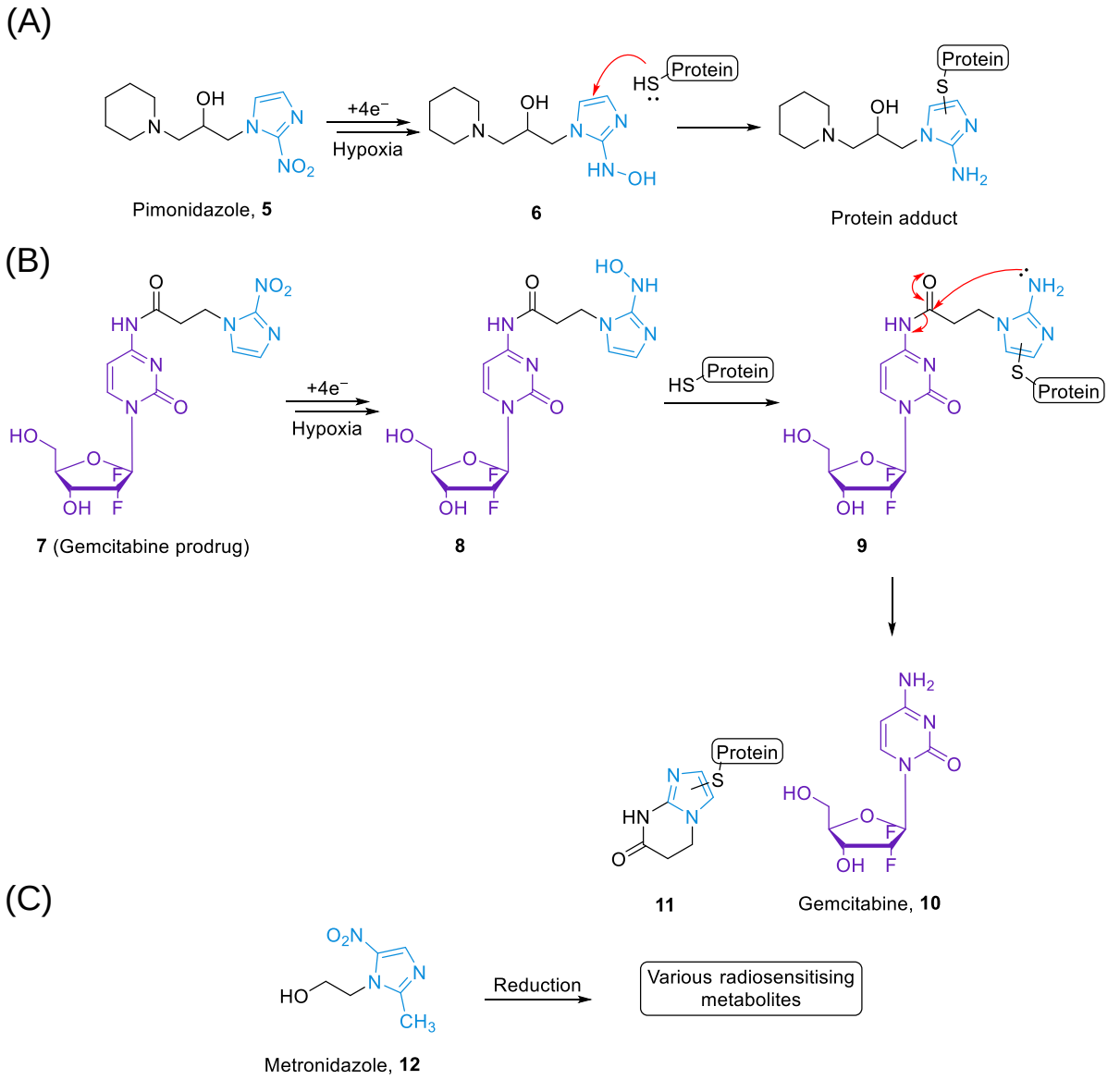
Nitroaromatics represent a heavily studied class of hypoxia-activated bioreductive compounds. Several nitroaromatic structures have been developed as bioreductive moieties; the nitrofuran,[44,45] nitrothiophene,[45,46] nitroquinoline,[47–50] nitrobenzyl,[51–56] and nitroimidazole groups.[45,57–60] These groups are reduced by one- or two-electron reductases to form a variety of intermediates (Scheme **2a**). One

significant advantage of the variety of nitroaromatic groups available is the option to tailor the properties of prodrugs by choosing the most appropriate of these groups. Each group has a different electrochemical reduction potential (Scheme **2b**),[61] and thus a different propensity towards biochemical reduction. This opens the possibility of these groups being reduced at different oxygen tensions.



Scheme 2: (A) General mechanism of the oxygen-sensitive reduction of nitroaryl groups, illustrated by the 2-nitroimidazole group. (B) Electrochemical reduction potentials of some nitroaryl bioreductive groups.[61]

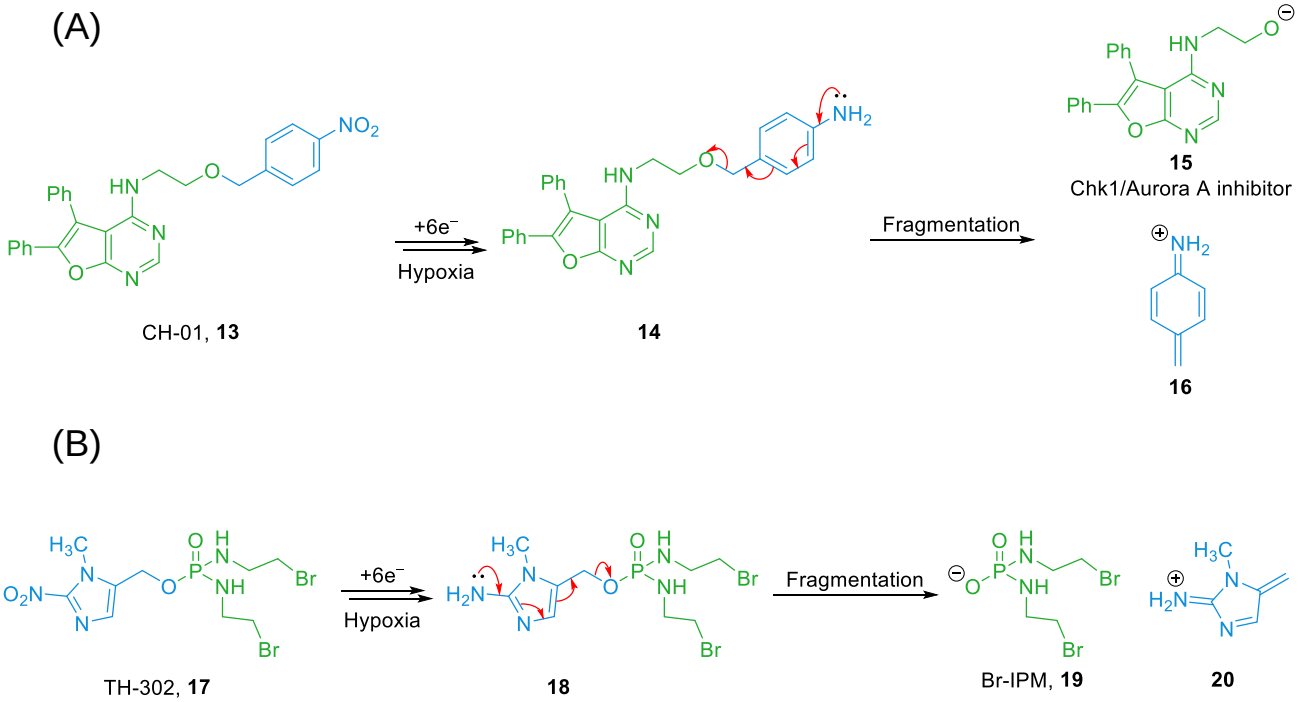
There are several mechanisms by which nitroaromatic bioreductive compounds exert their effects after reduction. The first is through the altered electronics of the aromatic ring. This may cause the molecule to become more reactive towards nucleophilic protein residues, as is the case for Pimonidazole **5**,[62] an immunohistochemical stain for hypoxia which binds to protein thiols after reduction in hypoxia. Others become radiosensitisers, such as metronidazole **12**.[19] 2-Nitroimidazole radiosensitisers such as metronidazole act in several ways, including depleting cellular stocks of protective thiols, undergoing radiolysis to form cytotoxins, or *via* production of damaging free radicals (so-called “electron affinity drugs”). Others become nucleophilic, such as **7** (Scheme **3b**),[59] which can then trigger other mechanisms such as intramolecular cyclisation.



Scheme 3: A selection of nitroaromatic bioreductive compounds whose activities are activated *via* nitro group reduction. (A) Pimonidazole **5**, a common immunohistochemical stain for hypoxia. Pimonidazole is reduced under hypoxia, and then reacts with intracellular thiol nucleophiles (such as L-glutathione and proteins). These adducts are then stained with fluorophore-tagged antibodies. (B) **7**, a prodrug form of gemcitabine **10**. Reduction in hypoxia unmasks the amino group as a latent nucleophile. Cyclisation of this nucleophile releases the cytotoxic cargo. (C) Metronidazole **12**, one of several 2-nitroimidazole radiosensitisers. Bioreduction under hypoxia produces several intermediates which then act in various ways to radiosensitise cells.

Another common mechanism by which nitroaromatic bioreductive groups act is *via* molecular fragmentation. Nitro groups are mesomerically electron-withdrawing, whereas its reduction metabolites (nitroso, hydroxylamine, amine) are all mesomerically electron-donating. This fundamental change in electronics can induce the molecule to undergo fragmentation, shown in Scheme **4**. This fragmentation

releases the bioreductive group (in the form of an alkylating agent), plus the attached "cargo" molecule. Cargo molecules can be various biologically-active agents including fluorophores,[44,52,54,63,64] cytotoxins,[33,65,66] or molecularly-targeted ligands.[51,52,67,68]



Scheme 4: Examples of hypoxia-activated bioreductive molecules which undergo molecular fragmentation after reduction. (A) CH-01 **13**, a hypoxia-activated prodrug which releases a dual-target kinase inhibitor.[51] (B) TH-302 **17**, a bioreductive prodrug form of Br-IPM, a phosphoramide-based nitrogen mustard which acts as a DNA crosslinker.[66]

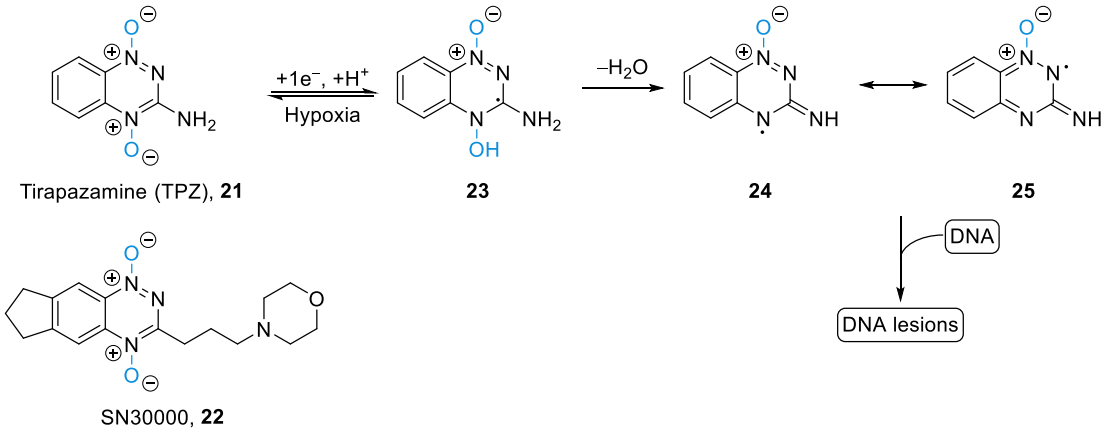
CH-01 **13** (Scheme **4a**) was developed by our group,[51] and is based upon a ligand which binds to both Checkpoint kinase 1 (Chk1) and Aurora A kinase, both of which are implicated as potential targets for the treatment of cancer.[69,70] We showed that appending the 4-nitrobenzyl bioreductive group to the terminal hydroxyl blocked a key interaction with Chk1, abrogating its binding affinity. Upon reduction of the 4-nitrobenzyl group under hypoxia fragmentation occurred, the parent ligand **15** was released, and its biological effect was exerted.

TH-302 **17** (Scheme **4b**) is a hypoxia-activated prodrug form of Br-IPM **19**, a phosphoramide nitrogen mustard which acts to crosslink DNA strands and induce DNA damage.[66,71,72] This cytotoxic agent has significantly impaired reactivity when the

2-nitroimidazole bioreductive group (shown in blue) is attached, reducing its toxicity to healthy, oxygenated cells. Upon reduction in hypoxia, molecular fragmentation again releases the active compound.

1.3.2.3 *N*-Oxide HAPs

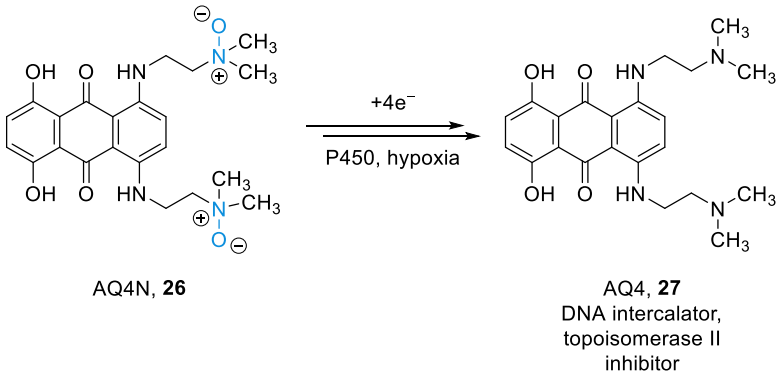
N-Oxide-containing molecules are another class of HAP which has gained considerable attention. There are two sub-classes of *N*-oxide prodrugs; aromatic and aliphatic *N*-oxides. The most significant aromatic *N*-oxide is SN30000 **22**,[73] which is an optimised analogue of the earlier prodrug tirapazamine (TPX **21**, Scheme **5**). TPZ acts by undergoing one-electron reduction under hypoxia to give the corresponding radical **23**, which then spontaneously decomposes to generate the benzotriazinyl radical **24/25**.[74] This radical then goes on to cause DNA lesions and associated toxicity.[75] TPZ has undergone extensive clinical trials as both combination therapy and in conjunction with radiotherapy; however, Phase III trials have shown disappointing results.[76,77]



Scheme 5: The structures of tirapazamine (TPZ, **21**) and SN30000 **22**, two HAPs that contain aromatic *N*-oxides. The mechanism by which TPZ induces DNA damage in hypoxia is also shown.[74,75]

The aliphatic *N*-oxide class of hypoxia-activated prodrug is represented by the compound AQ4N **26** (Scheme **6**), also known as banoxantrone.[27,78,79] AQ4N (while bearing resemblance to the quinone HAPs discussed in Chapter 1.3.2.1) also bears aliphatic *N*-oxides as its bioreductive component. Metabolism by P450 enzymes under

hypoxia converts the *N*-oxide to the corresponding amine giving AQ4 **27**,[36] a potent DNA intercalator and inhibitor of topoisomerase II.[79–81] AQ4N potentiates chemotherapies including cisplatin when co-administered,[82,83] and is in early-stage clinical trials.[84]

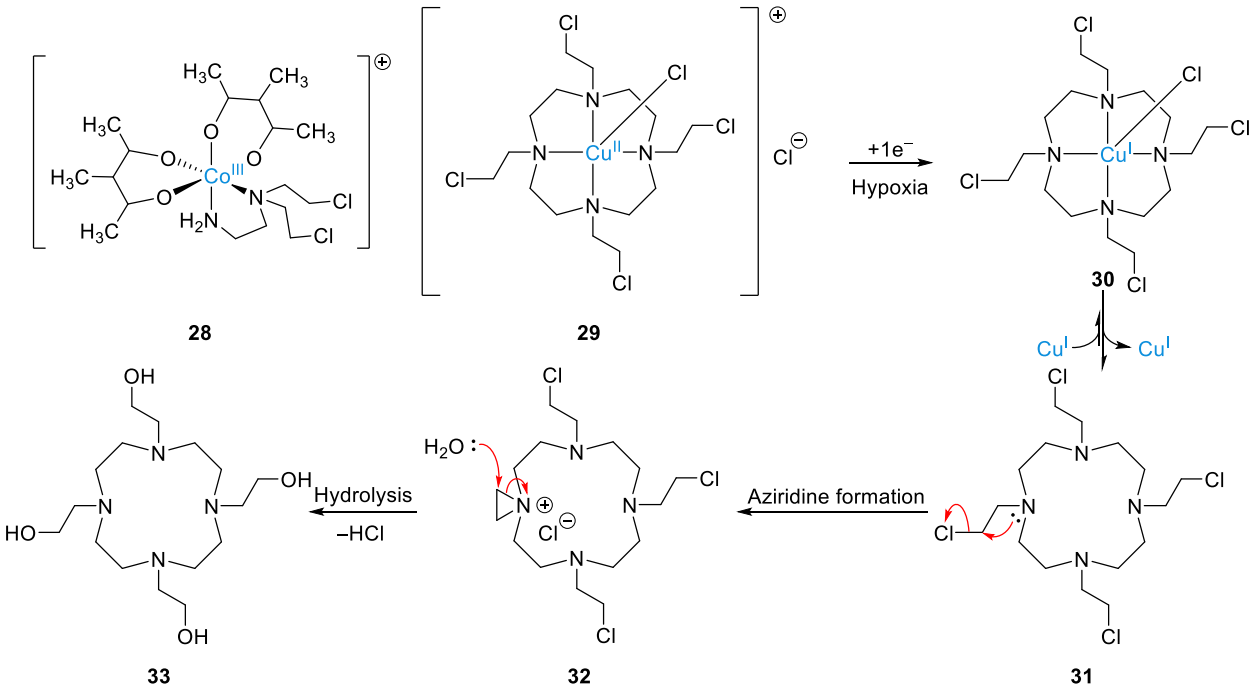


AQ4N, **26**

AQ4, **27**
DNA intercalator,
topoisomerase II
inhibitor

Scheme 6: The aliphatic *N*-oxide bioreductive drug AQ4N **26** and its active metabolite AQ4 **27**. Two-electron reduction of each *N*-oxide of AQ4N by cytochrome P450 enzymes gives the metabolite AQ4, which is a DNA intercalator ($K = 3.3\times10^6\ M^{-1}$)[79] and potent topoisomerase II inhibitor (total inhibition at 2 μM AQ4).[79]

1.3.2.4 Transition metal complex HAPs



28 **29** **30** **31** **32** **33**

Scheme 7: Two transition metal-based HAPs. Both metals (Co(III) in **28**, Cu(II) in **29**) are reduced under hypoxia to give less-stable complexes. The metals then decomplex from the ligands, which in turn makes the ligands become more reactive. In the case of **31**, the nitrogen atoms act like nitrogen mustards, undergoing intramolecular nucleophilic displacement of chloride and aziridinium formation. These aziridinium ions then undergo hydrolysis, leading to release of stoichiometric amounts of HCl.

Compared with these other classes of hypoxia-activated prodrugs, transition metal complexes have received relatively little attention. One early example used complexes of cobalt(III) with three bidentate ligands (such as **28**, Scheme **7**), one of which was a form of nitrogen mustard.[85] These complexes were tailored to have reasonable aqueous stability in the 3+ oxidation state, but to be much more labile to aqueous hydrolysis upon single-electron reduction from Co(III) to Co(II) under hypoxia. Dissociation of the metal from the complex occurs, releasing the reactive nitrogen mustard. These particular complexes suffered from poor aqueous solubility, but their principles were later built upon to produce multidentate nitrogen mustard complexes of Cu(II), such as **29** (Scheme **7**).[86] These complexes again had tuneable aqueous stability and increased cytotoxicity to hypoxic cells.

1.4 Cancer imaging

Medical imaging is one of the most crucial pillars of modern medicine. Imaging techniques can be used for many purposes, from initial diagnosis to disease staging to monitoring therapeutic interventions, as well to guide surgical intervention. Imaging is ubiquitous in the treatment of cancer and has found success in screening programmes for improving early diagnosis and intervention.

There are many modalities that have been invented and developed for medical imaging purposes. One of the earliest and most well-known is the use of X-rays, pioneered by German physicist Wilhelm Röntgen, which provides image contrast based on tissue density, and is a whole-body imaging technique.[87] Other whole-body techniques include Magnetic Resonance Imaging (MRI or sometimes simply MR), Computed Tomography (CT), Positron Emission Tomography (PET) and Single-Photon Emission Computed Tomography (SPECT). Other techniques include fluorescence imaging, Raman imaging, and photoacoustic (PA) imaging.

Some of these techniques can be used without the aid of chemical contrast agents and are entirely non-invasive.[88] Other techniques require the use of specialised contrast agents. This review does not cover all medical imaging techniques, but a select few which all make use of exogenous contrast agents to produce an imaging signal.

1.4.1 Contrast-enhanced imaging modalities

Whilst many imaging techniques can be performed without the use of contrast-enhancing chemicals (including CT and MRI), there are others which require exogenous chemical agents to provide an imaging signal. A selection of these modalities and their contras enhancing agents are discussed below.

1.4.1.1 Magnetic Resonance Imaging (MRI)

Magnetic Resonance Imaging (MRI or MR) is a nuclear imaging technique that is analogous to the Nuclear Magnetic Resonance (NMR) spectroscopy that is familiar to chemists. MRI relies on the intrinsic spin of certain atomic nuclei, and the polarisability of these spins in a powerful magnetic field.[88] When conducted without the use of exogenous contrast agents, MRI typically observes the nuclear spin of protons in the water which makes up the bulk mass of tissue.

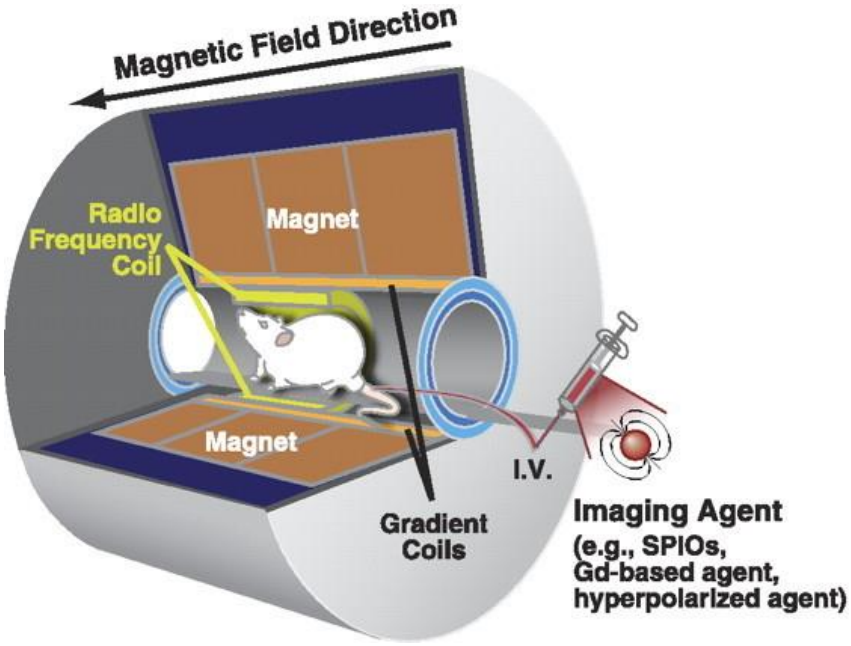
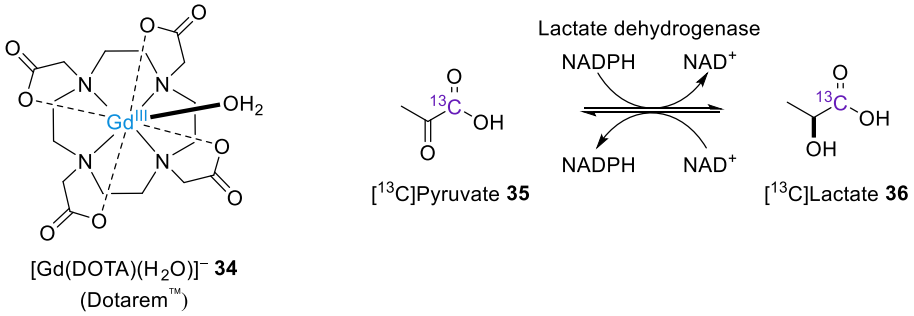


Figure 6: A general summary of practical magnetic resonance imaging. The subject is placed inside an electromagnet, with or without administration of an imaging (contrast) agent. The observed nuclei have their bulk magnetisation vector offset from the primary field vector by radiofrequency coils, and then decay of this magnetization is recorded. Image adapted from Gambhir and James, *Physiol. Rev.*, 2012, 897-975, under a Creative Commons (CC-BY) license.[88]

More advanced techniques rely on other properties of the observed endogenous molecules; for example, Diffusion-Weighted MRI (DW-MRI) measures the cellularity of tissue by detecting differences in the diffusion rates of bulk water. Blood Oxygen Level-Dependent MRI (BOLD-MRI), by contrast, measures differences in blood oxygen content. The iron centre of haemoglobin is paramagnetic when deoxygenated and diamagnetic when oxygen is bound.[89] This difference can be measured, and has been used to show physiological functions such as brain activity or oxygen delivery to perfused tumours.[90,91]

In addition to using endogenous molecules to produce an MRI signal, exogenous contrast agents are also frequently used. These include hyperpolarised gases and small molecules, such as hyperpolarised ^{13}C and ^{129}Xe MRI to analyse amino acid metabolism and airway perfusion, respectively.[92,93] Complexes of transition metals are also frequently used, the most common metal being gadolinium(III); all FDA-approved

clinical contrast agents are Gd(III)-chelates.[94] These complexes usually work *via* transfer of magnetisation to the bulk water around them, increasing local relaxivity. Complexes are optimised to have high Gd-binding constants, and rapid on-off rates for binding of a water molecule at the vacant co-ordination site.[95] This maximises the transfer of magnetisation to local water molecules. Other metals can be used, although none have yet been approved for clinical use. Amongst the other forms of contrast agent under study are super-paramagnetic iron oxide nanoparticles (SPIONs),[96] and perfluorinated lipids and micelles.[97,98] Some typical contrast agents are shown given in Figure **7**.



[Gd(DOTA)(H_2O)]$^-$ **34** (Dotarem™)

[^{13}C]Pyruvate **35**

[^{13}C]Lactate **36**

Figure 7: Structures of some MRI contrast agents. Dotarem™ **34** is penetrant of leaky vasculature and crosses the compromised blood-brain barrier (BBB). It is used to image lesions of the spine and brain. Hyperpolarized [^{13}C]Pyruvate **35** can monitor metabolic flux of pyruvate and lactate.[99]

Some of the key strengths of MRI as an imaging technique are its excellent tissue penetration; that often exogenous agents are not required; the use of non-ionising radiation; structural and functional information that can be gleaned; and the wide clinical applicability that illustrates its excellent safety profile.[88] Limitations include its lack of sensitivity compared with other techniques, resulting in large amounts of contrast agent being required. MRI also requires comparatively lengthy acquisition times for an adequate image, which can put it at odds with the rate of physiological processes as well as confounding factors such as an unfixed frame of reference (*i.e.* normal motion of living subjects).

1.4.1.2 Single-photon emission computed tomography (SPECT)

SPECT is a nuclear imaging technique that uses imaging agents that bear radionuclides that emit gamma rays.[100] These nuclides include ^{99m}Tc, ^{125}I and ^{11}In, which are usually incorporated into a molecule as either a coordination complex or covalently. The gamma rays emitted are highly penetrant of tissue and are detected externally; however, the single photon emitted from each nuclide means that calculating origin of detection is challenging. Modern SPECT apparatus use collimators to filter out diagonally incident photons, but this significantly reduces the sensitivity of SPECT.[88]

SPECT agents can be targeted to specific biological features such as overexpressed receptors associated with cancer, such as c-Met,[101] or monoclonal antibodies which bind extracellular receptors such as EFGR (Figure **8**).[102,103]

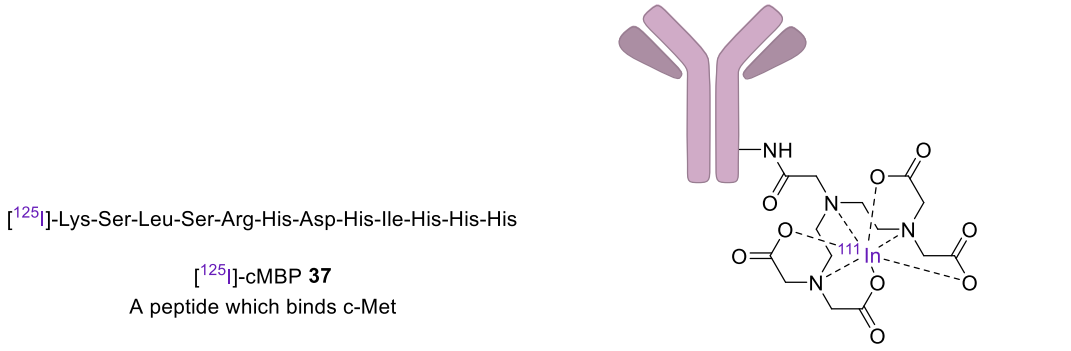


Figure 8: Examples of targeted SPECT imaging agents. [^{125}I]-cMBP **37** is a radiolabelled peptide which binds to c-Met, a receptor tyrosine kinase which is overexpressed in many cancers.[101] **38** is an anti-epidermal growth factor receptor (EGFR) monoclonal antibody (mAb), bioconjugated to a DPTA chelator which binds ^{111}In, a SPECT radionuclide.[102,103]

1.4.1.3 Positron emission tomography (PET)

Positron Emission Tomography (PET) is a widely-used clinical imaging technique, utilised for imaging of conditions such as Alzheimer's and Parkinson's disease,[104] cardiac conditions such as myocardial infarction and ischemia,[105,106] and many different forms of cancer.[107,108] PET imaging uses exogenous imaging agents which contain β-emitter radionuclides, such as ^{11}C, ^{18}F, ^{68}Ga, and ^{89}Zr.[109] The nuclide in question is unstable and undergoes β^+ decay, in which a proton decays into a neutron. This process is exoenergetic, with the energy being emitted in the form of both a neutrino ($\bar{\nu}_e$) and a high-energy positron (e^+, the antiparticle of an electron). In tissue, this positron travels a very short distance (up to a few millimetres)[110,111] before encountering an electron (electrons being abundant in tissue). When this antiparticle pair meet they are attracted to each other, collide and annihilate. The energy produced is emitted as two high-energy γ-photons of equal energies (≈ 511 keV) and with antiparallel vectors. These photons are highly penetrating of tissue and are emitted

from the body. In PET imaging, a tomographic detector can detect these emitted photons and correspondingly calculate their origin of emission.[112]

A major advantage of PET imaging is the nature of the radionuclides used. ^{11}C and ^{18}F, for example, can be incorporated into small-molecule drugs and imaging agents which can have relevant pharmacological behaviour. [^{18}F]-fluorodeoxyglucose (^{18}F-FDG **39**, or FDG), for example, is an antimetabolite analogue of glucose and is taken up by cells, both passively and *via* active transporters such as GLUT1.[113,114] These transporters are highly expressed by cells undergoing higher rates of glycolytic (anaerobic) metabolism, a characteristic of tumour cells and in particularly hypoxic tumour cells.[113] This preferential uptake allows FDG to accumulate in highly metabolically-active cells, such as those of a tumour. This gives an enhanced signal-to-noise ratio and provides functional information for the radiographer – in this case comparative rates of glycolysis.

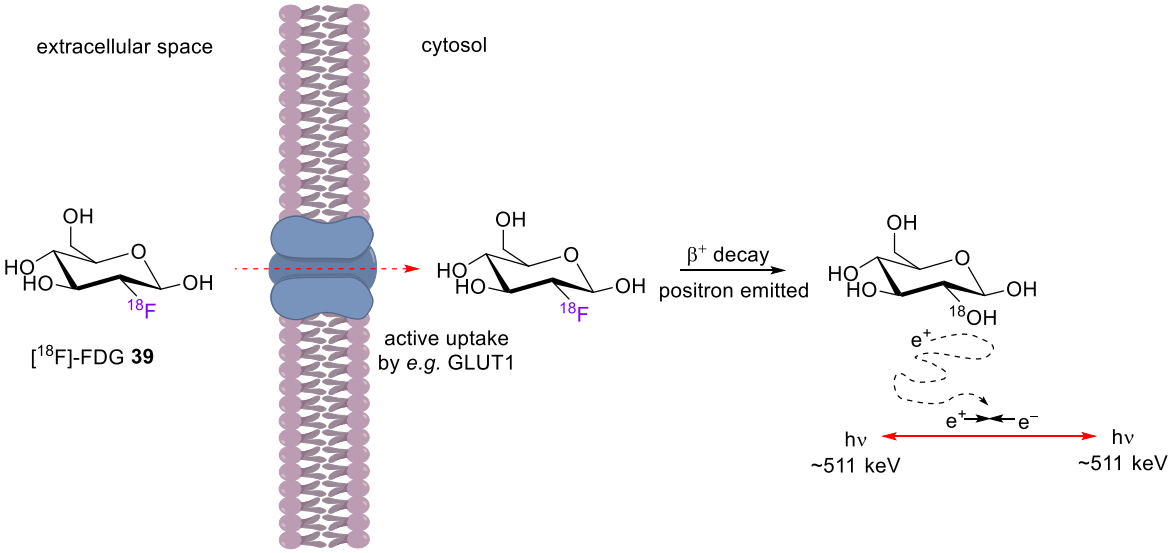


Figure 9: [^{18}F]-FDG as a PET imaging agent. As a glucose analogue, [^{18}F]-FDG is actively taken up by cells undergoing elevated levels of glycolysis, such as rapidly dividing tumour cells. The ^{18}F label then undergoes β^+ decay, and the emitted positron meets a nearby electron. The annihilation produces two antiparallel γ-photons of equal energy, which can then be detected.

By contrast, ^{68}Ga and ^{89}Zr are transition metals that cannot be incorporated into small molecules in the same manner as ^{18}F. They can, however, form complexes with

multidentate ligands, and these complexes can be further appended with other useful functionalities. For example, tethering a radionuclide complex to a monoclonal antibody for receptors such as Her2,[115] or ligands for extracellular receptors such as the human prostate-specific membrane antigen (PSMA)[116] can provide exquisite targeting properties to the imaging agent. Moreover, such bioconjugates often exhibit other advantageous properties over small-molecule tracers, such as enhanced biological stability, reduced toxicity and enhanced signal-to-background.

Despite the excellent tissue penetrance of PET imaging, this technique has limitations. PET provides no anatomical reference frame (*i.e.* PET signal does not provide an image of the whole body it is imaging), and so must be combined with other techniques, such as magnetic resonance imaging (MRI) or computed tomography (CT) to provide anatomical localisation. Spatial resolution of PET is also far lower than techniques such as optical (fluorescent, luminescent) imaging. Emitted positrons may travel up to a few millimetres before annihilating, and imprecision in detector equipment may further reduce resolution; as such, clinical PET has a spatial resolution of ~5–7 mm.[88]

Synthesis of radiolabelled ligands differs from conventional chemical synthesis. $^{18}F_2$ is produced in a cyclotron and must be rapidly converted into the desired fluorinating chemical reagent. These reagents include the $^{18}F_2$ directly, electrophilic $^{18}F^+$ reagents such as ^{18}F-NFSI and ^{18}F-SelectFluor®, nucleophilic $^{18}F^-$ reagents such as K^{18}F and H^{18}F, or deoxofluorinating reagents such as ^{18}F-DAST or ^{18}F-Deoxo-Fluor®. Once produced and adequately purified, these reagents must then be used in rapid fluorination reactions and the products purified. During this process the ^{18}F component of the sample is undergoing constant β^+ decay to ^{18}O, reducing the total activity of the sample and ultimately its usefulness as a dose of PET imaging agent.

Consequently, radiofluorination reactions are not optimised for yield or fluorine incorporation. Rather, they are optimised for their radiochemical yield (RCY) and the specific activity of the purified sample. Often, very small quantities of compound are required (< 1 μmol) to still retain a clinically useful activity. Reactions are often under forcing conditions, using low-volatility polar solvents such as DMF, DMA and NMP, and elevated temperatures (typically > 100 °C). Radiosynthesis using other PET radionuclides is also subject to similar consideration to those for ^{18}F radiolabelling.

1.4.1.4 Fluorescence imaging

Fluorescence is a phenomenon in which a molecule in a high-energy state releases some of that energy in the form of photons. The processes by which fluorescence occurs can be represented by a Jabłoński diagram, as shown in Figure **10** below.

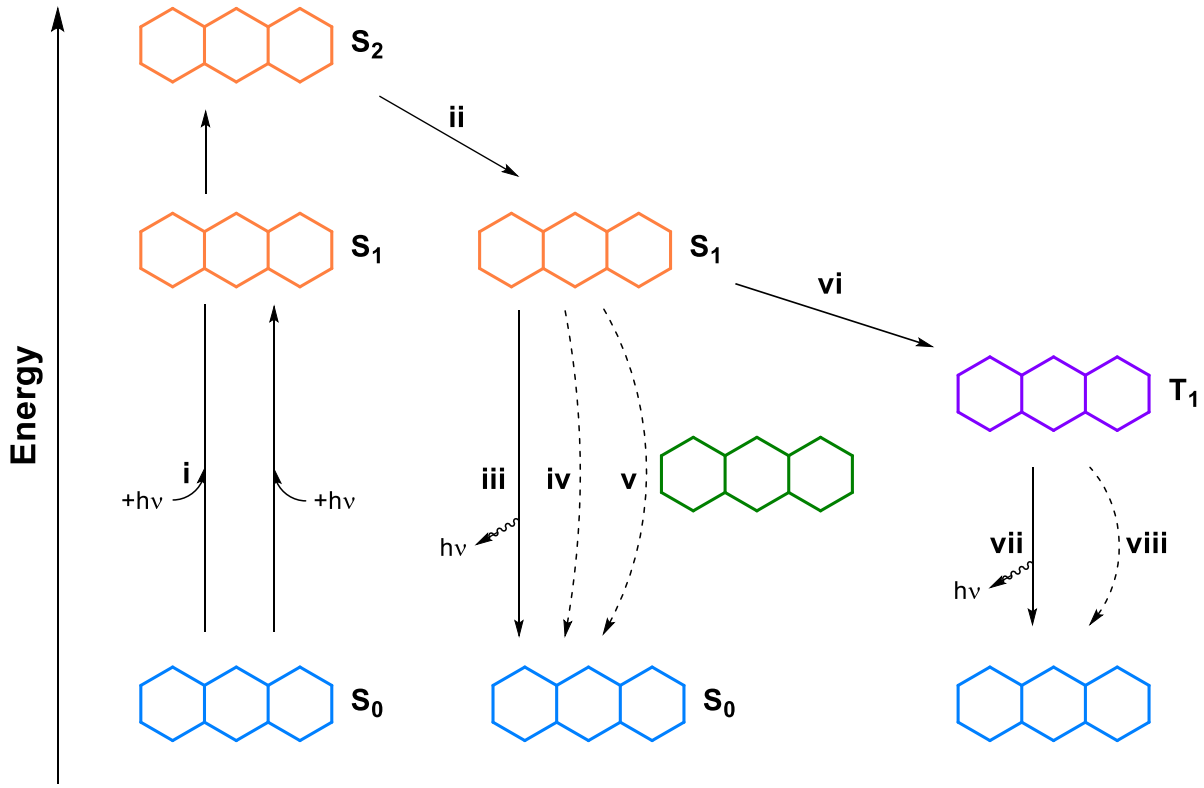


Figure 10: Jabłoński diagram illustrating the interaction of fluorophores and chromophores with incident photons. (i) absorption of a photon to give an excited state, (ii) internal conversion to S_1, (iii) fluorescence, (iv) nonradiative decay from a singlet state, (v) Förster resonance energy transfer (FRET), (vi) intersystem crossing from singlet state S_1 to triplet state T_1, (vii) phosphorescence, and (viii) nonradiative decay from a triplet state.

A fluorescent molecule begins in an energetic ground state, S_0, and one of its electrons is then excited to a higher energy singlet state S_1 by absorption of a photon with the correct quanta of energy (step i). If the absorbed photon is energetic enough to excite the molecule above S_1 (*i.e.* to S_2) the molecule may then lose some of this energy thermally *via* internal conversion processes (step ii), until it reaches S_1. From this state, there are 4 pathways by which the molecule may lose energy and return to the energetic ground state S_0. The first is fluorescence (step iii), in which the energy is emitted as a fluorescence photon – this is the process on which fluorescence imaging relies. However, other competing processes may also take place. Some molecules may undergo non-radiative decay, in which the energy is released thermally (step iv). Other molecules which are nearby in solution may also absorb the energy of the excited molecule (step v), a process known as Förster resonance energy transfer (FRET). If the S_1 state is long-lived, the molecule may undergo a "forbidden" transition to an excited triplet state T_1; this process requires the excited electron to change spin state, which is quantum mechanically disallowed but in practice may still occur (step vi). From this triplet state the molecule may relax back to the electronic ground state *via* emission of a photon (step vii). This process is known as phosphorescence, and emitted photons are typically lower in energy than the corresponding fluorescence photons. Finally, the triplet state T_1 may also return to the ground state *via* non-emissive processes (step viii).[117] Many fluorophores are designed to have "push-pull", or "donor-acceptor" electronics, which often result in suitable HOMO-LUMO gaps for them to exhibit fluorescence.[118]

The fluorescent properties of small molecules has been a mainstay of molecular and cell biology for many decades, and a great host of fluorescent probes have been developed.[119,120] These probes are used for many purposes, including monitoring

mitochondrial pH,[121] detecting changes in metal ion concentrations,[122] studying amyloid-β aggregates in neurodegenerative diseases,[123,124] and soluble ions.[125] Some examples are given below (Figure **11**).

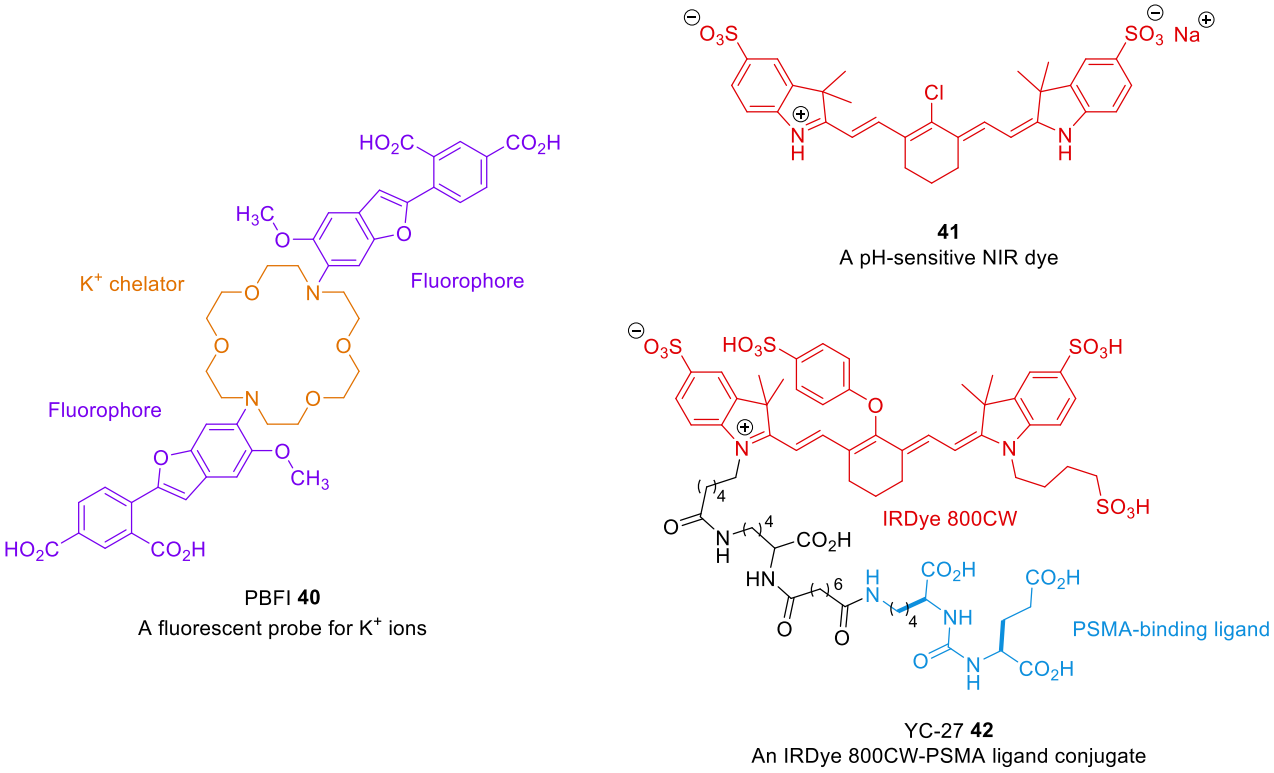


Figure 11: Some examples of fluorescent probes. PBFI **40** binds K^+/Na^+ *via* the crown ether (orange), and was the first fluorescent probe for K^+.[126] **41** is sensitive to protonation state.[127] YC-27 **42** is a conjugate of a commercial NIR dye (IRDye 800CW) with a prostate-specific membrane antigen (PSMA)-binding ligand.[128]

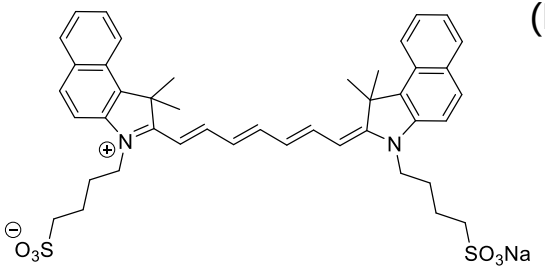
Fluorescence imaging has several advantages over other imaging techniques. Photons emitted by fluorophores are not confined to a single or small range of energies. Unlike PET imaging (where emitted gamma rays have a well-defined energy regardless of the emission source), fluorescence photons have energy ranges and emission maxima that are dependent on the identity of their emission source. Consequently, a broad palette of fluorophores has been developed, and many fluorophores can be used in a single experiment to highlight different cellular structures or processes, providing researchers with unprecedented detail. Fluorescence imaging

can also provide exquisite resolution, allowing minute processes and structures to be visualised on a sub-cellular level.[129]

Despite the many advantages that fluorescence imaging has in cellular imaging, it has some significant disadvantages when applied to biomedical imaging. The greatest amongst these is penetration depth: most fluorophores emit in the UV or visible range of the EM spectrum, and tissue is both highly absorbent of these wavelengths and causes significant scattering of photons.[88] This dramatically reduces the depth from which fluorescent signal can be detected, reducing its utility in whole-body imaging.

The challenge of tissue penetration can be partially overcome with the use of near-infrared (NIR) fluorophores. Photons with frequencies in the NIR range are more penetrating of tissue, and can be imaged at depths of up to ~1 cm. This makes them useful for preclinical experiments, as well as for topical imaging applications, and endoscopy.

(A)



Indocyanine green, ICG **43**

(B)

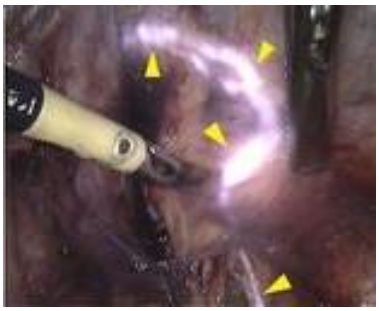


Figure 12: (A) The structure of indocyanine green (ICG, **43**), the only FDA-approved near-infrared fluorescent dye for clinical use. (B) Real-time intraoperative imaging of sentinel lymph nodes and lymphatic vessels (highlighted with yellow arrows) during the surgical resection of a gynaecological cancer in a female patient. Image adapted with permission under a Creative Commons Attribution 4.0 International License (https://creativecommons.org/licenses/by/4.0/) from Laios, Volpi, Tullis, *et al*. *BMC Res. Notes* **2015**, *8*, 608.[130]

An example of the utility of fluorescent medical imaging is the use of indocyanine green (ICG **43**, Figure **12a**), a polymethine NIR fluorophore which is the only FDA-approved fluorescent imaging agent for clinical use.[131] ICG is used for vascular imaging, but has also found use in real-time intraoperative surgery. Fluorophore

imaging, unlike other modalities, does not require bulky equipment and long acquisition times for imaging, and has been recently used in real-time for guiding surgery (Figure **12b**).[130]

1.4.2 Hypoxia imaging

An ongoing challenge in biomedical imaging is developing methods which can distinguish different types of tissue and identify cancerous lesions. One area of significant focus in recent years has been the use of targeted imaging agents which are selective for hypoxic tissue.[132,133] Identifying hypoxic tissue through imaging offers several advantages for treatment, including for cancer staging, stratification of patients for treatment, guiding surgery, and predicting response to therapy. Several strategies for identifying hypoxic tissue through imaging have been and continue to be explored, and these are summarised below.

Several approaches involve using the same hypoxia-targeting mechanism as hypoxia-activated prodrugs. A number of nitroimidazole-containing agents have been developed which target imaging agents to regions of hypoxia.[134] These include Pimonidazole **5**, (discussed in Chapter 1.3.2.2), PET imaging agents such as [^{18}F]-FMISO **44**, [^{18}F]-FAZA **45** and [^{18}F]-AmBF$_3$-Bu-2NI **46**, and fluorophore probes such as **47** (Figure **13a**).

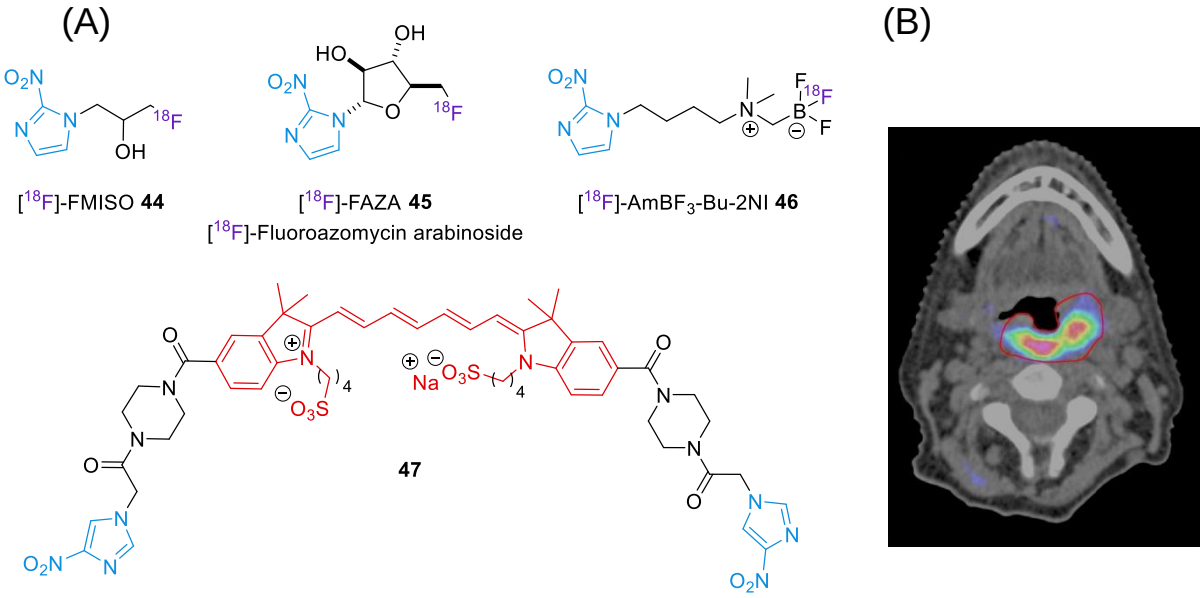
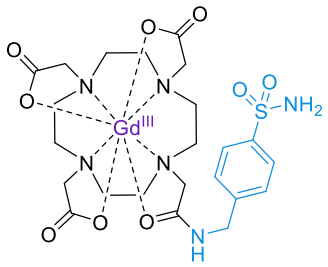


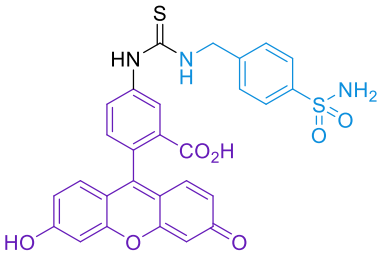
Figure 13: (A) Structures of some nitroimidazole-bearing hypoxia-targeted imaging agents. [^{18}F]-FMISO **44**,[135] [^{18}F]-FAZA **45**,[136] and [^{18}F]-AmBF$_3$-Bu-2NI **46**,[137] are all PET imaging agents, whilst **47** is a fluorescent imaging agent.[138] (B) [^{18}F]-FAZA PET imaging of a patient with oropharyngeal cancer. The red line illustrates the Gross Tumour Volume (GTV). Reused with permission from Mortensen *et al*., *Radiother. Oncol.*, 2012, 14-20.[139]

The nitroimidazole-based imaging agents described in Figure **13** above work *via* two distinct mechanisms. The ^{18}F PET imaging agents rely on reduction of the nitroimidazole under hypoxia leading to protein alkylation (*c.f.* Pimonidazole **5**), causing retention of the agent in hypoxic cells. The fluorescent imaging agent **47**, on the other hand, relies on intramolecular charge transfer (ICT) between the excited fluorophore and the nitroimidazole ring, which acts as an intramolecular quencher of fluorescence. Reduction under hypoxia gives the aminoimidazole and associated metabolites which no longer exhibit ICT, allowing unquenched fluorescence.[138]

Another strategy for targeting imaging agents to hypoxia is the exploitation of receptors and proteins which are overexpressed by hypoxic cancer cells. A variety of imaging modalities have been applied to ligands and antibodies for hypoxia-associated protein targets, including carbonic anhydrase IX (CAIX), examples of which are given in Figure **14** below.[140,141]



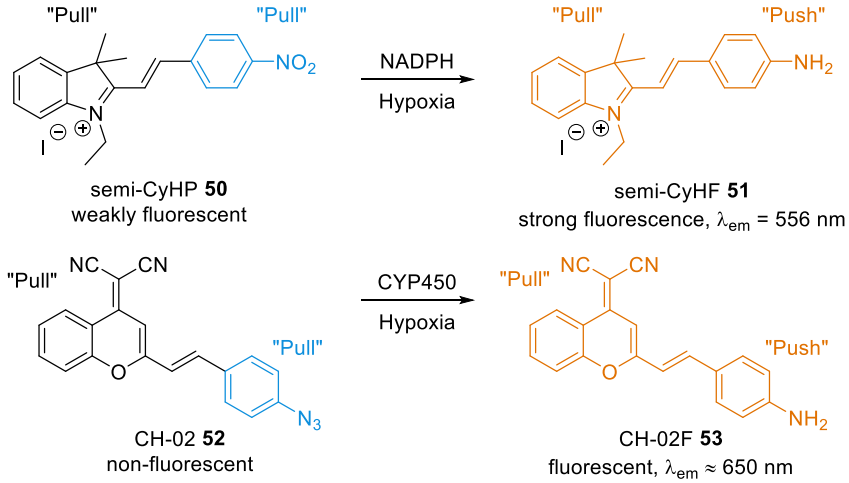
48
A CAIX-targeted MRI contrast agent



49
A CAIX-targeted fluorophore

Figure 14: Two imaging agents which target carbonic anhydrase IX (CAIX), a surrogate biomarker overexpressed on the surface of hypoxic cells.[142,143] **48** is a Gd(III) MRI contrast agent,[140] while **49** is a fluorophore.[141] Both bear benzenesulfonamide moieties, shown in blue, which bind to CAIX.

Another mechanism by which imaging agents are activated in hypoxia is *via* alteration of the molecule's electronics after metabolism. In a similar manner to HAPs that work *via* molecular fragmentation, conversion of an electron-withdrawing nitro group to an electron-donating metabolite may activate an imaging agent. One such example is the fluorophore **51** given below.



Scheme 8: A examples of hypoxia-activated fluorophores which relies on metabolism to alter their electronics.[144,145] **50** is a "pull-pull" molecule, which is weakly fluorescent. Metabolism under hypoxia converts it to **51** which is a "push-pull" molecule, which then exhibits strong fluorescence. CH-02 **52** also behaves in a similar manner, being reduced by cytochrome p450 oxidase enzymes under hypoxia to produce fluorophore CH-02F **53**.

1.5 Theranostic agents

A "theranostic" agent is the name given to a chemical entity designed to have both therapeutic efficacy and provide some form of diagnostic information to a clinician.[146] This concomitant imaging and therapeutic delivery is usually achieved by

combining a known therapeutic agent and an imaging probe with some form of targeting mechanism.

Theranostic agents may be, for example, bioresponsive materials such as nanoparticles or hydrogels which release the agent after certain stimuli, such as change in tissue pH.[147,148] Others may be targeted to certain tissues through use of antibody-drug conjugates or receptor-binding ligands.[149] Therapeutic modalities other than drug delivery may also be incorporated into theranostic agents, such as photothermal ablation of cancer cells.[150] A wide variety of theranostic agents have been developed over the last few years, however, very few have been developed to be responsive to tumour hypoxia.[151,152]

1.6 Aims

Developing new methods of treating cancer through targeted agents has become increasingly relevant in recent years. Many new chemotherapies are in development which target the molecular mechanisms on which cancer cells rely to thrive; however, these therapies often target processes which are also critical to the survival of healthy tissue. It therefore follows that methods of targeting these therapies to cancerous tissue selectively will bring about significant benefits in both treatment outcomes and patient quality of life. A highly promising method is targeting severe tissue hypoxia, which is found predominantly in solid tumours. To date, most efforts in this area have been focused on targeting chemotherapies that are broadly cytotoxic. We hypothesise that combining targeting strategies for tumour hypoxia with molecularly-targeted therapies will prove advantageous in delivering new generations of cancer-specific chemotherapies. One of our aims was therefore to apply bioreductive hypoxia-targeting motifs, primarily nitroaromatic groups, to ligands which are under pre-clinical or clinical investigation as molecular-targeted cancer therapies.

A further challenge to the development of hypoxia-activated prodrugs is an understanding of their behaviour *in vivo*. Hypoxic tumours often have heterogenous levels of perfusion and some regions may be significant distances from supplying vasculature. This can lead to poor exposure in some regions of a tumour to the HAP under study. To give better understanding of the behaviour and distribution of HAPs both *in vitro* and *in vivo*, we proposed to develop new hypoxia-targeted imaging probes which could be conjugated to therapeutic cargo molecules. These “theranostic agents” would have two significant roles; primarily, they would act as hypoxia-activated prodrugs which deliver the therapeutic cargo to hypoxic tissue selectively. Concomitantly, they would provide an activatable imaging signal which would report on localisation of delivery. In Chapters 3 and 4, we discuss our efforts towards new hypoxia-activated fluorescent agents which we hypothesised could form the basis of theranostic agents. In Chapter 5, we discuss the synthesis and evaluation of another hypoxia-activated fluorophore, and a potential theranostic agent based upon its scaffold.

Chapter 2
Towards Hypoxia-Activated Prodrug Forms of the Clinical Candidate Chk1 Inhibitor SAR020106

2.1 Checkpoint 1 Kinase (Chk1)

2.1.1 Structure and function

Checkpoint 1 kinase (Chk1, Figure **15**) is a serine/threonine kinase with a mass of ~54 kDa,[153] containing an N-terminal kinase domain, a flexible linker region, and a C-terminal region which in associated with regulation of Chk1 activity.[154,155] The kinase domain has a typical ATP binding cleft, found at the interface between the kinase two lobes of the kinase two-lobe fold.

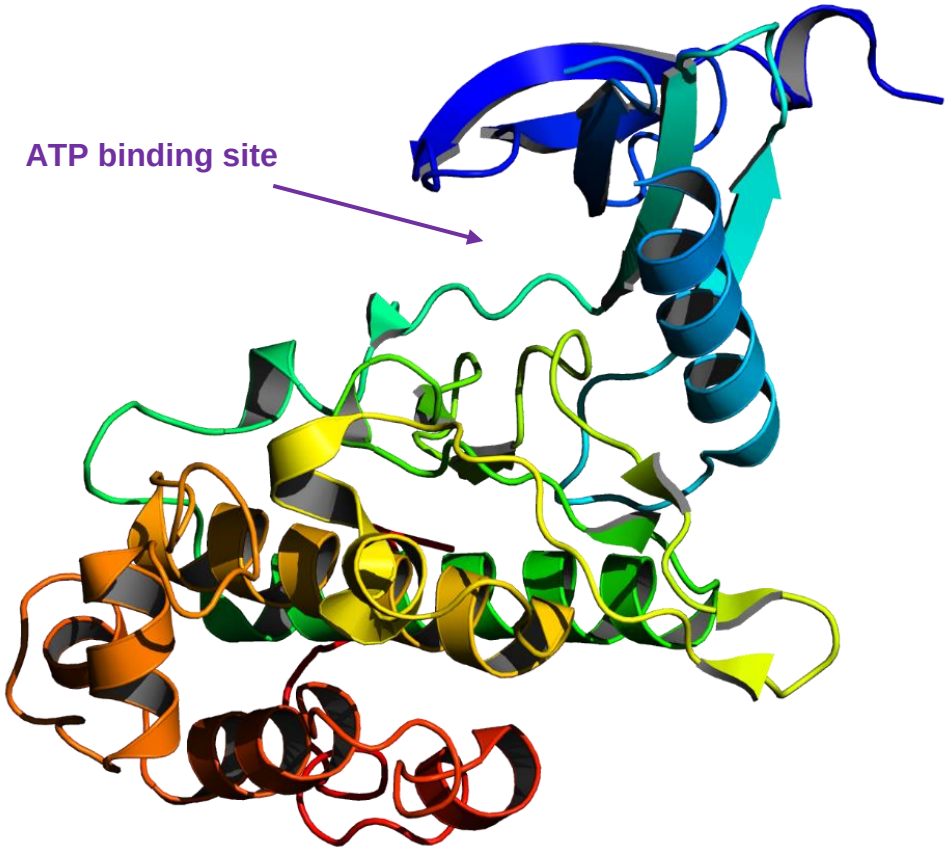


Figure 15: X-Ray crystal structure of *apo*-hChk1 (PDB: 1ia8).[156] The ATP binding site is highlighted.

Chk1 is involved in a number of signalling pathways (Figure **16**, below), and lies downstream of the phosphatidylinositol 3-kinase (PI3K) family.[157] Chk1 is directly

downstream of ataxia-telangiectasia mutated and rad3-related protein (ATR), a critical kinase involved in induction of the DNA damage response (DDR), the mechanism by which cells respond to DNA damage.[158] Chk1 phosphorylates several downstream target proteins, including the CDC25 family of phosphatases.[70] Phosphorylation of the CDC25 family inhibits dephosphorylation of the cyclin-dependent kinase (CDK) family.[159] Dephosphorylated CDKs help drive the cell cycle, and thus maintenance of CDK phosphorylation results in cell cycle arrest.[70] Both healthy and cancerous tissues use these cell cycle checkpoints to prevent progression to M-phase, allowing time for DNA repair before replication. In this way, Chk1 sits at a crucial point in the DDR signalling cascade.[159–161]

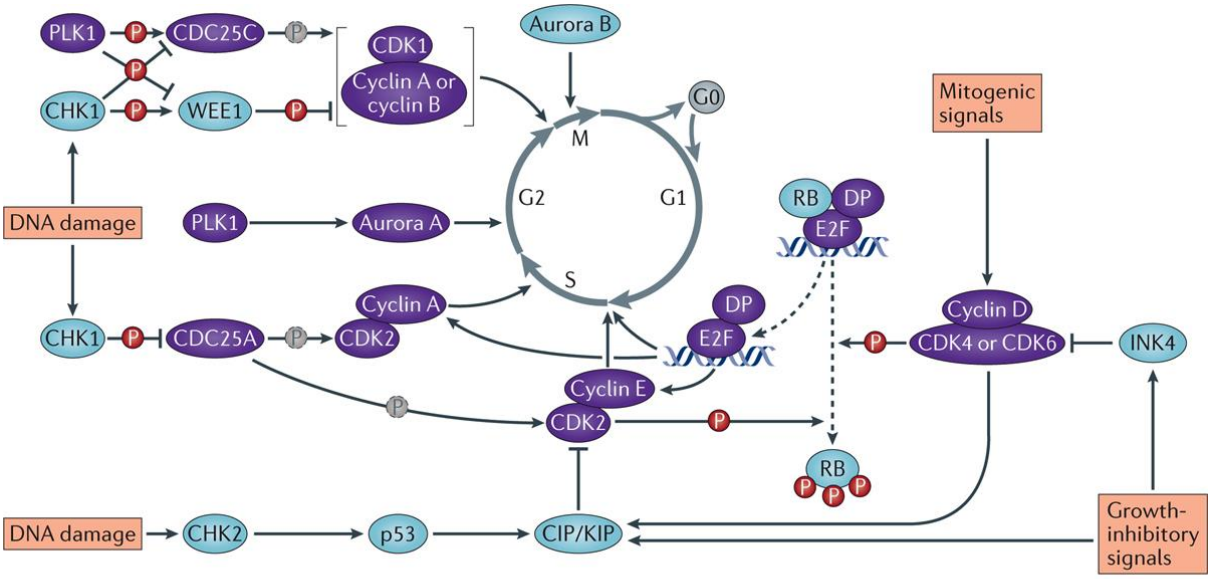


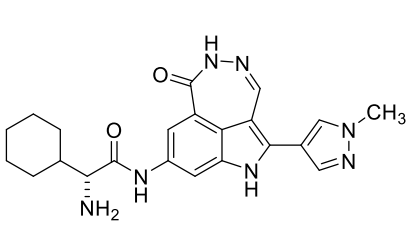
Figure 16: The cell cycle and select signalling pathways which control it progression or arrest. Reproduced with permission from Otto and Sicinski, *Nature Reviews Cancer*, 2017.[162]

Many cancer cells are functionally deficient in the tumour suppressor protein p53 through either mutation or deletion.[163] Cells that are p53-deficient lose control of the G1 checkpoint, making them heavily reliant on the G2 and S checkpoints. Chk1 is therefore a crucial effector of the DNA damage response, and it has been

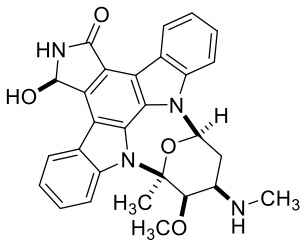
hypothesised that Chk1 inhibition may sensitise cells to both ionising radiation and DNA-damaging drugs.[157,164,165]

2.1.2 Inhibition of Chk1 as a therapeutic strategy

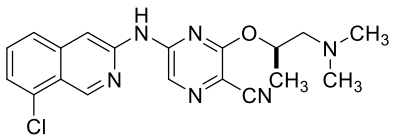
Inhibition of cell cycle checkpoints as a strategy for treatment of cancer has become a field of great interest.[164,165] By preventing cells from delaying their own cycle progression, it is hypothesised that cells will be forced to enter M-phase and undergo genome replication without first repairing damaged DNA. This should lead to exacerbation of intrinsic DNA damage, or that caused by ionising radiation and DNA-damaging agents, resulting in increased genomic instability and ultimately cell death.[166] To this end, a number of small-molecule inhibitors of Chk1 have recently been developed, and are in both preclinical and clinical development.[167–170] Many of these inhibitors are highly selective over the structurally-related Checkpoint 2 kinase (Chk2), and some examples of recent Chk1 inhibitors are given in Figure **17**, below.



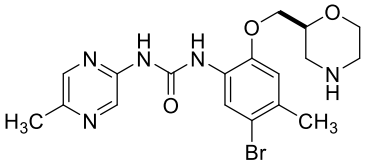
PF-00477736, **54**
Chk1 K_i = 0.49 nM
Chk2 K_i = 47 nM



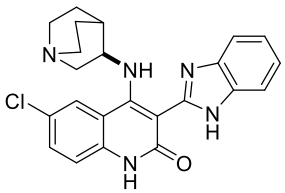
UCN-01, **55**
Chk1 IC_{50} = 11 nM
Ch2 IC_{50} = 1040 nM



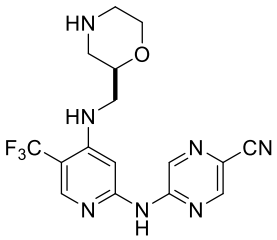
SAR020106, **56**
Chk1 IC_{50} = 13.3 nM
Chk2 IC_{50} > 10000 nM



LY2603618, **57**
Chk1 IC_{50} = 7 nM
Chk2 IC_{50} = 10000 nM



CHIR-124, **58**
Chk1 IC_{50} = 0.3 nM
Chk2 IC_{50} = 697 nM



CCT245737, **59**
Chk1 IC_{50} = 1.4 nM
Chk2 IC_{50} = 9030 nM

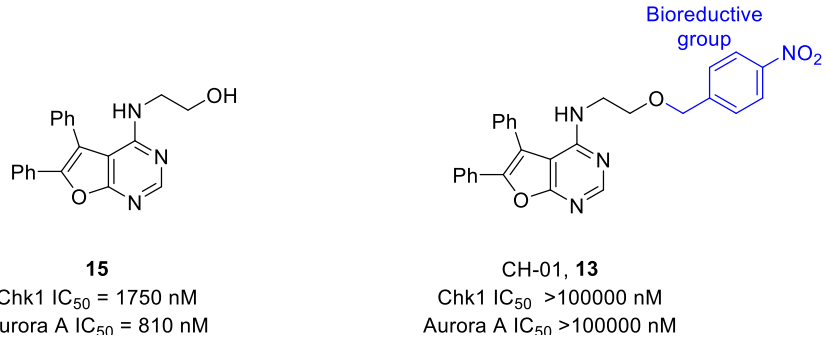
Figure 17: Some examples of clinical and preclinical Chk1 inhibitors PF-00477736 **54**,[171] UCN-01 **55**,[172,173] SAR020106 **56**,[170] LY2603618 **57**,[174] CHIR-124 **58**,[175] and CCT245737 **59**.[169] Their Chk1 and Chk2 inhibition constants (K_i) or IC_{50} values are given.

Inhibition of Chk1 sensitises cells to DNA damaging agents, such as SN-38 and gemcitabine,[168,176,177] as well as to radiotherapy.[178] Furthermore, Chk1 inhibitors are being clinically investigated as single agent therapeutics (NCT02514603, www.ClinicalTrials.gov). Inhibition of Chk1 interferes with the DNA damage response (DDR); in the context of hypoxia, this can result in accumulation of DNA damage and associated toxicity.[179,180] This evidence suggests that inhibition of Chk1 in the context of tumour hypoxia is a promising therapeutic strategy.

2.1.3 Targeted delivery of Chk1 inhibitors

Whilst suppression of the DDR *via* Chk1 inhibition appears promising, it is noteworthy that Chk1-mediated DNA repair mechanisms are also important in maintaining genomic integrity in healthy tissues.[181] It is thus desirable to target inhibitors of the DDR, including Chk1 inhibitors, to cancerous tissues selectively, while sparing healthy tissue. Consequently, it has been a focus of our research group to develop prodrugs which target Chk1 inhibitors to hypoxic regions of tumours. A proof-of-concept molecule, CH-01 **13** (Figure **18a**) was developed by Dr Cindy Cázares-Körner.[51,60] This was a prodrug form of dual Chk1/Aurora A kinase inhibitor **15**,[69] which sensitised cells to hypoxia/reoxygenation and was toxic to cancer cells in an oxygen-dependent manner (Figure **18b**).

(A)



15
Chk1 IC_{50} = 1750 nM
Aurora A IC_{50} = 810 nM

CH-01, **13**
Chk1 IC_{50} >100000 nM
Aurora A IC_{50} >100000 nM

(B)

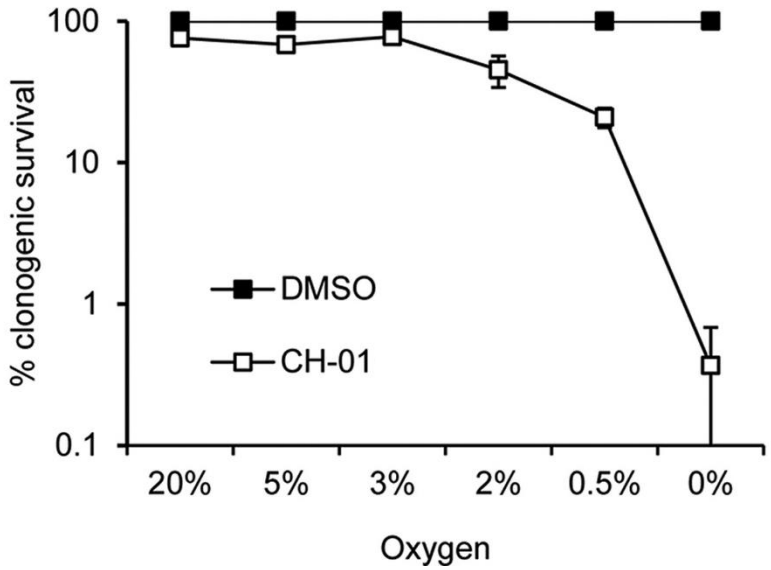


Figure 18: (A) Structures of Chk1/Aurora A kinase inhibitor **15**, and its prodrug form, CH-01 **13**. IC_{50} values are given for both Chk1 and Aurora A. These values were determined by our research group in a radioactive (^{33}P-ATP) filter-binding assay.[51] Literature IC_{50} values of **15** are 309 nM for Aurora A,[69] and 20400 nM for Chk1.[182] (B) Clonogenic survival assay for RKO cells treated with 25 μM CH-01 or DMSO at the stated oxygen tension for 24 hours, demonstrating that CH-01 **13** kills cancer cells in an oxygen-dependent manner.

Having demonstrated that a hypoxia-activated prodrug form of a Chk1 inhibitor can cause hypoxia-dependent toxicity in cancer cells, Dr Cázares-Körner then attempted to make hypoxia-activated prodrug forms of the clinical candidate Chk1 inhibitor SAR020106 **56**.[60] The X-ray crystal structure of SAR020106 **56** bound to Chk1 (PDB: 2ym8, Figure **19** below) showed that the secondary nitrogen atom bridging the two aryl portions of the molecule formed a crucial binding interaction with Glu85 in the ATP binding pocket. Dr Cázares-Körner hypothesised that this would be a suitable attachment point for the hypoxia-activated moiety, since blocking this interaction would

occlude binding, and fragmentation after metabolism under hypoxia would restore this binding interaction (Scheme **9**).

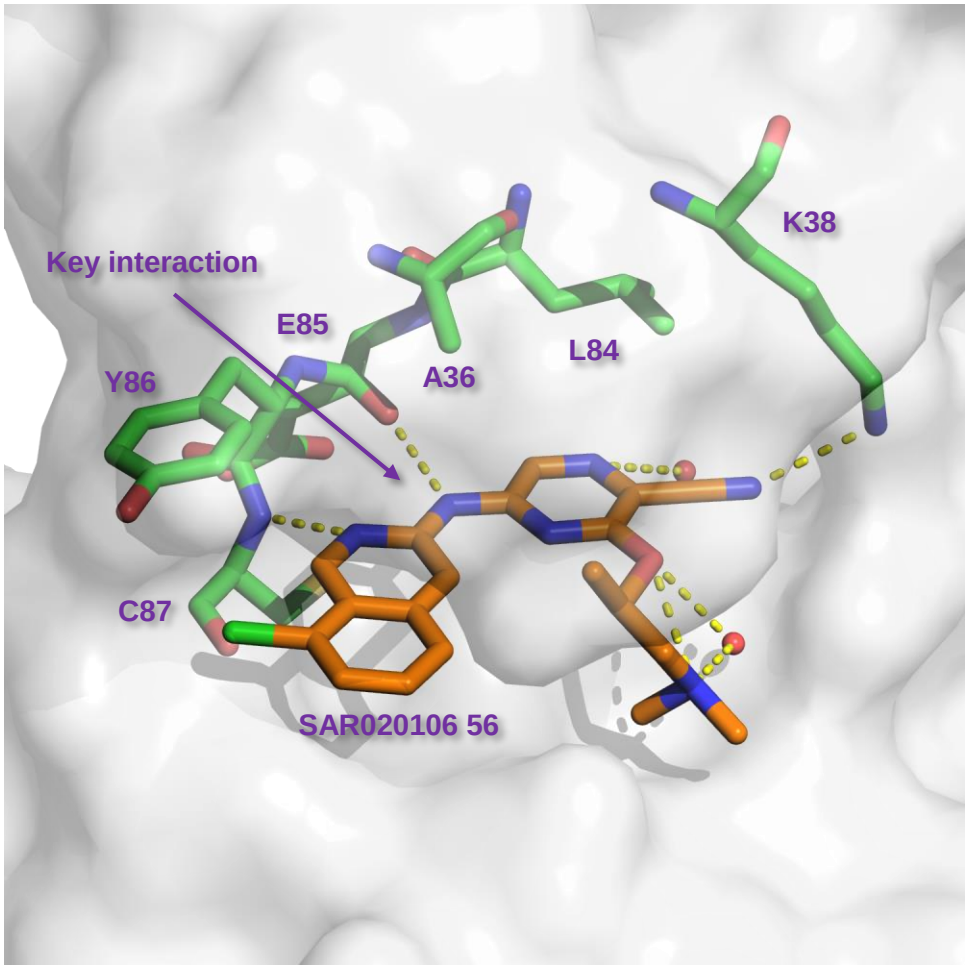
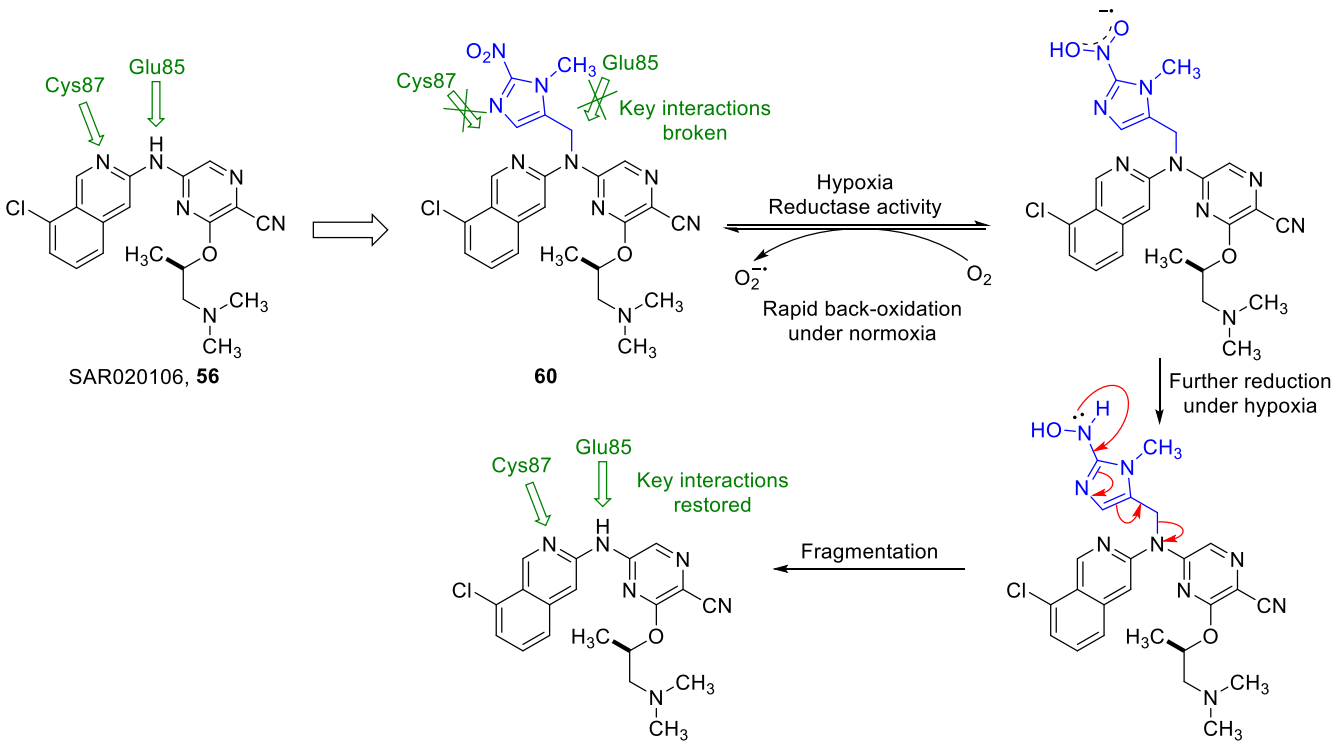


Figure 19: X-Ray crystal structure of SAR020106 **56** bound to the ATP pocket of Chk1 (PDB: 2ym8).[183] Chk1 is shown as a grey van der Waal surface. Key hydrogen-bonding interactions are shown as dashed yellow lines. Water molecules are shown as red spheres. SAR020106 is coloured as carbon = orange, nitrogen = blue, oxygen = red, chlorine = green. Key residues in the active site are shown as sticks (carbon = green).



Scheme 9: Proposed strategy for making SAR020106 **56** into a hypoxia-activated prodrug. Addition of the nitroimidazole moiety should block a key interaction with Glu85, preventing binding. Reduction of the nitroimidazole under hypoxia results in fragmentation, releasing the active inhibitor in hypoxic tissue.

The nitroimidazole prodrug **60** was successfully synthesised by Dr Cázares-Körner, however, it exhibited only a 57-fold lower affinity for Chk1.[60] Whilst **60** was nontoxic to cancer cells under normoxic conditions, no cytotoxicity was observed under hypoxia (as determined by a clonogenic survival assay). *In vitro* study of release of SAR020106 from **60** showed that, whilst the nitroimidazole was metabolised by cytochrome p450 reductase, this metabolite was stable in media and fragmentation was very slow (see Figure **20**).

We therefore hypothesised that the lack of cytotoxicity under hypoxia was a result of slow release of SAR020106 **56**. Rate of ligand release will compete with both drug efflux and metabolism in a cellular setting, and thus slow release likely results in peak exposure at a sub-efficacious concentration. This hypothesis explains the lack of a cytotoxicity towards cells treated with **60** under hypoxia.

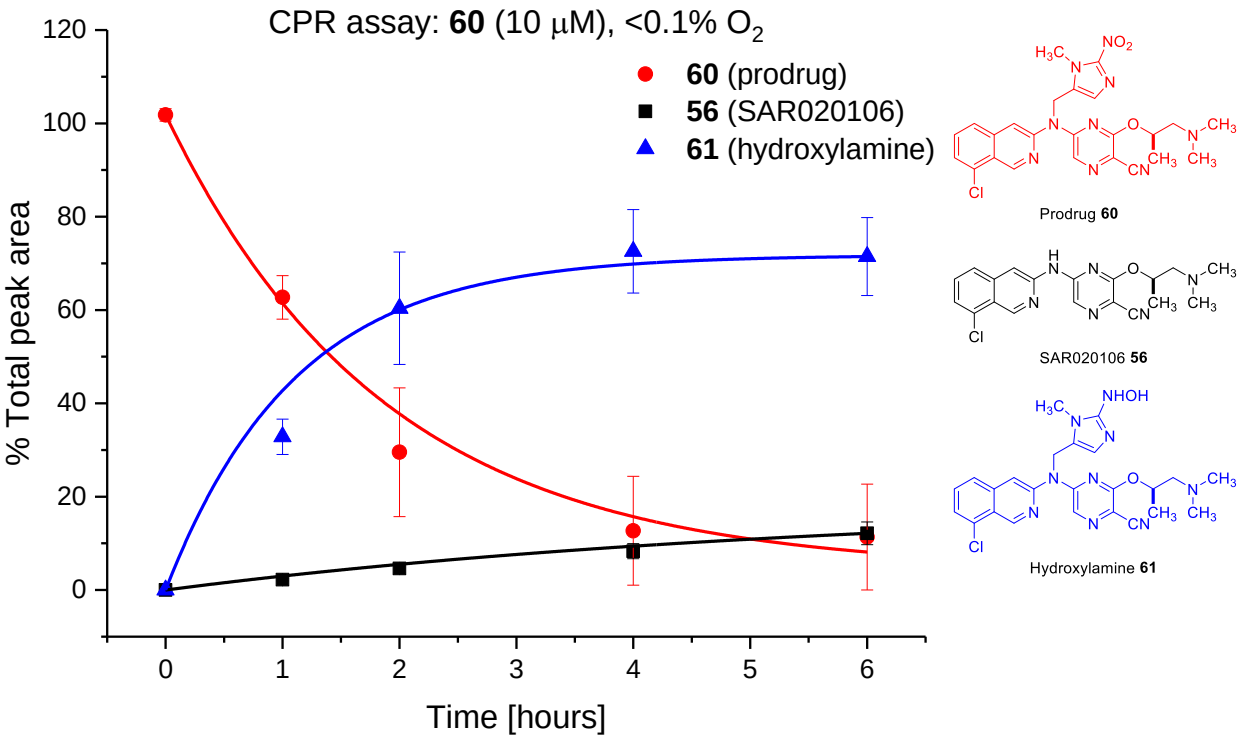


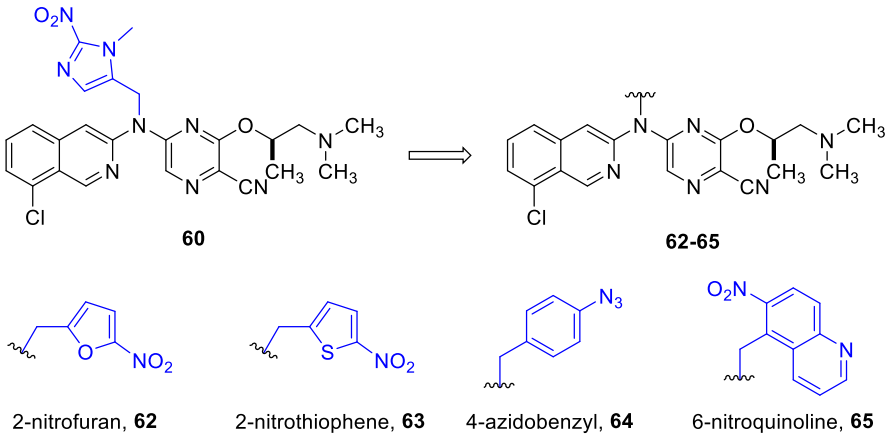
Figure 20: Reaction profile of prodrug **60** in the cytochrome p450 reductase assay. The prodrug **60** (red line) is metabolised quickly, producing the hydroxylamine intermediate **61** (blue line). This intermediate is stable, as indicated by slow release of cargo ligand SAR020106 **56** (black line).

2.2 Aims of the study

The work of Dr Cázares-Körner demonstrated that SAR020106 **56** could be effective in radiosensitising hypoxic cancer cells and exacerbate DNA damage from hypoxia/reoxygenation, as well as kill cells outright. Unfortunately, the nitroimidazole-based bioreductive prodrug form **60** she synthesised did not provide the desired selectivity of drug release under hypoxia.[60] Our hypothesis is that slow release of the drug is the reason for the lack of toxicity in hypoxic cancer cells.

To address the problem of slow compound release, we aimed to synthesise new analogues of SAR020106 **56** appended with alternative bioreductive groups. The reduction of each bioreductive group has a different kinetic behaviour, and it followed that the kinetics of fragmentation will also vary.[184] We therefore wished to synthesise a suite of SAR020106 analogues bearing different bioreductive groups, which could

then be studied *in vitro* for their reduction and fragmentation kinetics. Examples of the bioreductive groups we wished to use are given in Scheme **10** below.

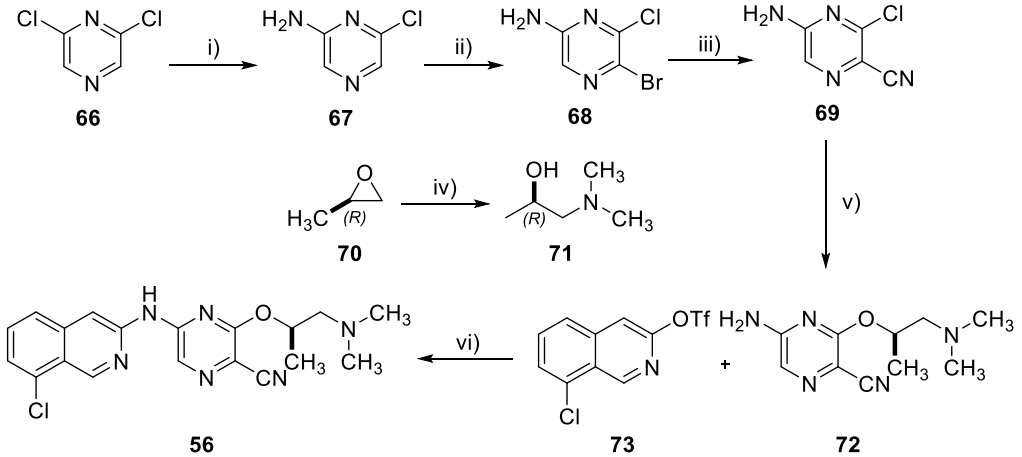


Scheme 10: Proposed alternative bioreductive groups to be appended to SAR020106 **56**.

2.3 Synthesis

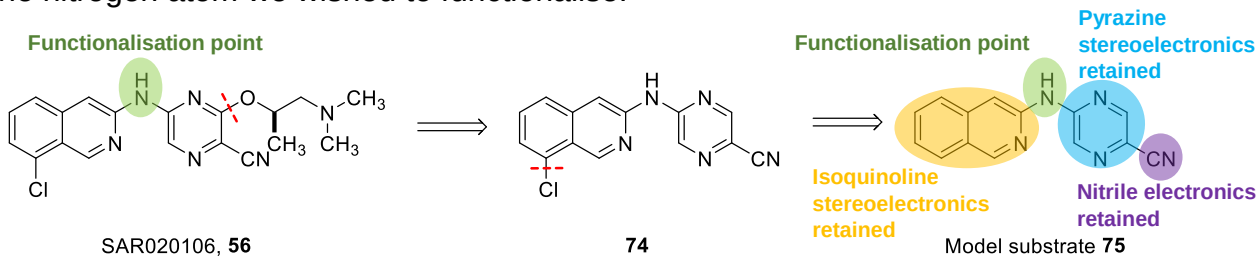
2.3.1 Synthesis of a model substrate

We began by synthesising a substrate to act as a model for SAR020106 **56**. **56** is a complex molecule with a 6-step synthesis (literature synthesis is shown in Scheme **11**),[183] and a 500 mg custom-synthesised batch had previously been purchased. Access to **56** for reactions was thus a limiting factor, and hence we chose to use a model substrate for initial studies.



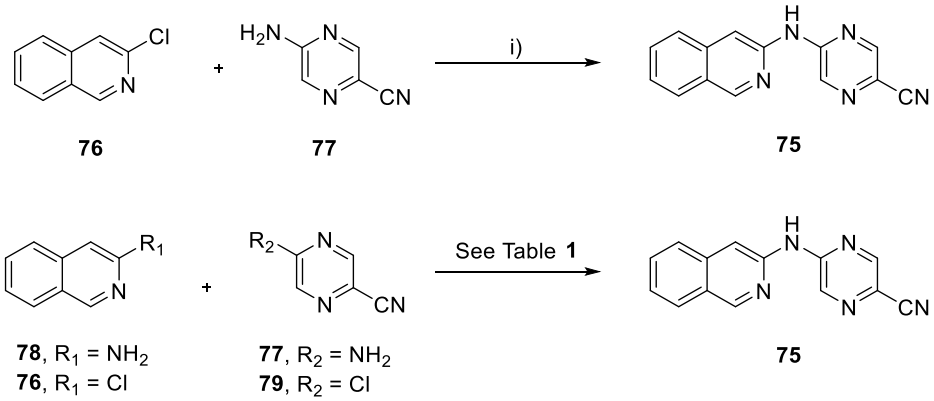
Scheme 11: Literature synthesis of SAR020106 **56**. *Reagents and conditions* i) aq. NH_3 (28%), 100 °C, overnight, 91%; ii) NBS, CH_2Cl_2, 0 °C, 1 hour, 42%; iii) CuI, 18-crown-6, $Pd(PPh_3)_4$, potassium cyanide, DMF, reflux, 3 hours, 82%; iv) $NHMe_2$ (40% in H_2O), 0 °C → 20 °C, 2 hours, 40%; v) **71**, NaH (60% in oil), 1,4-dioxane, 100 °C, overnight, 39%; vi) $Pd_2(dba)_3$, XantPhos, Cs_2CO_3, toluene, μW, 130 °C, 45 minutes, 45%.[183]

We designed the model substrate in such a way that it retained key features of SAR020106 **56**, whilst simplifying the synthesis and reagent cost (Scheme **12**). We therefore chose to remove the ether-linked pendant chain, since this likely has little steric of electronic effect on the overall molecule and significantly simplifies synthesis. We also chose to remove the 8-chloro substituent to the left-hand isoquinoline portion. Whilst this chlorine forms an important halogen-bonding interaction when binding to Chk1 and is a source of its selectivity,[183] it too has little steric or electronic effect on the nitrogen atom we wished to functionalise.



Scheme 12: Disconnection of SAR020106 **56**, simplifying the structure to a model substrate **75**, on which we wished to test alternative bioreductive groups.

Model substrate **75** still retains the key steric features of **56**, namely the isoquinoline and pyrazine moieties on either side of the amine we wished to functionalise. The isoquinoline, we speculated, would have similar electronic properties to the 8-chloroisoquinoline of **56**. More importantly, we retained the 4-cyano substituent to the pyrazine ring, which has a strongly electron-withdrawing effect on the aryl amine. Model substrate **75** is also a Chk1 inhibitor, with a Chk1 IC_{50} of 0.94 μM and a Chk2 IC_{50} of >100 μM, giving it >100-fold selectivity.[183]



Scheme 13: Literature synthesis of the model substrate **75**, and our attempts to find improved conditions. *Reagents and conditions*: i) $Pd(OAc)_2$, (±)-BINAP, NaO^tBu, toluene/DMF (4:1), 140 °C, microwave, 30 minutes, 7% yield (preparative HPLC)[185]; for other *reagents and conditions* see Table **1**.

Compound **75** had been synthesised in the literature using a Buchwald-Hartwig amination reaction between aminopyrazine **77** and 3-chloroisoquinoline **76**, as shown in Scheme **13**. The Buchwald-Hartwig reaction proved low-yielding in our hands (see Table **1**, entry **6**), possibly due to the poor nucleophilicity of aminopyrazine **77**, and so we looked for alternate coupling conditions.

Table 1: *Reagents and conditions* used to synthesise model substrate **75** in Scheme **13**.

Entry	R_1	R_2	Reagents	Solvent	T	Time	Yield
1	1 eq. NH_2	1.25 eq. Cl	$Pd(OAc)_2$, (S)-BINAP, NaO^tBu	Toluene	reflux	18 h	0%
2	1.5 eq. NH_2	1 eq. Cl	$Pd(OAc)_2$, (S)-BINAP, NaO^tBu	Toluene	reflux	19 h	26%
3	1.5 eq. NH_2	1 eq. Cl	$Pd(OAc)_2$, (S)-BINAP, NaO^tBu	Toluene	reflux	20 h	12%
4	1.5 eq. NH_2	1 eq. Cl	$Pd(OAc)_2$, (S)-BINAP, NaO^tBu	Toluene	80 °C	2 h	0%
5	1.5 eq. NH_2	1 eq. Cl	$Pd(OAc)_2$, (S)-BINAP, NaO^tBu	Toluene	80 °C	2 h	6%
6	1 eq. Cl	1 eq. NH_2	$Pd(OAc)_2$, (S)-BINAP, NaO^tBu	Toluene/DMF (2:1)	100 °C	21 h	19% (lit. 7%)[185]
7	1 eq. NH_2	1.1 eq. Cl	NaO^tBu	Toluene	80 °C	5 h	28%
8	1.5 eq. NH_2	1 eq. Cl	NaO^tBu	Toluene	80 °C	6 h	16%
9	1.5 eq. NH_2	1 eq. Cl	DIPEA	DME	reflux	18 h	51%
10	1.3 eq. NH_2	1 eq. Cl	DIPEA	DME	reflux	45 h	47%
11	1 eq. NH_2	1.1 eq. Cl	DIPEA	DME	reflux	41 h	26%

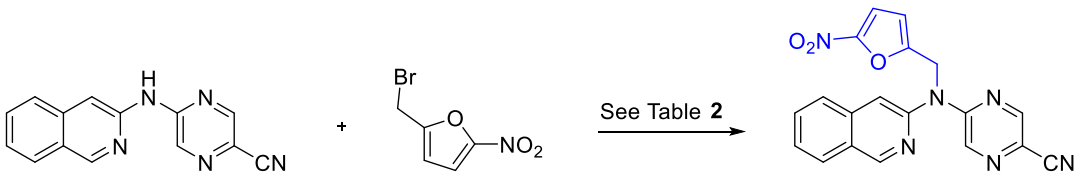
Buchwald-Hartwig couplings using pyrazine halide **79** and isoquinoline amine **78** resulted in yields that were both poor and variable, as demonstrated in Table **1** entries **1–5**. Cross-coupling between **76** and pyrazine amine **77** (Table **1**, entry **6**) was low yielding and not considered an improvement upon the other conditions used.

We next attempted to couple the two fragments using S_NAr chemistry, using sodium *t*-butoxide as a base. These conditions afforded the desired product in somewhat poor yield (Table **1**, entries **7** and **8**). However, the limited solubility of both reactants and reagents in the solvent gave us confidence that the reaction conditions could be further improved. Thus, the solvent was changed from toluene to 1,2-dimethoxyethane (DME), which whilst somewhat lower boiling, is significantly more polar and able to solubilise both reactants and base. The bulky non-nucleophilic organic base *N,N*-diisopropylethylamine (DIPEA) was chosen to replace sodium *t*-butoxide, since *t*-butoxide bases can be potentially nucleophilic. These new conditions afforded higher yields under milder conditions (Table **1**, entries **9–11**).

2.3.2 Synthesis of *N*-alkyl-linked prodrugs

2.3.2.1 2-Nitrofuranyl prodrugs

The 2-nitrofuranyl group can act a fragmenting bioreductive group that is sensitive to hypoxia.[44] It has been observed that this group can slowly fragment under normoxia, including in the absence of nitoreductase enzymes. This indicates that the 2-nitrofuran group may be advantageous over groups which fragment slowly. The electrochemical reduction potential of the nitrofuran is significantly lower than that of, for example, the nitrobenzyl group (−0.33 V for the furan *vs* −0.49 V for the benzyl).[61] This observation suggests that biochemical reduction may be more rapid, and that reduction/fragmentation could occur at higher dissolved oxygen concentrations *in vivo*.



75 **80** **62**

Scheme 14: Alkylation of model Chk1 inhibitor **75** with a 2-nitrofuranyl alkylating agent. *Reagents and conditions* are given in Table **2**, below.

Table 2: *Reagents and conditions* used to alkylate model substrate **75** with 2-nitro-5-(bromomethyl)furan **80** (Scheme **14**).

Entry	Eq. of **80**	Base	Solvent	Temperature	Time	Yield
1	1.1	Cs_2CO_3	DMF	40 °C	1 hour	0%
2	2	Cs_2CO_3	DMF	RT	24 hours	0%
3	2	Cs_2CO_3	DMF	0 °C	4 hours	0%
4	2	Cs_2CO_3	DMF	0 °C	5.5 hours	0%

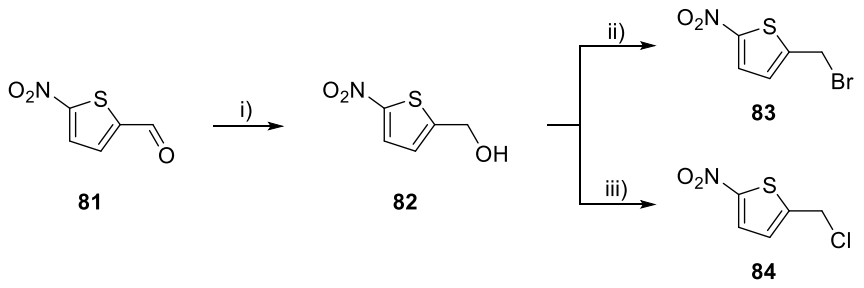
Test alkylation reactions were conducted on model substrate **75** and are listed in Table **2**. In all cases, a new product appeared to have formed by TLC analysis. However, this new product appeared to break down over longer time periods in solution (Table **2**, entries **1** and **2**). Cooling the reaction mixture to slow the rate of decomposition allowed the product to exist in solution for extended periods without decomposition (Table **2**, entries **3** and **4**), although it could not be detected by mass spectrometry, and attempts to isolate the product spot *via* silica gel chromatography proved unsuccessful. This might indicate the compound's instability on silica gel or might be due to the small scale of each reaction (~20 µmol of model substrate used per reaction). Nevertheless, it was not possible to determine whether the observed species was the desired product.

2.3.2.2 2-Nitrothiopheneyl prodrugs

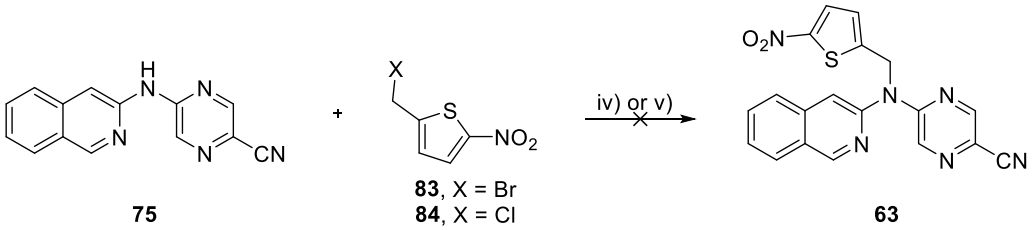
Analogous to the 2-nitrofuranyl group is the 2-nitrothiopheneyl group, which also undergoes biochemical reduction and fragmentation under low oxygen conditions.[46] The 2-nitrothiophene group has low electrochemical reduction potential (−0.39 V), and work conducted within our group (unpublished) has shown that 2-nitrothiopheneyl prodrugs fragment more rapidly than their 2-nitrofuranyl analogues. We therefore

wished to synthesise a 2-nitrothiopheneyl analogue of **75**, which could have more favourable fragmentation kinetics.

(A)



(B)



Scheme 15: Attempted synthesis of the 2-nitrothiopheneyl prodrug of **75**. *Reagents and conditions*: i) $NaBH_4$, MeOH, 0 °C, 3.5 hours, 70% yield; ii) PBr_3, CH_2Cl_2, 0 °C, 2.5 hours, then RT, 1 hour, 30% yield; iii) $SOCl_2$, pyridine, CH_2Cl_2, 0 °C, 2 hours, then RT, 20 hours, 49% yield; iv) **84**, Cs_2CO_3, DMF, RT, 3 hours, N.R.; v) **83**, C_2CO_3, DMF, RT, 3 hours, N.R.

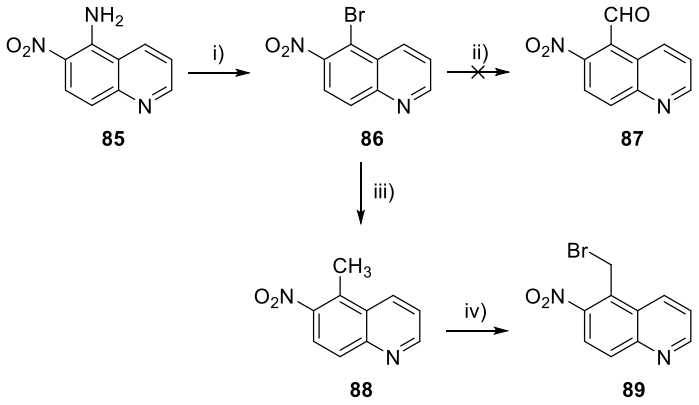
The 2-nitrothiophene alkylating agents **83** and **84** were not commercially available, and so were synthesised according to literature procedures.[64,186] In the case of the chloro analogue **84**, the published procedure could not be accessed in the literature,[186] and so an approximation of the conditions was made. The aldehyde **81** was readily reduced to the corresponding alcohol **82** by treatment with sodium borohydride in very good yield. Subsequent treatment with phosphorus tribromide afforded the bromide **83** in a low but acceptable yield (30%); treatment with thionyl chloride and pyridine afforded the chloride analogue **84** in somewhat higher yield (49%).

We then attempted to synthesise the 2-nitrothiophenyl prodrug form of model substrate **75** *via* an alkylation reaction, using either the chloride **84** or bromide **83**. In both cases, no reaction was observed by TLC analysis or mass spectrometry, and

decomposition of the alkylating agents in solution appeared to occur during the reactions.

2.3.2.3 6-Nitroquinoline prodrugs

It has been previously demonstrated that the 6-nitroquinoline group can undergo enzymatic reduction in hypoxia, followed by fragmentation to release a cargo compound. The nitroquinoline has the advantage of exhibiting 'switch-on' fluorescence. In its nitro form, it exhibits minimal fluorescence and is essentially 'switched off'; upon reduction to the corresponding aminoquinoline, a significant increase in fluorescence can be detected. This makes the nitroquinoline a particularly interesting hypoxia-activated group to study, since it can report on its own reduction by concomitant 'switch-on' of fluorescent signal. Work by Dr Liam O'Connor from this group has demonstrated this effect, by conjugating the nitroquinoline moiety to a BRD4 ligand.[49,50]



Scheme 16: Modified synthesis of the 6-nitroquinoline bioreductive fluorogenic moiety. *Reagents and conditions* i) CuBr (1.2 eq.), $NaNO_2$ (3 eq., 7.9 M in H_2O), HBr/H_2O (1:2), 3 hours, RT, 59% yield; ii) 1) PhLi (1 eq.), THF, −78 °C, 20 minutes, 2) ethyl formate (5 eq.), THF, −78 °C → RT, 16 hours, N.R.; iii) trimethylboroxine (1 eq.), K_2CO_3 (3 eq.), $Pd(dppf)Cl_2{\cdot}CH_2Cl_2$ (0.1 eq.), 1,4-dioxane, reflux, 3 hours, 92% yield; iv) NBS (2.8 eq.), AIBN (cat.), CCl_4, 70 °C, 16 hours, 92% yield.

The previous synthesis of the nitroquinoline alkylating agent **89** had been developed by Dr O'Connor. 5-Amino-6-nitroquinoline **85** is first brominated using a Sandmeyer reaction; diazotisation of the amine followed by addition of a copper(I) catalyst in aqueous hydrobromic acid results in a radical bromination at the 5-position

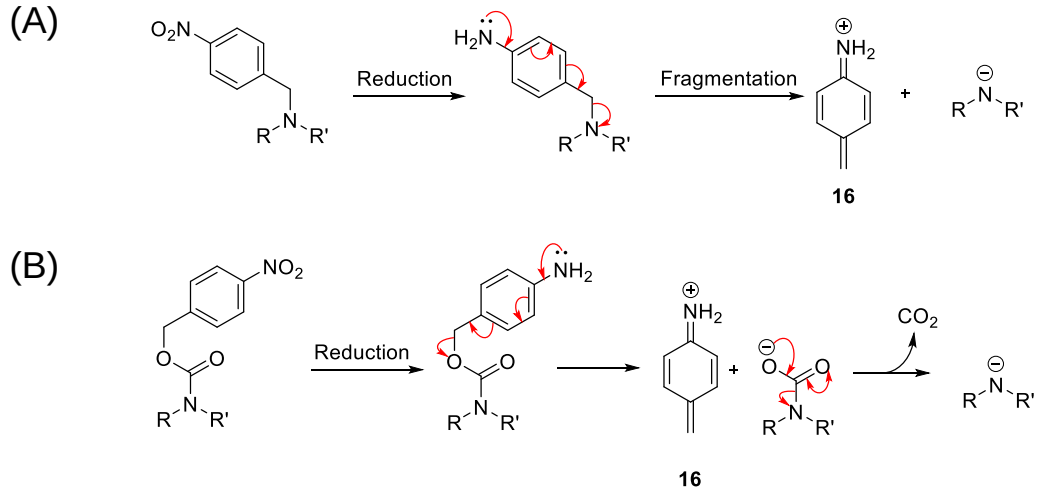
of the quinoline in good yield (Scheme **16**). In the original synthesis, Dr O'Connor then performed lithium-halogen exchange at the bromide using phenyllithium solution, which gave the 5-formyl analogue **87** upon treatment with ethyl formate. Despite several attempts this proved unsuccessful, with no product being isolated despite evidence for formation by TLC analysis. As an alternative to formylation, we performed a Suzuki coupling between 5-bromo-6-nitroquinoline **86** and trimethylboroxine, using the common palladium(II) salt, $Pd(dppf)Cl_2 \cdot CH_2Cl_2$, affording the 5-methyl analogue **88** in excellent yield. Subsequent radical bromination of the 5-methyl position, using *N*-bromosuccinimide (NBS) as a bromine source and catalytic AIBN as the radical initiator gave the corresponding benzylic bromide **89** in similarly excellent yield.

At this point in the project, given our lack of success in appending alkylating agents to the model substrate **75**, we chose not to pursue *N*-alkyl prodrugs further, instead focusing on prodrug variants with self-immolative linkers.

2.3.3 Synthesis of carbamate-linked bioreductives

As discussed above, *N*-alkylation of model substrate **75** proved challenging. We therefore decided to explore the use of linkers that did not rely solely on an *N*-alkyl bond, and so we initially chose to study carbamate-linked bioreductives.

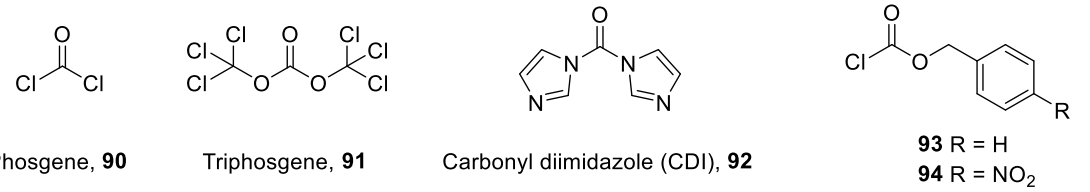
We hypothesise that one of the key problems with *N*-alkylated prodrugs of SAR020106 **56**, such as the one tested by Dr Cindy Cázares-Körner, is that breaking of the C-N bond to form a nitrogen anion is less energetically favourable than forming the corresponding oxy-anion. The use of a carbamate group as a linker offers the possibility of overcoming this problem.



Scheme 17: (A) Proposed mechanism of molecular fragmentation of an *N*-alkyl-linked bioreductive group. This mechanism produces the electrophile intermediate **16** and the tertiary nitrogen anion. (B) Proposed mechanism of fragmentation of a carbamate-linked bioreductive group. This mechanism produces the electrophile intermediate **16** *via* breaking of a C-O bond. The remaining carbamate anion then decomposes to release gaseous CO_2, breaking the C-N bond.

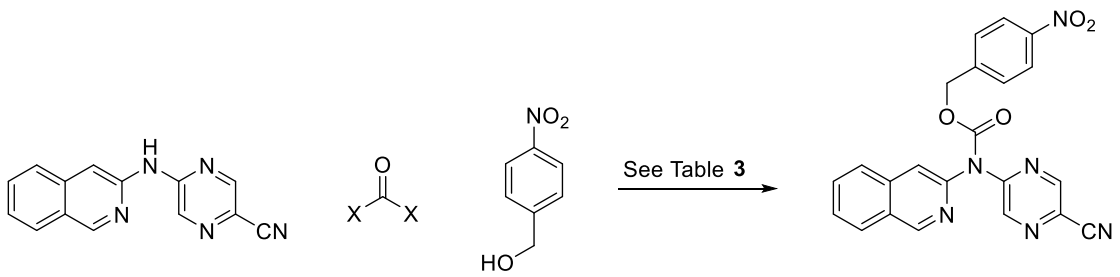
After reduction of an *N*-alkyl-linked moiety such as the nitrobenzyl group, molecular fragmentation produces the electrophile **16** as well as a nitrogen anion *via* C-N bond breakage (Scheme **17a**). By contrast, fragmentation of a carbamate-linked nitrobenzyl group can be viewed as a 2-stage process. First the electrophilic intermediate **16** is released *via* C-O bond cleavage, leaving a carbamate anion. This anion is unstable and cleaves the C-N bond to eliminate CO_2 and the nitrogen anion. This mechanism disconnects C-N bond cleavage from elimination of electrophile **16** and has the added entropic driving force of elimination of CO_2.

(A)



Phosgene, **90** Triphosgene, **91** Carbonyl diimidazole (CDI), **92** **93** R = H **94** R = NO_2

(B)



75 **90-92** **95** **96**

Scheme 18: Attempted synthesis of an *N*-carbamate-linked bioreductive form of the model substrate **75**. (A) Structures of carbamate-forming reagents used. (B) General reaction undertaken for the synthesis of carbamate-linked prodrugs. *Reagents and conditions* are given in Table **3**, below.

Table 3: Reagents and conditions used in the attempted synthesis of *N*-carbamate-linked prodrug forms of **75**.

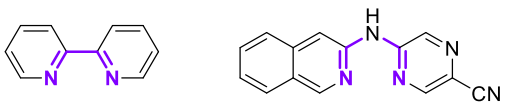
Entry	Reagents	Solvent	T	Time	Yield
1	1.5 eq. **95**, 1.5 eq. Phosgene **90** (20% in tol.), 3 eq. DIPEA	Toluene	0 °C → RT	5 h 45 m	N. R.
2	1.5 eq. **95**, 1.5 eq. Phosgene **90** (20% in tol.), 3 eq. DIPEA	Toluene	0 °C → RT	29 h	N. R.
3	1.5 eq. **95**, 1.5 eq. Phosgene **90** (20% in tol.), 3 eq. DIPEA	THF	0 °C → RT	3 d	N. R.
4	1 eq. **95**, ⅓ eq. Triphosgene **91**, 1.5 eq. pyridine	CH_2Cl_2	0 °C → RT	9 d	N. R.
5	1.1 eq. CDI **92**, then 1.1 eq. **95**	CH_2Cl_2	0 °C → RT	7 d	N. R.
6	2 eq. **94**	Pyridine	0 °C → RT	3 d	N. R.
7	1.2 eq. *n*-BuLi (2.5 M in hexanes), then 1.2 eq. **94**	THF	−78 °C → RT	3 d	N. R.
8	1.1 eq. $Cu(OTf)_2$, 1.2 eq. DIPEA, then 1.2 eq. **94**	THF	RT	26 h	N. R.
9	2 eq. Cs_2CO_3, then 1.5 eq. **94**	DMF	RT, then 50 °C	4 d	N. R.
10	1.1 eq. **93**, 1.1 eq. triethylamine	THF	0 °C → RT	2 d	N. R.
11	1.2 eq. ethyl chloroformate, 1.4 eq. DIPEA	THF	0 °C → RT	24 h	N. R.

Initially we chose to use reagents which act as carbonyl equivalents, to use as coupling reagents between the model substrate **75** and bioreductive component 4-nitrobenzyl alcohol **95**. We first used phosgene **90**, which acts as a carbonyl with two labile leaving groups, allowing it to couple two nucleophiles *via* a carbonyl group. Attempts using phosgene were not successful, either in apolar or polar solvents (Table **3**, entries **1**–**3**), with no product being detected by low-resolution mass spectrometry or TLC analysis. Likewise, triphosgene **91** (a stabilised phosgene equivalent which reacts in solution to release three equivalents of phosgene) did not

afford any of the desired product (Table **3**, entry **4**). Carbonyl diimidazole (CDI, **92**) is often used as an amide coupling reagent and is a safer analogue of phosgene; attempts at carbamate formation using CDI and 4-nitrobenzyl alcohol **95** also failed to form the desired product, as indicated by TLC and MS analysis.

Next, we turned to the use of chloroformate-based reagents. Chloroformates are the species formed in a reaction between an alcohol and phosgene, and many are stable solids that may be used directly to form carbamates. We attempted reactions using 4-nitrobenzyl chloroformate **94**, however, all proved unsuccessful (Table **3**, entries **6**–**9**), with the chloroformate reagent **94** appearing to degrade in solution over time. Pre-stirring the model substrate **75** with *n*-butyllithium solution to deprotonate the central nitrogen atom, followed by addition of chloroformate **94** was also unsuccessful (Table **3**, entry **7**).

To test whether the electron-poor nature or steric bulk of 4-nitrobenzyl chloroformate **94** was affecting its reactivity, we repeated the reaction using the more electron-rich benzyl chloroformate **93** (Table **3**, entry **10**), and the less bulky ethyl chloroformate (Table **3**, entry **11**). Both reactions also failed to afford any product, suggesting that both electronics and sterics may not have been significant factors in the lack of reactivity. Taken together, the above data suggest that even highly reactive reagents for forming carbamates were not reactive with model substrate **75**, implying that the unreactive nitrogen atom was the problem.

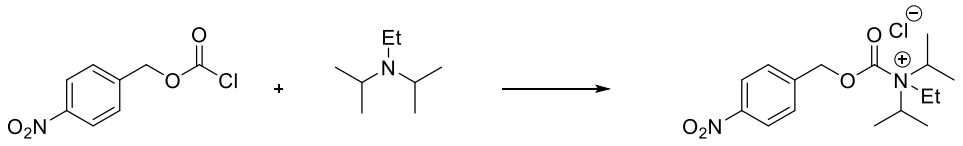


2,2'-bipyridine (BIPY, **97**) **75**

Figure 21: The structures of 2,2'-bipyridine (BIPY, **97**), a commonly-used metal-chelating ligand, and model substrate **75**. The similarities between their metal-binding motifs are highlighted in purple.

Since the lack of reactivity of the nitrogen atom appeared to be a hindrance to synthesis, we hypothesised an alternative way improving its reactivity. SAR020106 **56**

and model substrate **75** both have nitrogen-rich motifs which resemble organic chelators of metal ions, such as 2,2'-bipyridine (BIPY **97**, Figure **21**). Consequently, it was hypothesised that by first incubating **75** with a metal ion to cause chelation, a mild base would then be able to better deprotonate the central nitrogen atom and again improve its reactivity. To this end, **75** was stirred with the Lewis acid $Cu(OTf)_2$, followed by addition of DIPEA, then addition of 4-nitrobenzyl chloroformate **94**, however, this approach also afforded no desired product (Table **3**, entry **8**).



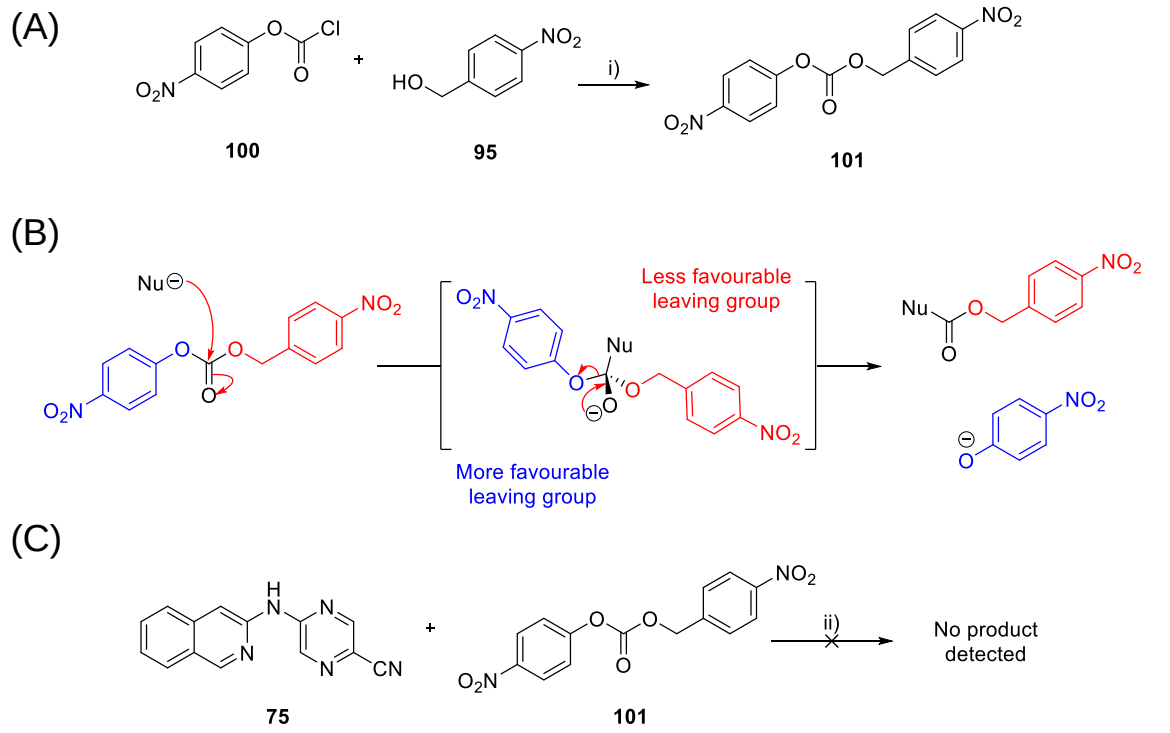
94 DIPEA **98** **99**, $[M-Cl]^+$ *m/z* = 309 Observed by LRMS

Scheme 19: Identity of a possible chloroformate-DIPEA adduct observed by low-resolution mass spectrometry.

During reactions using chloroformates and DIPEA, we had observed what appeared to be a stable adduct by low-resolution mass spectrometry (Scheme **19**). This adduct appeared to be formed by the addition of DIPEA to the chloroformate carbonyl, eliminating a chloride ion and forming a quarternary ammonium species **99**. We hypothesised that this adduct, if formed in solution, would be able to undergo reaction with substrate **75** to form the desired carbamate. However, if the adduct was very stable in solution this could possibly hinder reaction with the amine substrate **75**. Consequently, the non-nucleophilic inorganic base Cs_2CO_3 was used in place of DIPEA, in *N,N*-dimethylformamide (DMF), a solvent in which the base in mildly soluble. Pre-stirring **75** in DMF with Cs_2CO_3 followed by addition of chloroformate **94**, however, did not result in formation of any product (Table **3**, entry **9**).

The experiments detailed above suggested that the nitrogen atom of substrate **75** had poor reactivity towards activated carbonyl compounds. We therefore hypothesised that if reactions between the substrate and highly reactive reagents was

significantly less than the rate at which the reagents decompose in solution, this could explain why no product could be detected and isolated. Instead, we considered using a more stabilised reactant that would not decompose quickly in solution, allowing for more forcing conditions to be used over longer time periods.



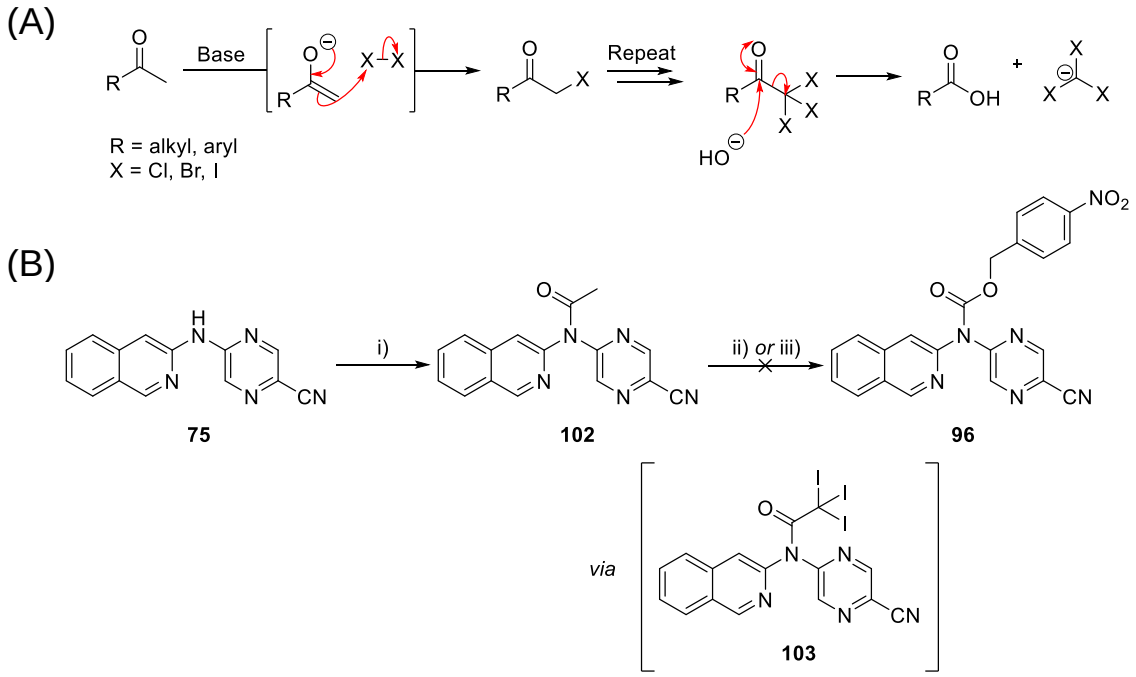
Scheme 20: (A) Synthesis of the 'mixed carbonate' **101** *Reagents and conditions* i) Pyridine, THF, 0 °C → RT, 19 hours, 52% yield; (B) Proposed mechanism by which a nucleophile could displace one of the carbonate substituents, eliminating the most stable leaving group; (C) Attempted reaction with mixed carbonate **101**. *Reagents and conditions* ii) DIPEA, THF, reflux, 13 days, N.R.

We therefore chose to use a "mixed carbonate" reagent **101**, in which the carbonate carbonyl has two different substituents, in this case the 4-nitrobenzyl and 4-nitrophenyl moieties. We proposed that nucleophilic attack at the carbonyl of **101** would form a tetrahedral intermediate oxyanion (Scheme **20b**), which then had three possible leaving groups. For this mixed carbonate, we proposed that the nitrophenyl would be the better leaving group. Negative charges on phenolic oxygen atoms are quite stable (the pK_a of phenol in water is ~10), and the inductively and mesomerically electron-withdrawing NO_2 group in the *para* position further stabilises this negative charge, such that the pK_a of 4-nitrophenol in water is ~7.15 (*i.e.* formation of the

4-nitrophenol anion is almost 1000× more favourable *vs* phenol alone). In this case, attack of the carbonate by the substrate would eliminate the 4-nitrophenyl moiety and result in formation of the desired carbamate.

We therefore synthesised the mixed carbonate **101** in a single step by treating 4-nitrobenzyl alcohol **95** with 4-nitrophenyl chloroformate **100** in pyridine, affording **101** in reasonable yield after recrystallisation (Scheme **20a**). However, reaction of carbonate **101** with model substrate **75** and DIPEA under reflux in THF did not afford the desired 4-nitrobenzyl carbamate product **96**, as determined by TLC and LRMS analysis. This result is not entirely surprising, since the carbonate **101** is recrystalised from boiling EtOH following purification. EtOH is a nucleophilic solvent, and for the carbonate to be stable at elevated temperature in EtOH suggests that it is highly unreactive toward even good, unhindered nucleophiles.

As an alternative approach, we proposed the use of the haloform reaction. This reaction uses base-catalysed enolate formation of methyl ketones, which then perform a nucleophilic attack on a molecular halogen (such as Cl_2, Br_2 and I_2).[188] Three sequential halogenations of the methyl ketone form the α-trihalomethyl ketone, which can then undergo nucleophilic attack to lose the corresponding haloform anion (*e.g.* CCl_3^-, the chloroform anion) as a leaving group (the mechanism of the haloform reaction is given in Scheme **21a**, below). We hypothesised that, if model substrate **75** could be made into an acetamide under forcing conditions, we could employ the haloform reaction to form the corresponding carbamate. Nucleophilic attack by 4-nitrobenzyl alcohol onto the trihalomethyl amide would then afford the desired carbamate.



Scheme 21: (A) The mechanism of a general haloform reaction, in which base-catalysed enolisation of an α-methyl ketone results in sequential monohalogenation. This α-trihalomethyl ketone is then susceptible to nucleophilic attack (in this case my hydroxide), with loss of the haloform anion as a leaving group. (B) Attempted Iodoform reactions on substrate **103**. *Reagents and conditions*: i) Ac_2O, reflux, 24 hours, 95% yield; ii) Cs_2CO_3, I_2, THF, RT, 3 hours, then reflux, 1.5 hours, then 4-nitrobenzyl alcohol **95**, reflux, 2 hours, N.R.; iii) 4-Nitrobenzyl alcohol **95**, I_2, NaOH, THF, RT, 6 hours, N.R.

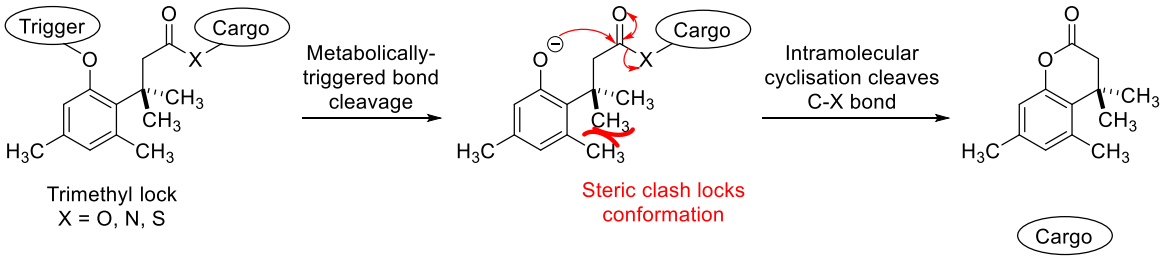
Acetylation of model substrate **75** was carried out under reflux in acetic anhydride, which led to excellent conversion to the presumed acetylated product **102** (as determined by TLC analysis). We subsequently attempted two iodoform reactions, using either cesium carbonate or sodium hydroxide as bases, and molecular iodine as the electrophile, in the presence of 4-nitrobenzyl alcohol **95** as a latent nucleophile. In both cases, however, neither reaction appeared to form the desired product. Some consumption of the starting material **102** was observed, including deacetylation to form **75**, but no apparent product was observed by TLC or mass spectrometry analysis.

2.3.4 Synthesis of trimethyl lock-based prodrug forms

Formation of carbamate-linked prodrug forms of SAR020106 **56** had proven unsuccessful, and so we wished to explore alternative prodrug linkers. As with the carbamate, the prodrug linker should separate molecular fragmentation into two distinct steps. In the first, the bioreductive group fragments post-metabolism to release

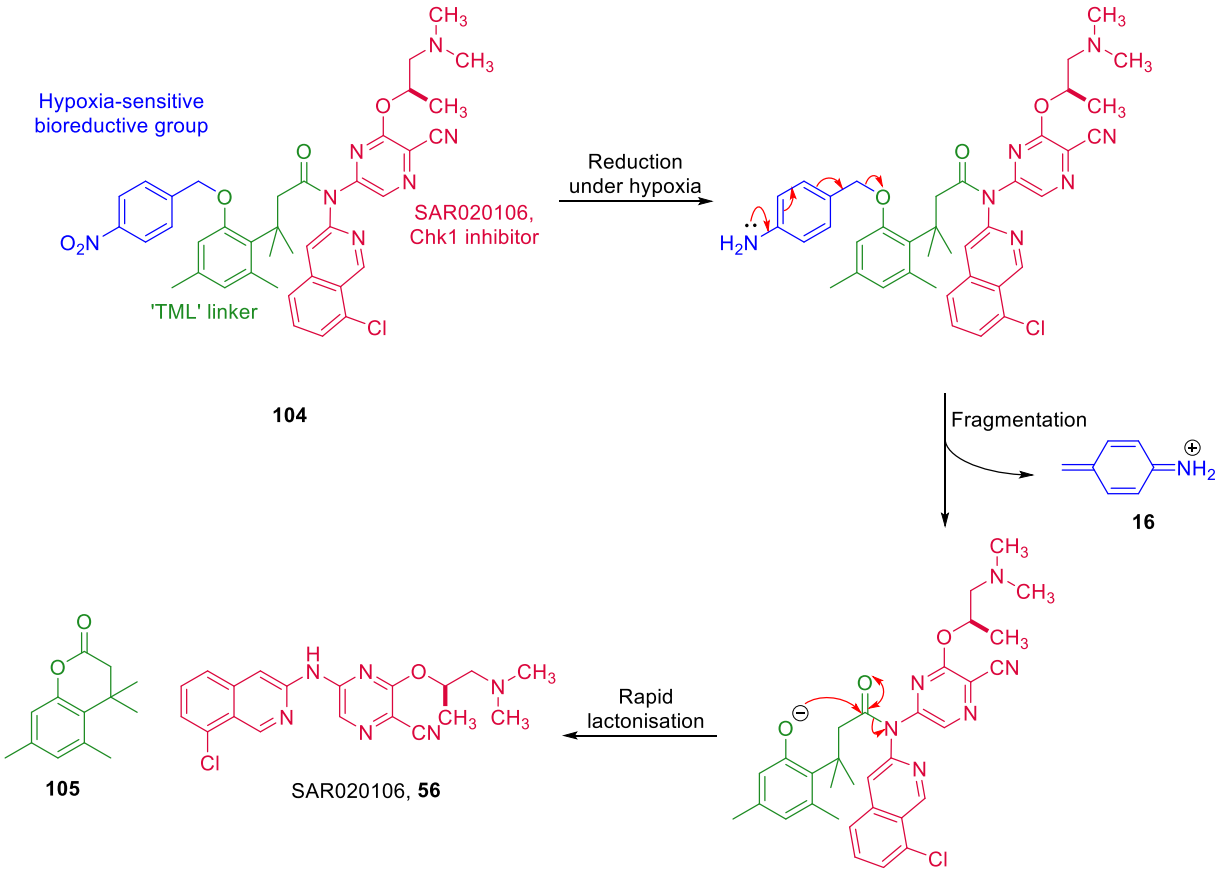
a relatively stable anion, aiding fragmentation kinetics. In the second, the nucleophile unmasked by this fragmentation undergoes some form of intramolecular fragmentation or nucleophilic attack, breaking the C-N bond that attaches the linker to the drug and releasing the active compound.

We chose to explore the so-called "trimethyl lock" system, which has been previously used as a "self-immolative" linker for prodrugs.[189] Variants of the trimethyl lock system have been triggered by various biochemical events, such as direct reduction of their quinone ring,[190] esterase cleavage,[191] and phosphatase cleavage.[192] Recently trimethyl lock systems that employ a bioreductive nitrobenzyl group have also been developed for release of a peptide,[193] as well as systems for delivering proteins into cell,[194] and even systems which form a fluorescent coumarin upon cyclisation.[195]



Scheme 22: General mechanistic concept of a "trimethyl lock" prodrug system. Initially, cleavage of the biologically responsive "trigger" released the phenolic anion. This latent nucleophile then performs intramolecular cyclisation into an ester or amide, forming a lactone and releasing the cargo molecule.

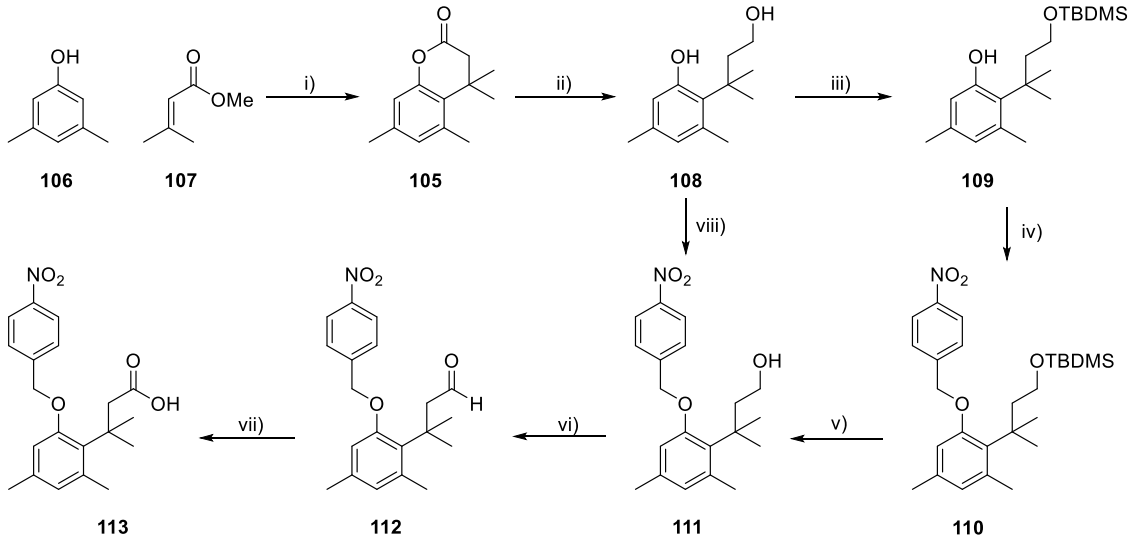
Scheme **22** above shows the general concept for a trimethyl lock prodrug system. The steric clash of the three methyl groups causes them to "lock" together, forcing the amide group to sit close to the phenolic oxygen which, when unmasked through metabolism, reacts with the amide rapidly due to the Thorpe-Ingold effect.[196,197] We hypothesised that such a system could be utilised with SAR020106 **56** - enzymatic reduction under hypoxia and fragmentation to release a hydroxy anion, followed by intramolecular lactonisation could cleave an amide bond to SAR020106 **56** and release the active inhibitor, as shown in Scheme **23**, below.



Scheme 23: Proposed bioreductive form of SAR020106 **56** based on a "trimethyl lock" linker system. The bioreductive component is attached to the phenolic oxygen of the trimethyl lock, whilst the cargo SAR020106 **56** is attached *via* an amide bond. After reduction under hypoxia, the bioreductive component fragments to release the latent nucleophilic phenoxy anion, which undergoes intramolecular cyclisation to form the lactone **105** and release the cargo molecule *via* C-N bond cleavage.

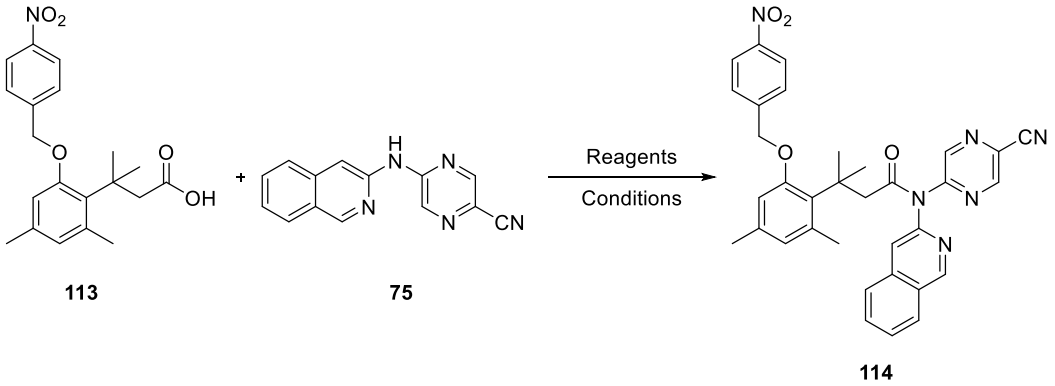
We began synthesis of the trimethyl lock system by following literature procedures (Scheme **24**, below). First, we synthesised the lactone **105** *via* electrophilic aromatic substitution of 3,5-dimethylphenol **106**, in a conjugate addition to 3,3'-dimethylacrylate **107**, which formed lactone **105** in excellent yield. Ring-opening of the lactone *via* reduction with lithium aluminium hydride gave the alcohol **108**, again in excellent yield. We then attached the bioreductive 4-nitrobenzyl group to the phenolic hydroxyl: initially, this was done by first protecting the primary alcohol with a *t*-butyldimethylsilyl (TBDMS) protecting group to give **109**, followed by alkylation of the phenol affording **110**, then removal of the TBDMS group to give **111**. However, we also attempted to selectively alkylate phenol **108**, using potassium carbonate as a

base under reflux in acetone, which gave the mono-alkylated product **111** with no evidence of alkylation at the primary alcohol. Jones-type oxidation of the alcohol using pyridinium chlorochromate (PCC) gave aldehyde **112** in very good yield, and a Pinnick-type oxidation gave the carboxylic acid **113** in reasonable yield.



Scheme 24: Synthesis of a nitrobenzyl-protected trimethyl lock precursor. *Reagents and conditions* i) $MeSO_3H$, 70 °C, 16 hours, 99% yield; ii) $LiAlH_4$, THF, 0 °C, 93% yield; iii) TBDMSCl, Et_3N, CH_2Cl_2, overnight; 89% yield iv) 4-Nitrobenzyl bromide, K_2CO_3, acetone, 50 °C, overnight, 92% yield; v) AcOH/THF/H_2O (3:1:1), RT, 2 hours, 89% yield; vi) PCC, CH_2Cl_2, RT, 3 hours, 70% yield; vii) NaH_2PO_4, NaOCl, MeCN, H_2O, −10 °C, 1 hour, then → RT, overnight, 53% yield.

With the carboxylic acid **113** in hand, we wished to perform an amide coupling to assemble the full prodrug. As previously discussed, we initially used the model substrate **75** to optimise the coupling chemistry before applying it to our drug of choice SAR020106 **56**. Attempted amide coupling procedures are given in Scheme **25** and Table **4**, below.



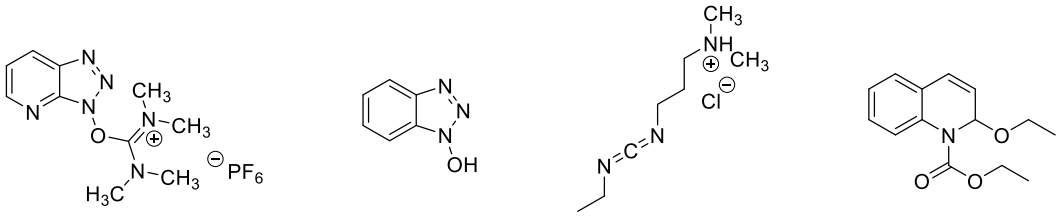
113 **75** **114**

Scheme 25: Attempted amide coupling of model substrate **75** with the trimethyl lock-based carboxylic acid **115**. *Reagent and conditions* are given in Table **4**, below.

Table 4: *Reagents and conditions* for amide couplings in the attempted synthesis of model bioreductive **114**, as depicted in Scheme **25**, above.

Entry	Reagents	Solvent	T	Time	Yield
1	Vac down, then CH_2Cl_2 and Et_3N	$SOCl_2$	30 °C	30 minutes	N. R.
2	Oxalyl chloride (1.5 eq.), DMF (cat.), DIPEA (1 eq.)	CH_2Cl_2	0 °C → RT	3 hours	N. R.
3	Oxalyl chloride (2 eq.), DMF (cat.), DIPEA (1 eq.)	THF	0 °C → RT → 40 °C	24 hours	N. R.
4	Oxalyl chloride (1.2 eq.), DMF (cat.), DMAP (1.5 eq.)	Pyr.	0 °C → 40 °C	24 hours	N. R.
5	HATU (1.5 eq.), DIPEA (1.5 eq.)	DMF	RT, then 40 °C	overnight, then 5 hours	N. R.
6	HOBt (2 eq.), EDC hydrochloride (2 eq.)	DMF	40 °C	2 days	N. R.
7	EEDQ (1.4 eq.)	Tol.	RT	overnight	N. R.
8	CDI (1.1 eq.), Et_3N (2 eq.)	THF	RT	3 hours	N. R.
9	Deoxo-Fluor® (1.1 eq.)	THF	0 °C → RT	3 days	N. R.
10	Cyanuric fluoride (0.5 eq.), Pyr. (0.5 eq.)	CH_2Cl_2	0 °C → RT	4 hours	N. R.
11	BTFFH (1.5 eq.), DIPEA (4.5 eq.), sealed tube	CH_2Cl_2	reflux	overnight	N. R.

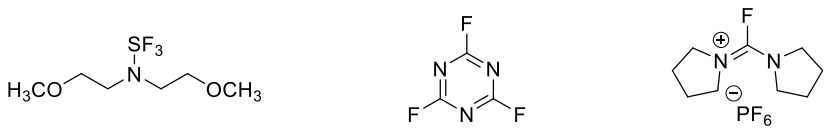
We began by attempting *in situ* formation of acid chlorides (Table **4**, entries **1**–**4**) of the carboxylic acid **113**, using both thionyl chloride (Table **4**, entry **1**) and oxalyl chloride (Table **4**, entries **2**–**4**). In each case, TLC analysis suggested that acid chloride formation had been successful; however, when treated with model substrate amine **75** no product was formed. We next attempted to use amide coupling reagents HATU **115**, HOBt **116** and EDC **117**, EEDQ **118**, and CDI **93** (the structures of which are given in Scheme **18** and Figure **22**). Again, none of these showed any formation of the desired product **114** by TLC or MS analysis (Table **4**, entries **5**–**8**).



HATU, **115** HOBt, **116** EDC HCl, **117** EEDQ, **118**

Figure 22: Structures of the amide coupling reagents used in Table **4**.

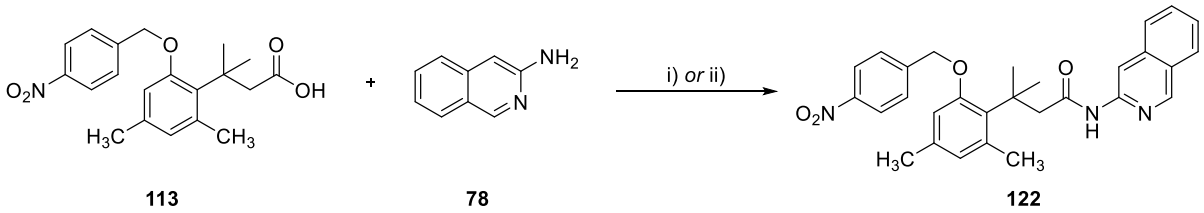
Given the lack of successful coupling observed with the trimethyl lock system and in carbamate formation, we hypothesised that the amine of model substrate **75** had poor nucleophilicity; delocalisation of the amine lone pair intothe aryl rings, plus the inductively electron withdrawing effect of the *para*-nitrile group contribute to reduced nucleophilicity. If this lack of nucleophilicity lead to slow reaction times, then decomposition of the coupling reagents could explain the lack of product formation. We therefore speculated that using a more stable coupling reagent could help improve reactivity. We chose to make acid fluorides of acid **113**; we hypothesised that since the C-F bond of an acid fluoride is stronger than the corresponding C-Cl bond of an acid chloride, this would improve its stability in solution. The electronegativity of fluorine would, however, make the carbonyl carbon significantly electron deficient, increasing its susceptibility to nucleophilic attack. We therefore attempted to make acid fluorides (Table **4**, entries **9**–**11**), using either Deoxo-Fluor® **119**, cyanuric fluoride **120** or BTFFH **121**, the structures of which are given in Figure **XX**, below. In each case, no acid fluoride was formed by TLC and MS analysis, and so this approach was not explored further.



Deoxo-Fluor®, **119** Cyanuric fluoride, **120** BTFFH, **121**

Figure 23: Structures of the acyl fluoride-forming reagents used in Table **4**, entries **9**–**11**.

Since it had proven challenging to directly couple model substrate **75** to the trimethyl lock system **113**, we investigated whether the coupling could be broken down into two stages. We thus attempted to couple 3-aminoisoquinoline **78**, one half of the model substrate, to acid **113** *via* an acid chloride-mediated coupling, shown in Scheme **26** below.



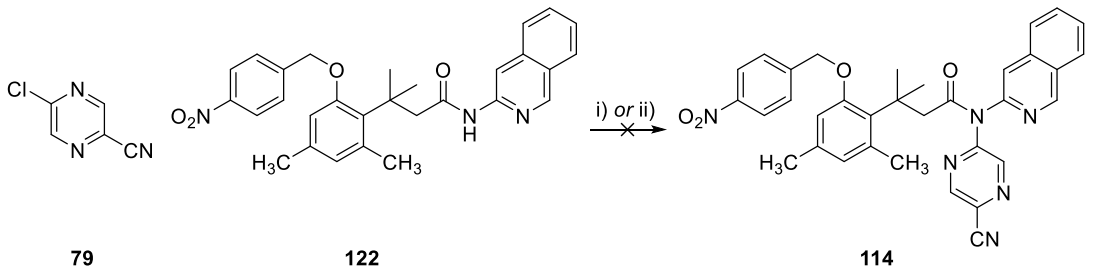
113 **78** **122**

Scheme 26: Synthesis of amide intermediate **122**. *Reagents and conditions:* i) Oxalyl chloride, DMF (cat.), Et_3N, THF, 0 °C → RT, 1 hour, 31% yield; ii) HATU, DIPEA, DMF, 90 °C, µW, 5 minutes, 40% yield.

Coupling of 3-aminoisoquinoline **78** to acid **113** was achieved using an acid chloride-mediated coupling in moderate yield; this yield was slightly improved upon by using a HATU-mediated amide coupling under microwave conditions in a sealed tube.

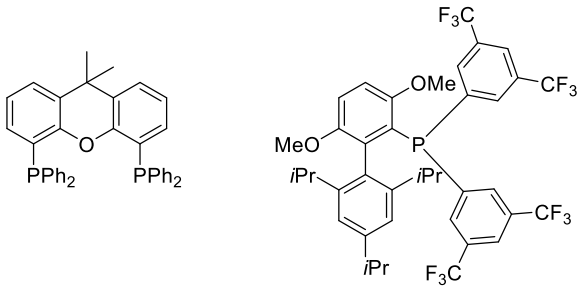
With compound **122** in hand, we considered methods of coupling the remaining pyrazine fragment of our model substrate. Buchwald-Hartwig couplings between primary amides and aryl halides have been reported,[198] and so we attempted to perform similar couplings.

(A)



79 **122** **114**

(B)

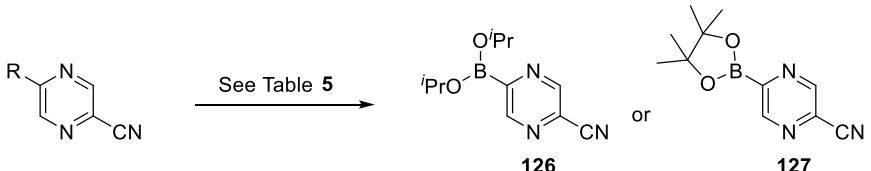


XantPhos, **123** JackiePhos, **124**

Scheme 27: (A) Attempted Buchwald-Hartwig couplings of amide **122** to chloropyrazine **79**. *Reagents and conditions*: i) $Pd_2(dba)_3$, XantPhos **123**, Cs_2CO_3, 1,4-dioxane, sealed tube, 80 °C, 7 days, N.R.; ii) $Pd_2(dba)_3$, JackiePhos **124**, K_2CO_3, 1,4-dioxane, 80 °C, 4 days, N.R. (B) Chemical structures of the ligands XantPhos (**123**) and JackiePhos (**124**) used in the Buchwald-Hartwig couplings.

Two sets of Buchwald-Hartwig conditions were employed to couple the pyrazine fragment of the model prodrug, both employing $Pd_2(dba)_3$ as catalyst, but with either the bidentate phosphine ligand XantPhos **123** or monodentate biaryl phosphine ligand JackiePhos **124**. In both cases, no evidence of reaction was observed by TLC, LRMS or ^{1}H NMR analysis.

The lack of reactivity in palladium-catalysed cross-couplings therefore led us to investigate the use of other transition metals. We chose to explore the Chan-Lam coupling, a copper-catalysed cross-coupling that can couple an aryl boronate to an amine or,[199] in some cases, an amide.[200]



125, R = H
79, R = Cl

126 **127**

Scheme 28: Attempted synthesis of pyrazine-boronates **126** or **127** for Chan-Lam couplings. *Reagents and conditions* are given in Table **5**, below.

Table 5: *Reagents and conditions* used to synthesise pyrazine-boronate reagents **128** or **129** as coupling partners for Cham-Lam reactions.

Entry	Reagents and Conditions	Solvent	T	Time	Yield
1	**79**, *n*-BuLi, 10 minutes, then $B(O^iPr)_3$	THF	−78 °C	10 minutes, overnight	N.R.
2	**79**, $B_2(pin)_2$, $Pd(dppf)Cl_2$, KOAc,, sealed tube, μW	Dioxane	120 °C	80 minutes	N.R.
3	**79**, $B_2(pin)_2$, $Pd_2(dba)_3$, $P(Cy)_3$, KOAc	Dioxane	80 °C	Overnight	N.R.
4	**125**, $B_2(pin)_2$, $[Ir(COD)Cl]_2$ (10 mol%), Me_4Phen (10 mol%)	MTBE	80 °C	1 hour	N.R.
5	**125**, $B_2(pin)_2$, $[Ir(COD)(OMe)]_2$ (3 mol%), Me_4Phen (3 mol%)	MTBE	80 °C	16 hours	N.R.

We attempted to synthesise a boronate analogue of the cyanopyrazine component of our model substrate. Using chloropyrazine **79**, we attempted lithium-halogen exchange using *n*-BuLi, followed by treatment with triisopropylboronate to afford the boronate ester **127** (Table **5**, entry **1**). TLC and LRMS analysis indicated no reaction had occurred, and so we instead employed Miyaura borylation (Table **5**, entries **2** and **3**), neither of which produced boronate **127**. We had noted that iridium-catalysed C-H borylation could be effective on several nitrogen-containing heterocycles,[201,202] and so we attempted C-H borylation of pyrazine **125**, using an iridium-cyclooctadienyl (COD) complex and tetramethylphenanthroline (Me_4Phen) as a ligand in methyl *t*-butyl ether (MTBE, Table **5**, entries **4** and **5**). Again, neither of these reactions appeared to afford the desired borylated product by TLC or LRMS analysis, and so no further exploration of Chan-Lam couplings was conducted.

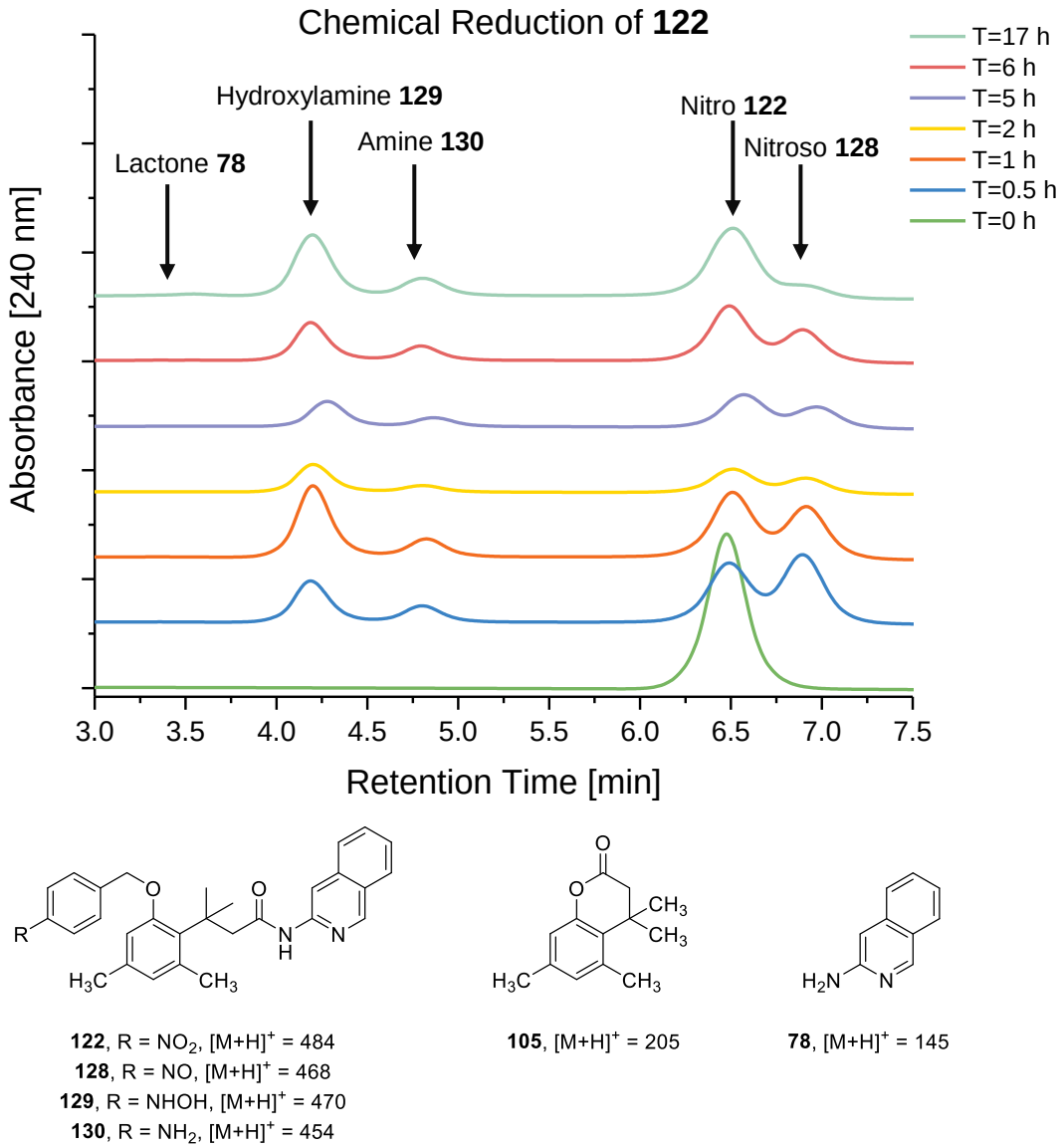
2.4 Testing of the 'trimethyl lock' platform

Whilst we had not synthesised our target bioreductive prodrug based on a trimethyl lock release system, we had in hand a somewhat related amide analogue, the isoquinolineamide **122**. We therefore chose to test this compound in both chemical reduction and nitroreductase assays, to assess its propensity to undergo reduction, fragmentation and cyclisation.[184] This would then serve as an indication of whether

this prodrug approach would be suitable for further study, in our pursuit of optimised prodrug forms of SAR020106 **56**.

2.4.1 Chemical reduction of 122

We first carried out a chemical reduction assay on **122**, which is a quick and simple initial test of the possible reductive behaviour of a substrate under reducing chemical conditions, as well as its propensity to fragment. The substrate was dissolved in DMF in the presence of a 10% *w/v* aqueous solution of ammonium chloride and is treated with zinc powder (see Chemical Experimental for details). Aliquots were taken during the reaction, added to neutral phosphate-buffered saline (PBS, pH 7.4), and analysed by HPLC-MS to assess the presence of new chemical species and their identities.



122, R = NO_2, $[M+H]^+$ = 484
128, R = NO, $[M+H]^+$ = 468
129, R = NHOH, $[M+H]^+$ = 470
130, R = NH_2, $[M+H]^+$ = 454

105, $[M+H]^+$ = 205

78, $[M+H]^+$ = 145

Figure 24: HPLC timecourse traces of the chemical reduction assay of trimethyl lock amide **122**. The identities of the peaks are given along with the associated molecular ion peak from the mass spectrum, and their structures are given below.

The above HPLC-MS analysis indicated that, as expected, the nitrobenzyl group of **122** underwent a slow chemical reduction to form various intermediates (nitroso **128**, hydroxylamine **129**, and amine **130**, Figure **24**). However, the peak observed for the amine **130** appeared to be comparatively stable, and no peak for the fragmented phenol was observed, nor one for the lactone **105**. This suggested that the amine reduction product **130** was stable under neutral aqueous conditions, and hence no cyclisation could occur to eject the cargo isoquinoline **78**.

2.5 Conclusions and Outlook

We began with the hypothesis that the lack of cytotoxicity caused by a hypoxia-activated prodrug form of Chk1 inhibitor SAR020106 **56** was due to poor fragmentation kinetics of the bioreductive group. We therefore set out to explore whether alternative bioreductive forms could be synthesised which had improved fragmentation kinetics, with the hypothesis that this would overcome the limitations of our first-generation prodrug.

Initially we began by designing a compound to act as a model for SAR020106 **56**, which retained the key features that influence the reactivity of the key nitrogen atom but had reduced chemical complexity and hence a simplified synthesis. This model substrate, **75**, was synthesised in good yield by both Buchwald-Hartwig coupling as well as S_NAr reactions. With the model substrate in hand, we attempted to append bioreductive groups to it which were alternatives to the 2-nitroimidazole previously employed.

Synthesis of alkylating agents to add the 2-nitrothiophene, 2-nitrofuran, 4-azidobenzyl and 6-nitroquinoline bioreductive groups was successful, however none of these could be alkylated to the nitrogen atom of **75**.

We also explored the use of more complex linkers between the model substrate and the bioreductive trigger. Several different synthetic strategies were employed to form the carbamate-linked nitrobenzyl prodrug, under the working hypothesis that the added driving force of CO_2 explusion upon fragmentation would aid fragmentation kinetics. Despite these efforts, however, no carbamate-linked bioreductives could be synthesised, suggesting either a lack of reactivity of the amine of **75**, or the instability of any carbamate species that formed.

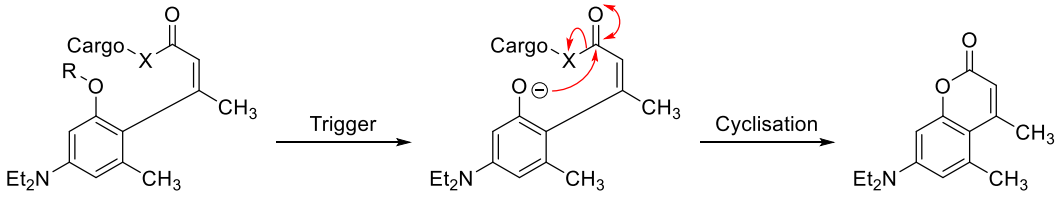
In the same vein as the carbamate-linked prodrug hypothesis, we also explored the use of the "trimethyl lock" linker. We synthesised a trimethyl lock intermediate, with a 4-nitrobenzyl trigger alkylated to the phenolic oxygen of the trimethyl lock core, and with a terminal carboxylic acid on the side chain. Efforts to synthesise the corresponding amide with model substrate **75**, however, proved unsuccessful. Amide coupling was achieved using the smaller fragment 3-aminoisoquinoline **78**, however, this amide could not be further alkylated using transition metal-catalysed couplings.

To test the hypothesis that the trimethyl lock system could aid fragmentation kinetics, we tested the simple amide analogue **122** under both chemical and biochemical reducing conditions. These assays indicated that, whilst the nitrobenzyl group was susceptible to reduction to the amine, no fragmentation and cyclisation occurred, with no detection of lactone **105**.

Insofar as prodrug forms of SAR020106 **56** are concerned, it may still be possible to synthesise better prodrug forms of this compound. However, there have recently been developed new inhibitors of Chk1, which have both superior pharmacodynamics and significantly better pharmacokinetic properties.[169,203] These compounds may prove more promising candidates for hypoxia-activated prodrugs as they move further forward in their clinical development. Moreover, the chemistry associated with converting them to bioreductive prodrugs may prove more tractable than SAR020106 has proven in our hands.

Despite the lack of cyclisation and concomitant release of cargo we observed for model trimethyl lock system **122**, such prodrug delivery systems still hold great promise in improving compound release for prodrugs. Alternative bioreductive groups have superior reduction kinetics to the 4-nitrobenzyl group and may prove to have superior fragmentation kinetics when applied to a trimethyl lock scaffold.

We later discuss the design and development of bioreductive prodrug moieties which also exhibit “switch-on” fluorescence when reduced under hypoxia, for use as potential theranostic agents. The trimethyl lock system may serve a purpose as such a theranostic agent; analogues of the trimethyl lock system have been studied which, upon cyclisation, produce fluorescent coumarins (see Scheme **29**, below).[195] Such a scaffold could prove useful for both enhanced drug release kinetics, as well as for its switch-on signal. This is, however, beyond the scope of the studies herein.



Coumarin 1, **131**
λ_{em} = 418 nm (THF)

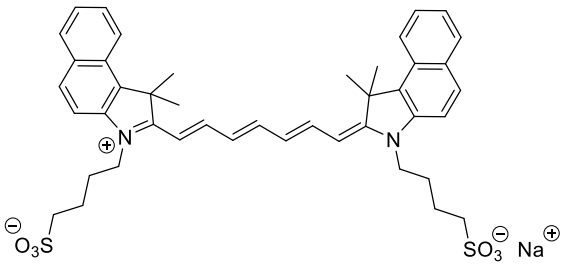
Scheme 29: Possible fluorogenic analogue of the trimethyl lock system. Coumarin 1 (**131**) is used as an example of a fluorescent cyclisation product.[204]

Chapter 3
A minimal, hypoxia-activated bioreductive fluorophore

3.1 Introduction

Drug-fluorophore conjugates are useful tools for studying drug behaviour both *ex vivo* and *in vivo*, with the fluorophore being used to report on the drug's localisation and distribution in cells and in tissue.[205] Fluorescence imaging is highly sensitive, and imaging can be achieved with concentrations in the nM to pM range,[88] which is complementary to typical efficacious exposure to clinical or pre-clinical drugs.

Despite the utility of drug-fluorophore conjugates, one clear limitation exists in their use for evaluation of drug pharmacokinetic and pharmacodynamics (PK/PD). Fluorophores with tissue-penetrating emission wavelengths are often large, conjugated structures with extended π-systems. Whilst this often improves their fluorescence properties, it is usually detrimental to their physicochemical properties. This quality results in poor solubility, high protein binding and a propensity to aggregation under physiological conditions. Moreover, these poor PK properties can be detrimental to their drug or antibody conjugate.[206] Indocyanine green **132**, for example, is the only clinically-approved fluorophore imaging agent; its structure contains two sulfonate groups, the purpose of which is only to aid solubility.[131]



Indocyanine green, ICG **132**

Figure 25: The structure of Indocyanine Green (ICG) **132**, the only FDA-approved fluorescent imaging agent.

A significant challenge in the development of drug molecules is optimising their PK properties, with candidate molecules often chosen as a compromise between binding affinity, *ex vivo* efficacy and pharmacokinetics.[207] It follows that conjugation of a fluorophore with poor PK, to a drug with a finely balanced PK profile, will usually result in a conjugate with poor PK properties.

Consequently, we hypothesised that finding new fluorophores which have both biologically-compatible fluorescence properties and improved PK properties would be beneficial to the field of drug-fluorophore conjugates. Keeping molecular weight as low as possible was our primary goal in minimising the impact of conjugation on the overall PK of the conjugate. This should allow any drug-fluorophore conjugates studied to behave similarly to the drug as a single agent.

We wished to combine this concept (*i.e.* minimising fluorophore impact on PK) with our interest in hypoxia-targeted drug delivery. Hence, we set out to find a new, low molecular weight scaffold that was fluorescent in the near-infrared ($\lambda_{em} \geq 650$ nm). Ideally, we wanted a scaffold which exhibited "switch-on" fluorescence, such that in one state it was non-emissive, until some environment-induced chemical change (such as metabolism) caused it to become fluorescent. These could be used as the basis for bioreductive prodrugs which would be minimally perturbing to the pharmacokinetic behaviour of their molecular cargoes.

3.2 Design of target molecules

To achieve our aim of a fluorophore which has a minimal impact on the PK properties of the attached drug cargo, we decided to use scaffolds which were of particularly low molecular weight. We therefore searched the literature for near-infrared fluorophores, looking for the smallest we could find.

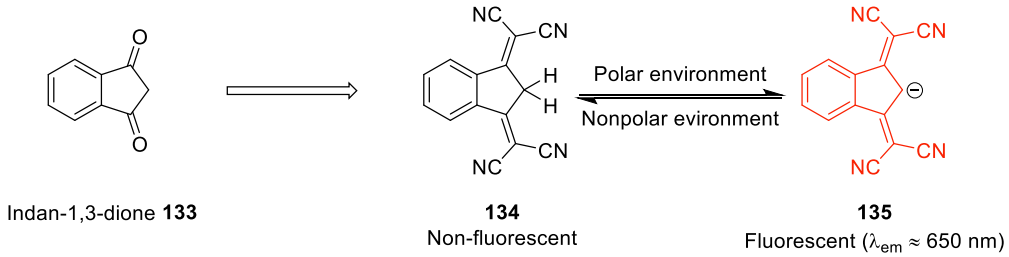


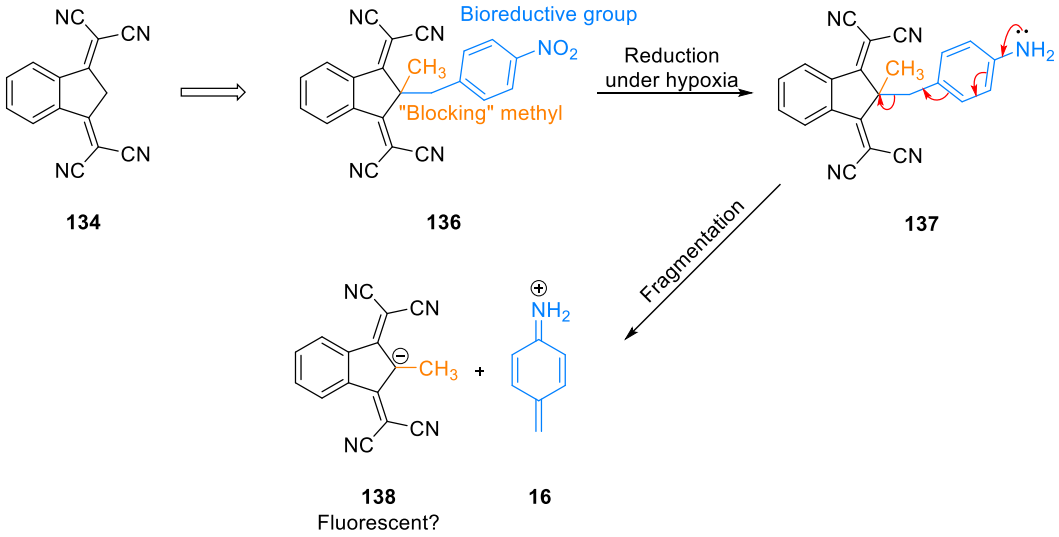
Figure 26: Structure of indan-1,3-dione **133**, the basis for electron-acceptor molecule **134**. Heo and coworkers showed that **134** appeared to undergo deprotonation in polar media, resulting in a fluorescent, presumably anionic species **135**.[208]

One of the molecules we found had been reported by Heo *et al*.[208] Based on the small molecule indan-1,3-dione **133**, compound **134** was designed as an electron acceptor component to be incorporated into merocyanine-type fluorophore structures. They found that **134**, when placed in polar organic solvents or basic aqueous solvent, appeared to undergo deprotonation. This resulted in a chemical species which had a significantly altered UV-Vis absorbance profile and was also fluorescent, with an emission maximum of ~650 nm. They hypothesised that deprotonation of **134** resulted in the methylene carbon atom acquiring sp^2 character, with the remaining proton lying in-plane. This placed the anion in a filled p-orbital perpendicular to the molecular plane, which overlaps with both dicyanovinylene moieties and the aryl ring to form an extended π-system. They calculated the change in energies of the HOMO and LUMO, finding that both appeared to be destabilised, but with much greater destabilisation of the HOMO than the LUMO, resulting in a reduced HOMO-LUMO gap.

Furthermore, Heo *et al*. used density functional theory (DFT) calculations of Gibbs free energy and enthalpy to estimate the dissociation constants (pK_a) for both

single and double deprotonation of **134**, estimating the first dissociation constant as ~4.1 (*c.f.* acetic acid pK_a ~4.8), and the second as being ~57.6, suggesting the conjugate base of monodeprotonated **134** was quite stable. Finally, they formed the **134**-human serum albumin (HSA) complex and used it to image both SCC7 cells and an SCC7 tumour xenograft in a mouse.

The properties described above fit well with our criteria for a starting-point molecule; **134** had a low molecular weight of 242 Da (*c.f.* ICG **132**, MW = 775 Da), appeared to exhibit "switch-on" fluorescence *via* formation of the anionic species **135**, and had been demonstrated to function as an NIR imaging agent in cells. We hypothesised that we could utilise the "switch-on" fluorescent behaviour of **134** to produce a hypoxia-activated imaging agent, which could then be incorporated into a theranostic agent.



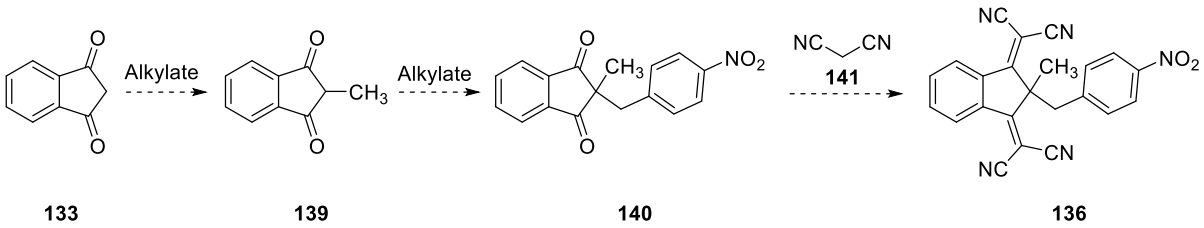
Scheme 30: Proposed modification to **134** to give a hypoxia-activated "switch-on" fluorophore, and mechanism of activation.

We hypothesised that addition of a hypoxia-sensitive bioreductive group, such as the 4-nitrobenzyl group shown in Scheme **30**, could provide the "switch-on" fluorescent signal we wanted. It has been demonstrated by us, and others, that when electron-withdrawing nitro groups are converted to electron-donating forms, such as amino and

hydroxylamino, molecular fragmentation can occur.[26,51] We proposed that this fragmentation mechanism could result in a negative charge being placed at the central methylene carbon atom of product **138**, which would then be fluorescent. Addition of a nitrobenzyl group at C2 of **134** would leave a single proton at this position which would still be highly acidic; hence, we proposed the addition of a methyl group at this position to block unwanted deprotonation and anion formation, and thus fluorescence.

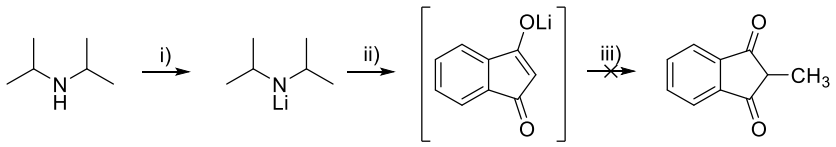
3.3 Synthesis

We began synthesis by following a similar procedure to Heo *et al*., who performed a Knoevenagel condensation between malononitrile **141** and indan-1,3-dione **133** to synthesise fluorophore **134**.[208] Taking indan-1,3-dione **133** as a starting material, we proposed to perform two monoalkylation reactions at the methylene carbon *via* enolate chemistry, then complete the synthesis with a Knoevenagel condensation, outlined in Scheme **31**.



Scheme 31: Proposed synthetic route to bioreductive "switch-on" fluorophore **136**.

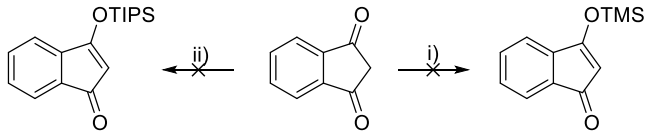
We identified overalkylation as a possible problem with this method, and so we began by attempting to form the enolate using the bulky, irreversible base lithium di*iso*-propylamide (LDA, formed *in situ*). We hoped to form the lithium enolate **144** exclusively, and then achieve single methylation by treatment with 1 equivalent of methyl iodide, shown in Scheme **32**. This approach proved unsuccessful, with TLC and MS analysis indicating the presence of remaining indan-1,3-dione **133** and no clear product.



142 **143** **144** **139**

Scheme 32: Attempted monoalkylation of **133**, using LDA **143** as a base. *Reagents and conditions*: i) *n*-BuLi, THF, −78 °C → RT, 1 hour; ii) Indan-1,3-dione **133**, THF, RT, 25 minutes; iii) Methyl iodide, THF, RT, 3 hours, N.R.

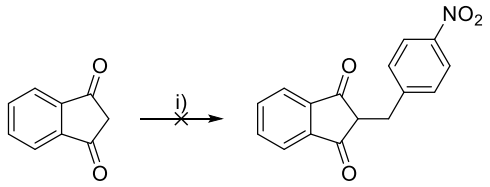
As an alternative to forming an enolate *in situ* for alkylation, we instead attempted to trap the enolate as a silyl enol ether, as shown in Scheme **33** below. Treatment of indan-1,3-dione **133** with base, followed by addition of either trimethylsilyl chloride (TMSCl) or tri*iso*-propylsilyl chloride (TIPSCl), did not form the corresponding silyl enol ethers **145** and **146**, respectively.



146 **133** **145**

Scheme 33: Attempted enolate trapping *via* formation of silyl enol ethers. *Reagents and conditions*. i) Et_3N, DMF, 0 °C, 20 minutes, then TMSCl, 0 °C → RT, 20 hours, N.R.; ii) Et_3N, imidazole, CH_2Cl_2, RT, 10 minutes, then TIPSCl, RT, 21 hours, N.R.

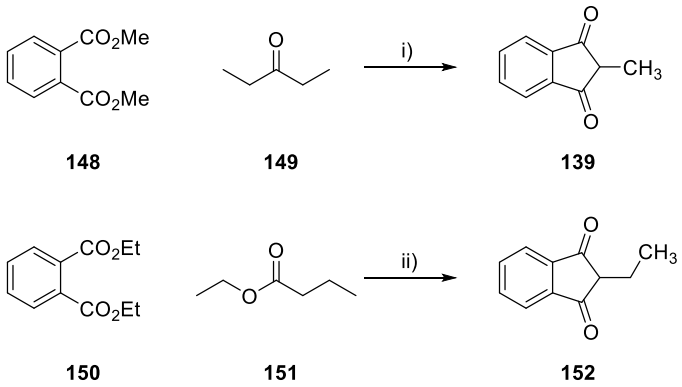
In all the preceding reactions, the aim was to initially alkylate with a methyl group. Since methyl groups are small, they provide little steric impediment to overalkylation. By contrast, the nitrobenzyl group is significantly larger; we therefore attempted to first alkylate **133** with a nitrobenzyl group in the first step, rather than a methyl group. We hypothesised that mono-alkylation with the bulky nitrobenzyl group would sterically block a second alkylation, allowing us to then attempt the methylation step (Scheme **34**, below). Again, this reaction was not successful, with only starting materials returned.



133 **147**

Scheme 34: Attempted alkylation of indan-1,3-dione **133** with a nitrobenzyl group. *Reagents and conditions*. i) K_2CO_3, DMF, RT, 30 minutes, then 4-nitrobenzyl bromide, RT, 18 hours, N.R.

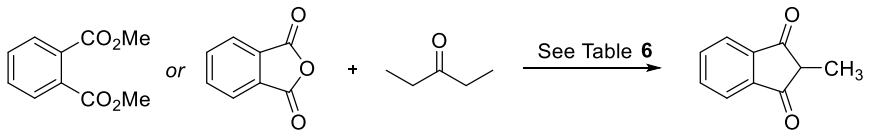
These attempts at alkylating indan-1,3-dione **133** proved unsuccessful, and so we considered alternate methods of synthesising differentially-alkylated analogues of **133**. Analysis of the literature identified two previous reports in which mono-alkylated indanediones had been synthesised without use of alkylation reactions.[209,210] Both methods involved forming an enolate (of a ketone or ester), which underwent a double sequential condensation onto a phthalate ester, forming monoalkylated indan-1,3-diones **139** and **152**.



Scheme 35: Literature syntheses of mono-alkylated indanediones. *Reagents and conditions*. i) NaH, benzene, reflux, 15 hours, then H_2O, conc. aqueous HCl, 68% yield;[209] ii) NaH, Bu_2O, reflux, 2 hours, then NaH, reflux, 4 hours, then 5% *v/v* aqueous HCl, 87% yield.[210]

These conditions appeared to offer a readily accessible method of producing differentially substituted indanedione derivatives, and so we attempted to synthesise **139** using the reported method. The set of conditions which afforded the methylated analogue **139** used benzene as a solvent, a known carcinogen which we were keen to avoid. Hence, we modified the reaction conditions to use the comparatively benign

solvent di-*n*-butyl ether from the synthesis of **152**, details of which can be found in Table **6** and Scheme **36**.



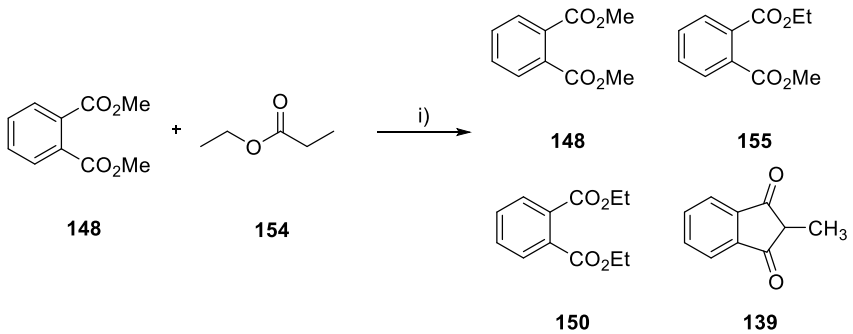
148 **153** **149** **139**

Scheme 36: Attempts to synthesise 2-methylindan-1,3-dione **139** *via* phthalate condensation. *Reagents and conditions* are given in Table **6**.

Table 6: Reagents and conditions used in the attempted synthesis of **139**.

Entry	Phthalate	Base	Solvent	Temperature	Time	Yield
1	**148**	NaH (60% in oil)	Toluene	80 °C	64 hours	0%
2	**153**	NaH (60% in oil)	Toluene	0 °C → RT	1.5 hours	0%
3	**153**	NaH (60% in oil)	THF	0 °C → RT	18 hours	0%
4	**153**	NaH (60% in oil)	DMF	0 °C → RT	1 hour	0%

In the first attempt (Table **6**, entry **1**), we replaced benzene with toluene, and the solution was heated at 80 °C for 3 days. Formation of a precipitate, an indication that the condensation had taken place, was not observed, and no product was observed by TLC and MS analysis. We repeated the reaction using phthalic anhydride **153** (Table **6**, entry **2**) which is more reactive, and at a lower temperature. This again proved unsuccessful, as did subsequent reactions using THF (Table **6**, entry **3**) or DMF (Table **6**, entry **4**) as solvents.

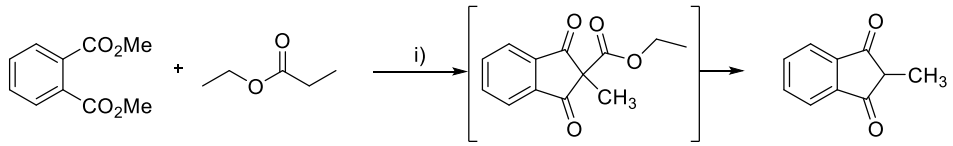


148 **154** **148** **155** **150** **139**

Scheme 37: First attempted synthesis of **139** using conditions modified from Tanaka *et al.*[210] *Reagents and conditions*: i) NaH, *n*-Bu_2O, reflux, 6 hours.

These unsuccessful efforts prompted us to adapt the conditions of Tanaka *et al.*,[210] using ethyl propionate **154** and dimethyl phthalate **148** in di-*n*-butyl ether, heated under reflux for 6 hours. During this time, the reaction mixture began to turn orange

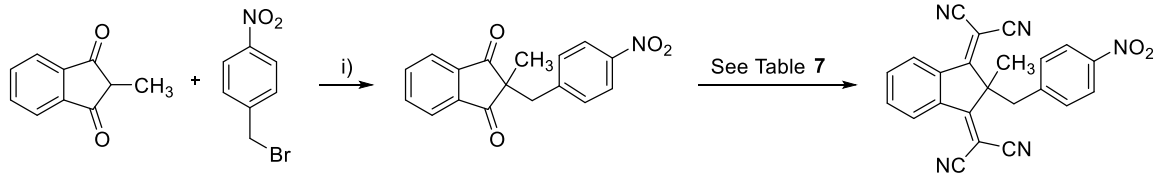
and the colour became progressively more intense. After concentrating the reaction mixture under reduced pressure, ^{1}H NMR analysis revealed the presence of dimethyl phthalate **148** starting material, the *mono*-transesterified ethyl methyl phthalate **155**, the *bis*-transesterified diethyl phthalate **150**, and the desired product **139**. Unfortunately, these impurities could not be separated by silica gel chromatography.



148 **154** **155** **139**

Scheme 38: Optimised conditions for synthesis of 2-methylindan-1,3-dione **139**. *Reagents and conditions*: i) NaH, *n*-Bu_2O, reflux, 2 hours, then H_2O, conc. aqueous HCl, 94% yield.

We had observed during the reaction that an orange precipitate had formed, and this also observed upon repeating the reaction. We hypothesised that this precipitate was the ester intermediate **157**, shown in Scheme **39**, however ^{1}H NMR analysis did not elucidate its identity. Suction filtration was used to collect the precipitate, which readily dissolved in water. Treatment of the solution with concentrated aqueous hydrochloric acid immediately caused brisk effervescence and formation of **141** as a precipitate, presumably as the result of acid-catalysed decarboxylation. The optimised conditions are given in Scheme **39**.



139 **156** **140** **136**

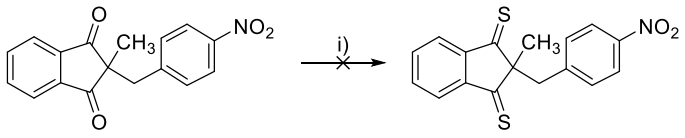
Scheme 39: Synthesis of a dialkylated indanedione **140** and attempted Knoevenagel condensation. *Reagents and conditions:* i) K_2CO_3, DMF, RT, 3 hours, 50% yield.

Table 7: Conditions for the attempted Knoevenagel condensation of malononitrile **141** with indanedione **140**.

Entry	Additive	Base	Solvent	Temperature	Time	Yield
1	-	NH_4OAc	EtOH	Reflux	30 hours	N.R.
2	-	NH_4OAc	Toluene	Reflux	3 hours	N.R.
3	$POCl_3$	Et_3N	$CHCl_3$	RT, then reflux	5 hours, then 17 hours	N.R.
4	Piperidine	-	EtOH	Reflux	7 hours	N.R.
5	10 mol% $Ga(OTf)_3$	Et_3N	CH_2Cl_2	−78 °C → RT	17 hours	N.R.
6	10 mol% $Ga(OTf)_3$	Et_3N	THF	RT	23 hours	N.R.
7	$BF_3{\cdot}Et_2O$	Et_3N	THF	RT	20 hours	N.R.

With the monosubstituted indanedione **139** in hand, we next attempted to introduce the nitrobenzyl bioreductive group. Pleasingly, alkylation of **139** with nitrobenzyl bromide **156** proceeded readily under mildly basic conditions in DMF (Scheme **39**). The last step was to incorporate the divinylnitrile groups *via* Knoevenagel condensation. This proved challenging, and no reactions were successful; conditions used are given in Table **7**.

We first attempted to use conventional condensation conditions from the literature, using ammonium acetate as a "buffered" base in refluxing ethanol (Table **7**, entry **1**), which did not give any reaction and returned only starting material. Repeating the reaction in toluene (Table **7**, entry **2**), to achieve a higher reflux temperature, also resulted in no reaction. We therefore attempted to activate the carbonyl oxygen atoms, starting with $POCl_3$ (Table **7**, entry **3**), however, no reaction was observed. Similarly, using piperidine to form iminium adducts at the carbonyls of **140** (Table **7**, entry **4**) was also unsuccessful. Finally, we attempted to use Lewis acids gallium(III) triflate (Table **7**, entries **5**&**6**) and boron trifluoride diethyletherate (Table **7**, entry **7**) to activate the carbonyl group, but again this was unsuccessful.



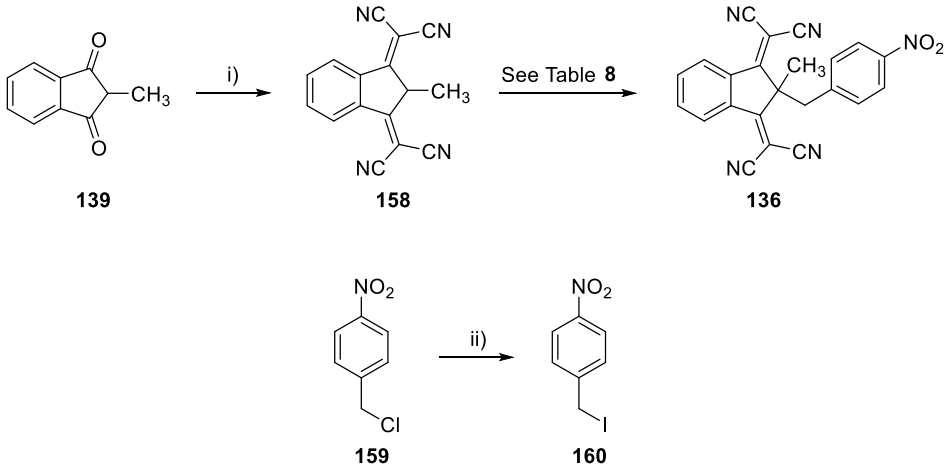
140 **157**

Scheme 40: Attempted synthesis of the thiocarbonyl analogue **157**. *Reagents and conditions*: i) P_2S_5, toluene, reflux, 3 hours, N.R.

As an alternative form of carbonyl activation, we hypothesised that the carbonyl groups could be converted to their thiocarbonyl analogues. The C=S bond of a thiocarbonyl group is weaker than the corresponding C=O bond of a carbonyl group, due to poor overlap between the carbon atom's small 2s and 2p valence orbitals with the sulfur atom's larger 3s and 3p valence orbitals. We therefore rationalised that these

weaker bonds would be more susceptible to nucleophilic attack and displacement by malononitrile. Unfortunately, attempting to synthesise the thiocarbonyl analogue **157** using phosphorus pentasulfide was not successful (Scheme **40**).

These experiments demonstrated that Knoevenagel condensation of malononitrile onto the carbonyls of **142** was a difficult reaction to achieve. We hypothesised that this was due to the presence of a quarternary carbon atom adjacent to the carbonyls, although it was not clear whether this was a consequence of steric crowding or some unusual mechanism for the condensation reaction. Consequently, we chose to explore an alternate method, performing the Knoevenagel condensation prior to installation of the second alkyl group.



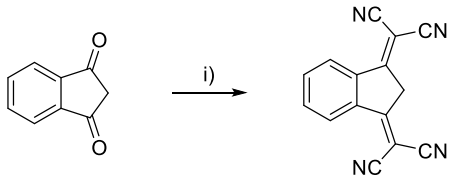
Scheme 41: Synthesis of small, bioreductive pro-fluorophore **136**. *Reagents and conditions*: i) Malononitrile, NH_4OAc, EtOH, reflux, 24 hours, 64% yield; ii) NaI, acetone, reflux, 2 hours 40 minutes, 96% yield.

Table 8: Reagents and conditions used for the alkylation of **158**.

Entry	Alkylating agent	Base	Solvent	Temperature	Time	Yield
1	**156**	Cs_2CO_3	DMF	RT	2 hours	N.R.
2	**156**	Cs_2CO_3	THF	RT	64 hours	N.R.
3	**156**	Cs_2CO_3	Toluene	RT, then reflux	2 hours, then 4 hours	N.R.
4	**156**	Et_3N	1,4-dioxane	Reflux	22 hours	N.R.
5	**156**	Et_3N	Toluene	Reflux	14 hours	Observed, not isolated
6	**160**	Et_3N	Toluene	Reflux	13 hours	25%

Knoevenagel condensation of malononitrile with monoalkylated indanedione **139** proceeded in good yield, indicating that the lack of reactivity for the disubstituted analogue **140** is directly related to the presence of the quarternary carbon atom. We next attempted to alkylate **158**, initially using mild alkylation conditions (Table **8**, entry **1**), which showed no sign of reaction by TLC analysis, despite the solution becoming intensely blue (indicative of formation of the anion of **158**).

Since it appeared that the anion of **158** was being formed in the presence of base, we considered the observed lack of reactivity. As discussed in Chapter 3.2, the pK_a of the unmethylated analogue **134** was estimated at ~4.2, meaning that the conjugate base (the anion) is highly stable in solution. The additional methyl group, we supposed, was unlikely to significantly alter the pK_a of the acidic proton of **158**, and hence the anion must also be highly stable in solution. We therefore hypothesised that the use of the polar solvent DMF was detrimental to the reaction, since the anion would be more stable in polar solvent and hence less nucleophilic. Changing solvent to THF (Table **8**, entry **2**), and then non-polar toluene (Table **8**, entry **3**) did not induce any reaction. Changing from caesium carbonate to triethylamine had no effect when conducted in 1,4-dioxane (Table **8**, entry **4**), however, in toluene we observed a new product by TLC (Table **8**, entry **5**). This product appeared to represent only a small amount of conversion, and the remaining alkylating agent appeared to decompose during the reaction. We hypothesised that using a more reactive alkylating agent could overcome this apparent slow conversion, and therefore synthesised 4-nitrobenzyl iodide **160** *via* a Finkelstein reaction from 4-nitrobenzyl chloride **159** (Scheme **41**), which proceeded in excellent yield. Using this alkylating agent, under reflux in toluene with triethylamine as a base thus afforded the final compound **136** in modest yield (Table **8**, entry **6**).



133 **134**

Scheme 42: Synthesis of literature fluorophore **134**. *Reagents and conditions:* i) Malononitrile, NH_4OAc, EtOH, reflux, 11 hours, 70% yield.

As a reference for UV-Vis and fluorescence characterisation, we also synthesised the literature fluorophore **134**, using a Knoevenagel condensation between malononitrile and indan-1,3-dione **133**, which proceeded in very good yield (Scheme **42**).

3.4 Characterisation

3.4.1 UV-Vis absorbance and fluorescence spectra

With the full protected pro-fluorophore scaffold in hand, we wished to measure the UV-Vis absorbance and fluorescence spectra of both the literature fluorophore **134** and our putative fluorophore **158**. It had been shown by Heo *et al.* that the unmethylated analogue **134** was fluorescent,[208] and we wished to see the effect of the additional methyl group on the molecule's fluorescence.

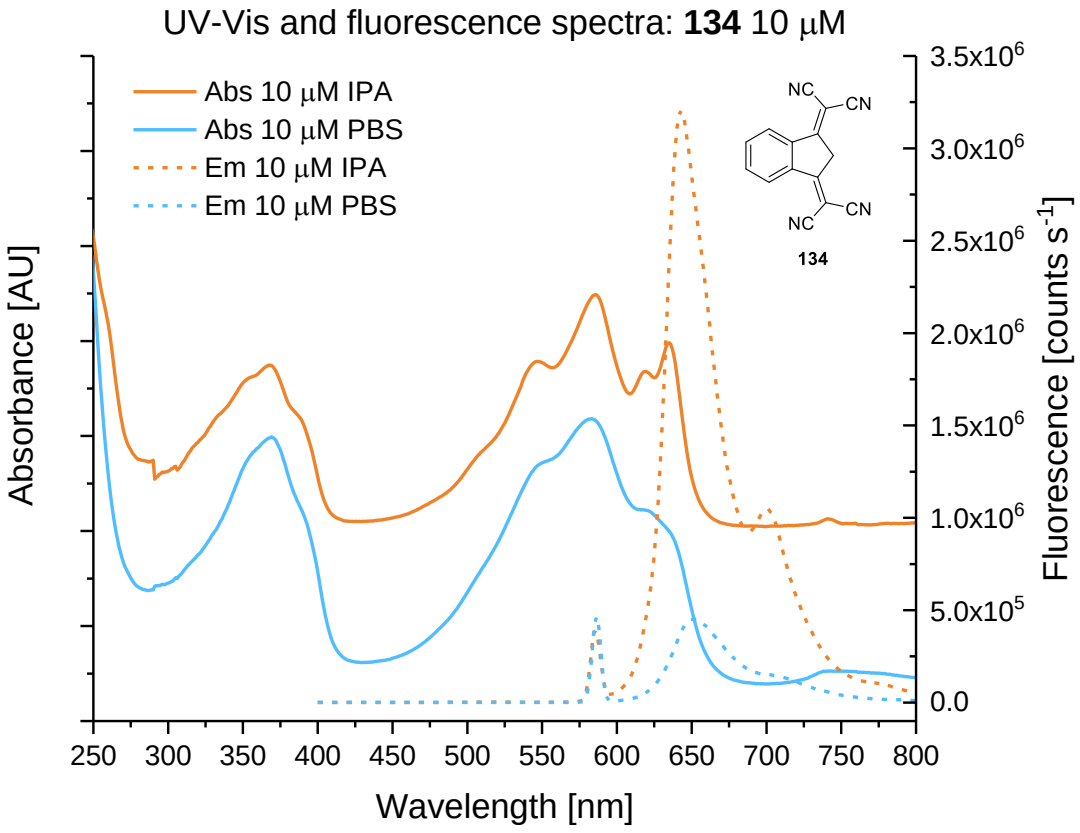


Figure 27: UV-Vis absorbance (solid lines) and fluorescence (dashed lines, λ_{ex} = 585 nm) spectra for literature compound **134.** Spectra were recorded at 10 μM in either *iso*-propanol (IPA, orange) or phosphate-buffered saline (PBS, blue).

Absorbance spectra (Figure **27**) showed that literature fluorophore **134** had an absorption maximum at 585 nm in IPA and, whilst the absorption curve was less well-defined in PBS, the absorption maximum was again at 585 nm. Both curves had similar shape and were comparable with literature spectra. Similar to the reported spectra of Heo *et al*., **134** had a fluorescence emission maximum at 643 nm in IPA (*c.f.* ~650 nm in acetone),[208] and as expected, the fluorescence intensity of **134** was significantly reduced in PBS (λ_{em} ≈ 651 nm).

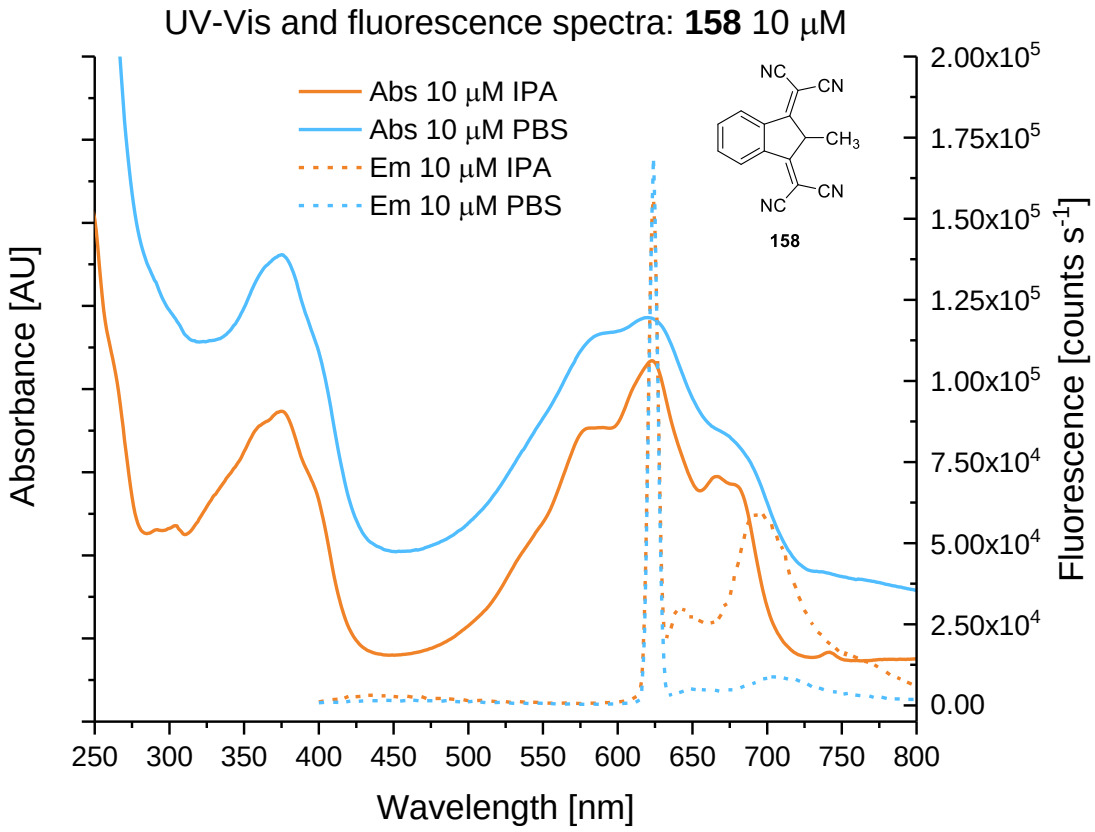


Figure 28: UV-Vis absorbance (solid lines) and fluorescence (dashed lines, λ_{ex} = 623 nm) spectra for methylated analogue **158** Spectra were recorded at 10 μM in either *iso*-propanol (IPA, orange) or phosphate-buffered saline (PBS, blue).

We then recorded the UV-Vis absorbance and fluorescence spectra of compound **158** (Figure **28**), our proposed fluorophore which would be released after metabolism under hypoxia. The UV-Vis absorbance spectra were comparable with those of parent compound **134**, with the absorption maxima in IPA and PBS shifted to ~623 nm. The fluorescence emission spectrum in IPA showed that, whilst **158** was still fluorescent in the NIR (λ_{em} ≈ 693 nm), the fluorescence intensity was >50-fold lower than that of the parent compound **134** at their respective emission maxima (~5.8 × 10^4 counts s^{-1} at 693 nm *vs* ~3.2 × 10^6 counts s^{-1} at 643 nm). Similarly, the fluorescence intensity of **158** was greatly reduced in PBS, such that it was approximately 50-fold lower than that of unmethylated analogue **134** (~9.1 × 10^3 counts s^{-1} at 652 nm *vs* ~4.5 × 10^5 counts s^{-1} at 706 nm).

The significant reduction in fluorescence intensity of methylated analogue **158** compared to the parent **134** was disappointing, since it suggested that **158** would not be bright enough to detect in imaging experiments. We therefore concluded that molecules based on methylated analogue **158** would not be useful for a theranostic imaging agent.

3.4.2 Chemical reduction of 136

Despite the diminished fluorescence of **158**, we nevertheless wished to test whether the scaffold **136** could act as an oxygen-sensitive bioreductive compound. We first subjected **136** to a chemical reduction assay, in which the compound is treated with zinc powder and ammonium chloride in DMF and analysed for metabolites and cargo release (in this case **158**) by HPLC-MS. This assay is typically the first step in a panel of assays we used to analyse potential bioreductive compounds.[184]

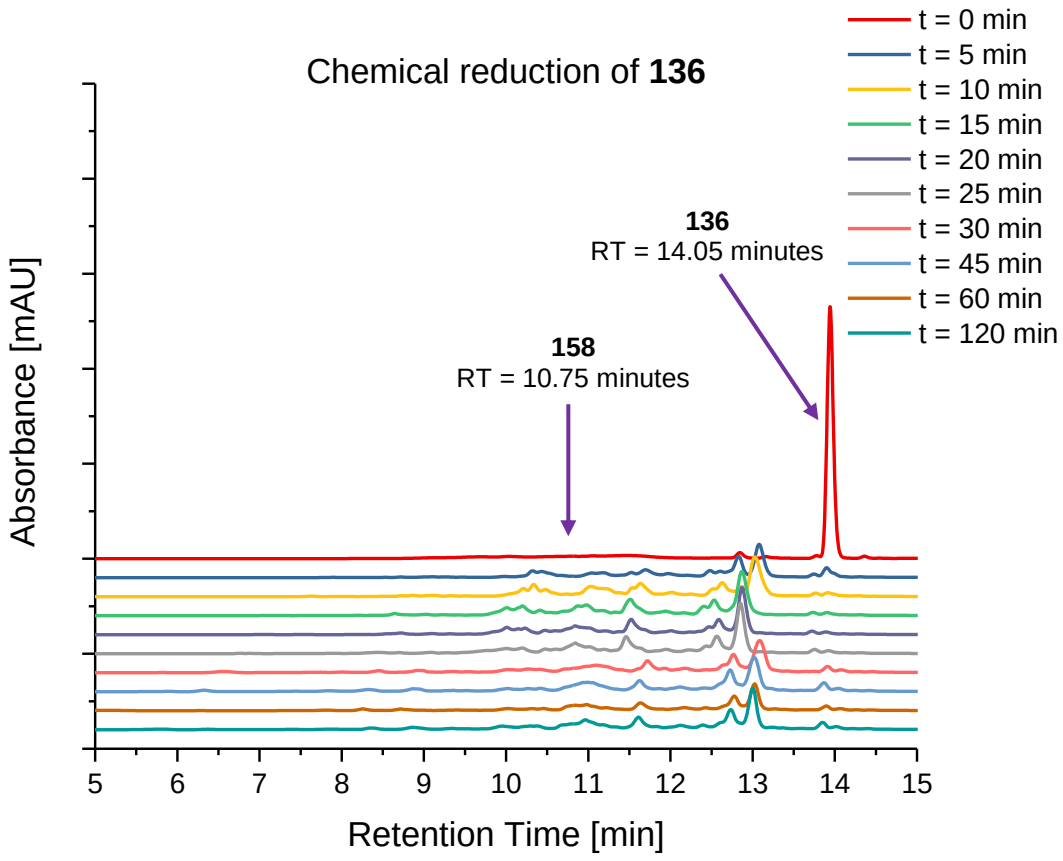


Figure 29: HPLC analysis of chemical reduction assay for protected compound **136**.

Analysis of the chemical reduction assay (Figure **29**) showed that **136** was highly unstable to chemically reducing conditions, which rapidly degraded **136** and produced a wide variety of products. We hypothesised this broad reactivity could be due to the presence of the four nitrile groups, which could be susceptible to reduction. Similarly, the electron-deficient tetrasubstituted olefins to which the nitriles were conjugated could also be unstable to chemical reduction.

Chemical reduction experiments can be useful as a quick, simple test of whether a potential bioreductive can be reduced, and if the reduced species can perform its function (*i.e.* releasing a cargo or becoming fluorescent). It is, however, conducted under a set of conditions which are not representative of a cellular environment, and as such a negative result is not necessarily indicative that the compound will not function as designed in a model of cellular hypoxia. We therefore took **136** forward to assess in a biochemical assay for oxygen-sensitive metabolism.

3.4.3 Enzymatic reduction of 136

We subjected **136** to a cytochrome p450 reductase (CPR) assay, the details of which can be found in Biological Materials and Methods.

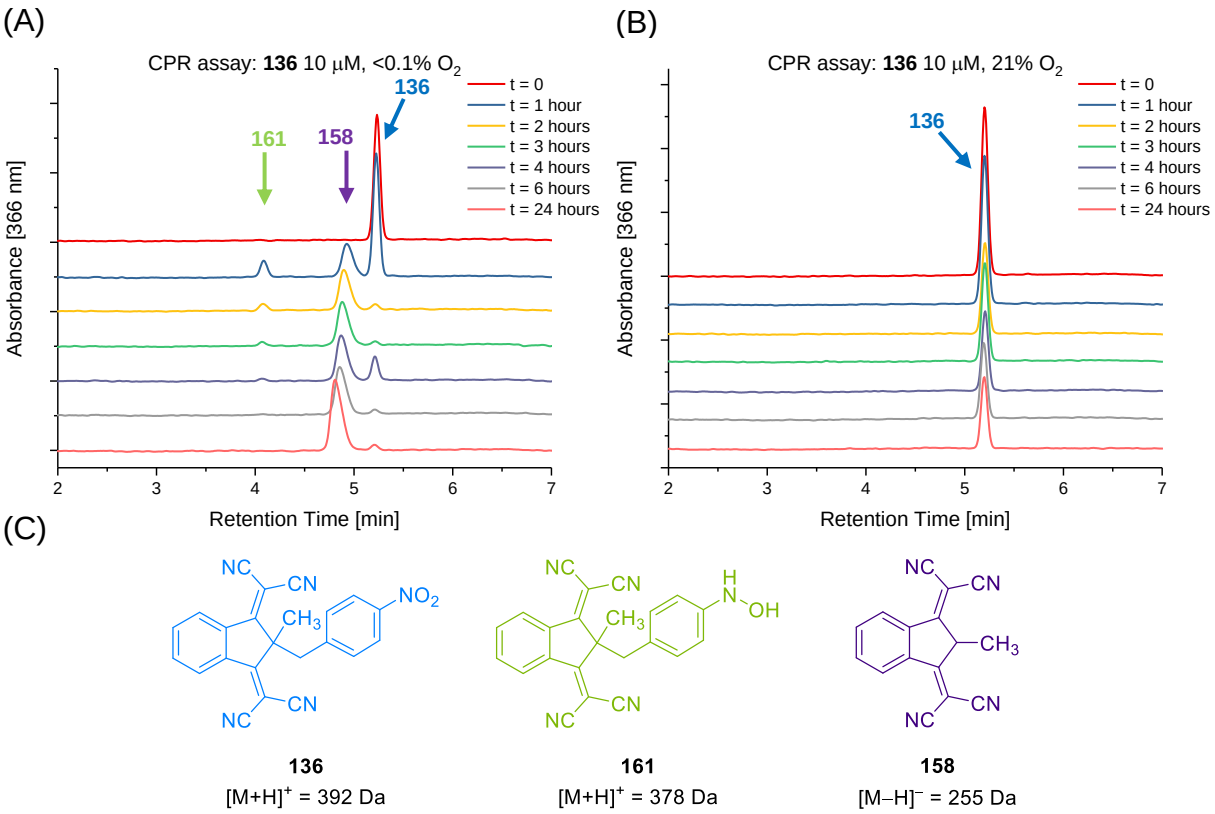


Figure 30: Enzymatic reduction of **136** under (A) anoxia and (B) normoxia. (C) Proposed identities of species observed by HPLC-MS.

We treated **136** to cytochrome p450 reductase (CPR) under anoxic (<0.1% O_2) and normoxic (~21% O_2) conditions, and analysed the mixture over a timecourse by HPLC-MS. For compound incubated under normoxic conditions (Figure **30b**) we observed no metabolism at all, with the HPLC peak remaining steady over the course of the assay. By contrast, **136** incubated under anoxic conditions appeared to be steadily metabolised, as indicated by a decrease in the substrate peak (Retention Time = 5.2 minutes, $[M+H]^+$ *m/z* = 392, Figure **30a**), with a concomitant appearance of the peak corresponding to the released "fluorophore" moiety **158** (Retention Time = 4.75 minutes, $[M-H]^-$ *m/z* = 255). We also observed a peak (Retention Time = 4.05 minutes, $[M+H]^+$ *m/z* = 378) appear rapidly, and then slowly disappear during the timecourse. This peak was identified as being the hydroxylamine intermediate **161**, given its observed mass, and our previous observation of hydroxylamine intermediates for metabolised nitrobenzyl groups.[51] These data support our hypothesis that the

nitrobenzyl group of **136** is metabolised by CPR in an oxygen-dependent manner, probably *via* a sequential single-electron reduction pathway, resulting in fragmentation and release of the "fluorophore" component.

3.5 Conclusions and Outlook

In this chapter we outlined a challenge for the development of theranostic agents, namely the perturbation of the ligand of interest's pharmacokinetic properties by appending large NIR fluorophores. We proposed a strategy to ameliorate the limitations imposed by large fluorophores, by using small (MW ≤ 250 Da) NIR fluorophores which have minimal impact of the PK properties of the studied ligands, a strategy we then set out to test.

We began by studying the literature, identifying a small-molecule fluorophore (MW = 242 Da) with NIR fluorescence ($\lambda_{em} \approx 650$ nm). This fluorophore appeared to have "switch-on" fluorescence, whereby the fluorescent species was the deprotonated, anionic form. We designed a molecule based upon this fluorophore, which we hypothesised would act as an oxygen-sensitive, bioreductive "switch-on" fluorophore.

The target molecule **136** was synthesised, and we analysed the "switch-on" fluorophore component of the molecule to determine its UV-Vis absorbance and fluorescence spectra. We found that addition of a methyl group at the C2 position of the literature fluorophore **134** significantly decreased its fluorescence. We nevertheless tested **136** to determine its susceptibility to oxygen-dependent metabolism. Whilst the molecule was degraded under chemically reducing conditions, it was selectively metabolised by cytochrome p450 reductase under anoxic conditions and unmetabolized under normoxic conditions, as we had hoped. Furthermore, the "fluorophore" cargo **158** was released *via* molecular fragmentation, showing that our hypothesised mechanism of "switch-on" was valid.

Whilst the molecule we developed transpired to lack fluorescence in its modified state, we believe this general approach is worth further investigation. **134** was shown to exhibit fluorescence in its anionic form due to an unusual narrowing of the HOMO-LUMO gap, and such effects may be key to finding other fluorophores which are near-infrared fluorescent while maintaining a small size. Whilst our interest was in finding a "switch-on" dye for environment-specific sensing, development of minimally-perturbing "always on" dyes will also be useful in drug-fluorophore for studying compound distribution and delivery.

It is also interesting to note that fragmentation of **136** to release **158** occurs *via* cleavage of a C–C bond. To the best of our knowledge, this is the first example of a nitroaryl HAP which fragments *via* C–C bond cleavage rather than C–O or C–N bond cleavage. This is likely due to the extreme stabilisation of the resultant carbanion of **158** and may provide an alternative strategy for design of new HAPs with C-linked bioreductive groups. This is, however, beyond the scope of this thesis.

Chapter 4
A new bioreductive near-infrared fluorophore for hypoxia imaging

Following on from the small fluorophore scaffold explored in Chapter 3, we wished to find other NIR fluorophore scaffolds which could be modified to exhibit 'switch-on' fluorescence in response to hypoxia. Moreover, we sought scaffolds which had been shown to have favourable imaging properties both in cells and in *in vivo* models.

4.1 Choice of scaffold

The most effective fluorophores for fluorescence imaging are those with emission maxima at wavelengths with the greatest tissue penetrance. Wavelengths longer than those of visible light (*i.e.* infrared light) are more penetrating of tissue than visible or ultraviolet light. Thus, near-infrared ($\lambda \geq 650$ nm) and infrared fluorophores are preferred for bioimaging applications; infrared fluorophores may have penetration depths of ~10 mm. Such fluorophores can be useful for preclinical imaging work, for fluorescent image-guided surgery,[211] and for endoscopy.[212,213]

We wished to develop a near-infrared fluorophore probe as an imaging agent for tumour hypoxia, which could then be incorporated into a hypoxia-responsive theranostic agent. As with previous work detailed herein, we hypothesised that fluorophores could be developed which exhibit minimal fluorescence until metabolised under hypoxia. We envisaged that a substrate bearing a nitroaryl or azidoaryl moiety may act as a non-emissive "pro-fluorophore", until metabolised by cytochrome p450 reductase (CPR) or related oxygen-inhibited enzymes.

Analysis of the literature identified an unusual benzopyrylium-based structure, published by Liu and coworkers,[214] with an intrinsic positively charged oxonium ion, shown in Figure **31**. This structure was based on that of the rhodamines, a family of

fluorescent dyes widely used for cellular imaging purposes. The amino analogue **163** is fluorescent, with an absorption maximum $\lambda_{abs} \approx 600$ nm and an emission maximum $\lambda_{em} \approx 725$ nm. This fluorophore emits in the NIR region and exhibits fluorescence upon two-photon excitation. Most importantly the azido analogue **165** had been synthesised, is non-fluorescent, and undergoes conversion to the fluorescent amine **163** upon exposure to hydrogen sulfide. The researchers also demonstrated its suitability for 'deep tissue' bioimaging applications, imaging rat liver sections at a depth of ~400 μm.

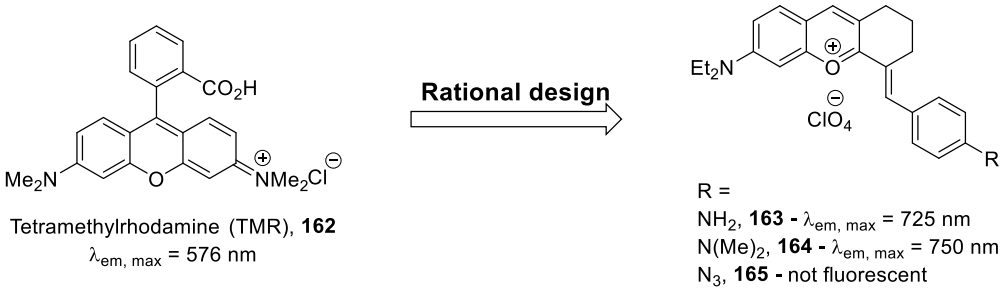


Figure 31: Design of benzopyrylium-based dyes by Liu and coworkers.[214]

Given the fluorogenic nature of these analogues, we hypothesised that this scaffold could be modified such that it became a hypoxia-activated fluorophore, *via* replacement of the azido group with a nitro group. As with the azide, the nitro group is electron-withdrawing, and we proposed that this too would eliminate any fluorescence. We hypothesised that the nitroaryl moiety would be a substrate for CPR or cytochrome p450 enzymes, and that metabolism in a hypoxic environment would produce the fluorescent amine **163**. Additionally, we further hypothesised that addition of an *ortho*-benzyl substituent linked *via* a heteroatom could allow the compound, once metabolised to an electron-donating analogue, to release some form of molecular cargo, such as a drug. This design hypothesis is shown in Figure **32**.

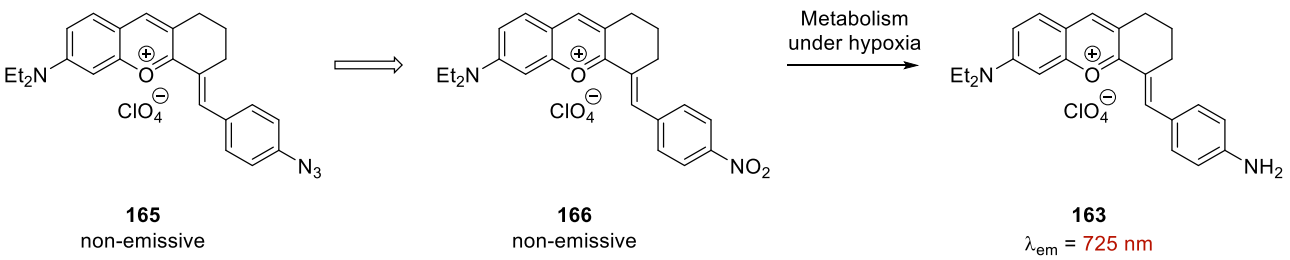
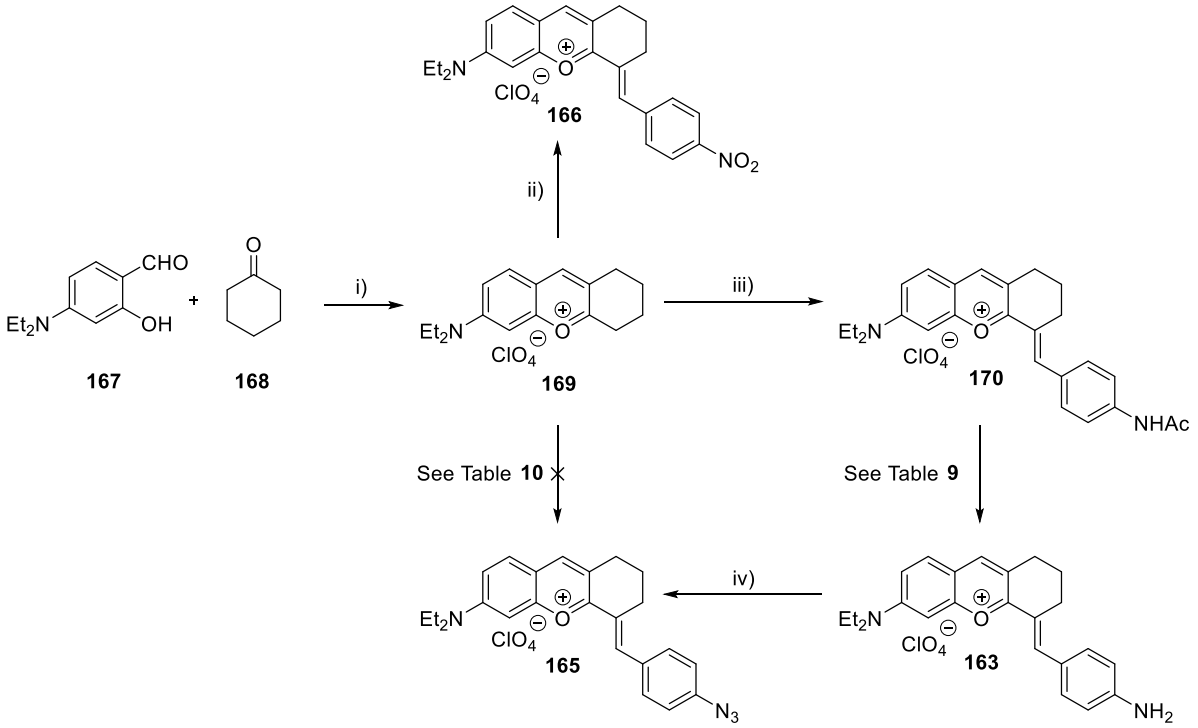


Figure 32: Proposed modification to **165** to produce a nitroaryl hypoxia-activated pro-fluorophore **165**.

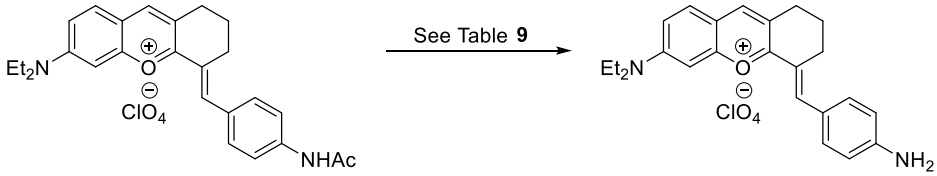
4.2 Synthesis of analogues



Scheme 43: Synthesis of fluorophore analogues. *Reagents and conditions:* i) conc. H_2SO_4, 0 °C → 90 °C, 1.5 hours, then H_2O, $HClO_4$, 0 °C, 85% yield; ii) 4-Nitrobenzaldehyde, AcOH, 110 °C, 1 hour, 79% yield; iii) 4-Acetamidobenzaldehyde, AcOH, 110 °C, 40 minutes, 39% yield; iv) $NaNO_2$ (aq.), EtOH, HCl (aq.), 0 °C, 30 minutes, then NaN_3 (aq.), 0 °C, 25 minutes, then RT, 16 hours, 20% yield.

All analogues in this series were synthesised from a common intermediate **169** (Scheme **43**), which was first synthesised *via* condensation of diethylaminosalicylaldehyde **167** with cyclohexanone **168** in hot, concentrated sulfuric acid. The reaction mixture was then poured into ice-water, and addition of perchloric acid caused core compound **169** to precipitate as the bright red-orange perchlorate salt. Further acid-catalysed condensation reactions with either 4-nitrobenzaldehyde or 4-acetamidobenzaldehyde afforded the nitro and acetamido derivatives **166** and **170**,

respectively. The acetamide of **170** was the removed *via* acid-catalysed hydrolysis (Scheme **44** and Table **9**).



170 **163**

Scheme 44: Hydrolysis of acetamide **170**. *Reagents and conditions* are given in Table **9** below.

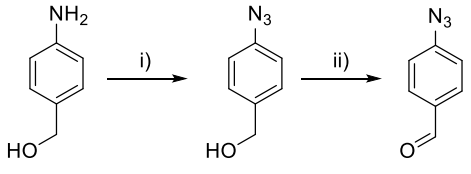
Table 9: Reagents and conditions used for hydrolysis of **170**.

Entry	Reagents and Solvent	Temperature	Time	Conversion
1	HCl (conc.)/EtOH (2:1)	90 °C	64 hours	0% (TLC and ^{1}H NMR)
2	HCl (conc.)/EtOH (2:1)	reflux	1 hour	0% (TLC and ^{1}H NMR)
3	HCl (4 M)/EtOH (1.8:1)	80 °C	5 hours	37% yield
4	10% $KOH_{(aq.)}$/EtOH (1:2)	RT	3 hours	0% (TLC)

Initially, we employed hydrolysis conditions that were similar to those used previously with a different arylacetamide.[145] Heating **170** in a 2:1 mixture of concentrated hydrochloric acid and ethanol did not afford **163**, but rather decomposed the product into a large number of side-products, as observed by TLC, after 2.5 days (Table **9**, entry **1**). Repeating this reaction under the same conditions for a shorter time (1 hour) also yielded several side-products (Table **9**, entry **2**). Thus, we turned to milder hydrolysis conditions; heating **170** in a 1.8:1 mixture of 4 M aqueous hydrochloric acid and ethanol afforded the amine **163** in 37% yield after 5 hours (Table **9**, entry **3**). To see if a better yield could be achieved using base-catalysed hydrolysis, **170** was also treated with a 1:2 mixture of 10% aqueous KOH solution in ethanol at room temperature (Table **9**, entry **4**). The starting material appeared stable during this time, so no further attempts at base-catalysed hydrolysis were made.

We also wished to synthesise the azido analogue **165**, which would then be evaluated alongside nitro compound **166** as a potential bioreductive, and several attempts were made to directly synthesise the azide *via* condensation reaction with 4-azidobenzaldehyde **171**. This is not a commercially available reagent but was readily

synthesised in two steps, shown in Scheme **45**. 4-aminobenzyl alcohol **171** was first converted to the diazonium salt using sodium nitrite, and this was then treated with sodium azide, displacing molecular nitrogen and affording 4-azidobenzyl alcohol **172**. This alcohol was then readily oxidised to 4-azidobezaldehyde **173** using pyridinium chlorochromate (PCC).



171 **172** **173**

Scheme 45: Synthesis of 4-azidobenzaldehyde as a coupling partner for condensation reactions. *Reagents and conditions*: i) 6 M aqueous HCl, $NaNO_2$, H_2O, 0 °C, 10 minutes, then NaN_3, H_2O, 0 °C, 10 minutes, then → RT, 1 hour, 83% yield; ii) PCC, CH_2Cl_2, RT, 30 minutes, 65% yield.

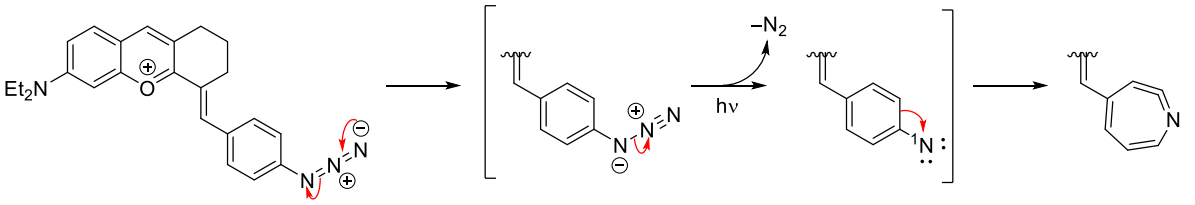
With azidoaldehyde **173** in hand, several attempts were made to produce a direct condensation with pyrylium intermediate **169**, the reagents and conditions for which are given in Table **10**.

Table 10: Reagents and conditions used to attempt direct condensation between aldehyde **173** and benzopyrylium compound **171**.

Entry	Additive	Solvent	Temperature	Time	Product
1	-	Acetic anhydride	reflux	135 minutes	Acetamide **170**
2	-	Acetic acid	RT	18 hours	Azide observed (LRMS), not isolated
3	-	Acetic acid	70 °C	22 hours	Azide observed (LRMS), not isolated
4	Piperidine	Acetonitrile	50 °C	22 hours	

Given the intrinsic positive charge held on the core of these molecules, reactions were monitored by low-resolution mass spectrometry as well as TLC. LRMS indicated the formation of a new product with an *m/z* $[M^+]$ = 357 Da, while the desired product **165** has a *m/z* $[M^+]$ = 385 Da, and the amine **163** has *m/z* $[M^+]$ = 359 Da. A plausible identity for this molecular ion is related to azide product **165**, which undergoes extrusion of N_2 to form a singlet nitrene, and subsequent ring expansion under the conditions of the mass spectrometer (Scheme **46**). This is a known phenomenon,[215] and suggests that some small amount of azide **165** was formed during the reaction;

nevertheless, this was not an appreciable amount and no azide was isolated from these condensation reactions.



165

m/z = 385

m/z
calc. = 357
observed = 357

Scheme 46: Proposed nitrogen extrusion mechanism of azide **165** under mass spectrometry ionisation, leading to observed mass ion.[215]

A major product was formed from the reaction performed under reflux in acetic anhydride which, after isolation, was identified as the acetamide analogue **170** by ^{1}H NMR and LRMS analysis (Figure **33**). This observation was interesting, since it indicated that a condensation between pyrylium core **169** and the aldehyde **171** had occurred. The forcing conditions of the reaction appeared to be causing a further side-reaction in which the azide decomposes *via* nitrogen extrusion to give singlet nitrene, similarly to the ring expansion mechanism, and is then acetylated by the acetic anhydride solvent; a proposed mechanism is shown in Scheme **47**.

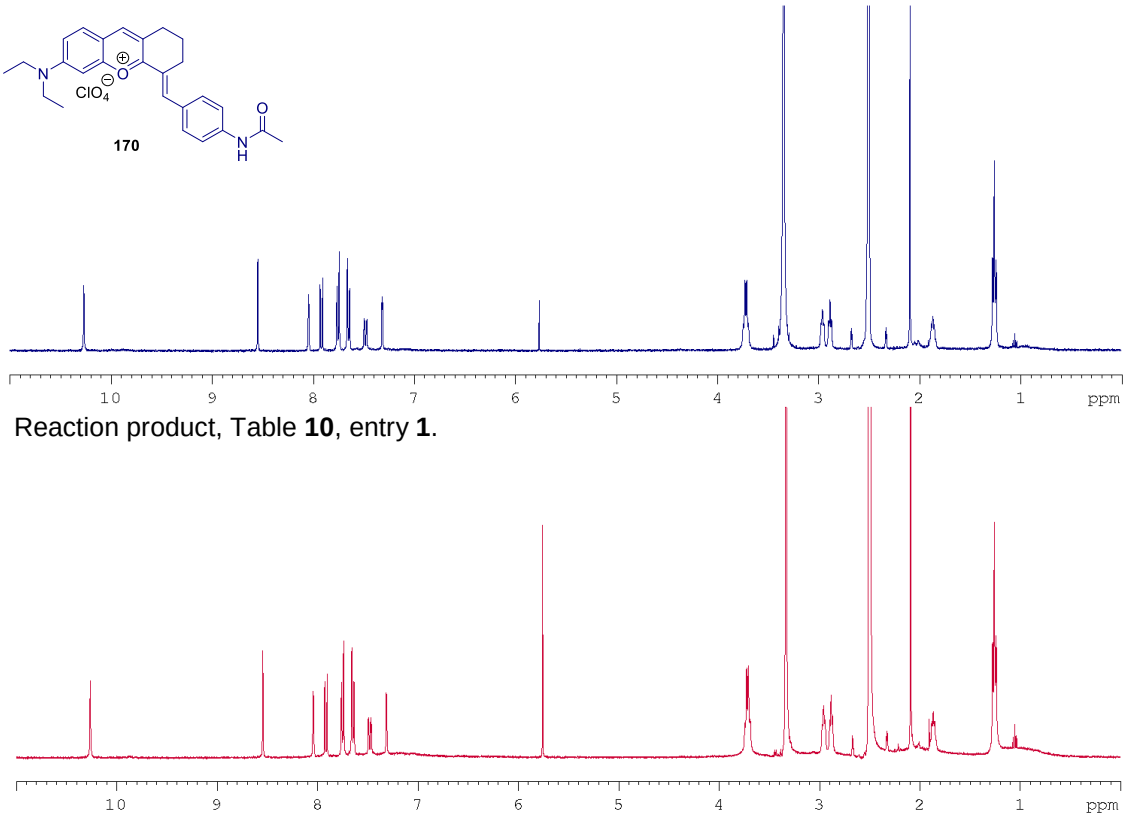
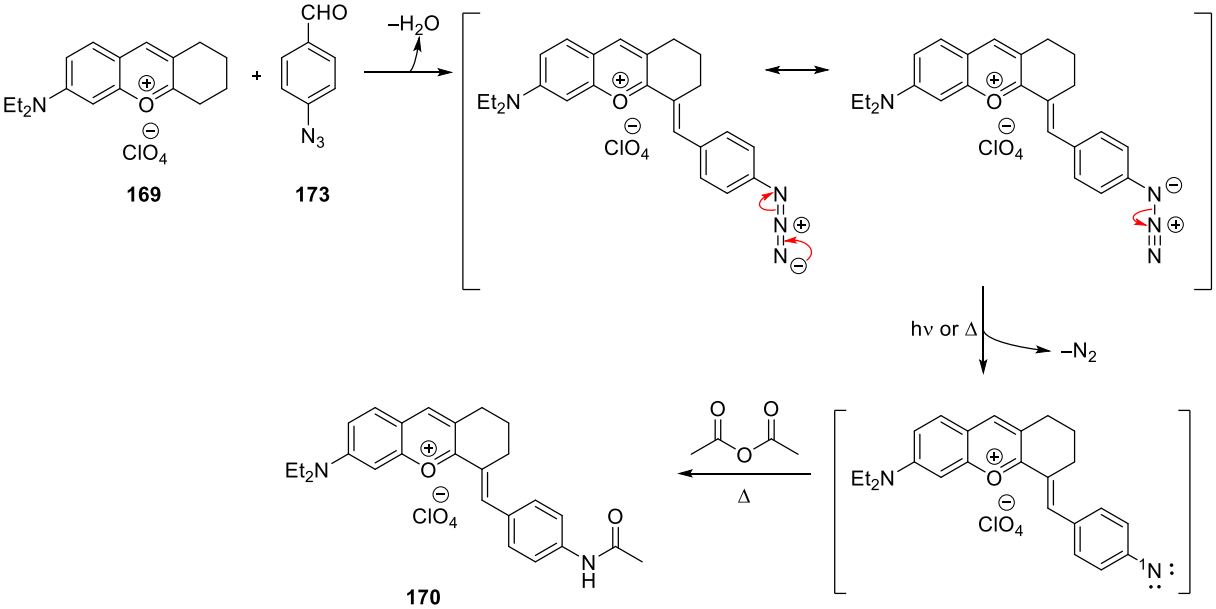


Figure 33: Stacked ^{1}H NMR spectra of (top) acetamide **170** and (bottom) the product isolated from Table **10**, entry **1**.



Scheme 47: Proposed mechanism of acetamide formation during condensation reaction.

Since the azide-bearing compound **165** appeared to be unstable under the harsh reaction conditions described above, we decided to use an alternative synthetic route.

Amine compound **163**, which had been previously synthesised, was converted to the azide analogue **165** using similar chemistry to that for aldehyde **173** (Scheme **45**). Treatment with sodium nitrite in aqueous acid formed the diazonium salt, which was then displaced by addition of sodium azide as a nucleophilic N_3 source, affording **165** in moderate yield after purification (Scheme **43**, above).

4.3 Characterisation

4.3.1 UV-Vis absorbance and fluorescence spectra

With the proposed pro-fluorophore **166** and fluorophore analogue **163** in hand, we first set about photophysical characterisation of these molecules. UV-Vis absorption spectra provide information on the absorbance maxima of the compounds; this information can be used to determine the best method of compound excitation for fluorescence microscopy. UV-Vis and fluorescence spectra were measured, and the curves are shown in Figure **34a**&**b**, respectively. These data are summarised in Table **11**.

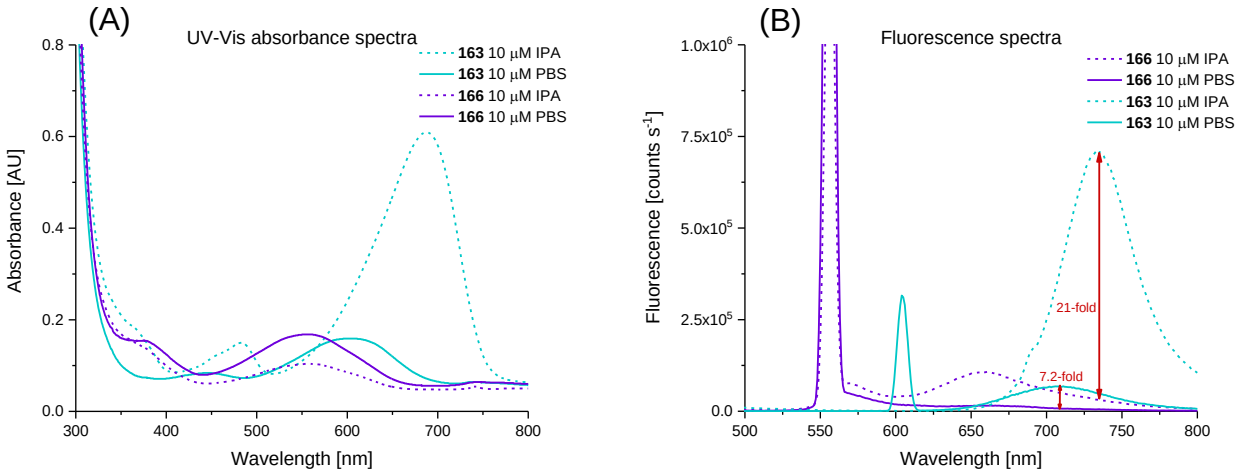


Figure 34: (A) UV-Vis absorbance spectra and (B) fluorescence spectra of nitro compound **166** (violet) and amine compound **163** (teal), recorded at 10 μM in phosphate-buffered saline (PBS, solid line) and 5 μM in *iso*-propyl alcohol (IPA, dashed line). For fluorescence spectra, the excitation wavelength for each compound was at its absorption maximum, which are given in Table **11** below. Scattered excitation photons can be observed in the fluorescence spectra at 555 nm (nitro **165**), 604 nm (amine **163**, PBS), and as a shoulder to the emission peak at 688 nm (amine **163**, IPA).

Table 11: Summary of photophysical for compounds **163** and **166**. Extinction coefficients were calculated using the Beer-Lambert Law ($A_\lambda = \varepsilon_\lambda \times c \times l$) at the stated concentration at the absorbance maximum wavelength.

Compound	Concentration	Solvent	$\lambda_{abs,\ max}$	$\lambda_{em,\ max}$	Stokes' shift	ε (λ_{max})
Nitro **166**	10 μM	IPA	555 nm	657 nm	102 nm	10.4×10^3
Nitro **166**	10 μM	PBS	555 nm	657 nm	102 nm	10.7×10^3
Amine **163**	10 μM	IPA	688 nm	734 nm	46 nm	60.9×10^3
Amine **163**	10 μM	PBS	604 nm	708 nm	104 nm	7.1×10^3

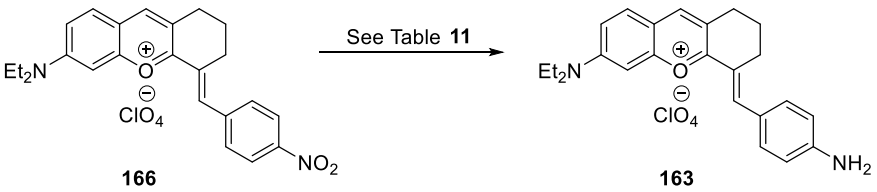
It is notable that the fluorescence emission for nitro compound **166** was non-negligible both in IPA and PBS, contrary to our expectation. It is possible that the change in frontier orbital energies caused by switching from electron-donating amine to electron-withdrawing nitro are not sufficient to completely abrogate the possibility of fluorescence. Nevertheless, these data show that amine **163** does indeed fluoresce in the near-infrared region (λ_{em} ≈ 708 nm in PBS), that it has a large Stokes' shift (≈ 100 nm), and that it has a reasonable molar extinction coefficient ε. Strong absorbance and emission for compounds in PBS is very important for fluorophores that are used as bioimaging tools, since many fluorophores are almost entirely quenched in an aqueous environment. Large Stokes' shifts are also advantageous for bioimaging purposes; they minimise the overlap between excitation and emission photon wavelengths, which allows excitation photons to be filtered out without significant loss of emission signal. Most pleasingly, there was a 21-fold increase in absolute fluorescence of the amine compound **163** in IPA *vs* that of the nitro compound **166**, and a 7.2-fold increase in PBS.

4.3.2 Chemical reduction assay

As outlined in our protocol paper on the testing of bioreductive substances, the primary assay for quickly assessing the suitability of the molecule for bioreductive studies is to perform a chemical reduction.[184] The substrate is dissolved in *N,N*-dimethylformamide (DMF) combined with 10% aqueous ammonium chloride solution. A sample is taken, and then zinc powder is added. The zinc acts as a catalyst

for the reduction of the aryl nitro group, and the reaction can be monitored by thin-layer chromatography or HPLC.

However, during the synthesis of the amine fluorophore **163**, we attempted to convert the readily-accessible nitro compound **166** *via* nitro reduction using Beauchamp-type conditions, summarised in Scheme **48** and Table **12**. It was observed that the substrate **166** was stable to these conditions. This is perhaps unsurprising, since the electron-donating aryl diethylamino group is in conjugation with the aryl nitro group, reducing its affinity for electrons and hence making it resistant to electron-based reduction by metals such as iron or zinc. As such, the substrate was taken forward to enzymatic studies without using the chemical reduction assay.



Scheme 48: Attempted chemical reduction of pro-fluorophore **166**. Conditions are summarised in Table **12**.

Table 12: Conditions used to convert nitro compound **166** into amine fluorophore **163**.

Entry	Reagents	Solvent	Temperature	Time	Conversion
1	Fe powder, $NH_4Cl_{(s)}$	H_2O/THF/MeOH (1:1:2)	50 °C	5 h	0% (TLC and ^1H NMR)
2	Zn powder, 10% aq. NH_4Cl	DMF	RT	16 h	0% (TLC and ^1H NMR)

4.3.3 Enzymatic reduction assay

As with other compounds developed as hypoxia-responsive agents, nitro compound **166** was assessed in a cytochrome p450 reductase assay to determine whether it was a substrate for these oxygen-sensitive enzymes.[184] Details of this assay can be found in Biological Materials and Methods. Assays were analysed by HPLC-MS, the traces of which are shown below.

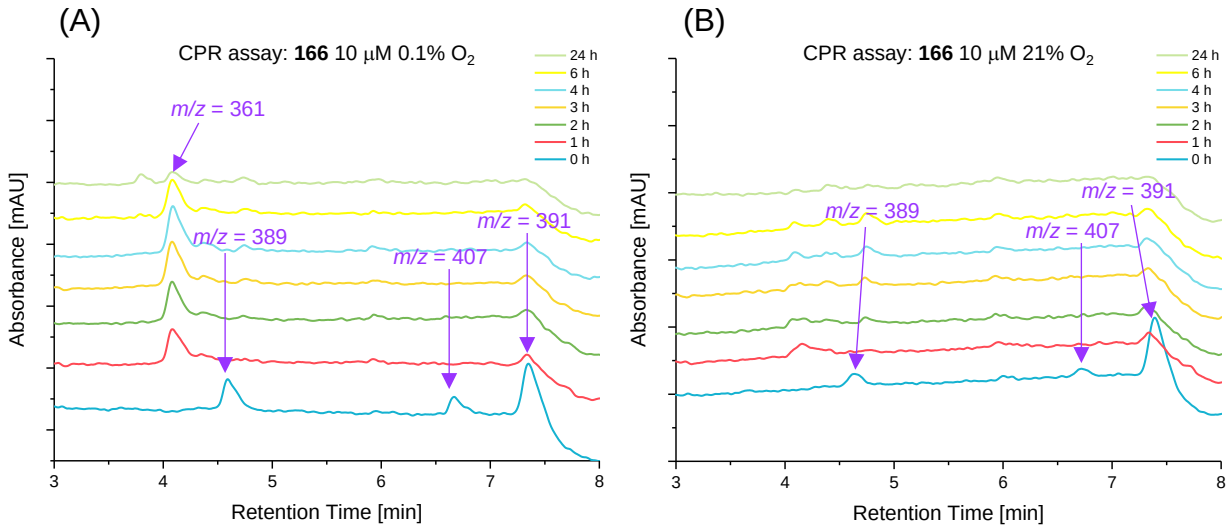


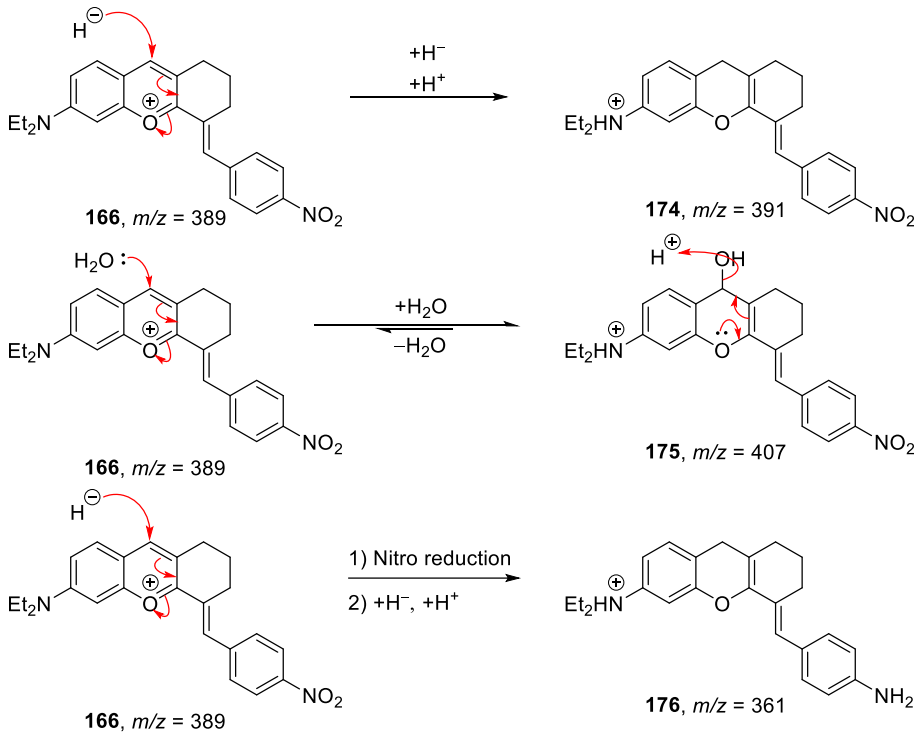
Figure 35: Analytical HPLC-MS traces for an *in vitro* CPR assay on compound **166**, under (A) hypoxia (<0.1% O_2), and (B) normoxia (21% O_2). Molecular ion peak *m/z* values are annotated to each major peak.

These initial data suggested that nitro pro-fluorophore **166** was unstable to the assay conditions, since the parent compound peak was rapidly consumed, and several new peaks were formed. However, closer inspection of the mass ions associated with each peak suggested plausible identities for each species. The peak containing *m/z* = 389 (RT ≈ 4.6 min) corresponded to the pro-fluorophore **166**, which was rapidly consumed (even after 1 hour), and a new peak (*m/z* = 361, RT ≈ 4.1 min) appeared equally rapidly. This peak was not the corresponding amino compound **163** ([M^+] *m/z* = 359) but appeared to be related to it with the addition of two protons. Likewise, another new peak (present even in the t=0 sample, RT ≈ 7.3 min) had an associated mass of *m/z* = 391 – equivalent to the starting nitro compound **166** with the addition of two protons. A final new peak (RT ≈ 6.7 min) had an $[M]^+$ ion with *m/z* = 407, equivalent to parent compound **166** plus 18 Da.

4.3.4 Identification of new species

We hypothesised that some of these species were the result of hydride addition to the core of the molecule, on which there are three positions which lie in a 1,4-relationship with the positively-charged oxonium ion in the core, effectively behaving as three related activated α,β-unsaturated carbonyl systems. It is plausible

that any hydride source present may act as a nucleophile, adding to the 1,4-system and neutralising the positive charge on the molecule, adding 1 Da in mass. With the molecules in a neutral state they could further ionise by protonation, likely at the diethylamino nitrogen atom, giving species **175**. We speculated that this species was the **166** $[M+2H]^+$ ion observed by mass spectrometry. These data suggest that the parent molecule **166** underwent undesired reactivity. With this reactivity in mind, interpretation of the other HPLC peaks became less complicated. We hypothesised that the peak containing *m/z* = 361 was the result of this unwanted metabolism, plus the desired metabolism of the nitro group of **166**: desired amine metabolite **163** would have *m/z* = 359, addition of nucleophilic hydride and subsequent protonation would give species **176**, with a corresponding *m/z* = 361, as observed. We further hypothesise that the peak with molecular ion *m/z* = 407 (RT ≈ 6.7 min) was the product of the addition of a molecule of water to nitro compound **166**, producing compound **175**. This addition, followed by protonation to form a cation, would add 18 Da in mass, resulting in a species with molecular weight 407 Da, which was observed in the mass spectrum of the final peak. These species and their mechanisms of formation are summarised in Scheme **49**, below.



Scheme 49: Possible identities of species observed by HPLC-MS in the cytochrome p450 reductase (CPR) assay, and the mechanisms by which they are formed.

The peak for the 'hydrate' species **175** was initially present in the t=0 sample, but then absent after even 1 hour of assay time. We theorised that this was due to the reversibility of the addition of water to **166**, compared with the irreversibility of the addition of an H^- ion.

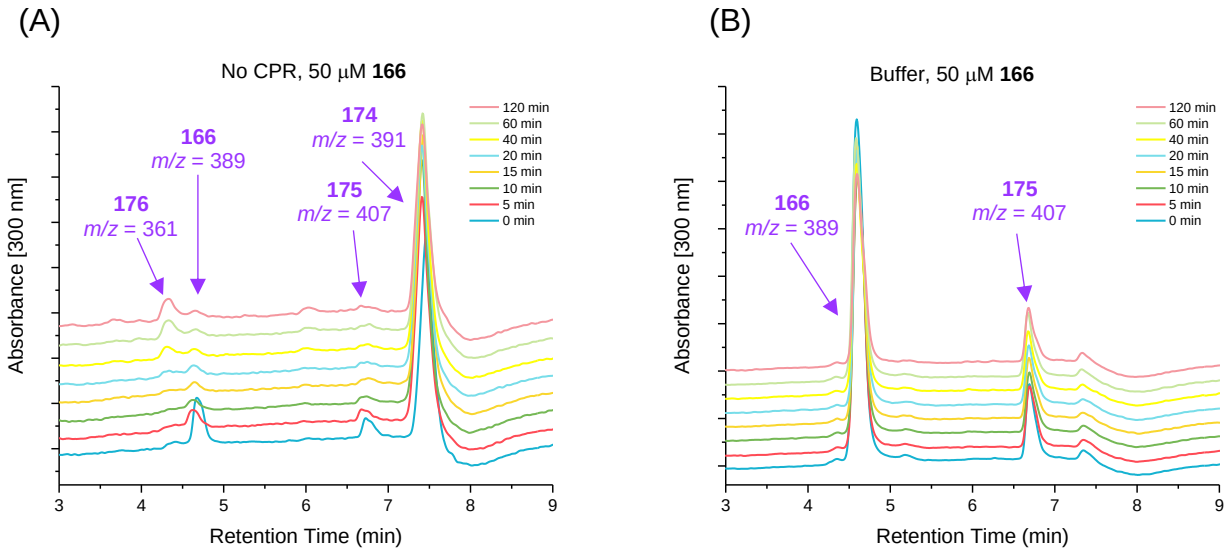


Figure 36: (A) Repeat of CPR assay with no CPR added, with substrate **166** at 50 µM. (B) Repeat of CPR assay with no CPR or NADPH regeneration system added, *i.e* compound in buffer, with substrate **166** at 50 µM.

To elucidate the nature of these species, control experiments were conducted (Figure **36a**&**b**). Repeating the assay in the absence of the CPR enzyme (Figure **36a**) no longer produced a peak corresponding to amine **176**, although peaks for conjugate addition and attack by water remained. A solution in buffer, without addition of the NADPH-regeneration system ($NADP^+$, glucose-6-phosphate, glucose-6-phosphate dehydrogenase) or CPR enzyme (Figure **36b**), prevented the formation of conjugate addition products associated with hydride attack, leaving only peaks for the parent compound **166** and the proposed hydrate, **175**. The ratio of peak areas between the parent nitro compound **166** and the "hydrated" species **175** remained constant, suggesting that addition of water was indeed reversible and that an equilibrium mixture had formed.

4.3.5 Susceptibility to biological nucleophiles

Whilst these data show that compound **166** reversibly forms an adduct upon nucleophilic attack of water, they also indicate that either form may still act as a substrate for cytochrome p450 reductase. This enzyme uses both FAD^+ and FMN as cofactors, and the initial electron donor to these bound cofactors is NADPH **178**. NADPH is endogenous to mammalian cells, and so its presence in the cytoplasm posed a potential risk to **166** and other compounds from this series. However, the assay detailed above is an *in vitro* experiment that is not representative of the cellular environment. Cells contain many chemical species which may act as nucleophiles, one of the most common being L-glutathione (GSH, **177**); GSH is estimated to be at millimolar (~1–2 mM) concentrations in many cell types, and up to 10 mM in hepatocytes.[216] Given such nucleophiles may pose a risk to pro-fluorophore **166**'s stability in the cellular milieu, we studied the susceptibility of **166** to nucleophilic attack by both NADPH **178** and L-GSH **177**.

We first studied the reactivity of compound **166** towards nucleophilic attack by NADPH. Compound **166** has 4 positions in which it is plausible that nucleophilic attack could occur (Figure **37**, below). Position 4, indicated in red, forms the end of an α,β-unsaturated activate carbonyl system. Position 4', indicated in blue, also forms the end of another α,β-unsaturated activate carbonyl system. Position 2, marked in red, could likewise be susceptible to attack by hard nucleophiles. Finally, position 1'' indicated in green forms the end of a 1,6-system that is in conjugation with the aryl-nitro group. It is also plausible, although perhaps less likely, that nucleophilic attack could occur at this position also.

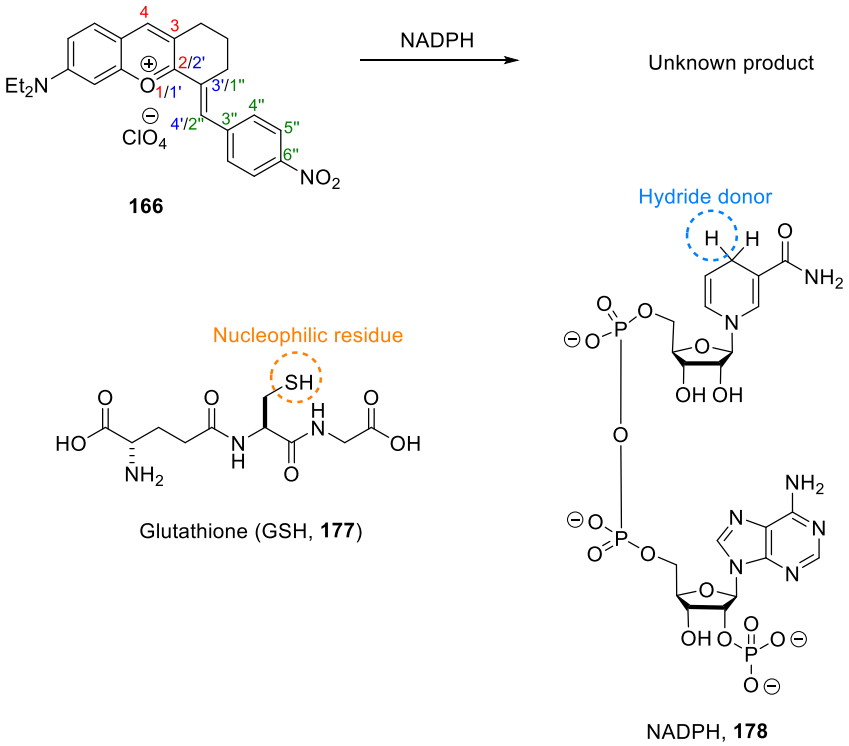


Figure 37: Reaction of **166** with NADPH **178** led to unidentified products. The structures of biologically-relevant nucleophiles studied, NADPH **178** and L-glutathione **177**, are shown.

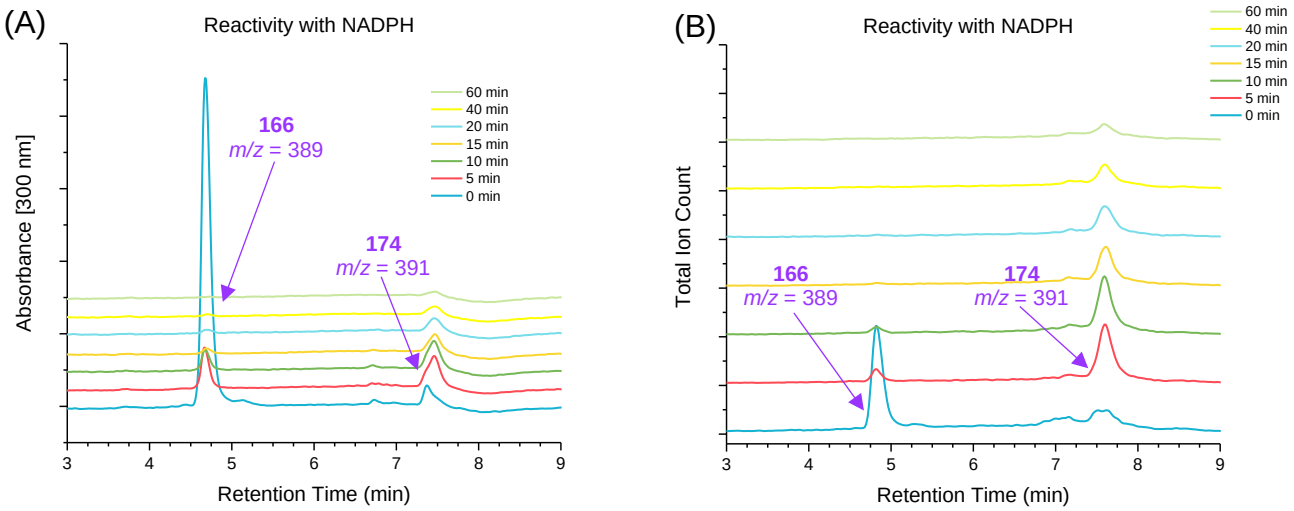
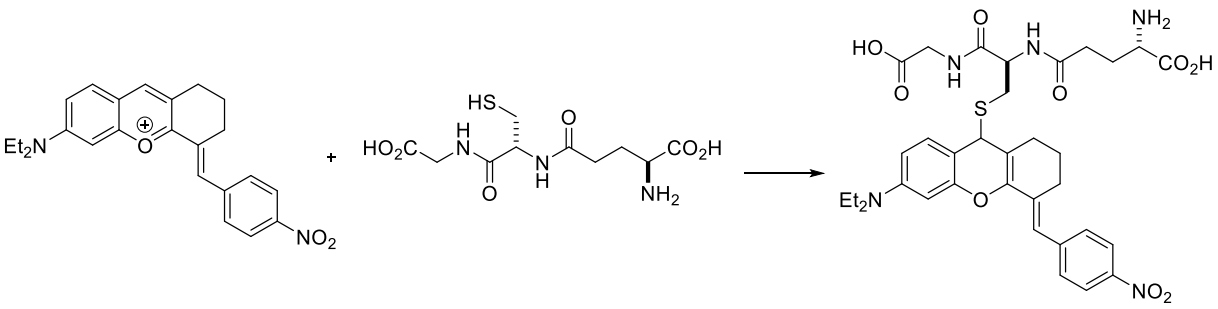


Figure 38: NADPH reactivity assay for pro-fluorophore **166** at 50 µM. After the t=0 sample was taken, a bolus of NADPH was added (4 eq.) and samples were taken at the indicated times and analysed by HPLC-MS. A detailed procedure can be found in Table **21** in Biological Materials and Methods. (A) UV-Vis chromatogram at 300 nm. (B) Total Ion Count (TIC) chromatogram for ions between 200 and 700 Da.

A solution of **166** in PBS was shaken at 37 °C, with aliquots taken before NADPH was added (t = 0 min), and then at indicated intervals after addition of a bolus of 4 equivalents of NADPH solution. HPLC-MS analysis, shown in Figure **38**, demonstrated that **166** was rapidly degraded by NADPH. Interestingly the metabolite **174** was only transiently stable, forming rapidly and then being further metabolised. This phenomenon is demonstrated by both the UV-Vis chromatogram (Figure **38a**) and mass spectrogram (Figure **38b**). The rapid formation of **174** gave us confidence that the presence of high concentrations of NADPH, rather than unwanted enzyme activity, were a cause of the complex mixture produced in the CPR assay.

This assay was repeated using L-glutathione in place of NADPH as the biological nucleophile. As discussed, L-GSH is abundant in eukaryotic cells and performs many functions, including the detoxification of exogenous electrophiles. We supposed that GSH may interfere with use of compounds based upon **166** as cellular imaging tools if they were susceptible to attack by nucleophiles such as GSH, forming adducts such as **179** (Scheme **50**).



166
MW = 389

L-GSH **177**
MW = 307

179
MW = 695

Scheme 50: Proposed adduct formation by nucleophilic 1,4-addition of L-glutathione **177** to pro-fluorophore **166**.

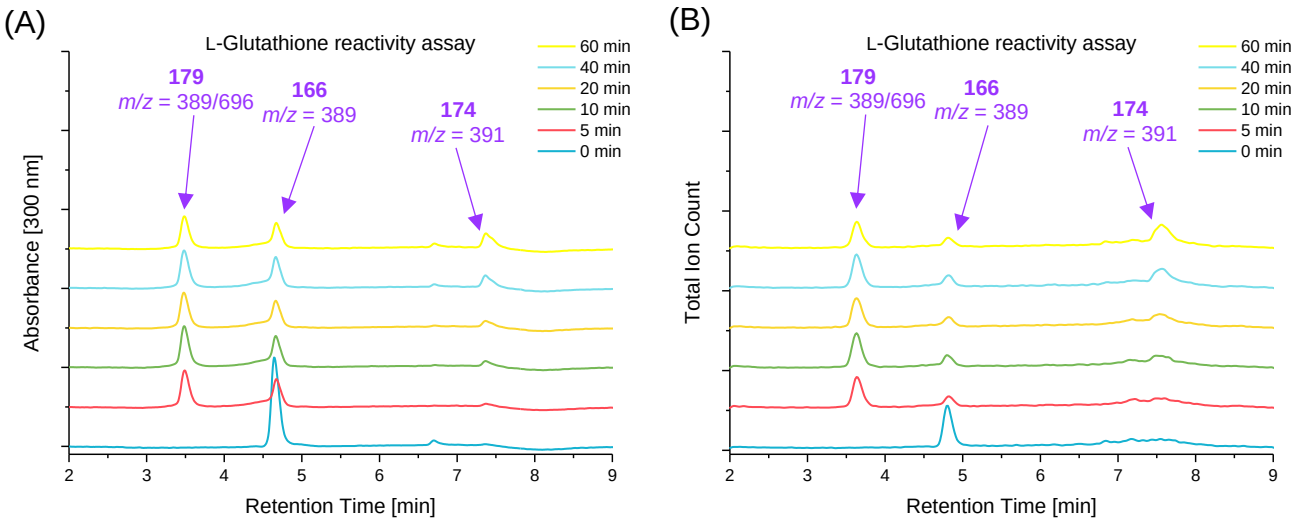


Figure 39: L-Glutathione reactivity assay. (A) UV-Vis chromatogram at 300 nm. (B) Total ion count (TIC) mass spectrometry chromatogram.

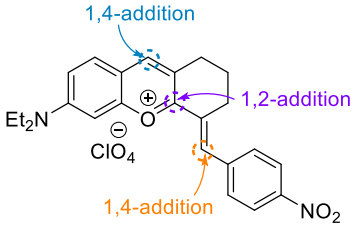
We repeated the NADPH assay protocol, using L-GSH in place of NADPH as the nucleophilic source (experimental conditions are given in Table **22** in Biological Materials and Methods). HPLC-MS analysis (Figure **39a**&**b**) demonstrated that **166** rapidly formed an adduct upon exposure to L-GSH. Mass spectrometry revealed that this new species had molecular ions [M^+] = 389 Da (parent **166**) and 696 Da (the mass of proposed L-glutathione adduct **179**). This suggested the species was indeed **179** ([M+H]$^+$ = 696 Da), and that this species was readily able to fragment back to the parent compound **166** ([M]$^+$ = 389 Da) under the ionising conditions of the mass spectrometer. Pleasingly, despite use of a large excess of L-GSH, only a fraction of the available **166** appeared to remain near-constant in height and area ratio, indicating

steady-state concentrations of each species. Since the nucleophile is in large excess, this indicates that a dynamic equilibrium exists between **179** and **166**/free GSH, suggesting that this type of nucleophilic attack, like that of water but unlike NADPH, is reversible. We found this result encouraging, since it indicated that nucleophilic attack by intracellular nucleophiles such as L-GSH would not necessarily interfere with use of **166** as a hypoxia-sensitive fluorophore.

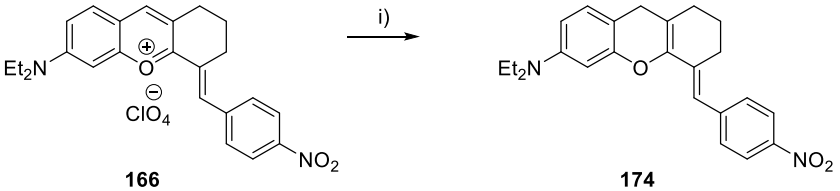
4.3.6 Chemical reduction by hydride ions

Pro-fluorophore **166** has three positions of its structure which form an activated conjugate acceptor system with the pyrylium ion (Scheme **51a**, below). We hypothesised and demonstrated that conjugate addition of nucleophiles such as water, hydride and L-glutathione to **166** could occur, but had no direct evidence of the site of addition. To verify that conjugate additions occurred, and verify the site of addition, **166** was treated to the chemical hydride reductant sodium borohydride in organic solvent (Scheme **51b**, below).

(A)



(B)



Scheme 51: (A) Possible sites of nucleophile addition to the scaffold of **166**. (B) Synthesis of hydride reduction product of **166**. *Reagents and conditions*: i) $NaBH_4$, MeCN, RT, 15 min, 76% yield.

Compound **166** was dissolved in acetonitrile giving a deep purple solution. Addition of sodium borohydride powder led to rapid decolouration of the solution. This indicated that the highly conjugated molecular orbitals which gave rise to the colour of

the compound had been disrupted, consistent with the hypothesis that conjugate addition had occurred resulting in the reduction of at least one double bond. TLC analysis indicated that **166** had been totally consumed, and that one new product with much lower polarity had formed. The product of reduction was not visible to the naked eye on the TLC plate without UV visualisation or chemical staining, unlike the parent compound which was deep purple. Interestingly the spots of reduction product on the TLC plate developed a deep purple colour upon exposure to air over a period of hours. Low-resolution mass spectrometry of these (now purple) spots revealed an $[M]^+$ molecular ion with $m/z = 389$, identical to that of the starting material **166**. This suggested that the pyrylium species is in fact quite stable compared with the "reduced" form, evidenced by this apparent propensity to undergo oxidation on silica gel in air. This was corroborated by the silica gel column used to purify "reduced" product **174**; the initially colourless silica gel began to turn bright purple over the course of a few hours of exposure to air.

This product **174** was isolated in very good yield after aqueous workup and silica gel chromatography and was analysed by ^{1}H NMR to determine the site of hydride addition.

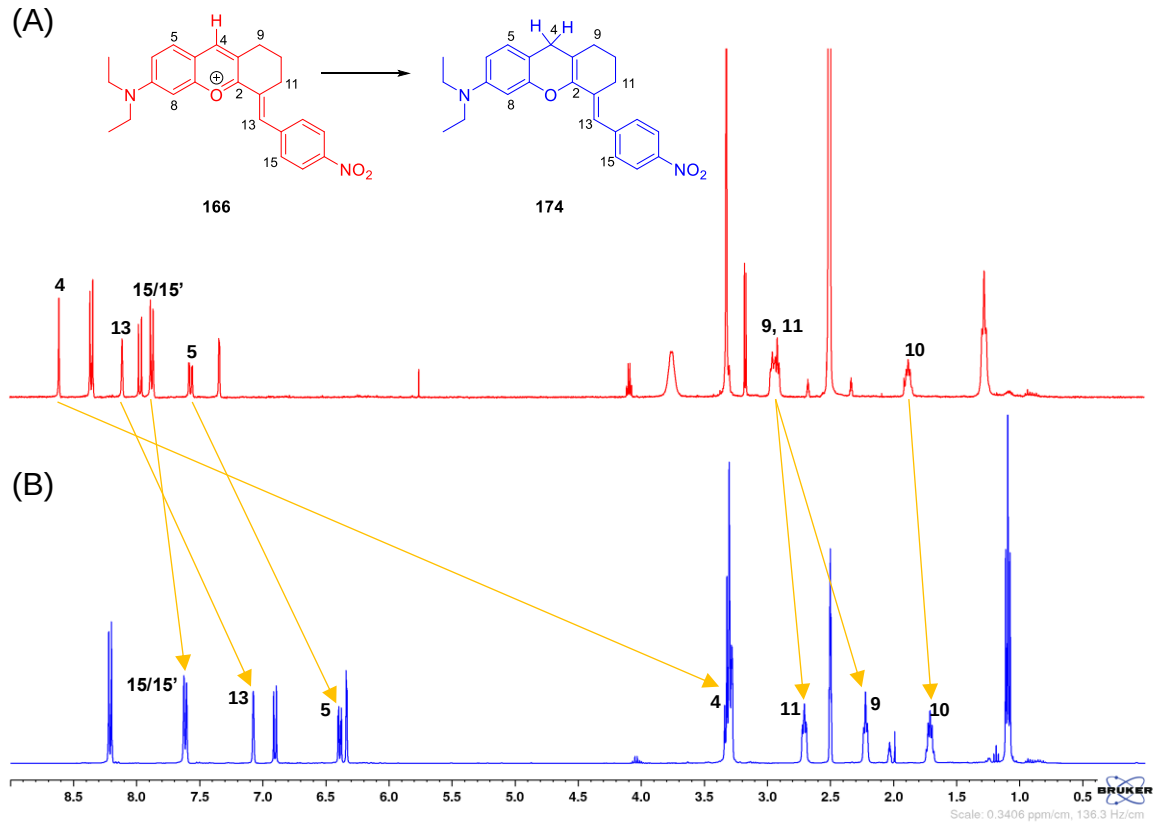


Figure 40: ^{1}H NMR analysis of chemical hydride reduction of **166**. (A) ^{1}H NMR spectrum of pro-fluorophore **166**. (B) ^{1}H NMR spectrum of reduction product **174**. Spectra were recorded on a Bruker Avance III 400 MHz spectrometer, samples were in D6-DMSO.

^{1}H NMR spectra gave evidence for hydride addition to the C4 position of **166**. The chemical shifts for the resonances of protons attached to the 4-nitrophenyl ring (marked **15/15'**), for example, are barely perturbed, moving from $\delta_H \approx 7.87$ ppm to $\delta_H \approx 7.62$ ppm ($\Delta\delta_H \approx 0.25$ ppm). If hydride addition had occurred in closer proximity (*i.e.* at C13), one might expect the change in chemical shift ($\Delta\delta_H$) to be greater. Likewise, the resonance for the proton attached to C13 moved from $\delta_H \approx 8.11$ ppm to $\delta_H \approx 7.07$ ppm ($\Delta\delta_H \approx 1.04$ ppm). This change is larger, likely due to the C12–C13 double bond being directly conjugated to the oxonium cation carbonyl, yet this shift is much smaller than might be expected had hydride attack taken place at C13.

Additionally, the C13 resonance had an integration still equal to 1 proton, suggesting no additional proton had been added there. The strongest evidence for the location of hydride addition came from the resonance for the proton at C4. This shifted from $\delta_H \approx 8.61$ ppm to $\delta_H \approx 3.29$ ppm ($\Delta\delta_H \approx 5.32$ ppm), a change dramatically larger than for any other proton resonance, with the integration for this proton signal changing from 1 to 2 protons. Taken together, this provides evidence that **166** undergoes hydride attack at C4.

4.3.7 Cellular permeability assay

Oxygen-dependent reductase analysis had demonstrated that, whilst it appeared **166** was reduced in an oxygen-dependent manner, other processes were occurring simultaneously which may interfere with use as an imaging probe. These experiments were conducted *in vitro* and did not accurately recreate the complex milieu of the intracellular environment; thus, we chose to continue our studies of **166** and **163** in a cellular environment.

As with any small-molecule studies in cells, an important question to answer is that of membrane permeability. Many small molecules, whether developed as probes, drugs, fluorophores or for other functions, often fail if they cannot penetrate cell membranes. This is particularly problematic for molecules which contain ionisable centres that bear charge at physiological pH, or molecules with an intrinsic charge. Since compounds based upon **166** and **163** all contain an intrinsic positive charge, by way of the benzopyrylium cation, we were particularly interested in establishing the permeability of our compounds.

To give a qualitative analysis of the permeability of compound **163**, we conducted a cellular permeability assay which was analysed by HPLC-MS. Cultured monolayers of OE21 cells were treated with **163** (50 μM) for 3 hours under normoxia. An aliquot of

supernatant media was taken for analysis, then the cells were washed, trypsinised, scraped, spun down in a lysis extraction mix (1:1 MeOH/MeCN), lysed by sonication, and the lysis mixture analysed by HPLC-MS. The results of this experiment are shown in Figure **41**, below.

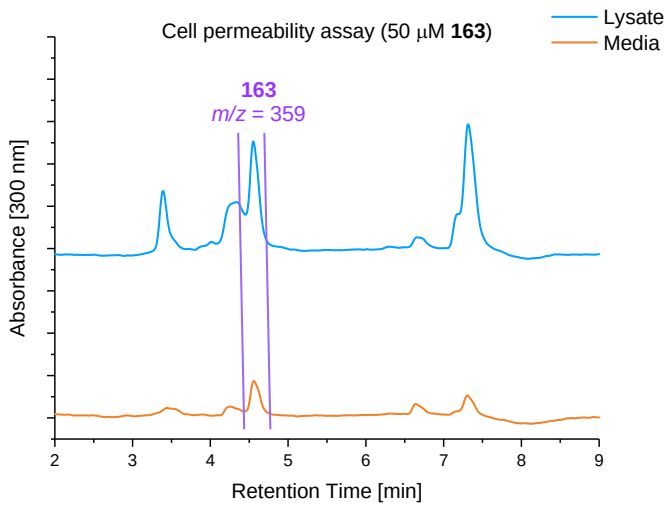


Figure 41: HPLC-MS analysis of cellular permeability assay for compound **163**, which shows that compound **163** is found in both the media and cell lysate after incubation, demonstrating membrane permeability.

The permeability assay demonstrated that compound **163** could indeed penetrate the cell membrane despite its intrinsic positive charge. With this encouraging data in hand, we continued to study **166** in cells.

4.3.8 Cellular imaging of hypoxia

Having demonstrated that amine fluorophore **163** was able to penetrate cell membranes, we wished to determine whether it could then be detected *via* fluorescence microscopy. This would help serve as a positive control for experiments in which pro-fluorophore **166** was monitored for its conversion to fluorophore **163**. Moreover, the most common fluorophores used for fluorescence microscopy emit in the ultraviolet or visible regions of the electromagnetic spectrum, whereas our fluorophore emitted in the near-infrared. We therefore also wished to determine the optimal microscope parameters for detection of the fluorophore.

OE21 cells were cultured on microscope cover slips and treated with amine fluorophore **163** at 1 μM for 3 hours at the indicated oxygen tension. The cells were then washed, fixed, transferred to microscope slides, stained with 4′,6-diamidino-2-phenylindole (DAPI, a fluorescent dye for staining nuclei of live cells) and imaged. Representative images are shown in Figure **42**, below. These data indicate that fluorophore **163** was cell permeable, confirming the literature observation.[214] Moreover, it could be imaged in cells even at low concentrations, and changes in cellular oxygen tension did not appear to interfere with the compound's fluorescence.

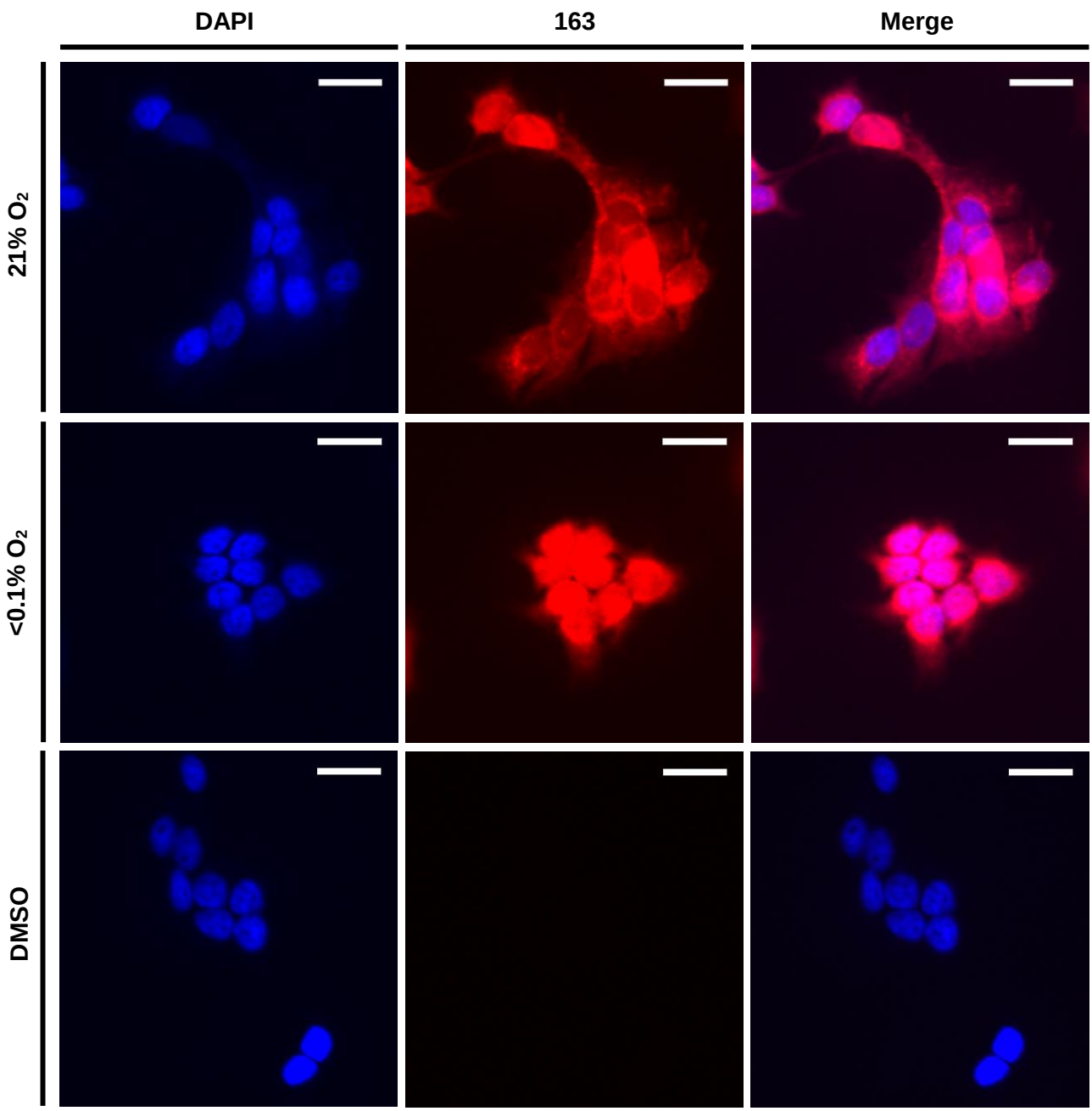


Figure 42: Fluorescence microscopy images of OE21 cells treated with 1 μM **163** or DMSO for 3 hours at the indicated oxygen tension. Scale bar = 25 μm. Images taken using a Nikon Ti-E fluorescence microscope.

Having established that the amine fluorophore **163** was indeed cell penetrant and could be used for fluorescence microscopy purposes, we then wished to determine whether nitro analogue **166** could indeed act as a hypoxia-responsive pro-fluorophore. *In vitro* experiments had suggested that oxygen-sensitive reductase enzymes such as cytochrome p450 reductase could metabolise the nitro group to the corresponding

amine as hypothesised, with the caveat that the molecule was also susceptible to conjugate addition by intracellular nucleophiles. We nevertheless persevered in testing nitro compound **166** to determine whether it was indeed suitable for hypoxia imaging.

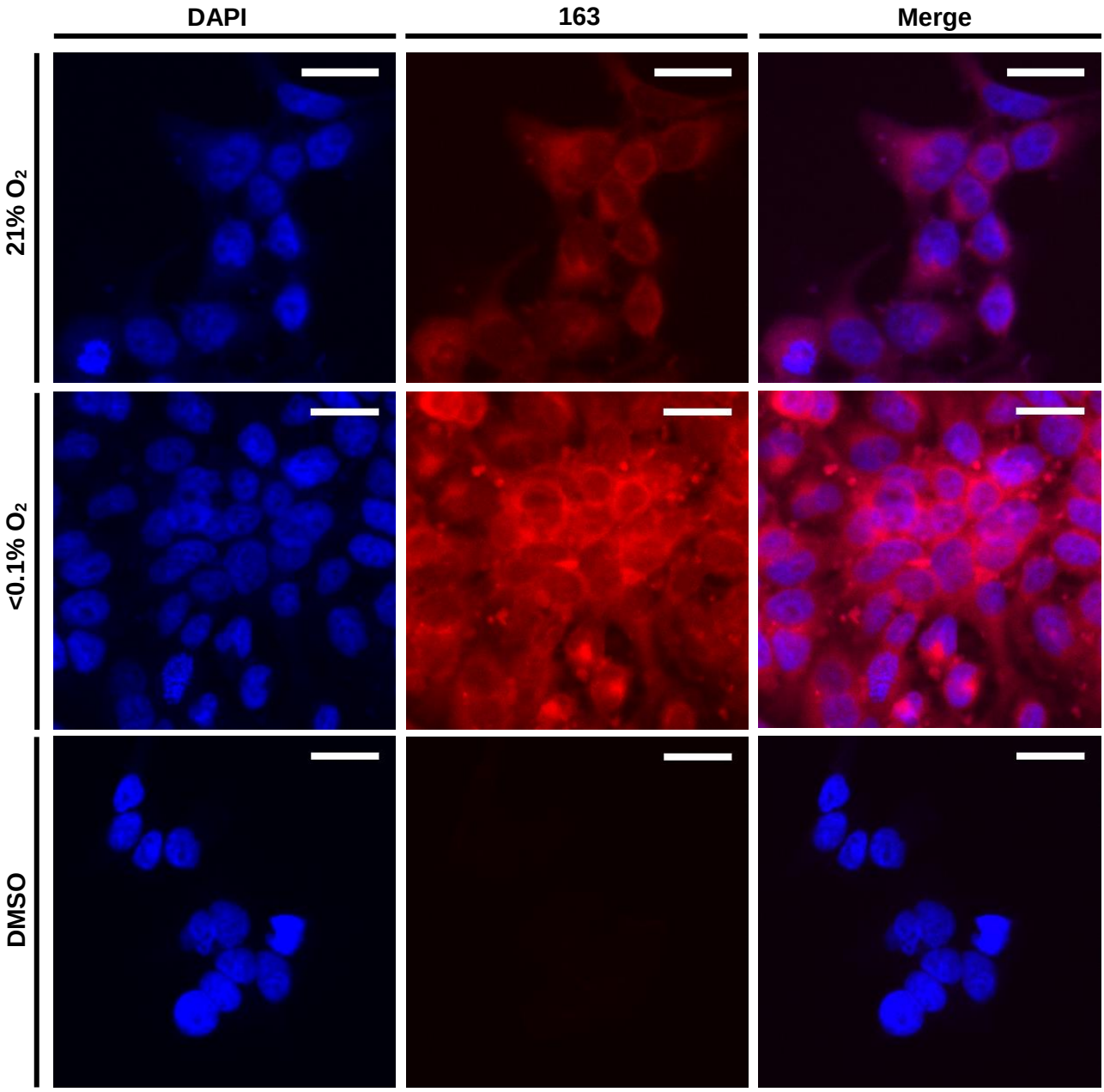


Figure 43: Fluorescence microscopy images of OE21 cells treated with 10 μM **166** or DMSO for 6 hours at the stated oxygen tension. Scale bar = 25 μm. Images taken using a Nikon Ti-E fluorescence microscope.

OE21 cells were treated with nitro **166** or DMSO for 6 hours under normoxia (21% O_2) or hypoxia (<0.1% O_2), then washed, fixed, stained with DAPI and imaged by fluorescence microscopy (Figure **43**). Cells treated under normoxic conditions

appeared to show a small amount of background fluorescence that was not present in the DMSO control, and we devised several plausible explanations for this observation. The small amount of intrinsic fluorescence observed in the fluorescence spectrum of compound **166** was significant enough to detect by fluorescence microscopy. Alternatively, there may be other oxygen-insensitive metabolic processes that partially contribute to the metabolism of **166**. Another plausible explanation is that adducts formed by nucleophilic attack of *e.g.* L-glutathione to **166** also display some intrinsic fluorescence which is also detectable in the filter for amine **163**. Nevertheless, it can be clearly seen that cells treated with **166** and cultured under hypoxia exhibited a significantly greater fluorescence signal that those cultured under normoxia or treated with DMSO. This suggested that **166** did indeed act as an oxygen-sensitive pro-fluorophore and could be used as a hypoxia sensor in cells.

To investigate whether the background fluorescence observed in cells under normoxic conditions was the result of metabolism or intrinsic fluorescence, we incubated nitro **166** in cell-free PBS at 10 μM and 50 μM for 30 minutes. These samples were then analysed using fluorescence microscopy, and representative images are shown below in Figure **44**.

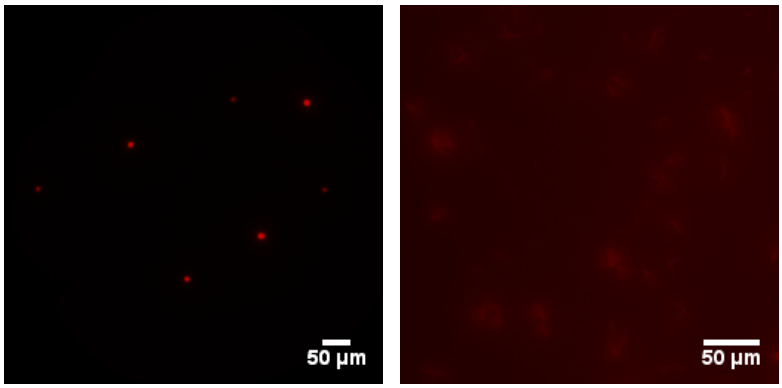


Figure 44: Fluescence microscopy images of nitro **166** incubated in PBS for 30 minutes. Left: 10 μM. Right: 50 μM. Small spots of fluorescing compound aggregate can be seen at 10 μM, whilst a fluorescent background and larger aggregates can be seen 50 μM. Images taken using a Nikon Ti-E fluorescence microscope.

This experiment demonstrated that high concentrations of unmetabolised nitro compound **166** could cause a fluorescent background signal, suggesting that the fluorescence observed in cells treated with **166** under hypoxia could be partially attributed to intrinsic fluorescence.

4.4 Concluding remarks and future direction

In this chapter we have shown the development of a new compound, based upon a pre-existing but highly understudied scaffold, which is compatible with use as a fluorescent hypoxia imaging probe. We began by following an established synthetic procedure to synthesise the amine fluorophore **163**, and by adapting it to synthesise the pro-fluorophore **166**.

Having synthesised these analogues, we characterised the photophysical properties of amino compound **163** and nitro compound **166**. We found that, contrary to expectation, nitro analogue **166** had some intrinsic fluorescence. This appeared to be recapitulated by fluorescence microscopy, where background fluorescence in cells treated with this compound under normoxia also showed some fluorescence, although we proposed alternative explanations for this.

The nitro compound **166** was further tested *in vitro* as a substrate for the oxygen-sensitive enzyme cytochrome p450 reductase. It was observed that whilst it appeared to act as a substrate as we had intended (with reduction of the aryl nitro group to the amine), the molecule was also susceptible to other forms of metabolism under these assay conditions. It was demonstrated through further *in vitro* experiments that NADPH was a major cause of this metabolism, through hydride addition to the core of the molecule *via* conjugate addition. We showed that whilst this addition appeared to be irreversible, other reactions such as addition of water or L-glutathione appeared to be

reversible. The site of reactivity on the molecule was confirmed by chemical treatment of **166** with hydride reductant sodium borohydride.

Despite the apparent susceptibility of **166** to conjugate addition reactions, it was demonstrated that it was stable in media and able to penetrate cell membranes. Finally, we demonstrated that **166** can indeed act as an imaging probe in cells, culminating in a demonstration that, whilst background fluorescence was present in normoxia, there was a significant increase in fluorescence for cells in hypoxia.

Whilst it is beyond the scope of this chapter, we propose that **166** could be further modified for use as a hypoxia-activated fluorogenic prodrug. Appending a benzylic group *ortho* to the aryl nitro hypoxia trigger could allow for the attachment of a drug cargo. Such a molecule could act, as with other hypoxia-activated prodrugs discussed herein and elsewhere, to deliver a cargo molecule upon conversion of the aryl nitro to an aryl amine.

Chapter 5
Towards bioreductive, hypoxia-activated theranostic agents

5.1 Theranostic agents

A “theranostic” agent, a portmanteau of “therapeutic” and “diagnostic”, is the name given to a chemical entity designed to have both therapeutic efficacy and provide some form of diagnostic information.[146] This is usually achieved by combining a known therapeutic agent and an imaging probe with a targeting mechanism. These may be, for example, bioresponsive materials such as nanoparticles or hydrogels which release the agent after certain stimuli, such as change in tissue pH.[127] Others may be targeted to certain tissues through use of antibody-drug conjugates or receptor-binding ligands.[115,116,128,206]

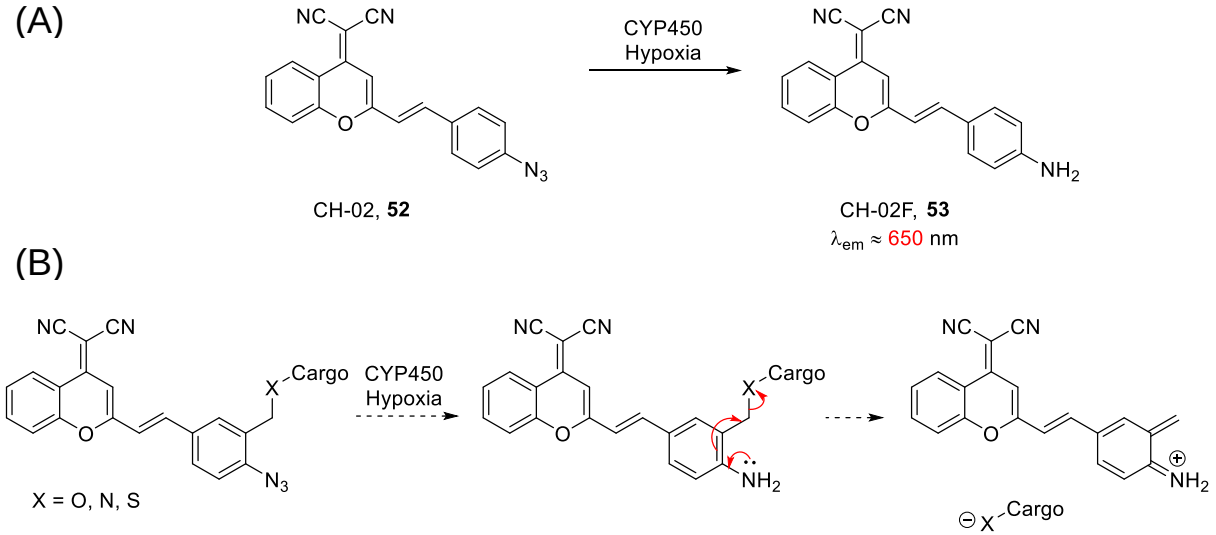
A wide variety of theranostic agents have been developed over the last few years,[146–148,151,152] however, relatively few have been developed to be responsive to hypoxia. Of those that are, most do not respond to the oxygen levels of the environment; rather, they respond to other hypoxia-associated (but not dependent) features, such as pH.[53,127] We therefore wished to use our method of hypoxia-selective metabolism as the trigger for a hypoxia-activated theranostic agent.

5.2 Design of compounds

5.2.1 Near-infrared (NIR) scaffolds

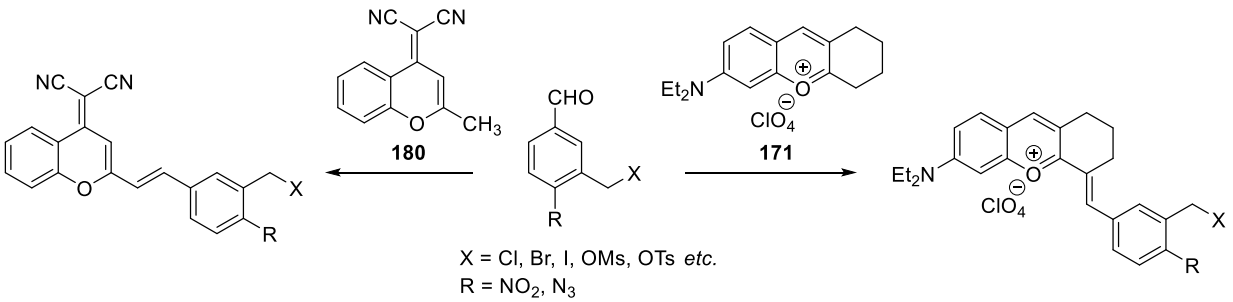
One limitation of fluorescence-based biomedical imaging probes is the tissue penetration of the fluorescent signal (*vide infra*). It is therefore preferable if the imaging probe emits photons which have the greatest possible depth of penetration into tissue. These are photons in the near-infrared (NIR) region of the spectrum, with $\lambda_{em} \geq 650$ nm. To form the basis of a fluorescent theranostic agent, we wished to use fluorophore scaffolds which emitted in the NIR region.

Previous work, conducted by Dr Liam O'Connor in our group, identified a known near-infrared fluorophore CH-02F **53** (λ_{em} ≈ 650 nm), the precursor form of which bore an azidoaryl moiety. This compound, CH-02 **52**, had been previously studied as a hydrogen sulfide sensor in cells.[217] Unlike more classical nitroaryl moieties, **52** was not a substrate for human cytochrome p450 reductase (CPR). Instead, a sub-family of cytochrome p450 oxidase enzymes were implicated as being responsible for the cellular activation of **52** under hypoxia, *via* binding of the azide moiety to their heme cofactor in the absence of oxygen.[187] We wished to use this scaffold as one possible basis for development of an NIR theranostic agent.



Scheme 52: (A) CH-02 **52**, an arylazide-based NIR pro-fluorophore developed by Dr Liam O'Connor.[145] (B) Proposed modification of **52** to form a theranostic prodrug platform.

As discussed in Chapter 4, we developed a new NIR hypoxia-sensitive imaging probe based upon a benzopyrylium scaffold. We further propose that this compound **166** could be adapted to also function as an NIR theranostic agent. Conveniently, both CH-02 **52** and **166** were synthesised using similar condensation chemistry using similar benzaldehyde derivatives. We speculated that both fluorophore scaffolds could be synthesised from a common, or closely related intermediate, outlined in Scheme **53**.

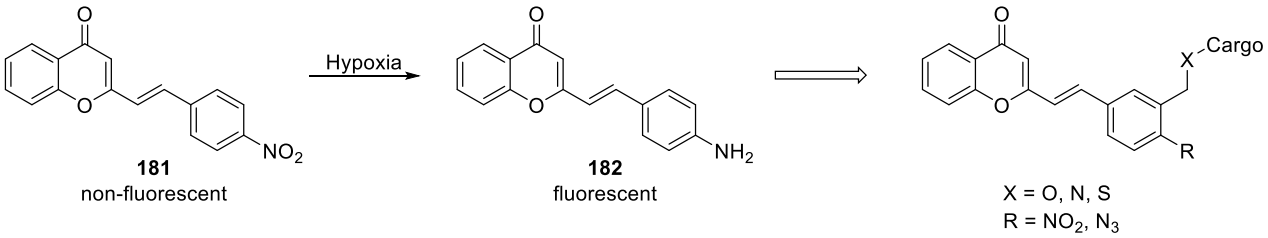


Scheme 53: Proposed synthesis of NIR theranostic agents from common intermediates.

The reasons for having theranostic agents based on multiple fluorophore cores was twofold. We were firstly aware of the limitations of compounds designed to be substrates for cytochrome p450 reductase and P450 enzymes; as with all small-molecule ligands, there are steric and electronic factors which affect binding affinity. Furthermore, it was clear to us that not all nitroaryl and azidoaryl compounds are intrinsically substrates for these enzymes; it therefore seemed sensible to have inherent scope for diversity in our compounds. Secondly, we were conscious of the synthetic challenges associated with our fluorophores. Dr Liam O'Connor had found that synthesis of analogues of **52** was non-trivial; synthesis of the nitro analogue proved highly challenging.[49] By having multiple scaffolds we hoped to allow ourselves flexibility based on synthetic tractability.

5.2.2 Visible-wavelength scaffold

During his synthesis of analogues of **52**, Dr O'Connor synthesised the chromanone analogues **181** and **182** (Scheme **54**).[49] He incidentally observed that **182** appeared to be highly fluorescent at a visible wavelength, although subsequent reactions he attempted on these compounds were unsuccessful and no further study was conducted. We hypothesised that these compounds could also act as hypoxia-responsive fluorophores and could also be used as the basis for visible-wavelength theranostic agents.



Scheme 54: Chromanone analogues as proposed hypoxia-responsive theranostic agents.

Although visible wavelength fluorophores are less useful for *in vivo* applications, they are useful for *in vitro* study and enable proof-of-concept studies. Visible wavelength fluorophores are typically much brighter than NIR fluorophores, since they typically have far greater fluorescence quantum yields (Φ_{FL}).[117] Visible-wavelength fluorophores may still be studied in a cellular setting, which can provide information on their possible behaviour *in vivo*. This is relevant in the context of hypoxia-activated prodrugs; if fluorescent signal is concomitant with release of the biologically active cargo, then *in vitro* fluorescent signal can provide both qualitative and quantitative measures of compound release. This information can then be used to better evaluate *in vivo* efficacy of the compounds in question.

5.2.3 Target compounds

We designed our target theranostic agents to have 3 components: a fluorogenic component which would non-emissive until metabolised under hypoxia; a biologically active cargo molecule, the activity of which could be abrogated once incorporated into the agent; and a hypoxia-sensitive 'trigger' functional group. We chose to use nitroaryl and/or azidoaryl groups as hypoxia-sensitive trigger moieties, since they have been well-studied by us and others.[26,28,51,145]

We wished our theranostic delivery platform to be broadly applicable to a range of biologically-active compounds, including clinical anticancer agents. As a proof-of-principle, we chose to use **184**, a small-molecule ligand for the BET family of bromodomain-containing proteins. This protein family are involved in epigenetic

regulation of gene expression and have important roles in many types of cancer; their inhibition results in a well-demonstrated cytotoxic phenotype.[218–220] **184** was developed in our research group by Dr Laura Jennings,[221] following on from the work of Dr David Hewings,[222,223] and had a well-established SAR around its binding to BET bromodomains. More discussion of both the BET family of proteins and analogues of ligand **184** can be found in Chapter 6.1.3 and 6.2.

Each of the three fluorophore cores chosen are typically synthesised *via* condensation of the "acceptor" component with an aryl aldehyde. We therefore wished, if possible, to design synthetic routes to these agents which involved condensation with a common aldehyde intermediate. A summary of our compound design is given in Figure **45**, below.

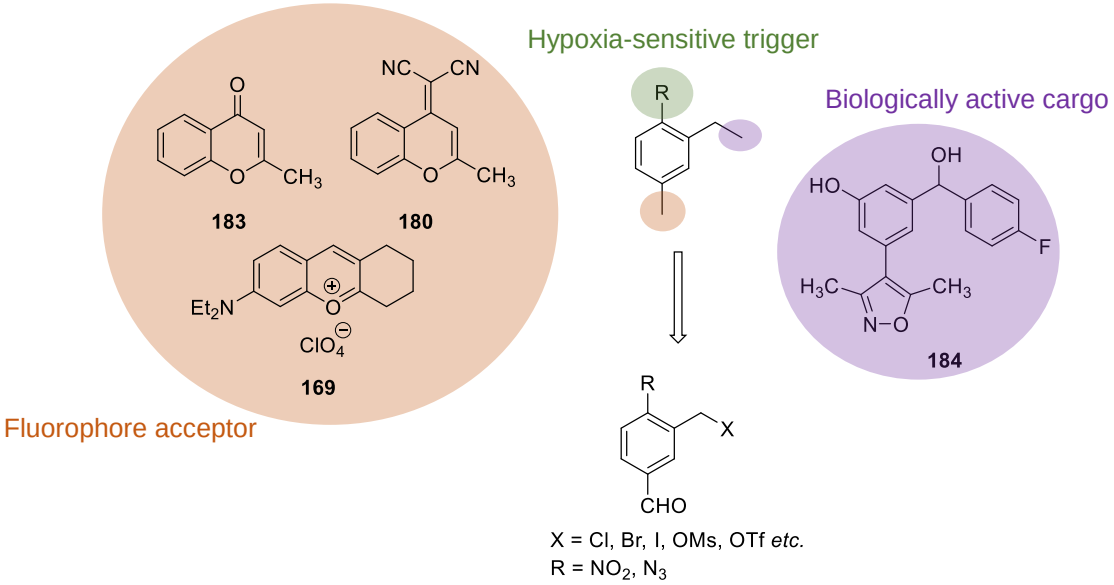
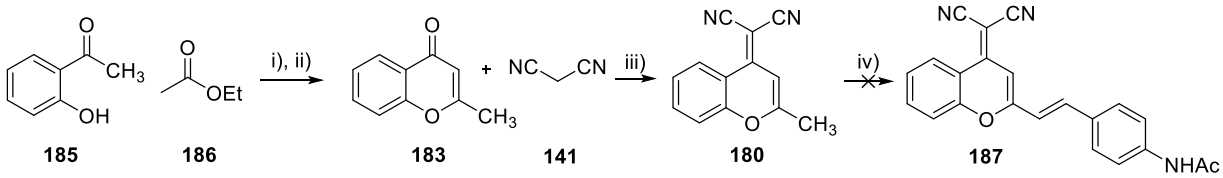


Figure 45: Design strategy for a family of hypoxia-sensitive theranostic agents, possibly synthesised from a common intermediate.

5.3 Synthesis

5.3.1 Synthesis of near-infrared fluorophores

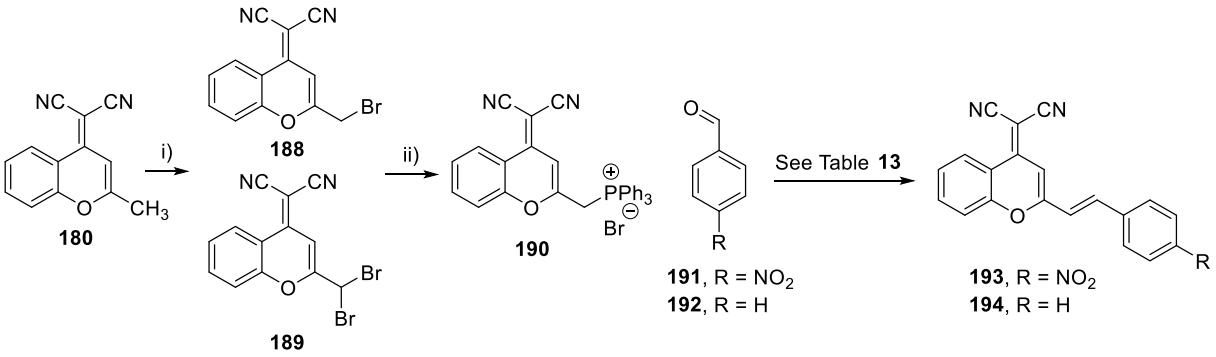
The original synthesis of fluorophore **53** had proven challenging,[49] requiring the use of piperidine and acetic acid as additives to aid condensation *via* imine formation of the aldehyde coupling partner. These conditions required sub-stoichiometric amounts of acid and amine, gave only moderate yields and were highly sensitive to variation in quantity; addition of excess piperidine, for example, led to nucleophilic attack of piperidine at one of the nitrile groups. We were therefore concerned that the sensitivity of these coupling conditions would not be ideal for synthesis of more diverse analogues and may result in unnecessary consumption of late-stage material.



Scheme 55: Synthesis of "acceptor" **180** and attempted aldehyde condensations. *Reagents and conditions*. i) Na, RT, 2 hours; ii) H_2SO_4/AcOH/H_2O (1:4:10), reflux, 16 hours, 38%-48% over 2 steps; iii) Ac_2O, 140 °C, 2 hours, then MeOH, 50 °C, 1 hour, 61%-70%; iv) 4-Acetamidobenzaldehyde, AcOH (0.8 eq.), piperidine (0.5 eq.), toluene, reflux, 24 hours, N.R.

Initially, resynthesis of **53** was attempted using the original conditions. 2'-hydroxyacetophenone **185** was first treated with sodium metal in ethyl acetate at room temperature to affect an aldol-type condensation, presumably through generation of small quantities of "dry" sodium hydroxide to act as a base. Subsequent heating under reflux in strongly acidic solution led to dehydration and formation of chromanone "acceptor" **183**, which then underwent a Knoevenagel condensation with malononitrile **141** to furnish "acceptor" core **180** in good yield. Attempts at condensation of 4-acetamidobenzaldehyde with core **180** proved unsuccessful despite several attempts. Our synthetic strategy involved this critical coupling step between acceptor **180** and a functionalised benzaldehyde derivative, and we therefore attempted to find alternate conditions to affect this transformation.

The desired condensation reaction was a form of olefination, and we therefore turned to alternate methods of forming olefins. We hypothesised that Wittig olefination could afford the desired coupling. Previous attempts to afford the nitro analogue of **52** had proven unsuccessful, hence the use of the azido analogue **53**; we hypothesised that Wittig olefination might tolerate a range of aldehyde substrates, allowing us access to the nitro compound. We therefore synthesised the triphenylphosphonium salt of **180**, first *via* radical bromination at the methyl group (resulting in both mono- and dibromination products **188** and **189**, respectively), followed by displacement of the bromide upon treatment with triphenylphosphine, giving **190** in very good yield (Scheme **56**).



Scheme 56: Synthesis of phosphonium salts and attempted Wittig reactions. *Reagents and conditions*: i) AIBN, NBS, CCl_4, 70 °C, sealed tube, dark, 21–72 hours, 38%–60% **188**, 0%–28% **189**; ii) **188**, PPh_3, toluene, reflux, 1–2 hours, 72–77%.

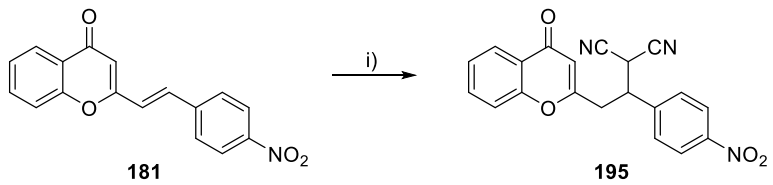
Table 13: Attempted Wittig reactions. Solutions of **190** in the solvent were cooled, base added, and stirred. After this time, a solution of the aldehyde was added dropwise, and allowed to warm to RT.

Entry	R	Base	Solvent	Temperature	Time	Yield
1	NO_2	1 eq. *n*-BuLi	Anh. THF	−78 °C; → RT	5 min; 1 hour	N.R.
2	NO_2	1.2 eq. *n*-BuLi	Anh. THF	−78 °C; → RT	15 min; 1 hour	N.R.
3	NO_2	1.2 eq. *n*-BuLi	Anh. THF	−78 °C; → RT	30 min; 2 hours	N.R.
4	NO_2	1.1 eq. NaHMDS	Anh. THF	−78 °C; → RT	10 min; 1 hour	N.R.
5	H	1.1 eq. LiHMDS	Anh. THF	−78 °C; → RT	15 min; 1 hour	N.R.

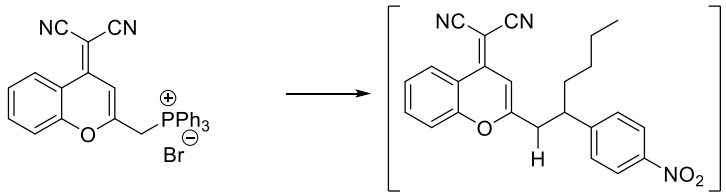
With the phosphonium salt **190** in hand we attempted to perform Wittig olefinations. Attempts at formation of the ylide using strong bases *n*-BuLi (Table **13**, entries **1**–**3**), sodium hexamethyldisilamide (NaHMDS, Table **13**, entry **4**) or lithium hexamethyldisilamide (LiHMDS, Table **13**, entry **5**), followed by treatment with

4-nitrobenzaldehyde **191**, were not successful. Despite a stark colour change upon addition of base to the suspension of triphenylphosphonium salt **190** (indicating possible formation of a stable anion in solution), no products were observed by TLC, mass spectrometry, or ^{1}H NMR analysis of the crude mixture. Wittig reactions are renowned for their sensitivity to trace amounts of water, and so in all cases tetrahydrofuran freshly distilled over sodium metal was used; the triphenylphosphonium salt was dried in a heated tube under high vacuum for a minimum of 24 hours before use – despite these efforts, no reaction was observed. To test whether the electron-deficient nature of 4-nitrobenzaldehyde was hindering the reaction, we repeated the reaction using distilled benzaldehyde (Table **13**, entry **5**). Again, no reaction was observed. These results suggested that the reaction was not forming due to the reactivity of the ylide. The pKa of the relevant proton is sufficiently low to allow deprotonation by strong bases such as butyllithium or HMDS salts, and we concluded that the resulting ylide is too stabilised by conjugation into the nitriles of the substrate, reducing its nuceophilicity.

(A)



(B)



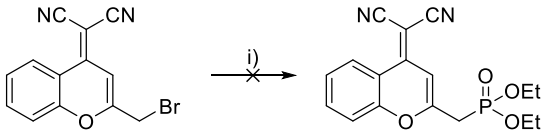
Exact Mass = 399

Detected $[M-H]^-$ = 398

Scheme 57: (A) 1,6-Addition adducts observed by Dr Liam O'Connor.[49] *Reagents and conditions*: i) $BF_3{\cdot}Et_2O$ (1.2 eq.), malononitrile (1.2 eq.), NaH (2 eq.), THF, RT, 1 hour, 16% yield. (B) Adduct observed by low-resolution mass spectrometry during Wittig reaction in Table **13**, entry **1**.

During Dr O'Connor's work, he observed that chromenone compound **181** underwent conjugate addition to the olefin during an attempted Knoevenagel condensation, forming adduct **195** shown in Scheme **57a**. Consistent with observation, a species was observed by low-resolution mass spectrometry during the reaction in Table **13**, entry **1**. This species had *m/z* = 398 in negative-mode electrospray ionisation, and we hypothesised that this may have been species **196**, shown in Scheme **57b**. *n*-BuLi can act as nucleophile, adding a butyl chain to an electrophilic position of some molecules. This species was not clearly observed by TLC and was not isolated, so its identity has not been proven and is only speculative. Whilst this suggested that olefination may indeed have occurred, alternate methods of olefination were instead explored.

We attempted to synthesise the diethylphosphonate ester **197** for use in a Horner-Wadsworth-Emmons (HWE) reaction *via* an Arbuzov reaction between bromide **188** and triethyl phosphite (Scheme **58**). This proved unsuccessful, as no product was detected by TLC, ^{1}H or ^{31}P NMR analysis.



188 **197**

Scheme 58: Attempted Arbuzov reactions to form the Horner-Wadsworth-Emmons substrate **197**. *Reagents and conditions*: i) Triethyl phosphite, toluene, reflux or RT, 12 hours, N.R.

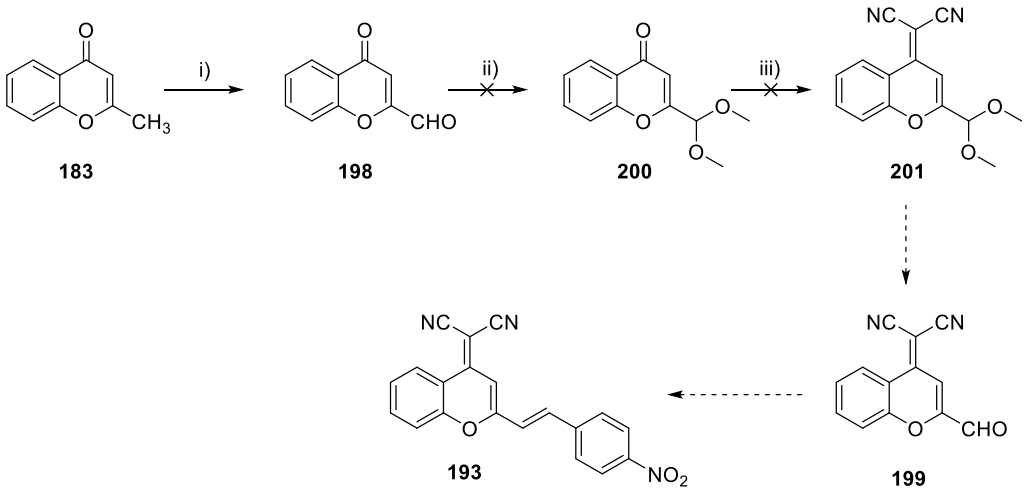
Both the Wittig and Horner-Wadsworth-Emmons reactions use two components – an alkylphosphorus-based ylide and a carbonyl-containing group, such as a ketone or aldehyde. The reactions described above aimed to use benzaldehyde derivatives as the carbonyl coupling partners, forming the ylide from the "acceptor" portion of the fluorophore. Having had little success with this approach we attempted to switch the

coupling partners, such that the "acceptor" moiety bore the carbonyl coupling partner and the phosphorus ylide was formed from the corresponding benzylic bromide.



Scheme 59: Riley oxidations of chromanone **183** and "acceptor" **180**. *Reagents and conditions:* i) SeO_2, xylenes, 165 °C, sealed tube, 16 hours, 29%–30% yield; ii) SeO_2, xylenes, 165 °C, sealed tube, 16 hours, N.R.

We attempted Riley oxidations, using selenium dioxide to oxidise the allylic methyl, on both the chromanone **183** and "acceptor" moiety **180**. As shown in Scheme **59**, "acceptor" **180** did not undergo any reaction but the chromanone **183** did, affording aldehyde **198** in modest yield.



Scheme 60: Proposed alternative synthesis of olefins *via* Wittig chemistry. *Reagents and conditions:* i) SeO_2, xylenes, 165 °C, sealed tube, 29%–30%; ii) *p*-TSA, $HC(OMe)_3$, MeOH, RT, 3 hours, N.R.

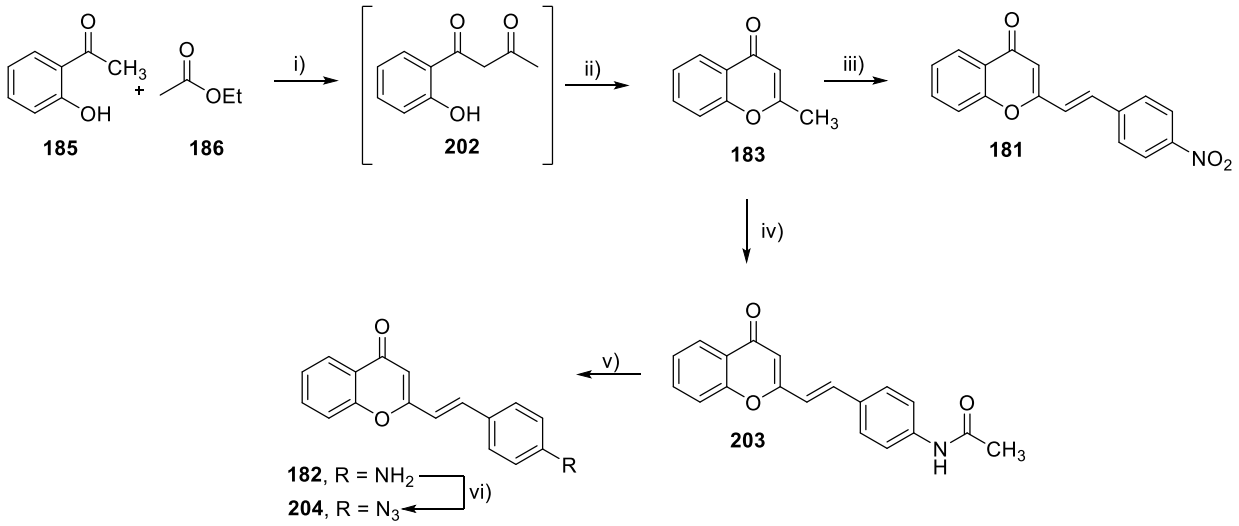
We determined that aldehyde **198** needed to undergo Knoevenagel condensation with malononitrile prior to any type of Wittig or HWE olefination; once the olefin was installed, we suspected that it would undergo conjugate addition from malononitrile as observed previously (*vide supra*). Thus, we chose to use a protecting group for the aldehyde which would be stable during the Knoevenagel condensation and could then be readily removed. Protecting the aldehyde as the dimethoxyacetal

200 using common conditions of methanol and *p*-TSA was not successful, and so the subsequent Knoevenagel condensation could not be conducted.

These data indicate that alternate olefin reactions to form analogues of **52** were similarly challenging to the original method. As described in Chapter 4, we had developed a facile synthesis of another class of hypoxia-sensitive fluorophore, and we therefore chose to use this scaffold as the initial basis for synthesis of an NIR theranostic agent.

5.3.2 Synthesis of visible-wavelength fluorophores

It was observed during earlier studies that **182**, the chromenone analogue of **53**, appeared to exhibit strong visible-wavelength fluorescence, where as its nitro analogue **181** did not.[49] We wished to investigate these compounds, to determine whether the amino form was indeed fluorescent and the nature of this fluorescence, and whether nitro- or azido- analogues could be used as new hypoxia-sensitive fluorogens.



Scheme 61: Synthesis of chromene-based compounds. *Reagents and conditions*: i) Na metal, RT, 1.5 hours, then ii) H_2O/AcOH/H_2SO_4 (10:4:1), reflux, 16 hours, 48% over 2 steps; iii) 4-Nitrobenzaldehyde, NaOMe, MeOH, reflux, 1.5 hours, 68%; iv) 4-Acetamidobenzaldehyde, NaOMe, MeOH, reflux, 16 hours, 39%; v) 4 M aqueous HCl/EtOH (2:1), reflux, 16 hours, 44%; vi) 2 M aqueous $NaNO_2$, H_2O/conc. HCl (2:1), 0 °C, 15 minutes, then 1.1 M aqueous NaN_3, 0 °C, 15 minutes, then RT, 45 minutes, 47%.

Synthesis of compounds **181**, **182** and **204** was readily achieved using similar chemistry from a common intermediate. Firstly, a base-catalysed, water-free enolate α-alkylation was conducted between 2'-hydroxyacetophenone **185** and ethyl acetate **186**, acting as both reactant and solvent. This was performed using sodium metal, acting as both a drying agent and a source of sodium hydroxide as a base to catalyse the reaction. The initial reaction intermediate **202** was not isolated, but instead subjected to an acid-catalysed condensation, resulting in production of the chromenone core **183** in good yield. This common intermediate compound was then coupled to the appropriate aldehyde in a base-catalysed condensation reaction under relatively mild conditions (sodium methoxide under reflux in methanol) to afford the nitro and acetamide compound **181** and **203**, respectively. Acetamide **203** was then subjected to acid-catalysed hydrolysis, affording amine **182** in reasonable yield. Finally, azide compound **204** was synthesised *via* formation of the diazonium salt intermediate, then displacement by the azide anion nucleophile using sodium azide, affording **204** in reasonable yield (Scheme **61**).

5.4 Photophysical characterisation

With fluorophore **182**, as well as putative pro-fluorophores **181** and **204** in hand, we first performed photophysical characterisation to determine their UV-Vis absorbance and fluorescence emission spectra.

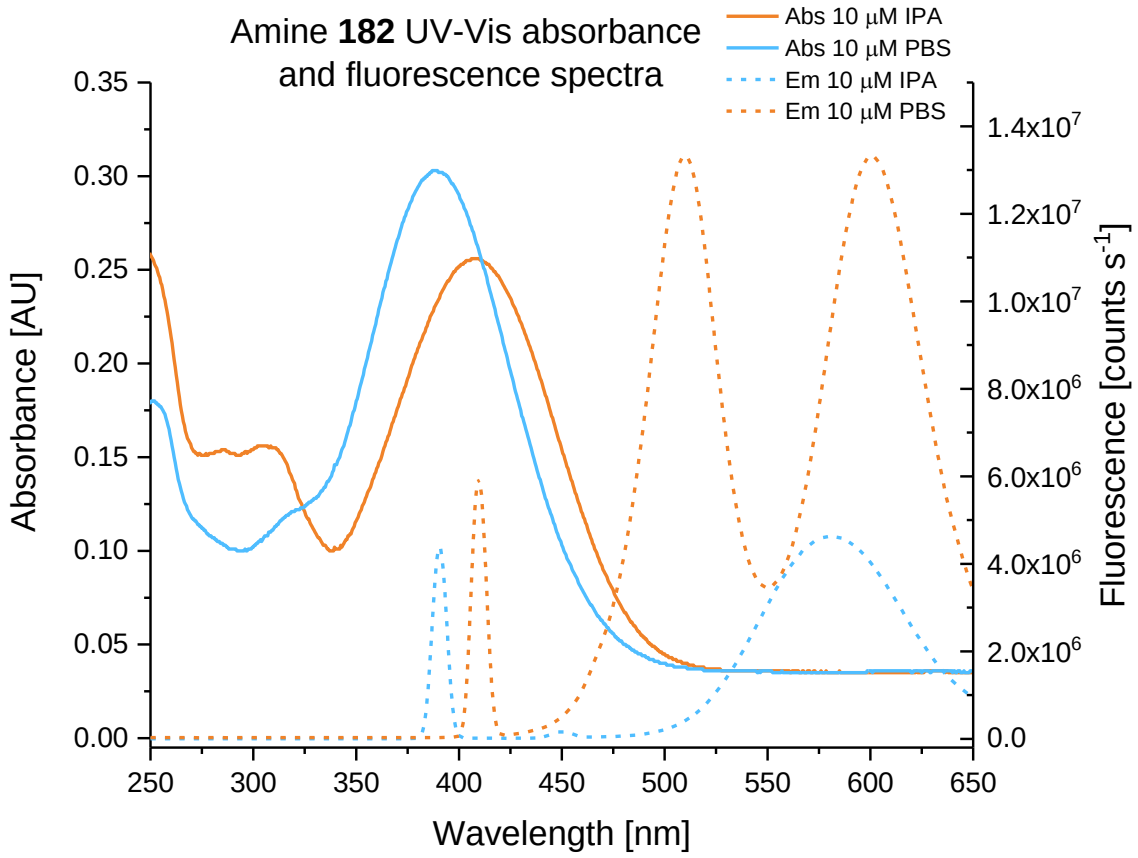


Figure 46: UV-Vis absorbance (solid lines) and fluorescence emission (dashed lines) spectra for amino-chromanone **182**. Data were recorded at 10 μM in either *iso*-propyl alcohol (IPA, orange) or phosphate buffered saline (PBS, blue) at pH 7.4. Compounds were excited at their absorbance maxima (409 nm in IPA, 389 nm in PBS).

The amine **182** had similar UV-Vis absorbance spectra in both IPA and PBS, with absorption maxima at 409 nm and 389 nm, respectively. **182** also exhibited strong fluorescence in both IPA and, pleasingly, PBS. Interestingly, in IPA the amine has two emission maxima at λ_{em} = 510 nm and 600 nm (dashed blue line). While interesting, the more important observation is the amine's emission in PBS, which is strong and has a maximum at λ_{em} = 580 nm, in the yellow region of the electromagnetic (EM) spectrum. This result was crucial, since it demonstrates that amine **182** should be

fluorescent in a physiological medium such as cytoplasm, a key feature of a biological imaging probe that is not organelle targeted.

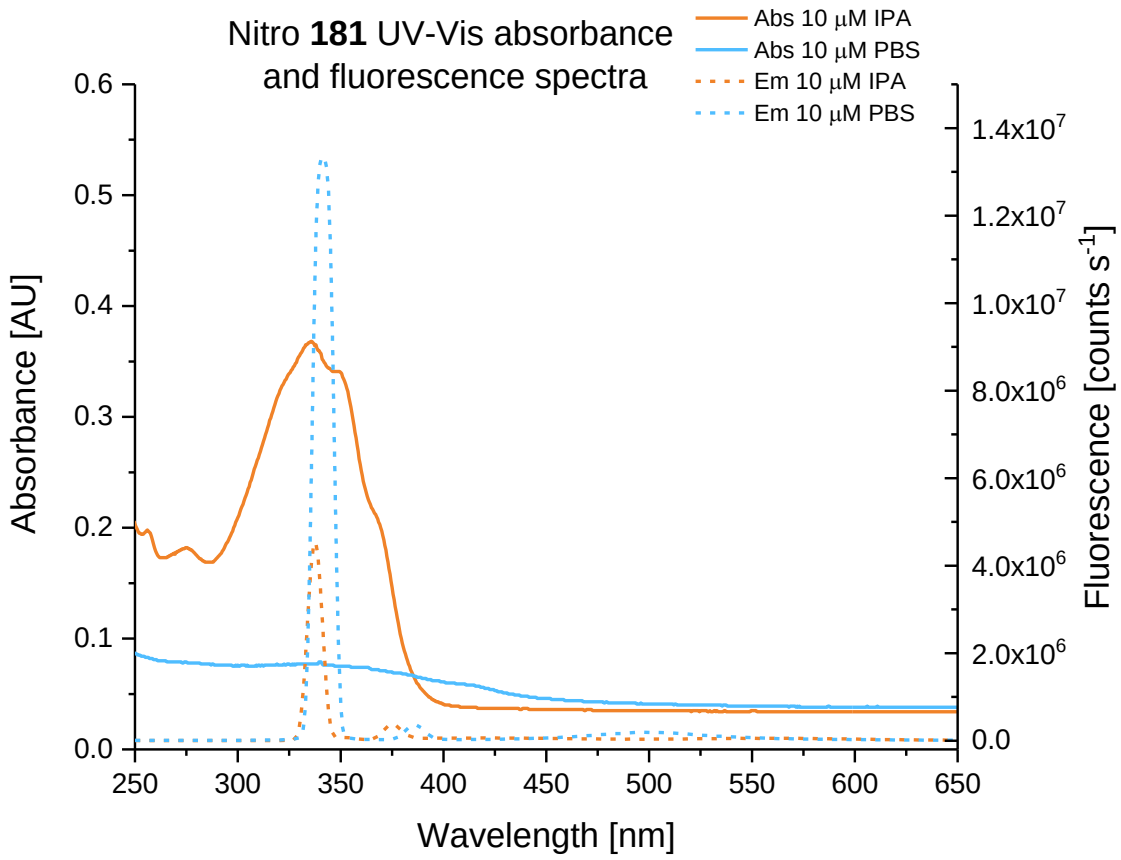


Figure 47: UV-Vis absorbance (solid lines) and fluorescence emission (dashed lines) spectra for nitro-chromanone **181**. Data were recorded at 10 μM in either *iso*-propyl alcohol (IPA, orange) or phosphate buffered saline (PBS, blue) at pH 7.4. Compounds were excited at their absorbance maxima (335 nm in IPA, 339 nm in PBS).

By contrast, nitro **181** shows a significant decrease in absorbance in PBS, compared with IPA. In PBS, **181** has a broad, featureless absorbance spectrum with no sharp maxima. Despite this, the absorbance maximum was similar in both media, with λ_{abs} = 335 nm and 339 nm in IPA and PBS, respectively. Pleasingly, **181** exhibited almost no background fluorescence in both IPA and PBS; the fluorescence appeared slightly greater in PBS, but significantly less intense than that of amine **182**.

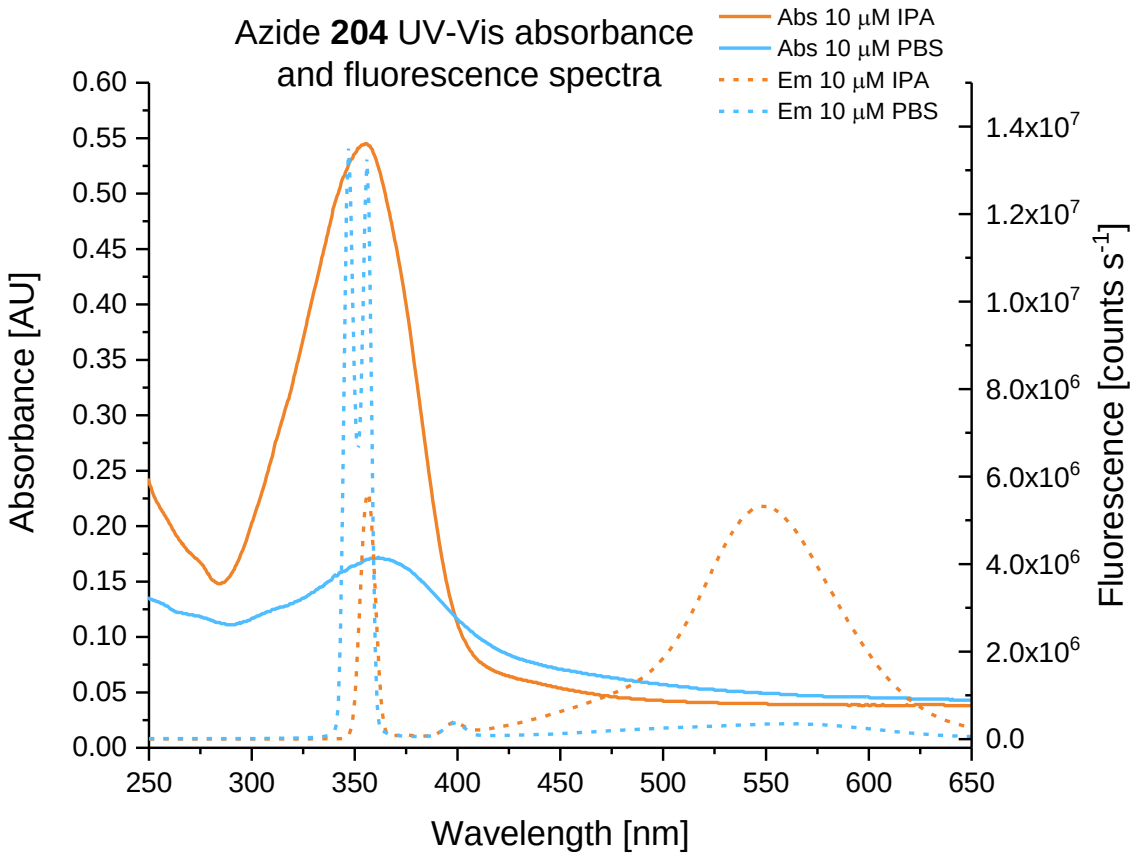


Figure 48: UV-Vis absorbance (solid lines) and fluorescence emission (dashed lines) spectra for azido-chromanone **204**. Data were recorded at 10 μM in either *iso*-propyl alcohol (IPA, orange) or phosphate buffered saline (PBS, blue) at pH 7.4. Compounds were excited at their absorbance maxima (355 nm in IPA, 362 nm in PBS).

Like the nitro analogue **181**, azido compound **204** exhibited similar UV-Vis absorbance spectra whether in IPA or PBS, with absorbance maxima at λ_{abs} = 355 nm and 362 nm respectively. Contrary to our expectation, **204** in IPA exhibited strong fluorescence with an emission maximum at λ_{em} = 549 nm. We had hypothesised that electron-withdrawing groups (such as $-NO_2$ or $-N_3$) would alter the molecular orbital energy levels such that the HOMO-LUMO gap was no longer small enough for fluorescence photons to be emitted. This appeared to hold true for nitro **181**, although not for the azide. **204** had significantly decreased fluorescence in PBS, with an emission maximum at λ_{em} = 555 nm. Since the emission intensity was far lower than that of the amine, **204** may still be considered "fluorogenic" if the azide is efficiently

metabolised to the amine in a biological context. Nevertheless, we proceeded with biological imaging of these compounds with a degree of added caution. A summary of the UV-Vis and fluorescence data for compounds **181**, **182** and **204** is given in Table **14**, below.

Table 14: Summary of the UV-Vis absorbance and fluorescence properties of compounds **181**, **182** and **204**.

Compound	Concentration	Solvent	$\lambda_{abs,\ max}$	$\lambda_{em,\ max}$	Stokes' shift
Amine **182**	10 μM	IPA	409 nm	510/600 nm	101/191 nm
Amine **182**	10 μM	PBS	389 nm	580 nm	191 nm
Nitro **181**	10 μM	IPA	335 nm	-	-
Nitro **181**	10 μM	PBS	339 nm	497 nm	158 nm
Azide **204**	10 μM	IPA	355 nm	549 nm	194 nm
Azide **204**	10 μM	PBS	362 nm	555 nm	193 nm

5.5 Enzymatic reduction studies of chromenone-based compounds

Having established that amine **182** was indeed strongly fluorescent in the yellow region of the EM spectrum, and maintained this fluorescence in aqueous media, we next wished to assess whether the nitro- and azido-profluorophores **181** and **204** were metabolic substrates for cytochrome p450 reductase (CPR), and whether their metabolism was oxygen-dependent.

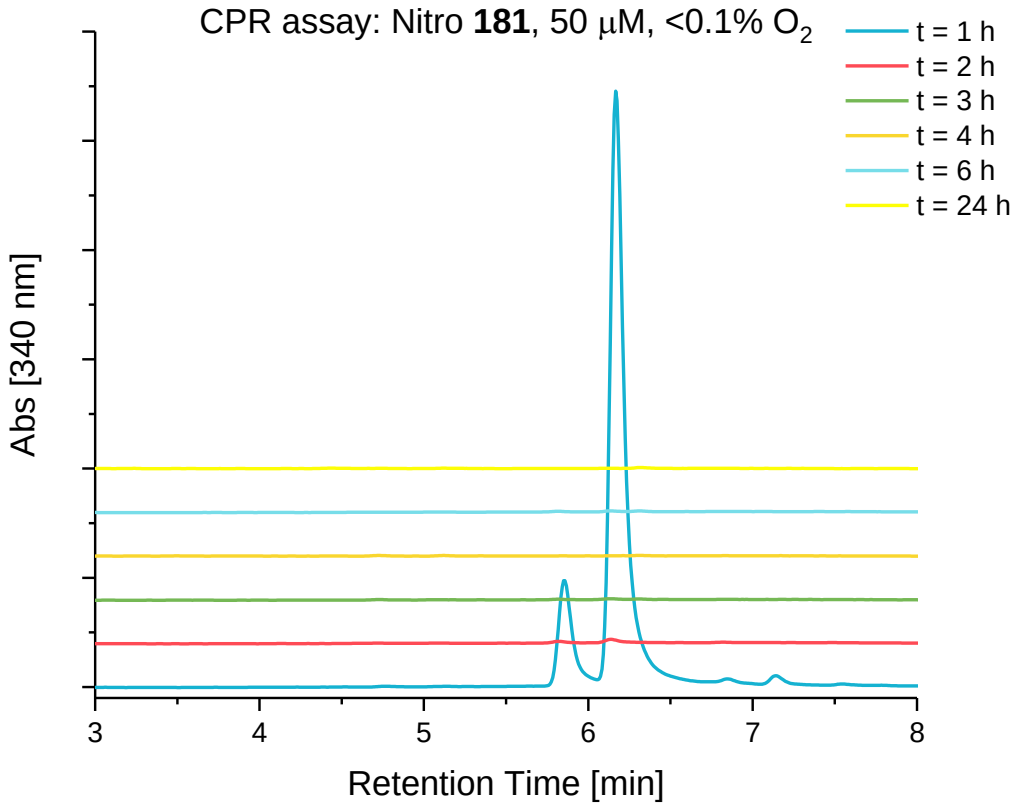


Figure 49: Cytochrome p450 reductase assay of nitro-chromanone **181** under anoxic conditions. Samples of compound **181** were incubated in PBS in the presence of cytochrome p450 reductase and an NADPH regeneration system, under hypoxic (pO_2 <0.1%) conditions. Aliquots were taken at the indicated timepoints and analysed by HPLC-MS.

Subjecting both compounds to the CPR assay yielded unusual results. The nitro-chromanone appeared to be stable for 1 hour under hypoxia, but at subsequent timepoints almost no compound could be detected. We speculated that this could be due to compound aggregation; we had observed that nitro-chromanone **181** was very poorly soluble in organic solvent and could not be made into a stock solution of 10 mM

concentration in DMSO (5 mM was, however, achievable). Furthermore, the azido-chromanone **204** appeared to be generally unstable, breaking down into multiple unidentified products.

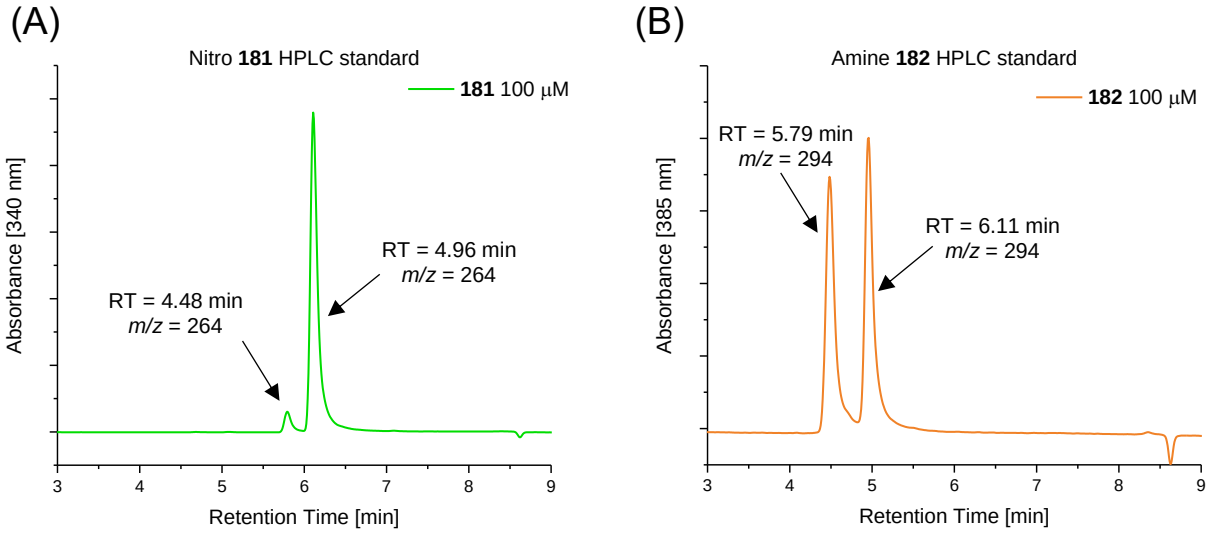


Figure 50: HPLC-MS traces of standards of (A) nitro **181** and (B) amine **182**. The molecular ion masses for each peak are shown.

More interesting to us was the apparent impurity of our compounds. Whilst attempting to run standard concentrations of amino- and nitro-chromanones **182** and **181**, we observed that there appeared to be two peaks in the HPLC traces (Figure **50a**&**b**). The ratios of the peaks changed depending on which wavelength the chromatogram was recorded at. This was surprising, since the compounds appeared to be single components by TLC, ^{1}H and ^{13}C NMR, and the molecular ions associated with each HPLC-MS peak was identical and corresponded to the $[M+H]^{+}$ ion for the compound.

Since each peak contained identical masses, which corresponded to the masses for the correct structure, we speculated that the condensation reaction had perhaps formed a mixture of both the *E*- and *Z*-alkenes. This would be consistent with each species having identical mass as well as having different UV-Vis absorption properties, as evidenced by the varying HPLC peak areas when observed at different wavelengths. However, this hypothesis did not appear consistent with ^{1}H NMR data

for each compound. 1,2-disubstituted olefins can usually be distinguished between *cis*- and *trans*-geometry by the chemical shifts of, coupling constant between, the vinylic olefin protons. Analysing the ^{1}H NMR spectra for each compound, we noticed that only one set of olefin protons were present, which suggested the presence of only a single geometric isomer. Furthermore, the olefin protons of both nitro **181** and amine **182** had similar, large coupling constants (J = 16.1 Hz and 16.0 Hz, respectively), suggesting the *trans*-olefin products (Figure **51**, below).

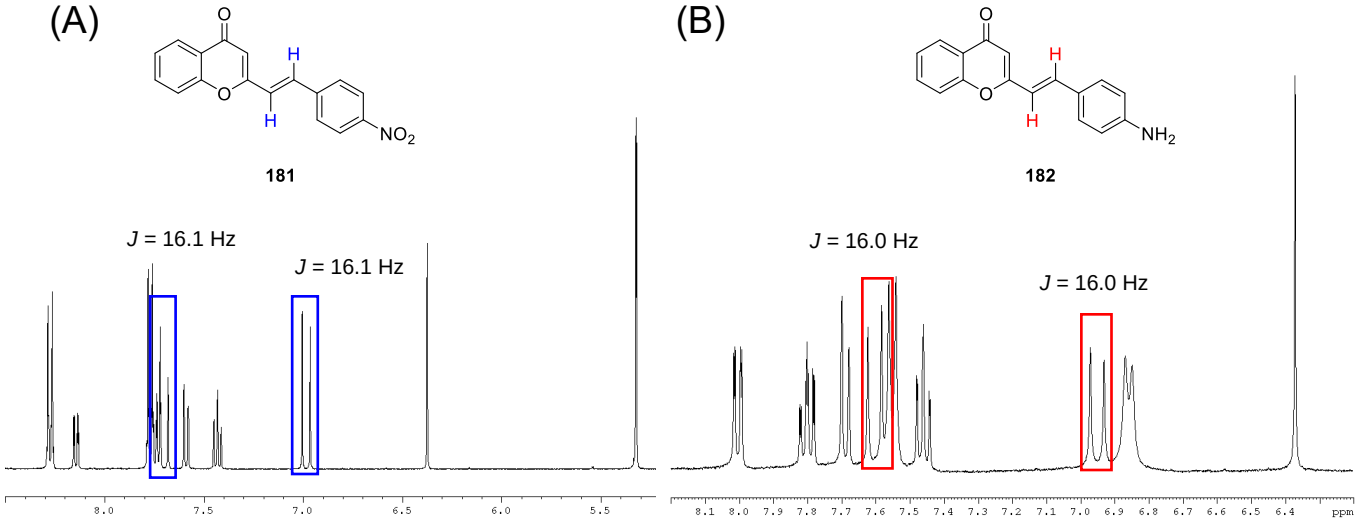
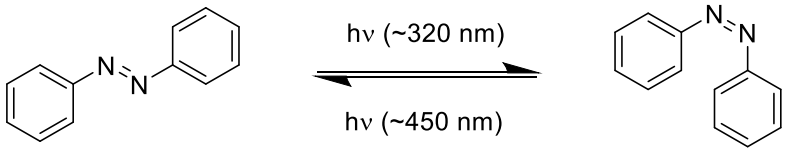


Figure 51: ^{1}H NMR analysis of nitro-chromanone **181** and amino-chromanone **182**. Olefin protons are shown in blue (nitro) and red (amino), with coupling constants highlighted. Spectra were recorded on a Bruker Avance III 400 MHz spectrometer in DMSO-D6.

It seemed unlikely that the condensation reaction to form **181** and **182** could form both the *cis*- and *trans*-isomers. The Aldol-type product formed loses a molecule of water typically *via* an E1cB mechanism in which an antiperiplanar proton to the hydroxyl is abstracted concomitantly with loss of the -OH group. Whilst the two protons at the α-position to the hydroxyl can both act as the antiperiplanar proton lost, there is free rotation about the C-C bond which will predominantly adopt a conformation that gives a *trans*-olefin product. We therefore speculated whether the presence of these two species was caused by photoisomerism.

5.6 Chromenone photoisomerisation



trans-azobenzene **205** *cis*-azobenzene **206**

Figure 52: Photo-induced isomerisation of azobenzene. The rate of interconversion between the two isomers is such that the sterically disfavoured *cis* isomer is transiently stable.[224]

Some compounds have a propensity to switch between isomeric forms after excitation by photons of the correct energy. Azobenzene **205** is a classic example of this; the two phenyl rings typically sit *trans* to each other, until the molecule is excited by photons of the correct wavelength (~340 nm), wherein it switches to the *cis*-conformation **206**.[224] If left in the dark, the *cis*- conformation relaxes thermally back to the *trans*-conformation, or this switch can be photoinduced by irradiation with light at 450 nm (see Figure **52**).

To test whether photoisomerisation was indeed the cause of the two peaks observe by HPLC-MS, we analysed samples of each compound before and after UV irradiation. Samples of nitro-chromanone **181** and amino-chromanone **182** were made up in acetonitrile and analysed by HPLC-MS. Directly after analysis, the sample vials were irradiated at 365 nm in a UV box for 10 minutes, and then analysed by HPLC-MS again; the results are shown below in Figure **53a**&**b**.

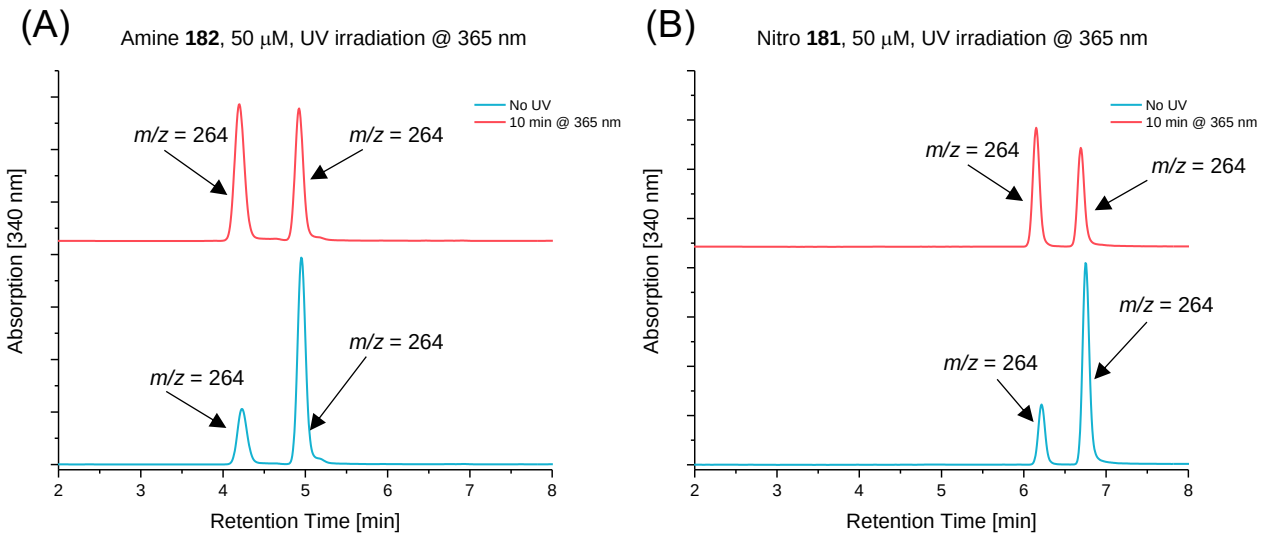


Figure 53: HPLC chromatograms of (A) amino-chromanone **182** and (B) nitro-chromanone **181** before and after UV irradiation at 365 nm. Molecular ion peak masses associated with each peak are annotated.

From these data, it can be clearly seen that irradiation with UV light at 365 nm for 10 minutes is sufficient to induce a change in the areas of each species' HPLC peak. This suggests interconversion between the two species that is induced by light, and thus that some form of photoisomerization between the two species. Attempts were made to isolate each species separately by reverse-phase C-18 semi-preparative HPLC; this was not successful, neither species was retained on the column, and it was therefore not possible to isolate each species to perform NMR analysis. As such, we cannot definitively state whether this apparent photoisomerism is indeed *cis*/*trans* isomerism of the olefin.

5.7 Cellular imaging

The reductase assays discussed in Chapter 5.5 provided no useful evidence of the propensity of either nitro-chromanone **181** or azido-chromanone **204** to be reduced by reductase enzymes under hypoxia or normoxia. These agents were ultimately designed to act as imaging probes, and therefore we wished to test whether they could be used to image cells. We hypothesised that comparison of the nitro and azide compounds under normoxia and hypoxia could indicate whether these compounds were metabolised to the amino-fluorophore **182**, and whether there was an oxygen-dependent difference in this metabolism.

5.7.1 Imaging of amine 182 in cells

We initially tested whether the amino-fluorophore **182** could penetrate cells and be detected by fluorescence microscopy. OE21 cells were treated with 10 μM **182** for 3 hours, then imaged by fluorescence microscopy. Representative images are shown in Figure **54** below.

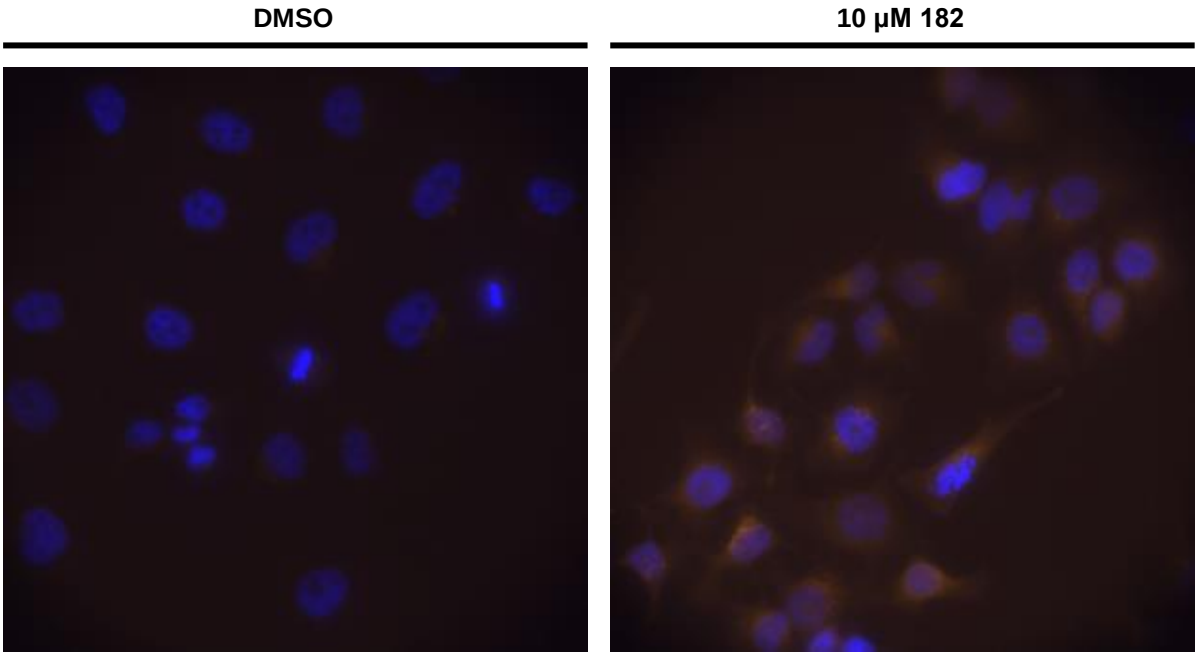


Figure 54: Fluorescence microscopy images of OE21 cells treated with either DMSO (left) or 10 μM amino-chromanone **182** (right, yellow) under atmospheric oxygen tension for 3 hours. Cell nuclei are stained with DAPI (blue).

These initial experiments showed that amino-chromanone **182** could indeed penetrate into cells and be detected *via* fluorescence microscopy.

5.7.2 Imaging of cellular hypoxia

Having demonstrated that amino-chromanone **182** can be detected in cells by fluorescence microscopy, we wished to test whether the nitro- and azido- analogues **181** and **204** were converted to amine **182** in a cellular context, and whether this conversion appeared to be oxygen-dependent.

We treated OE21 cells with either nitro-chromanone **181** or azido-chromanone **204** at 25 μM and incubated them under normoxia (~21% O_2) or anoxia (< 0.1% O_2) for 6 hours, then stained with DAPI and imaged, initially using a Nikon Ti-E fluorescence microscope, with representative images shown in Figure **55**, below.

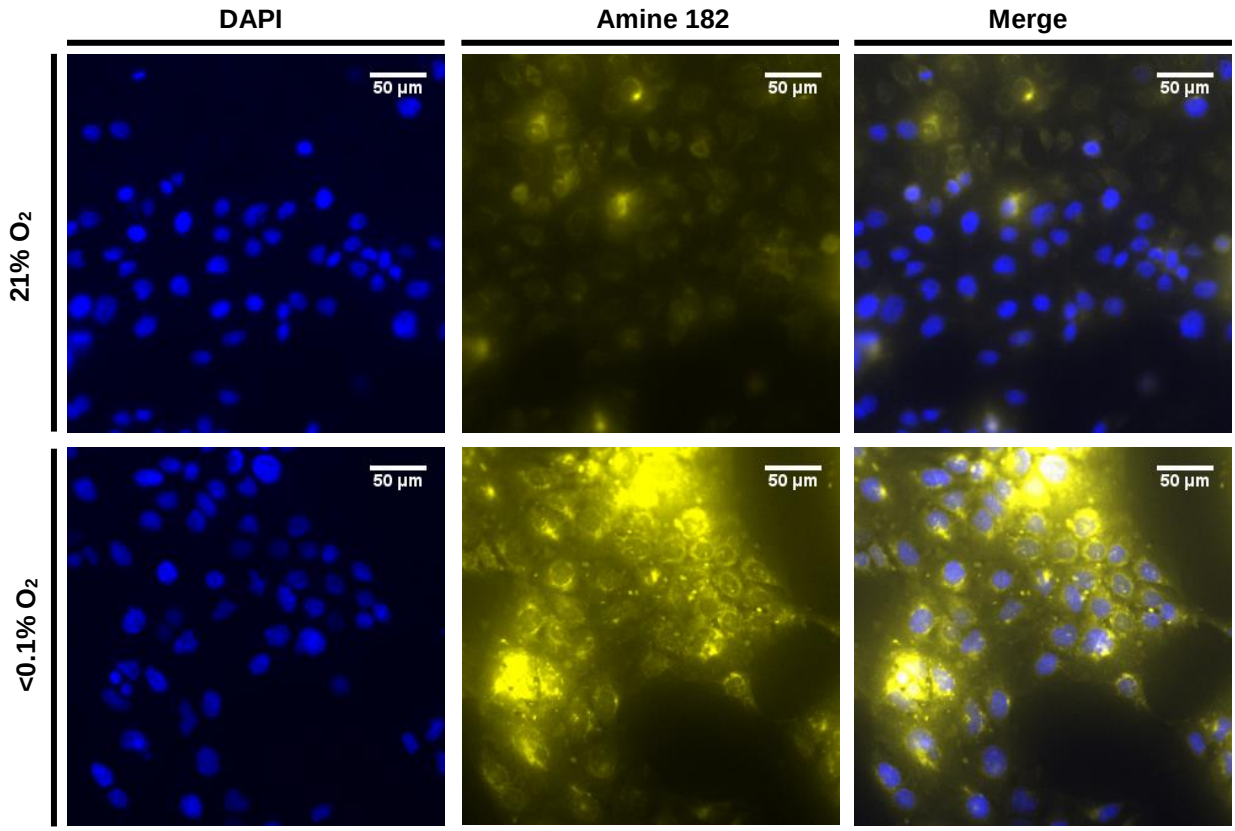


Figure 55: Fluorescence microscopy images of OE21 cells treated with 25 μM nitro-chromanone **181** and incubated at the indicated oxygen tension for 6 hours. Cell nuclei are stained with DAPI (blue), amine **182** is coloured yellow.

Nitro-chromanone **181** appeared to exhibit some background fluorescence under normoxic conditions, suggesting either an oxygen-insensitive metabolism to a fluorescent species or some intrinsic instability in the compound. Cells treated in anoxic conditions, however, appeared to show a significant increase in fluorescent signal. This suggests that metabolism of **181** to the amino-fluorophore **182** is greatly increased under hypoxia, consistent with our hypothesis.

The amine fluorophore **182** has some overlap in its emission spectrum to that of DAPI, the live-cell nuclear counterstain used in these experiments. To separate interference between signal from **182** and DAPI, we repeated this imaging experiment using a confocal microscope, employing linear unmixing to distinguish between the signals for the two fluorophores.

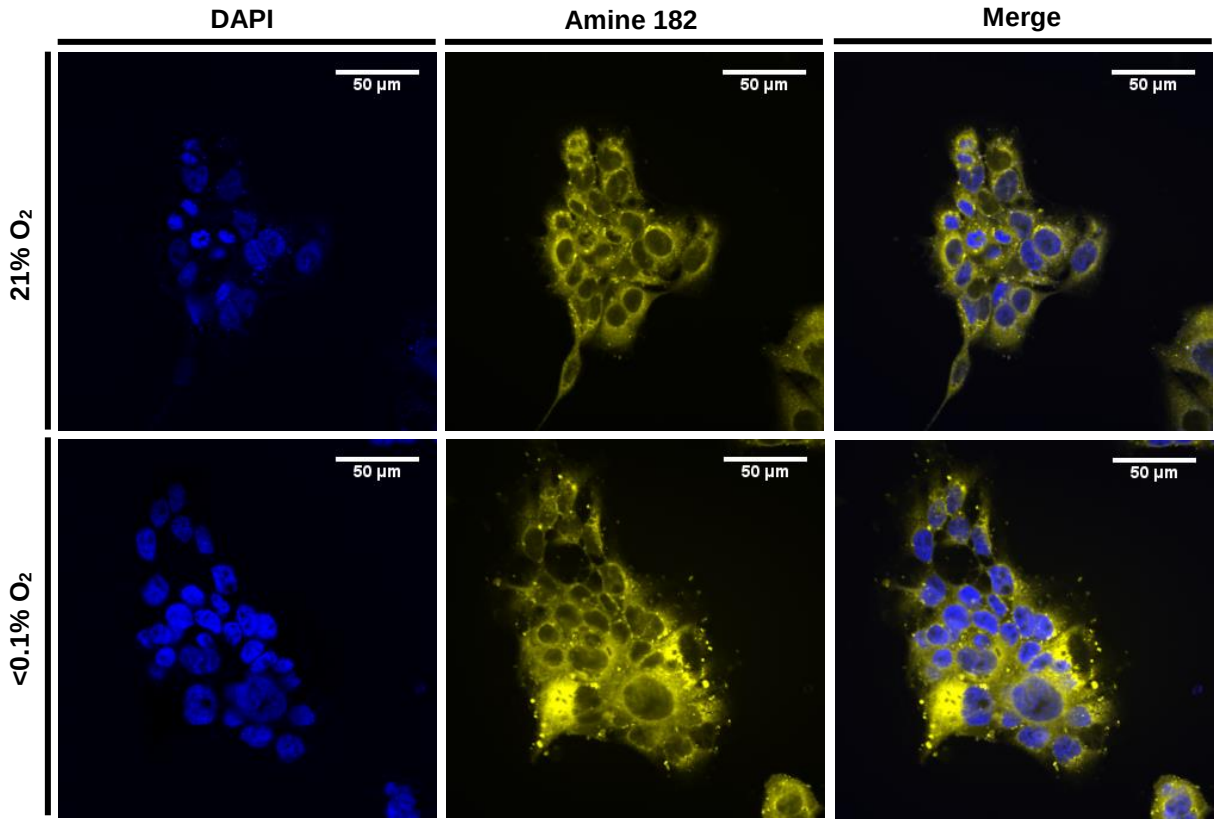


Figure 56: Confocal microscopy images of OE21 cells treated with 25 µM nitro-chromanone **181** and incubated at the indicated oxygen tension for 6 hours. Cell nuclei are stained with DAPI (blue), amine **182** is coloured yellow. Individual channels were created by linear unmixing of the spectra of DAPI-only or amine-only cells.

Disappointingly, confocal microscopy experiments appeared to show that there was only minor difference between the fluorescent signal of **181**-treated cells under normoxia or hypoxia. These experiments were repeated with the azido-chromanone **204** and imaged by both fluorescence and confocal microscopy; representative images are shown in Figure **57**, below.

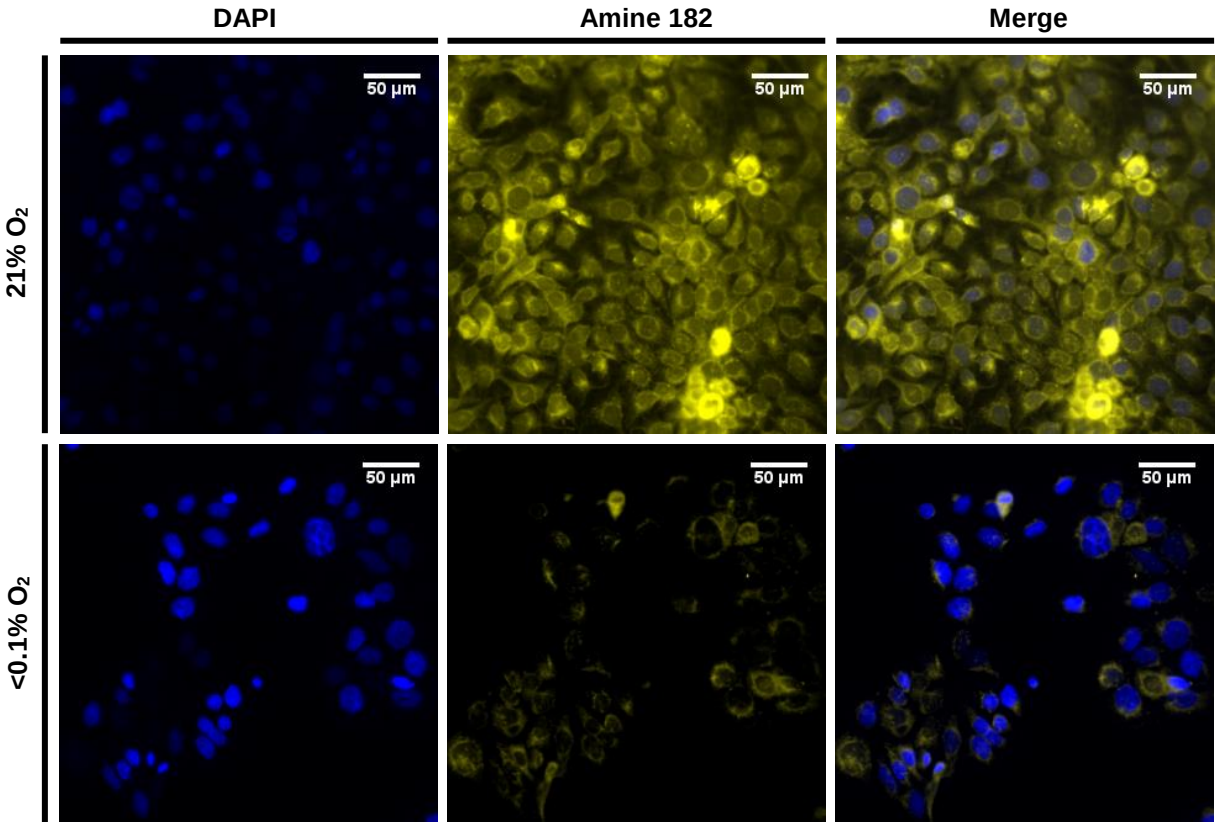


Figure 57: Fluorescence microscopy images of OE21 cells treated with 25 µM azido-chromanone **204** and incubated at the indicated oxygen tension for 6 hours. Cell nuclei are stained with DAPI (blue), amine **182** is coloured yellow.

Fluorescence microscopy images for cells treated with azide **204** appeared to show that, contrary to our expectation, significantly more fluorescence was observed when cells were treated under normoxia than those treated under hypoxia. This suggested either greater metabolic activation of **204** by normoxic cells than hypoxic cells, or some other metabolism in hypoxic cells which destroys the fluorescent species.

Intrigued by this unexpected result, we again repeated these imaging experiments for analysis by confocal microscopy. Linear unmixing was again used to separate the signals of DAPI and amine **181**. It is notable from fluorimetry experiments shown in Chapter 5.4 that azide **204** appears to exhibit strong intrinsic fluorescence in organic solvent and maintains some fluorescence in PBS. This intrinsic signal, when viewed alongside the intrinsic instability of organic azides, led us not to attempt unmixing of background azide signal; unmixing requires control samples which have been treated with a single fluorescent agent, which can have its characteristic spectrum in the medium of interest recorded. This reference spectrum is then used to separate out individual signals from a mixture in an image. Since we could not definitively state that the fluorescent signal from cells treated only with azide **204** under normoxia came from a single component (the azide), and not from amine impurity, unmixing would likely remove some of the amine signal. Nevertheless, we repeated the experiments and analysed the samples by confocal microscopy.

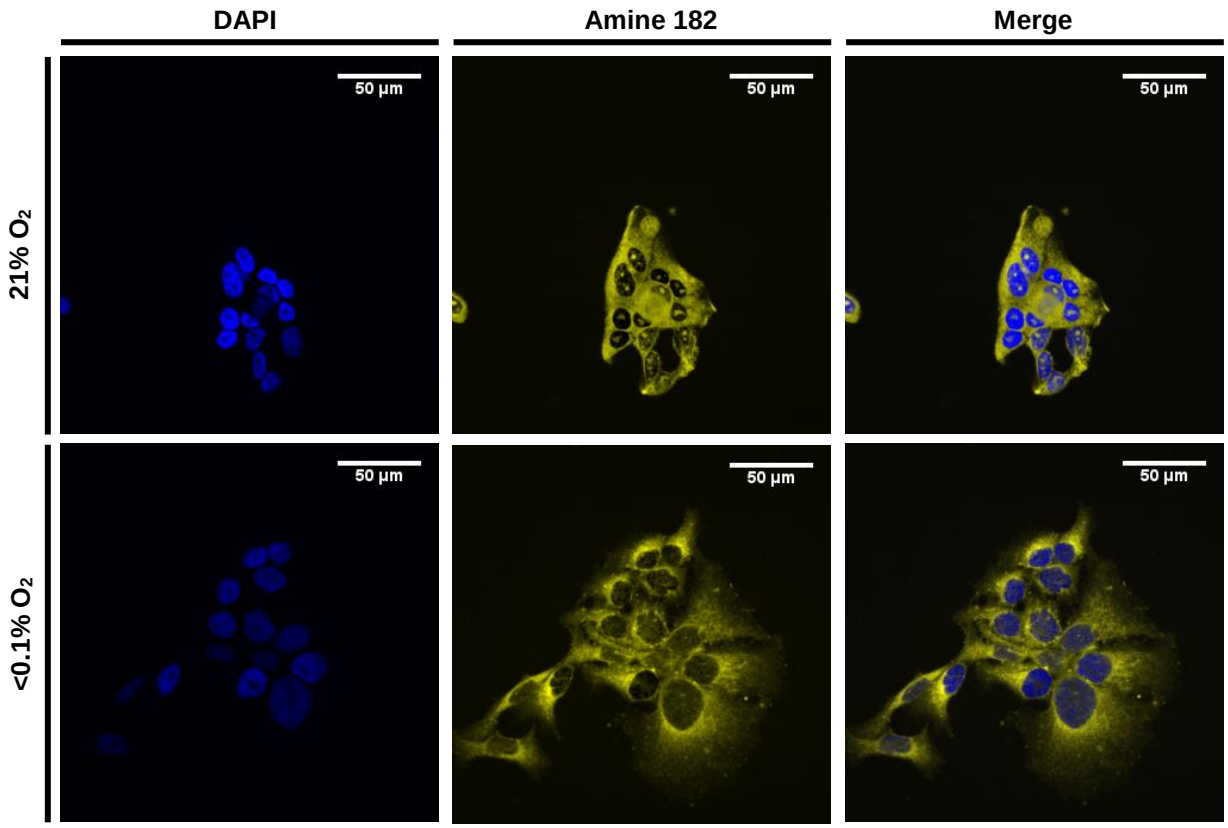


Figure 58: Confocal microscopy images of OE21 cells treated with 25 µM azido-chromanone **204** and incubated at the indicated oxygen tension for 6 hours. Cell nuclei are stained with DAPI (blue), amine **182** is coloured yellow. Individual channels were created by linear unmixing of the spectra of DAPI-only or amine-only cells.

Confocal microscopy experiments appeared to show an increase in fluorescence in cells treated under both normoxia and hypoxia, further suggesting that metabolism of azide **204** is not oxygen-dependent. The cells also appeared to display aberrant morphology, typified by expanded and multi-compartment nuclei. This may indicate that the given concentration of **204** (25 µM) was enough to induce toxicity to these cells, although this was far from definitive.

5.8 Fluorescence-activated cell sorting (FACS) analysis

Microscopy experiments provided somewhat disappointing data, and it appeared that out hypothesis that these chromenone-based molecules could be selectively metabolised under hypoxia was incorrect. We therefore wished to quantify the extent to which nitro-chromenone **181** and azido-chromanone **204** were converted to amino-chromanone **182** in cells, under normoxia and anoxia. We attempted to do this using Fluorescence-Activated Cell Sorting (FACS), a form of flow cytometry which uses the fluorescence properties of cells passing through the cytometer to divide them into different populations and count them.

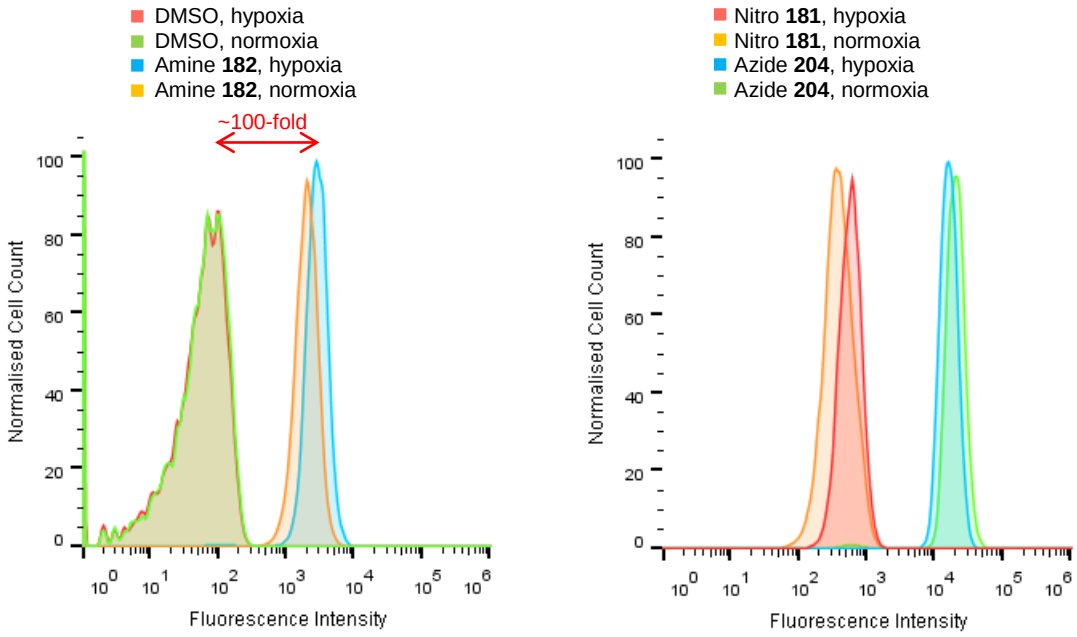


Figure 59: FACS analysis of chromene-based compounds in OE21 cells. (A) Control samples showing the fluorescence intensities of cells treated with DMSO (normoxia, hypoxia) or 25 μM amine fluorophore **182** (normoxia, hypoxia). (B) Samples treated with either 25 μM nitro-chromenone **181** (normoxia, hypoxia) or 25 μM azido-chromanone **204** (normoxia, hypoxia). All samples were incubated for 6 hours.

FACS analysis of OE21 cells treated with 25 μM amine **182** (Figure **59**, left) showed a ~100-fold increase in signal over cells treated with DMSO, indicating that FACS would be a suitable technique for assessing whether **181** or **204** had differential activation between hypoxic and normoxic cells. However, whilst cells treated with nitro

181 showed an increase in fluorescent signal over the DMSO control, there appeared to be little difference between cells incubated under normoxia *vs* hypoxia, suggesting that metabolism of **181** to a fluorescent species was not necessarily oxygen-dependent. Curiously, azide **204** appeared to exhibit greater fluorescence than cells treated with amine **182** alone, and again we observed no significant difference between cells treated under normoxia or hypoxia.

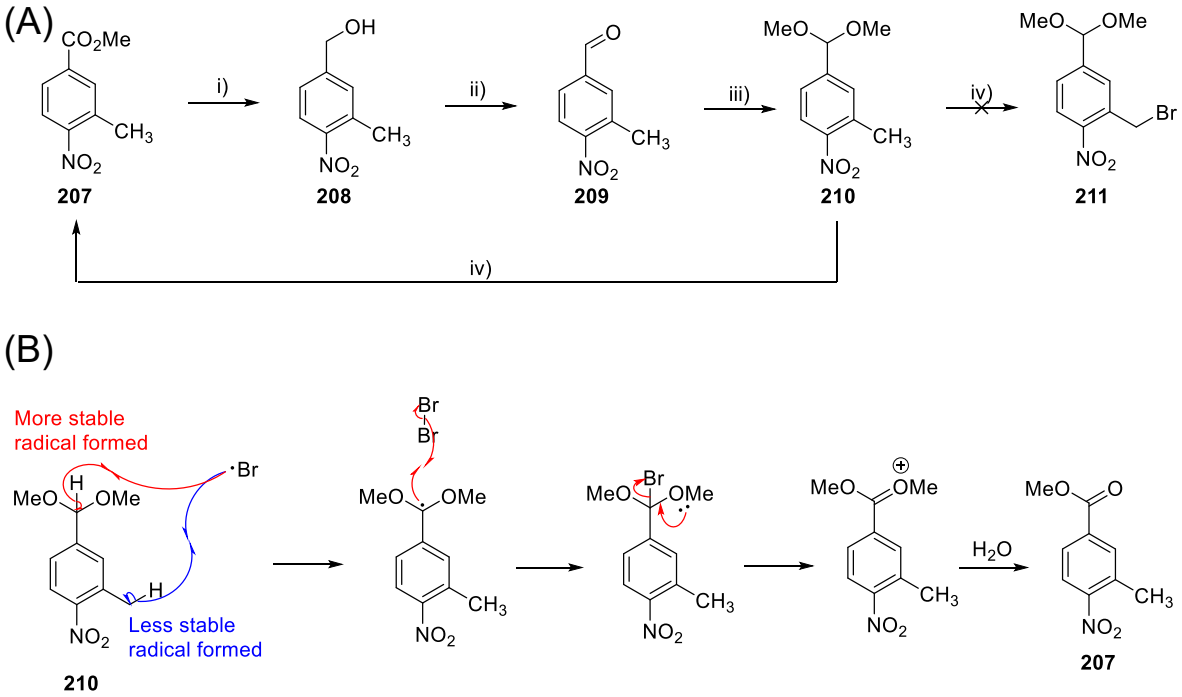
5.9 Synthesis of theranostic fluorophore-drug conjugates

From the data presented above, it appeared that activation of chromanone-based pro-fluorophores occurred both under normoxia and hypoxia, with conflicting evidence as to whether there was a preference for activation under hypoxia over normoxia. Nevertheless, we wished to synthesise a full drug-fluorophore conjugate to see whether this class of pro-fluorophore could be used to successfully deliver a bioactive cargo molecule in an environment-selective manner.

Previous synthetic efforts by Dr Liam O'Connor towards a drug-fluorophore conjugate base upon CH-02 **52** had proven unsuccessful. He attempted to use a nitroaryl starting material bearing 2 carboxylate groups, and then selectively manipulate their oxidation states such that one was at the aldehyde level, whilst the other was at the alcohol level. This proved fruitless; selective reduction of one carboxylate over another was challenging, and despite employing protecting groups he was not able to find compatible reaction conditions to achieve his functionalised molecule.[49]

Because of the difficulties this work had demonstrated, an alternate method was proposed. Rather than manipulating the oxidation state of benzylic C-O bonds, a substituent which is entirely unoxidised (*i.e.* a benzylic methyl group) was instead used. It has been shown that aryl methyl groups can be oxidised using strong oxidants,

and that they can also be directly appended with good leaving groups using radical chemistry to install halides, such as bromine or chlorine.

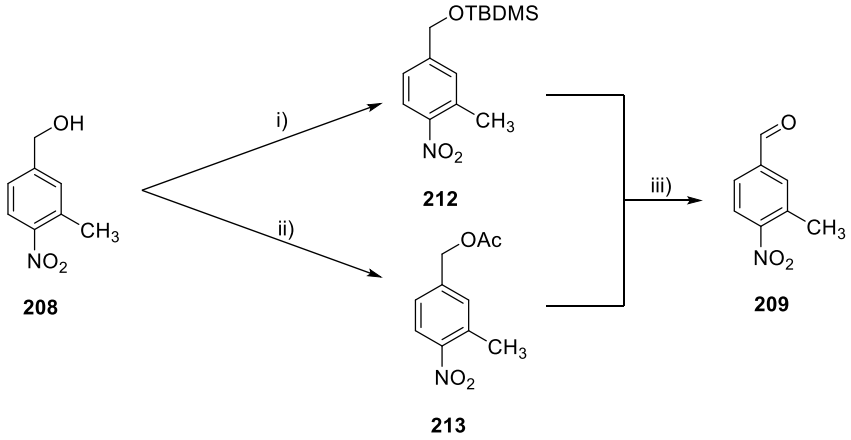


Scheme 62: (A) Attempted synthesis of multifunctionalised benzene. *Reagents and conditions:* i) DIBAL-H (1 M in hexanes), THF, 0 °C, 45 minutes, then RT, 2 hours, 88%; ii) MnO_2, CH_2Cl_2, reflux, 3 hours, 89%; iii) Trimethyl orthoformate, *p*-TSA, MeOH, RT, 24 hours, 87%; iv) NBS, AIBN, CCl_4, 70 °C, 2 hours. (B) Possible mechanism of radical bromination-induded oxidation of dimethyoxyacetal **210**.

Starting material **207** was chosen; it has the desired substitution pattern relative to the aryl nitro group, a benzylic methyl group that is activated towards radical halidation (due to the presence of an *ortho* nitro group), has a carboxylate group whose oxidation state can be manipulated using well-established and robust chemistry, and is inexpensive. Reduction of the methyl ester of **207** to benzylic alcohol **208** using sodium borohydride, followed by partial oxidation to aldehyde **209** under mild conditions using manganese dioxide afforded the desired oxidation state of this group. It was thought that a free aldehyde would not tolerate radical halidation, and that the condensed fluorophore moieties would also have undesired side-reactivity under radical conditions; thus, protecting groups were employed. The dimethoxy acetal **210** was readily synthesised in excellent yield; however, radical bromination did not

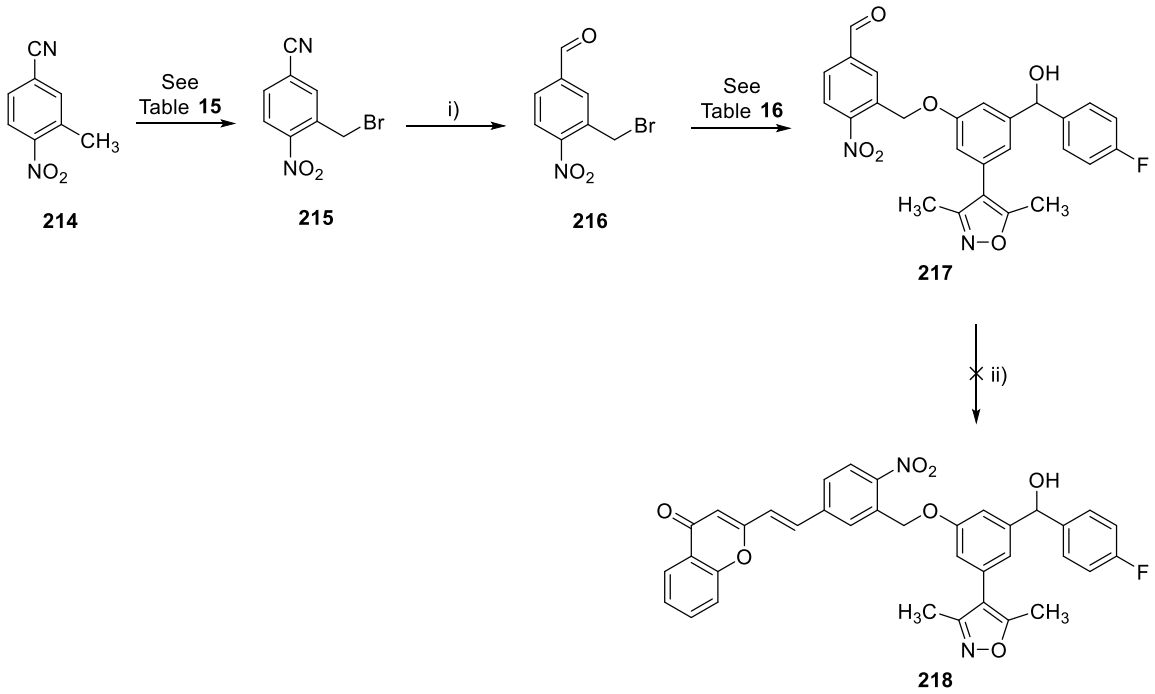
afforded a single bromination of the benzylic methyl group but resulted in oxidation of the acetal to afford a methyl ester, possibly *via* the mechanism shown in Scheme **62b**.

We chose therefore to use other protecting group strategies. Alcohol **208** was protected with both a *tert*-butyldimethylsilyl (TBDMS) group, and as an acetate ester. Again, attempts to radically brominate this species led to loss of the protecting groups and re-oxidation, in these cases to the aldehyde, shown in Scheme **63**.



Scheme 63: Alternative protecting group strategies. *Reagents and conditions:* i) TBDMSCl, Et_3N, CH_2Cl_2, RT, 16 hours, 68%; ii) AcCl, Et_3N, CH_2Cl_2, RT, 1 hour, 82%; iii) NBS, $(PhCO_2)_2$, CCl_4, reflux, 48 hours (**212**) or 45 minutes (**213**).

Given these difficulties, and alternative approach was proposed. The carbon atom of a nitrile group is in a high oxidation state. Nitrile groups are also unreactive towards many reducing agents and are relatively inert to many other types of reaction. It was hypothesised that a nitrile group would be stable to radical bromination chemistry, as well as to oxidative reactions that produce acids and aldehydes from methyl groups. 4-Nitro-3-carboxylbenzonitrile derivatives are not generally commercially available and are not readily synthesised from commercial starting materials; thus, 4-nitro-3-methylbenzonitrile **214** was chosen as the inexpensive starting material.



Scheme 64: Attempted synthesis a bioreductive, fluorogenic prodrug. *Reagents and conditions*: i) DIBAL-H (1 M in *n*-hexane), toluene, 0 °C, 1 h, then RT, 1 h, 14%–60% (n=4); ii) **183**, NaOMe, MeOH, reflux, 24 hours, decomposition.

Radical bromination was first conducting using azobisisobutyronitrile (AIBN) as the radical initiator, heating overnight at 60 °C (Table **15,** entry **1**). This failed to produce any reaction, as determined by ^{1}H NMR spectroscopy. The initiator was changed to benzoyl peroxide, however, heating at 60 °C again did not produce any reaction (Table **15**, entry **2a**). Raising the temperature of the mixture to reflux did produce some discernible change in the crude reaction mixture by ^{1}H NMR spectroscopy, although the products were not isolated (Table **15**, entry **2b**). Heating under reflux overnight (Table **15**, entry **3**) led to a small yield of the monobromo product, but a much more significant amount of the dibromo product after purification. The use of a 300 W UV lamp as a heating source slightly improved yield (Table **15**, entry **4**), and subsequent reactions with shorter reaction times led to further improved yields (Table **15**, entries **5**–**8**).

Table 15: Reagents and conditions for the radical bromination of benzonitrile derivative **214**.

Entry	Reagents	Solvent	T	Time	Yield
1	NBS (1.2 eq.), AIBN (0.1 eq.)	CCl_4	60 °C	16 hours	N.R.
2a	NBS (1.1 eq.), $(PhCO_2)_2$ (0.05 eq.)	CCl_4	60 °C	3 hours	N.R.
2b	As above	CCl_4	80 °C	16 hours	Not purified
3	NBS (1.1 eq.), $(PhCO_2)_2$ (0.1 eq.)	CCl_4	Reflux	24 hours	23% monobromo, 40% dibromo
4	NBS (1.1 eq.), $(PhCO_2)_2$ (0.1 eq.)	CCl_4	Reflux (300 W UV)	6 hours	33% monobromo, 20% recovered SM
5	NBS (1.4 eq.), $(PhCO_2)_2$ (0.1 eq.), HBr (0.05 eq.)	CCl_4	Reflux (300 W UV)	16 hours	Mostly dibromo (^{1}H NMR)
6	NBS (2 eq.), $(PhCO_2)_2$ (0.1 eq.)	CCl_4	Reflux (300 W UV)	4 hours	32% monobromo, 19% dibromo
7	NBS (1.4 eq.), $(PhCO_2)_2$ (0.05 eq.)	CCl_4	Reflux (300 W UV)	24 hours	24% monobromo, dibromo N.D.
8	NBS (1.2 eq.), $(PhCO_2)_2$ (0.1 eq.)	CCl_4	Reflux	4 hours	41% monobromo, dibromo N.D.

Brominated compound **215** was then treated with di-*iso*-butylaluminium hydride (DIBAL-H) solution, a bulky reducing agent which is known to reduce nitrile groups to aldehydes (rather than further reducing them to alcohols) *via* co-ordination of the aluminium species to the nitrile nitrogen, forming an imino-aluminate species upon single hydride transfer. This species is stable to further reduction but is readily hydrolysed by the addition of water (most often in aqueous workup). The use of aqueous sodium potassium tartrate solution to both quench the reaction and scavenge aluminium salts appeared to give low yields (14%), possibly due to alkylation of the product benzylic bromide onto the free hydroxyls of tartaric acid under basic conditions. Quenching with 0.1 M aqueous hydrochloric acid solution provided improved yields (50%–60%).

We then attempted to alkylate **184** with benzyl bromide **216** under mild, basic conditions in polar organic solvent. This proved challenging; alkylation appeared to take place slowly, but both starting materials also appeared to decompose over time. Conditions are given in Table **16**, overleaf.

Table 16: Attempted alkylation reactions for appending multifunctional trigger **216** to ligand **217**.

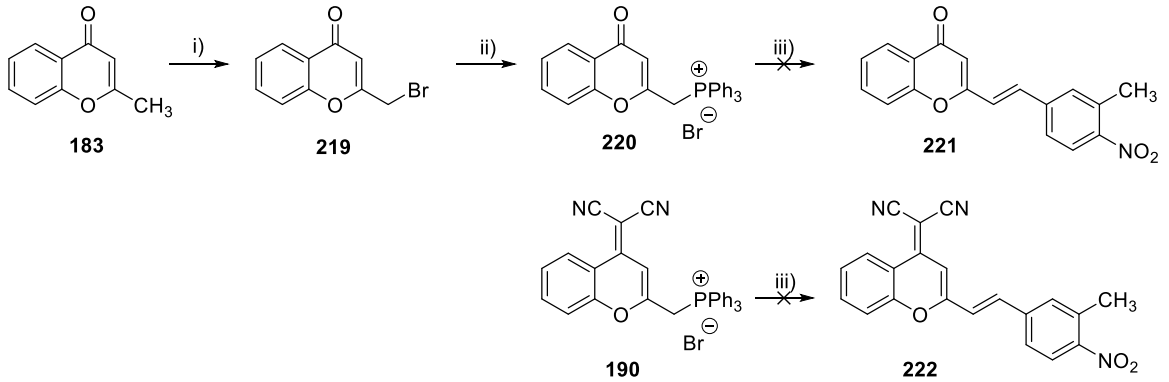
Entry	Base	Solvent	T	Time	Yield
1a	K_2CO_3	DMF	0 °C	1 hours	N.R.
1b	K_2CO_3	DMF	RT	20 minutes	Decomposed
2	K_2CO_3	Acetone	RT	17 hours	Decomposed
3	K_2CO_3	Acetone	RT	3 hours	<10% (unclean)
4	Cs_2CO_3	Acetone	RT	2 hours	18% (unclean)

Initially we attempted alkylation in highly polar solvent (DMF), at 0 °C to avoid decomposition of reactants. Whilst we did not observe significant decomposition, no product appeared to form at all. Increasing the temperature to RT led to decomposition of both starting materials (Table **16** entries **1a** and **1b**). Switching to acetone, a less polar solvent, reduced the apparent rate of decomposition and appeared to show some slow formation of product by TLC. However, this reaction was left to go to completion, which resulted in decomposition of what appeared to have been a product spot (Table **16**, entry **2**). Repeating the reaction for a shorter period resulted in some formation of what appeared to be a product spot. This was, however, isolated in very low yield and with remaining impurities, after 3 attempts at purification by normal-phase column chromatography (Table **16**, entry **3**). A final attempt, using similar conditions but with Cs_2CO_3 in place of K_2CO_3 as a base, resulted in isolation of a small amount of what appeared to be product, but again this could not be sufficiently purified by silica gel chromatography (Table **16**, entry **4**).

With a small amount of impure material in hand, we attempted the final condensation reaction with chromenone core **183** using our standard conditions of refluxing sodium methoxide in methanol. This, however, failed to produce the desired compound, and the aldehyde intermediate **217** again decomposed over time (Scheme **64**).

The strategy described above involved synthesis of a nitroaryl “core”, which would first be alkylated onto the ligand **184** and the coupled to chromenone core **183**

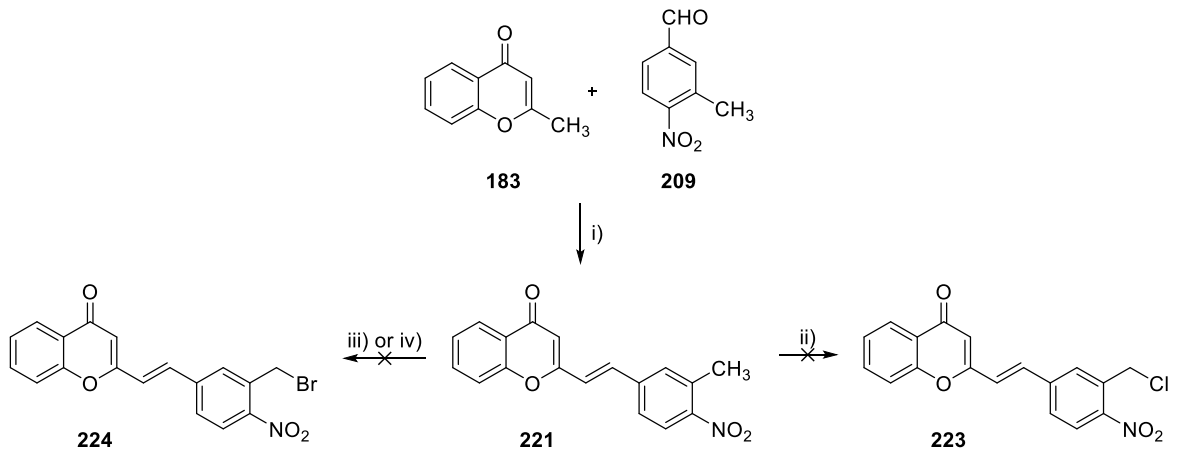
in the final step. We elected to approach from the other direction, namely coupling the nitroaryl core to the chromenone **183** first, then alkylation of the ligand onto the *ortho*-benzylic handle last.



Scheme 65: Attempted Wittig reactions to form pro-fluorophores with benzyl handles. *Reagents and conditions*: i) NBS, AIBN, CCl_4, reflux, 9 hours, 25% yield (+19% dibromination); ii) PPh_3, toluene, reflux, 16 hours, 68% yield; iii) **209**, KHMDS (0.7 M in toluene), distilled THF, 0 °C, 1.5 hours, then RT, 18 hours, N.R.

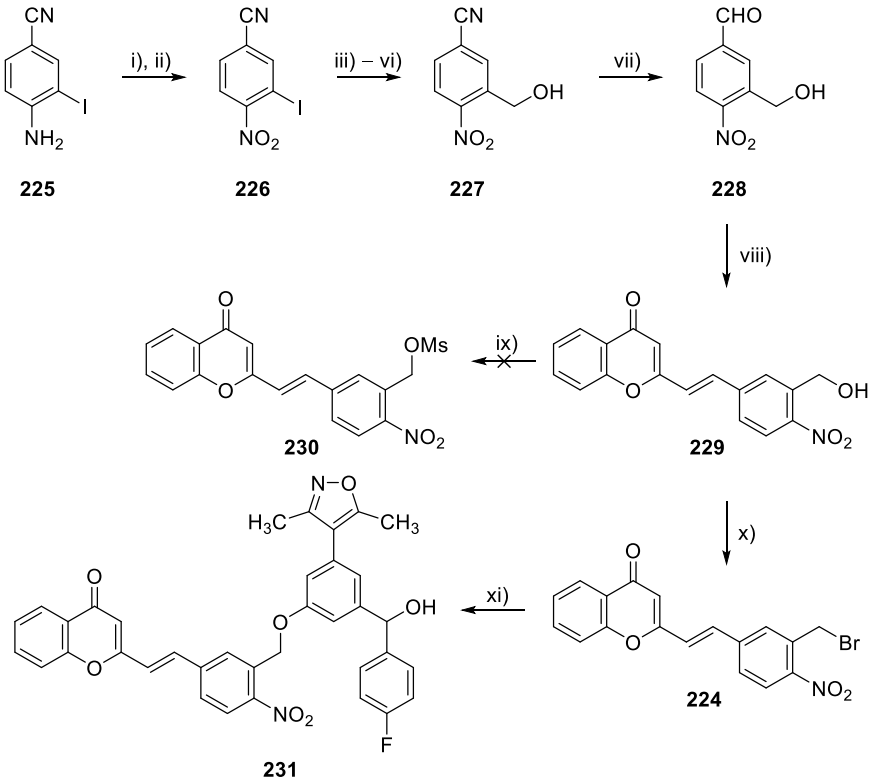
The triphenylphosphonium salt **190** had been previously synthesised while exploring an alternate route to analogues of CH-02 **52**, using Wittig chemistry. We therefore synthesised the chromenone analogue **220** in reasonable yield, *via* radical bromination of the vinyl methyl group to give **219**, followed by displacement with triphenylphosphine (Scheme **65**). Attempts at performing Wittig reactions between both **220** and **190**, and the functionalised aldehyde **209** were conducted in parallel. Potassium hexaethyldisilamide (KHMDS) was used as the base, and the reactions were performed at 0 °C, however, both proved unsuccessful, likely for the same reason of poor ylide nucleophilicty as we had previously speculated.

Witting chemistry had proven unsuccessful in our hands for this class of molecules, and we there returned to the condensation chemistry that had proven successful in the synthesis of the original fluorophore molecules. Accordingly, chromeone **183** was subjected to a condensation reaction with functionalised benzaldehyde **209**, which afforded the corresponding nitro-chromenone **221** in good yield (Scheme **66**).



Scheme 66: Attempted synthesis of a functionalised nitro-chromenone. *Reagents and conditions*: i) NaOMe, MeOH, reflux, 3 hours, 61–73% yield (n=2); ii) LiHMDS (1 M in THF), THF, 0 °C, 1 hour, then NCS, 0 °C → RT, 1 hour, N.R; iii) NBS, AIBN, CCl_4, reflux, 22 hours, N.R; iv) NBS, $(PhCO_2)_2$, CCl_4, reflux, 5 hours, N.R.

We next attempted to convert the benzylic methyl group to functional handle with which we could form an alkylating agent. Radical bromination of vinylic and benzylic methyl groups had proven successful for us previously, and so we attempted radical bromination of **221** using a common set of reagents. Use of either AIBN or benzoyl peroxide under reflux in carbon tetrachloride did not, however, afford the desired product **224**, but rather a complicated reaction mixture without any apparent benzylic peaks by ^{1}H NMR analysis. As an alternative, we attempted direct deprotonation of the benzylic methyl group by use of the strong, non-nucleophilic base LiHMDS. Addition of LiHMDS to a suspension of **221** in THF caused a colour change (yellow to deep green), suggesting anion formation. Addition of recrystalized *N*-chlorosuccinimide (NCS, an electrophilic source of Cl^+), however, did not afford the corresponding benzyl chloride **223**.



Scheme 67: Synthesis of drug-profluorophore conjugate **231**. *Reagents and conditions*: i) $NaNO_2$, H_2SO_4, H_2O, 0 °C, 1 hour; ii) $NaNO_2$, $CuSO_4$, H_2O, reflux, 2 hours, 41% over 2 steps; iii) PhMgCl (1 M in 2-MeTHF), THF, −40 °C, 10 minutes; iv) anhydrous DMF, −40 °C → RT, 1 hour; v) H_2O, RT, 20 minutes; vi) $NaBH_4$, EtOH, RT, 1.5 hours, 80% over 4 steps; vii) DIBAL-H (1 M in hexanes), toluene, 0 °C, 1 hour, 45% yield; viii) **183**, NaOMe, MeOH, reflux, 34–56% yield; ix) see Table **17**; x) 48% aqueous HBr, 90 °C, 5 hours, 81% yield; xi) Cs_2CO_3, DMF, RT, 5 hours, 22% yield.

We turned to an alternative method, based the chemistry of Knochel,[225] in which electron-deficient aryl halides are converted to benzylic alcohols *via* the use of Grignard exchange. Initially we took amino-functionalised aryl iodide **225** and performed a Sandmeyer nitration reaction. The amine was first converted to the corresponding diazonium salt *via* treatment with aqueous sodium nitrite in acidic solution. The diazonium salt was then transferred to a hot solution of concentrated sodium nitrite, with the presence of $CuSO_4$ as a catalyst. Whilst this reaction was not high yielding, it could be carried out on a large scale (~4.5 g), providing ample amounts of the intermediate **226**. We next applied the Knochel conditions to **226**, following the literature procedure.[225] Treatment of **226** with phenylmagnesium chloride formed the Grignard reagent rapidly. Initially we wished to treat this intermediate with

para-formaldehyde to directly access the benzyl alcohol **227**. This reaction did not occur, seemingly due to the lack of solubility of solid *para*-formaldehyde. Reactions conducted either cold (0 °C), at RT or 40 °C did not yield any product, and so we sought a different electrophilic source of a benzyl alcohol. We first used anhydrous DMF as a formylating agent, which we then quenched with water to hydrolyse any dimethyliminium salt formed. The aldehyde intermediate was isolated, indicating to us that the Grignard exchange-formylation step was successful. Repeating the exchange reaction, we did not isolate further aldehyde intermediate, but rather treated the product with sodium borohydride *in situ*, affording the desired benzyl alcohol **227** in excellent yield over 4 steps in one pot.

Subsequently we treated benzyl alcohol **227** with DIBAL-H solution, producing aldehyde **228** in reasonable yield. This aldehyde was readily coupled to chromenone core **183** to give **229** in excellent yield using standard base-catalysed condensation conditions. Attempts to alkylate this species by first forming the mesylate **230** failed, and a list of conditions are given in Table **17**, below. We attribute this lack of reactivity to the poor solubility of **229**.

Table 17: Reagents and conditions used to attempt to form mesylate **230**.

Entry	Reagents	Solvent	T	Time	Yield
1	MsCl, DIPEA	CH_2Cl_2	0 °C	2 hours	N.R.
2	Ms_2O	Pyridine	RT; 50 °C	1 hour; 45 minutes	N.R.

In place of a mesylate alkylating agent, we chose to synthesise a benzylic halide instead. Following conditions previously used by Dr Liam O'Connor,[49] heating of **229** in 48% aqueous HBr displaced the benzylic hydroxyl group with a bromide, affording alkylating agent **224** in excellent yield. Pleasingly, alkylation of **184** with **224** occurred readily, and the full conjugate **231** was synthesised in 22% yield after chromatography.

5.10 Photophysical characterisation of drug-fluorophore conjugate

With drug-fluorophore conjugate **231** in hand, we wished to characterise its UV-Vis absorbance and fluorescence emission spectra. A crucial part of the design of our theranostic agents is that they do not exhibit any fluorescence in their unmetabolised state, and only become fluorescent once metabolised under hypoxia. Equally, it is useful to determine whether the conjugate's absorption spectra has any overlap with the emission spectra of the fluorophore – this can lead to the self-quenching phenomenon.

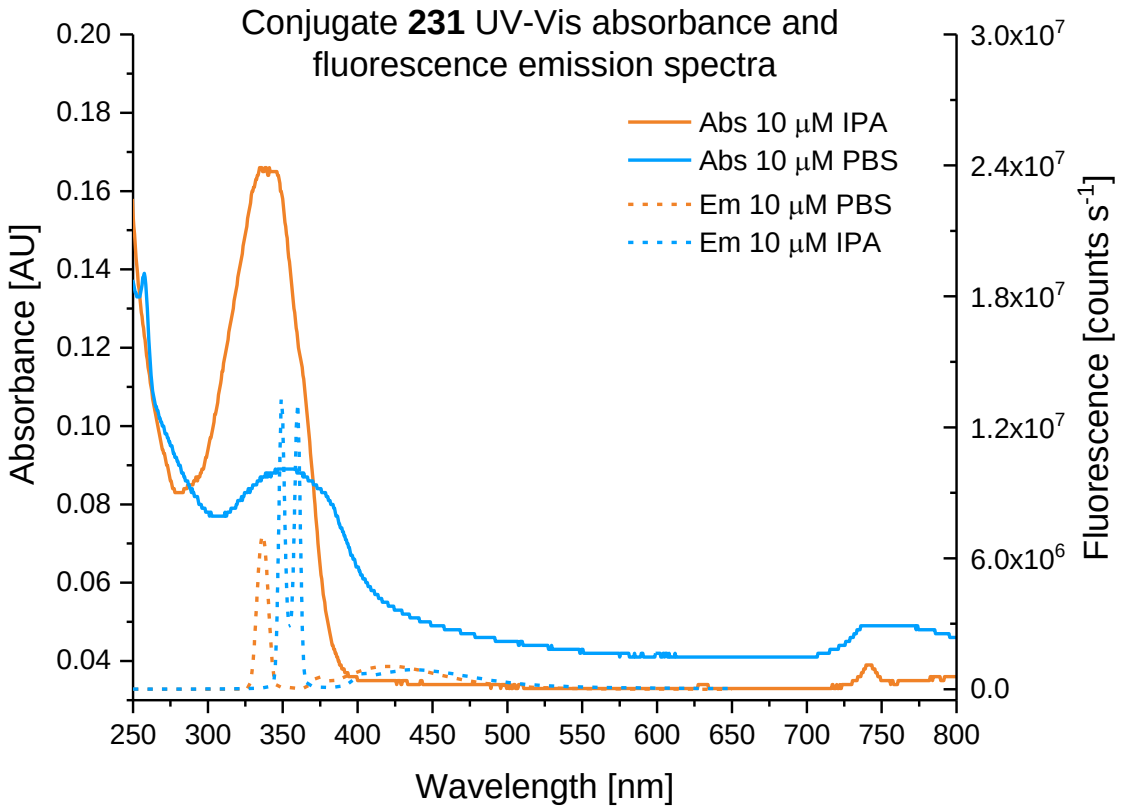


Figure 60: UV-Vis absorbance (solid lines) and fluorescence emission (dashed lines) spectra for drug-fluorophore conjugate **231**. Data were recorded at 10 μM in either *iso*-propyl alcohol (IPA, orange) or phosphate buffered saline (PBS, blue) at pH 7.4. Absorbance spectra are shown as solid lines, fluorescence emission spectra are shown as dashed lines. Emission spectra were obtained by exciting at the absorbance maxima (340 nm in IPA, 354 nm in PBS).

Absorbance spectra indicated no particularly strong absorbance for the conjugate **231** in the emission range of the fluorophore, with absorbance maxima at 340 nm and 354 nm in IPA and PBS, respectively. Interestingly, the conjugate seemed

to exhibit a small amount of intrinsic fluorescence in both IPA and PBS, with emission maxima at 420 nm and 440 nm, respectively. These were not particularly strong, however, and far from the emission wavelengths of the fluorophore, and thus conjugate emission was not considered a problem for cell imaging experiments.

5.11 Enzymatic reduction studies of drug-fluorophore conjugate 231

As before, we wished to assess conjugate **231** in its ability to be a substrate for oxygen-sensitive reductase enzymes, namely cytochrome p450 reductase (CPR). We therefore subjected **231** to a CPR assay, comparing effects between normoxia and hypoxia.

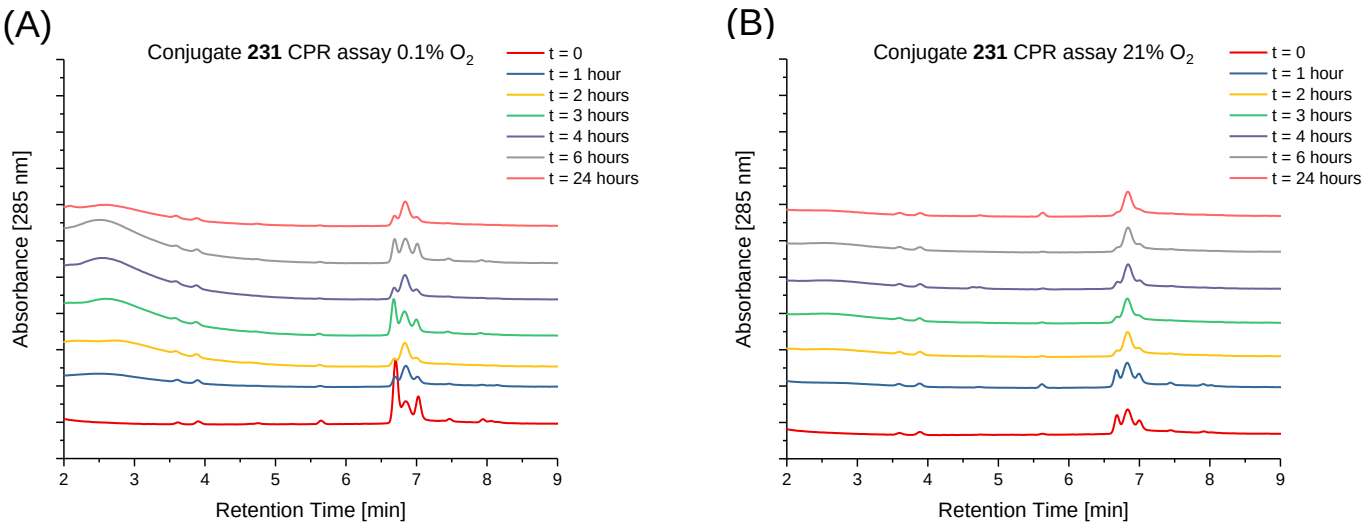


Figure 61: Cytochrome p450 reductase assay of conjugate **231** under (A) anoxic (<0.1% O_2) or (B) normoxic (21% O_2) conditions.

As with the nitro and aminochromanone compounds **181** and **182**, conjugate **231** appeared as two peaks by HPLC. We hypothesised that this was also due to the photoisomerisation properties of the nitrochromanone. Both peaks (RT = 6.70 min and 7.03 min) were consumed during the assay, although no clear increase in the peak for ligand **184** appeared (RT = 3.55 min). No other significant peaks appeared which could be identified as metabolites by mass spectrometry, suggesting that **231** was simply unstable. This was concurrent with our observations during synthesis of **231** – after column chromatography and purification as a single component by TLC, the isolated

solid changed colour over time. Further TLC analysis would indicate the appearance of a small, close-running impurity, suggesting some form of degradation. Moreover, there appeared to be no significant difference between the compound's behaviour under normoxia or anoxia in the cytochrome p450 reductase assay.

Conjugate **231** therefore appeared to be unstable, and we could not adequately assess whether it could act as a bioreductive prodrug platform.

5.12 Concluding remarks and future work

In this chapter we have shown the development of a family of fluorogenic compounds and made efforts towards applying them as theranostic agents.

Initially, we attempted to synthesise analogues of the previously studied hypoxia-activated fluorophore CH-02 **52**, to which we wished to append biologically active cargo molecules. This synthesis proved challenging, and we were not successful in developing NIR-emissive theranostic agents based upon CH-02 **52**. However, we identified a related chromenone-based scaffold, and developed a synthesis of the fluorescent amino form **182**, the non-fluorescent nitro form **181**, and the intermediately fluorescent azido form **204**, giving us a direct analogue of CH-02.

We examined the photophysical properties of these chromenone compounds, found that the amine was fluorescent in the yellow region of the visible spectrum, and that the nitro analogue was non-fluorescent, with the azide being somewhat intermediate. CPR assay results suggested that the nitro compound was consumed rapidly, and we could not account for all the missing compound; this may be due to aggregation, given its poor solubility. Interestingly, it appeared that the seemingly "pure" nitro and amino analogues **181** and **182** had some impurity, which we hypothesised was a mixture of *cis* and *trans* isomers – we used UV irradiation

experiments to demonstrate that this may indeed be the case and may be triggered by photoisomerisation.

We then tested the aminochromenone **182** as an imaging agent in cells, and pleasingly found that it could be imaged in cells by fluorescence microscopy. The nitro and azido analogues were then tested, which gave us mixed results. Fluorescence microscopy appeared to show that the nitro had some small amount of metabolism under normoxia, but that this was greater in hypoxia. However, confocal microscopy seemed to demonstrate that there was little difference between normoxia and hypoxia. By contrast, the azido fluorophore **204** appeared to exhibit greater fluorescence in cells incubated under normoxia, than those under hypoxia. This result was seen in both fluorescence and confocal microscopy experiments.

To try and quantify the difference in fluorescent signal between treated cells under normoxia and hypoxia, we used Fluorescence-assisted Cell Sorting (FACS) analysis. Whilst we could readily separate control populations (cells treated with DMSO *vs.* treated with amine **182**), we saw no discernible difference between nitro-treated cells under normoxia or hypoxia. Unusually, not only was there little apparent difference between cells treated with azido-treated cells under normoxia or hypoxia, but these cells appeared to be more fluorescent than those treated with amine fluorophore **182** alone. We can only speculate on the reason for this, however this may be due to the intrinsic fluorescence of the azide. Flow cytometers do not filter single emission wavelengths, but rather ranges of wavelengths. It may be that the emission grating of the flow cytometer does not wholly cover the spectral emission range of amine **182** but does more adequately cover azide **204**.

Having shown that fluorophores of this scaffold appeared to be activated in cells, we then developed a synthetic route which allowed us to assemble a full

drug-profluorophore conjugate, **231**, bearing a bioreductive group, a fluorogenic moiety and a cargo ligand that we wished to be released. We subsequently tested the conjugate in a CPR assay, and whilst the results were inconclusive, it appeared that none of the ligand **231** was released.

The future direction of this work is to use alternative fluorophore scaffolds to assemble theranostic agents. The route developed to key aldehyde intermediate **228** is critical to this: the new NIR fluorophore developed in Chapter 4, for example, is also synthesised *via* condensation with an aryl aldehyde, and so too is CH-02. We believe it is eminently possible to, with slight modifications, use this chemistry to assemble other drug-fluorophore conjugates for use as theranostic agents.

Moreover, future work is not limited to either the fluorophore scaffolds, nor bioactive ligands detailed herein. Had conjugate **231** proved successful in delivering a cargo, we would have modified the cargo to be more drug-like; either a late-stage clinical candidate with a therapeutic relevance to us (*e.g.* a Chk1 inhibitor), or a clinically-approved agent with which there would be clear advantages in targeting to hypoxia. Such molecules would then be progressed towards *in vivo* models of cancer, using their fluorogenic properties *ex vivo* to assess delivery and distribution in 2D and 3D tissue culture models.

Chapter 6
Towards an ^{18}F-PET imaging probe for BET proteins

6.1 Introduction

6.1.1 Dual-modal imaging

All imaging modalities have advantages and disadvantages; some only provide structural information with no detail on biological function. Others may be highly penetrant of tissue but lacking in spatial or temporal resolution, such as MRI, PET or SPECT (Single Photon Emission Computed Tomography). By contrast, high-resolution techniques such as fluorescence may lack sufficient penetration depth for deep tissue and whole-body imaging. Despite each technique often requiring a different imaging agent, the imaging signals are not necessarily mutually exclusive. For example, there is no interference between PET and CT (computed tomography) signals, and thus PET-CT is a fast-growing multi-modality imaging technique that is routinely performed in major cancer centres. Since the goal of any medical imaging technique is to provide radiographers and clinicians with the greatest amount of information to better inform clinical decision-making, it is therefore advantageous to develop agents which can provide complementary imaging signals.

6.1.2 Positron Emission Tomography (PET) imaging

Positron Emission Tomography (PET) is a widely-used clinical imaging technique, utilised for imaging of conditions such as Alzheimer's and Parkinson's disease,[104] cardiac conditions such as myocardial infarction and ischemia,[105,106] and many different forms of cancer.[107,108] A detailed discussion of PET imaging can be found in Chapter 1.4.1.3. We chose PET imaging a complimentary modality to fluorescence imaging, since it has excellent tissue penetrance and widespread clinical utility.

6.1.3 The BET family of bromodomain-containing proteins

Bromodomain-containing proteins are a class of epigenetic "reader" proteins. Bromodomains are bundles of 4 right-handed α-helices which form a binding pocket; this pocket recognises acetylation marks on specific lysine residues of many different proteins, including acetylation of histone protein tails.[226] They are involved in the recruitment of protein complexes that control the transcription of many crucial genes, and their aberrant function is implicated in many different diseases, including some cancers and immunoinflammatory diseases.[227] Of these proteins, one of the most studied groups is the so-called Bromodomain and Extra-Terminal (BET) family of tandem bromodomain-containing proteins, which includes BRD2, BRD3, BRD4, and the testes-specific BRDT.

Complexes containing BRD4 are involved in the driving of certain cancers including acute myeloid leukaemia (AML).[218] Moreover, the protein produced by fusion of the *NUTM1* and *BRD4* or *BRD3* genes *via* chromosomal translocation has been found to cause NUT midline carcinoma (NMC), a rare form of cancer with almost no chance of survival, mean survival of less than 1 year, and limited palliative treatments.[228] Inhibition of the acetyl-lysine recognition function of these proteins – particularly BRD4 – exhibits a powerful cellular phenotype. (+)-JQ1, one of the original and most-studied BET inhibitors, has shown promising results in treating several cancers, including NMC,[229] *MYC*-driven cancers,[218] and pancreatic ductal adenocarcinoma (PDAC, in combination with histone deacylase inhibitors).[220]

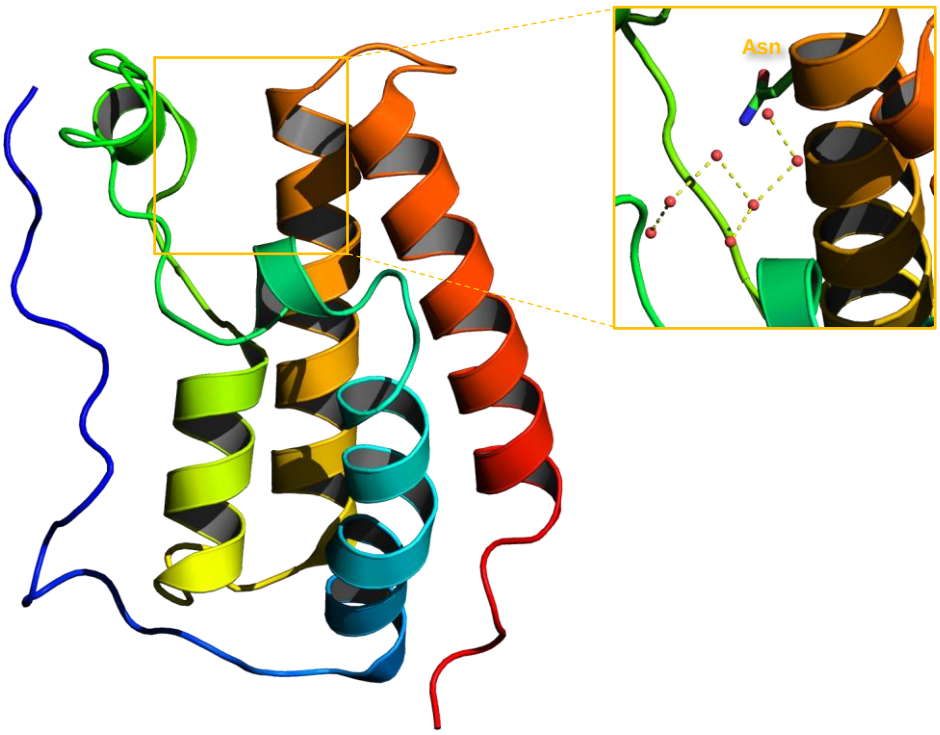


Figure 62: X-Ray crystal structure of *apo*-BRD4(1) (PDB: 4lyi),[230] with a detailed view of the acetyl-lysine binding site (inset). The network of water molecules (red spheres) in the binding site are shown as yellow dashed lines. The conserved asparagine, which acts to recognise acetyl-lysine, is shown as coloured sticks. Image created using PyMOL.[231]

6.2 Compound design

Our research group has a prior interest in bromodomain-containing proteins.[221,223,232–234] We have previously developed a series of ligands for the BET proteins, based on the 3,5-dimethylisoxazole scaffold as an acetyl-lysine mimetic (Figure **63**).[221] We, and others, have shown that inhibition of BRD4 has a profound cell-killing effect in several cancer cell lines.[221] Given our previous experience with BET ligands, and their demonstrated cell-killing ability in cancer, we chose these dimethylisoxazole-based ligands as biologically-active component of our proof-of-concept compounds.

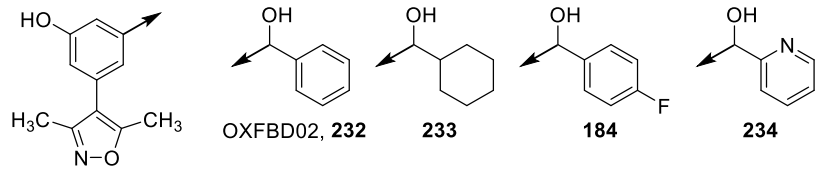


Figure 63: Selected BET bromodomain ligands based on the 3,5-dimethylisoxazole acetyl-lysine mimetic.[221] IC_{50} values were determined using an AlphaScreen™ assay.[235]

To target these ligands to hypoxia we again chose to use fluorogenic, hypoxia-activated bioreductive moieties. The use of a hypoxia-responsive bioreductive moiety, appended at a critical attachment point, should abrogate protein binding and fluorescent signal in normoxia. Upon metabolism in hypoxia the parent compound would be released, giving environment-specific activity. The metabolised group would become fluorescent, switching on one of the imaging signals.

To provide dual-modal imaging, we envisaged molecules which could incorporate both a PET radionuclide and a fluorogenic group. Our chosen radionuclide was ^{18}F, since its inactive sister isotope ^{19}F is commonly incorporated into drugs and other small molecules during SAR studies (^{19}F being isosteric with ^{1}H). Moreover, Gouverneur and coworkers have recently developed methodology to allow late-stage radiofluorination of drugs and drug-like molecules.[236] This method uses pinacolboronate esters as the functional handle for fluorination, with substoichiometric amounts of a copper(II) salt and a nucleophilic source of $^{18}F/^{19}F$. Finally, SAR studies around our dimethylisoxazole ligands had shown that fluorine atoms were well tolerated on the aryl ring which occupies the so-called 'WPF shelf' of the bromodomain binding pocket, and thus the ^{18}F compound should have comparable binding affinity to its ^{19}F analogue **184**.[221]

Several fluorogenic groups are known; for these studies we envisaged the use of the 6-nitroquinoline moiety.[49,50] This group acts as a hypoxia-sensitive bioreductive

group, which released a fluorescent species upon metabolism under hypoxia.[50] A summary of the molecular design is given in Figure **64**.

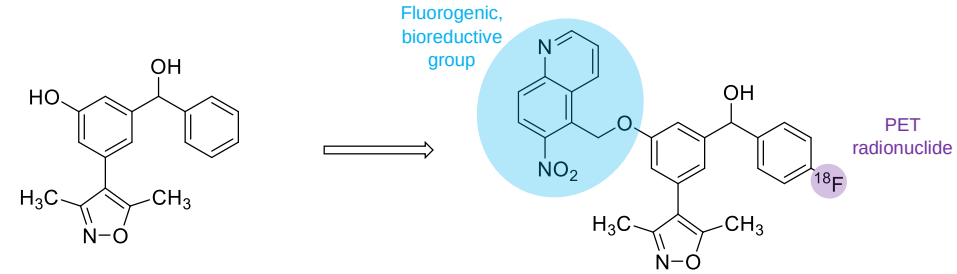


Figure 64: Design of BET ligands for dual-modal hypoxia imaging.

When designing prodrugs, choice of attachment point is critical. Functionalisation of the chosen part of the molecule must have at least one of two effects; it must either disrupt a crucial bonding interaction with its protein target (dramatically reducing affinity), or it must induce a steric clash with protein. This steric clash should prevent the molecule adopting a favourable binding conformation to the protein, also significantly reducing affinity.

For the dimethylisoxazole-based ligands, we chose to block the phenolic hydroxyl group. The X-ray crystal structure of the parent ligand OXFBD02 **232** bound to the first bromodomain of BRD4 [BRD4(1), Figure **65**] shows that the phenolic hydroxyl points into the narrow ZA channel, forming a hydrogen bond with a network of conserved water molecules.[222,223] We hypothesised that attaching a large moiety here would both remove the hydrogen-binding interaction, as well as occupying too much space to fit into the channel. By contrast, the secondary hydroxyl group points away from the protein into surrounding solvent. Studies of both enantiomers of these molecules showed no difference in binding affinity for BRD4(1), and thus we concluded that blocking this position would also have no effect and fail to make a prodrug.

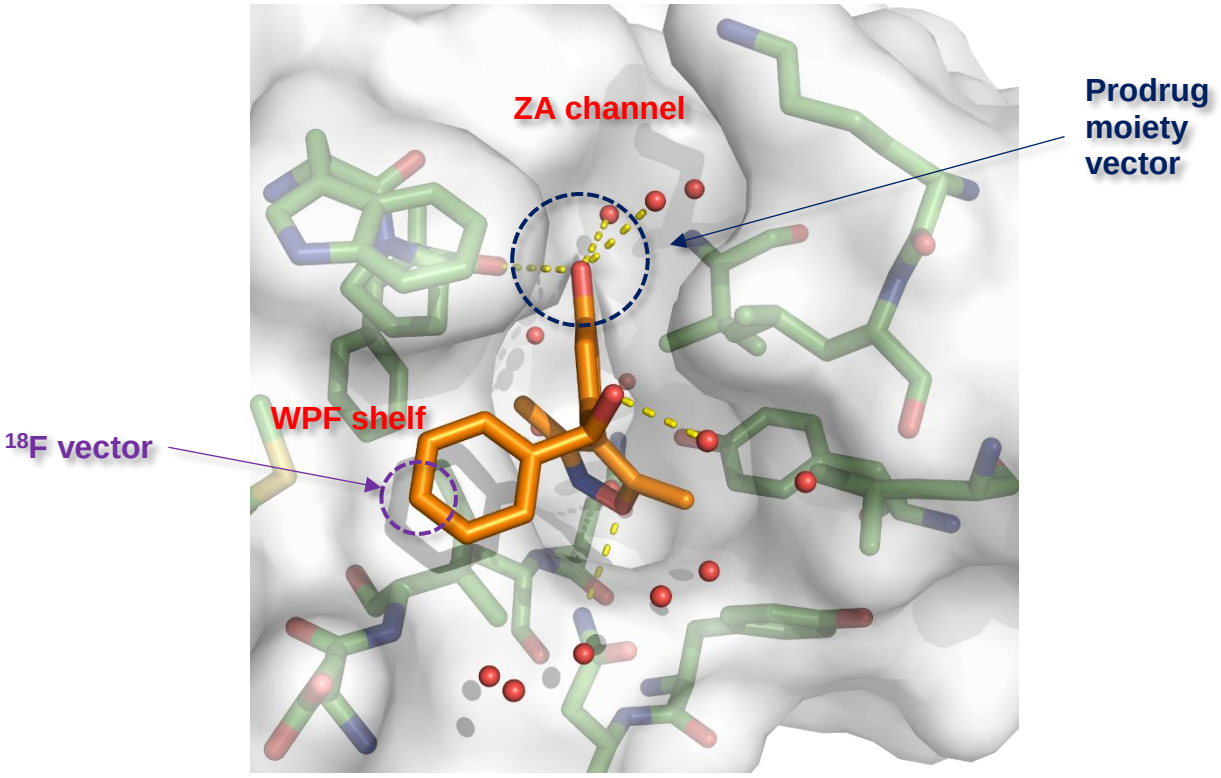
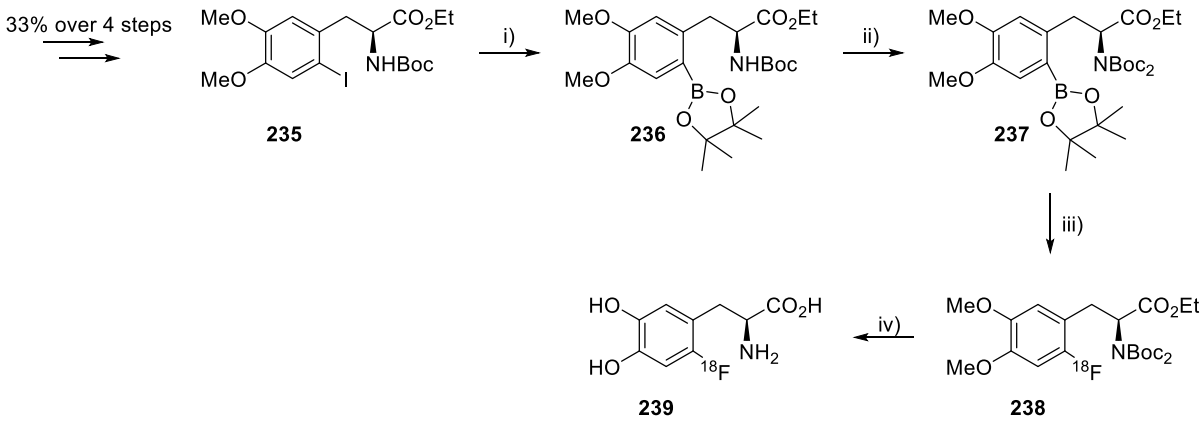


Figure 65: X-Ray crystal structure of OXFBD02 **232** (carbon = orange, oxygen = red, nitrogen = blue) bound to the first bromodomain of BRD4 [BRD4(1), PDB: 4j0s].[223] Local water molecules are represented as red spheres. Polar contacts are shown as dashed yellow lines. Only binding site residues are shown for clarity (carbon = green, oxygen = red, nitrogen = blue, sulfur = yellow). Image created using PyMOL.[231]

6.3 Development of a radiosynthesis-compatible route to ^{18}F BET probes

To produce radiofluorinated analogues of OXFBD02 **232**, the synthesis of the molecule needed to be designed in such a way that (radio)fluorination occurred as late as possible in the synthesis. Ideally, radiofluorination occurs in the final synthetic step, or as the penultimate step followed by a rapid removal of protecting groups. Several late-stage fluorination methods have been developed, including methods from the groups of Ritter,[237,238] Sanford,[239–241] and others.[242] One such method employs a Chan-Lam-type coupling, in which an aryl-, vinyl- or alkyl-pinacolboronate ester [B(pin)] is converted to the corresponding fluoride in the presence of an F^- source and a simple Cu(II) catalyst.[236] This method was very effective for late-stage installation of ^{19}F in drug molecules and for ^{18}F labelling, as demonstrated by their synthesis of 6-[^{18}F]Fluoro-L-DOPA, shown in Scheme **68**.

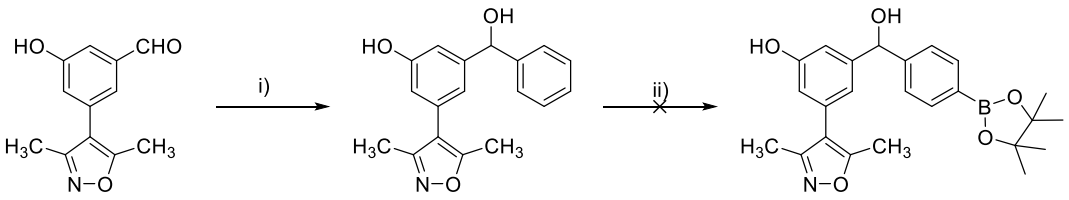


Scheme 68: Gouverneur's synthesis of [18F]F-L-DOPA.[236] Intermediate **235** was synthesised using their previously reported method.[242] *Reagents and conditions*: i) B_2pin_2, $Pd(dppf)Cl_2{\cdot}CH_2Cl_2$, KOAc, DMF, 80 °C, 18 hours, 62%; ii) $(Boc)_2O$, 4-DMAP, Et_3N, MeCN, RT, 18 hours, 53% yield; iii) $[Cu(OTf)_2(py)_4]$, $[^{18}F]KF/K_{222}$ (3 GBq), DMF, 110 °C, 20 min, RCY = 55% ± 23% (*n* = 2); iv) 57% aq. HI, 130 °C, 10 min, >95% conversion, *ee* > 99%.

6.3 Synthesis

6.3.1 Ir-catalysed C-H borylation

To install the required pinacolboronate ester moiety, a few strategies were explored. A current topic of interest in synthetic organic chemistry is C-H activation, and its potential to allow for late-stage functionalisation of complex molecules. One such class of C-H activation is C-H borylation, of which several Ir-catalysed reactions exist. It was envisaged that an Ir-catalysed C-H borylation reaction could be employed to directly functionalise OXFBD02 **232** and its analogues. Such C-H borylations have been demonstrated to occur often with excellent regioselectivity, to proceed under mild conditions and with low catalyst loading, as well as being tolerant of other functional groups. Consequently, OXFBD02 was synthesised from intermediate **240**, and Ir-catalysed C-H borylation was attempted, as shown in Scheme **69**.



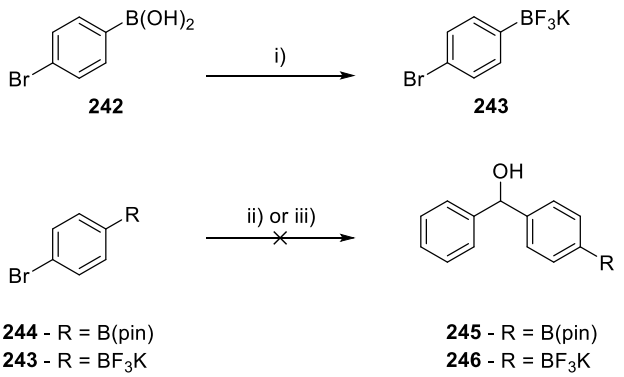
240 **232** **241**

Scheme 69: Attempted direct C-H borylation of OXFBD02 **232**. *Reagents and conditions:* i) Phenylmagnesium bromide (3 eq., 1 M in THF), THF, 0 °C, 1 hour, then RT, 45 minutes, 66% yield; ii) HBPin (1.5 eq.), $[Ir(OMe)(cod)]_2$ (0.25 mol%), 2,3,7,8-tetramethyl-1,10-phenanthroline (0.5 mol%), THF, 50 °C, 2 days, N.R.

This borylation proved unsuccessful, despite monitoring by TLC and LRMS analysis over the course of 2 days. Given this result, along with other unsuccessful borylations on other substrates using similar methodology (see Chapter 2.3.4), it was decided that an alternate method should be explored.

6.3.2 Direct Grignard reaction with pendant boronate species

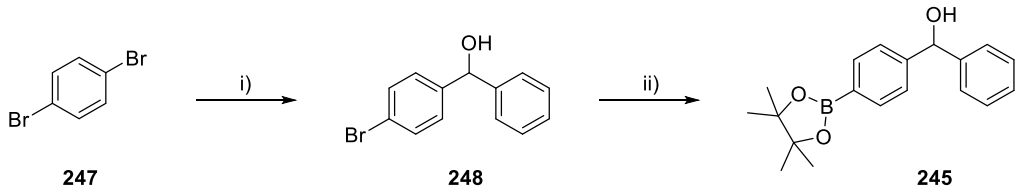
The synthesis of OXFBD02 **232**, and many of its analogues, involves addition of organomagnesium salts to the aldehyde intermediate **240**. We hypothesised that this strategy could be conducted using an organomagnesium reagent with the boronate group pre-installed, using an aryl bromide as a starting material. Given that pincolboronate esters are not always stable to some reaction conditions, such as those of the Grignard reaction,[243] the potassium trifluoroborate analogue **243** was also synthesised from the corresponding boronic acid **242** in excellent yield (Scheme **70**).[244] To test this hypothesis, attempts to form Grignard reagents with both pinacolboroate ester **244** and trifluoroborate salt **243** were made, followed by trapping with benzaldehyde. Neither attempt was successful, and it was noted that the solid magnesium did not appear to completely dissolve over the course of the Grignard reagent formation. This indicates that the substrates were not forming Grignard reagent under these conditions.



Scheme 70: Test reactions to install a synthetic handle suitable for (radio)fluorination. *Reagents and conditions* i) KHF_2 (5 eq.), H_2O/MeOH (1:2), 0 °C → RT, 1 hour, 99%; ii) **244** (2.2 eq.), Mg (2 eq.), I_2 (cat.), THF, reflux, 3.5 hours, then → 0 °C, benzaldehyde, THF, 0 °C → RT, 45 minutes, N.R.; iii) **243**, *n*-BuLi (1 eq.), THF, −78 °C, 1 hour, then benzaldehyde, −78 °C, 10 minutes, then −78 °C → RT, 30 minutes, then KHF_2 (5 eq., 4.5 M in H_2O), RT, 10 minutes, N.R.

6.3.3 Miyaura borylation

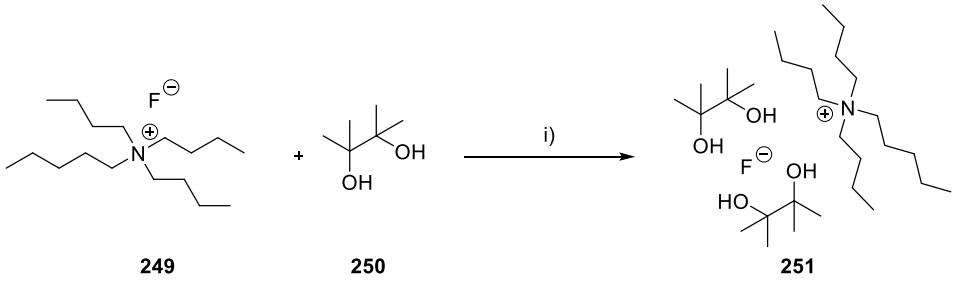
An alternative to a Grignard reagent is an organolithium reagent, which can often be made *via* lithium-halogen exchange between an organolithium base, such as *n*-BuLi, and an aryl, alkyl or vinyl halide. 1,4-Dibromobenzene **247** was chosen as a test substrate, along with benzaldehyde. Mono-lithiation of **247**, using *n*-BuLi, followed by addition of benzaldehyde afforded the nucleophilic addition product **248**. Subsequent Miyaura borylation using bis(pinacolato)diboron [$B_2(pin)_2$] and the common catalyst Pd(dppf)Cl_2 afforded the desired pinacolboronate ester compound **245** in good yield (Scheme **71**).



Scheme 71: Model system for installation of pinacolboronate ester. *Reagents and conditions* i) 1,4-Dibromobenzene (1.1 eq.), *n*-BuLi (1.11 eq.), THF, −78 °C, 15 minutes, then benzaldehyde (1 eq.), −78 °C, 1 hour, 74%; ii) $B_2(pin)_2$ (1.5 eq.), KOAc (3 eq.), Pd(dppf)Cl_2·CH_2Cl_2 (0.1 eq.), 1,4-dioxane, reflux, 16 hours, 55%.

Nucleophilic fluorination to incorporate ^{18}F often uses K^{18}F as the fluorinating reagent, since its production in a radiochemical laboratory is more facile than other, more complex reagents. However, for the purposes of testing nucleophilic

fluorination conditions using ^{19}F it is often easier to employ TBAF(pin)$_2$ **251** as the fluoride source. TBAF(pin)$_2$ is commercially available but was also readily synthesised from TBAF **249** and pinacol **250** in good yield (Scheme **72**).

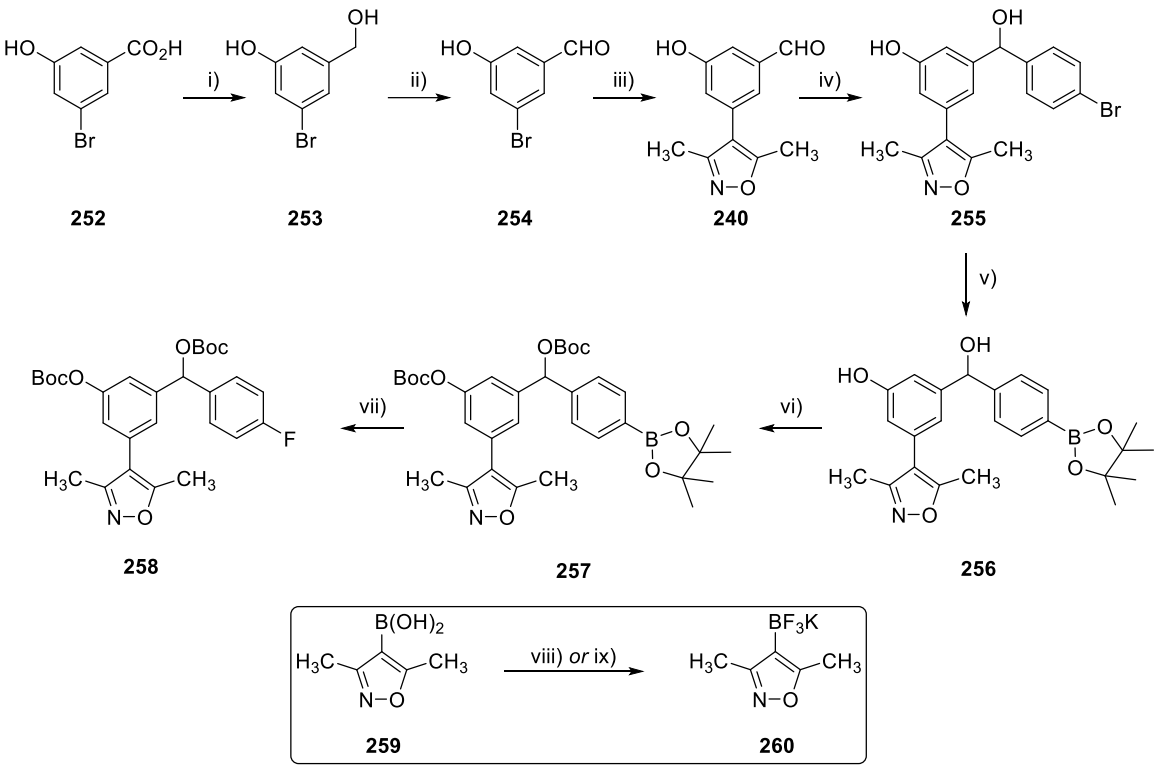


249 **250** **251**

Scheme 72: Synthesis of fluorinating agent TBAF(pin)$_2$ **251**. *Reagents and conditions* i) n-Hexane, reflux, 2 hours, 66%.

6.3.4 Synthesis of fluorination precursor

With promising conditions to install the pinacolboronate handle identified, synthesis of the OXFBD02-fluorination precursor **257** was conducted (Scheme **73**). Key intermediate **240** was synthesised *via* reduction of acid **252** to alcohol **253**, partial oxidation to aldehyde **254**, and subsequent Suzuki coupling with trifluoroborate salt **260**. The 4-bromophenyl ring was then successful installed *via* mono-lithiation of 1,4-dibromobenzene **247** and organolithium addition to afford **255**, which then underwent Miyaura borylation to afford pinacolboronate ester compound **256**. Since free hydroxyl groups have been shown to be detrimental to the nucleophilic fluorination conditions (Dr Sean Preshlock, *personal communication*), the hydroxyls of **256** were protected with *t*-butyl carbonate (Boc) groups in excellent yield, giving the diBoc-protected compound **257.** Test fluorination reactions were conducted, which resulted in incorporation of ^{19}F into the product **258**, as determined by ^{19}F NMR.



Scheme 73: Synthesis of a fluorinated BET inhibitor precursor **258**. *Reagents and conditions*: i) BH_3·THF (1 M in THF), THF, 0 °C → RT, 3 hours, 93%; ii) MnO_2, $CHCl_3$ 70 °C, 2 hours, 69%; iii) **254**, $Pd(OAc)_2$, Na_2CO_3, RuPhos, EtOH, 80 °C, 5 hours, 78%; iv) 1,4-Dibromobenzene, *n*-BuLi, THF, −78 °C, 10 minutes, then **240**, THF, −78 °C → RT, 1 hour, 81%; v) $Pd(dppf)Cl_2$, KOAc, 1,4-dioxane, 85 °C, 16 hours, 76%; vi) $(Boc)_2O$, 4-DMAP, CH_2Cl_2, 0 °C → RT, 1 hour, 69%; vii) $[Cu(OTf)_2(py)_4]$, TBAF(pin)$_2$, DMA, 110 °C, 20 min ~20% F^- incorporation by ^{19}F NMR; viii) KHF_2, H_2O, MeOH, 0 °C → RT, 10 minutes, 84%; ix) KF (10 M in H_2O), MeCN, RT, 40 minutes, then L-(−)-tartaric acid (1.37 M in THF), RT, 1.5 hours, 74%.

6.3.4 Radiolabelling-compatible fluorination studies

As discussed previously, successful radiolabelling is foremost determined by speed of reaction and radiochemical incorporation in that time. Reactions must produce a useful quantity of radioactive material rapidly, so that the product may be sufficiently purified for experimental or clinical dose without undergoing significant decay. To determine whether radiofluorination-like reactions could be conducted on derivatives of OXFBD02 **232**, labelling-relevant fluorination conditions were applied to test substrate **257**. A sample of **257** was dissolved in DMA, along with copper(II) catalyst $[Cu(OTf)_2(py)_4]$ and fluoride source **251**, and the mixture was heated at 110 °C for 20 minutes. Reaction monitoring by ^{19}F NMR showed that the corresponding fluorinated product had indeed been formed and internal standard 4-fluoroanisole **261**

indicated ~20% of total fluoride had been incorporated. These promising results indicate that ^{18}F can indeed be incorporated into derivatives of OXFBD02 to produce PET imaging agents.

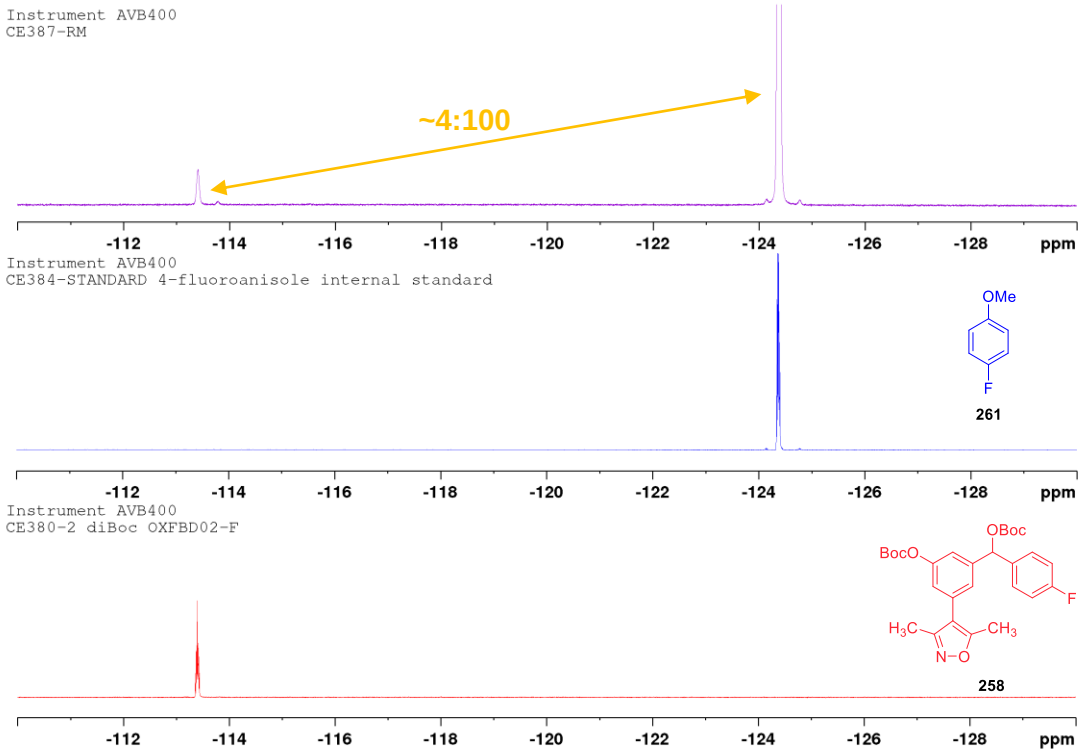


Figure 66: Cold (^{19}F) fluorination of precursor **257** using radiofluorination-compatible conditions. Incorporation of ^{19}F is quantified using 4-fluoroanisole **261** as an internal standard for integration. A reference sample of product **258** was synthesised using previously developed chemistry. *Reagents and conditions:* i) 4-Fluoroanisole **261** (1 eq.), $[Cu(OTf)_2(py)_4]$ (1.33 eq.), $TBAF(pin)_2$ **251** (0.2 eq.), DMA, 110 °C, 20 minutes, approx. 20% incorporation of total ^{19}F.

The ^{19}F fluorination experiment indicated that **257** was a suitable substrate for radiofluorination. Since biological activity has already been demonstrated for the ^{19}F analogue, we concluded that this would make a suitable proof-of-concept molecule for a dual-modal theranostic agent.

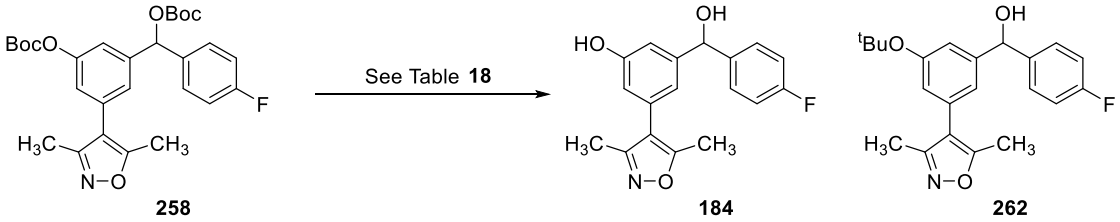
6.3.5 Radiosynthesis-compatible removal of Boc protecting groups

Our chosen radiofluorination conditions required the substrate's hydroxyl groups to be protected. As with the radiolabelling step, any subsequent synthetic steps must

be rapid and selective, and ideally require no extra purification steps. We therefore wished to find conditions to remove the Boc protecting groups in a rapid and selective manner, ideally with reagents which could be added direction to the radiofluorination mixture.

Perhaps the most common reagent used to remove a Boc group is 2,2,2-trifluoroacetic acid (TFA), a strong organic acid that is also volatile. TFA is often used to rapidly remove Boc groups by the mechanism shown in Scheme **74** and can then be removed *in vacuo* along with solvent, and hence we chose to start with this reagent.

It should be noted that the mechanism of Boc deprotection using a Brønsted produces a *t*-butyl cation as a side product. This is known to be problematic, since nucleophilic functional groups may attack this cation and become alkylated with a *t*-butyl group. In the case of OXFBD02 analogues, we anticipated that either the phenolic or alcoholic hydroxyl groups could become alkylated to give the *t*-butyl ether. To avoid this, the use of a cation scavenger additive was explored – in this case, triisopropylsilane (TIPS-H) was chosen. The test reaction is shown in Scheme **75**, and the conditions are given in Table **18**.



258 **184** **262**

Scheme 74: Test reaction to determine ideal deprotection conditions. Reagents and conditions are given in Table **18**.

Table 18: Reagents and conditions used during optimisation of Boc deprotection for radiosynthesis.

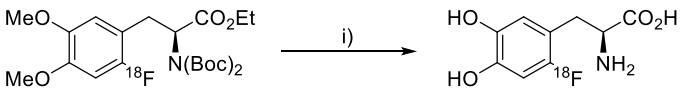
Entry	Reagent	Additive	Solvent	Conc of substrate (M)	Temp.	Time (min)	Conversion **184**	Conversion **262**
1	TFA	TIPS-H	CH_2Cl_2	0.12	RT	60	~5%	~25%
2	HCl (4 M in dioxane)	-	Dioxane	0.32	Reflux	60	~10%	~60%
3	HCl (4 M in dioxane)	-	Dioxane	0.50	Reflux	60	~15%	~65%
4	HCl (4 M in dioxane)	TIPS-H	Dioxane	0.075	90 °C	60	0%	~85%
5	57% $HI_{(aq.)}$	-	DMA	0.15	130 °C	20	Mixture of products	
6	57% $HI_{(aq.)}$	-	DMA	0.15	50 °C	20	SM stable	
7	57% $HI_{(aq.)}$	-	DMA	0.15	90 °C	5	Majority **184**. 44% isolated yield	

For entry **1**, monitoring by TLC indicated that very little of the desired product **184** was formed over a 1-hour timecourse. A new, low polarity product appeared to form by TLC, and this was thought to be the *tert*-butyl ether by-product **262**, although ^{1}H NMR analysis could not definitively confirm this. In the final dual-modal ligand the phenolic hydroxyl will be protected by the bioreductive group, so this is unlikely to cause a problem. *t*-butylation of the secondary alcohol may still prove problematic, however, hence the need for a deprotection that does not form *t*-butyl by-products. Moreover, significant amounts of starting material appeared to be present even after 1 hour of reaction; this is not rapid enough to be feasible for radiosynthesis.

It had been reported that 4 M hydrochloric acid in dioxane at elevated temperatures can be used to remove Boc protecting groups from phenols without significant *t*-butyl ether formation. Two reactions of this type were attempted without

the use of a cation scavenger (Table **18**, entries **2** and **3**), and these showed significant consumption of starting material by TLC over a 1-hour timecourse. Again, only a small amount of desired product **184** was formed, and the same byproduct (presumed to be **262**) was formed to a much greater extent. Addition of a cation scavenger (Table **18**, entry **4**) did not appear to improve the amount of product formed. It must be noted, however, that these reactions were performed on small scales (~10 mg **258**), and so the quantities used may not have been accurate enough to prevent undesired reactions.

It was noted that Gouverneur and coworkers, in their publication detailing the fluorination conditions upon which this synthesis is based, had applied their methodology to the synthesis of 6-[^{18}F]fluoro-L-DOPA **239**. L-DOPA is an important non-proteogenic amino acid used in humans and animals as a precursor in the biosynthesis of important neurotransmitters such as dopamine and adrenaline.[245] The radiolabelled analogue is used as a radiotracer in both neurology and oncology. This synthesis required the use of protecting groups, including Boc groups for the primary amine, ethyl ester for the carboxylic acid, and methyl ethers for the catechol moiety, which were removed post-fluorination. They achieved this *via* a global deprotection using 57% aqueous hydroiodic acid at 130 °C for 10 minutes, as outlined in Scheme **75**.



238 **239**

Scheme 75: Deprotection step of the Gouverneur synthesis of 6-[^{18}F]fluoro-L-DOPA.[236] *Reagents and conditions*. i) 57% $HI_{(aq.)}$, DMA, 130 °C, 10 min, >95% conversion, *ee* >99%.

These conditions were applied to substrate **258** (Table **18**, entries **5**–**7**). Initially, the reaction was performed at identical temperature (130 °C) and monitored by TLC analysis. At this temperature, removal of both Boc groups was rapid (<5 minutes), but

multiple products formed alongside the desired product **184**. The reaction was repeated at the lower temperature of 50 °C, but this proved ineffective, with the starting material appearing to be stable even after 20 minutes. Pleasingly, a repeat reaction with an intermediate temperature of 90 °C led to rapid removal of both Boc groups (<5 minutes), with minimal formation of side products. Aqueous workup and silica gel chromatography after 40 minutes led to isolation of **184** in 44% yield, although TLC analysis indicated significantly higher conversion. During radiosynthesis the final compound is usually isolated *via* radioHPLC, a form of HPLC which detects species based on their radiation emission. It was thus concluded that the high conversion and reasonable yield by conventional purification indicated these conditions were more than acceptable for a radiosynthetic protocol.

The conditions used in the Gouverneur synthesis are harsh,[236] presumably to afford the global deprotection. Removal of amine-protecting Boc groups and hydrolysis of ethyl esters is often trivial chemistry, however, cleavage of methyl ethers, converting methoxy groups to phenols, is more challenging and often requires strong Lewis acids such as boron tribromide. The use of extremely strong acid HI ($pK_a \approx -9.5 \pm 1.0$, *c.f.* HCl $pK_a \approx -5.9 \pm 0.4$)[246] combined with elevated temperatures is likely required for this demethylation. It is possible that this is advantageous in avoiding formation of *t*-butyl ether side products; they may indeed be formed, but then readily cleaved by the harsh reaction conditions.

6.4 Concluding remarks

In conclusion, we demonstrated that the synthesis of OXFBD02 and its analogues could be modified to allow the installation of pinacolboronate ester functional group, and that this group can undergo fluorination reactions. Importantly, the reaction conditions are analogous to those used in radiosynthesis to install the PET radionuclide ^{18}F. We demonstrated by ^{19}F NMR that precursor **257** underwent ~20% $^{19}F^-$ incorporation during the 20-minute reaction time, which is sufficient for achieving a useful radiochemical yield during radiosynthesis. Furthermore, we found that the substrate could undergo efficient post-radiolabelling deprotection using aqueous hydroiodic acid at elevated temperature, meaning that a radiotracer analogue of **184** could theoretically be synthesised.

Due to time constraints, no radiosynthesis was performed using precursor **257**, and as such we cannot state with certainty an average radiochemical yield. Consequently [^{18}F]-**184** was not used for any PET imaging studies during this project. Despite this, we are confident that application of the chemistry developed herein will allow the production of radiolabelled **184**, which may act as a PET imaging probe for BET proteins. As previously shown by our group, hypoxia-sensitive bioreductive groups can be attached to the phenolic hydroxyl group of OXFBD02 **232** analogues, and such molecules can act as hypoxia-sensitive prodrugs. Addition of a fluorogenic prodrug moiety, such as the 6-nitroquinoline group, will therefore produce a proof-of-concept dual-modal PET-NIR theranostic agent for hypoxic tumours, although this is beyond the scope of this dissertation.

Chapter 7
Conclusions and Outlook

7.1 Conclusions

One of the two main aims of this study was to build upon our earlier work of exploring the use of hypoxia-activated prodrug (HAP) strategies to improve the effectiveness of molecularly-targeted therapies. We wished to continue our study of prodrug forms of the Checkpoint 1 kinase (Chk1) inhibitor SAR020106 **56**.[183] Chk1 inhibition interferes with the cellular response to DNA damage, which is of interest as a therapeutic target as well as a potentiator of cytotoxin- and radiation-induced DNA damage.

In Chapter 2, we focused on earlier work conducted in our group by Dr Cindy Cázares-Körner.[60] Dr Cázares-Körner produced a prototypical 2-nitroimidazole prodrug analogue of SAR020106, but this was shown to have slow fragmentation kinetics and hence no phenotypic response. We performed extensive synthetic studies to form alternative prodrug forms of SAR020106, with the aim of comparing their biochemical reduction and fragmentation kinetics. These alternate forms were designed to increase the entropic driving force associated with fragmentation and compound release and included using carbamate linkages to the bioreductives as well as the “trimethyl lock” system. Despite these efforts, no new prodrug forms could be synthesised. There may be several reasons for this outcome, including steric crowding or the electron-deficient nature of the crucial amine. We observed that the biaryl-amine of a compound which models SAR020106 was exceptionally unreactive towards the formation of amide linkages. Indeed, highly forcing conditions (heating under reflux in neat acetylating reagent acetic anhydride) were required to form an amide-linked

compound. Nevertheless, we were unable to synthesise any new prodrug forms of SAR020106.

The other aim of these studies was to combine hypoxia-targeting approaches with bioimaging. To aid the study of the behaviour and distribution of targeted prodrugs in *in vivo* settings, we wished to develop new hypoxia-targeted imaging agents which could then be incorporated into hypoxia-activated theranostic agents.

In Chapter 3, we designed a hypoxia-activated, "switch-on" fluorophore which was based on a low molecular weight near-infrared scaffold from the literature.[208] This molecule was to serve as the basis for theranostic agents in which metabolism under hypoxia would release both the activated fluorophore and a biologically-relevant cargo molecule. We synthesised the prototypical hypoxia-activated molecule which, whilst highly unstable to chemically-reducing conditions, was metabolised by cytochrome p450 reductase in an oxygen-dependent manner to release the fluorophore component. It transpired, however, that our addition of a methyl group in place of a proton (to block unwanted deprotonation and hence fluorescent "switch-on") dramatically reduced the fluorescence of the released fluorophore. This prevented this class of compound from being taken forward as a theranostic platform, however it did provide an interesting observation. To the best of our knowledge, this is the first example of the fragmentation of a hypoxia-activated group which proceeds *via* the breaking of a C–C bond. We speculate that this fragmentation occurs because the product carbanion is exceptionally highly stabilised *via* delocalisation into a highly conjugated π-orbital system. This may expand the scope for utilisation of hypoxia-activated groups, allowing their attachment to carbon atoms at a crucial position of a molecule if there are no convenient heteroatoms available. However, this

would presumable require the carbanion generated to also be highly stabilised, which is perhaps unlikely for most therapeutically relevant molecules.

In Chapter 4, we explored an alternate NIR fluorophore scaffold as a potential hypoxia-activated theranostic platform. We chose a fluorophore based on the unusual benzopyrylium scaffold, which had originally been utilised as a hydrogen sulfide sensor.[214] We synthesised the analogous compound with an aryl-nitro group in place of the original aryl-azide. We tested this compound for its oxygen-dependent bioreductive potential in an *in vitro* assay, which showed that the molecule was unstable. More detailed analysis by HPLC-MS demonstrated that the fluorophore acted as a conjugate acceptor and underwent conjugate addition by several chemical species in our assays. We observed that the scaffold underwent an irreversible conjugate addition from the hydride donated by NADPH, whilst the addition of other nucleophiles such as L-glutathione appeared to be reversible. We showed *via* ^{1}H NMR analysis that conjugate addition of hydride from $NaBH_4$ occurred on the pyrylium ring in a 1,4-relationship to the oxonium ion. Curiously, it appeared that this reduced species could be re-oxidised to the benzopyrylium on silica gel upon brief exposure to air, indicating the apparent thermodynamic stability of the benzopyrylium scaffold. We undertook work in cells to demonstrate that the fluorophore and pro-fluorophore were penetrant of cell membranes and using fluorescence microscopy demonstrated that the nitro analogue was preferentially activated in hypoxic cancer cells to the fluorophore. We conclude that whilst this scaffold has potential for use as a probe for cellular hypoxia, its susceptibility to spontaneous reaction with intracellular nucleophiles limits its utility.

In Chapter 5, we turned to a NIR fluorophore scaffold which had been developed in our group by Dr Liam O'Connor. This styryl-chromenone-derived fluorophore had

been shown to be activated under hypoxia by cytochrome p450 oxidase enzymes *via* a novel mechanism involving their heme cofactor.[145] We attempted to synthesise analogues of this fluorophore to which a biologically-active cargo molecule had been appended. This synthesis proved challenging, and we were unable to produce a potential theranostic agent based upon the fluorophore. We also explored the synthesis of close analogues of the fluorophore which emitted in the visible range, rather than the NIR. We synthesised the aryl-nitro and aryl-azide analogues as potential hypoxia-activated prodrugs, as well as the parent aryl-amine fluorophore. Biochemical assays proved challenging, as the compounds could not be detected *via* HPLC-MS in assay samples, possibly because of aggregation. We also observed that the amino and nitro analogues appeared to exist as two distinct species by HPLC analysis, whereas other analyses such as ^{1}H NMR and TLC had indicated single species. These species appeared to undergo interconversion when subjected to UV irradiation, suggesting photoisomerisation between the *E*- and *Z*-isomers; attempts to isolate each species *via* preparative HPLC were not successful. We next evaluated both the nitro and azido analogues as hypoxia-activated imaging agents in OE21 cells. The nitro analogue appeared to show some preferential activation under hypoxia although fluorescence was observed under both normoxia and hypoxia by fluorescence microscopy. Interestingly, this selectivity was not observed in confocal microscopy experiments. Curiously, the azide analogue appeared to undergo minimal activation under hypoxia but showed significantly more fluorescence under normoxia. We next synthesised an analogue of the aryl-nitro fluorophore to which was conjugated a ligand for the BET family of bromodomain-containing proteins. This compound proved to be highly unstable and could not be adequately evaluated in biochemical assays, and thus it was not progressed further.

These studies focused on the use of near-infrared fluorescent imaging probes which, whilst having superior properties for preclinical imaging over visible fluorophores, are still limited in their utility *in vivo*. In Chapter 6, therefore, we sought to incorporate an additional imaging modality to enable deep-tissue imaging. We chose positron emission tomography and proposed to incorporate the PET radionuclide ^{18}F into one of our group's bromodomain ligands.[221] We modified the synthesis of these ligands to allow the installation of a pinacolboronate ester, which we then used as a synthetic handle for incorporation of ^{19}F, as demonstrated by ^{19}F NMR. The fluorination chemistry required the use of protecting groups for the ligand's hydroxyl groups, which we accomplished using Boc groups. We then developed a rapid deprotection of both Boc groups that avoided undesired side-products. The fluorination chemistry employed is applicable to radiosynthesis of ^{18}F-PET imaging agents,[236] and thus the synthesis developed will, we propose, be able to produce PET imaging probes based on our BET ligands. These probes could be combined with a hypoxia-activated, fluorogenic prodrug platform to achieve dual-modal imaging as well as targeted delivery of a biologically active agent.

7.2 Future Outlook

Strategies which deliver molecularly-targeted therapies to specific tissues continue to hold a great deal of promise for the future of medicinal chemistry, particularly in the field of cancer. Limited successes in the clinic have spurred research which seeks to improve our understanding of the subtleties and challenges that face the field. Using imaging probes to study the behaviour of targeted drugs offers a wealth of information to aid the development of these therapies. Particularly, the field of fluorophore chemistry is beginning to develop a strong understanding of the nature of molecular fluorescence. This is leading to new generations of fluorophores, rationally

designed in much the way that medicinal chemists rationally design drugs.[247–249] The new fluorophores are being optimised for biological applications and will serve as excellent tools for the design of environment-sensitive probes, such as hypoxia-activated fluorophores.

Alongside the use of new biocompatible fluorophores, a focus of environment-sensitive theranostic agents will likely be on drugs that are already used clinically. As this document was being prepared, Liu and coworkers published a theranostic agent which was metabolised in hypoxia to release both a fluorophore and the clinical anticancer agent 5-fluorodeoxyuridine (FDU).[250] They demonstrated its utility in both cancer cell spheroid and xenograft murine models, and such an approach will likely be applicable to other clinical therapies.

Chemistry Experimental

General experimental

Chemicals

Chemicals were purchased from Acros UK, Sigma-Aldrich UK, Alfa Aesar UK, Fluorochem UK, or Fisher UK. Where appropriate and if not stated otherwise, all non-aqueous reactions were performed in a flame-dried flask under an inert atmosphere of nitrogen or argon.

Analytical thin-layer chromatography

The progress of all reactions was monitored by analytical thin-layer chromatography (TLC). TLC analysis was carried out using normal-phase Merck Geduran® silica gel 60 F_{254} aluminium-supported chromatography sheets. Visualisation was by absorption of UV light (λ_{max} 254 nm and 365 nm), or thermal development after treatment with one of the following: (a) ethanolic phosphomolybic acid (PMA), (b) ethanolic ninhydrin, or (c) aqueous potassium permanganate, potassium carbonate and sodium hydroxide.[251]

NMR spectroscopy

^{1}H NMR spectra were recorded on Bruker AV400 (400 MHz), Bruker AV500 (500 MHz), or Bruker DPX 200 (200 MHz) using the solvents stated in parentheses as a reference for internal deuterium lock. The chemical shift data for each signal are given as δ_H in units of parts per million (ppm) relative to the residual solvent signal, where δ_H (Solvent) is as follows: 5.32 ppm (CD_2Cl_2), 7.26 ppm ($CDCl_3$), 2.05 ppm (acetone-D6), 2.50 ppm (DMSO-D6), 1.94 ppm (CD_3CN), 3.31 ppm (MeOH-D4), as determined by Fulmer *et al*.[252] The multiplicity of each signal is indicated by: s (singlet); br s (broad singlet); d (doublet); t (triplet); q (quartet); qn (quintet), dd (doublet of doublets); or m (multiplet). The number of protons (n) for a given resonance signal is indicated by nH. Coupling constants (*J*) are quoted in Hz and are recorded to the

nearest 0.1 Hz. Identical proton coupling constants (*J*) are averaged in each spectrum and reported to the nearest 0.1 Hz. The coupling constants are determined by analysis using Bruker TopSpin software.

^{13}C NMR spectra were recorded on Bruker AV400 (101 MHz) or Bruker AVII 500 (126 MHz) spectrometers with broadband proton decoupling and internal deuterium lock. The chemical shift data for each signal are given as δ_C in units of parts per million (ppm) relative to the residual solvent signal, where δ_C (Solvent) is as follows: 53.84 ppm (CD_2Cl_2), 77.16 ppm ($CDCl_3$), 29.84 & 206.26 ppm (acetone-D6), 39.52 ppm (DMSO-D6), 1.32 & 118.26 ppm (CD_3CN), 49.00 ppm (MeOH-D4), as determined by Fulmer *et al*.[252]

^{19}F NMR spectra were recorded on a Bruker AV400 (376 MHz) or Bruker AV500 (470 MHz) spectrometer using a broadband proton decoupling pulse sequence and deuterium internal lock. The chemical shift for each signal is given as δ_F in units of parts per million relative to trifluoromethane where δ_F = 0.00 ppm.

^{31}P NMR was recorded on a Bruker AV400 (162 MHz) spectrometer with broadband proton decoupling and internal deuterium lock. The chemical shift data are given as δ_P in units of parts per million (ppm) relative to.

UV-Vis spectrophotometry

UV/Vis spectra were measured on a LAMBDA 25 UV/Vis System (Perkin-Elmer, Massachusetts, USA), excitation range 200 - 800 nm, 1 nm bandwidth, and processed using UV WinLab software (Perkin-Elmer, Massachusetts, USA) or Shimadzu UV-2600 UV-Vis Spectrophotometer (Shimadzu Corporation, Kyoto, Japan) and plotted using OriginPro 2015 or OriginPro 2017 (OriginLab Corporation, Massachusetts,

USA). Samples were evaluated in either a 500 µL or 1000 µL quartz cuvette and analysed across the indicated wavelengths.

Fluorescence spectroscopy

Fluorescence spectra were measured on an LS-55 Fluorescence Spectrophotometer (Perkin-Elmer, Massachusetts, USA), LS-50B Fluorescence Spectrophotometer (Perkin-Elmer, Massachusetts, USA), or Horiba FluoroMax®-4 Fluorescence Spectrophotometer (Horiba Instruments Ltd, USA), and plotted using OriginPro 2015 or OriginPro 2017 (OriginLab Corporation, Massachusetts, USA). Samples were evaluated in either a 500 µL or 1 mL quartz cuvette, and excited at the indicated wavelength.

Mass spectrometry

Spectra were acquired on a Micromass LCT Premier Spectrometer, VG platform spectrometer, or Agilent 6120 spectrometer (low resolution). Electrospray ionisation spectra were obtained on Micromass LCT Premier and Bruker MicroTOF spectrometers, operating in positive or negative mode as indicated, from solutions of MeOH or MeCN. *m/z* values are reported in Daltons and followed by their percentage abundance in parentheses. Electron ionisation/field ionisation (EI/FI) was carried out on a Waters GCT with a temperature programmed solids probe inlet. Samples were introduced in glass tips directly into the source where they were vaporised and analysed. In EI the ionisation is by electron impact, electrons being provided by a filament. In FI the ionisation is in an intense electric field that causes quantum electron tunnelling of a valence electron.

Low-resolution mass spectra (LRMS) were recorded using an Agilent 6120 Quadrupole LC-MS spectrometer (ES), or a Waters/Micromass LCT Premier spectrometer (ES). *m/z* values are reported in Daltons.

High-resolution mass spectra (HRMS) were acquired using the following apparatus: electrospray ionisation (ESI) and atmospheric pressure chemical ionisation (APCI) were recorded using a Thermo Orbitrap Exactive spectrometer operating in either positive or negative mode; chemical ionisation (CI) gas chromatography-mass spectra (GCMS) was recorded using an Agilent 7200 Accurate Mass Q-TOF spectrometer operating in either positive or negative mode. All samples were made into solutions in methanol, water or acetonitrile.

Melting points

Melting points on recrystallised samples were determined using a Leica Galen III hot stage microscope and are uncorrected. The solvent of crystallisation is shown in parentheses.

Infrared spectra

Infrared (IR) spectra were obtained from neat samples, either as thin films, solids or liquids (as indicated) using a diamond ATR module. The spectra were recorded on a Bruker Tensor 27 spectrometer. Absorption maxima are reported in wavenumbers (cm^{-1}) and are classified as broad (br), strong (s), medium (m) or weak (w).

Analytical HPLC for compound purity

Analytical HPLC was carried out on a PerkinElmer Flexar system with a Binary LC Pump and UV/Vis LC Detector. For determination of compound purity, a reversed-phase Dionex Acclaim® 120 column (C18, 5 µm, 120 Å, 4.6 × 150 mm) was

employed, using gradient methods of between 15 and 25 minutes, at flow rates of either 1.5 mL min^{-1} (Methods B, C and D) or 1.0 mL min^{-1} (Method A). Eluents of H_2O/MeCN 95:5 (A) and MeCN/H_2O 95:5 (B) (Method A), or H_2O/MeCN 100:0 (A) and MeCN/H_2O 100:0 (B) (Methods B, C and D) were used. All sample were detected at 254 nm, except when detected at 365 nm, as stated. Samples were injected by dissolving in MeCN, sometimes with the aid of DMSO (final concentration <10% *v/v* DMSO) and were injection volumes were 10 µL in all cases. The methods used are described below:

Method A

Step length (minutes)	Elapsed time (minutes)	%A	%B
1	1	100	0
10	11	0	100
3	14	0	100
1	15	100	0
5	20	100	0

Method B

Step length (minutes)	Elapsed time (minutes)	%A	%B
5	5	95	5
5	10	5	95
5	15	5	95

Method C

Step length (minutes)	Elapsed time (minutes)	%A	%B
5	5	95	5
5	10	5	95
15	25	5	95

Method D

Step length (minutes)	Elapsed time (minutes)	%A	%B
5	5	95	5
15	20	5	95
5	25	5	95

Silica gel flash column chromatography

Flash column chromatography was performed by hand using Merck Geduran® silica gel 60 (40-63 µm) under a positive pressure of nitrogen.

Automated silica gel flash column chromatography

Automated silica gel flash column chromatography was performed on a Biotage® SP4® system equipped with 4-rack autocollector and dual-wavelength UV-Vis detector. Samples were loaded neat, or adsorbed onto Celite®, onto appropriately-sized Biotage® SNAP KP-Sil silica gel cartridges, or Telos silica gel cartridges, as indicated.

Anhydrous solvents

Anhydrous solvents were obtained under the following conditions: anhydrous DMF, anhydrous MeOH and anhydrous EtOH were purchased from Sigma-Aldrich UK in SureSeal™ bottles and used without further purification; anhydrous THF, CH_2Cl_2 and Et_2O were dried using an MBraun SPS-800 system and stored over activated 3 Å molecular sieves under an argon or nitrogen atmosphere. Where stated, THF was distilled over sodium metal, using benzophenone as an indicator.

Microwave reactions

Reactions with microwave irradiation were carried out in a CEM Explorer 48 100 W microwave synthesiser using variable power input to achieve and maintain the indicated temperature.

Concentration *in vacuo*

In vacuo refers to the use of a Büchi® or Heidolph® rotary evaporator attached to a diaphragm pump.

Petroleum ether

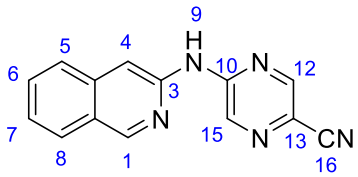
Petroleum ether refers to the fraction boiling between 40–60 °C unless otherwise stated.

Zinc reduction studies

Zinc reduction was performed using Zn dust (Sigma-Aldrich), NH_4Cl (Fisher Scientific), and DMF (Sigma-Aldrich). t=0 refers to the aliquot taken before the addition of zinc dust. To a solution of substrate (2 mg, 1 eq.) in DMF (2 mL), was added aq. NH_4Cl (20 µL, 10% w/v) and zinc dust (30 eq.). The reaction mixture was stirred at ambient temperature for 16 hours. Aliquots (200 µL) were taken at the indicated time intervals, the solution filtered through Supelco® Iso-Disc™ PTFE-4-4 Filter Tips (4 mm × 0.45 µm) to remove zinc and analysed by HPLC.

Synthetic procedures

5-(Isoquinolin-3-ylamino)pyrazine-2-carbonitrile (75)



***via* Buchwald-Hartwig coupling:**

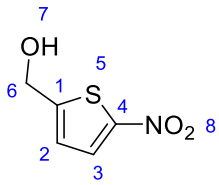
To a flame-dried microwave vial under Ar was added 3-aminoisoquinoline (43 mg, 0.3 mmol, 1 eq.), 2-chloro-5-cyanopyrazine (63 mg, 0.45 mmol, 1.5 eq.), $Pd(OAc)_2$ (3.3 mg, 0.015 mmol, 0.05 eq.), (*S*)-BINAP (11.1 mg, 0.018 mmol, 0.06 eq.), and sodium *tert*-butoxide (57 mg, 0.6 mmol, 2 eq.). Dry toluene (1.5 mL) was added, and the vessel was sealed. The suspension was degassed with a flow of Ar and sonication for 10 minutes, and the reaction mixture was heated under reflux for 20 hours. The reaction mixture was diluted with EtOAc, filtered through Celite®, and concentrated *in vacuo* to afford a brown residue. The residue was taken up in EtOAc and washed with water (1 × 20 mL) and brine (2 × 20 mL). The organic phase was separated, dried over Na_2SO_4, filtered, and concentrated *in vacuo* to afford a yellow residue, which was adsorbed onto Celite®, loaded onto silica gel and purified by flash column chromatography (2:8 EtOAc/petroleum ether) to afford the title compound as a pale yellow solid (8.9 mg, 0.036 mmol, 12% yield): R_f: 0.32 (EtOAc/petroleum ether 3:7); mp 218–221 °C (EtOAc); ^{1}H NMR (500 MHz; DMSO-D6) δ_H 11.02 (1H, s, *H*-9) 9.21 (1H, s, *H*-1) 8.81 (1H, d, *J* 1.3, *H*-12) 8.71 (1H, d, *J* 1.3, *H*-15) 8.49 (1H, s, *H*-4) 8.08 (1H, d, *J* 8.3, *H*-8) 7.91 (1H, d, *J* 8.3, *H*-5) 7.73 (1H, ddd, *J* 8.3, 6.9, 1.3, *H*-6) 7.54 (1H, ddd, *J* 8.2, 6.9, 1.1, *H*-7); ^{13}C NMR (125 MHz; DMSO-D6) δ_C 152.0 (*C*-10), 151.6 (*C*-1), 147.38 (*C*-3), 147.27 (*C*-12), 137.2 (*C*-4'), 137.0 (*C*-15), 131.2 (*C*-6), 127.8 (*C*-8), 126.2 (*C*-5), 125.7 (*C*-7), 125.5 (*C*-8'), 117.6 (*C*-13), 117.4 (*C*-16), 106.3 (*C*-4); LRMS

m/z (ES+) 248 $[M+H]^+$ (100%), (ES−) 246 $[M-H]^-$ (100%). These data are in good agreement with the literature.[183]

***via* nucleophilic aromatic substitution:**

To a flame-dried flask under Ar was added 3-aminoisoquinoline (21 mg, 0.143 mmol, 1 eq.) and 2-chloro-5-cyanopyrazine (30 mg, 0.215 mmol, 1.5 eq.), which was dissolved in 1,2-dimethoxyethane (0.5 mL) and stirred to give a yellow solution. DIPEA (40 µL, 0.229 mmol, 1.6 eq.) was added, and the reaction mixture was heated at 80 °C for 4 hours, then 95 °C for 66 hours. The reaction mixture was diluted with EtOAc, washed with water (2 × 15 mL) and brine (2 × 15 mL), and the organic layer was separated. The organic phase was dried over Na_2SO_4, filtered, and concentrated *in vacuo* to afford a brown residue. The residue was adsorbed onto Celite®, loaded onto silica gel and purified by flash column chromatography eluting in 10%–25% EtOAc/petroleum ether, affording the title compound as an off-white solid (18 mg, 0.073 mmol, 51% yield). The data match those for the method above.

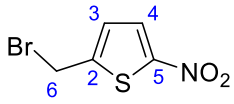
(5-Nitrothiophen-2-yl)methanol (82)



To a flame-dried flask under Ar was added 5-nitrothiophene-2-carboxaldehyde (1.0 g, 6.36 mmol, 1 eq.), which was dissolved in methanol (20 mL) and stirred to give a brown solution. The solution was cooled to 0 °C and powdered $NaBH_4$ (361 mg, 9.55 mmol, 1.5 eq.) was added, causing brisk effervescence. The mixture was stirred at 0 °C for 3.5 hours, then neutralised with addition of 1 M aqueous HCl solution. Water, EtOAc and brine were added to aid separation, the mixture was shaken and the organic component was separated. The aqueous component was extracted twice more with

EtOAc (2 × 40 ml), and the combined organic components were washed with brine (3 × 50 mL) and separated. The organic component was dried over $MgSO_4$, filtered, and concentrated *in vacuo* to afford a brown oil. The oil was dissolved in CH_2Cl_2, loaded onto silica gel and purified by flash column chromatography eluting in 2%–5% MeOH in CH_2Cl_2. The appropriate fractions were collected and concentrated *in vacuo* to afford the title compound as a brown oil (706 mg, 4.43 mmol, 70% yield): R_f: 0.60 (MeOH/CH_2Cl_2 1:9); $\bar{\nu}_{max}$ (solid) cm^{-1} 3371 (br), 3107 (w), 2871 (br), 1538 (m, N-O), 1493 (s), 1433 (m), 1324 (s, N-O), 1205 (w), 1155 (m), 1033 (m), 1015 (m), 813 (s), 575 (w), 733 (s), 678 (s), 627 (w); ^1H NMR (400 MHz; $CDCl_3$) δ_H 7.82 (1H, d, *J* 4.1, *H*-3) 6.94 (1H, d, *J* 4.1, *H*-2) 4.88 (2H, d, *J* 5.8, *H*-6) 2.19 (1H, t, *J* 5.8, *H*-7); LRMS *m/z* (ES−) 158 $[M-H]^-$ (100%). These data are in good agreement with the literature.[45]

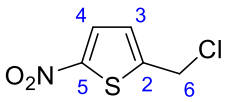
2-(Bromomethyl)-5-nitrothiophene (83)



To a flame-dried flask under argon containing (5-nitrothiophen-2-yl)methanol (200 mg, 1.26 mmol, 1 eq.) was added CH_2Cl_2 (20 mL), affording a brown solution which was stirred and cooled to 0 °C. PBr_3 (177 µL, 1.88 mmol, 1.5 eq.) was added dropwise, and the mixture was stirred at 0 °C for 2.5 hours, and then warmed to RT and stirred for a further 1 hour. The mixture was again cooled to 0 °C and quenched by addition of saturated aqueous $NaHCO_3$ solution. The biphasic mixture was separated, and the aqueous layer was extracted with CH_2Cl_2 (2 × 30 mL). The organic layers were combined and washed with saturated aqueous $NaHCO_3$ solution (1 × 30 mL) and brine (3 × 30 mL). The organic layer was separated, dried over Na_2SO_4, filtered, and concentrated *in vacuo* to afford a pale pink oil. The oil was dissolved in CH_2Cl_2 and purified over a plug of silica gel, eluting with CH_2Cl_2. The eluent was concentrated *in*

vacuo to afford the title compound as a yellow oil (83.5 mg, 0.376 mmol, 30% yield): R_f: 0.92 (MeOH/CH_2Cl_2 1:9); $\bar{\nu}_{max}$ (solid) cm^{-1} 3106 (w), 1720 (w), 1538 (m, N-O), 1496 (s), 1439 (m), 1427 (m), 1352 (m), 1332 (s, N-O), 1237 (w), 1212 (m), 1181 (m), 1128 (m), 1091 (w), 1028 (m), 909 (w), 868 (w), 812 (s), 755 (w), 731 (s), 685 (w), 620 (m); ^{1}H NMR (400 MHz; $CDCl_3$) δ_H 7.72 (1H, d, *J* 4.1, *H*-4) 6.99 (1H, d, *J* 4.1, *H*-3) 4.55 (2H, s, *H*-6); LRMS *m/z* not detected; HRMS *m/z* GCMS (NH_3 CI) [Found: $[M(^{79}Br)+NH_4]^+$ 238.9483 (50%), $C_5H_8(^{79}Br)N_2O_2S^+$ requires 238.9484; $[M(^{81}Br)+NH_4]^+$ 240.9458; $C_5H_8(^{81}Br)N_2O_2S^+$ requires 240.9464]. These data are in good agreement with the literature.[46]

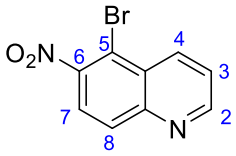
2-(Chloromethyl)-5-nitrothiophene (84)



To a flame-dried flask under Ar was added (5-nitrothiophen-2-yl)methanol (200 mg, 1.26 mmol, 1 eq.), which was dissolved in CH_2Cl_2 (9 mL) to give a brown solution. Distilled pyridine (305 µL, 3.77 mmol, 3 eq.) was added, the mixture was stirred and cooled to 0 °C for ~10 minutes. $SOCl_2$ (273 µL, 3.77 mmol, 3 eq.) was added dropwise, and the mixture was stirred at 0 °C for 2 hours, then warmed to RT and stirred for a further 20 hours. More pyridine (305 µL, 3.77 mmol, 3 eq.) and $SOCl_2$ (273 µL, 3.77 mmol, 3 eq.), and the mixture was left to stir at RT for 24 hours. The mixture was quenched with addition of water and brine and partitioned with CH_2Cl_2. The mixture was shaken and separated, and the aqueous component was further extracted with CH_2Cl_2 (3 × 40 mL). The organic components were combined, dried over $MgSO_4$, filtered, and concentrated *in vacuo* to afford a brown oil. The oil was dissolved in CH_2Cl_2 and filtered through a plug of silica gel, eluting with CH_2Cl_2. The solvent was removed *in vacuo* to afford the title compound as a brown oil (110 mg,

0.62 mmol, 49% yield): R_f: 0.88 (MeOH/CH_2Cl_2 1:9); $\bar{\nu}_{max}$ (solid) cm^{-1} 3108 (w), 1541 (m, N-O), 1499 (s), 1435 (m), 1334 (s, N-O), 1265 (m), 1185 (m), 1126 (w), 1111 (w), 1031 (m), 900 (w), 814 (s), 756 (w), 732 (s), 708 (m), 665 (w), 631 (w); ^{1}H NMR (400 MHz; $CDCl_3$) δ_H 7.80 (1H, d, *J* 4.1, *H*-4) 7.04 (1H, d, *J* 4.1, *H*-3) 4.73 (2H, s, *H*-6); LRMS *m/z* not detected; HRMS *m/z* GCMS (NH_3 CI) [Found: $[M(^{35}Cl)+NH_4]^+$ 194.9989 (50%); $C_5H_8(^{35}Cl)N_2O_2S^+$ requires 194.9990; $[M(^{37}Cl)+NH_4]^+$ 196.9957 (50%); $C_5H_8(^{37}Cl)N_2O_2S^+$ requires 196.9960]. These data are in good agreement with the literature.[186]

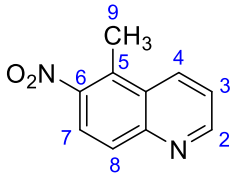
5-Bromo-6-nitroquinoline (86)



To a flask containing water (25 mL) and HBr solution (10.4 mL, 48 wt% in water) was added 5-amino-6-nitroquinoline (500 mg, 2.64 mmol, 1 eq.) and copper(I) bromide (455 mg, 3.17 mmol, 1.2 eq.). The mixture was stirred to give an orange-brown solution, and an aqueous solution of $NaNO_2$ (1 mL, 547 mg, 7.93 mmol, 3 eq., 7.9 M), dropwise, causing effervescence and orange fumes to evolve. The reaction mixture was stirred at RT for 24 hours, then quenched with addition of saturated aqueous $NaHCO_3$ solution bringing the mixture to pH 7. Saturated aqueous EDTA solution (30 mL) was added and the mixture was stirred for 20 minutes. The reaction mixture was extracted with EtOAc (5 × 60 mL), and the combined organic components were washed with saturated EDTA solution (3 × 30 mL), saturated aqueous $Na_2S_2O_3$ solution (3 × 30 mL), and brine (3 × 30 mL). The organic phase was separated, dried over $MgSO_4$, filtered, and concentrated *in vacuo* to afford a brown residue. The residue was adsorbed onto Celite®, loaded onto silica gel and purified by flash column

chromatography in 20%–24% EtOAc/petroleum ether. The fractions were collected and concentrated *in vacuo* to afford a fluffy, off-white solid (394 mg, 1.56 mmol, 59% yield): R_f: 0.39 (EtOAc/petroleum ether 2:3); mp 138–141 °C (*i*-PrOH) [lit. 138–140 °C (EtOAc)][49]; ^{1}H NMR (400 MHz; $CDCl_3$) δ_H 9.07 (1H, dd, *J* 4.2, 1.6, *H*-2) 8.78 (1H, d, *J* 8.7, *H*-4) 8.22 (1H, d, *J* 9.1, *H*-7) 8.00 (1H, d, *J* 9.1, *H*-8) 7.67 (1H, dd, *J* 8.7, 4.2, *H*-3); LRMS *m/z* (ES+) 255 [M(^{79}Br)+H]$^+$ (50%), 257 [M(^{81}Br)+H]$^+$ (50%). These data are in good agreement with the literature.[49,50]

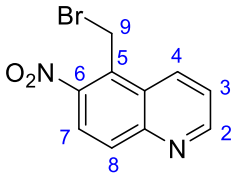
5-Methyl-6-nitroquinoline (88)



To a flask was added 5-bromo-6-nitroquinoline (250 mg, 0.992 mmol, 1 eq.), Pd(dppf)Cl_2·CH_2Cl_2 (81 mg 0.099 mmol, 0.1 eq.), and K_2CO_3 (411 mg, 2.98 mmol, 3 eq.). 1,4-Dioxane (3 mL) was added, followed by trimethylboroxine (138 μL, 0.992 mmol, 1 eq.). The mixture was stirred, and the resulting suspension was heated under reflux 2 hours and 45 minutes. The mixture was cooled to RT, filtered through a pad of Celite®, washed through with EtOAc, and concentrated *in vacuo*. The residue was dissolved in EtOAc, adsorbed onto Celite®, loaded onto a 25 g Biotage SNAP silica gel cartridge and purified by flash column chromatography on a Biotage SP4, eluting with 25%–40% EtOAc/petroleum ether. The fractions were collected and concentrated *in vacuo* to afford the title compound as an off-white solid (172 mg, 0.914 mmol, 92% yield): R_f: 0.32 (EtOAc/petroleum ether 1:1); mp 132–135 °C (sub.)(EtOAc) [lit. 166–167 °C][253]; $\bar{\nu}_{max}$ (solid) cm^{-1} 1601 (m, C=N), 1580 (m), 1518 (s, N-O), 1496 (s), 1410 (m), 1389 (m), 1314 (s), 1213 (s, methyl C-H), 1169 (w), 1144 (w), 1077 (w), 1042 (w), 965 (w), 892 (w), 867 (w), 830 (m), 802 (s), 777 (m), 737 (m),

699 (m), 652 (w), 613 (m); ^{1}H NMR (400 MHz; $CDCl_3$) δ_H 9.06 (1H, dd, *J* 4.2, 1.6, *H*-2) 8.56 (1H, dd, *J* 8.7, 1.6, *H*-4) 8.08 (1H, d, *J* 9.2, *H*-7) 8.05 (1H, d, *J* 9.2, *H*-8) 7.60 (1H, dd, *J* 8.7, 4.2, *H*-3) 2.86 (3H, s, *H*-9); ^{13}C NMR (101 MHz; $CDCl_3$) δ_C 152.6 (C-2), 149.2 (C-8'), 147.9 (C-6), 134.1 (C-4), 130.5 (C-8), 129.4 (C-5), 127.8 (C-4'), 124.0 (C-7), 122.5 (C-3), 14.3 (C-9); LRMS *m/z* (ES+) 189 $[M+H]^+$ (100%); HRMS *m/z* (ESI+) [Found 189.06589; $C_{10}H_9N_2O_2$ requires 189.06585]; HPLC (Method B) Retention Time = 8.44 minutes, purity 99.4%. These data are in good agreement with the literature.[253]

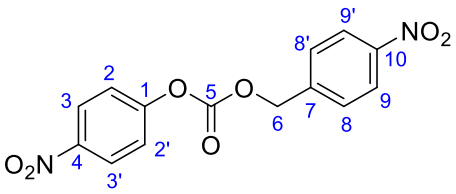
5-(Bromomethyl)-6-nitroquinoline (89)



To a flame-dried 2 mL–5 mL microwave vial was added 5-methyl-6-nitroquinoline (150 mg, 0.797 mmol, 1.0 eq.), *N*-Bromosuccinimide (225 mg, 1.435 mmol, 1.8 eq.) and AIBN (6.5 mg, 0.0399 mmol, 0.05 eq.). The vessel was sealed and coated with aluminium foil, and anhydrous CCl_4 (2.66 mL) was added. The mixture was stirred in the dark at 70 °C for 24 hours, by which time TLC analysis indicated that the reaction was not complete. Further *N*-bromosuccinimide (47 mg, 0.300 mmol) and AIBN (6.5 mg, 0.0399 mmol) was added, the vessel was resealed and heated at 70 °C for a further 5 hours. Further *N*-bromosuccinimide (47 mg, 0.300 mmol) and AIBN (6.5 mg, 0.0399 mmol) was added, the vessel was resealed and heated at 70 °C for 18 hours, by which time ^{1}H NMR analysis indicated 94% conversion to the *mono*-bromo product. The reaction mixture was diluted with $CHCl_3$, washed with saturated aqueous $NaHCO_3$ solution (1 × 20 mL), water (1 × 20 mL) and brine (3 × 20 mL). The layers were separated, and the organic phase was dried over anhydrous Na_2SO_4, filtered, and concentrated *in vacuo* to afford an orange-brown crystalline solid (192 mg,

0.718 mmol, 90% yield): R_f: 0.32 (EtOAc/petroleum ether 1:1); mp 112-115 °C ($CHCl_3$) [lit. 112-114 °C (EtOAc)][49]; ^{1}H NMR (400 MHz; $CDCl_3$) δ_H 9.11 (1H, dd, *J* 4.2, 1.6, *H*-2) 8.67 (1H, d, *J* 8.8, *H*-4) 8.25 (1H, d, *J* 9.2, *H*-7) 8.14 (1H, d, *J* 9.2, *H*-8) 7.70 (1H, dd, *J* 8.8, 4.2, *H*-3) 5.11 (2H, s, *H*-9); LRMS *m/z* (ES+) 267 [M(^{79}Br)+H]$^+$ (50%), 269 [M(^{81}Br)+H]$^+$ (50%). These data are in good agreement with the literature.[49,50]

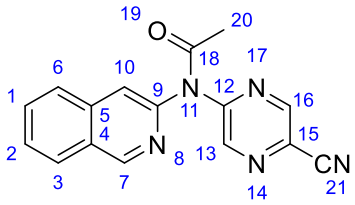
4-Nitrobenzyl-(4-nitrophenyl) carbonate (101)



To a flame-dried flask under Ar was added 4-nitrophenyl chloroformate (550 mg, 2.55 mmol, 1.5 eq.), which was dissolved in anhydrous THF (20 mL). The solution was stirred and cooled to 0 °C, and anhydrous pyridine (206 µL, 2.55 mmol, 1.5 eq.) was added causing a colourless precipitate to form. The mixture was stirred at 0 °C for 20 minutes, and then a solution of 4-nitrobenzyl alcohol (260 mg, 1.70 mmol, 1 eq.) in anhydrous THF (7 mL) was added *via* cannulation. The mixture was warmed to room temperature and stirred for 19 hours, and then diluted with CH_2Cl_2. The organic phase was washed with 1 M aqueous HCl (3 × 25 mL) and brine (1 × 25 mL), and the combined aqueous phases were re-extracted with CH_2Cl_2 (3 × 20 mL). The combined organic phases were dried over $MgSO_4$, filtered, and concentrated *in vacuo* to afford a yellow oil, which was dissolved in EtOAc and precipitated by addition of *n*-hexane. The resulting precipitate was filtered and recrystallised from EtOAc to afford the title compound as an off-white, crystalline solid (285 mg, 0.89 mmol, 52% yield): R_f: 0.54 (EtOAc/petroleum ether 3:7); mp 125–126 °C (EtOAc) [lit. 125–126 °C (EtOAc/*n*-hexane)][254]; ^{1}H NMR (500 MHz; $CDCl_3$) δ_H 8.26-8.31 (4H, m, *H*-9&9'&3&3') 7.60-7.64 (2H, m, *H*-8&8') 7.38-7.41 (2H, m, *H*-2&2') 5.39 (2H, s, *H*-6); ^{13}C NMR (125 MHz;

$CDCl_3$) δ_C 155.3 (C-4) 152.3 (C-5) 148.2 (C-10) 145.6 (C-1) 141.2 (C-7) 128.8 (C-8&8') 125.4 (C-9&9') 124.1 (C-3&3') 121.7 (C-2&2') 69.1 (C-6); LRMS *m/z* (ES+) 341 $[M+Na]^+$ (100%). These data are in good agreement with the literature.[254,255]

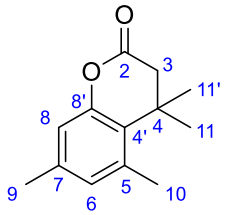
_N_-(5-Cyanopyrazin-2-yl)-_N_-(isoquinolin-3-yl)acetamide (102)



To a flame-dried flask under Ar was added 5-(isoquinolin-3-ylamino)pyrazine-2-carbonitrile (5 mg, 0.02 mmol, 1 eq.). Acetic anhydride (1 mL) was added, and the mixture was stirred to form a suspension, which was heated under reflux for 2 days. The reaction mixture was cooled to room temperature and diluted with $CHCl_3$. The organic phase was washed with saturated aqueous $NaHCO_3$ solution (2 × 30 mL) and water (1 × 30 mL), separated, dried over $MgSO_4$, filtered, and concentrated *in vacuo*. The residue was adsorbed onto Celite®, loaded onto silica gel and purified by flash column chromatography eluting in 20%–40% EtOAc/petroleum ether, with appropriate fractions collected and concentrated *in vacuo* to afford the title compound as a pale, sticky oil which was precipitated from CH_2Cl_2 as a colourless solid (5.5 mg, 0.019 mmol, 95% yield): R_f: 0.15 (EtOAc/petroleum ether 3:7); mp 170–173 °C (CH_2Cl_2); $\bar{\nu}_{max}$ (solid) cm^{-1} 2921 (w, br), 2853 (w), 2233 (w, C≡N), 1697 (s, C=O), 1625 (m), 1593 (m), 1579 (m), 1560 (m), 1523 (m), 1494 (w), 1461 (s), 1442 (s), 1358 (s), 1340 (m), 1315 (m), 1261 (s), 1230 (s), 1212 (s), 1164 (m), 1131 (w), 1013 (s), 970 (w), 947 (m), 916 (m), 889 (m), 847 (m), 799 (w), 781 (s), 753 (w), 697 (w), 656 (w), 621 (m); ^1H NMR (500 MHz; $CDCl_3$) δ_H 9.51 (1H, d, *J* 1.4, *H*-16) 9.28 (1H, s, *H*-7) 8.45 (1H, d, *J* 1.4, *H*-13) 8.10 (1H, d, *J* 8.1, *H*-6) 7.91 (1H, d, *J* 8.1, *H*-3) 7.82 (1H, ddd, *J* 8.2, 6.8, 1.2, *H*-2) 7.75 (1H, ddd, *J* 8.2, 6.8, 1.2, *H*-1) 7.72 (1H, s, *H*-10) 2.16 (3H, s, *H*-20);

^{13}C NMR (125 MHz; $CDCl_3$) δ_C 171.4 (*C*-18) 153.5 (*C*-7) 152.8 (*C*-15) 147.4 (*C*-9) 145.9 (*C*-13) 141.6 (*C*-16) 137.4 (*C*-4) 131.6 (*C*-2) 128.8 (*C*-1) 128.4 (*C*-5) 127.9 (*C*-6) 127.0 (*C*-3) 124.8 (*C*-12) 120.5 (*C*-10) 115.7 (*C*-21) 25.2 (*C*-20); LRMS (ES+) *m/z* 290 $[M+H]^+$ (100%), 312 $[M+Na]^+$ (75%); HRMS *m/z* (ESI+) [Found: 290.10359; $C_{16}H_{12}N_5O^+$ requires 290.10364]; HPLC (Method B) Retention Time = 8.51 minutes, purity 98.5%.

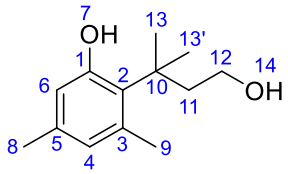
4,4,5,7-Tetramethylchroman-2-one (105)



To a flame-dried flask under Ar was added 3,5-dimethylphenol (5.0 g, 40.9 mmol, 1 eq.). Methanesulfonic acid (10 mL) was added, and the mixture was stirred to give a brown suspension. Ethyl 3,3-dimethylacrylate (6.83 mL, 49.1 mmol, 1.2 eq.) was added, and the mixture was heated at 70 °C for 16 hours. The mixture was cooled to RT, and then poured into a separating funnel with water. The aqueous was extracted with EtOAc (3 × 60 mL), and the combined organic components were washed with saturated aqueous $NaHCO_3$ solution (1 × 70 mL) and brine (1 × 70 mL). The organic component was separated, dried over Na_2SO_4, filtered, and concentrated *in vacuo* to afford a yellow-brown oil. The oil was adsorbed onto Celite®, loaded onto silica gel and purified by flash column chromatography in 5%–10% EtOAc/petroleum ether. The fractions were collected and concentrated *in vacuo* to afford the title compound as an off-white crystalline solid (7.72 g, 37.8 mmol, 92% yield): R_f: 0.65 (EtOAc/petroleum ether 1:4); mp 96–97 °C (EtOAc); ^{1}H NMR (400 MHz; $CDCl_3$) δ_H 6.74 (2H, s, *H*-6&8) 2.59 (2H, s, *H*-3) 2.46 (3H, s, *H*-9) 2.27 (3H, s, *H*-10) 1.43 (6H, s, *H*-11&11'); ^{13}C NMR (400 MHz; $CDCl_3$) δ_C 168.6 (C-2) 151.7 (C-8'), 137.8 (C-7), 136.2 (C-4'), 129.6 (C-8)

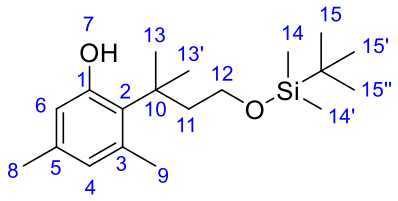
126.8 (C-5), 116.4 (C-6), 45.9 (C-3) 35.2 (C-4), 27.9 (C-11&11') 23.2 (C-9) 20.7 (C-10); LRMS *m/z* (ES+) 205 $[M+H]^+$ (29%), 227 $[M+Na]^+$ (100%). These data are in good agreement with the literature.[194,256]

2-(4-Hydroxy-2-methylbutan-2-yl)-3,5-dimethylphenol (108)



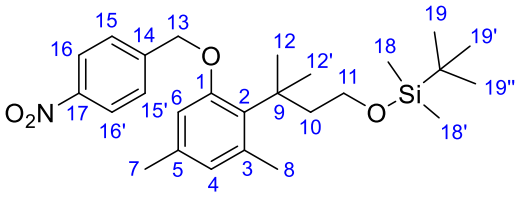
To a flame-dried flask under Ar was added $LiAlH_4$ solution (2.28 mL, 4.56 mmol, 1.5 eq., 2 M in THF), which was stirred and cooled to 0 °C. To this was added a solution of 4,4,5,7-tetramethylchroman-2-one (621 mg, 3.04 mmol, 1 eq.) in distilled THF (3.56 mL), dropwise. The solution was stirred at 0 °C for 2 hours, then warmed to RT and stirred for a further 3 hours. The reaction mixture was cooled to 0 °C and the reaction quenched by slow addition of EtOAc. The mixture was diluted with water which caused colourless insoluble salts to precipitate. These salts were filtered through a plug of Celite® and the filtrate was concentrated *in vacuo* to afford a yellow oil, which crystallised upon high-vacuum drying to afford the title compound as an off-white solid (592 mg, 2.84 mmol, 93% yield): R_f: 0.57 (EtOAc/petroleum ether 1:1); mp 94–96 °C (EtOAc) °C; ^{1}H NMR (400 MHz; $CDCl_3$) δ_H 6.50 (1H, s, *H*-6) 6.34 (1H, s, *H*-4) 5.49 (1H, s, *H*-7) 3.62 (2H, t, *J* 7.2, *H*-12) 2.47 (3H, s, *H*-8) 2.22 (2H, t, *J* 7.2, *H*-11) 2.17 (3H, s, *H*-9) 1.55 (6H, s, *H*-13&13'); LRMS *m/z* (ES+) 231 $[M+Na]^+$ (100%), (ES−) 207 $[M-H]^-$ (100%). These data are in good agreement with the literature.[194,257]

2-(4-((*t*-Butyldimethylsilyl)oxy)-2-methylbutan-2-yl)-3,5-dimethylphenol (109)



To a flame-dried flask under an argon atmosphere was added 2-(4-hydroxy-2-methylbutan-2-yl)-3,5-dimethylphenol (2.20 g, 10.6 mmol, 1 eq.) and TBDMSCl (3.91 g, 21.1 mmol, 2 eq.), which were then dissolved in CH_2Cl_2 (50 mL) and stirred to give a pale solution. Triethylamine (4.41 mL, 31.7 mmol, 3 eq.) was added, and the reaction mixture was stirred at RT for 20 hours. Celite® was added to the reaction mixture, which was then concentrated *in vacuo.* The solid was loaded onto silica gel and purified by flash column chromatography eluting in 2%–4% Et_2O in petroleum ether. The fractions were collected and concentrated *in vacuo* to afford the title compound as a colourless crystalline solid (3.06 g, 9.47 mmol, 89% yield): R_f: 0.45 (Et_2O/petroleum ether 1:19); mp 110–111 °C (Et_2O); $\bar{\nu}_{max}$ (solid) cm^{-1} 3298 (br, -OH) 3018 (w), 2952 (m), 2924 (m), 2896 (m), 2855 (m), 1614 (w), 1575 (w), 1469 (m), 1441 (m), 1413 (w), 1388 (w), 1360 (w), 1340 (w), 1304 (w), 1260 (m), 1207 (m, C-O), 1184 (m), 1070 (s), 1046 (s, -OH), 1027 (s), 1006 (m), 988 (m), 952 (w), 938 (w), 872 (m), 831 (s), 782 (s), 750 (m), 671 (m), 651 (w); ^{1}H NMR (400 MHz; $CDCl_3$) δ_H 6.48 (1H, s, *H*-6) 6.40 (1H, s, *H*-4) 5.55 (1H, s, *H*-7) 3.58 (2H, t, *J* 7.0, *H*-12) 2.44 (3H, s, *H*-8) 2.17 (3H, s, *H*-9) 2.10 (2H, t, *J* 7.0, *H*-11) 1.53 (6H, s, *H*-13&13') 0.86 (9H, s, *H*-15&15'&15'') 0.00 (6H, s, *H*-14&14'); LRMS *m/z* (ES+) 345 $[M+Na]^+$ (100%), (ES−) 321 $[M-H]^-$ (100%). These data are in good agreement with the literature.[194,257]

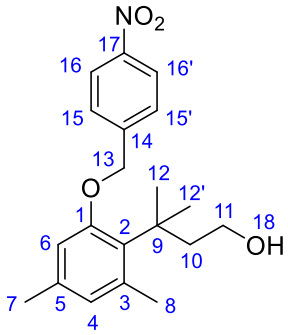
_t_-Butyl(3-(2,4-dimethyl-6-((4-nitrobenzyl)oxy)phenyl)-3-methylbutoxy)dimethylsilane (110)



To a flame-dried flask under Ar was added 2-(4-((*t*-butyldimethylsilyl)oxy)-2-methylbutan-2-yl)-3,5-dimethylphenol (1.5 g, 4.65 mmol, 1 eq.), 4-nitrobenzyl bromide (1.11 g, 5.12 mmol, 1.1 eq.), and K_2CO_3 (708 mg, 5.12 mmol, 1.1 eq.). Acetone (46.5 mL) was added, and the mixture was stirred resulting in a pale solution with a colourless suspension. The mixture was heated under reflux for 18 hours, then allowed to cool and filtered under reduced pressure. The solid components were washed with acetone, and the filtrate was concentrated *in vacuo* onto Celite® and loaded onto silica gel. The crude material was then purified by flash column chromatography, eluting with 2% Et_2O in petroleum ether. Fractions were collected and concentrated *in vacuo* to afford the title compound as an off-white solid (1.96 g, 4.28 mmol, 92% yield): R_f: 0.63 (Et_2O/petroleum ether 1:9); mp 81–84 °C (petroleum ether); $\bar{\nu}_{max}$ (solid) cm^{-1} 3705 (w), 2952 (m), 2925 (m), 2856 (m), 2361 (m), 2342 (m), 2160 (m), 2029 (m), 1978 (m), 1609 (m), 1564 (m), 1515 (s, N-O), 1470 (m), 1436 (m), 1409 (m), 1383 (m), 1342 (s, N-O), 1304 (m), 1256 (s), 1221 (m), 1197 (m), 1177 (m), 1090 (m), 1072 (s), 1049 (s), 1033 (s), 1008 (m), 985 (w), 939 (w), 915 (m), 897 (m), 872 (m), 855 (m), 829 (s), 773 (s), 754 (m), 726 (m), 708 (m), 670 (w), 657 (w); ^{1}H NMR (500 MHz; $CDCl_3$) δ_H 8.31 (2H, d, *J* 8.6, *H*-16&16') 7.68 (2H, d, *J* 8.6, *H*-15&15') 6.64 (1H, s, *H*-6) 6.62 (1H, s, *H*-4) 5.20 (2H, s, *H*-13) 3.55 (2H, t, *J* 7.7, *H*-11) 2.56 (3H, s, *H*-7) 2.28 (3H, s, *H*-8) 2.19 (2H, t, *J* 7.7, *H*-10) 1.58 (6H, s, *H*-12&12') 0.88 (9H, s, *H*-19&19'&19'') 0.00 (6H, s, *H*-18&18'); ^{13}C NMR (125 MHz; $CDCl_3$) δ_C 158.1 (C-1) 147.5 (C-17) 145.0 (C-14) 138.0 (C-5) 135.9 (C-3) 131.6 (C-2) 128.1 (C-15&15') 127.9 (C-16&16') 127.7 (C-19) 123.9

(C-4) 112.6 (C-6) 70.0 (C-13) 61.3 (C-11) 45.7 (C-10) 39.9 (C-9) 32.2 (C-12&12') 25.9 (C-8) 20.7 (C-7) 18.2 (C-20&20'&20'') −5.3 (C-18&18'); LRMS *m/z* (ES−) 456 $[M-H]^-$ (100%); HRMS *m/z* (ESI+) [Found 480.25394; $C_{26}H_{39}O_4N^{23}NaSi^+$ requires 480.25406], (ESI−) [Found 456.25747; $C_{26}H_{38}O_4NSi^-$ requires 456.25756]; HPLC (Method C) Retention Time = 18.80 minutes, purity 99.5%.

3-(2,4-Dimethyl-6-((4-nitrobenzyl)oxy)phenyl)-3-methylbutan-1-ol (111)



from TBDMS-protected substrate 109

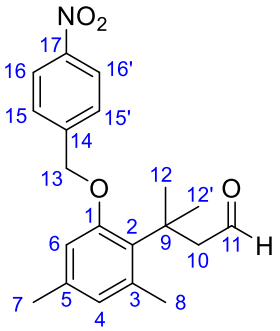
To a flask containing *t*-butyl(3-(2,4-dimethyl-6-((4-nitrobenzyl)oxy)phenyl)-3-methylbutoxy)dimethylsilane (493 mg, 1.08 mmol, 1 eq.) was added a mixture of THF (3 mL), acetic acid (3 mL) and water (1 mL), which was stirred to give a colourless suspension. The mixture was stirred at RT for 18 hours, and the reaction mixture was concentrated *in vacuo*. The residue was redissolved in EtOAc and washed with water (1 × 50 mL), saturated aqueous $NaHCO_3$ solution (1 × 50 mL), and brine (1 × 50 mL). The organic phase was separated, dried over Na_2SO_4, filtered, and concentrated *in vacuo* to afford a yellow oil. The oil was dissolved in Et_2O, adsorbed onto Celite®, loaded onto silica gel and purified by flash column chromatography, eluting with 10%–60% Et_2O/petroleum ether. Fractions were collected and concentrated *in vacuo* to afford the title compound as a clear yellow oil which became an off-white solid upon high-vacuum drying (334 mg, 0.973 mmol, 90% yield): R_f: 0.15–0.5 (Et_2O/petroleum ether 1:1, streaky); mp 77–80 °C (EtOAc); $\bar{\nu}_{max}$ (solid) cm^{-1} 3310 (br, O-H), 2921 (w), 2363 (w), 2160 (w), 2029 (w), 1604 (w), 1565 (w), 1516 (m, N-O), 1450 (w), 1390 (w),

1342 (s, N-O), 1300 (m), 1260 (m), 1212 (w), 1177 (m), 1113 (w), 1082 (m), 1030 (m), 986 (m), 862 (w), 839 (s), 824 (m), 739 (s), 681 (w); ^{1}H NMR (500 MHz; $CDCl_3$) δ_H 8.27 (2H, d, *J* 8.7, *H*-16&16') 7.63 (2H, d, *J* 8.7, *H*-15&15') 6.60 (1H, s, *H*-6) 6.58 (1H, s, *H*-4) 5.17 (2H, s, *H*-13) 3.56 (2H, t, *J* 7.4, *H*-11) 2.52 (3H, s, *H*-7) 2.22 (3H, s, *H*-8) 2.17 (2H, t, *J* 7.4, *H*-10) 1.54 (6H, s, *H*-12&12'); ^{13}C NMR (125 MHz; $CDCl_3$) δ_C 158.2 (C-1), 147.6 (C-17), 144.9 (C-14), 138.0 (C-5), 136.3 (C-3), 131.3 (C-2), 128.3 (C-15&15'), 127.9 (C-16&16'), 123.9 (C-4), 112.8 (C-6), 70.0 (C-13), 61.2 (C-11), 45.6 (C-10), 39.8 (C-9), 32.3 (C-12&12'), 25.9 (C-8), 20.7 (C-7); LRMS *m/z* (ES+) 366 $[M+Na]^+$ (100%), (ES−) 342 $[M-H]^-$ (100%); HRMS *m/z* (ESI+) [Found 366.16757; $C_{20}H_{25}O_4NNa^+$ requires 366.16758]; HPLC (Method C) Retention Time = 14.28 minutes, purity 92.2%.

from unprotected phenol/primary alcohol 108

To a flame-dried flask under Ar was added 2-(4-hydroxy-2-methylbutan-2-yl)-3,5-dimethylphenol (400 mg, 1.92 mmol, 1 eq.), 4-nitrobenzyl bromide (498 mg, 2.30 mmol, 1.2 eq.), and K_2CO_3 (398 mg, 2.88 mmol, 1.5 eq.). Dry acetone (4 mL, dried over anhydrous K_2CO_3 overnight) was added, and the mixture was stirred to give a clear colourless solution with a colourless suspension. The mixture was heated at 50 °C for 21 hours, then cooled to RT. The suspension was filtered under reduced pressure and washed with acetone. The liquor was concentrated *in vacuo* onto Celite®, loaded onto a 10 g Biotage® SNAP silica gel cartridge and purified by flash column chromatography on a Biotage® SP4 system, eluting in 20%–50% EtOAc/petroleum ether. The appropriate fractions were collected and concentrated *in vacuo* to afford the title compound as an off-white solid (527 mg, 1.535 mmol, 80% yield). These data match those for the method describe above.

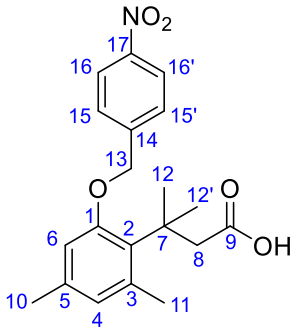
3-(2,4-Dimethyl-6-((4-nitrobenzyl)oxy)phenyl)-3-methylbutanal (112)



To a flame-dried flask under Ar was added 3-(2,4-dimethyl-6-((4-nitrobenzyl)oxy)phenyl)-3-methylbutan-1-ol (270 mg, 0.786 mmol, 1 eq.), which was dissolved in dry CH_2Cl_2 (2 mL) and stirred to give a colourless solution. Celite® was added, followed by PCC (339 mg, 1.57 mmol, 2 eq.), portionwise, to give a deep brown, sludgy mixture. The mixture was stirred at RT for 3 hours, and then filtered through a plug of Celite® and concentrated *in vacuo* to afford a brown residue. The residue was taken up in CH_2Cl_2, adsorbed onto Celite®, loaded onto silica gel and purified by flash column chromatography eluting in 10% Et_2O/petroleum ether. Fractions were collected and concentrated *in vacuo* to afford the title compound as a colourless solid (185 mg, 0.542 mmol, 70% yield): R_f: 0.70 (Et_2O/petroleum ether 1:1); mp 87–91 °C (Et_2O); $\bar{\nu}_{max}$ (solid) cm^{-1} 2921 (w), 2724 (w), 2163 (w), 1720 (s, C=O), 1606 (m), 1564 (w), 1518 (s, N-O), 1477 (w), 1447 (m), 1408 (m), 1392 (w), 1342 (s, N-O), 1300 (m), 1256 (m), 1212 (m), 1172 (w), 1141 (m), 1110 (m) 1082 (s), 1015 (m), 985 (m), 863 (w), 839 (s), 733 (s); ^{1}H NMR (500 MHz; $CDCl_3$) δ_H 9.52 (1H, s, *H*-11) 8.27 (2H, d, *J* 8.5, *H*-16&16') 7.60 (2H, d, *J* 8.5, *H*-15&15') 6.63 (1H, s, *H*-6) 6.58 (1H, s, *H*-4) 5.15 (2H, s, *H*-13), 2.91 (2H, d, *J* 2.1, *H*-10) 2.54 (3H, s, *H*-7) 2.23 (3H, s, *H*-8) 1.61 (6H, s, *H*-12&12'); ^{13}C NMR (125 MHz; $CDCl_3$) δ_C 158.3 (C-1) 147.7 (C-17) 145.0 (C-14) 138.1 (C-5) 136.4 (C-3) 131.4 (C-2) 128.4 (C-15/15') 128.0 (C-4) 124.1 (C-16/16') 112.9 (C-6) 70.2 (C-13) 61.4 (C-10) 45.7 (C-12/12') 40.0 (C-9) 32.4 (C-) 26.0

(C-7) 20.9 (C-8); LRMS *m/z* (ES+) 364 $[M+Na]^+$ (100%); HRMS *m/z* (ES^+) [Found: ($M+Na^+$) 364.15186. $C_{20}H_{23}O_4NNa^+$ requires 364.15193]; HPLC (Method B) Retention Time = 12.15 minutes, purity 97.3%.

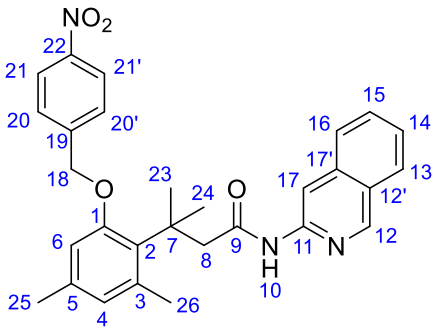
3-(2,4-Dimethyl-6-((4-nitrobenzyl)oxy)phenyl)-3-methylbutanoic acid (113)



To a flask containing 3-(2,4-dimethyl-6-((4-nitrobenzyl)oxy)phenyl)-3-methylbutanal (830 mg, 2.43 mmol, 1 eq.) was added MeCN (2.5 mL) and water (1.25 mL), which was stirred to give a suspension. To this was added NaH_2PO_4 (91 mg, 0.66 mmol, 0.27 eq.) and H_2O_2 (203 µL), followed by a solution of $NaOCl_2$ (407 mg, 4.50 mmol, 1.85 eq.) in water (3.65 mL). The reaction mixture was stirred at RT for 20 hours, then further H_2O_2 (500 µL) was added and the mixture was stirred for a further 4 hours. Further H_2O_2 (500 µL) was added, and the mixture was stirred for a further 3 hours. The reaction was then quenched by slow addition of saturated aqueous $Na_2S_2O_3$ solution and acidified with 1 M aqueous HCl. The mixture was extracted into EtOAc (3 × 50 mL), and the combined organic layers were washed with brine (1 × 50 mL). The layers were separated, and the organic component was dried over Na_2SO_4, filtered, and concentrated *in vacuo* onto Celite®. The crude material was then purified by silica gel chromatography, the product eluting in 20%–50% Et_2O/petroleum ether. Fractions were collected and concentrated *in vacuo* to afford the title compound as a fluffy colourless solid (465 mg, 1.30 mmol, 53% yield): R_f: 0.15–0.49 (Et_2O/petroleum ether 1:1, streaky); mp 178–180 °C (Et_2O); $\bar{\nu}_{max}$ (solid) cm^{-1} 2919 (m, br, CO_2H), 1699

(s, C=O), 1609 (m), 1562 (w), 1518 (s, N-O), 1476 (w), 1423 (w), 1398 (m), 1380 (m), 1344 (m, N-O), 1297 (s), 1284 (w), 1258 (m), 1234 (m), 1188 (m), 1166 (m), 1124 (m), 1108 (w), 1064 (s), 1030 (w), 1014 (m), 984 (w), 938 (m), 873 (w), 852 (s), 825 (s), 749 (s), 704 (s), 679 (w), 664 (w), 630 (w); ^{1}H NMR (400 MHz; $CDCl_3$) δ_H 8.25 (2H, d, *J* 8.7, *H*-16&16') 7.61 (2H, d, *J* 8.7, *H*-15&15') 6.59 (1H, s, *H*-6) 6.56 (1H, s, *H*-4) 5.16 (2H, s, *H*-13) 2.96 (2H, s, *H*-8) 2.53 (3H, s, *H*-10) 2.21 (3H, s, *H*-11) 1.62 (6H, s, *H*-12&12'); ^{13}C NMR (101 MHz; DMSO-D6) δ_C 173.3 (C-11), 157.5 (C-1), 147.0 (C-17), 145.3 (C-14), 137.1 (C-5), 135.2 (C-3), 130.4 (C-2), 128.4 (C-15&15'), 127.4 (C-19), 123.6 (C-4), 112.7 (C-6), 69.3 (C-13), 46.7 (C-10), 39.2 (C-9), 31.6 (C-12&12'), 25.2 (C-8), 20.3 (C-7); LRMS *m/z* (ES−) 356.1 $[M-H]^-$ (100%); HRMS *m/z* (ESI+) [Found 380.14716; $C_{20}H_{23}O_5NNa^+$ requires 380.14684]; HPLC (Method B) Retention Time = 11.17 minutes, purity 98.4%.

3-(2,4-Dimethyl-6-((4-nitrobenzyl)oxy)phenyl)-*N*-(isoquinolin-3-yl)-3-methylbutanamide (122)

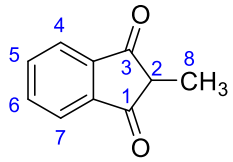


To a flame-dried flask under Ar was added 3-(2,4-dimethyl-6-((4-nitrobenzyl)oxy)phenyl)-3-methylbutanoic acid (30 mg, 0.084 mmol, 1 eq.), which was dissolved in anhydrous THF (0.5 mL) and stirred to give a colourless solution. The mixture was cooled to 0 °C and oxalyl chloride (8.5 µL, 0.10 mmol, 1.2 eq.) was added followed by DMF (1 drop), causing mild effervescence. The mixture was stirred and warmed to RT over 30 minutes. From a separate flame-dried flask under Ar was added a solution of 3-aminoisoquinoline (12 mg, 0.084 mmol, 1 eq.) and triethylamine

(17.5 µL, 0.126 mmol, 1.5 eq.) in anhydrous THF (0.5 mL), dropwise. This caused the solution to become deep yellow-orange, and a colourless precipitate to form. The mixture was stirred at room temperature for 100 minutes, then quenched with addition of water causing the precipitate to dissolve. The mixture was extracted into EtOAc (3 × 20 mL), and the combined organic fractions were washed with 1 M aqueous HCl (1 × 15 mL), saturated aqueous $NaHCO_3$ solution (1 × 15 mL) and brine (1 × 15 mL). The organic layer was separated, dried over anhydrous Na_2SO_4, filtered, and concentrated *in vacuo* to afford a yellow oil. The oil was dissolved in $CHCl_3$, adsorbed onto Celite®, loaded onto silica gel and purified by flash column chromatography eluting with 10%–15% EtOAc/petroleum ether. The fractions were collected and concentrated *in vacuo* to afford a yellow glassy solid which was further purified by semi-preparative HPLC, with the appropriate fractions lyophilised to afford the title compound as a colourless solid (6.1 mg, 12.6 µmol, 15% yield): R_f: 0.55 (EtOAc/petroleum ether 2:3); mp 160–161 °C (H_2O); $\bar{\nu}_{max}$ (solid) cm^{-1} 2918 (w, br), 1694 (m, C=O), 1629 (m), 1601 (m), 1521 (s, N-O), 1485 (m), 1450 (m), 1345 (s, N-O), 1324 (m), 1300 (m), 1258 (m), 1184 (m), 1116 (m), 1069 (m), 1015 (w), 959 (w), 930 (w), 881 (m), 850 (m), 825 (m), 750 (s), 738 (s), 704 (m), 690 (m), 630 (w); ^{1}H NMR (500 MHz; $CDCl_3$) δ_H 8.80 (1H, s, *H*-12) 8.38 (1H, s, *H*-17) 8.17 (2H, d, *J* 8.6, *H*-21&21') 7.77 (1H, d, *J* 8.3, *H*-16) 7.68 (1H, d, *J* 8.4, *H*-13) 7.57 (2H, d, *J* 8.6, *H*-20&20') 7.53 (1H, t, *J* 7.5, *H*-15) 7.37 (1H, t, *J* 7.5, *H*-14) 6.57 (1H, s, *H*-6) 6.56 (1H, s, *H*-4) 5.16 (2H, s, *H*-18) 2.96 (2H, s, *H*-8) 2.47 (3H, s, *H*-25) 2.16 (3H, s, *H*-26) 1.63 (6H, s, *H*-23&24); ^{13}C NMR (125 MHz; $CDCl_3$) δ_C 170.6 (C-9) 157.6 (C-11) 150.9 (C-1) 146.2 (C-22) 144.4 (C-19) 138.2 (C-17') 137.9 (C-5) 136.7 (C-3) 130.7 (C-15) 130.3 (C-2) 128.7 (C-20/20') 128.1 (C-13) 127.4 (C-12) 126.7 (C-14) 125.6 (C-12') 124.1 (C-21/21') 112.6 (C-6) 107.4 (C-17) 70.0 (C-18) 50.9 (C-8) 40.4 (C-7) 32.1 (C-23/24) 25.8

(C-25) 20.9 (C-26); LRMS *m/z* (ES+) 484.1 $[M+H]^+$ (100%); HRMS *m/z* (CI+) [Found 484.2231; $C_{29}H_{30}N_3O_4^+$ requires 484.2231]; HPLC (Method B) Retention Time = 12.83 minutes, purity 100.0%.

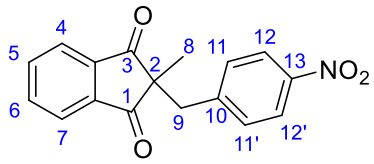
2-Methylindan-1,3-dione (139)



To a flame-dry flask under argon was added sodium hydride (3.20 g, 80 mmol, 4 eq., 60% in mineral oil). The sodium hydride was washed twice with hexane (2 × 20 mL, removed *via* cannulation), and then di-*n*-butyl ether (30 mL, dried over sieves) was added, giving a light grey suspension upon stirring. To this suspension was added dimethyl phthalate (4.76 mL, 20 mmol, 1 eq.), and then ethyl propionate (4.60 mL, 40 mmol, 2 eq.). The mixture was then heated under reflux for 2 hours, during which time the mixture turned bright orange and a solid orange crust formed. The reaction mixture was cooled on ice, the solid was collected by suction filtration, and washed with di-*n*-butyl ether affording a bright orange powder after drying. The powder was dissolved in distilled water (60 mL) to give an intense, deep orange solution. The solution was acidified with concentrated aqueous HCl (~15 mL), causing the solution to effervesce vigorously and turn pale yellow and cloudy. A bright yellow precipitate formed which was collected by suction filtration. The collected precipitate was dried under high vacuum to afford the title compound as a bright yellow solid (2.99 g, 18.7 mmol, 94% yield): R_f 0.56 (EtOAc/petroleum ether/AcOH 3:7:0.1); mp 84–86 °C (H_2O) [lit. 84–85 °C (H_2O)][258]; $\bar{\nu}_{max}$ (solid) cm^{-1} 3270 (br, w), 2935 (br, w), 1742 (s), 1710 (s), 1658 (m), 1572 (w), 1452 (w), 1369 (m), 1229 (br, s), 1166 (br, m), 1121 (br, m), 1079 (br, m), 1033 (br, s), 904 (br, w), 800 (w), 742 (w), 692 (w), 638 (w); ^1H NMR (400 MHz;

$CDCl_3$) δ_H 8.01–7.96 (2H, m, *H*-4&7) 7.88–7.82 (2H, m, *H*-5&6) 3.08 (1H, q, *J* 7.8, *H*-2) 1.44 (3H, d, *J* 7.8, *H*-8); ^{13}C NMR (101 MHz; $CDCl_3$) δ_C 201.2 (*C*-1&3) 142.0 (*C*-3'&7') 135.8 (*C*-5&6) 123.4 (*C*-4&7) 48.9 (*C*-2) 10.5 (*C*-8); LRMS *m/z* (ES−) 159 $[M-H]^-$ (100%). These data are in good agreement with the literature.[258,259]

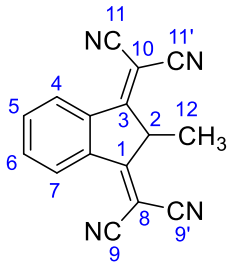
2-Methyl-2-(4-nitrobenzyl)-1H-indene-1,3(2H)-dione (140)



To a flame-dry flask under argon was added 2-methylindan-1,3-dione (50 mg, 0.312 mmol, 1 eq.). The material was dissolved in anhydrous DMF (0.5 mL), which was stirred to give a clear yellow solution. K_2CO_3 (86 mg, 0.624 mmol, 2 eq.) was added, causing the solution to turn deep orange. In a separate flame-dry flask under argon was added 4-nitrobenzyl bromide (81 mg, 0.375 mmol, 1.2 eq.), which was dissolved in DMF (0.25 mL), resulting in a pale straw-coloured solution. This solution was transferred to the reaction flask *via* cannulation, rinsed with further DMF (0.25 mL) and transferred again, causing the reaction mixture to turn cloudy and yellow. The reaction mixture was stirred at ambient temperature for 3 hours. The reaction mixture was then acidified by the addition of 1 M aqueous HCl and extracted with EtOAc (3 × 10 mL). The organic components were combined and washed with brine (3 × 30 mL), separated, dried over $MgSO_4$, filtered, and concentrated *in vacuo* to afford a pale yellow crystalline solid. The solid was dissolved in Et_2O, adsorbed onto Celite®, loaded onto silica gel, and purified by flash column chromatography eluting in 20–30% Et_2O/petroleum ether. The appropriate fractions were combined and concentrated *in vacuo* to afford the title compound as a colourless powder (46 mg, 0.156 mmol, 50% yield); R_f: 0.23 (3:7 EtOAc/petroleum ether); mp 119–122 °C (Et_2O); $\bar{\nu}_{max}$ (solid) cm^{-1}

1744 (m), 1704 (s, C=O), 1598 (m), 1503 (s, N-O), 1435 (w), 1378 (w), 1340 (s, N-O), 1288 (w), 1205 (m), 1186 (m), 1155 (m), 1108 (w), 1017 (m), 999 (m), 913 (m), 862 (m), 849 (m), 795 (s), 750 (m), 725 (s), 698 (s), 645 (m); ^{1}H NMR (500 MHz; $CDCl_3$) δ_H 7.94 (2H, dt, *J* 8.8, 1.9, *H*-12&12') 7.87 (2H, ddd, *J* 3.1, 6.6, 1.4, *H*-4&7) 7.78 (2H, ddd, *J* 3.1, 6.6, 1.4, *H*-5&6) 7.21 (2H, dt, *J* 8.8, 1.9, *H*-11&11') 3.27 (2H, s, *H*-9) 1.44 (3H, s, *H*-8); ^{13}C NMR (126 MHz; $CDCl_3$) δ_C 203.1 (*C*-1&3) 146.9 (*C*-13) 143.7 (*C*-10) 141.1 (*C*-3'&7') 136.1 (*C*-5&6) 130.8 (*C*-11&11') 123.4 (*C*-12&12') 123.3 (*C*-4&7) 55.7 (*C*-2) 40.3 (*C*-9) 20.8 (*C*-8); LRMS *m/z* (ES+) 318 $[M+Na]^+$ (100%); HRMS *m/z* (ESI+) [Found: 318.07376, $C_{17}H_{13}NO_4Na^+$ requires 318.07368]; HPLC (Method A) Retention Time 12.99 min, purity 99.6%.

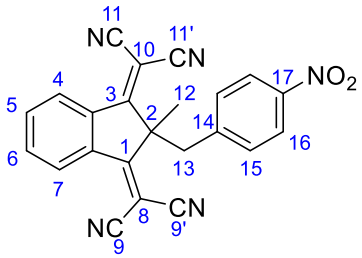
2,2'-(2-Methyl-1*H*-indene-1,3(2*H*)-diylidene)dimalononitrile (158)



To a flame-dry flask under Ar was added 2-methylindan-1,3-dione (1.0 g, 6.24 mmol, 1 eq.), which was dissolved in anhydrous ethanol (20 mL) and stirred to give a bright yellow solution. To this was added ammonium acetate (1.44 g, 18.73 mmol, 3 eq.), causing the solution to bright orange, and then malononitrile (1.24 g, 18.73 mmol, 3 eq.) which caused the solution to turn deep brown. The mixture was heated under reflux for 24 hours, causing the solution to turn an intense deep blue. The mixture was cooled and acidified with addition of concentrated HCl, causing the solution to turn brown, with a deep brown precipitate forming. The precipitate was collected by suction filtration, washed with 1 M aqueous HCl, and dried *in vacuo*. The resulting solid was dissolved in acetone, loaded onto silica gel, and purified by flash column

chromatography with the product eluting in 20%–50% acetone/petroleum ether. The fractions were combined and concentrated *in vacuo* to afford the title compound as a deep brown crystalline solid (1.03 g, 4.01 mmol, 64% yield): R_f: 0.29 (acetone/petroleum ether 1:1); mp >350 °C (acetone); $\bar{\nu}_{max}$ (solid) cm^{-1} 2186 (s, C≡N), 1693 (w, C=C), 1462 (m), 1401 (s), 1379 (s), 1317 (m), 1275 (m), 1218 (w), 1165 (w), 1091 (s), 1005 (m), 749 (w), 685 (m); ^{1}H NMR (500 MHz; $CDCl_3$) δ_H 8.66–8.60 (2H, m, *H*-4&7) 7.95–7.89 (2H, m, *H*-5&6) 4.38 (1H, q, *J* 7.4, *H*-2) 1.73 (3H, d, *J* 7.4, *H*-12); ^{13}C NMR (126 MHz; $CDCl_3$) δ_C 171.1 (*C*-1&3) 138.9 (*C*-3'&7') 136.4 (*C*-5&6) 127.2 (*C*-4&7) 111.7 (*C*-9&11) 111.5 (*C*-9'&11') 78.8 (*C*-8&10) 47.9 (*C*-2) 18.8 (*C*-12); LRMS *m/z* (ES−) 255 $[M-H]^-$ (100%); HRMS *m/z* (ESI−) [Found 255.0674; $C_{16}H_7N_4^-$ requires 255.0665]; HPLC (Method A) Retention Time = 10.79 minutes, 90.7%.

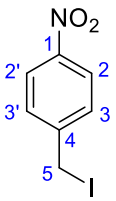
2,2'-(2-Methyl-2-(4-nitrobenzyl)-1*H*-indene-1,3(2*H*)-diylidene)dimalononitrile (136)



To a flame-dry flask under an argon atmosphere was added 2,2'-(2-methyl-1*H*-indene-1,3(2*H*)-diylidene)dimalononitrile (100 mg, 0.390 mmol, 1 eq.) and 4-nitrobenzyl iodide (113 mg, 0.429 mmol, 1.1 eq.). To this was added dry toluene (2 mL), and the mixture was stirred to give a dark brown suspension. Triethylamine (65 µL, 0.468 mmol, 1.2 eq.) was added, causing the solution to turn an intense dark blue, and the solution was heated under reflux for 13 hours. The reaction mixture was cooled to RT, diluted with EtOAc, and shaken with 1 M aqueous HCl. The layers were separated, and the aqueous component was extracted twice more with EtOAc (2 × 20 mL). The organic components were combined, washed with saturated aqueous $NaHCO_3$ solution

(1 × 40 mL), and then brine (1 × 40 mL). The organic component was then separated, dried over $MgSO_4$, filtered, and concentrated *in vacuo* to afford a deep purple residue from which purple crystals formed. The residue was dissolved in EtOAc, adsorbed onto Celite®, loaded onto silica gel, and purified by flash column chromatography using 10%–23% EtOAc/*n*-hexane. The appropriate fractions were combined and concentrated *in vacuo*, affording a yellow solid. This solid was triturated with Et_2O three times, and then dried *in vacuo* to afford the title compound as a yellow solid (38 mg, 0.096 mmol, 25% yield): R_f: 0.65 (EtOAc/*n*-hexane/AcOH 2:3:0.1); mp 238–239 °C (EtOAc); $\bar{\nu}_{max}$ (solid) cm^{-1} 2225 (m, C≡N), 1585 (m), 1556 (s), 1518 (s, N–O), 1463 (w), 1442 (w), 1388 (w), 1346 (s), 1317 (m), 1273 (m), 1237 (m), 1198 (w), 1177 (w), 1113 (w), 1012 (w), 960 (w), 910 (m), 880 (m), 862 (s), 848 (s), 805 (w), 776 (s), 752 (s), 717 (m), 693 (s), 842 (w); ^{1}H NMR (500 MHz; $CDCl_3$) δ_H 8.64 (2H, dd, *J* 3.1, 6.2, *H*-4&7) 7.99 (2H, dt, *J* 8.9, 2.0, *H*-16&16') 7.82 (2H, dd, *J* 3.1, 6.2, *H*-5&6) 7.14 (2H, dt, *J* 8.9, 2.0, *H*-15&15') 4.00 (2H, s, *H*-13) 2.16 (3H, s, *H*-12); ^{13}C NMR (126 MHz; $CDCl_3$) δ_C 171.7 (*C*-1&3) 146.5 (*C*-17) 140.0 (*C*-14) 137.9 (*C*-3'&7') 135.9 (*C*-5&6) 128.6 (*C*-15&15') 125.5 (*C*-4&7) 122.9 (*C*-16&16') 111.22 (*C*-9&11) 111.16 (*C*-9'&11') 77.5 (*C*-8&10) 56.1 (*C*-2) 39.5 (*C*-13) 21.9 (*C*-12); LRMS *m/z* not detected; HRMS *m/z* (EI+) [Found 391.1069; $C_{23}H_{14}N_5O_2^+$ requires 391.1064]; HPLC (Method A) Retention Time = 13.80 min, purity 96.4%.

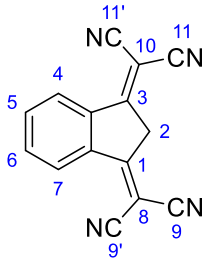
1-(Iodomethyl)-4-nitrobenzene (182)



To a flame-dry flask under Ar was added 4-nitrobenzyl chloride (500 mg, 2.91 mmol, 1 eq.), followed by sodium iodide (4.37 g, 29.1 mmol, 10 eq.). Acetone (7.5 mL) was

added and stirred to give a colourless suspension in a yellow solution. The mixture was heated under reflux for 160 minutes, then cooled to RT. Water was added, and the mixture was extracted with EtOAc (3 × 30 mL). The combined organic components were washed with brine (50 mL), dried over Na_2SO_4, filtered, and concentrated *in vacuo* to afford the title compound as a fluffy, pale brown solid (738 mg, 2.81 mmol, 96% yield): R_f: 0.53 (EtOAc/petroleum ether 1:9); mp 126–128 °C (EtOAc) [lit. 125-126 °C (CH_2Cl_2)][260]; $\bar{\nu}_{max}$ (solid) cm^{-1} 1933 (w), 1594 (m), 1515 (m, N–O), 1417 (w), 1340 (s), 1321 (s, N-O), 1157 (m), 1106 (m), 854 (s, Ar C-H), 797 (s), 751 (s), 693 (s), 629 (w); ^1H NMR (400 MHz; $CDCl_3$) δ_H 8.16 (2H, d, *J* 8.7, *H*-2&2') 7.56 (2H, d, *J* 8.7, *H*-3&3') 4.48 (2H, s, *H*-5); ^{13}C NMR (101 MHz; CDCl3) δ_C 147.3 (*C*-1) 146.9 (*C*-4) 129.7 (*C*-2&2') 124.3 (*C*-3&3') 2.2 (*C*-5); LRMS *m/z* not detected. These data are in good agreement with the literature.[260–262]

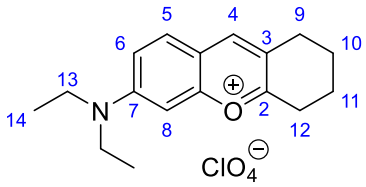
2,2'-(1*H*-indene-1,3(2*H*)-diylidene)dimalononitrile (134)



To a flame-dry flask under Ar was added indan-1,3-dione (500 mg, 3.42 mmol, 1 eq.) and anhydrous ethanol (10 mL). The mixture was stirred to give a suspension, and to this was added ammonium acetate (264 mg, 3.42 mmol, 1 eq.) causing the solution to turn orange. Malononitrile (678 mg, 10.26 mmol, 3 eq.) was added, and the solution was heated under reflux for 10 hours. The now-deep purple reaction mixture was cooled to RT and acidified by addition of 1 M aqueous HCl, causing the solution to turn pale brown and a grey suspension to form. The suspended material was collected by suction filtration, washed with 1 M aqueous HCl, and dried *in vacuo*. The material was

taken up in acetone, loaded onto silica gel and purified by flash column chromatography, the product eluting in 20%–50% acetone in petroleum ether. The appropriate fractions were collected and concentrated *in vacuo* to afford the title compound as a deep purple solid (585 mg, 2.41 mmol, 70% yield): R_f: 0.55 (acetone/petroleum ether 1:1); m.p. >300 °C (acetone/petroleum ether) [lit. 263–266 °C][263]; $\bar{\nu}_{max}$ (solid) cm^{-1} 3493 (w, br), 2190 (m, br, C≡N), 1630 (w, C=C), 1557 (w), 1479 (s), 1451 (s), 1397 (m), 1302 (m), 1241 (m), 1185 (m), 1123 (s), 1083 (m), 895 (w), 786 (m), 743 (s), 658 (m); ^{1}H NMR (400 MHz; acetone-D6) δ_H 8.05-8.00 (2H, m, *H*-4&7) 7.40-7.36 (2H, m, *H*-5&6) 5.88 (1H, s, *H*-2); ^{13}C NMR (101MHz; acetone-D6) δ_C 159.4 (*C*-1&3) 139.6 (*C*-4'&7') 130.4 (*C*-5&6) 122.6 (*C*-4&7) 119.0 (*C*-9'&11') 118.7 (*C*-9&11) 103.9 (*C*-2) 51.6 (*C*-8&10); LRMS *m/z* (ES^-) 241 $[M-H]^-$ (100%). With the exception of the melting point, these data are in good agreement with the literature.[208,263]

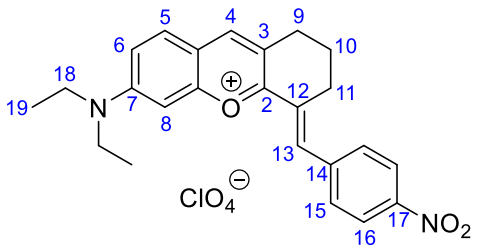
6-(Diethylamino)-1,2,3,4-tetrahydroxanthylium perchlorate (169)



To a flame-dried flask under argon was added concentrated aqueous H_2SO_4 (26 mL), which was stirred. Cyclohexanone (2.02 mL, 20 mmol, 2 eq.) was added dropwise, and the solution was cooled to 0 °C. 4-(Diethylamino)-salicylaldehyde (1.93 g, 10 mmol, 1 eq.) was added in one portion, and the mixture was stirred vigorously until the resulting solution was deep brown. The solution was then heated at 90 °C for 90 minutes, during which time the solution turned a deep red colour. The solution was cooled to RT, poured onto ice (~200 g), and stirred. To the resulting intense red solution was added ice-cold aqueous $HClO_4$ (2.42 mL, 70% *v/v*), causing a fine

precipitate to form. The precipitate was filtered under reduced pressure, washed with ice-cold water, and dried under high vacuum to afford the title compound as a bright red powder (3.02 g, 8.49 mmol, 85% yield): R_f: 0.90–0.42 (1:19 EtOH/CH_2Cl_2); mp 164–168 °C (H_2O) [lit. 173–175 °C][264]; ^{1}H NMR (400 MHz, $CDCl_3$) δ_H 8.42 (1H, s, *H*-4) 7.92 (1H, d, *J* 9.6, *H*-5) 7.28 (1H, dd, *J* 9.5, 2.4, *H*-6) 6.82 (1H, d, *J* 2.4, *H*-8) 3.65 (4H, q, *J* 7.3, *H*13&13') 3.03 (2H, t, *J* 6.4, *H*-12) 2.85 (2H, t, *J* 6.1, *H*-9) 2.04–1.95 (2H, m, *H*-11) 1.91–1.83 (2H, m, *H*-10) 1.32 (6H, t, *J* 7.3, *H*-14&14'); ^{13}C NMR (101 MHz, $CDCl_3$) δ_C 170.8 (C-2) 160.1 (C-8') 156.6 (C-7) 150.6 (C-4) 133.1 (C-5) 122.4 (C-4') 119.7 (C-8) 118.8 (C-6) 95.3 (C-3) 46.5 (C-13/13') 29.2 (C-9) 26.3 (C-10) 21.5 (C-11) 21.3 (C14/14') 12.6 (br, C-12?); LRMS *m/z* 256 $[M-ClO_4]^+$ (100%); HRMS *m/z* [Found: 256.16963; $C_{17}H_{22}NO^+$ requires 256.16959]; due to the salt nature of this compound, HPLC purity could not be determined. These data are in good agreement with the literature, except for the melting point.[214,264]

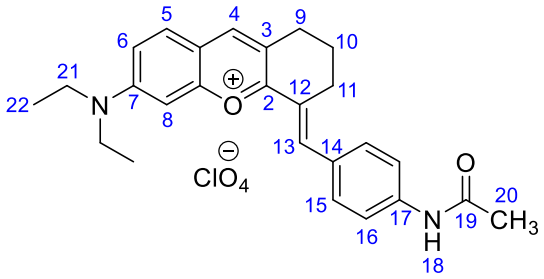
(*E*)-6-(Diethylamino)-4-(4-nitrobenzylidene)-1,2,3,4-tetrahydroxanthylium (166)



To a flask was added 6-(diethylamino)-1,2,3,4-tetrahydroxanthylium perchlorate (300 mg, 0.843 mmol, 1 eq.) and 4-nitrobenzaldehyde (178 mg, 1.179 mmol, 1.4 eq.). Glacial acetic acid (84.3 mL) was added and the mixture was stirred, giving a deep red solution. The mixture was heated at 110 °C for 24 hours, then concentrated *in vacuo* onto Celite® and purified by flash silica gel chromatography, eluting in 1%–7% EtOH/CH_2Cl_2. The fractions were collected and concentrated *in vacuo* and dried under high vacuum to afford the title compound as a deep purple solid (360 mg, 0.736 mmol,

87% yield): R_f: 0.38–0.27 (1:19 EtOH/CH_2Cl_2); mp 189–190 °C (H_2O); $\bar{\nu}_{max}$ (solid) cm^{-1} 1637 (m), 1606 (m), 1592 (m), 1577 (m), 1510 (s), 1475 (s), 1452 (m), 1409 (m), 1379 (s), 1354 (w), 1336 (s), 1295 (s), 1268 (m), 1246 (m), 1214 (m), 1183 (m), 1134 (m), 1082 (s, br), 1008 (m), 921 (w), 903 (m), 878 (m), 852 (s), 819 (s), 791 (w), 757 (w), 729 (w), 704 (m), 693 (m), 656 (w), 621 (s), 606 (m); ^{1}H NMR (400 MHz, CD_3CN) δ_H 8.31 (2H, d, *J* 8.9, *H*-16/16') 8.27 (1H, s, *H*-4) 8.06 (1H, s, *H*-13) 7.83–7.76 (3H, m, *H*-5/15/15') 7.38 (1H, dd, *J* 9.5, 2.4, *H*-6) 7.11 (1H, d, *J* 1.8, *H*-8) 3.75–3.66 (4H, m, *H*-18/18') 3.00–2.95 (2H, m *H*-9) 2.91 (2H, t, *J* 6.1, *H*-11) 1.32 (6H, t, *J* 7.1, *H*-19/19'); LRMS *m/z* (ES+) 389 $[M-ClO_4]^+$ (100%); HRMS *m/z* [Found: 389.18608; $C_{24}H_{25}O_3N_2^+$ requires 389.18597]; due to the salt nature of this compound, HPLC purity could not be determined.

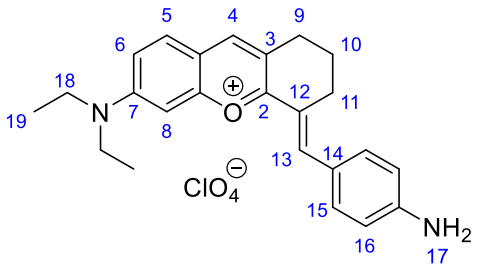
(*E*)-4-(4-Acetamidobenzylidene)-6-(diethylamino)-1,2,3,4-tetrahydroxanthylium perchlorate (170)



To a flame-dried flask under Ar was added 6-(diethylamino)-1,2,3,4-tetrahydroxanthylium perchlorate (356 mg, 1.0 mmol, 1 eq.) and 4-acetamidobenzaldehyde (196 mg, 1.2 mmol, 1.2 eq.), which was dissolved in acetic anhydride (3 mL) to give a bright red solution. The mixture was heated at 140 °C for 5 hours, during which time the solution became deep blue. The mixture was cooled to 0 °C, then concentrated *in vacuo* to dryness. The residue was redissolved in a mixture of MeOH/CH_2Cl_2, and again concentrated *in vacuo* onto Celite®. The crude material was then purified by flash silica gel chromatography, eluting in 2%–10% EtOH/CH_2Cl_2. The fractions were concentrated *in vacuo* to afford the title compound as a deep purple

solid (156 mg, 0.389 mmol, 39% yield): R_f: 0.31–0.12 (1:19 EtOH/CH_2Cl_2); mp 214–217 °C (EtOH); $\bar{\nu}_{max}$ (solid) cm^{-1} 3313 (w), 2968 (w), 1686 (m), 1634 (m), 1587 (w), 1560 (w), 1542 (m), 1502 (m), 1474 (m), 1460 (m), 1402 (m), 1355 (w), 1334 (m), 1311 (m), 1267 (m), 1212 (w), 1178 (m), 1153 (m), 1132 (w), 1102 (s), 1070 (s), 1004 (m), 965 (w), 920 (w), 881 (w), 863 (w), 832 (m), 797 (m), 733 (w), 705 (m), 655 (m), 621 (s); ^{1}H NMR (400 MHz, DMSO-D6) δ_H 10.25 (1H, s, *H*-18) 8.54 (1H, s, *H*-4) 8.04 (1H, s, *H*-13) 7.91 (1H, d, *J* 9.5, *H*-5) 7.75 (2H, d, *J* 8.7, *H*-16&16') 7.65 (2H, d, *J* 8.7, *H*-15&15') 7.48 (1H, dd, *J* 9.5, 2.2, *H*-6) 7.31 (1H, d, *J* 2.2, *H*-8) 3.72 (4H, q, *J* 7.0, *H*-21&21') 2.96 (2H, t, *J* 5.4, *H*-9) 2.88 (2H, t, *J* 6.0, *H*-11) 2.09 (3H, s, *H*-20) 1.91–1.83 (2H, m, *H*-10) 1.26 (6H, t, *J* 7.0, *H*-22&22'); LRMS *m/z* (ES+) 401 $[M-ClO_4]^+$ (100%); HRMS *m/z* [Found: 401.22233; $C_{26}H_{29}O_2N_2^+$ requires 401.22235]; due to the salt nature of this compound, HPLC purity could not be determined.

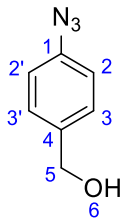
(*E*)-4-(4-Aminobenzylidene)-6-(diethylamino)-1,2,3,4-tetrahydroxanthylium perchlorate (163)



A flask was charged with a sample of (*E*)-4-(4-acetamidobenzylidene)-6-(diethylamino)-1,2,3,4-tetrahydroxanthylium (100 mg), which was dissolved in a mixture of EtOH (5.2 mL) and 4 M aqueous HCl (9.36 mL). The mixture was stirred to give a deep purple solution, which was then heated under reflux (~80 °C) for 5 hours. The solution was diluted with water and neutralised with saturated aqueous $NaHCO_3$ solution, causing the solution to turn dark turquoise. The mixture was extracted with CH_2Cl_2, dried over Na_2SO_4, filtered and concentrated *in vacuo* onto Celite®. The crude material was then purified by flash silica gel column chromatography, eluting in 2%–

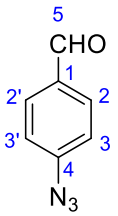
5% EtOH/CH_2Cl_2. The fractions were collected and concentrated *in vacuo* to afford a dark turquoise solid. This solid was dissolved in MeCN/H_2O (1:1) and loaded onto a DOWEX 50WX8 column, which had been pre-equilibrated with MeCN/H_2O (1:1). The column was flushed with ~5 CVs of MeCN/H_2O (1:1), and then the product was eluted with ~10 CVs of MeCN/6% aqueous $HClO_4$ (1:1). The fractions were collected, the volatile components removed *in vacuo*, and the remaining orange aqueous component was extracted into CH_2Cl_2. The organic layer was separated, dried over Na_2SO_4, filtered, and concentrated *in vacuo* to afford the title compound as a dark turquoise solid (42 mg, 0.117 mmol, 37% yield): R_f: 0.0–0.48 (EtOH/CH_2Cl_2 1:9, streaky); mp 165 °C–166 °C (H_2O); $\bar{\nu}_{max}$ (solid) cm^{-1} 3378 (s, br, -NH2), 1641 (w, br, C=O), 1482 (w), 1268 (w), 1046 (w), 1024 (s), 991 (s), 826 (m), 763 (m); ^{1}H NMR (400 MHz, DMSO-D6) δ_H 8.34 (1H, s, *H*-4) 8.05 (1H, s, *H*-13) 7.80 (1H, d, *J* 9.4, *H*-5) 7.55 (2H, d, *J* 8.7, *H*-15&15') 7.31 (1H, dd, *J* 9.4, 2.3, *H*-6) 7.20 (1H, d, *J* 2.3, *H*-8) 6.70 (2H, d, *J* 8.7, *H*-16&16') 6.48 (2H, s br, *H*-17) 3.65 (4H, q, *J* 7.1, *H*-18&18') 2.92 (2H, t, *J* 5.8, *H*-9) 2.83 (2H, t, *J* 5.8, *H*-11) 1.86 (2H, q, *J* 5.8, *H*-10) 1.23 (6H, t, *J* 7.1, *H*-19&19'); ^{13}C NMR (101 MHz, DMSO-D6) δ_c 165.1, 158.3, 155.1, 153.2, 146.9, 140.8, 135.4, 131.7, 123.5, 123.3, 121.8, 117.1, 117.0, 114.4, 96.0, 45.6, 27.6, 27.5, 21.4, 13.0; LRMS *m/z* (ES+) 359 $[M-ClO_4]^+$ (100%); HRMS *m/z* (ESI+) [Found 359.21171;$C_{24}H_{27}N_2O^+$ requires 359.21179]; due to the salt nature of this compound, HPLC purity could not be determined. These data are in good agreement with the literature, except for ^{13}C NMR, for which there is a consistent ~5 ppm downfield shift for the reported resonances. This discrepancy is accounted for by differences in calibration of the reference solvent.[214]

4-(Hydroxymethyl)azidobenzene (172)



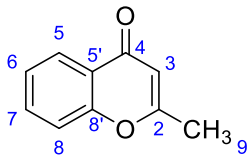
To a 3-necked flask fitted with two dropping funnels was added 4-aminobenzyl alcohol (1.0 g, 8.12 mmol, 1 eq.) which was dissolved in 6 M aqueous HCl (5.33 mL) and stirred to give a brown solution. The mixture was cooled to 0 °C, and from one funnel was added a solution of $NaNO_2$ (566 mg, 8.20 mmol, 1.01 eq.) in water (2.87 mL) dropwise over 5 minutes. The mixture was stirred at 0 °C for 10 minutes, then a solution of NaN_3 (533 mg, 8.20 mmol, 1.01 eq.) in water (2.87 mL) was added dropwise, causing brisk effervescence. The mixture was stirred at 0 °C for 10 minutes, then warmed to RT and stirred for 1 hour. The mixture was then diluted with water and extracted with Et_2O (2 × 60 mL). The combined organic components were washed with water (2 × 40 mL), separated, dried over Na_2SO_4, filtered, and concentrated *in vacuo* to give a brown oil. The oil was dissolved in EtOAc and concentrated *in vacuo* onto Celite®. The crude material was loaded onto a 25 g Biotage® SNAP silica gel cartridge and purified by automated flash column chromatography on a Biotage® SP4 system, eluting in 10%–40% EtOAc/petroleum ether. The fractions were collected and concentrated *in vacuo* to afford the title compound as a yellow oil (1.0 g, 6.70 mmol, 83% yield): R_f: 0.57 (EtOAc/petroleum ether 1:1); $\bar{\nu}_{max}$ (solid) cm^{-1} 3323 (br, O-H), 2362 (w), 2101 (s, N_3), 1608 (w), 1582 (w), 1506 (s), 1419 (w), 1280 (s), 1009 (m), 812 (m), 772 (m); ^1H NMR (400 MHz, $CDCl_3$) δ_H 7.36 (2H, d, *J* 8.6, *H*-2&2') 7.02 (2H, d, *J* 8.6, *H*-3&3') 4.67 (2H, s, *H*-5) 1.66 (1H, br s, *H*-6); LRMS *m/z* not detected; HRMS *m/z* not detected. These data are in good agreement with the literature.[265]

4-Azidobenzaldehyde (173)



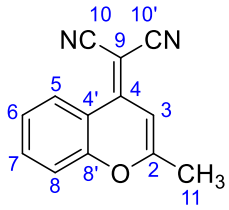
To a flask containing 4-azidobenzyl alcohol (2.08 g, 13.94 mmol, 1.0 eq.) under Ar was added CH_2Cl_2 (61.6 mL) and Celite® (~30 g), and the mixture was stirred vigorously to give a suspension. Pyridinium chlorochromate (5.11 g, 23.70 mmol, 1.7 eq.) was added, causing the solution to turn brown rapidly. The mixture was stirred at RT for 2 hours, then filtered through a pad of Celite® and washed through with CH_2Cl_2. The filtrate was concentrated *in vacuo* onto Celite®, loaded onto silica gel and purified by flash column chromatography, the product eluting with 5%–20% Et_2O/petroleum ether. The fractions were collected and concentrated *in vacuo* to afford the title compound as a clear yellow liquid (1.94 g, 13.18 mmol, 95% yield): R_f: 0.62 (CH_2Cl_2); $\bar{\nu}_{max}$ (solid) cm^{-1} 2408 (w), 2362 (w), 2109 (s, br, -N_3), 1690 (C=O), 1595 (s), 1577 (s), 1501 (m), 1424 (w), 1390 (w), 1280 (s), 1211 (s), 1164 (s), 1125 (m), 1108 (m), 1010 (w), 851 (m), 822 (s), 781 (m), 684 (w), 614 (w); ^{1}H NMR (400 MHz, $CDCl_3$) δ_H 9.94 (1H, s, *H*5) 7.88 (2H, ddd, *J* 8.5, 2.3, 1.9, *H*3/3') 7.16 (2H, ddd, *J* 8.5, 2.3, 1.9, *H*2/2'); ^{13}C NMR (101 MHz, $CDCl_3$) δ_C 190.7 (C5) 146.4 (C4) 133.4 (C1) 131.7 (C3/3') 119.6 (C2/2'); LRMS *m/z* not detected; HRMS *m/z* (APCI MS) not detected. These data are in good agreement with the literature.[266–268]

2-Methyl-4*H*-chromen-4-one (183)



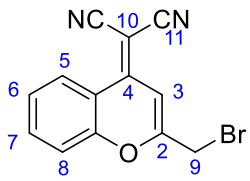
To a flame-dried flask under Ar was added EtOAc (667 mL), which was stirred. 2'-Hydroxyacetophenone (24.10 mL, 200.0 mmol, 1.00 eq.) was added, followed by cut pieces of sodium metal (12.87 g, 560 mmol, 2.80 eq.) portionwise. The solution began to gain a yellow-green colour and was stirred at RT for 1.5 hours. During the reaction time, the solution became bright yellow, a fine suspension formed, and the mixture became warm. The precipitate was collected by suction filtration (~67 g) and redissolved in water (156 mL) to give a yellow solution. Glacial acetic acid (62 mL), then concentrated aqueous H_2SO_4 (16 mL) was added, and the solution was stirred and heated under reflux for 16 hours, during which time the solution turned orange. The heat was removed, and ice-cold water (100 mL) was added. The solution was neutralised with addition of solid $NaHCO_3$ (~200 g). The solution was extracted with toluene (3 × 400 mL), washed with brine (3 × 300 mL), separated, dried over Na_2SO_4, filtered, and concentrated *in vacuo* to afford a brown solid. The solid was dissolved in EtOAc, adsorbed onto Celite®, loaded onto silica gel and purified by flash column chromatography, eluting with 50% Et_2O/petroleum ether. The fractions were combined and concentrated *in vacuo* to afford the title compound as an off-white solid (15.52 g, 96.9 mmol, 48% yield): R_f: 0.18 (Et_2O/petroleum ether 1:1); mp 58–61 °C (Et_2O) [lit. 55–56 °C][269]; ^{1}H NMR (400 MHz; $CDCl_3$) δ_H 8.18 (1H, dd, *J* 8.1, 1.6, *H*-5) 7.64 (1H, ddd, *J* 8.5, 6.9, 1.6, *H*-7) 7.42 (1H, d, *J* 8.5, *H-8*) 7.38 (1H, ddd, *J* 8.1, 7.2, 1.0, *H-6*) 6.18 (1H, d, *J* 0.7, *H*-3), 2.39 (3H, d, *J* 0.7, *H*-9); LRMS *m/z* (ES+) 161 $[M+H]^+$ (100%).These data are in agreement with the literature.[49,187,269]

2-(2-Methyl-4*H*-chromen-4-ylidene)malononitrile (180)



To a flame-dried flask under Ar was added 2-methyl-4*H*-chromen-4-one (2.0 g, 12.5 mmol, 1.0 eq.) and malononitrile (8.2 g, 125 mmol, 10.0 eq.). Acetic anhydride (12.5 mL) was added and the mixture was stirred, giving an intense deep red colour. The solution was heated under reflux for 2 hours, during which time is turned an intense red-brown. The mixture was cooled to 50 °C, methanol (30 mL) was added, and the mixture was stirred for 1 hour. The mixture was cooled to RT, and the volatile components were removed *in vacuo*. Et_2O was added causing a precipitate to form, which was collected by suction filtration. The filtrate was dried under reduced pressure to afford the title compound as a fine red-brown powder (1.82 g, 8.74 mmol, 70% yield): R_f 0.26 (1:4 EtOAc/petroleum ether); mp 185–188 °C (Et_2O) [lit. 184–186 °C (MeOH)][187]; ^{1}H NMR (400 MHz, $CDCl_3$) δ_H 8.92 (1H, dd, *J* 8.7, 1.4, *H*-5) 7.72 (1H, ddd, *J* 8.1, 7.5, 1.4, *H*-7) 7.43–7.48 (2H, m, *H*-8/*H*-6) 6.72 (1H, s, *H*-3) 2.44 (3H, s, *H*-11); LRMS *m/z* (ES+) 209 $[M+H]^+$ (100%). These data are in good agreement with the literature.[49,187]

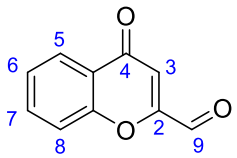
2-(2-(Bromomethyl)-4*H*-chromen-4-ylidene)malononitrile (188)



To a flame-dried microwave vial under argon was added 2-(2-methyl-4*H*-chromen-4-ylidene)malononitrile (100 mg, 0.480 mmol, 1.0 eq.), *N*-bromosuccinimide (171 mg, 0.961 mmol, 2.0 eq.), and AIBN (7.9 mg, 0.048 mmol, 0.1 eq.). CCl_4 (1.92 mL) was

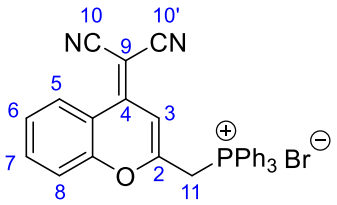
added, and the mixture was stirred to give a dark suspension. The vessel was sealed and heated at 70 °C for 22 hours. Additional *N*-bromosuccinimide (85.5 mg, 0.480 mmol, 1.0 eq.) and AIBN (7.9 mg, 0.048 mmol, 0.1 eq.) was added, the vessel was resealed and heated at 70 °C for 5 hours. The reaction mixture cooled to RT, diluted with $CHCl_3$ (50 mL) and washed with water (2 × 30 mL) and brine (2 × 40 mL). The organic component was separated, dried over $MgSO_4$, filtered, and concentrated *in vacuo* onto Celite®. The crude material was then purified by flash column silica gel chromatography, eluting with toluene. The appropriate fractions were collected and concentrated *in vacuo* to afford the title compound as a yellow solid (52 mg, 0.181 mmol, 38% yield): R_f: 0.46 (1:3 EtOAc/petroleum ether); mp 182–185 °C (toluene); $\bar{\nu}_{max}$ (solid) cm^{-1} 2219 (m, C≡N), 2204 (m), 1637 (s, C=C), 1613 (m), 1519 (s), 1456 (m), 1424 (w), 1398 (s), 1333 (m), 1324 (m), 1270 (m), 1224 (m), 1200 (w), 1147 (w), 1126 (m), 1041 (w), 972 (s), 918 (m), 890 (m), 875 (m), 862 (m), 799 (m), 769 (s), 746 (s), 688 (m), 665 (s), 640 (s), 617 (m); ^{1}H NMR (400 MHz, $CDCl_3$) δ_H 8.92 (1H, dd, *J* 8.4, 1.5, *H*5) 7.76 (1H, ddd, *J* 8.4, 7.1, 1.5, *H*7) 7.54–7.47 (2H, m, *H*6&8) 6.94 (1H, s, *H*3) 4.29 (2H, s, *H*9); ^{13}C NMR (126 MHz, $CDCl_3$) δ_C 158.0 (C4) 152.8 (C2) 152.6 (C4') 135.4 (C7) 126.7 (C6) 126.0 (C5) 119.0 (C8) 117.5 (C8') 116.0 (C11') 114.9 (C11) 106.8 (C3) 65.9 (C10) 26.6 (C9); LRMS *m/z* (ES−) 285 $[M(^{79}Br)-H]^-$ (50%), 287 $[M(^{81}Br)-H]^-$ (50%); HRMS *m/z* (ESI−) [Found 284.96695; $C_{13}H_6ON_2{}^{(79)}Br^-$ requires 284.96690; 286.96492; $C_{13}H_6ON_2{}^{(81)}Br^-$ requires 286.96485]; HPLC (Method B) Retention Time = 10.43 minutes, purity 97.4%.

4-Oxo-4*H*-chromene-2-carbaldehyde (198)



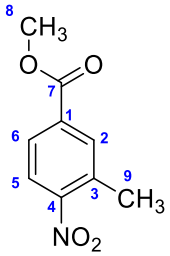
To a flame-dried V-shaped vial under argon was added 2-methyl-4*H*-chromen-4-one (100 mg, 0.624 mmol, 1.0 eq.) and SeO_2 (95 mg, 0.937 mmol, 1.5 eq.). The vessel was sealed and purged with Ar, then xylenes (0.624 mL) were added. The mixture was stirred and heated at 165 °C for 16 hours. The mixture was cooled to RT, filtered through a pad of Celite® and washed through with $CHCl_3$. The solution was concentrated *in vacuo* to give an orange residue, which was adsorbed onto Celite®, loaded onto silica gel and purified by flash column chromatography, eluting in 30%–50% EtOAc/petroleum ether. The fractions were collected and concentrated *in vacuo* to afford the title compound as an orange solid (32 mg, 0.184 mmol, 29% yield): R_f 0.49 (1:4 EtOAc/CH_2Cl_2); mp 120–123 °C (EtOAc); $\bar{\nu}_{max}$ (solid) cm^{-1} 3065 (w), 2919 (w), 2160 (m, br), 2032 (m), 1977 (m), 1703 (m), 1651 (s), 1607 (s), 1570 (w), 1461 (s), 1406 (m), 1385 (m), 1302 (m), 1216 (m), 1165 (w), 1114 (s), 1081 (m), 1020 (w), 995 (w), 962 (s), 884 (s), 863 (m), 815 (w), 778 (m), 755 (s), 721 (m), 675 (m), 619 (m); ^{1}H NMR (400 MHz, $CDCl_3$) δ_H 9.80 (1H, s, *H*-9) 8.21 (1H, dd, *J* 8.0, 1.7, *H*-5) 7.78 (1H, ddd, *J* 8.7, 7.2, 1.7, *H*-7) 7.61 (1H, d, *J* 8.7, *H*-8) 7.47 (1H, ddd, *J* 8.0, 7.2, 1.1, *H*-6) 6.91 (1H, s, *H*-3); ^{13}C NMR (101 MHz; $CDCl_3$) δ_C 185.6 (C3) 178.4 (C4) 156.2 (C2) 155.8 (C8') 135.4 (C7) 126.3 (C3) 126.1 (C5) 125.0 (C4') 119.0 (C6) 117.1 (C8); LRMS *m/z* (ES+) 175 $[M+H]^+$ (22%), 207 $[M+CH_3OH+H]^+$ (100%), 229 $[M+CH_3OH+Na]^+$ (59%); HRMS *m/z* (ESI+) [Found: 175.03903; $C_{10}H_7O_3^+$ requires 175.03897].

((4-(Dicyanomethylene)-4*H*-chromen-2-yl)methyl)triphenylphosphonium bromide (190)



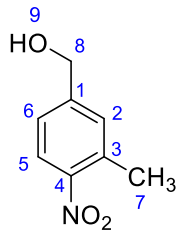
To a flame-dried flask under Ar was added 2-(2-(bromomethyl)-4*H*-chromen-4-ylidene)malononitrile (50 mg, 0.174 mmol, 1 eq.) and toluene (1.75 mL), which was stirred to give a yellow solution. Triphenylphosphine (46 mg, 0.174 mmol, 1 eq.) was added, and the mixture was heated under reflux for 1 hour, during which time a pale off-white precipitate formed. The mixture was cooled to RT, and the precipitate was collected by suction filtration and washed with ice-cold toluene. The precipitate was dried under reduced pressure to afford the title compound as an off-white powder (69 mg, 0.126 mmol, 69% yield): R_f: 0.79 (1:1 EtOAc/petroleum ether); mp 200 °C (dec)(toluene); $\bar{\nu}_{max}$ (solid) cm^{-1} 3040 (w), 3005 (w), 2848 (w), 2749 (w), 2214 (m, C≡N), 2203 (m), 1627 (s, C=C), 1609 (m), 1586 (w), 1520 (s), 1482 (m), 1454 (m, C-P), 1437 (m), 1401 (m), 1330 (w), 1260 (w), 1220 (w), 1176 (w), 1112 (s), 996 (w), 972 (m), 893 (w), 864 (m), 804 (m), 775 (s), 718 (s), 688 (s), 656 (w), 616 (w), 606 (m); ^{1}H NMR (400 MHz, CD_3CN) δ_H 8.75 (2H, dd, *J* 8.4, 1.4, *H*-5) 7.88-7.94 (3H, m, Ar*H*) 7.69-7.78 (14H, m, Ar*H* & *H*-7) 7.53 (1H, ddd, *J* 8.7, 7.3, 1.3, *H*-6) 7.01 (1H, dd, *J* 8.5, 1.1, *H*-8) 6.75 (1H, d, *J* 3.0, *H*-3) 4.85 (2H, d, *J* 15.3, *H*-11); ^{31}P NMR (162 MHz, CD_3CN) δ_P 22.20 (s); LRMS *m/z* 469 $[M-Br]^+$ (100%); HRMS *m/z* (ESI+) [Found 469.14621; $C_{31}H_{22}N_2OP^-$ requires 469.14643]; due to the salt nature of this compound, HPLC purity could not be determined.

Methyl 3-methyl-4-nitrobenzoate (207)



Methanol (25.6 mL) was added to a flask containing 3-methyl-4-nitrobenzoic acid (4.0 g, 22.1 mmol) and stirred, resulting in an off-white suspension. To this suspension was added concentrated H_2SO_4 (0.51 mL), and the mixture was heated under reflux for 3.5 hours, during which time the mixture became a clear yellow-brown solution. The solution was cooled to RT, causing an off-white suspension to form. The suspension was dissolved by addition of CH_2Cl_2, and the organic component was washed with saturated aqueous $NaHCO_3$ solution (3 × 50 mL). The layers were separated, and the organic layer was dried over $MgSO_4$, filtered, and concentrated *in vacuo*. The resulting crude product was dissolved in CH_2Cl_2 and filtered through a plug of silica gel, washing through with CH_2Cl_2. The eluent was concentrated *in vacuo* and dried under high vacuum to afford the title compound as a colourless solid (3.80 g, 19.5 mmol, 88% yield): R_f: 0.81 (EtOAc/petroleum ether 1:1); mp 79–81 °C (CH_2Cl_2) [lit. 41–43 °C (CH_2Cl_2)][270]; ^{1}H NMR (400 MHz, $CDCl_3$) δ_H 8.03 (1H, m, *H*-5) 8.01–7.95 (2H, m, *H*-2 & *H*-6) 3.96 (3H, s, *H*-8) 2.63 (3H, s, *H*-9); LRMS *m/z* not detected; HRMS *m/z* (APCI−) [Found 195.05341; $C_9H_9O_4N^-$ requires 195.05371]. These data are in good agreement with the literature, with the exception of the melting point.[270,271]

(3-Methyl-4-nitrophenyl)methanol (208)



***via* borane reduction:**

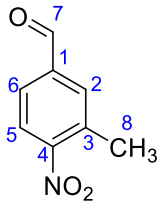
To a flame-dried flask under argon was added 3-methyl-4-nitrobenzoic acid (9.06 g, 50.0 mmol, 1.0 eq.). The material was dissolved in anhydrous THF (50 mL) and stirred. The solution was cooled to 0 °C, and BH_3·THF (50 mL, 50.0 mmol, 1.0 eq., 1 M in THF) was added slowly, causing effervescence. The solution was stirred at 0 °C for 5 minutes, then warmed to RT and stirred for 64 hours, by which time a colourless suspension had formed. The mixture was quenched with addition of methanol (~10 mL) and concentrated *in vacuo*. The residue was redissolved in CH_2Cl_2 and filtered through a pad of silica gel. The eluent was concentrated *in vacuo* to afford the title compound as an off-white solid (7.68 g, 47.0 mmol, 94% yield): R_f: 0.40 (1:1 EtOAc/petroleum ether) [lit. 0.42 (1:1 EtOAc/*n*-hexane)][272]; mp 34–36 °C (CH_2Cl_2) [lit. 60–61 °C][273]; ^{1}H NMR (400 MHz, $CDCl_3$) δ_H 7.99 (1H, d, *J* 8.3, *H*-2) 7.36–7.30 (2H, m, *H*1 & *H*-5) 4.77 (2H, s, *H*-7) 2.62 (3H, s, *H*-9); LRMS *m/z* not detected; HRMS *m/z* (APCI−) [Found 166.05069; $C_8H_8O_3N^-$ requires 166.05097]. These data are in good agreement with the literature, with the exception of the melting point.[272,273]

***via DIBAL-H reduction of ester 207*:**

To a flame-dried flask under Ar was added methyl 3-methyl-4-nitrobenzoate (3.5 g, 17.9 mmol, 1.0 eq.), which was dissolved in anhydrous THF (70 mL) and stirred, giving a yellow solution. The solution was cooled to 0 °C, and a solution of DIBAL-H (44.8 mL, 44.8 mmol, 2.5 eq., 1 M in *n*-hexane) was added slowly. The reaction mixture was stirred at 0 °C for 45 minutes, then warmed to RT and stirred for 2 hours. The reaction

was quenched with addition of saturated aqueous potassium sodium tartrate, and the mixture was left to stir at RT overnight, resulting in a yellow biphasic mixture. The mixture was extracted with EtOAc (3 × 50 mL), and the organic components were combined and washed with brine (3 × 50 mL). The organic phase was separated, dried over $MgSO_4$, filtered, and concentrated *in vacuo* to give a yellow oil. The oil was dissolved in EtOAc and adsorbed onto Celite®. The material was loaded onto a 50 g Biotage® SNAP silica gel cartridge and purified by automated flash column chromatography, the product eluting with 10%–40% EtOAc/petroleum ether. The fractions were collected and concentrated *in vacuo* to afford the title compound as an orange oil (2.62 g, 15.67 mmol, 88% yield). The data match those for the method above.

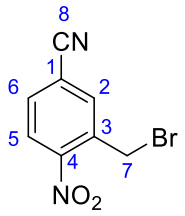
3-Methyl-4-nitrobenzaldehyde (209)



To a flask containing (3-methyl-4-nitrophenyl)methanol (2.62 g, 15.67 mmol, 1 eq.) was added CH_2Cl_2 (200 mL), which was stirred to afford a clear yellow solution. MnO_2 powder (13.62 g, 156.7 mmol, 10.0 eq.) was added, and the mixture was heated under reflux for 2.5 hours, after which time TLC analysis showed the reaction to be complete. The mixture was cooled to RT and filtered through a pad of Celite®, eluting with CH_2Cl_2. The solution was concentrated *in vacuo* onto Celite®, loaded onto a 50 g Biotage® SNAP silica gel column, and purified on a Biotage® SP4 system eluting in 10%–30% EtOAc/petroleum ether. The fractions were concentrated *in vacuo* to afford the title compound as an orange solid (2.32 g, 14.05 mmol, 89% yield): R_f: 0.45 (3:7 EtOAc/petroleum ether); mp 65–66 °C (EtOAc); ^{1}H NMR (400 MHz, $CDCl_3$) δ_H 10.09

(1H, s, *H*-7) 8.06 (1H, d, *J* 8.2, *H*-5) 7.88–7.84 (2H, m, *H*-2/6) 2.66 (3H, s, *H*-8); LRMS *m/z* not detected; HRMS *m/z* not detected. These data are in good agreement with the literature.[274]

3-(Bromomethyl)-4-nitrobenzonitrile (215)



***via* oil-bath heating:**

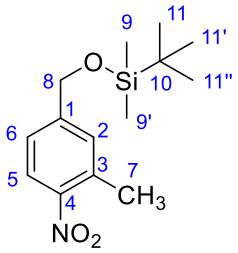
To a flame-dried flask under Ar was added 3-methyl-4-nitrobenzonitrile (1.0 g, 6.17 mmol, 1.0 eq.), which was dissolved in CCl_4 (12.3 mL). *N*-Bromosuccinimide (1.32 g, 7.40 mmol, 1.2 eq.) was added, followed by benzoyl peroxide (199 mg, 0.62 mmol, 0.1 eq.). The mixture was stirred and heated under reflux for 4 hours. The mixture was then cooled, diluted with CH_2Cl_2, and washed with water (2 × 30 mL) and brine (3 × 40 mL). The layers were separated, and the organic component was dried over Na_2SO_4, filtered, and concentrated *in vacuo* onto Celite®. The material was loaded onto a 50 g Biotage® SNAP silica gel column and purified by automated flash column chromatography on a Biotage® SP4, eluting with a gradient of 5%–20% Et_2O/petroleum ether. The fractions were collected and concentrated *in vacuo* to afford the title compound as a yellow solid (611 mg, 2.53 mmol, 41% yield): R_f: 0.40 (Et_2O/petroleum ether 3:7); mp 70–73 °C ($CHCl_3$); $\bar{\nu}_{max}$ (solid) cm^{-1} 3119 (w), 3073 (w), 3061 (w), 3042 (w), 3000 (w), 2922 (w), 2857 (w), 2237 (w, C≡N), 1603 (w), 1581 (m), 1523 (s, N-O), 1478 (m), 1440 (m), 1340 (s, N-O), 1307 (m), 1285 (m), 1234 (m), 1222 (m), 1159 (m), 1123 (m), 943 (w), 905 (m), 879 (w), 851 (s), 833 (s), 766 (m), 718 (w), 690 (s), 654 (m); ^{1}H NMR (500 MHz, DMSO-D6) δ_H 8.12 (1H, d, *J* 8.4, *H*-5) 7.92 (1H, d, *J* 1.8, *H*-2) 7.79 (1H, dd, *J* 8.4, 1.8, *H*-6) 4.79 (2H, s, *H*-7); ^{13}C NMR

(125 MHz, $CDCl_3$) δ_C 150.3 (C4) 136.4 (C2) 134.4 (C3) 133.2 (C6) 126.3 (C5) 117.7 (C1) 116.4 (C8) 27.0 (C7); LRMS *m/z* not detected; HRMS *m/z* (GCMS CH_4 CI) [Found: 240.9601; $C_8H_6{}^{(79)}BrN_2O_2^+$ requires 240.9607; 242.9580; $C_8H_6{}^{(81)}BrN_2O_2^+$ requires 242.9587]; HPLC (Method B) Retention Time = 9.23 minutes, purity 93.7%.

***via* UV lamp heating:**

To a flame-dried flask under Ar was added 3-methyl-4-nitrobenzonitrile (500 mg, 3.08 mmol, 1.0 eq.), *N*-bromosuccinimide (604 mg, 3.39 mmol, 1.1 eq.) and benzoyl peroxide (100 mg, 0.31 mmol, 0.1 eq.). CCl_4 (62 mL) was added, and the mixture was stirred to give a solution with colourless suspension. The mixture was then loosely coated in foil and heated under reflux with a 300 W ultraviolet lamp at approximately 5 cm distance. The mixture was heated for 6 hours, and then cooled to RT. The mixture was diluted with $CHCl_3$, washed with water (50 mL), saturated aqueous Na_2CO_3 solution (50 mL), and brine (50 mL). The organic phase was separated, dried over $MgSO_4$, filtered, and concentrated *in vacuo* onto Celite®. The material was loaded onto a 40 g Telos silica gel column and purified by automated flash column chromatography on a Biotage® SP4 system, eluting with 5%–20% Et_2O/petroleum ether. The appropriate fractions were collected and concentrated *in vacuo* to afford the title compound as a yellow solid (244 mg, 1.01 mmol, 33% yield). The data match those for the previously described method.

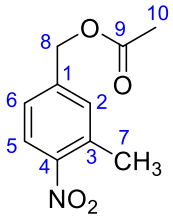
***t*-Butyldimethyl((3-methyl-4-nitrobenzyl)oxy)silane (212)**



To a flame-dried flask under Ar was added (3-methyl-4-nitrophenyl)methanol (1.01 g, 6.03 mmol, 1.0 eq.), to which CH_2Cl_2 (30 mL) was added, giving an off-white

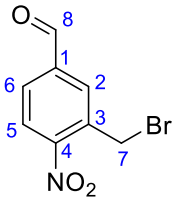
suspension. Triethylamine (1.84 mL, 13.3 mmol, 2.0 eq.) was added, causing the remaining suspended material to dissolve. TBDMSCl (1.0 g, 6.63 mmol, 1.1 eq.) was added, and the mixture was stirred at RT for 18 hours. Further TBDMSCl (0.27 g, 1.81 mmol, 0.3 eq.) was added, and the mixture left to stir at RT for a further 3 hours. The reaction was quenched with addition of methanol (5 mL), diluted with EtOAc (30 mL), and washed with water (3 × 50 mL) and brine (3 × 50 mL). The organic component was separated, dried over $MgSO_4$, filtered, and concentrated *in vacuo* to afford a brown oil. The oil dissolved in EtOAc, adsorbed onto Celite®, loaded onto a 25 g Biotage® SNAP silica gel column, and purified by automated flash silica gel chromatography, eluting with 10% EtOAc/petroleum ether. The fractions were collected and concentrated *in vacuo* and then dried under high vacuum to afford the title compound as a yellow oil (1.15 g, 4.09 mmol, 68% yield): R_f: 0.88 (EtOAc/petroleum ether 3:7); $\bar{\nu}_{max}$ (solid) cm^{-1} 2954 (w), 2930 (w), 2857 (w), 1614 (w), 1591 (w), 1519 (s, N-O), 1462 (w), 1412 (w), 1341 (s, N-O), 1255 (s, CH_3), 1164 (m), 1102 (s), 1006 (w), 934 (w), 832 (s), 777 (s), 749 (s), 670 (w), 637 (w); ^{1}H NMR (400 MHz, DMSO-D6) δ_H 7.98 (1H, d, *J* 9.1, *H*-5) 7.30-7.26 (2H, m, *H*-6 & *H*-2) 4.76 (2H, s, *H*-8) 2.61 (3H, s, *H*-7) 0.85 (9H, s, *H*-10/10'/10'') 0.12 (6H, s, *H*-9/9'); ^{13}C NMR (101 MHz, $CDCl_3$) δ_C 148.0 (C-4) 147.4 (C-1) 133.9 (C-3) 129.9 (C-2) 125.0 (C-6) 124.2 (C-5) 64.1 (C-8) 26.0 (C-11/11'/11'') 20.9 (C-10) 18.5 (C-7) −5.2 (C-9/9'); LRMS *m/z* not detected; HRMS *m/z* (APCI+) [Found 282.15198; $C_{14}H_{24}O_3NSi^+$ requires 282.15200]; HPLC (Method B) Retention Time = 13.53 minutes, purity 100.0%.

3-Methyl-4-nitrobenzyl acetate (213)



To a flame-dried flask under Ar was added (3-methyl-4-nitrophenyl)methanol (300 mg, 1.80 mmol, 1.0 eq.), to which was added CH_2Cl_2 (18 mL), giving a suspension. Triethylamine (374 µL, 2.69 mmol, 1.5 eq.) was added, causing the suspension to fully dissolve. Acetyl chloride (153 µL, 2.15 mmol, 1.2 eq.) was added, and the mixture was stirred at RT for 1 hour. The mixture was diluted with CH_2Cl_2, washed with 1 M aqueous HCl (2 × 80 mL), and the layers were separated. The organic component was dried over $MgSO_4$, filtered, and concentrated *in vacuo*. The crude material was redissolved in CH_2Cl_2, adsorbed onto Celite®, loaded onto a 25 g Biotage® SNAP silica gel column, and purified by automated flash silica gel chromatography, the product eluting with a gradient of 20%–50% EtOAc/petroleum ether. The fractions were collected and concentrated *in vacuo* to afford the title compound as a yellow oil (310 mg, 1.48 mmol, 82% yield): R_f: 0.65 (EtOAc/petroleum ether 1:1); $\bar{\nu}_{max}$ (solid) cm^{-1} 1740 (s, C=O), 1615 (w), 1591 (w), 1518 (s, N-O), 1451 (w), 1375 (w), 1343 (s, N-O), 1311 (w), 1219 (s, CH_3), 1169 (w), 1035 (m, br), 886 (w), 836 (s), 740 (m), 695 (w), 659 (w); ^{1}H NMR (400 MHz, DMSO-D6) δ_H 7.98 (1H, d, *J* 8.7, *H*-5) 7.33-7.29 (2H, m, *H*-2 & *H*-6) 5.13 (2H, s, *H*-8) 2.61 (3H, s, *H*-7) 2.14 (3H, s, *H*-10); ^{13}C NMR (101 MHz, $CDCl_3$) δ_C 170.7 (C-9) 148.9 (C-4) 141.1 (C-1) 134.2 (C-3) 132.1 (C-2) 126.2 (C-6) 125.2 (C-5) 64.9 (C-8) 21.0 (C-7) 20.7 (C-10); LRMS *m/z* not detected; HRMS *m/z* not detected; HPLC (Method B) Retention Time = 11.32 minutes, purity = 100.0%.

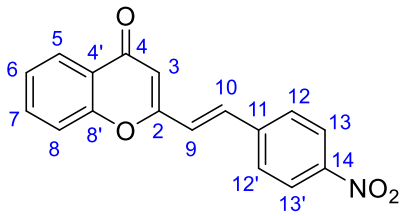
3-(Bromomethyl)-4-nitrobenzaldehyde (216)



To a flame-dried flask under Ar was added 3-(bromomethyl)-4-nitrobenzonitrile (300 mg, 1.24 mmol, 1.0 eq.). The material was dissolved in dry toluene (12.4 mL) and stirred, affording a yellow solution. The solution was cooled to 0 °C and DIBAL-H solution (1.49 mL, 1.49 mmol, 1.2 eq., 1 M in *n*-hexane) was added dropwise, causing the solution to turn bright yellow. The mixture was stirred at 0 °C for 45 minutes, then quenched with addition of 0.1 M aqueous HCl (10 mL), causing a colourless precipitate to form. The mixture was stirred at 0 °C for 1 hour, and then filtered through Celite® and washed through with EtOAc, and the organic component was then washed with brine (2 × 40 mL). The organic phase was separated, dried over Na_2SO_4, filtered, and concentrated *in vacuo*. The residue was taken up in EtOAc and adsorbed onto Celite®, loaded onto a silica gel column and purified by flash column chromatography in 10% EtOAc/petroleum ether. The fractions were concentrated *in vacuo* to afford the title product as a yellow solid (182 mg, 0.746 mmol, 60% yield): R_f: 0.45 (EtOAc/petroleum ether 3:7); mp 82–85 °C (EtOAc); $\bar{\nu}_{max}$ (solid) cm^{-1} 3384 (w), 3111 (w), 3064 (w), 3039 (w), 2999 (w), 2960 (w), 2852 (w), 1695 (w), 1665 (s, C=O), 1606 (w), 1585 (m), 1525 (s, N-O), 1440 (m, -CH_2-), 1416 (m), 1341 (s, N-O), 1314 (s), 1291 (w), 1236 (w), 1219 (s), 1169 (w), 1121 (s), 1068 (w), 1005 (w), 978 (w), 945 (w), 901 (w), 880 (w), 847 (m), 834 (s), 780 (s), 766 (s), 695 (m), 670 (w), 646 (m), 628 (m); ^{1}H NMR (400 MHz, $CDCl_3$) δ_H 10.12 (1H, s, *H*-8) 8.15 (1H, d, *J* 8.3, *H*-5) 8.10 (1H, d, *J* 1.8, *H*-2) 7.99 (1H, dd, *J* 8.3, 1.8, *H*-6) 4.85 (2H, s, *H*-7); ^{13}C NMR (101 MHz, $CDCl_3$) δ_C 189.7 (C8) 139.3 (C4) 134.0 (C1) 133.5 (C3) 130.3 (C2&6) 126.3 (C5) 27.7 (C7); LRMS *m/z* not

detected; HRMS *m/z* not detected; HPLC (Method B) Retention Time = 9.07 minutes, purity = 100.0%.

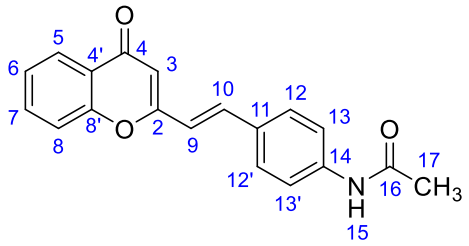
(*E*)-2-(4-Nitrostyryl)-4*H*-chromen-4-one (181)



To a flame-dried flask under Ar was added NaOMe (337 mg, 6.24 mmol, 5.0 eq.) and MeOH (22.3 mL), which was stirred at RT for 10 minutes. 2-Methyl-4*H*-chromen-4-one (200 mg, 1.25 mmol, 1.0 eq.) was added and stirred at RT for 5 minutes, during which time the solution turned yellow. 4-Nitrobenzaldehyde (226 mg, 1.50 mmol, 1.2 eq.) was added, and the mixture was heated under reflux for 1.5 hours, during which time the mixture turned brown and a precipitate formed. The mixture was cooled to RT and filtered, and the filtrate was washed with ice-cold MeOH and dried *in vacuo* to afford a fluffy off-white solid (251 mg, 0.856 mmol, 68% yield): R_f: 0.15–0.81 (EtOAc); mp 280–282 °C (MeOH) [lit. 282.6–283.0 °C][275]; $\bar{\nu}_{max}$ (solid) cm^{-1} 1645 (m, C=C), 1624 (m, C=O), 1590 (m), 1563 (w), 1509 (m, N-O), 1465 (m), 1392 (m), 1337 (s, N-O), 1313 (m), 1279 (w), 1243 (w), 1223 (w), 1172 (w), 1123 (w), 1107 (m), 1025 (m), 975 (w), 891 (m), 863 (m), 843 (m), 829 (m), 773 (m), 761 (m), 749 (m), 691 (m), 675 (m), 652 (w), 631 (w); ^{1}H NMR (500 MHz, CD_2Cl_2) δ_H 8.27 (2H, ddd, *J*, *H*-13/13') 8.14 (1H, dd, *J* 7.9, 1.6, *H*-5) 7.77 (2H, ddd, *J*, *H*-12/12') 7.74 (1H, ddd, *J*, *H*-6) 7.70 (1H, d, *J* 16.1, *H*-10) 7.59 (1H, d, *J* 8.4, *H*-8) 7.43 (1H, ddd, *J*, *H*-7) 6.98 (1H, d, *J* 16.1, *H*-9) 6.37 (1H, s, *H*-3); ^{13}C NMR (125 MHz, CD_2Cl_2) δ_c 178.3 (C4) 160.8 (C2) 156.4 (C8') 148.5 (C14) 141.8 (C11) 134.4 (C6) 134.2 (C10) 128.6 (C12/C12') 125.8 (C5) 125.6 (C7) 124.99 (C9) 124.59 (C13/C13') 124.55 (C4') 118.4 (C8) 112.4 (C3); LRMS *m/z* (ES+) 294 $[M+H]^+$ (100%); HRMS *m/z* (ESI+) [Found: 294.07607; $C_{17}H_{12}NO_4^+$ requires

294.07608]; HPLC (Method C, 365 nm) Retention Time = 10.43 minutes, purity 100.0%. These data are in good agreement with the literature.[49,275]

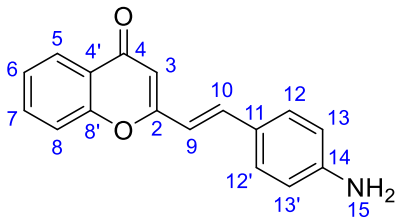
(*E*)-*N*-(4-(2-(4-Oxo-4*H*-chromen-2-yl)vinyl)phenyl)acetamide (203)



To a flame-dried flask under Ar was added NaOMe (337 mg, 6.24 mmol, 5.0 eq.) and methanol (22.3 mL), which was stirred to give a suspension. After 5 minutes, 2-methyl-4*H*-chromen-4-one (200 mg, 1.25 mmol, 1.0 eq.) was added, causing the suspension to turn yellow. After a further 10 minutes, 4-acetamidobenzaldehyde (244 mg, 1.50 mmol, 1.2 eq.) was added, and the mixture was heated under reflux for 16 hours, during which time a yellow precipitate formed. The mixture was cooled to 0 °C, and the precipitate was collected by suction filtration. The solid was washed with a small amount of ice-cold methanol (~10 mL), and then dried under reduced pressure and *in vacuo* to afford the title compound as a yellow powder (149 mg, 0.488 mmol, 39% yield): R_f 0.43 (EtOAc); mp 300 °C (MeOH); $\bar{\nu}_{max}$ (solid) cm^{-1} 3313 (w), 1731 (w), 1694 (s, C=O), 1617 (s, C=C), 1591 (s, C=O), 1573 (m), 1553 (m), 1474 (m), 1462 (m), 1414 (s), 1383 (m), 1356 (m), 1325 (m), 1307 (m), 1283 (m), 1260 (m), 1240 (m), 1223 (m), 1164 (w), 1124 (s), 1045 (s), 1022 (s), 980 (w), 969 (s), 946 (w), 889 (w), 846 (s), 834 (s), 820 (s), 775 (m), 741 (m), 722 (m), 702 (w), 672 (w), 652 (w), 631 (w); ^{1}H NMR (500 MHz, DMSO-D6) δ_H 10.18 (1H, s, H-15) 8.01 (1H, dd, *J* 7.9, 1.7, *H*-5) 7.81 (1H, ddd, *J* 8.5, 7.2, 1.8, *H*-6) 7.70 (1H, d, *J* 8.3, *H*-8), 7.67 (4H, s, *H*-12/12'/13/13') 7.64 (1H, d, *J* 16.3, *H*-10) 7.47 (1H, dd, *J* 7.2, 7.9, *H*-7) 7.10 (1H, d, *J* 16.3, *H*-9) 6.43 (1H, s, *H*-3) 2.07 (3H, s, *H*-17); ^{13}C NMR (125 MHz, DMSO-D6) δ_C 177.0 (C-4), 168.7 (C-16), 162.1 (C-2), 155.5 (C-8'), 140.9 (C-10), 136.3 (C-14), 134.3 (C-7), 129.7 (C-

11), 128.7 (C-12/12'), 125.3 (C-5), 124.8 (C-4'), 123.6 (C-6), 119.1 (C-13/13'), 118.8 (C-9), 118.2 (C-8), 109.6 (C-3), 24.1 (C-17); LRMS *m/z* (ES+) 306 $[M+H]^+$ (100%), (ES−) 304 $[M-H]^-$ (100%); HRMS *m/z* (ES^+) [Found: 306.11256, $C_{19}H_{16}NO_3^+$ requires 306.11247].

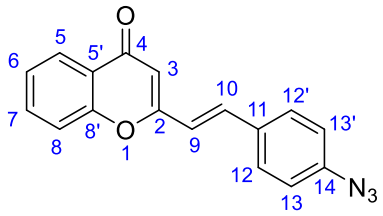
(*E*)-2-(4-Aminostyryl)-4*H*-chromen-4-one (182)



(*E*)-*N*-(4-(2-(4-Oxo-4*H*-chromen-2-yl)vinyl)phenyl)acetamide (100 mg, 0.328 mmol, 1.0 eq.) was added to a flask, to which was then added ethanol (3.28 mL) and 4 M aqueous HCl (6.56 mL), which was stirred to give a yellow suspension. The mixture was heated under reflux for 16 hours, and then cooled to 0 °C which caused a pale precipitate to form. The precipitate was collected by suction filtration, washed with ice-cold ethanol (~10 mL), dried under reduced pressure and then *in vacuo* to afford the title compound as a fluffy yellow solid (38 mg, 0.144 mmol, 44% yield): R_f: 0.20 (acetone/petroleum ether 3:7); mp 208–210 °C (EtOH); $\bar{\nu}_{max}$ (solid) cm^{-1} 3443 (w, br), 2723 (w), 2544 (w), 2161 (w), 1629 (m, C=C), 1608 (m, C=O), 1585 (s, NH_2), 1550 (m), 1513 (m), 1463 (s), 1430 (w), 1382 (s), 1321 (w), 1305 (w), 1247 (m), 1226 (m), 1175 (m), 1124 (w), 1067 (w), 1028 (w), 983 (w), 964 (s), 891 (m), 881 (m), 860 (m), 818 (s), 783 (m), 699 (s), 674 (w), 643 (w), 610 (m); ^{1}H NMR (500 MHz, DMSO-D6) δ_H 8.01 (1H, dd, *J* 8.0, 1.7, H-5) 7.81 (1H, ddd, *J* 8.4, 7.1, 1.7, H-6) 7.70 (1H, d, *J* 8.4, H-8) 7.67-7.62 (3H, m, H-12/12'/9) 7.47 (1H, ddd, *J* 8.0, 7.1, 1.0, H-7) 7.10-7.03 (3H, m, H-13/13'/10) 6.41 (1H, s, H-3); ^{13}C NMR (125 MHz, DMSO-D6) δ_C 176.9 (C-4) 162.2 (C-2) 155.5 (C-8') 136.4 (C-14) 134.2 (C-4') 129.4 (C-12/12') 125.2 (C-7) 124.8 (C-8) 123.6 (C-6) 119.2 (C-10) 118.2 (C-5) 118.0 (C-13/13') 109.3 (C-3); LRMS *m/z* (ES+)

264 $[M+H]^+$ (100%); HRMS *m/z* (ESI+) [Found: 264.10176; $C_{17}H_{14}NO_2^+$ requires 264.10191]; HPLC (Method B, 365 nm) Retention Time = 8.96 minutes, purity 99.6%.

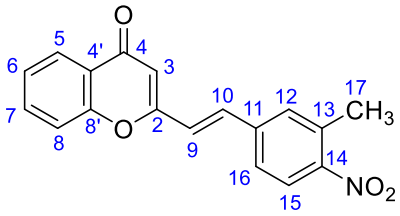
(*E*)-2-(4-Azidostyryl)-4*H*-chromen-4-one (204)



(*E*)-2-(4-Aminostyryl)-4*H*-chromen-4-one (100 mg, 0.38 mmol, 1.0 eq.) was added to a flask, followed by water (3.8 mL). The mixture was stirred giving a yellow suspension, which was cooled to 0 °C. Concentrated aqueous HCl (1.9 mL) was added dropwise, causing the suspension to become cloudy and pale. A solution of $NaNO_2$ (29 mg, 0.42 mmol, 1.1 eq.) in water (0.209 mL, 2 M) was added, dropwise, causing the mixture to become bright yellow. The mixture was stirred at 0 °C for 15 minutes, then a solution of NaN_3 (30 mg, 0.46 mmol, 1.2 eq.) in water (0.415 mL, 1.1 M) was added dropwise, causing brisk effervescence. The mixture was stirred at 0 °C for 15 minutes, then warmed to RT and stir for 45 minutes, during which time the mixture became orange and frothy. The mixture was then diluted with water and extracted with CH_2Cl_2 (3 × 40 mL). The organic components were separated, combined, dried over Na_2SO_4, filtered, and concentrated *in vacuo*. The crude material was dissolved in CH_2Cl_2, adsorbed onto Celite®, loaded onto a silica gel column and purified by flash column chromatography, the product eluting in 20% acetone in petroleum ether. The appropriate fractions were collected and concentrated *in vacuo* to afford the title compound as an orange solid (52 mg, 0.180 mmol, 47% yield): R_f: 0.47 (acetone/petroleum ether 2:3); mp N.D. (organic azide); $\bar{\nu}_{max}$ (solid) cm^{-1} 2118 (m, N=N=N), 2079 (m), 1624 (s, C=O), 1596 (s), 1561 (m), 1504 (m), 1464 (m), 1388 (s), 1290 (s), 1244 (m), 1223 (m), 1177 (m), 1126 (s), 1025 (w), 970 (s), 890 (w), 850

(w), 832 (w), 803 (m), 772 (s), 757 (s), 708 (w), 675 (w), 652 (w); ^{1}H NMR (500 MHz, MeCN-D3) δ_H 8.07 (1H, dd, *J* 7.9, 1.6, *H-5*) 7.76 (1H, ddd, *J* 8.5, 7.2, 1.6, *H-7*) 7.71–7.66 (3H, m, *H*-9&12/12') 7.61 (1H, d, *J* 8.5, *H-8*) 7.43 (1H, ddd, *J* 7.9, 7.2, 1.0, *H-6*) 7.13 (2H, dt, *J* 8.6, 2.0, *H*-13/13') 6.95 (1H, d, *J* 16.2, *H*-10) 6.29 (1H, s, *H*-3); ^{13}C NMR (125 MHz, MeCN-D3) δ_C 178.6 (C-4) 162.9 (C-2) 157.0 (C-8') 142.4 (C-14) 136.5 (C-10) 135.0 (C-11) 133.2 (C-7) 130.3 (C-12&12') 126.04 (C-13&13') 125.95 (C-5) 125.0 (C-5') 121.1 (C-6) 120.6 (C-8) 119.0 (C-9) 111.1 (C-3); LRMS *m/z* (ES+) 312 $[M+Na]^+$; HRMS *m/z* (ESI+) [Found: 290.09261; $C_{17}H_{12}N_3O_2^+$ requires 290.09240].

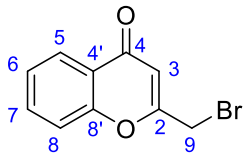
(*E*)-2-(3-Methyl-4-nitrostyryl)-4*H*-chromen-4-one (221)



To a flame-dried flask under Ar was added 2-methyl-4*H*-chromen-4-one (265 mg, 1.65 mmol, 1 eq.), 3-methyl-4-nitrobenzaldehyde (300 mg, 1.81 mmol, 1.1 eq.) and NaOMe (178 mg, 3.30 mmol, 2 eq.). Methanol (16.5 mL) was added, and the mixture was stirred and heated under reflux for 5 hours, during which time a precipitate formed. The mixture was cooled to RT and the precipitate collected by suction filtration. The solid was washed with ice-cold methanol, then ice-cold water, then ice-cold methanol, and then dried under high vacuum to afford the title compound as a fluffy yellow solid (370 mg, 1.20 mmol, 73% yield): R_f: 0.50 (EtOAc/petroleum ether 1:4); mp 242–243 °C (MeOH); $\bar{\nu}_{max}$ (solid) cm^{-1} 1650 (s, C=O), 1632 (s, C=C), 1611 (m), 1580 (m, N-O), 1464 (m), 1391 (m), 1333 (s), 1319 (s, N–O), 1244 (w), 1221 (w), 1171 (w), 1157 (w), 1123 (w), 1075 (w), 1042 (w), 1023 (w), 976 (m), 900 (w), 875 (w), 840 (s), 772 (m), 757 (s), 695 (w), 675 (w), 648 (w); ^{1}H NMR (400 MHz, $CDCl_3$) δ_H 8.21 (1H, dd, *J* 7.8, 1.7, *H*-5) 8.06 (1H, d, *J* 8.5, *H*-16) 7.72 (1H, ddd, *J* 8.3, 7.2, 1.7, *H*-7) 7.60 (1H, d,

J 16.0, *H*-9) 7.58–7.53 (3H, m, *H*-8&12&15) 7.43 (1H, ddd, *J* 7.8, 7.2, 1.0, *H*-6) 6.90 (1H, d, *J* 16.0, *H*-10) 6.40 (1H, s, *H*-3) 2.68 (3H, s, *H*-17); ^{13}C NMR (101 MHz, DMSO-d6) δ_C 177.1 (C-4) 160.9 (C-2) 155.5 (C-8') 148.7 (C-14) 139.7 (C-11) 134.5 (C-7) 134.0 (C-10) 133.7 (C-15) 131.9 (C-13) 126.2 (C-16) 125.4 (C-5) 125.3 (C-9) 124.9 (C-12) 124.5 (C-4') 123.5 (C-6) 118.2 (C-8) 111.3 (C-3) 19.8 (C-17); LRMS *m/z* not detected; HRMS *m/z* (ESI+) [Found: 308.09162; $C_{18}H_{14}O_4N^+$ requires 308.09173]; HPLC (Method D) Retention Time = 17.09 minutes, purity 93.3%.

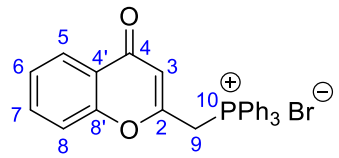
2-(Bromomethyl)-4*H*-chromen-4-one (219)



To a flame-dried flask under Ar was added 2-methyl-4*H*-chromen-4-one (500 mg, 3.12 mmol, 1.0 eq.), *N*-bromosuccinimide (833 mg, 4.68 mmol, 1.5 eq.) and AIBN (51 mg, 0.312 mmol, 0.1 eq.). CCl_4 (10 mL) was added, and the mixture was stirred to give a colourless solution with a colourless suspension. The mixture was heated under reflux for 5.5 hours, then cooled to RT. Further *N*-bromosuccinimide (416 mg, 2.34 mmol, 0.75 eq.) and AIBN (25 mg, 0.156 mmol, 0.05 eq.) was added, and the mixture was heated under reflux for 2 hours. The mixture was cooled to RT and diluted with $CHCl_3$ (50 mL). The organic components were washed with water (1 × 50 mL) and brine (2 × 50 mL), separated, dried over Na_2SO_4, filtered, and concentrated *in vacuo* to afford a yellow oil. The oil was dissolved in EtOAc, adsorbed onto Celite®, loaded onto silica gel and purified by flash column chromatography, eluting in 2%–10% EtOAc/toluene. The fractions were collected and concentrated in vacuo to afford the title compound as an off-white solid (189 mg, 0.791 mmol, 25% yield): R_f: 0.20 (1:4 EtOAc/petroleum ether); mp 128–131 °C ($CHCl_3$) [lit. 110–112 °C (ligroin)][276]; $\bar{\nu}_{max}$ (solid) cm^{-1} 3068 (w), 3038 (w), 2977 (w), 1656 (s, C=O), 1631 (s, C=C), 1574 (m),

1463 (m), 1431 (w), 1412 (w), 1385 (s), 1334 (w), 1304 (w), 1221 (m), 1172 (w), 1151 (w), 1139 (w), 1118 (m), 1089 (w), 1024 (w), 969 (m), 907 (w), 878 (m), 841 (m), 785 (m), 752 (s), 701 (m), 677 (s), 666 (m); ^{1}H NMR (500 MHz, $CDCl_3$) δ_H 8.18 (1H, dd, *J* 8.0, 1.7, *H*-5) 7.69 (1H, ddd, *J* 8.4, 7.2, 1.7, *H*-7) 7.49 (1H, d, *J* 8.4, *H*-8) 7.41 (1H, dd, *J* 8.0, 7.2, *H*-6) 6.41 (1H, s, *H*-3) 4.28 (2H, s, *H*-9); ^{13}C NMR (126 MHz; $CDCl_3$) δ_C 178.2 (C-4) 162.6 (C-2) 156.6 (C-8') 134.3 (C-7) 125.9 (C-5) 125.6 (C-6) 123.8 (C-4') 118.2 (C-8) 111.5 (C-3) 27.5 (C-9); LRMS *m/z* (ES+) 239 $[M(^{79}Br)+H]^+$ (50%), 241 $[M(^{81}Br)+H]^+$ (50%); HRMS *m/z* (ESI+) [Found: 238.97037; $C_{10}H_8O_2{}^{(79)}Br^+$ requires 238.97022, 240.96816; $C_{10}H_8O_2{}^{(81)}Br^+$ requires 240.96817]. These data are not in agreement with the literature.[276]

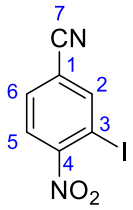
((4-Oxo-4*H*-chromen-2-yl)methyl)triphenylphosphonium bromide (220)



To a flame-dried flask under Ar was added 2-(bromomethyl)-4*H*-chromen-4-one (100 mg, 0.42 mmol, 1 eq.), which was dissolved in toluene (4.2 mL) and stirred to give a clear yellow solution. PPh_3 (121 mg, 0.46 mmol, 1.1 eq.) was added, and the mixture was heated under reflux for 16 hours, during which time a precipitate formed. The mixture was cooled to RT and the precipitate was collected by suction filtration, which was then dried under high vacuum to afford the title compound as a deep purple solid (144 mg, 0.287 mmol, 68% yield): R_f: 0.80 (EtOAc/petroleum ether 1:9); mp 300–303 °C (toluene); $\bar{\nu}_{max}$ (solid) cm^{-1} 3013 (w), 2852 (w), 2752 (w), 1641 (s, C=O), 1602 (w, C=C), 1571 (w), 1484 (w), 1462 (m, C-P), 1438 (s), 1381 (s), 1320 (s), 1305 (w), 1212 (m), 1165 (w), 1109 (s), 1027 (w), 996 (m), 966 (m), 900 (w), 883 (m), 834 (m), 793 (w), 771 (m), 747 (s, ArC-H), 722 (s, ArC-H), 689 (s, ArC-H), 618 (m), 608 (m);

^{1}H NMR (400 MHz, $CDCl_3$) δ_H 8.06 (1H, d, *J* 8.0, *H*-5) 8.02–7.90 (5.5H, m, Ar-H) 7.84–7.78 (3.5H, m, Ar-H) 7.72–7.65 (6H, m, Ar-H) 7.55–7.50 (1H, m, *H*-7) 7.34 (1H, t, *J* 7.8, *H*-6) 6.79 (1H, d, *J* 8.4, Ar-H) 6.54 (1H, d, *J* 2.5, Ar-H) 5.91 (2H, d, *J* 15.0, *H*-9); ^{31}P NMR (376 MHz; DMSO-D6) δ_P 22.18 (s); LRMS *m/z* (ES+) 421 $[M-Br]^+$ (100%); 841 $[2M-H-Br]^+$ (22%); HRMS *m/z* (ESI+) [Found: 421.13527; $C_{28}H_{22}O_2P^+$ requires 421.13519]; HPLC (Method B) Retention Time = 17.30 minutes, purity 97.7%.

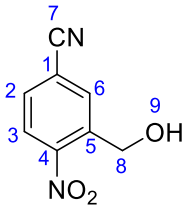
3-Iodo-4-nitrobenzonitrile (226)



4-Amino-3-iodobenzonitrile (1.5 g, 6.15 mmol, 1 eq.) was added to a 2-necked flask fitted with a dropping funnel. 2 M aqueous H_2SO_4 (31 mL) was added, and the mixture was stirred to give a dark brown suspension. The suspension was cooled to 0 °C, and from the dropping funnel a solution of $NaNO_2$ (1.01 g, 14.6 mmol, 2.4 eq.) in water (3.37 mL) was added dropwise over 10 minutes. The mixture was stirred at 0 °C for 1 hour, then transferred to a flask containing a stirring solution of $NaNO_2$ (8.49 g, 123 mmol, 20 eq.) and $CuSO_4 \cdot 5H_2O$ (77 mg, 0.31 mmol, 0.05 eq.) in water (40 mL) at 85 °C portionwise, causing brisk effervescence and evolution of an orange-brown gas. The mixture was heated under reflux for 2 hours, then cooled to RT and extracted with CH_2Cl_2. The organic component was washed with water (2 × 30 mL), then brine (3 × 40 mL), then saturated aqueous K_2CO_3 solution (2 × 40 mL). The mixture was separated, dried over $MgSO_4$, filtered, and concentrated *in vacuo* to afford a brown residue. The residue was redissolved in EtOAc and concentrated *in vacuo* onto Celite®. The crude material was loaded onto a 50 g Biotage® SNAP silica gel cartridge and purified by automated flash column chromatography on a Biotage® SP4 system,

eluting in 3%–10% EtOAc/petroleum ether. The fractions were collected and concentrated *in vacuo* to afford the title compound as a colourless solid (700 mg, 2.55 mmol, 41% yield): R_f: 0.72 (1:4 EtOAc/petroleum ether); mp 163–164 °C (EtOAc); $\bar{\nu}_{max}$ (solid) cm^{-1} 3064 (w, ArC-H), 2923 (w), 2228 (s, C≡N), 1762 (w), 1571 (m), 1528 (m, N-O), 1460 (s), 1440 (w), 1363 (s, N-O), 1269 (w), 1253 (s), 1186 (m), 1141 (w), 1084 (m), 1005 (s), 959 (w), 883 (s), 823 (s), 807 (s), 688 (m), 664 (m); ^{1}H NMR (400 MHz, $CDCl_3$) δ_H 8.10 (1H, d, *J* 1.9, *H*-2) 8.00 (1H, d, *J* 8.2, *H*-5) 7.29 (1H, dd, *J* 8.2, 1.9, *H*-6); ^{13}C NMR (101 MHz, $CDCl_3$) δ_C 141.9 (C-2) 140.1 (C-5) 131.8 (C-6) 116.8 (C-4) 114.9 (C-7) 113.3 (C-1) 108.8 (C-3); LRMS *m/z* not detected; HRMS *m/z* not detected.

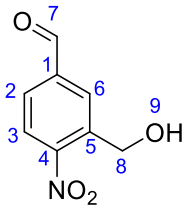
3-(Hydroxymethyl)-4-nitrobenzonitrile (227)



To a flame-dried flask under Ar was added 3-iodo-4-nitrobenzonitrile (500 mg, 1.82 mmol, 1.0 eq.), which was dissolved in anhydrous THF (9.1 mL) and stirred. The solution was cooled to −40 °C and 1 M phenylmagnesium chloride solution in 2-MeTHF (2.19 mL, 2.19 mmol, 1.2 eq.) was added, causing the solution to turn bright yellow. The solution was stirred at −40 °C for 15 minutes, then anhydrous DMF (0.283 mL, 3.65 mmol, 1.0 eq.) was added dropwise. The solution was warmed to RT and stirred for 3 hours. Water (0.1 mL) was added, causing a grey precipitate to form. The suspension was stirred for 10 minutes, then a solution of $NaBH_4$ (69 mg, 1.82 mmol, 1.0 eq.) in EtOH (1 mL) was added dropwise, causing effervescence and the solution to turn yellow. The mixture was stirred at RT for 20 minutes, then diluted with EtOAc (100 mL). The mixture was washed with brine (2 × 150 mL), and the

organic layer was separated and dried over Na_2SO_4, filtered, and concentrated *in vacuo*. The residue was dissolved in EtOAc, adsorbed onto Celite®, loaded onto a 10 g Biotage® SNAP column and purified by automated silica gel chromatography in 2%–20% EtOAc/petroleum ether. The fractions were collected and concentrated *in vacuo* to afford the title compound as a colourless solid (213 mg, 0.777 mmol, 43% yield): R_f: 0.33 (1:4 EtOAc/petroleum ether); mp 137–140 °C (EtOAc); $\bar{\nu}_{max}$ (solid) cm^{-1} 3462 (s, br, O-H), 2235 (s, C≡N), 1583 (m), 1557 (w), 1460 (m, N-O), 1445 (m), 1427 (m), 1395 (w), 1299 (m, N-O), 1275 (w), 1240 (w), 1221 (w), 1131 (w), 1110 (w), 1055 (s), 1025 (w), 1010 (s), 891 (s), 821 (s), 736 (w), 719 (w), 696 (m); ^{1}H NMR (400 MHz, $CDCl_3$) δ_H 7.94 (1H, d, *J* 8.0, *H*-3) 7.79 (1H, d, *J* 2.0, *H*-6) 7.26 (1H, dd, *J* 8.0, 2.0, *H*-2) 4.69 (2H, d, *J* 5.8, *H*-8) 2.07 (1H, t, *J* 5.8, *H*-9); LRMS *m/z* not detected; HRMS *m/z* not detected; HPLC (Method B) Retention Time = 7.95 minutes, purity 100.0%.

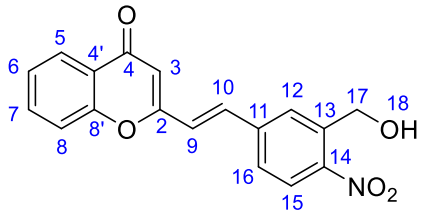
3-(Hydroxymethyl)-4-nitrobenzaldehyde (228)



To a flame-dried flask under Ar was added 3-(hydroxymethyl)-4-nitrobenzonitrile (110 mg, 0.620 mol, 1.0 eq.). Toluene (6.2 mL) was added, the mixture was stirred, and the stirring suspension was cooled to 0 °C. 1 M DIBAL-H solution in *n*-hexane (1.30 mL, 1.30 mmol, 2.1 eq.) was added dropwise, and the mixture was stirred at 0 °C for 30 minutes. The reaction was quenched by addition of 1 M aqueous HCl (10 mL) and stirred for 20 minutes. The mixture was extracted into EtOAc (3 × 50 mL) and washed with a saturated aqueous solution of Rochelle's salt (3 × 50 mL). The layers were separated, and the organic layer was dried over Na_2SO_4, filtered, and concentrated *in vacuo*. The residue was dissolved in EtOAc, adsorbed onto Celite®,

loaded onto a 10 g Biotage® SNAP silica gel column, and purified by automated flash chromatography on a Biotage® SP4 system, eluting with a gradient of 10%–50% EtOAc/petroleum ether. The fractions were collected and concentrated *in vacuo* to afford the title compound as a colourless solid (50 mg, 0.276 mmol, 45% yield): R_f: 0.76 (EtOAc/petroleum ether 2:3); mp 60–62 °C (EtOAc); ^{1}H NMR (400 MHz, $CDCl_3$) δ_H 10.00 (1H, s, *H*-7) 8.02 (1H, d, *J* 8.1, *H*-3) 7.97 (1H, d, *J* 2.1, *H*-6) 7.50 (1H, dd, *J* 8.1, 2.1, *H*-2) 4.75 (2H, s, *H*-8) 2.12 (1H, s, *H*-9); LRMS *m/z* not detected; HPLC (Method B) Retention Time = 7.55 minutes, purity 97.9%.

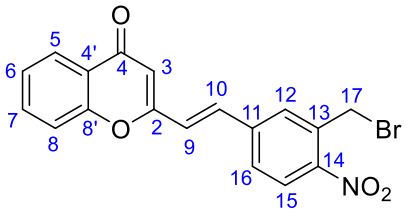
(*E*)-2-(3-(Hydroxymethyl)-4-nitrostyryl)-4*H*-chromen-4-one (229)



To a flame-dried flask under Ar was added 3-(hydroxymethyl)-4-nitrobenzaldehyde (144 mg, 0.795 mmol, 1.0 eq.), which was dissolved in MeOH (10.5 mL) and stirred to give a clear yellow solution. NaOMe (86 mg, 1.59 mmol, 2.0 eq.) and 2-methyl-4*H*-chromen-4-one (153 mg, 0.954 mmol, 1.2 eq.) were added, and the resulting suspension was heated under reflux for 18 hours, during which time a yellow precipitate formed. The mixture was cooled to RT and the precipitate was collected by suction filtration. The solid was washed with ice-cold MeOH (10 mL), then ice-cold water (10 mL), then ice-cold MeOH again (10 mL). The solid was then dried under reduced pressure to afford the title compound as a fluffy yellow solid (149 mg, 0.461 mmol, 58% yield): mp 242–243 °C (MeOH); $\bar{\nu}_{max}$ (solid) cm^{-1} 1628 (s, C=O), 1611 (s, C=C), 1582 (m), 1564 (m, N-O), 1482 (w), 1462 (m), 1402 (m), 1357 (w, N-O), 1321 (w), 1247 (w), 1222 (w), 1179 (w), 1152 (w), 1127 (m), 1067 (m, br, O-H), 1009 (m), 973 (s), 877 (m), 838 (w), 804 (m), 774 (m), 754 (m), 675 (w), 650 (w), 631

(w); ^{1}H NMR (400 MHz, DMSO-D6) δ_H 8.02 (1H, dd, *J* 7.9, 1.6, *H*-5) 7.90 (1H, d, *J* 8.0, *H*-15) 7.83 (1H, ddd, *J* 8.4, 7.1, 1.6, *H*-7) 7.80 (1H, d, *J* 2.0, *H*-12) 7.74 (1H, d, *J* 7.9, *H*-8) 7.72 (1H, d, *J* 16.2, *H*-9) 7.48 (1H, ddd, *J* 8.4, 7.9, 1.0, *H*-6) 7.40 (1H, dd, *J* 8.0, 2.0, *H*-16) 7.28 (1H, d, *J* 16.2, *H*-10) 6.54 (1H, s, *H*-3) 5.59 (1H, br s, *H*-18) 4.45 (2H, br s, *H*-17); LRMS *m/z* not detected; HRMS *m/z* not detected; HPLC (Method D) Retention Time = 15.57 minutes, 70.8% purity. Due to the poor solubility of this compound, ^{13}C NMR spectra could not be measured.

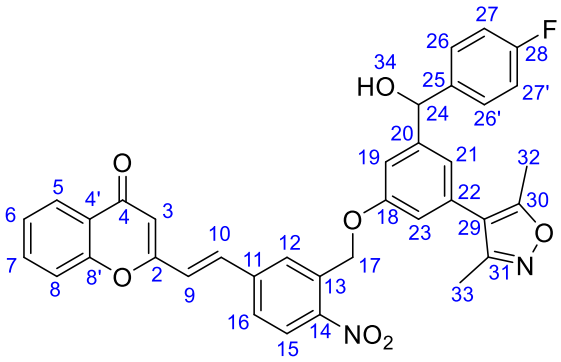
(*E*)-2-(3-(Bromomethyl)-4-nitrostyryl)-4*H*-chromen-4-one (224)



To a flask containing (*E*)-2-(3-(hydroxymethyl)-4-nitrostyryl)-4*H*-chromen-4-one (50 mg, 0.155 mmol, 1.0 eq.) was added 48% *v/v* aqueous HBr (6.2 mL), which was stirred to give an orange suspension. The suspension was stirred at 80 °C for 2.5 hours, then cooled to 0 °C and collected by suction filtration. The solid was washed with ice-cold water (10 mL), then dried *in vacuo* to afford the title compound as an orange solid (43 mg, 0.111 mmol, 72% yield): R_f: 0.59 (1:1 EtOAc/petroleum ether); mp 242-244 °C (H_2O); $\bar{\nu}_{max}$ (solid) cm^{-1} 1677 (s, C=O), 1611 (m, C=C), 1589 (w), 1564 (w), 1473 (m, N-O), 1462 (s), 1437 (w), 1389 (s, N-O), 1313 (w), 1244 (w), 1216 (m), 1172 (w), 1121 (m), 1014 (m), 970 (m), 958 (s), 877 (m), 862 (m), 827 (m), 803 (m), 773 (s), 754 (s), 719 (w), 702 (w), 676 (w), 663 (w), 617 (w); ^{1}H NMR (400 MHz, $CDCl_3$) δ_H 8.22 (1H, dd, *J* 8.0, 1.6, *H*-5) 7.92 (1H, d, *J* 8.2, *H*-15) 7.73 (1H, ddd, *J* 8.4, 7.1, 1.6, *H*-7) 7.68 (1H, d, *J* 2.1, *H*-12) 7.60–7.54 (2H, m, *H*-8/9) 7.44 (1H, m, *H*-6) 7.22 (1H, dd, *J* 8.2, 2.1, *H*-16) 6.87 (1H, d, *J* 16.0, *H*-10), 6.55 (1H, s, *H*-3) 4.63 (2H, s, *H*-17); ^{13}C NMR (126 MHz, DMSO-D6) δ_C 177.1 (C) 161.5 (C) 155.5 (C) 144.5 (C) 139.2 (C)

135.8 (C) 135.0 (C) 134.3 (C) 127.6 (C) 126.6 (C) 125.3 (C) 124.8 (C) 123.5 (C) 121.2 (C) 118.3 (C) 110.4 (C) 98.5 (C) 67.1 (C); LRMS *m/z* not detected; HRMS *m/z* not detected; HPLC (Method B, 365 nm) Retention Time = 10.15 minutes, purity 96.6%.

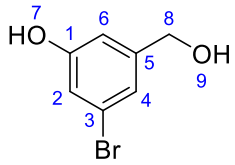
(*E*)-2-(3-((3-(3,5-Dimethylisoxazol-4-yl)-5-((4-fluorophenyl)(hydroxy)methyl)phenoxy)methyl)-4-nitrostyryl)-4*H*-chromen-4-one (231)



To a flame-dried flask under Ar was added a sample of 3-(3,5-dimethylisoxazol-4-yl)-5-((4-fluorophenyl)(hydroxy)methyl)phenol (24 mg, 0.078 mmol, 1.2 eq.), which was dissolved in anhydrous DMF (1.3 mL). Cs_2CO_3 (42 mg, 0.129 mmol, 2.0 eq.) was added and the mixture was stirred at RT for 5 minutes, during which time the solution turned pale yellow. To this stirring solution was added a solution of (*E*)-2-(3-(bromomethyl)-4-nitrostyryl)-4*H*-chromen-4-one (25 mg, 0.065 mmol, 1.0 eq.) in anhydrous DMF (1.3 mL), dropwise. The mixture was stirred at RT for 16 hours, then diluted with EtOAc (10 mL) and washed with brine (4 × 30 mL). The layers were separated, and the organic components were dried over $MgSO_4$, filtered, and concentrated *in vacuo*. The residue was taken up in $CHCl_3$, loaded onto silica gel and purified by flash column chromatography, eluting in $CHCl_3$. The fractions were collected and concentrated *in vacuo* to afford the title compound as a glassy, colourless solid (25 mg, 0.0404 mmol, 62% yield). R_f: 0.36 (Et_2O/$CHCl_3$ 1:4); ^{1}H NMR (400 MHz, $CDCl_3$) δ_H 8.20 (1H, dd, *J* 8.0, 1.6, *H*-5) 7.92 (1H, d, *J* 8.1, *H*-15) 7.72–7.67 (2H, m, *H*-7&12) 7.58–7.51 (2H, m, *H*-16&9) 7.44–7.35 (3H, m, *H*-6&27&27') 7.28 (1H,

m, *H*-8) 7.09–6.99 (3H, m, *H*-23&26&26') 6.87 (1H, s, *H*-19) 6.82 (1H, d, *J* 15.9, *H*-10) 6.76 (1H, s, *H*-21) 6.34 (1H, s, *H*-3) 5.87 (1H, d, *J* 3.2, *H*-24) 5.09 (2H, s, *H*-17) 2.37 (3H, s, *H*-32) 2.22 (3H, s, *H*-33); ^{13}C NMR (101 MHz, $CDCl_3$) δ_C 178.6, 165.5, 161.3, 158.9, 158.6, 156.1, 146.2, 140.2, 139.8, 135.64, 135.58, 134.1, 132.3, 128.42, 128.34, 128.2, 127.9, 125.9, 125.3, 124.3, 121.7, 120.4, 118.0, 116.4, 115.8, 115.6, 114.8, 112.5, 111.3, 98.5, 75.4, 74.1, 11.8, 11.0. Note: this compound was highly unstable, and it was not possible to obtain full characterisation data.

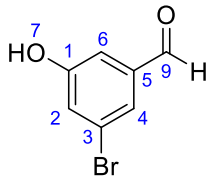
3-Bromo-5-(hydroxymethyl)phenol (253)



A flame-dried flask under Ar was charged with 3-bromo-5-hydroxybenzoic acid (5.0 g, 23.0 mmol, 1 eq.), which was dissolved in anhydrous THF (23 mL) to give a deep brown solution. The solution was stirred and cooled to 0 °C, and BH_3·THF (25.3 mL, 25.3 mmol, 1.1 eq.) was added, causing gas to evolve. The reaction mixture was warmed to RT and stirred for 2 hours. The reaction mixture was cooled to 0 °C, quenched with addition of methanol (25 mL), and volatile components were removed *in vacuo*. The residue was dissolved in EtOAc, adsorbed onto Celite®, loaded onto silica gel, and purified by flash column chromatography eluting in 20%–50% EtOAc/petroleum ether. Appropriate fractions were collected and concentrated *in vacuo* to afford the title compound as an off-white solid (4.34 g, 21.38 mmol, 93% yield): R_f: 0.57 (EtOAc/petroleum ether, 1:1); mp 89–90 °C (EtOAc) [lit. 88–89 °C ($CHCl_3$)][222]; $\bar{\nu}_{max}$ (solid) cm^{-1}: 3362 (br, OH), 1611 (w), 1572 (s), 1489 (w, ArC=C), 1441 (s), 1415 (m), 1367 (m), 1334 (m), 1277 (s), 1219 (m), 1153 (s), 1099 (m), 1043 (s), 988 (s), 950 (s), 826 (s, br), 682 (s), 647 (s, C-Br); ^{1}H NMR (400 MHz; DMSO-D6) δ_H 9.79 (1H, s, *H*-7) 6.90 (1H, s, *H*-2) 6.79 (1H, t, *J* 2.1, *H*-6) 6.72 (1H, s, *H*-4) 5.23

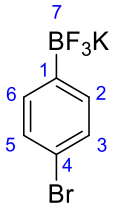
(1H, t, *J* 5.9, *H*-9) 4.40 (2H, d, *J* 5.9, *H*-8); ^{13}C NMR (101 MHz; DMSO-D6) δ_C 158.9 (C-1) 147.0 (C-5) 122.0 (C-3) 120.0 (C-4) 116.7 (C-2) 112.8 (C-6) 62.6 (C-8); LRMS *m/z* (ES−) 201 [M(^{79}Br)−H]$^-$ (50%), 203 [M(^{81}Br)−H]$^-$ (50%). These data are in good agreement with the literature.[222]

3-Bromo-5-hydroxybenzaldehyde (254)



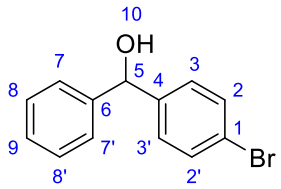
A flask containing a sample of 3-bromo-5-(hydroxymethyl)phenol (4.34 g, 21.38 mmol, 1.0 eq.) was placed under N_2. To this was added $CHCl_3$ (116 mL), forming a pale straw-coloured solution. Activated MnO_2 powder (5.57 g, 64.14 mmol, 3 eq.) was added, giving a black suspension. The reaction mixture was heated to 70 °C and stirred for 24 hours. The reaction mixture was filtered through Celite®, eluting with methanol. The filtrate was concentrated *in vacuo*, loaded onto silica gel, and purified by flash silica gel chromatography, the product eluting in 5%–30% EtOAc/petroleum ether. The fractions were collected and concentrated *in vacuo* to afford the title compound as an off-white powder (2.96 g, 14.72 mmol, 69% yield): R_f 0.50 (EtOAc/petroleum ether 3:7); mp 149–151 °C (EtOAc) [lit. 133–135 °C (Et_2O)]; ^{1}H NMR (400 MHz; DMSO-D6) δ_H 10.48 (1H, br s, *H-7*), 9.87 (1H, s, *H*-9) 7.51 (1H, t, *J* 1.3, *H*-6) 7.26 (1H, t, *J* 2.1, *H*-4) 7.24 (1H, dd, *J* 2.1, 1.3, *H*-2); ^{13}C NMR (101 MHz; DMSO-D6) δ_C 192.5 (C-9) 159.6 (C-1) 139.4 (C-5) 124.4 (C-2) 123.6 (C-4) 123.1 (C-3) 115.0 (C-6); LRMS *m/z* (ES−) 199 [M(^{79}Br)−H]$^-$ (50%), 201 [M(^{81}Br)−H]$^-$ (50%). These data are in good agreement with the literature.[222]

Potassium (4-bromophenyl)trifluoroborate (243)



To a flame-dried flask under an Ar atmosphere was added 4-bromophenylboronic acid (2.06 g, 10.3 mmol, 1 eq.), which was dissolved in methanol (20 mL), cooled to 0 °C and stirred to give a colourless solution. A solution of KHF_2 (4.01 g, 51.3 mmol, 5 eq.) in water (11.4 mL) was added slowly, causing a flocculent colourless precipitate to form. The mixture was left to stir at 0 °C for 10 minutes, then warmed to RT and stir for 1 hour. The volatile components were removed *in vacuo*, and the sludgy residue was further dried under high vacuum overnight. The solid was purified by continuous Soxhlett extraction with MeCN (150 mL) for 2 days. The solvent was removed *in vacuo*, and the residue was dissolved in hot acetone (10 mL). Et_2O (50 mL) was added, causing the product to precipitate as a colourless solid which was collected by suction filtration and dried *in vacuo*, affording the title compound as a colourless solid (2.71 g, 10.3 mmol, 100% yield): R_f not detected by UV or chemical staining; mp >300 °C (Acetone/Et_2O) [lit. >200 °C (Acetone/Et_2O)][244]; $\bar{\nu}_{max}$ (solid) cm^{-1} 1580 (w, Ar C=C), 1383 (w), 1232 (w), 1211 (m), 1065 (w), 949 (s, br), 933 (s, br), 840 (w), 808 (s), 626 (w); ^1H NMR (400 MHz; acetone-D6) δ_H 7.40 (2H, d, *J* 8.2, *H*-3&5) 7.23 (2H, d, *J* 8.2, *H*-2&6); ^{19}F NMR (376 MHz; acetone-D6) δ_F −142.93–−143.49 (m, *F*-7); LRMS *m/z* (ES−) 223 $[M(^{79}Br)-K]^-$ (50%), 225 $[M(^{81}Br)-K]^-$ (50%); HRMS *m/z* (ES−) [Found 222.95472; $C_6H_4B^{(79)}BrF_3^-$ requires 222.95470; 224.95253; $C_6H_4B^{(81)}BrF_3^-$ requires 224.95265]. These data are in good agreement with the literature.[244]

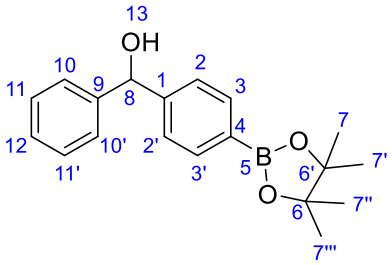
(4-Bromophenyl)(phenyl)methanol (248)



To a flame-dried flask under Ar was added 1,4-dibromobenzene (2.36 g, 10 mmol, 1.11 eq.), which was dissolved in anhydrous THF (20 mL) and stirred to give a colourless solution. The solution was cooled to −78 °C and *n*-BuLi (4 mL, 10 mmol, 1.11 eq., 2.5 M in *n*-hexane) was added dropwise, causing the solution to turn off-white and cloudy. The mixture was stirred at −78 °C for 15 minutes, and then benzaldehyde (916 µL, 9.01 mmol, 1 eq.) was added dropwise, causing the solution to become clear and yellow. The solution was stirred at −78 °C for 1 hour, then the reaction was quenched with addition of 10% *w/v* aqueous NH_4Cl solution. The mixture was warmed to RT, and then extracted with CH_2Cl_2 (3 × 60 mL). The organic layers were combined, dried over Na_2SO_4, filtered, and concentrated *in vacuo* to afford a yellow oil. The residue was dissolved in EtOAc, adsorbed onto Celite®, loaded onto silica gel and purified by flash column chromatography, eluting with 5%–10% EtOAc/petroleum ether. The fractions were collected and concentrated *in vacuo* to afford the title compound as a colourless oil which formed colourless crystals after prolonged exposure to atmosphere (1.76 g, 6.69 mmol, 74% yield): R_f: 0.20 (EtOAc/petroleum ether 1:9); mp 53–54 °C; $\bar{\nu}_{max}$ (solid) cm^{-1} 3383 (br, s, O-H), 1912 (w), 1591 (w), 1486 (s), 1447 (s), 1394 (w), 1336 (w), 1310 (s), 1269 (s), 1180 (s), 1106 (s), 1072 (w), 1033 (s), 1008 (s), 921 (w), 857 (s), 837 (s), 805 (s), 786 (s), 757 (s), 738 (s), 714 (s), 697 (s), 660 (s), 618 (s); ^{1}H NMR (500 MHz; $CDCl_3$) δ_H 7.46 (2H, ddd, *J* 8.5, 1.9, 2.4, *H*-3&3') 7.36-7.34 (4H, m, Ar-H) 7.30-7.25 (3H, m, Ar-H); ^{13}C NMR (125 MHz; $CDCl_3$) δ_C 143.4 (C-6) 142.7 (C-4) 131.6 (C-2&2'), 128.7 (C8&8'), 128.2 (C-3&3'), 127.9 (C-7&7'),

126.5 (C-9), 121.4 (C-1), 75.7 (C-5); LRMS *m/z* not detected; HRMS *m/z* not detected. These data are in agreement with the literature.[277]

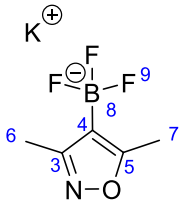
Phenyl(4-(4,4,5,5-tetramethyl-1,3,2-dioxaborolan-2-yl)phenyl)methanol (245)



To a flask charged with (4-bromophenyl)(phenyl)methanol (100 mg, 0.38 mmol, 1 eq.), bis(pinacolato)diboron (145 mg, 0.57 mmol, 1.5 eq.) and KOAc (112 mg, 1.14 mmol, 3 eq.) was added degassed 1,4-dioxane (3.3 mL). The mixture was stirred to give a colourless solution, and to this was added $Pd(dppf)Cl_2 \cdot CH_2Cl_2$ (31 mg, 0.038 mmol, 0.1 eq.), causing the solution to become an orange suspension. The suspension was heated to 85 °C for 1.5 hours, during which time the suspension became deep brown. The mixture was cooled to RT, filtered through a pad of Celite®, washed through with EtOAc and concentrated *in vacuo*. The resultant brown residue was dissolved in EtOAc, adsorbed onto Celite®, loaded onto a 10 g Biotage® SNAP Silica Gel cartridge and purified by automated flash column chromatography on Biotage® SP4, the product eluting in 10%–50% EtOAc/petroleum ether. The fractions were collected and concentrated *in vacuo* to afford the title compound as a clear, colourless oil (65 mg, 0.21 mmol, 55% yield): R_f: 0.47 (EtOAc/petroleum ether 2:3); ^{1}H NMR (500 MHz; $CDCl_3$) δ_H 7.79 (2H, d, *J* 8.1, *H*-2&2') 7.41–7.30 (6H, m, Ar-H) 7.27–7.25 (1H, m, Ar-H) 5.84 (1H, s, *H*-8) 1.33 (12H, s, *H*-7&7'&7''&7'''); ^{13}C NMR (126 MHz; $CDCl_3$) δ_C 146.8 (C-9) 143.7 (C-1) 135.0 (C-3/3') 128.5 (C-11/11') 127.7 (C-2/2') 126.6 (C-10/10') 125.8 (C-12) 83.8 (C-4?) 83.5 (C-6/6') 76.3 (C-8) 24.9 (C-7/7'/7''/7'''); ^{11}B NMR

(161 MHz; $CDCl_3$) δ_B 34.1–27.4 (br s, *B*-5); LRMS *m/z* not detected; HRMS *m/z* (GCMS Ammonia CI) [Found 308.1699; $C_{19}H_{23}BO_3^+$ requires 310.18493].

Potassium (3,5-dimethylisoxazol-4-yl)trifluoroborate (260)

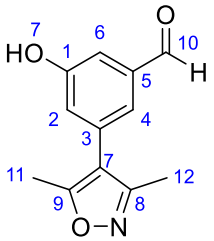


Molander Method:[278] A suspension of 3,5-dimethylisoxazol-4-yl boronic acid (2.0 g, 14.2 mmol, 1.0 eq.) in MeOH (10 mL) was stirred and cooled to 0 °C. To this suspension was added KHF_2 (3.55 g, 45.4 mmol, 3.2 eq.), followed by water (9.6 mL), dropwise. The reaction mixture was warmed to RT and stirred for 10 minutes. The volatile components were removed under reduced pressure, and the resulting sludgy solid was purified by continuous Soxhlett extraction in acetone (350 mL) for 17 hours. The solution was cooled, concentrated *in vacuo* and redissolved in acetone (150 mL). The product was then precipitated by addition of Et_2O (200 mL), filtered, and dried under reduced pressure to afford the title compound as a colourless powder (2.40 g, 11.84 mmol, 84% yield): mp >300 °C (acetone/Et_2O) [lit. >275 °C][222]; ^{1}H NMR (400 MHz; DMSO-D6) δ_H 2.19 (3H, s, *H*-7) 2.04 (3H, s, *H*-6); ^{19}F NMR (376 MHz; DMSO-D6) δ_F −134.2–−134.8 (m); LRMS *m/z* (ES−) 164 $[M-K]^-$ (100%); HRMS *m/z* (ES−) observed 164.04993 [$C_5H_6BF_3NO^-$ requires 164.05000]. These data are in good agreement with the literature.[278]

Lloyd-Jones Method:[279] To a stirring suspension of 3,5-dimethylisoxazol-4-yl boronic acid (5.0 g, 35.5 mmol, 1 eq.) in MeCN (142 mL) was added a solution of KF (14.2 mL, 142 mmol, 4 eq., 10 M in water), causing the suspension to dissolve. The solution was stirred at RT for 40 min, and then a solution of (L)-(−)-tartaric acid (53 mL, 72.7 mmol, 2.05 eq., 1.37 M in THF) was added causing a flocculent colourless precipitate to form.

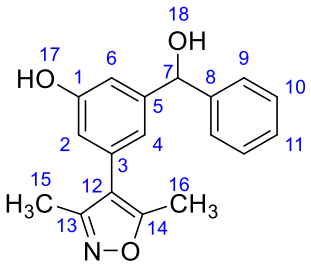
The suspension was stirred at RT for 1.5 hours, and then the precipitate was filtered under reduced pressure. The mother liquor was concentrated *in vacuo* to afford the title compound as a colourless powder (5.38 g, 26.4 mmol, 74% yield). Data match those for the product of the method above.

3-(3,5-Dimethylisoxazol-4-yl)-5-hydroxybenzaldehyde (240)



To a flame-dried flask under Ar was added 3-bromo-5-hydroxybenzaldehyde (1.22 g, 6.09 mmol, 1 eq.), potassium (3,5-dimethylisoxazol-4-yl)trifluoroborate (1.36 g, 6.70 mmol, 1.1 eq.), $Pd(OAc)_2$ (41 mg, 0.183 mmol, 3 mol%), RuPhos (171 mg, 0.365 mmol, 6 mol%), and Na_2CO_3 (1.29 g, 12.2 mmol, 2 eq.). Ethanol (12.1 mL) (thoroughly degassed with N_2 flow and sonication) was added, and the mixture was heated under reflux for 16 hours. The mixture was cooled to RT, filtered through a pad of Celite®, and concentrated *in vacuo*. The resulting brown residue was dissolved in EtOAc, adsorbed onto Celite®, loaded onto a 50 g Biotage® SNAP silica gel column, and purified by flash column chromatography eluting with 20%–50% EtOAc/petroleum ether with ~1% AcOH. The appropriate fractions were collected and concentrated *in vacuo* to afford the title compound as an off-white solid (944 mg, 4.35 mmol, 71% yield): R_f: 0.58 (EtOAc/*n*-hexane 1:1); mp 184–190 °C (EtOAc) [lit. 184–187 °C][222,223]; ^{1}H NMR (400 MHz; $CDCl_3$) δ_H 9.99 (1H, s, *H*-10) 7.35–7.32 (2H, m, *H*-2 and *H*-4) 7.02 (1H, t, *J* 2.0, *H*-6) 2.44 (3H, s, *H*-11) 2.30 (3H, s, *H*-12); LRMS *m/z* (ES^-) 216 $[M-H]^-$, 433 $[2M-H]^-$. These data are in good agreement with the literature.[221–223]

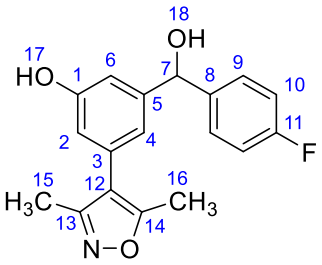
3-(3,5-Dimethylisoxazol-4-yl)-5-(hydroxy(phenyl)methyl)phenol (232)



To a flame-dried flask under Ar was added 3-(3,5-dimethylisoxazol-4-yl)-5-hydroxybenzaldehyde (250 mg, 1.02 mmol, 1 eq.), which was dissolved in anhydrous THF (20 mL). The mixture was stirred, giving a yellow solution which was cooled to 0 °C. Phenylmagnesium bromide solution (3.06 mL, 3.06 mmol, 3 eq., 1 M in THF) was added dropwise, causing the solution to turn slightly green. The solution was stirred at 0 °C for 35 minutes, then warmed to RT. The reaction was quenched with addition of 1 M aqueous HCl (10 mL), and the volatile components were removed *in vacuo*. The remaining aqueous solution was extracted with EtOAc (3 × 35 mL), and the combined organic phases were washed with water, (2 × 20 mL) and brine (2 × 20 mL). The organic layer was separated, dried over $MgSO_4$, filtered, and concentrated *in vacuo*. The resulting yellow residue was triturated with Et_2O (3 × 10 mL), and the resulting off-white solid was dissolved in EtOAc and adsorbed onto Celite®. The crude material was loaded onto a 25 g Biotage® SNAP silica gel column and purified by flash column chromatography on a Biotage® SP4 system, the compound eluting in 10%–80% EtOAc/$CHCl_3$. The fractions were collected and concentrated *in vacuo* to afford the title compound (188 mg, 0.637 mmol, 62% yield) as a colourless solid: R_f: 0.40 (1:1 EtOAc/petroleum ether); mp 187-189 °C ($CHCl_3$) [lit. 187-188 °C ($CHCl_3$)][223]; ^{1}H NMR (400 MHz; acetone-D6) δ_H 7.48–7.44 (2H, m, Ar-H) 7.34–7.29 (2H, m, Ar-H) 7.24–7.19 (1H, m Ar-H) 6.93–6.90 (1H, m, *H*-2) 6.88–6.86 (1H, m *H*-4) 6.67–6.65 (1H, m, *H*-6) 5.78 (1H, s, *H*-7) 2.36 (3H, s, *H*-11) 2.19 (3H, s,

H-12); LRMS *m/z* (ES−) 294 $[M-H]^-$ (100%), 589 $[2M-H]^-$ (23%). These data are in good agreement with the literature.[223]

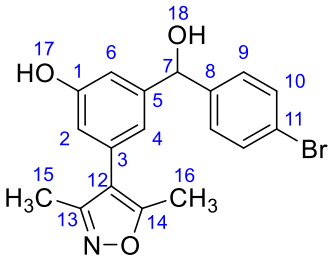
3-(3,5-Dimethylisoxazol-4-yl)-5-((4-fluorophenyl)(hydroxy)methyl)phenol (184)



To a flame-dry 2-necked flask under Ar, fitted with a dropping funnel, was added Mg turnings (63 mg, 2.59 mmol) and a single crystal of iodine. To this was added dry THF (5 mL, distilled over sodium), and the mixture was stirred. To the dropping funnel was added a solution of 4-fluorobromobenzene (314 µL, 2.85 mmol) in THF (5 mL). The solution was added dropwise at RT, and the funnel rinsed with further THF (0.5 mL). The mixture was then heated under reflux with stirring for 1 hour. At this time, the Mg turnings had dissolved, and the solution had become cloudy. The solution was cooled to 0 °C, and from a separate flame-dry flask under Ar was transferred an ice-cooled solution of 3-(3,5-dimethylisoxazol-4-yl)-5-hydroxybenzaldehyde (94 mg, 0.433 mmol) in THF (10 mL) *via* cannulation, causing the Grignard solution to turn orange and cloudy. The mixture was warmed to RT and stir for 16 hours. The reaction was then quenched with addition of water and neutralised with 1 M aqueous HCl (~1 mL). The volatile components were removed *in vacuo*, and the remaining aqueous solution was extracted with EtOAc (3 × 30 mL). The combined organic components were washed with brine (30 mL), dried over $MgSO_4$, filtered, and concentrated *in vacuo* to afford a pale brown oil. The oil was dissolved in EtOAc, adsorbed onto Celite®, loaded onto silica gel and purified by flash column chromatography, the product eluting in 25%–40% EtOAc/petroleum ether. The fractions were collected and concentrated *in vacuo*

to afford a colourless oil, from which the title compound was precipitated by addition of $CHCl_3$ as a colourless crystalline solid (98 mg, 0.313 mmol, 72% yield): R_f: 0.26 (EtOAc/petroleum ether 1:1); mp 67–71 °C ($CHCl_3$); $\bar{\nu}_{max}$ (solid) cm^{-1} 3202 (s, br), 1595 (s), 1544 (w), 1507 (s), 1421 (s), 1322 (s), 1256 (s), 1221 (s), 1156 (s), 1081 (m), 1035 (m), 1014 (m), 998 (m), 964 (m), 856 (s), 840 (s), 782 (s), 701 (s), 675 (s); ^1H NMR (400 MHz; MeOH-D4) δ_H 7.42–7.38 (2H, m, *H*-19 & *H*-21) 7.08–7.03 (2H, m, *H*-18 & *H*-22) 6.83–6.81 (1H, m, *H*-2) 6.78–6.77 (1H, m, *H*-4) 6.62–6.61 (1H, m, *H*-6) 5.74 (1H, s, *H*-8) 2.37 (3H, s, *H*-15) 2.21 (3H, s, *H*-14); ^{19}F NMR (377 MHz; MeOH-D4) δ_F −117.74 (m); LRMS *m/z* (ES−) 312 $[M-H]^-$ (29%); 625 $[2M-H]^-$ (100%). These data are in good agreement with the literature.[221]

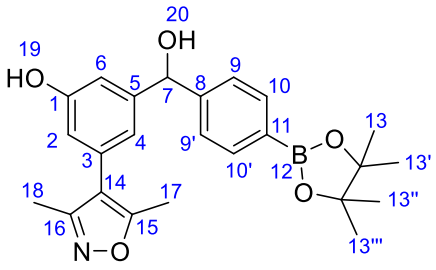
3-((4-Bromophenyl)(hydroxy)methyl)-5-(3,5-dimethylisoxazol-4-yl)phenol (255)



To a flame-dried flask under Ar was added 1,4-dibromobenzene (1.34 g, 5.69 mmol, 3 eq.), which was dissolved in anhydrous THF (59.6 mL) and stirred to give a clear, colourless solution which was cooled to −78 °C. To the stirring solution was added *n*-BuLi solution (2.50 mL, 6.26 mmol, 3.3 eq., 2.5 M in *n*-hexane), dropwise. The solution was stirred at −78 °C for 10 minutes, then warmed to RT. A solution of 3-(3,5-dimethylisoxazol-4-yl)-5-hydroxybenzaldehyde (412 mg, 1.90 mmol, 1 eq.) in anhydrous THF (10 mL) was added dropwise, causing the solution to turn yellow, and stirred at RT for 1 hour. The reaction was quenched with addition of methanol, and the volatile components were removed *in vacuo*. The residue was dissolved in MeOH, adsorbed onto Celite®, loaded onto a 25 g Biotage® SNAP silica gel cartridge, and

purified by automated silica gel chromatography on a Biotage® SP4, eluting with 30%–60% EtOAc/petroleum ether. The fractions were collected and concentrated *in vacuo* to afford the title compound as an amorphous yellow solid (559 mg, 1.49 mmol, 78% yield): R_f: 0.24 (EtOAc/petroleum ether 2:3); $\bar{\nu}_{max}$ (solid) cm^{-1} 3250 (m, br, O-H), 2929 (w), 2853 (w), 2360 (w), 2160 (w), 2028 (w), 1631 (m), 1595 (s), 1487 (m), 1423 (s), 1324 (m, ArO-H), 1256 (m), 1203 (m), 1148 (w), 1107 (w), 1039 (w), 1010 (m), 965 (w), 909 (m), 851 (m), 828 (m), 804 (m), 766 (w), 731 (s), 655 (w), 620 (w); ^{1}H NMR (400 MHz; $CDCl_3$) δ_H 7.48 (2H, d, *J* 8.4, *H*-19&21) 7.27 (2H, d, *J* 8.4, *H*-18&22) 6.83 (1H, s, *H*-2) 6.79 (1H, s, *H*-6) 6.64 (1H, s, *H*-4) 5.78 (1H, d, *J* 2.9, *H*-9) 5.19 (1H, s, *H*-7) 2.37 (3H, s, *H*-15) 2.23 (3H, s, *H*-14); ^{13}C NMR (101 MHz, $CDCl_3$) δ_C 165.6 (C-14) 158.7 (C-1) 156.6 (C-13) 145.9 (C-5) 142.5 (C-8) 132.2 (C-10/10') 131.8 (C-3) 128.3 (C-9/9') 121.8 (C-11) 119.5 (C-12) 116.4 (C-4) 115.5 (C-6) 112.9 (C-2) 75.4 (C-7) 11.7 (C-16) 10.9 (C-15); LRMS *m/z* not detected; HRMS *m/z* (GCMS NH_3 CI) [Found 374.0388; $C_{18}H_{17}{}^{(79)}BrNO_3^+$ requires 374.0386; 376.0372; $C_{18}H_{17}{}^{(81)}BrNO_3^+$ requires 376.0366]; HPLC (Method B) Retention Time = 9.08 minutes, purity 93.9%.

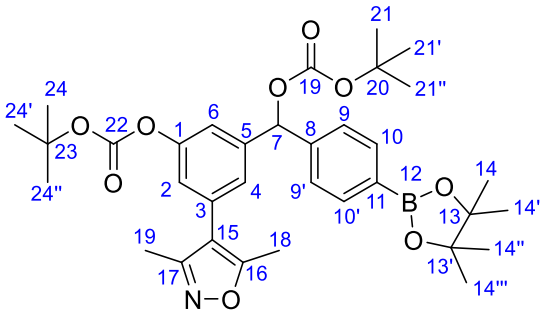
3-(3,5-Dimethylisoxazol-4-yl)-5-(hydroxy(4-(4,4,5,5-tetramethyl-1,3,2-dioxaborolan-2-yl)phenyl)methyl)phenol (256)



To a flask under a nitrogen atmosphere was added bis(pinacolato)diboron (254 mg, 1.00 mmol, 1.5 eq.), potassium acetate (197 mg, 2.00 mmol, 3 eq.), and Pd(dppf)Cl_2·CH_2Cl_2 (55 mg, 0.0668 mmol, 0.1 eq.). To this was added a solution of 3-((4-bromophenyl)(hydroxy)methyl)-5-(3,5-dimethylisoxazol-4-yl)phenol (250 mg, 0.668 mmol, 1 eq.) in degassed 1,4-dioxane (2.9 mL), and the resulting solution was

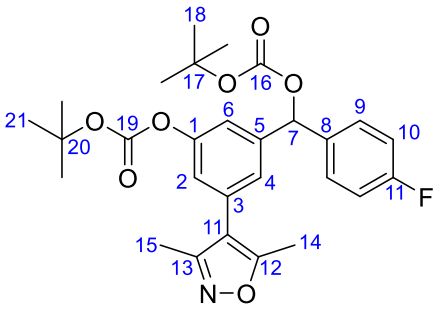
stirred and heated at 85 °C for 2 hours. The mixture was cooled to RT, filtered through a pad of Celite®, washed through with EtOAc, and concentrated *in vacuo* to afford a brown residue. The residue was dissolved in EtOAc, adsorbed onto Celite®, loaded onto a 25 g Biotage® SNAP silica gel cartridge and purified on a Biotage® SP4 system eluting with 20%–30% EtOAc/petroleum ether. The appropriate fractions were collected and concentrated *in vacuo* to afford the title compound as a viscous, pale brown oil (213 mg, 0.506 mmol, 76% yield): R_f: 0.24 (EtOAc/petroleum ether 2:3); $\bar{\nu}_{max}$ (solid) cm^{-1} 3270 (br, O-H), 2978 (w), 1595 (m), 1514 (w), 1399 (w, -CH_3), 1359 (s), 1320 (m), 1257 (w -CH_3), 1203 (w, C-O), 1142 (s, C-O), 1086 (s), 1043 (w), 1019 (m), 962 (m), 856 (s), 824 (m), 798 (m), 707 (m), 672 (m), 658 (s), 609 (w); ^{1}H NMR (400 MHz; $CDCl_3$) δ_H 7.80 (2H, d, *J* 8.1, *H*-9&9') 7.40 (2H, d, *J* 8.1, *H*-10&10') 6.84 (1H, s, *H*-2) 6.80 (1H, s, *H*-6) 6.62 (1H, s, *H*-4) 5.82 (1H, d, *J* 3.3, *H*-7) 5.34 (1H, s, *H*-20) 2.35 (3H, s, *H*-17) 2.21 (3H, s, *H*-18) 1.33 (12H, s, *H*-13&13'&13''&13'''); ^{13}C NMR (101 MHz; $CDCl_3$) δ_C 165.6 (C-15) 158.8 (C-1) 156.7 (C-16) 146.6 (C-5) 146.0 (C-8) 135.2 (C-10/10') 131.9 (C-3) 125.9 (C-9/9') 119.4 (C-14) 116.6 (C-4) 115.4 (C-6) 113.0 (C-2) 84.1 (C-12/12') 76.0 (C-7) 24.9 (C13/13'/13''/13'''?) 24.7 (C13/13'/13''/13'''?) 11.7 (C-17) 10.9 (C-18) ; LRMS *m/z* (ES+) 422 $[M+H]^+$, 444 $[M+Na]^+$; (ES−) 420 $[M-H]^-$ 456 $[M+Cl]^-$;HPLC (Method B) Retention Time = 9.62 minutes, purity 89.3%.

(3-((*t*-Butoxycarbonyl)oxy)-5-(3,5-dimethylisoxazol-4-yl)phenyl)(4-(4,4,5,5-tetramethyl-1,3,2-dioxaborolan-2-yl)phenyl)methyl *t*-butyl carbonate (257)



To a flame-dried flask under Ar was added a solution of 3-(3,5-dimethylisoxazol-4-yl)-5-(hydroxy(4-(4,4,5,5-tetramethyl-1,3,2-dioxaborolan-2-yl)phenyl)methyl)phenol (100 mg, 0.237 mmol, 1 eq.) in anhydrous CH_2Cl_2 (790 µL). 4-DMAP (1.4 mg, 0.012 mmol, 0.05 eq.) was added, and the solution was stirred and cooled to 0 °C. Boc_2O (131 µL, 0.57 mmol, 2.4 eq.) was added dropwise, and the solution was stirred at 0 °C for 5 minutes, then warmed to RT and stirred for 1 hour. The solution was then diluted with CH_2Cl_2 and washed with 1 M aqueous HCl (1 × 15 mL) and water (2 × 15 mL). The layers were separated, and the organic phase was dried over $MgSO_4$, filtered, and concentrated *in vacuo* to afford the title compound as a viscous oil (116 mg, 0.187 mmol, 69% yield): R_f: 0.75 (EtOAc/petroleum ether 1:1); $\bar{\nu}_{max}$ (solid) cm^{-1} 2979 (w), 1744 (m), 1612 (w), 1457 (w), 1397 (w, -CH_3), 1360 (m), 1323 (w), 1270 (s, -CH_3), 1245 (s), 1142 (s, C-O), 1088 (m), 1021 (w), 963 (w), 858 (m), 784 (w), 701 (w), 658 (w); ^{1}H NMR (400 MHz; $CDCl_3$) δ_H 7.73 (2H, d, *J* 8.1, *H*-10&10') 7.31 (2H, d, *J* 8.1, *H*-9&9') 7.11 (1H, t, *J* 1.8, *H*-2) 6.97 (1H, m, *H*-4) 6.94 (1H, t, *J* 1.8, *H*-6) 6.58 (1H, s, *H*-7) 2.27 (3H, s, *H*-18) 2.15 (3H, s, *H*-19) 1.48 (9H, s, *H*-24&24'&24'') 1.40 (9H, s, *H*-12&21'&21'') 1.26 (10.5H, s, *H*-14&14'&14''&14'''); LRMS *m/z* (ES+) 622 $[M+H]^+$ (100%); HRMS *m/z* (ESI+) [Found 644.29988; $C_{34}H_{44}O_9NBNa^+$ requires 644.30013].

3-(((*t*-Butoxycarbonyl)oxy)(4-fluorophenyl)methyl)-5-(3,5-dimethylisoxazol-4-yl)phenyl *t*-butyl carbonate (258)



To a flame-dried flask under argon was added XX (20 mg, 0.064 mmol, 1 eq.), followed by dry CH_2Cl_2 (213 µL) to give a suspension which was stirred. 4-DMAP (0.4 mg, 9.19 µL, 5 mol%) was added, and the mixture was cooled to 0 °C, and Boc_2O (35 µL, 0.153 mmol, 2.4 eq.) dropwise. The mixture was stirred at 0 °C for 10 minutes, then warmed to RT and stirred overnight. The mixture was then diluted with CH_2Cl_2, washed with 1 M aqueous HCl (1 × 10 mL) and water (2 × 10 mL). The organic component was separated, dried over $MgSO_4$, filtered and concentrated *in vacuo*. The residue was dissolved in EtOAc, adsorbed onto Celite®, loaded onto silica gel and purified by flash column chromatography eluting in 30% EtOAc/petroleum ether to afford the title compound as a colourless oil (19.6 mg, 0.038 mmol, 59% yield): R_f: 0.82 (EtOAc/petroleum ether 1:1); $\bar{\nu}_{max}$ (solid) cm^{-1} 2981 (w), 1744 (m, br), 1633 (w), 1607 (w), 1510 (w) 1416 (w), 1395 (w), 1370 (w), 1270 (s C-O), 1244 (s, CH_3), 1141 (s), 1086 (m), 1036 (w), 982 (w), 842 (m), 785 (m), 695 (w), 666 (w), 616 (w); ^{1}H NMR (400 MHz; $CDCl_3$) δ_H 7.38–7.32 (2H, m, *H*-10&10') 7.18–7.15 (1H, m, *H*-2) 7.08–7.01 (4H, m, *H*-4, *H*-6, *H*-9&9') 6.64 (1H, s, *H*-7) 2.37 (3H, s, *H*-14) 2.23 (3H, s, *H*-15) 1.55 (9H, s, *H*-21&21'&21'') 1.47 (9H, s, *H*-18&18'&18''); ^{13}C NMR: (101 MHz; $CDCl_3$) δ_C 165.8 (C) 164.0 (C) 161.5 (C) 158.5 (C) 152.8 (C) 151.58 (C) 151.51 (C) 142.3 (C) 135.36 (C) 135.33 (C) 132.2 (C) 129.17 (C) 129.09 (C) 124.7 (C) 121.5 (C) 118.9 (C) 115.89 (C) 115.78 (C) 115.67 (C) 84.1 (C) 83.1 (C) 78.3 (C) 27.90 (C) 27.82 (C) 11.7 (C) 10.9 (C); ^{19}F NMR (377 MHz; DMSO-D6) δ_F −113.90 (m); LRMS *m/z* (ES+) 514

$[M+H]^+$ (100%) 536 $[M+Na]^+$ (45%); HRMS *m/z* (ESI+) [Found 536.20496; $C_{28}H_{32}O_7NFNa^+$ requires 536.20550]; HPLC (Method B) Retention Time = 12.50 minutes, purity 91.3%.

Biological Materials and Methods

General biological laboratory and cell culture reagents

Laboratory plastic ware was supplied by CoStar® and Corning®. Table **19** describes the general biological laboratory reagents used. All glassware was autoclaved prior to use.

Table 19: General biological laboratory reagents

Name	Supplier
Acetonitrile	Sigma-Aldrich UK
DMSO (dimethyl sulfoxide)	Sigma-Aldrich UK
Ethanol	Sigma-Aldrich UK
FBS (fetal bovine serum)	Autogen Bioscience
Paraformaldehyde	Thermo-Fisher
PBS (phosphate-buffered saline)	Fisher Scientific
ProLong® GOLD Antifade	Invitrogen/Life Technologies
ProLong® GOLD Antifade with DAPI	Invitrogen/Life Technologies
RPMI medium	Sigma-Aldrich UK
Trypsin 0.05% EDTA	Sigma-Aldrich UK

Hypoxia treatment

Hypoxia treatment was carried out using a Bactron II anaerobic chamber (Shel Lab®), or a Bactron EZ anaerobic chamber (Shel Lab®). These chambers are under a positive pressure of an anaerobic nitrogen gas mixture (90% N_2/5% CO_2/5% H_2). No oxygen is supplied to this chamber; however, it is not possible to guarantee 0% oxygen due to potential leaks. It is estimated that the oxygen concentration at a given time is no higher than 0.1%. Therefore, the oxygen tension for experiments carried out in these chambers will be referred to as <0.1% O_2 throughout the text. For experiments performed in the anaerobic chamber, glass dishes for plating cells, and glass vials for enzymatic assays were used. This is because plastic can retain oxygen. For indicated fluorescent or confocal microscopy experiments, cell culture and treatment was performed using Falcon Corning® 4-well chamber slides (Fisher Scientific, product code 10384501), which are composed partly of plastic.

Enzyme treatment

All purified enzymes used were purchased from Cypex Limited (Dundee, UK) and were used as supplied. Purified cytochrome p450 reductase (cat.no CYP004) was purchased individually. An NADPH regenerating system was used in each assay. Solution A (20×, Corning®, 451220) and Solution B (200×, Corning®, 451200) were used as supplied. Solution A and Solution B comprise the following:

a) Solution A: 26 mM NADP+, 66 mM $MgCl_2$, 66 mM glucose-6-phosphate in H_2O.
b) Solution B: 40 units/mL glucose-6-phosphate dehydrogenase in 5 mM sodium citrate.

In all cases, Millipore™ water and 0.5 M K_2HPO_4 buffer (BD Gentest™) were used. The composition of 1 mL of assay solution for a typical assay with cytochrome p450 reductase is detailed in Table **20**. Volumes of cytochrome p450 reductase solution were varied between batches to provide a final concentration of 92 pmol mL^{-1}. Volumes of substrate were varied by stock concentration to provide a final concentration of 10 μM unless otherwise stated. Volumes of H_2O were varied to ensure the overall volume was 1 mL.

Table 20: Format of a typical 1 mL NADPH reductase assay.

Substance	Volume in 1 mL assay	Final concentration
0.5 M K_2HPO_4	200 μL	100 mM
Solution A (20×)	50 μL	1×
Solution B (200×)	10 μL	1×
H_2O	730 μL	-
Cytochrome p450 reductase (8.1 nmol mL^{-1})	11.4 μL	92 pmol mL^{-1}
Substrate (10 mM in DMSO)	1 μL	10 μM

Substrates were introduced to the assay volume last, and t=0 aliquots taken at this time. Aliquots (50 μL) were taken at the desired time points, and any reaction

quenched by addition into MeCN (50 µL). Samples were then centrifuged at 17000 × *g* for 10 minutes, and the supernatant analysed by HPLC-MS.

Cell lines and culture

OE21 oesophageal cells were used for these studies. Cells came from Public Health England. OE21 cells were cultured in RPMI medium supplemented with 10% FBS, in a standard humidified incubator at 37 °C and 5% CO_2. All experiments were performed at a cell confluency of 65–75%.

Cells were cultured with 100 Units/mL penicillin and 0.1 mg/mL streptomycin. Penicillin-Streptomycin solution (Sigma-Aldrich, 100×, cat. no. P4333) was aliquoted (5 mL), and stored at −20 °C. When required, the aliquot was thawed at ambient temperature, and added to media (500 mL) directly.

Cells were passaged 3–4 times per week. A cell suspension was prepared by removal of the medium, washing with PBS (×3), followed by addition of Trypsin-EDTA solution for 5 minutes to trypsinise the cells. The Trypsin-EDTA solution was inactivated by the addition of fresh media. The cell density was determined by addition of cell suspension (10 µL) to a Neuenbauer haemocytometer chamber. Cells were counted in the standard manner. The desired number of cells for each experiment was then seeded into fresh media.

Cells were routinely tested for the presence of mycoplasma using the PlasmoTest™ kit (InvivoGen). Cells were grown in antibiotic-free media for 24 hours, then harvested when 90–100% confluent. Cells were then heated for 15 minutes at 100 °C. The resulting suspension (50 µL) was added to HEK-Blue cells (200 µL, 1–3.5×10^5 cells/mL) in HEK-Blue™ detection medium (InvivoGen). Cells were plated, in duplicate in a 96-well plate, together with positive and negative controls provided by

the manufacturer. The plates were then incubated under normal tissue culture conditions for 24 hours. After this time, the wells were examined for the appearance of a blue colour, which indicated the presence of lipoprotein expressed by bacteria and mycoplasma. A pink colour indicated a negative result, suggesting the absence of mycoplasma.

Cryopreservation of cell lines

Cells were grown to 70% confluence, trypsinised with Trypsin-EDTA solution, and resuspended in 5 mL of fresh media. The cells were pelleted by centrifugation at 4500 × *g* for 5 minutes at ambient temperature. The media supernatant was removed, and the cell pellet resuspended in 1 mL of freezing media (10% FBS, 80% media, 10% DMSO) and stored in a 1.5 mL cryovial (ThermoScientific Nunc™, cat. no. 5001-1020) for freezing. The vial was insulated by wrapping with tissue, before transfer to liquid N_2 for long-term storage.

When required, cells were removed from liquid N_2, rapidly thawed in a water bath at 37 °C and transferred to 5 mL of pre-warmed media. Cells were pelleted by centrifugation at 4500 × *g* for 5 minutes at ambient temperature. The supernatant was removed, and the pelleted cells were resuspended in fresh media. The cell suspension was then transferred to a 75 cm^3 flask and incubated under normal conditions.

Compound treatments of cells

Cells were treated with the indicated compounds, at the indicated concentrations, as a solution made in fresh media. Compounds were stored as stock solutions in DMSO at 5, 10 or 30 mM as indicated. Stock solutions were stored in the dark at −20 °C. Compound stocks in DMSO were diluted in media at a minimum of 1:500 to the desired concentration, such that the overall DMSO concentration was ≤ 0.2% in the media.

Cell permeability analysis by HPLC-MS

OE21 cells were seeded into 6 cm glass dishes at a density of 0.5–1.0×10^6 cells per dish in a total of 3 mL of medium. Cells were incubated for 15 hours, then treated as indicated above with either compound or vehicle control (typically DMSO), at ambient oxygen pressure for the indicated time. An aliquot of media (200 µL) was taken and added to MeCN (200 µL) for HPLC-MS analysis. The remaining media was removed, the cells were washed with PBS (×3), and then harvested by scraping in 1 mL PBS. The cells were pelleted by centrifugation at 2500 × *g* for 10 minutes, the supernatant removed, and resuspended in a lysis mix (1:1 MeCN/MeOH, 200 µL). The cells were then lysed by 2 × 20 second bursts of sonication. The resulting debris was pelleted by centrifugation at 4000 × *g* for 10 minutes, and an aliquot of supernatant (100 µL) was taken and added to MeCN (100 µL) for HPLC-MS analysis.

Cellular metabolism analysis by HPLC-MS

OE21 cells were seeded into 6 cm glass dishes at a density of 0.5–1.0×10^6 cells per dish in a total of 3 mL of medium. Cells were incubated for 15 hours, then treated as indicated above with either compound or vehicle control (typically DMSO), at the indicated oxygen pressure for the indicated time. The media was removed, the cells were washed with PBS (×4), and then harvested by scraping in 1 mL PBS. The cells were pelleted by centrifugation at 2500 × *g* for 10 minutes, the supernatant removed, and resuspended in a lysis mix (1:1 MeCN/MeOH, 200 µL). The cells were then lysed by 2 × 20 second bursts of sonication. The resulting debris was pelleted by centrifugation at 4000 × *g* for 10 minutes, and an aliquot of supernatant (100 µL) was taken and added to MeCN (100 µL) for HPLC-MS analysis.

Compound 166 reactivity with NADPH

NADPH tetrasodium salt powder (Sigma-Aldrich UK, cat. no. N7505) was made up to a 10 mM solution in Millipore™ water. In all cases, Millipore™ water and 0.5 M K_2HPO_4 buffer (BD Gentest™) were used. Assays were conducted in a 1.5 mL Eppendorf vial, shaken at 1000 rpm at 37 °C. The composition of 1 mL of assay solution for a typical assay with NADPH is detailed in Table **21**.

Substance	Volume in 1 mL assay	Final concentration
0.5 M K_2HPO_4	200 µL	100 mM
H_2O	775 µL	-
NADPH solution (10 mM)	20 µL	200 µM
Substrate (10 mM in DMSO)	5 µL	50 µM

Table 21: Typical conditions for a 1 mL NADPH reactivity assay of compound **166**.

All substances except for NADPH were introduced to the assay vessel, and an aliquot (50 µL) was taken to represent time t=0. After addition of NADPH solution, aliquots were taken and added to MeCN (50 µL) for HPLC-MS analysis.

Compound 166 reactivity with L-glutathione (GSH)

L-glutathione reduced powder (Sigma-Aldrich UK, cat. no. G4251) was made up to a 50 mM solution in Millipore™ water. In all cases, Millipore™ water and 0.5 M K_2HPO_4 buffer (BD Gentest™) were used. Assays were conducted in a 1.5 mL Eppendorf vial, shaken at 1000 × *g* at 37 °C. The composition of 1 mL of assay solution for a typical assay with L-glutathione is detailed in Table **22**.

Table 22: Typical conditions for a 1 mL L-GSH reactivity assay of compound **166**.

Substance	Volume in 1 mL assay	Final concentration
0.5 M K_2HPO_4	200 µL	100 mM
H_2O	775 µL	-
L-GSH solution (50 mM)	20 µL	1 mM
Substrate (10 mM in DMSO)	5 µL	50 µM

All substances except for L-glutathione were introduced to the assay vessel, and an aliquot (50 µL) was taken to represent time t=0. After addition of NADPH solution, aliquots were taken and added to MeCN (50 µL) for HPLC-MS analysis.

Fluorescence microscopy

0.5–1×10^6 cells were seeded in 6 cm glass dishes containing cover slips and left to adhere for 16 hours. The media was removed and replaced with fresh media containing the desired compound and the stated concentration (or vehicle control), and the cells treated under 21% or <0.1% O_2 for the stated time. After this time, the media was removed, and the cells were washed with PBS (1×) for 5 minutes, twice. The cells were fixed with 4% paraformaldehyde solution (4% *w/v* paraformaldehyde, PBS) for 10 minutes at ambient temperature, then washed twice with PBS for 5 minutes. The cover slips were carefully removed and mounted onto slides with ProLong® Gold mounting medium containing DAPI (Invitrogen/Life Technologies). The slides were left to dry for 24 hours and sealed with nail varnish before analysis using either a Ti-E (Nikon Instruments) inverted fluorescence microscope, or LSM780 Airyscan (Carl Zeiss Microscopy Ltd) confocal microscope.

Alternatively, 1–10×10^4 cells per well were seeded into 4-well chamber slides in 300 µL of media. The slides were incubated for 2 hours for cells to adhere, then filled to 1000 µL of media, and incubated for 16 hours. The media was removed and replaced with media supplemented with the desired compound at the stated concentration. The slides were then incubated at either 21% or <0.1% O_2 for the stated time. After this time, the media was removed, and the chambers washed with PBS for 5 minutes, twice. The cells were fixed with 4% paraformaldehyde solution (4% *w/v* paraformaldehyde, PBS) for 10 minutes at ambient temperature, then washed twice with PBS for 5 minutes. The chambers were removed, and the slides were mounted

with cover slips using ProLong® Gold mounting medium, with or without DAPI. The slides were left to dry for 24 hours and sealed with nail varnish before analysis using either a Ti-E (Nikon Instruments) inverted fluorescence microscope, or LSM780 Airyscan (Carl Zeiss Microscopy Ltd) confocal microscope.

Fluorescence-activated cell sorting (FACS)

$0.5–1\times10^6$ cells were seeded in 6 cm dishes and left to adhere for 16 hours. After this time, the media was removed and replaced with fresh media supplemented with the desired compound at the stated concentration. The cells were then incubated at either 21% or <0.1% O_2 for 3 hours. Following treatment, the media was removed, the cells washed with PBS thrice, and then incubated with Trypsin-EDTA solution for 1 minute. The trypsin was removed and kept, and fresh Trypsin-EDTA solution was added. After a further 5 minutes incubation, the trypsin was neutralised by addition of media, and the cells were pelleted by centrifugation at 4500 × *g* for 5 minutes. The media was removed, the cells resuspended in PBS for 5 minutes, then pelleted by centrifugation at 4500 × *g* for 5 minutes. The supernatant was removed, and the cells resuspended in ice-cold ethanol. FACS analysis was then performed using an Attune NxT Flow Cytometer (Thermofisher Scientific) and analysed using FlowJo v10 (FlowJo LLC).

Bibliography

(1) World Health Organisation Cancer Statistics http://www.who.int/en/news-room/fact-sheets/detail/cancer (accessed Jul 25, 2018).
(2) Cancer Research UK Cancer Statistics https://www.cancerresearchuk.org/health-professional/cancer-statistics-for-the-uk (accessed Jul 25, 2018).
(3) Quaresma, M.; Coleman, M. P.; Rachet, B. *Lancet* **2015**, *385*, 1206–1218.
(4) Net Ten-Year Survival Trends by Cancer Type https://www.cancerresearchuk.org/health-professional/cancer-statistics/survival/common-cancers-compared#heading-Three (accessed Jul 25, 2018).
(5) Hanahan, D.; Weinberg, R. A. *Cell* **2000**, *100*, 57–70.
(6) Hanahan, D.; Weinberg, R. A. *Cell* **2011**, *144*, 646–674.
(7) Burrell, R. A.; McGranahan, N.; Bartek, J.; Swanton, C. *Nature* **2013**, *501*, 338–345.
(8) Gerlinger, M.; Rowan, A. J.; Horswell, S.; Larkin, J.; Endesfelder, D.; Gronroos, E.; Martinez, P.; Matthews, N.; Stewart, A.; Tarpey, P. et al. *N. Engl. J. Med.* **2012**, *366*, 883–892.
(9) Vaupel, P.; Mayer, A. *Cancer Metastasis Rev.* **2007**, *26*, 225–239.
(10) Nordsmark, M.; Bentzen, S. M.; Rudat, V.; Brizel, D.; Lartigau, E.; Stadler, P.; Becker, A.; Adam, M.; Molls, M.; Dunst, J. et al. *Radiother. Oncol.* **2005**, *77*, 18–24.
(11) Ramachandran, S.; Ient, J.; Göttgens, E.-L.; Krieg, A.; Hammond, E. *Genes* **2015**, *6*, 935–956.
(12) Harris, A. L. *Nat. Rev. Cancer* **2002**, *2*, 38–47.
(13) Heiden, M. G. Vander; Cantley, L. C.; Thompson, C. B.; Mammalian, P.; Exhibit, C.; Metabolism, A. *Science* **2009**, *324*, 1029.
(14) Bristow, R. G.; Hill, R. P. *Nat. Rev. Cancer* **2008**, *8*, 180–192.
(15) Tannock, I. F. *Br. J. Radiol.* **1972**, *45*, 515–524.
(16) Olive, P. L.; Vikse, C.; Trotter, M. J. *Int. J. Radiat. Oncol.* **1992**, *22*, 397–402.
(17) Cosse, J.-P.; Michiels, C. *Anticancer. Agents Med. Chem.* **2008**, *8*, 790–797.
(18) Brown, J. M.; Giaccia, A. J. *Cancer Res.* **1998**, *58*, 1408–1416.
(19) Wardman, P. *Clin. Oncol.* **2007**, *19*, 397–417.
(20) Jain, R. K. *Cancer Cell* **2014**, *26*, 605–622.
(21) Peng, F.; Xu, Z.; Wang, J.; Chen, Y.; Li, Q.; Zuo, Y.; Chen, J.; Hu, X.; Zhou, Q.; Wang, Y. et al. *PLoS One* **2012**, *7*, 1–10.
(22) Sorensen, A. G.; Batchelor, T. T.; Zhang, W. T.; Chen, P. J.; Yeo, P.; Wang, M.; Jennings, D.; Wen, P. Y.; Lahdenranta, J.; Ancukiewicz, M. et al. *Cancer Res.* **2009**, *69*, 5296–5300.
(23) Jain, R. K. *Science* **2005**, *307*, 58–62.
(24) Reynolds, A. R.; Hart, I. R.; Watson, A. R.; Welti, J. C.; Silva, R. G.; Robinson, S. D.; Da Violante, G.; Gourlaouen, M.; Salih, M.; Jones, M. C. et al. *Nat. Med.* **2009**, *15*, 392–400.
(25) Wilson, W. R.; Hay, M. P. *Nat. Rev. Cancer* **2011**, *11*, 393–410.
(26) Guise, C. P.; Mowday, A. M.; Ashoorzadeh, A.; Yuan, R.; Lin, W. H.; Wu, D. H.; Smaill, J. B.; Patterson, A. V.; Ding, K. *Chin. J. Cancer* **2014**, *33*, 80–86.
(27) McKeown, S. R.; Cowen, R. L.; Williams, K. J. *Clin. Oncol.* **2007**, *19*, 427–442.
(28) Hunter, F. W.; Wouters, B. G.; Wilson, W. R. *Br. J. Cancer* **2016**, *114*, 1071–1077.

(29) Xia, C.; Panda, S. P.; Marohnic, C. C.; Martasek, P.; Masters, B. S.; Kim, J.-J. P. *Proc. Natl. Acad. Sci. USA* **2011**, *108*, 13486–13491.
(30) Lienhart, W. D.; Gudipati, V.; MacHeroux, P. *Arch. Biochem. Biophys.* **2013**, *535*, 150–162.
(31) Iyanagi, T. *Biochem. Biophys. Res. Commun.* **2005**, *338*, 520–528.
(32) Garner, A. P.; Paine, M. J.; Rodriguez-Crespo, I.; Chinje, E. C.; Ortiz De Montellano, P.; Stratford, I. J.; Tew, D. G.; Wolf, C. R. *Cancer Res.* **1999**, *59*, 1929–1934.
(33) Guise, C. P.; Abbattista, M. R.; Tipparaju, S. R.; Lambie, N. K.; Su, J.; Li, D.; Wilson, W. R.; Dachs, G. U.; Patterson, A. V. *Mol. Pharmacol.* **2012**, *81*, 31–40.
(34) Walton, M. I.; Workman, P. *Biochem. Pharmacol.* **1987**, *36*, 887–896.
(35) Miskiniene, V.; Dickancaite, E.; Nemeikaite, A.; Cenas, N. *IUBMB Life* **1997**, *42*, 391–397.
(36) Raleigh, S. .; Wanogho, E.; Burke, M. D.; McKeown, S. .; Patterson, L. . *Int. J. Radiat. Oncol.* **1998**, *42*, 763–767.
(37) Hay, M. P.; Hicks, K. O.; Wang, J. In *Tumor Microenvironment and Cellular Stress*; Koumenis, C., Hammond, E., Giaccia, A., Eds.; Springer New York: New York, NY, 2014; pp 111–145.
(38) Foehrenbacher, A.; Secomb, T. W.; Wilson, W. R.; Hicks, K. O. *Front. Oncol.* **2013**, *3*, 33–35.
(39) Wilson, W. R.; Hicks, K. O.; Pullen, S. M.; Ferry, D. M.; Helsby, N. A.; Patterson, A. V. *Radiat. Res.* **2007**, *167*, 625–636.
(40) Moore, H. W.; Czerniak, R. *Med. Res. Rev.* **1981**, *1*, 249–280.
(41) Bolton, J. L.; Trush, M. A.; Penning, T. M.; Dryhurst, G.; Monks, T. J. *Chem. Res. Toxicol.* **2000**, *13*, 135–160.
(42) Danson, S.; Ward, T. H.; Butler, J.; Ranson, M. *Cancer Treat. Rev.* **2004**, *30*, 437–449.
(43) Ross, D.; Siegel, D. In *Methods in Enzymology*; 2004; Vol. 382, pp 115–144.
(44) Li, Z.; Li, X.; Gao, X.; Zhang, Y.; Shi, W.; Ma, H. *Anal. Chem.* **2013**, *85*, 3926–3932.
(45) Winn, B. A.; Shi, Z.; Carlson, G. J.; Wang, Y.; Nguyen, B. L.; Kelly, E. M.; Ross, R. D.; Hamel, E.; Chaplin, D. J.; Trawick, M. L. et al. *Bioorg. Med. Chem. Lett.* **2017**, *27*, 636–641.
(46) Thomson, P.; Naylor, M. a; Everett, S. a; Stratford, M. R. L.; Lewis, G.; Hill, S.; Patel, K. B.; Wardman, P.; Davis, P. D. *Mol. Cancer Ther.* **2006**, *5*, 2886–2894.
(47) Rajapaske, A.; Gates, K. S. *J. Org. Chem.* **2012**, *77*, 3531–3537.
(48) Rajapakse, A.; Linder, C.; Morrison, R. D.; Sarkar, U.; Leigh, N. D.; Barnes, C. L.; Daniels, J. S.; Gates, K. S. *Chem. Res. Toxicol.* **2013**, *26*, 555–563.
(49) O'Connor, L. University of Oxford, 2016.
(50) Conway, S.; O'Connor, L.; Hammond, E. WO 2015/071665 A1, 2015.
(51) Cazares-Körner, C.; Pires, I. M.; Swallow, I. D.; Grayer, S. C.; O'Connor, L. J.; Olcina, M. M.; Christlieb, M.; Conway, S. J.; Hammond, E. M. *ACS Chem. Biol.* **2013**, *8*, 1451–1459.
(52) Chevalier, A.; Zhang, Y.; Khdour, O. M.; Kaye, J. B.; Hecht, S. M. *J. Am. Chem. Soc.* **2016**, *138*, 12009–12012.
(53) Nakata, E.; Yukimachi, Y.; Kariyazono, H.; Im, S.; Abe, C.; Uto, Y.; Maezawa, H.; Hashimoto, T.; Okamoto, Y.; Hori, H. *Bioorganic Med. Chem.* **2009**, *17*, 6952–6958.
(54) Huang, B.; Chen, W.; Kuang, Y.-Q.; Liu, W.; Liu, X.-J.; Tang, L.-J.; Jiang, J.-H.

Org. Biomol. Chem. **2017**, *15*, 4383–4389.
(55) Gruber, T. D.; Krishnamurthy, C.; Grimm, J. B.; Tadross, M. R.; Wysocki, L. M.; Gartner, Z. J.; Lavis, L. D. *ACS Chem. Biol.* **2018**.
(56) Zhou, Y.; Bobba, K. N.; Lv, X. W.; Yang, D.; Velusamy, N.; Zhang, J. F.; Bhuniya, S. *Analyst* **2017**, *142*, 345–350.
(57) Jin, C.; Wen, S.; Zhang, Q.; Zhu, Q.; Yu, J.; Lu, W. *ACS Med. Chem. Lett.* **2017**, *8*, 762–765.
(58) O'Connor, L. J.; Cazares-Körner, C.; Saha, J.; Evans, C. N. G.; Stratford, M. R. L.; Hammond, E. M.; Conway, S. J. *Org. Chem. Front.* **2015**, *2*, 1026–1029.
(59) Ikeda, Y.; Hisano, H.; Nishikawa, Y.; Nagasaki, Y. *Mol. Pharm.* **2016**, *13*, 2283–2289.
(60) Cazares-Körner, C. University of Oxford, 2015.
(61) Wardman, P. *Environ. Health Perspect.* **1985**, *64*, 309–320.
(62) Varia, M. A.; Calkins-Adams, D. P.; Rinker, L. H.; Kennedy, A. S.; Novotny, D. B.; Fowler, W. C.; Raleigh, J. A. *Gynecol. Oncol.* **1998**, *71*, 270–277.
(63) Xu, J.; Sun, S.; Li, Q.; Yue, Y.; Li, Y.; Shao, S. *Analyst* **2015**, *140*, 574–581.
(64) Li, Z.; Gao, X.; Shi, W.; Li, X.; Ma, H. *Chem. Commun.* **2013**, *49*, 5859.
(65) Phillips, R. M. *Cancer Chemother. Pharmacol.* **2016**, *77*, 441–457.
(66) Meng, F.; Evans, J. W.; Bhupathi, D.; Banica, M.; Lan, L.; Lorente, G.; Duan, J.-X.; Cai, X.; Mowday, a M.; Guise, C. P. et al. *Mol. Cancer Ther.* **2012**, *11*, 740–751.
(67) Karnthaler-Benbakka, C.; Groza, D.; Koblmüller, B.; Terenzi, A.; Holste, K.; Haider, M.; Baier, D.; Berger, W.; Heffeter, P.; Kowol, C. R. et al. *ChemMedChem* **2016**, *11*, 2410–2421.
(68) Naughtonb, D. P.; Down, C. *Bioorganic Med. Chem. Lett.* **1999**, *9*, 2031–2036.
(69) Coumar, M. S.; Tsai, M.-T.; Chu, C.-Y.; Uang, B.-J.; Lin, W.-H.; Chang, C.-Y.; Chang, T.-Y.; Leou, J.-S.; Teng, C.-H.; Wu, J.-S. et al. *ChemMedChem* **2010**, *5*, 255–267.
(70) McNeely, S.; Beckmann, R.; Bence Lin, A. K. *Pharmacol. Ther.* **2014**, *142*, 1–10.
(71) Hart, C. P.; Duan, J.; Meng, F.; Sun, J. D.; Jung, D.; Kroll, S. M.; Curd, J. G.; Matteucci, M. 2009.
(72) Chawla, S. P.; Cranmer, L. D.; Van Tine, B. A.; Reed, D. R.; Okuno, S. H.; Butrynski, J. E.; Adkins, D. R.; Hendifar, A. E.; Kroll, S.; Ganjoo, K. N. *J. Clin. Oncol.* **2014**, *32*, 3299–3309.
(73) Anderson, R. F.; Yadav, P.; Patel, D.; Reynisson, J.; Tipparaju, S. R.; Guise, C. P.; Patterson, A. V; Denny, W. A.; Maroz, A.; Shinde, S. S. et al. *Org. Biomol. Chem.* **2014**, *12*, 3386–3392.
(74) Shinde, S. S.; Maroz, A.; Hay, M. P.; Patterson, A. V.; Denny, W. A.; Anderson, R. F. *J. Am. Chem. Soc.* **2010**, *132*, 2591–2599.
(75) Scott Daniels, J.; Gates, K. S.; Tronche, C.; Greenberg, M. M. *Chem. Res. Toxicol.* **1998**, *11*, 1254–1257.
(76) Williamson, S. K.; Crowley, J. J.; Lara, P. N.; McCoy, J.; Lau, D. H. M.; Tucker, R. W.; Mills, G. M.; Gandara, D. R.; Granados, B. *J. Clin. Oncol.* **2005**, *23*, 9097–9104.
(77) Rischin, D.; Peters, L. J.; O'Sullivan, B.; Giralt, J.; Fisher, R.; Yuen, K.; Trotti, A.; Bernier, J.; Bourhis, J.; Ringash, J. et al. *J. Clin. Oncol.* **2010**, *28*, 2989–2995.
(78) McKeown, S.; Hejmadi, M.; McIntyre, I.; McAleer, J.; Patterson, L. *Br. J. Cancer* **1995**, *72*, 76–81.

(79) Patterson, L. H. *Cancer Metastasis Rev.* **1993**, *12*, 119–134.
(80) Hejmadi, M.; McKeown, S.; Friery, O.; McIntyre, I.; Patterson, L.; Hirst, D. *Br. J. Cancer* **1996**, *73*, 499–505.
(81) Smith, P. J.; Blunt, N. J.; Desnoyers, R.; Giles, Y.; Patterson, L. H. *Cancer Chemother. Pharmacol.* **1997**, *39*, 455–461.
(82) Friery, O. P.; Gallagher, R.; Murray, M. M.; Hughes, C. M.; Galligan, E. S.; McIntyre, I. A.; Patterson, L. H.; Hirst, D. G.; McKeown, S. R. *Br. J. Cancer* **2000**, *82*, 1469–1473.
(83) Gallagher, R.; Hughes, C. M.; Murray, M. M.; Friery, O. P.; Patterson, L. H.; Hirst, D. G.; McKeown, S. R. *Br. J. Cancer* **2001**, *85*, 625–629.
(84) Albertella, M. R.; Loadman, P. M.; Jones, P. H.; Phillips, R. M.; Rampling, R.; Burnet, N.; Alcock, C.; Anthoney, A.; Vjaters, E.; Dunk, C. R. et al. *Clin. Cancer Res.* **2008**, *14*, 1096–1104.
(85) Ware, D. C.; Palmer, B. D.; Wilson, W. R.; Denny, W. A. *J. Med. Chem.* **1993**, *36*, 1839–1846.
(86) Parker, L. L.; Lacy, S. M.; Farrugia, L. J.; Evans, C.; Robins, D. J.; O'Hare, C. C.; Hartley, J. A.; Jaffar, M.; Stratford, I. J. *J. Med. Chem.* **2004**, *47*, 5683–5689.
(87) Whitmore, G. F. *Radiat. Res.* **1995**, *144*, 148.
(88) James, M. L.; Gambhir, S. S. *Physiol. Rev.* **2012**, *92*, 897–965.
(89) Logothetis, N. K.; Wandell, B. A. *Annu. Rev. Physiol.* **2004**, *66*, 735–769.
(90) Boussida, S.; Traoré, A. S.; Durif, F. *PLoS One* **2017**, *12*, e0176512.
(91) Hectors, S. J.; Wagner, M.; Bane, O.; Besa, C.; Lewis, S.; Remark, R.; Chen, N.; Fiel, M. I.; Zhu, H.; Gnjatic, S. et al. *Sci. Rep.* **2017**, *7*, 2452.
(92) Hesketh, R. L.; Brindle, K. M. *Curr. Opin. Chem. Biol.* **2018**, *45*, 187–194.
(93) Wang, Z.; Robertson, S. H.; Wang, J.; He, M.; Virgincar, R. S.; Schrank, G. M.; Bier, E. A.; Rajagopal, S.; Huang, Y. C.; O'Riordan, T. G. et al. *Med. Phys.* **2017**, *44*, 2415–2428.
(94) Caravan, P.; Ellison, J. J.; McMurry, T. J.; Lauffer, R. B. *Chem. Rev.* **1999**, *99*, 2293–2352.
(95) Caravan, P. *Chem. Soc. Rev.* **2006**, *35*, 512–523.
(96) Artemov, D.; Mori, N.; Okollie, B.; Bhujwalla, Z. M. *Magn. Reson. Med.* **2003**, *49*, 403–408.
(97) Mulder, W. J. M.; Strijkers, G. J.; van Tilborg, G. A. F.; Griffioen, A. W.; Nicolay, K. *NMR Biomed.* **2006**, *19*, 142–164.
(98) Kaberov, L. I.; Verbraeken, B.; Riabtseva, A.; Brus, J.; Radulescu, A.; Talmon, Y.; Stepanek, P.; Hoogenboom, R.; Filippov, S. K. *Macromolecules* **2018**, *51*, 6047–6056.
(99) Day, S. E.; Kettunen, M. I.; Gallagher, F. A.; Hu, D.-E.; Lerche, M.; Wolber, J.; Golman, K.; Ardenkjaer-Larsen, J. H.; Brindle, K. M. *Nat. Med.* **2007**, *13*, 1382–1387.
(100) Wadas, T. J.; Wong, E. H.; Weisman, G. R.; Anderson, C. J. *Chem. Rev.* **2010**, *110*, 2858–2902.
(101) Kim, E. M.; Park, E. H.; Cheong, S. J.; Lee, C. M.; Kim, D. W.; Jeong, H. J.; Lim, S. T.; Sohn, M. H.; Kim, K.; Chung, J. *Nucl. Med. Biol.* **2009**, *36*, 371–378.
(102) Goldenberg, A.; Masui, H.; Divgi, C.; Kamrath, H.; Pentlow, K.; Mendelsohn, J. *J. Natl. Cancer Inst.* **1989**, *81*, 1616–1625.
(103) Divgi, C. R.; Welt, S.; Kris, M.; Real, F. X.; Yeh, S. D. J.; Gralla, R.; Merchant, B.; Schweighart, S.; Unger, M.; Larson, S. M. et al. *JNCI J. Natl. Cancer Inst.* **1991**, *83*, 97–104.

(104) Silverman, D. H. S.; Small, G. W.; Chang, C. Y.; Lu, C. S.; de Aburto, M. A. K.; Chen, W.; Czernin, J.; Rapoport, S. I.; Pietrini, P.; Alexander, G. E. et al. *JAMA* **2001**, *286*, 2120.
(105) Armbrecht, J. J.; Buxton, D. B.; Schelbert, H. R. *Circulation* **1990**, *81*, 1594–1605.
(106) Janssens, S.; Dubois, C.; Bogaert, J.; Theunissen, K.; Deroose, C.; Desmet, W.; Kalantzi, M.; Herbots, L.; Sinnaeve, P.; Dens, J. et al. *Lancet* **2006**, *367*, 113–121.
(107) Gambhir, S. S. *Nat. Rev. Cancer* **2002**, *2*, 683–693.
(108) Farwell, M. D.; Pryma, D. A.; Mankoff, D. A. *Cancer* **2014**, *120*, 3433–3445.
(109) Massoud, T. F.; Gambhir, S. S. *Genes Dev.* **2003**, 545–580.
(110) Levin, C. S.; Hoffman, E. J. *Phys. Med. Biol.* **1999**, *44*, 781–799.
(111) Moses, W. W. *Nucl. Instruments Methods Phys. Res. Sect. A Accel. Spectrometers, Detect. Assoc. Equip.* **2011**, *648*, 1–14.
(112) *Emission Tomography: The Fundamentals of PET and SPECT*, 1st ed.; Wernick, M. N., Aarsvold, J. N., Eds.; Academic Press, 2004.
(113) Ancey, P.-B.; Contat, C.; Meylan, E. *FEBS J.* **2018**, *285*, 2926–2943.
(114) Fass, L. *Mol. Oncol.* **2008**, *2*, 115–152.
(115) Dijkers, E. C.; Oude Munnink, T. H.; Kosterink, J. G.; Brouwers, A. H.; Jager, P. L.; de Jong, J. R.; van Dongen, G. A.; Schröder, C. P.; Lub-de Hooge, M. N.; de Vries, E. G. *Clin. Pharmacol. Ther.* **2010**, *87*, 586–592.
(116) Afshar-Oromieh, A.; Malcher, A.; Eder, M.; Eisenhut, M.; Linhart, H. G.; Hadaschik, B. A.; Holland-Letz, T.; Giesel, F. L.; Kratochwil, C.; Haufe, S. et al. *Eur. J. Nucl. Med. Mol. Imaging* **2013**, *40*, 486–495.
(117) Lavis, L. D.; Raines, R. T. *ACS Chem. Biol.* **2008**, *3*, 142–155.
(118) Klymchenko, A. S. *Acc. Chem. Res.* **2017**, *50*, 366–375.
(119) Terai, T.; Nagano, T. *Curr. Opin. Chem. Biol.* **2008**, *12*, 515–521.
(120) Giepmans, B. N. G.; Adams, S. R.; Ellisman, M. H.; Tsien, R. Y. *Science* **2006**, *312*, 217–224.
(121) Li, P.; Xiao, H.; Cheng, Y.; Zhang, W.; Huang, F.; Zhang, W.; Wang, H.; Tang, B. *Chem. Commun.* **2014**, *50*, 7184.
(122) Mao, L.; Jiang, Q.; Wang, F.; Zhao, Y.; Guo, Z. *Analyst* **2015**, *140*, 197–203.
(123) Hintersteiner, M.; Enz, A.; Frey, P.; Jaton, A.-L.; Kinzy, W.; Kneuer, R.; Neumann, U.; Rudin, M.; Staufenbiel, M.; Stoeckli, M. et al. *Nat. Biotechnol.* **2005**, *23*, 577–583.
(124) Fu, H.; Peng, C.; Liang, Z.; Dai, J.; Liu, B.; Cui, M. *Chem. Commun.* **2016**.
(125) Yuan, L.; Lin, W.; Zheng, K.; He, L.; Huang, W. *Chem. Soc. Rev.* **2013**, *42*, 622–661.
(126) Minta, A.; Tsien, R. Y. *J. Biol. Chem.* **1989**, *264*, 19449–19457.
(127) Lee, H.; Akers, W.; Bhushan, K.; Bloch, S.; Sudlow, G.; Tang, R.; Achilefu, S. *Bioconjug. Chem.* **2011**, *22*, 777–784.
(128) Chen, Y.; Dhara, S.; Banerjee, S. R.; Byun, Y.; Pullambhatla, M.; Mease, R. C.; Pomper, M. G. *Biochem. Biophys. Res. Commun.* **2009**, *390*, 624–629.
(129) Huang, B.; Babcock, H.; Zhuang, X. *Cell* **2010**, *143*, 1047–1058.
(130) Laios, A.; Volpi, D.; Tullis, I. D. C.; Woodward, M.; Kennedy, S.; Pathiraja, P. N. J.; Haldar, K.; Vojnovic, B.; Ahmed, A. A. *BMC Res. Notes* **2015**, *8*, 608.
(131) Alander, J. T.; Kaartinen, I.; Laakso, A.; Pätilä, T.; Spillmann, T.; Tuchin, V. V.; Venermo, M.; Välisuo, P. *Int. J. Biomed. Imaging* **2012**, *2012*, 1–26.
(132) Krohn, K. a; Link, J. M.; Mason, R. P. *J. Nucl. Med.* **2008**, *49*, 129S–148S.
(133) Liu, J.; Bu, W.; Shi, J. *Chem. Rev.* **2017**, *117*, 6160–6224.

(134) Nunn, A.; Linder, K.; Strauss, H. W. *Eur. J. Nucl. Med.* **1995**, *22*, 265–280.
(135) Koh, W. J.; Rasey, J. S.; Evans, M. L.; Grierson, J. R.; Lewellen, T. K.; Graham, M. M.; Krohn, K. A.; Griffin, T. W. *Int. J. Radiat. Oncol. Biol. Phys.* **1992**, *22*, 199–212.
(136) Postema, E. J.; McEwan, A. J. B.; Riauka, T. A.; Kumar, P.; Richmond, D. A.; Abrams, D. N.; Wiebe, L. I. *Eur. J. Nucl. Med. Mol. Imaging* **2009**, *36*, 1565–1573.
(137) Nunes, P. S. G.; Zhang, Z.; Kuo, H.-T.; Zhang, C.; Rousseau, J.; Rousseau, E.; Lau, J.; Kwon, D.; Carvalho, I.; Bénard, F. et al. *J. Label. Compd. Radiopharm.* **2018**, *61*, 370–379.
(138) Abuteen, A.; Zhou, F.; Dietz, C.; Mohammad, I.; Smith, M. B.; Zhu, Q. *Dye. Pigment.* **2016**, *126*, 251–260.
(139) Mortensen, L. S.; Johansen, J.; Kallehauge, J.; Primdahl, H.; Busk, M.; Lassen, P.; Alsner, J.; Sørensen, B. S.; Toustrup, K.; Jakobsen, S. et al. *Radiother. Oncol.* **2012**, *105*, 14–20.
(140) Rami, M.; Montero, J.-L.; Dubois, L.; Lambin, P.; Scozzafava, A.; Winum, J.-Y.; Supuran, C. T. *New J. Chem.* **2010**, *34*, 2139.
(141) Dubois, L.; Lieuwes, N. G.; Maresca, A.; Thiry, A.; Supuran, C. T.; Scozzafava, A.; Wouters, B. G.; Lambin, P. *Radiother. Oncol.* **2009**, *92*, 423–428.
(142) Becker, H. M.; Klier, M.; Deitmer, J. W. *Carbonic Anhydrase: Mechanism, Regulation, Links to Disease, and Industrial Applications*; Frost, S. C., McKenna, R., Eds.; Subcellular Biochemistry; Springer Netherlands: Dordrecht, 2014; Vol. 75.
(143) McDonald, P.; Winum, J.; Supuran, C.; Dedhar, S. *Oncotarget* **2012**, *3*, 84–97.
(144) Yuan, J.; Xu, Y.-Q.; Zhou, N.-N.; Wang, R.; Qian, X.-H.; Xu, Y.-F. *RSC Adv.* **2014**, *4*, 56207–56210.
(145) O'Connor, L. J.; Mistry, I. N.; Collins, S. L.; Folkes, L. K.; Brown, G.; Conway, S. J.; Hammond, E. M. *ACS Cent. Sci.* **2017**, *3*, 20–30.
(146) Kelkar, S. S.; Reineke, T. M. *Bioconjug. Chem.* **2011**, *22*, 1879–1903.
(147) Janib, S. M.; Moses, A. S.; MacKay, J. A. *Adv. Drug Deliv. Rev.* **2010**, *62*, 1052–1063.
(148) Li, Z.; Barnes, J. C.; Bosoy, A.; Stoddart, J. F.; Zink, J. I. *Chem. Soc. Rev.* **2012**, *41*, 2590.
(149) Tung, C.-H.; Lin, Y.; Moon, W. K.; Weissleder, R. *ChemBioChem* **2002**, *3*, 784.
(150) Xiao, Q.; Zheng, X.; Bu, W.; Ge, W.; Zhang, S.; Chen, F.; Xing, H.; Ren, Q.; Fan, W.; Zhao, K. et al. *J. Am. Chem. Soc.* **2013**, *135*, 13041–13048.
(151) Wu, J. B.; Shi, C.; Chu, G. C. Y.; Xu, Q.; Zhang, Y.; Li, Q.; Yu, J. S.; Zhau, H. E.; Chung, L. W. K. *Biomaterials* **2015**, *67*, 1–10.
(152) Hu, M.; Yang, C.; Luo, Y.; Chen, F.; Yang, F.; Yang, S.; Chen, H.; Cheng, Z.; Li, K.; Xie, Y. *J. Mater. Chem. B* **2018**, *6*, 2413–2416.
(153) Sanchez, Y.; Wong, C.; Thoma, R. S.; Richman, R.; Wu, Z.; Piwnica-Worms, H.; Elledge, S. J. *Science* **1997**, *277*, 1497–1501.
(154) Walker, M.; Black, E. J.; Oehler, V.; Gillespie, D. A.; Scott, M. T. *Oncogene* **2009**, *28*, 2314–2323.
(155) Palermo, C.; Hope, J. C.; Freyer, G. A.; Rao, H.; Walworth, N. C. *PLoS One* **2008**, *3*, e1427.
(156) Chen, P.; Luo, C.; Deng, Y.; Ryan, K.; Register, J.; Margosiak, S.; Tempczyk-Russell, A.; Nguyen, B.; Myers, P.; Lundgren, K. et al. *Cell* **2000**, *100*, 681–692.
(157) Bartek, J.; Lukas, J. *Cancer Cell* **2003**, *3*, 421–429.

(158) Shiloh, Y. *Nat. Rev. Cancer* **2003**, *3*, 155–168.
(159) Nilsson, I.; Hoffmann, I. In *Progress in Cell Cycle Research*; Meijer, L., Jézéquel, A., Ducommun, B., Eds.; Springer US: Boston, MA, 2000; pp 107–114.
(160) Kastan, M. B.; Bartek, J. *Nature* **2004**, *432*, 316–323.
(161) Elledge, S. J. *Science* **1996**, *274*, 1664–1672.
(162) Otto, T.; Sicinski, P. *Nat. Rev. Cancer* **2017**, *17*, 93–115.
(163) Bensaad, K.; Vousden, K. H. *Nat. Med.* **2005**, *11*, 1278–1279.
(164) Ma, C. X.; Janetka, J. W.; Piwnica-Worms, H. *Trends Mol. Med.* **2011**, *17*, 88–96.
(165) Ronco, C.; Martin, A. R.; Demange, L.; Benhida, R. *MedChemComm* **2017**, *8*, 295–319.
(166) Gorgoulis VG, Vassiliou LV, Karakaidos P, Zacharatos P, Kotsinas A, Liloglou T, Venere M, Ditullio RA Jr, Kastrinakis NG, Levy B, Kletsas D, Yoneta A, Herlyn M, Kittas C, H. T. *Nature* **2005**, 907–913.
(167) Gazzard, L.; Appleton, B.; Chapman, K.; Chen, H.; Clark, K.; Drobnick, J.; Goodacre, S.; Halladay, J.; Lyssikatos, J.; Schmidt, S. et al. *Bioorganic Med. Chem. Lett.* **2014**, *24*, 5704–5709.
(168) Doi, T.; Yoshino, T.; Shitara, K.; Matsubara, N.; Fuse, N.; Naito, Y.; Uenaka, K.; Nakamura, T.; Hynes, S. M.; Lin, A. B. *Anti-cancer Drugs* **2015**, *26*, 1043–1053.
(169) Walton, M. I.; Eve, P. D.; Hayes, A.; Henley, A. T.; Valenti, M. R.; Brandon, A. K. D. H.; Box, G.; Boxall, K. J.; Tall, M.; Matthews, T. P. et al. *Oncotarget* **2016**, *7*.
(170) Walton, M. I.; Eve, P. D.; Hayes, A.; Valenti, M.; De Haven Brandon, A.; Box, G.; Boxall, K. J.; Aherne, G. W.; Eccles, S. A.; Raynaud, F. I. et al. *Mol. Cancer Ther.* **2010**, *9*, 89–100.
(171) Blasina, A.; Hallin, J.; Chen, E.; Arango, M. E.; Kraynov, E.; Register, J.; Grant, S.; Ninkovic, S.; Chen, P.; Nichols, T. et al. *Mol. Cancer Ther.* **2008**, *7*, 2394–2404.
(172) Graves, P. R.; Yu, L.; Schwarz, J. K.; Gales, J.; Sausville, E. A.; O'Connor, P. M.; Piwnica-Worms, H. *J. Biol. Chem.* **2000**, *275*, 5600–5605.
(173) Garrett, M. D.; Collins, I. *Trends Pharmacol. Sci.* **2011**, *32*, 308–316.
(174) King, C.; Diaz, H.; Barnard, D.; Barda, D.; Clawson, D.; Blosser, W.; Cox, K.; Guo, S.; Marshall, M. *Invest. New Drugs* **2014**, *32*, 213–226.
(175) Tse, A. N.; Rendahl, K. G.; Sheikh, T.; Cheema, H.; Aardalen, K.; Embry, M.; Ma, S.; Moler, E. J.; Ni, Z. J.; Lopes de Menezes, D. E. et al. *Clin. Cancer Res.* **2007**, *13*, 591–602.
(176) Zabludoff, S. D.; Deng, C.; Grondine, M. R.; Sheehy, A. M.; Ashwell, S.; Caleb, B. L.; Green, S.; Haye, H. R.; Horn, C. L.; Janetka, J. W. et al. *Mol. Cancer Ther.* **2008**, *7*, 2955–2966.
(177) Matthews, D. J.; Yakes, M.; Chen, J.; Tadano, M.; Bornheim, L.; Clary, D. O.; Tai, A.; Wagner, J. M.; Miller, N.; Kim, Y. D. et al. *Cell Cycle* **2007**, *6*, 104–110.
(178) Borst, G. R.; McLaughlin, M.; Kyula, J. N.; Neijenhuis, S.; Khan, A.; Good, J.; Zaidi, S.; Powell, N. G.; Meier, P.; Collins, I. et al. *Int. J. Radiat. Oncol. Biol. Phys.* **2013**, *85*, 1110–1118.
(179) Hammond, E. M.; Dorie, M. J.; Giaccia, A. J. *Cancer Res.* **2004**, *64*, 6556–6562.
(180) Hammond, E. M.; Denko, N. C.; Dorie, M. J.; Abraham, R. T.; Giaccia, A. J. *Mol. Cell. Biol.* **2002**, *22*, 1834–1843.

(181) Sancar, A.; Lindsey-Boltz, L. A.; Ünsal-Kaçmaz, K.; Linn, S. *Annu. Rev. Biochem.* **2004**, *73*, 39–85.
(182) Foloppe, N.; Fisher, L. M.; Howes, R.; Kierstan, P.; Potter, A.; Robertson, A. G. S.; Surgenor, A. E. *J. Med. Chem.* **2005**, *48*, 4332–4345.
(183) Reader, J. C.; Matthews, T. P.; Klair, S.; Cheung, K.-M. J.; Scanlon, J.; Proisy, N.; Addison, G.; Ellard, J.; Piton, N.; Taylor, S. et al. *J. Med. Chem.* **2011**, *54*, 8328–8342.
(184) O'Connor, L. J.; Cazares-Körner, C.; Saha, J.; Evans, C. N. G.; Stratford, M. R. L.; Hammond, E. M.; Conway, S. J. *Nat. Protoc.* **2016**, *11*, 781–794.
(185) Collins, I.; Reader, J. C.; Williams, D. H.; Klair, S. S.; Scanlon, J. E.; Piton, N.; Cherry, M. WO2009103966 (A1), 2009.
(186) Newcombe, P.; Norris, R. *Aust. J. Chem.* **1979**, *32*, 2647.
(187) O'Connor, L. J.; Mistry, I. N.; Collins, S. L.; Folkes, L. K.; Brown, G.; Conway, S. J.; Hammond, E. M. *ACS Cent. Sci.* **2017**, *3*, 20–30.
(188) Fuson, R. C.; Bull, B. A. *Chem. Rev.* **1934**, *15*, 275–309.
(189) Levine, M. N.; Raines, R. T. *Chem. Sci.* **2012**, *3*, 2412.
(190) Huang, S.-T.; Lin, Y.-L. *Org. Lett.* **2006**, *8*, 265–268.
(191) Greenwald, R. B.; Choe, Y. H.; Conover, C. D.; Shum, K.; Wu, D.; Royzen, M. *J. Med. Chem.* **2000**, *43*, 475–487.
(192) Zhou, W.; Andrews, C.; Liu, J.; Shultz, J. W.; Valley, M. P.; Cali, J. J.; Hawkins, E. M.; Klaubert, D. H.; Bulleit, R. F.; Wood, K. V. *ChemBioChem* **2008**, *9*, 714–718.
(193) Shigenaga, A.; Ogura, K.; Hirakawa, H.; Yamamoto, J.; Ebisuno, K.; Miyamoto, L.; Ishizawa, K.; Tsuchiya, K.; Otaka, A. *ChemBioChem* **2012**, *13*, 968–971.
(194) Andersen, K. A.; Smith, T. P.; Lomax, J. E.; Raines, R. T. *ACS Chem. Biol.* **2016**, *11*, 319–323.
(195) Wang, B.; Zhang, H.; Wang, W. *Bioorganic Med. Chem. Lett.* **1996**, *6*, 945–950.
(196) Okoh, O. A.; Klahn, P. *ChemBioChem* **2018**, *19*, 1668–1694.
(197) Jung, M. E.; Piizzi, G. *Chem. Rev.* **2005**, *105*, 1735–1766.
(198) Yin, J.; Buchwald, S. L. *Org. Lett.* **2000**, *2*, 1101–1104.
(199) Qiao, J.; Lam, P. *Synthesis* **2011**, *2011*, 829–856.
(200) Rossi, S. A.; Shimkin, K. W.; Xu, Q.; Mori-Quiroz, L. M.; Watson, D. A. *Org. Lett.* **2013**, *15*, 2314–2317.
(201) Preshlock, S. M.; Ghaffari, B.; Maligres, P. E.; Krska, S. W.; Maleczka, R. E.; Smith, M. R. *J. Am. Chem. Soc.* **2013**, *135*, 7572–7582.
(202) Harrisson, P.; Morris, J.; Marder, T. B.; Steel, P. G. *Org. Lett.* **2009**, *11*, 3586–3589.
(203) Osborne, J. D.; Matthews, T. P.; McHardy, T.; Proisy, N.; Cheung, K.-M. J.; Lainchbury, M.; Brown, N.; Walton, M. I.; Eve, P. D.; Boxall, K. J. et al. *J. Med. Chem.* **2016**, *59*, 5221–5237.
(204) Rusalov, M. V.; Druzhinin, S. I.; Uzhinov, B. M. *J. Fluoresc.* **2004**, *14*, 193–202.
(205) Uddin, M. J.; Crews, B. C.; Ghebreselasie, K.; Marnett, L. J. *Bioconjug. Chem.* **2013**, *24*, 712–723.
(206) Cilliers, C.; Nessler, I.; Christodolu, N.; Thurber, G. M. *Mol. Pharm.* **2017**, *14*, 1623–1633.
(207) Van de Waterbeemd, H.; Smith, D. A.; Beaumont, K.; Walker, D. K. *J. Med. Chem.* **2001**, *44*, 1313–1333.
(208) Heo, J.; Lim, C.-K.; Whang, D. R.; Shin, J.; Jeong, S. Y.; Park, S. Y.; Kwon, I. C.; Kim, S. *Chem. Eur. J.* **2012**, *18*, 8699–8704.

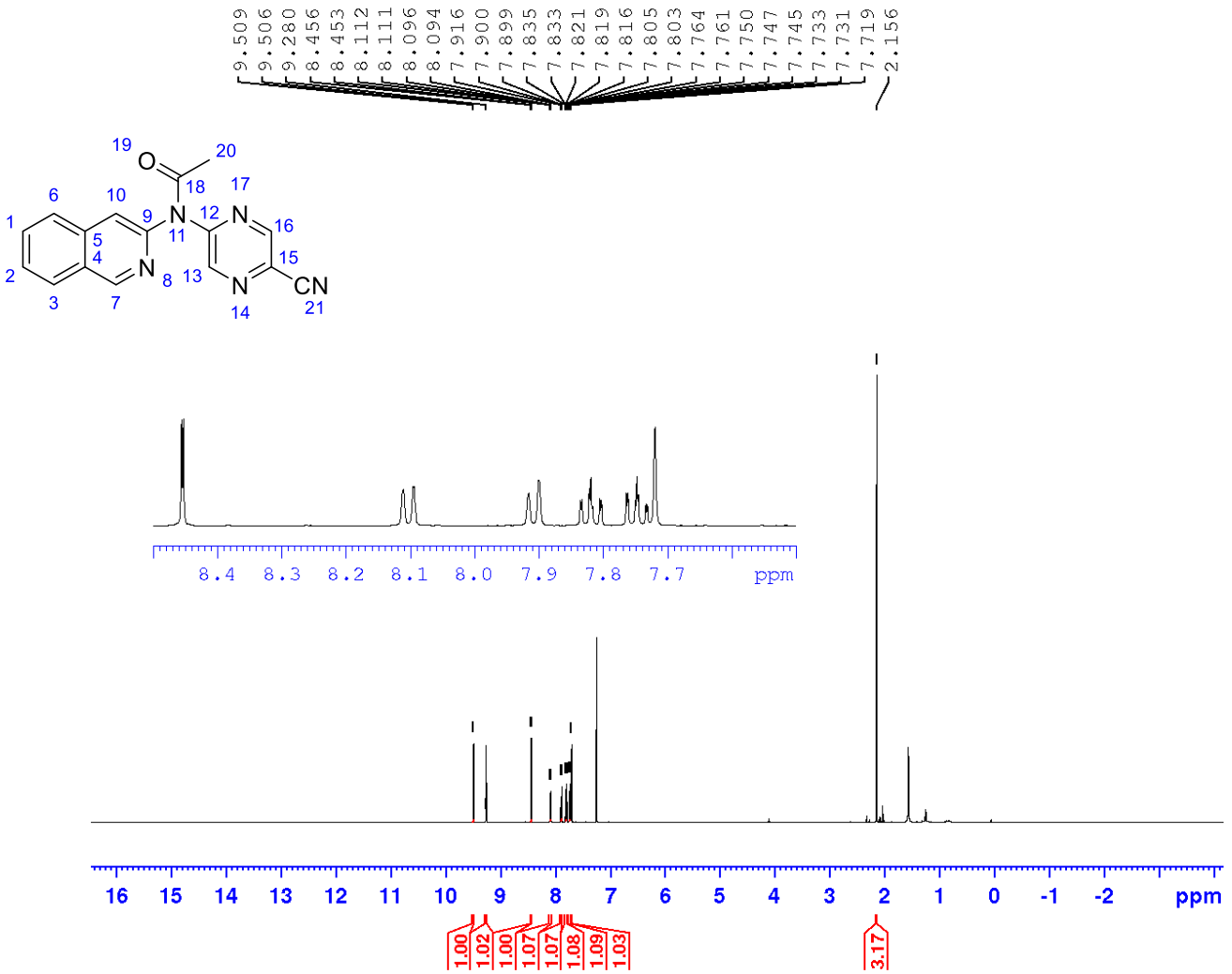
(209) Mosher, W. A.; Soeder, R. W. *J. Org. Chem.* **1967**, *1*, 1960–1962.
(210) Tanaka, K.; Hosokawa, A.; Yoshida, K. *Synthesis* **1999**, *1999*, 249–253.
(211) Sonn, G. A.; Behesnilian, A. S.; Jiang, Z. K.; Zettlitz, K. A.; Lepin, E. J.; Bentolila, L. A.; Knowles, S. M.; Lawrence, D.; Wu, A. M.; Reiter, R. E. *Clin. Cancer Res.* **2016**, *22*, 1403–1412.
(212) Vahrmeijer, A. L.; Hutteman, M.; van der Vorst, J. R.; van de Velde, C. J. H.; Frangioni, J. V. *Nat. Rev. Clin. Oncol.* **2013**, *10*, 507–518.
(213) Borotto, E.; Englender, J.; Pourny, J.; Naveau, S.; Chaput, J.; Lecarpentier, Y. *Gastrointest. Endosc.* **1999**, *50*, 684–688.
(214) Zhou, L.; Wang, Q.; Tan, Y.; Lang, M. J.; Sun, H.; Liu, X. *Chem. Eur. J.* **2017**, *23*, 8736–8740.
(215) Marcinek, A.; Leyva, E.; Whitt, D.; Platz, M. S. *J. Am. Chem. Soc.* **1993**, *115*, 8609–8612.
(216) Giustarini, D.; Colombo, G.; Garavaglia, M. L.; Astori, E.; Portinaro, N. M.; Reggiani, F.; Badalamenti, S.; Aloisi, A. M.; Santucci, A.; Rossi, R. et al. *Free Radic. Biol. Med.* **2017**, *112*, 360–375.
(217) Sun, W.; Fan, J.; Hu, C.; Cao, J.; Zhang, H.; Xiong, X.; Wang, J.; Cui, S.; Sun, S.; Peng, X. *Chem. Commun.* **2013**, *49*, 3890–3892.
(218) Mertz, J. A.; Conery, A. R.; Bryant, B. M.; Sandy, P.; Balasubramanian, S.; Mele, D. A.; Bergeron, L.; Sims, R. J. *Proc. Natl. Acad. Sci. USA* **2011**, *108*, 16669–16674.
(219) Filippakopoulos, P.; Qi, J.; Picaud, S.; Shen, Y.; Smith, W. B.; Fedorov, O.; Morse, E. M.; Keates, T.; Hickman, T. T.; Felletar, I. et al. *Nature* **2010**, *468*, 1067–1073.
(220) Mazur, P. K.; Herner, A.; Mello, S. S.; Wirth, M.; Hausmann, S.; Sánchez-Rivera, F. J.; Lofgren, S. M.; Kuschma, T.; Hahn, S. A.; Vangala, D. et al. *Nat. Med.* **2015**, *21*, 1163–1171.
(221) Jennings, L. E.; Schiedel, M.; Hewings, D. S.; Picaud, S.; Laurin, C. M. C.; Bruno, P. A.; Bluck, J. P.; Scorah, A. R.; See, L.; Reynolds, J. K. et al. *Bioorg. Med. Chem.* **2018**, *26*, 2937–2957.
(222) Hewings, D. S. University of Oxford, 2014.
(223) Hewings, D. S.; Fedorov, O.; Filippakopoulos, P.; Martin, S.; Picaud, S.; Tumber, A.; Wells, C.; Olcina, M. M.; Freeman, K.; Gill, A. et al. *J. Med. Chem.* **2013**, *56*, 3217–3227.
(224) Beharry, A. A.; Woolley, G. A. *Chem. Soc. Rev.* **2011**, *40*, 4422.
(225) Sapountzis, I.; Knochel, P. *Angew. Chemie Int. Ed.* **2002**, *41*, 1610–1611.
(226) Filippakopoulos, P.; Knapp, S. *FEBS Lett.* **2012**, *586*, 2692–2704.
(227) Belkina, A. C.; Denis, G. V. *Nat. Rev. Cancer* **2012**, *12*, 465–477.
(228) French, C. A. *J. Clin. Pathol.* **2010**, *63*, 492–496.
(229) Wang, R.; You, J. *J. Biol. Chem.* **2015**, *290*, 2744–2758.
(230) Lucas, X.; Wohlwend, D.; Hügle, M.; Schmidtkunz, K.; Gerhardt, S.; Schüle, R.; Jung, M.; Einsle, O.; Günther, S. *Angew. Chemie Int. Ed.* **2013**, *52*, 14055–14059.
(231) Schrodinger LLC. 2015.
(232) Sekirnik née Measures, A. R.; Hewings, D. S.; Theodoulou, N. H.; Jursins, L.; Lewendon, K. R.; Jennings, L. E.; Rooney, T. P. C.; Heightman, T. D.; Conway, S. J. *Angew. Chemie Int. Ed.* **2016**, *55*, 8353–8357.
(233) Hay, D.; Fedorov, O.; Filippakopoulos, P.; Martin, S.; Philpott, M.; Picaud, S.; Hewings, D. S.; Uttakar, S.; Heightman, T. D.; Conway, S. J. et al. *MedChemComm* **2013**, *2*, 140–144.

(234) Hewings, D. S.; Wang, M.; Philpott, M.; Fedorov, O.; Uttarkar, S.; Filippakopoulos, P.; Picaud, S.; Vuppusetty, C.; Marsden, B.; Knapp, S. et al. *J. Med. Chem.* **2011**, *54*, 6761–6770.
(235) Philpott, M.; Yang, J.; Tumber, T.; Fedorov, O.; Uttarkar, S.; Filippakopoulos, P.; Picaud, S.; Keates, T.; Felletar, I.; Ciulli, A. et al. *Mol. Biosyst.* **2011**, *7*, 2899.
(236) Tredwell, M.; Preshlock, S. M.; Taylor, N. J.; Gruber, S.; Huiban, M.; Passchier, J.; Mercier, J.; Génicot, C.; Gouverneur, V. *Angew. Chemie Int. Ed.* **2014**, *53*, 7751–7755.
(237) Tang, P.; Furuya, T.; Ritter, T. *J. Am. Chem. Soc.* **2010**, *132*, 12150–12154.
(238) Lee, E.; Kamlet, A. S.; Powers, D. C.; Neumann, C. N.; Boursalian, G. B.; Furuya, T.; Choi, D. C.; Hooker, J. M.; Ritter, T. *Science* **2011**, *334*, 639–642.
(239) Ye, Y.; Schimler, S. D.; Hanley, P. S.; Sanford, M. S. *J. Am. Chem. Soc.* **2013**, *135*, 16292–16295.
(240) Ye, Y.; Sanford, M. S. *J. Am. Chem. Soc.* **2013**, *135*, 4648–4651.
(241) Ichiishi, N.; Brooks, A. F.; Topczewski, J. J.; Rodnick, M. E.; Sanford, M. S.; Scott, P. J. H. *Org. Lett.* **2014**, *16*, 3224–3227.
(242) Stenhagen, I. S. R.; Kirjavainen, A. K.; Forsback, S. J.; Jørgensen, C. G.; Robins, E. G.; Luthra, S. K.; Solin, O.; Gouverneur, V. *Chem. Commun.* **2013**, *49*, 1386.
(243) Molander, G. A.; Ellis, N. *Acc. Chem. Res.* **2007**, *40*, 275–286.
(244) Molander, G. A.; Sandrock, D. L. *J. Am. Chem. Soc.* **2008**, *130*, 15792–15793.
(245) Lindemann, L.; Hoener, M. C. *Trends Pharmacol. Sci.* **2005**, *26*, 274–281.
(246) Trummal, A.; Lipping, L.; Kaljurand, I.; Koppel, I. A.; Leito, I. *J. Phys. Chem. A* **2016**, *120*, 3663–3669.
(247) Grimm, J. B.; English, B. P.; Chen, J.; Slaughter, J. P.; Zhang, Z.; Revyakin, A.; Patel, R.; Macklin, J. J.; Normanno, D.; Singer, R. H. et al. *Nat. Methods* **2015**, *12*, 244–250.
(248) Lavis, L. D.; Raines, R. T. *ACS Chem. Biol.* **2014**, *9*, 855–866.
(249) Lavis, L. D. *Biochemistry* **2017**, *56*, 5165–5170.
(250) Liu, W.; Liu, H.; Peng, X.; Zhou, G.; Liu, D.; Li, S.; Zhang, J.; Wang, S. *Bioconjug. Chem.* **2018**, acs.bioconjchem.8b00511.
(251) Pirrung, M. C. In *The Synthetic Organic Chemist's Companion*; John Wiley & Sons, Inc., 2007; pp 171–172.
(252) Fulmer, G. R.; Miller, A. J. M.; Sherden, N. H.; Gottlieb, H. E.; Nudelman, A.; Stoltz, B. M.; Bercaw, J. E.; Goldberg, K. I. *Organometallics* **2010**, *29*, 2176–2179.
(253) Claret, P. A.; Osborne, A. G. *Tetrahedron* **1977**, *33*, 1765–1767.
(254) Warnecke, A.; Kratz, F. *J. Org. Chem.* **2008**, *73*, 1546–1552.
(255) Matikonda, S. S.; Fairhall, J. M.; Tyndall, J. D. A.; Hook, S.; Gamble, A. B. *Org. Lett.* **2017**, *19*, 528–531.
(256) Huvelle, S.; Alouane, A.; Le Saux, T.; Jullien, L.; Schmidt, F. *Org. Biomol. Chem.* **2017**, *15*, 3435–3443.
(257) Liu, R.; Aw, J.; Teo, W.; Padmanabhan, P.; Xing, B. *New J. Chem.* **2010**, *34*, 594.
(258) Morwry, D. T.; Ringwald, E. L.; Renoll, M. *J. Am. Chem. Soc.* **1949**, *71*, 120–122.
(259) Kirchwehm, Y.; Damme, A.; Kupfer, T.; Braunschweig, H.; Krueger, A. *Chem. Commun.* **2012**, *48*, 1502–1504.
(260) Lee, J. C.; Park, J. Y.; Yoo, E. S. *Synth. Commun.* **2004**, *34*, 2095–2099.

(261) Mirjafari, A.; Mohammadpoor-Baltork, I.; Moghadam, M.; Tangestaninejad, S.; Mirkhani, V.; Khosropour, A. R. *Tetrahedron Lett.* **2010**, *51*, 3274–3276.
(262) Ding, R.; He, Y.; Wang, X.; Xu, J.; Chen, Y.; Feng, M.; Qi, C. *Molecules* **2011**, *16*, 5665–5673.
(263) Kim, S.-H.; Kim, S.-H.; Son, Y.-A. *Mol. Cryst. Liq. Cryst.* **2011**, *538*, 320–326.
(264) Kanitz, A.; Hartmann, H.; Czerney, P. *J. für Prakt. Chemie/Chemiker-Zeitung* **1998**, *340*, 34–44.
(265) Spletstoser, J. T.; Flaherty, P. T.; Himes, R. H.; Georg, G. I. *J. Med. Chem.* **2004**, *47*, 6459–6465.
(266) Liu, T.; Lin, J.; Li, Z.; Lin, L.; Shen, Y.; Zhu, H.; Qian, Y. *Analyst* **2015**, *140*, 7165–7169.
(267) Schimler, S.; Sanford, M. *Synlett* **2016**, *27*, 2279–2284.
(268) Zeng, Y.-S.; Gao, R.-C.; Wu, T.-W.; Cho, C.; Tan, K.-T. *Bioconjug. Chem.* **2016**, *27*, 1872–1879.
(269) Shaw, A. Y.; Chang, C.-Y.; Liau, H.-H.; Lu, P.-J.; Chen, H.-L.; Yang, C.-N.; Li, H.-Y. *Eur. J. Med. Chem.* **2009**, *44*, 2552–2562.
(270) Antoine, M.; Marchand, P.; Baut, G. Le; Czech, M.; Gunther, E.; Antoine, M.; Marchand, P.; Baut, G. Le; Czech, M.; Baasner, S. et al. *J. Enzyme Inhib. Med. Chem.* **2008**, *23*, 686–695.
(271) Costero, A. M.; Parra, M.; Gil, S.; Gotor, R. *Chem. Asian J.* **2010**, *5*, 1573–1585.
(272) Dhanoa, D. S.; Bagley, S. W.; Chang, R. S. L.; Lotti, V. J.; Chen, T. B.; Kivlighn, S. D.; Zingaro, G. J.; Siegl, P. K. S.; Patchett, A. A.; Greenlee, W. J. *J. Med. Chem.* **1993**, *36*, 4239–4249.
(273) Hay, M. P.; Sykes, B. M.; Denny, W. A.; O'Connor, C. J. *J. Chem. Soc. Perkin Trans. 1* **1999**, No. 19, 2759–2770.
(274) Kumar, S.; Chang, T.; Liu, T. *Tetrahedron* **2008**, *64*, 2586–2595.
(275) Barros, A. I. R. N. A.; Silva, A. M. S. *Magn. Reson. Chem.* **2009**, *47*, 885–896.
(276) Gobbi, S.; Hu, Q.; Zimmer, C.; Engel, M.; Belluti, F.; Rampa, A.; Hartmann, R. W.; Bisi, A. *J. Med. Chem.* **2016**, *59*, 2468–2477.
(277) Padmanaban, M.; Biju, A. T.; Glorius, F. *Org. Lett.* **2011**, *13*, 98–101.
(278) Molander, G. A.; Canturk, B.; Kennedy, L. E. *J. Org. Chem.* **2009**, *74*, 973–980.
(279) Lennox, A. J. J.; Lloyd-Jones, G. C. *Angew. Chemie - Int. Ed.* **2012**, *51*, 9385–9388.

APPENDICES

^{1}H NMR spectrum of *N*-(5-Cyanopyrazin-2-yl)-*N*-(isoquinolin-3-yl)acetamide (75)



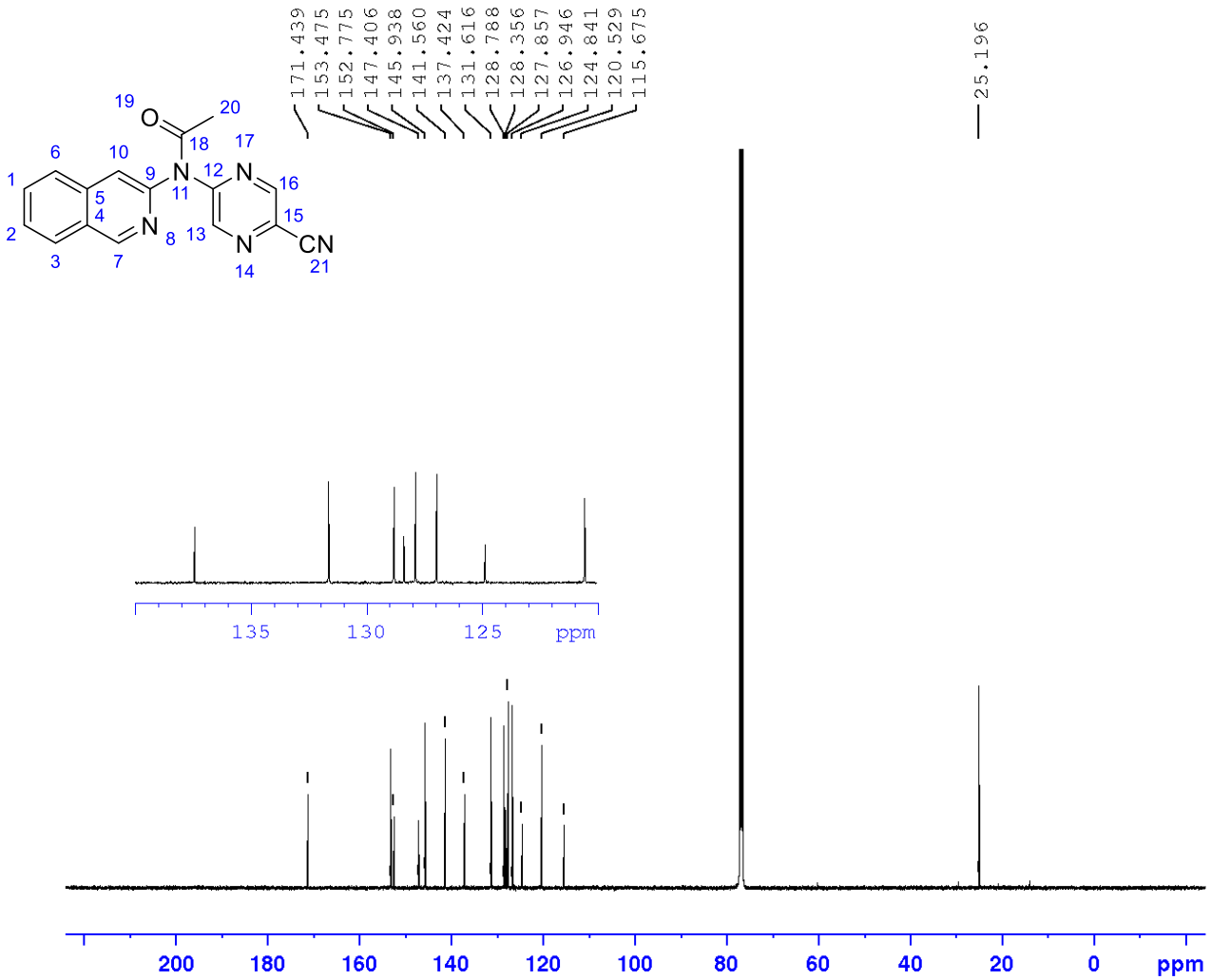

```
Current Data Parameters
NAME        CE175-01_500
EXPNO                  1
PROCNO                 1

F2 - Acquisition Parameters
Date_           20151020
Time               20.40
INSTRUM          avc500
PROBHD   5 mm CPDUL 13C
PULPROG             zg30
TD                 65536
SOLVENT            CDCl3
NS                    16
DS                     4
SWH            10330.578 Hz
FIDRES          0.157632 Hz
AQ             3.1719425 sec
RG                  3.56
DW                48.400 usec
DE                10.00 usec
TE                298.0 K
D1            1.00000000 sec
TD0                    1

======== CHANNEL f1 ========
SFO1         500.3030896 MHz
NUC1                 1H
P1                15.00 usec
PLW1          7.99830008 W

F2 - Processing parameters
SI                 65536
SF           500.3000130 MHz
WDW                   EM
SSB       0
LB                 0.30 Hz
GB        0
PC                 1.00
```

^{13}C NMR spectrum of *N*-(5-Cyanopyrazin-2-yl)-*N*-(isoquinolin-3-yl)acetamide (75)




```
Current Data Parameters
NAME         CE175-01_500
EXPNO                   4
PROCNO                  1

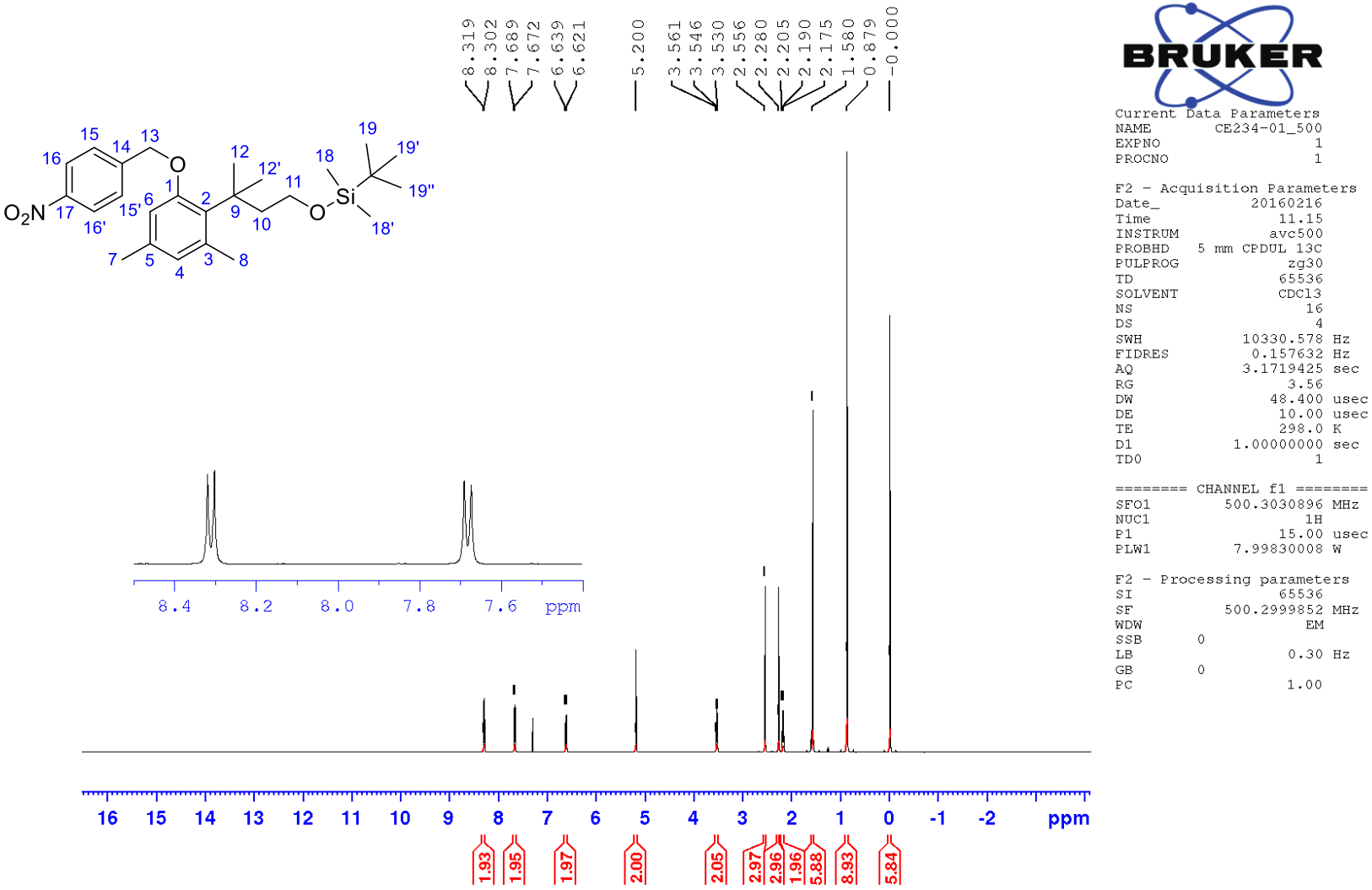
F2 - Acquisition Parameters
Date_           20151020
Time               22.15
INSTRUM          avc500
PROBHD   5 mm CPDUL 13C
PULPROG          zgpg30
TD                65536
SOLVENT           CDCl3
NS                 1024
DS                    2
SWH           31250.000 Hz
FIDRES         0.476837 Hz
AQ             1.0485760 sec
RG                  912
DW                16.000 usec
DE                18.00 usec
TE                298.0 K
D1             2.00000000 sec
D11            0.03000000 sec
TD0                   1

======== CHANNEL f1 ========
SFO1         125.8131152 MHz
NUC1                 13C
P1                 10.00 usec
PLW1         20.18400002 W

======== CHANNEL f2 ========
SFO2         500.3020012 MHz
NUC2                 1H
CPDPRG[2          waltz16
PCPD2              80.00 usec
PLW2          7.99830008 W
PLW12         0.28119001 W
PLW13         0.17996000 W

F2 - Processing parameters
SI                  32768
SF           125.8005351 MHz
WDW                   EM
SSB       0
LB                  1.00 Hz
GB        0
PC                  1.40
```

^{1}H NMR spectrum of *t*-Butyl(3-(2,4-dimethyl-6-((4-nitrobenzyl)oxy)phenyl)-3-methylbutoxy)dimethylsilane (110)



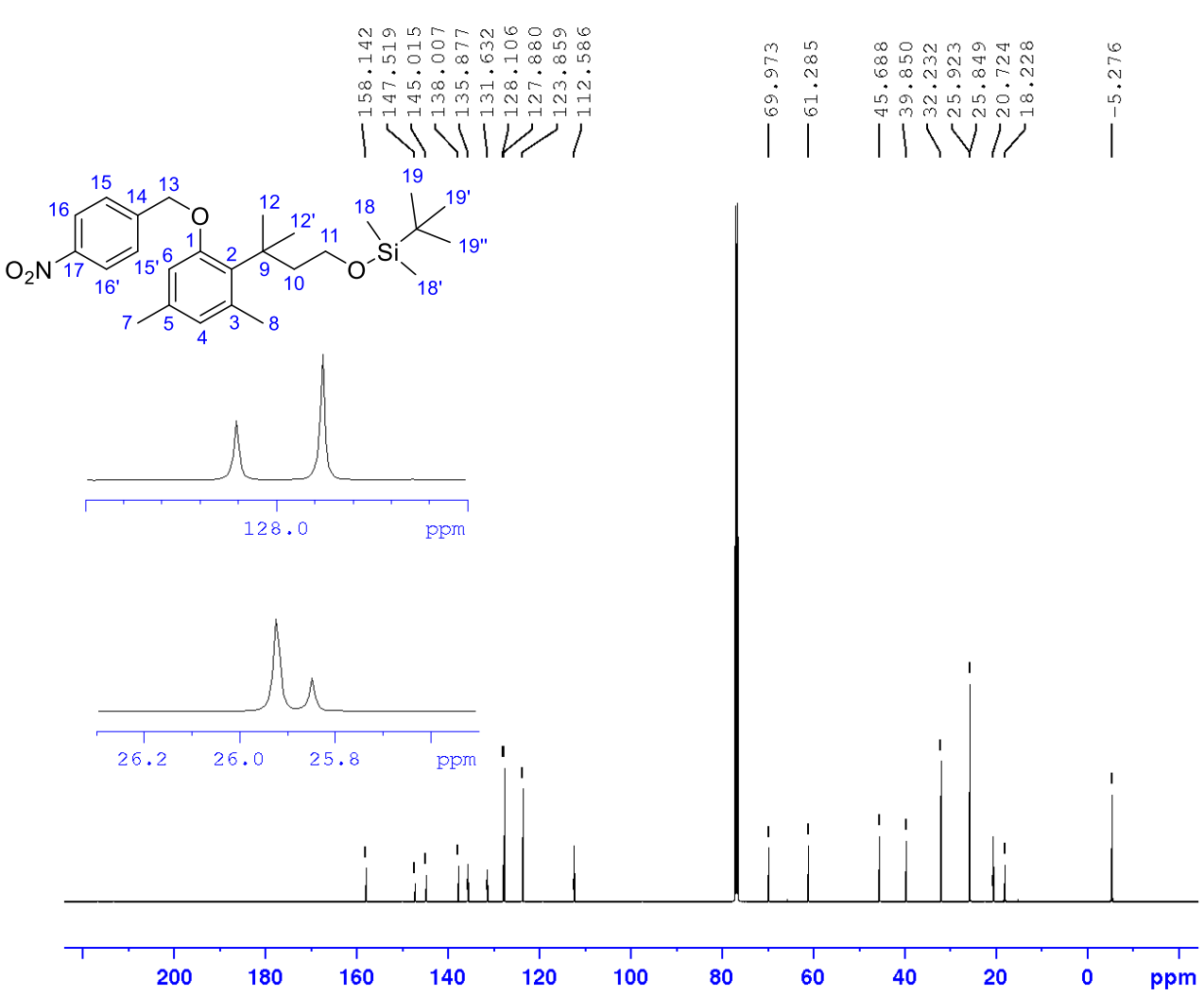

```
Current Data Parameters
NAME        CE234-01_500
EXPNO                  1
PROCNO                 1

F2 - Acquisition Parameters
Date_           20160216
Time               11.15
INSTRUM          avc500
PROBHD   5 mm CPDUL 13C
PULPROG             zg30
TD                 65536
SOLVENT            CDCl3
NS                    16
DS                     4
SWH            10330.578 Hz
FIDRES          0.157632 Hz
AQ             3.1719425 sec
RG                  3.56
DW                 48.400 usec
DE                 10.00 usec
TE                 298.0 K
D1            1.00000000 sec
TD0                    1

======== CHANNEL f1 ========
SFO1         500.3030896 MHz
NUC1                 1H
P1                15.00 usec
PLW1          7.99830008 W

F2 - Processing parameters
SI                 65536
SF           500.2999852 MHz
WDW                  EM
SSB       0
LB                 0.30 Hz
GB        0
PC                 1.00
```

^{13}C NMR spectrum of *t*-Butyl(3-(2,4-dimethyl-6-((4-nitrobenzyl)oxy)phenyl)-3-methylbutoxy)dimethylsilane (110)




```
Current Data Parameters
NAME        CE234-01_500
EXPNO                  4
PROCNO                 1

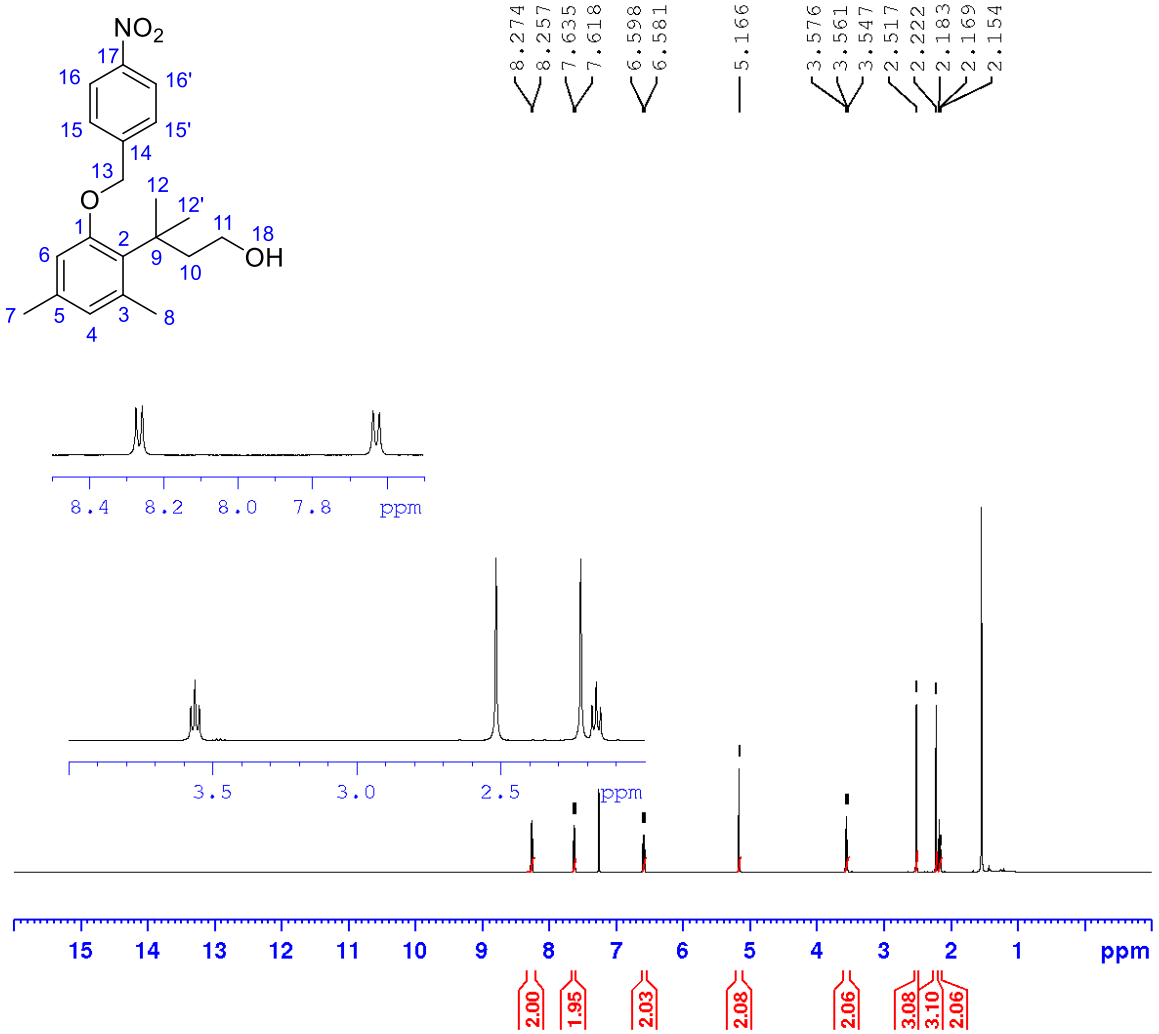
F2 - Acquisition Parameters
Date_           20160216
Time               12.41
INSTRUM          avc500
PROBHD   5 mm CPDUL 13C
PULPROG          zgpg30
TD                65536
SOLVENT           CDCl3
NS                 1024
DS                    2
SWH           31250.000 Hz
FIDRES         0.476837 Hz
AQ            1.0485760 sec
RG                  912
DW               16.000 usec
DE               18.00 usec
TE               298.0 K
D1            2.00000000 sec
D11           0.03000000 sec
TD0                   1

======== CHANNEL f1 ========
SFO1         125.8131152 MHz
NUC1               13C
P1               10.00 usec
PLW1         20.18400002 W

======== CHANNEL f2 ========
SFO2         500.3020012 MHz
NUC2               1H
CPDPRG[2         waltz16
PCPD2            80.00 usec
PLW2          7.99830008 W
PLW12         0.28119001 W
PLW13         0.17996000 W

F2 - Processing parameters
SI                32768
SF           125.8005351 MHz
WDW                EM
SSB       0
LB               1.00 Hz
GB        0
PC               1.40
```

^{1}H NMR spectrum of 3-(2,4-Dimethyl-6-((4-nitrobenzyl)oxy)phenyl)-3-methylbutan-1-ol (111)



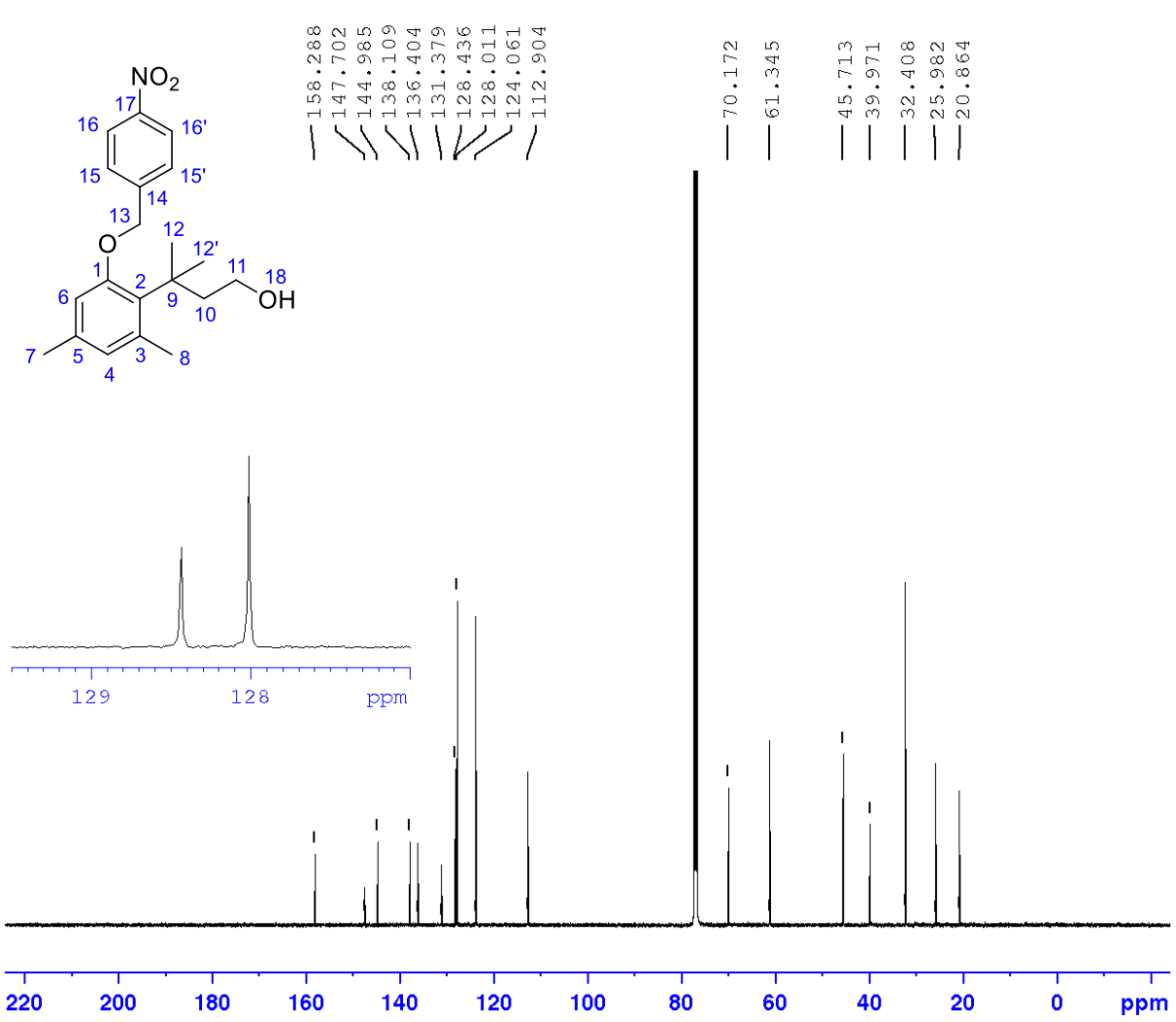

```
Current Data Parameters
NAME        CE238-01_500
EXPNO                  1
PROCNO                 1

F2 - Acquisition Parameters
Date_           20160217
Time               17.40
INSTRUM          avc500
PROBHD   5 mm CPDUL 13C
PULPROG             zg30
TD                 65536
SOLVENT            CDCl3
NS                    16
DS                     4
SWH            10330.578 Hz
FIDRES          0.157632 Hz
AQ             3.1719425 sec
RG                  3.56
DW                48.400 usec
DE                10.00 usec
TE                298.0 K
D1            1.00000000 sec
TD0                    1

======== CHANNEL f1 ========
SFO1         500.3030896 MHz
NUC1                 1H
P1                15.00 usec
PLW1          7.99830008 W

F2 - Processing parameters
SI                 65536
SF           500.3000134 MHz
WDW                  EM
SSB       0
LB                0.30 Hz
GB        0
PC                1.00
```

^{13}C NMR spectrum of 3-(2,4-Dimethyl-6-((4-nitrobenzyl)oxy)phenyl)-3-methylbutan-1-ol (111)




```
Current Data Parameters
NAME        CE238-01_500
EXPNO                  4
PROCNO                 1

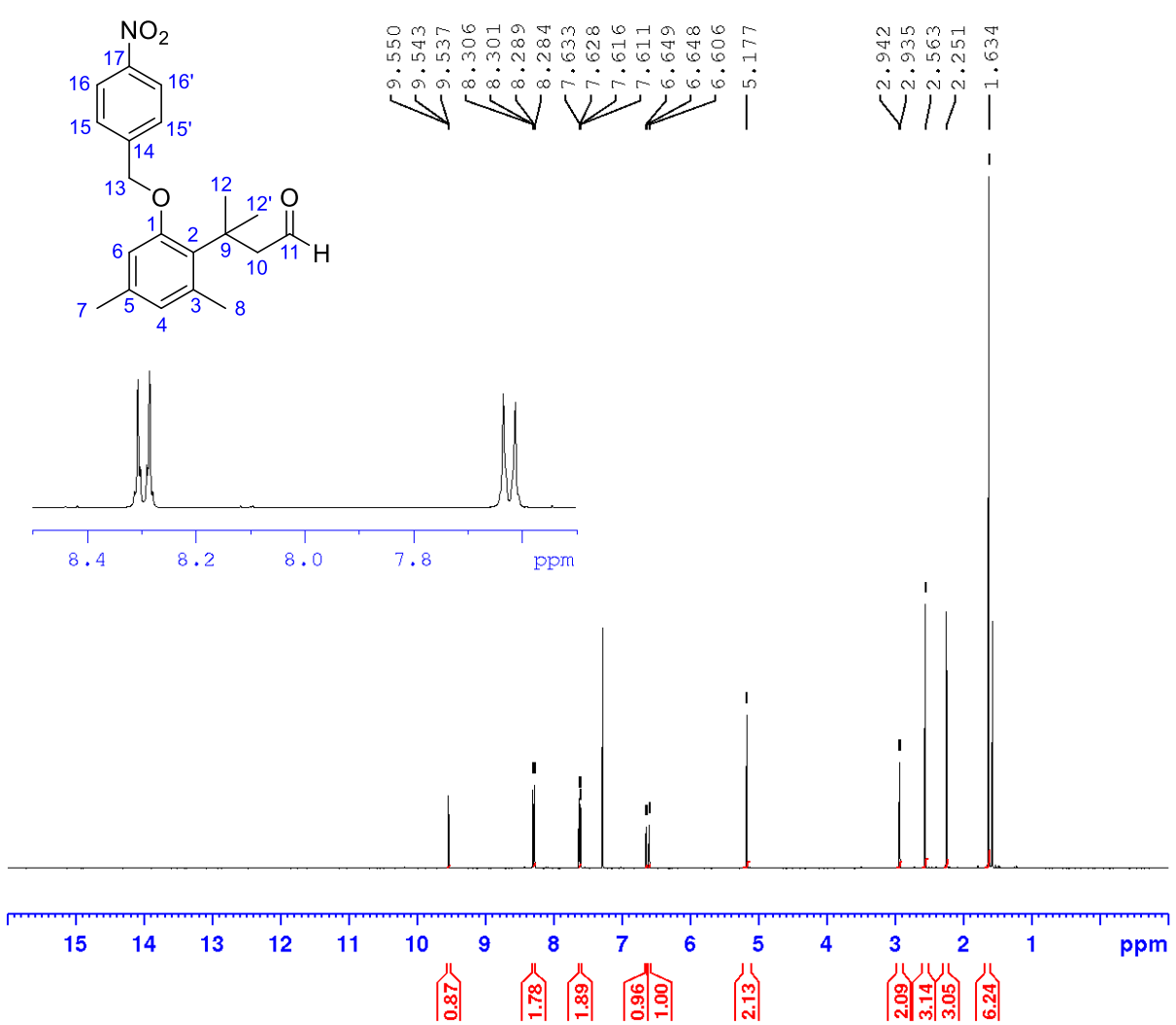
F2 - Acquisition Parameters
Date_           20160217
Time               19.19
INSTRUM          avc500
PROBHD   5 mm CPDUL 13C
PULPROG          zgpg30
TD                65536
SOLVENT           CDCl3
NS                 1024
DS                    2
SWH           31250.000 Hz
FIDRES         0.476837 Hz
AQ            1.0485760 sec
RG                  912
DW               16.000 usec
DE               18.00 usec
TE                298.0 K
D1           2.00000000 sec
D11          0.03000000 sec
TD0                   1

======== CHANNEL f1 ========
SFO1         125.8131152 MHz
NUC1                13C
P1                10.00 usec
PLW1         20.18400002 W

======== CHANNEL f2 ========
SFO2         500.3020012 MHz
NUC2                1H
CPDPRG[2         waltz16
PCPD2             80.00 usec
PLW2          7.99830008 W
PLW12         0.28119001 W
PLW13         0.17996000 W

F2 - Processing parameters
SI                 32768
SF           125.8005185 MHz
WDW                  EM
SSB       0
LB                1.00 Hz
GB        0
PC                1.40
```

^{1}H NMR spectrum of 3-(2,4-Dimethyl-6-((4-nitrobenzyl)oxy)phenyl)-3-methylbutanal (112)

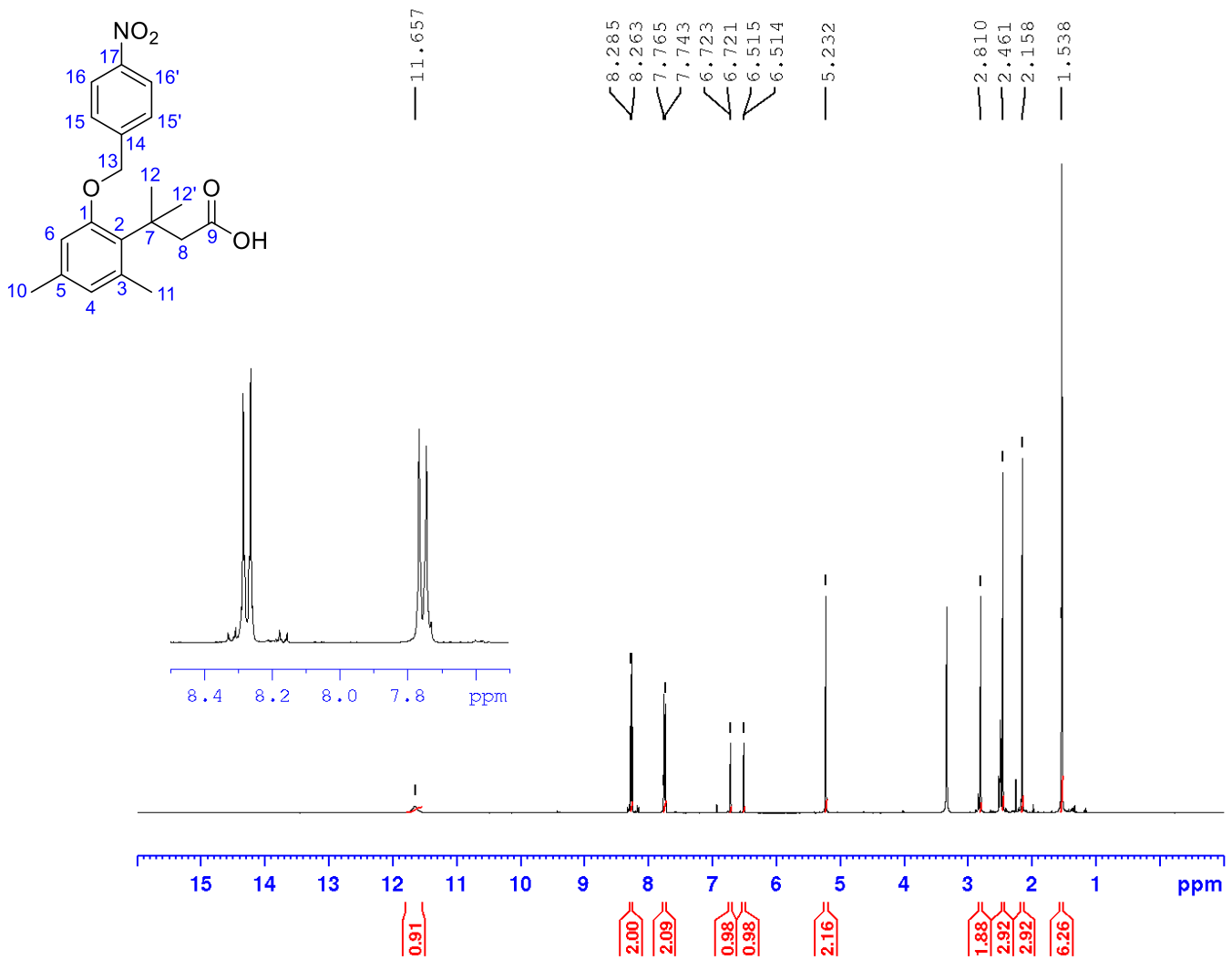



```
Current Data Parameters
NAME                  CE257-01
EXPNO                        1
PROCNO                       1

F2 - Acquisition Parameters
Date_              20160315
Time                   10.08 h
INSTRUM              avg400
PROBHD    Z108618_0816 (
PULPROG                zg60
TD                    65536
SOLVENT               CDCl3
NS                       16
DS                        2
SWH                8012.820 Hz
FIDRES            0.244532 Hz
AQ                4.0894465 sec
RG                   184.19
DW                   62.400 usec
DE                    6.50 usec
TE                   293.8 K
D1              1.00000000 sec
TD0                       1
SFO1           400.2024012 MHz
NUC1                    1H
P1                   14.00 usec
PLW1           14.00000000 W

F2 - Processing parameters
SI                    32768
SF             400.2000000 MHz
WDW                     EM
SSB         0
LB                    0.30 Hz
GB          0
PC                    1.00
```

^{1}H NMR spectrum of 3-(2,4-Dimethyl-6-((4-nitrobenzyl)oxy)phenyl)-3-methylbutanoic acid (113)

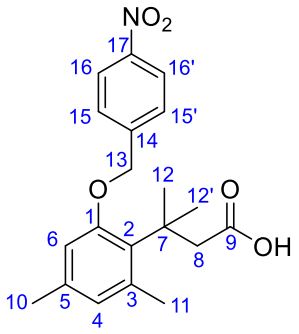


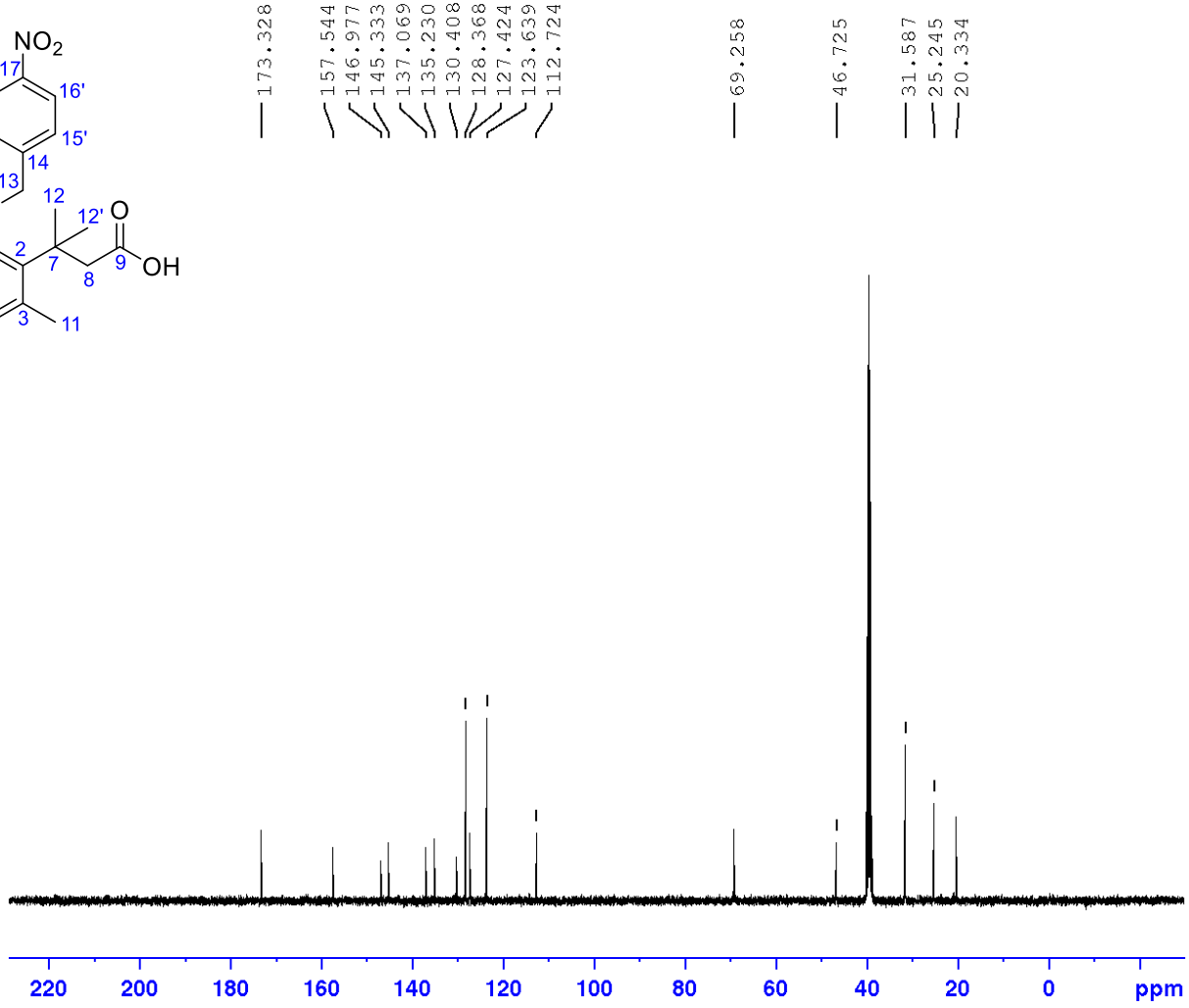

```
Current Data Parameters
NAME        CE315-1_FULL
EXPNO                 10
PROCNO                 1

F2 - Acquisition Parameters
Date_           20160929
Time                20.00 h
INSTRUM           avh400
PROBHD   Z108618_0873 (
PULPROG             zg60
TD                 65536
SOLVENT             DMSO
NS                    16
DS                     2
SWH              8012.820 Hz
FIDRES           0.244532 Hz
AQ               4.0894465 sec
RG                  53.51
DW                 62.400 usec
DE                  6.50 usec
TE                 296.5 K
D1            1.00000000 sec
TD0                    1
SFO1         400.1324008 MHz
NUC1                  1H
P1                 14.00 usec
PLW1         14.36999989 W

F2 - Processing parameters
SI                 32768
SF           400.1300034 MHz
WDW                  EM
SSB       0
LB                 0.30 Hz
GB        0
PC                 1.00
```

^{13}C NMR spectrum of 3-(2,4-Dimethyl-6-((4-nitrobenzyl)oxy)phenyl)-3-methylbutanoic acid (113)



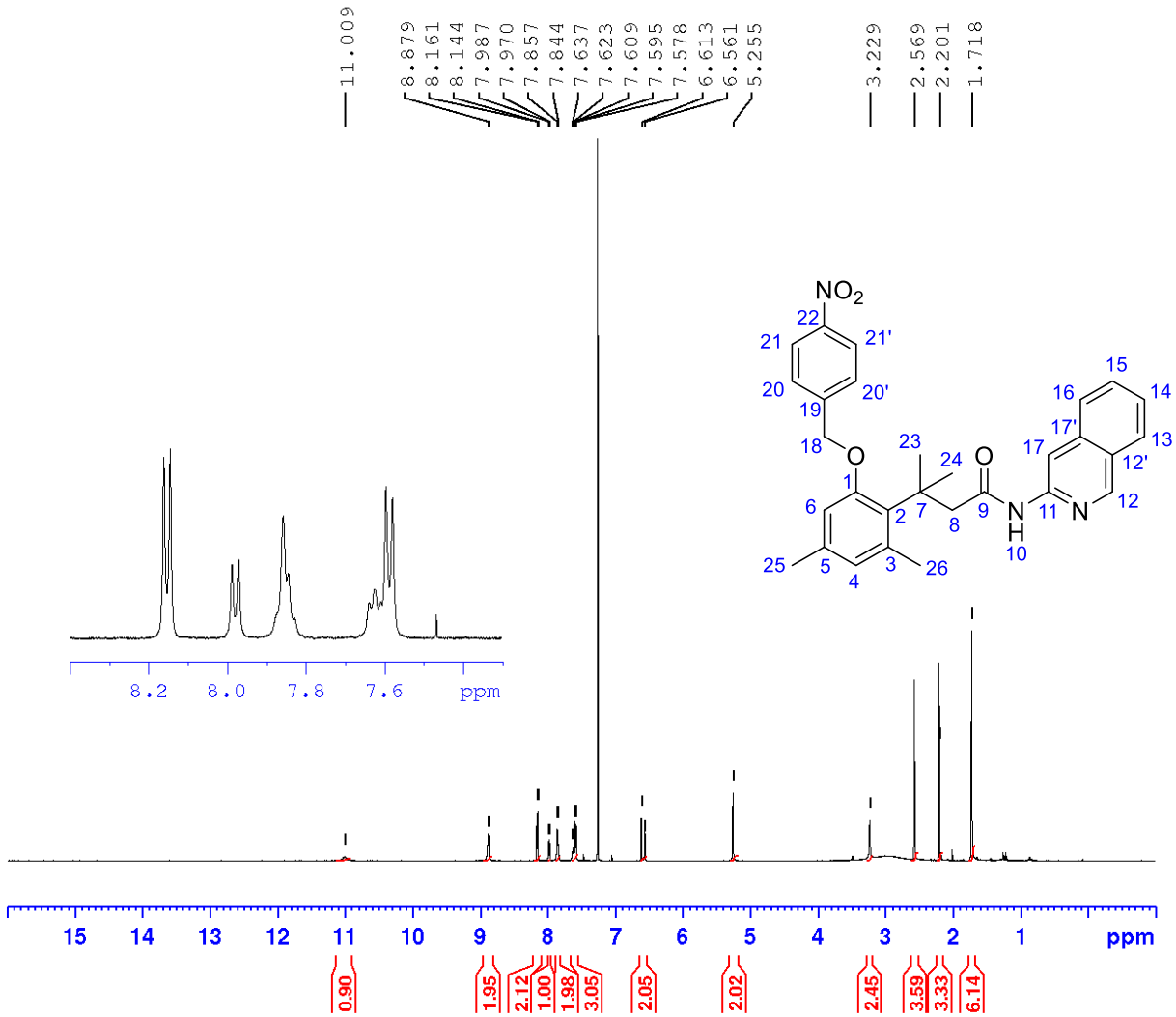



```
Current Data Parameters
NAME        CE315-1_FULL
EXPNO                 13
PROCNO                 1

F2 - Acquisition Parameters
Date_           20160929
Time               20.24 h
INSTRUM          avh400
PROBHD   Z108618_0873 (
PULPROG          zgpg30
TD              32768
SOLVENT           DMSO
NS                  256
DS                    4
SWH           26041.666 Hz
FIDRES         1.589457 Hz
AQ            0.6291456 sec
RG               197.18
DW               19.200 usec
DE                6.50 usec
TE               297.6 K
D1           1.00000000 sec
D11          0.03000000 sec
TD0                   1
SFO1        100.6228298 MHz
NUC1               13C
P1                10.00 usec
PLW1        47.86100006 W
SFO2        400.1316005 MHz
NUC2               1H
CPDPRG[2        waltz16
PCPD2             90.00 usec
PLW2        14.36999989 W
PLW12        0.34660661 W
PLW13        0.17371930 W

F2 - Processing parameters
SI                32768
SF          100.6128158 MHz
WDW                EM
SSB       0
LB                1.00 Hz
GB        0
PC                1.40
```

^{1}H NMR spectrum of 3-(2,4-Dimethyl-6-((4-nitrobenzyl)oxy)phenyl)-*N*-(isoquinolin-3-yl)-3-methylbutanamide (122)



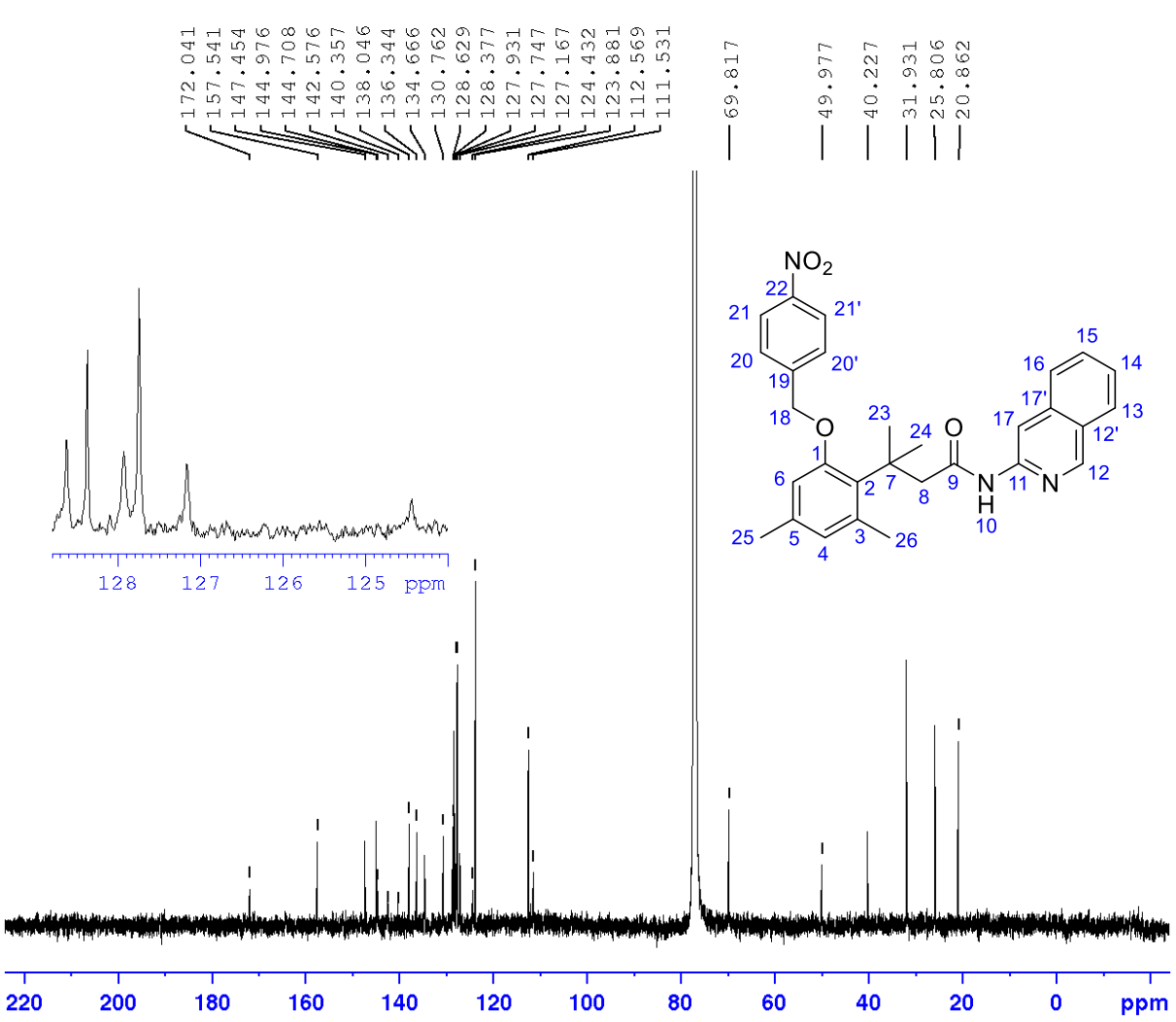

```
Current Data Parameters
NAME      CE273-02_SP_500
EXPNO                   1
PROCNO                  1

F2 - Acquisition Parameters
Date_           20160427
Time                3.33
INSTRUM          avc500
PROBHD   5 mm CPDUL 13C
PULPROG             zg30
TD                 65536
SOLVENT            CDCl3
NS                    16
DS                     4
SWH           10330.578 Hz
FIDRES         0.157632 Hz
AQ            3.1719425 sec
RG                     4
DW                48.400 usec
DE                10.00 usec
TE                298.0 K
D1           1.00000000 sec
TD0                    1

======== CHANNEL f1 ========
SFO1         500.3030896 MHz
NUC1                   1H
P1                 15.00 usec
PLW1          7.99830008 W

F2 - Processing parameters
SI                 65536
SF           500.3000136 MHz
WDW                   EM
SSB       0
LB                 0.30 Hz
GB        0
PC                 1.00
```

^{13}C NMR spectrum of 3-(2,4-Dimethyl-6-((4-nitrobenzyl)oxy)phenyl)-*N*-(isoquinolin-3-yl)-3-methylbutanamide (122)




```
Current Data Parameters
NAME      CE273-02_SP_500
EXPNO                   4
PROCNO                  1

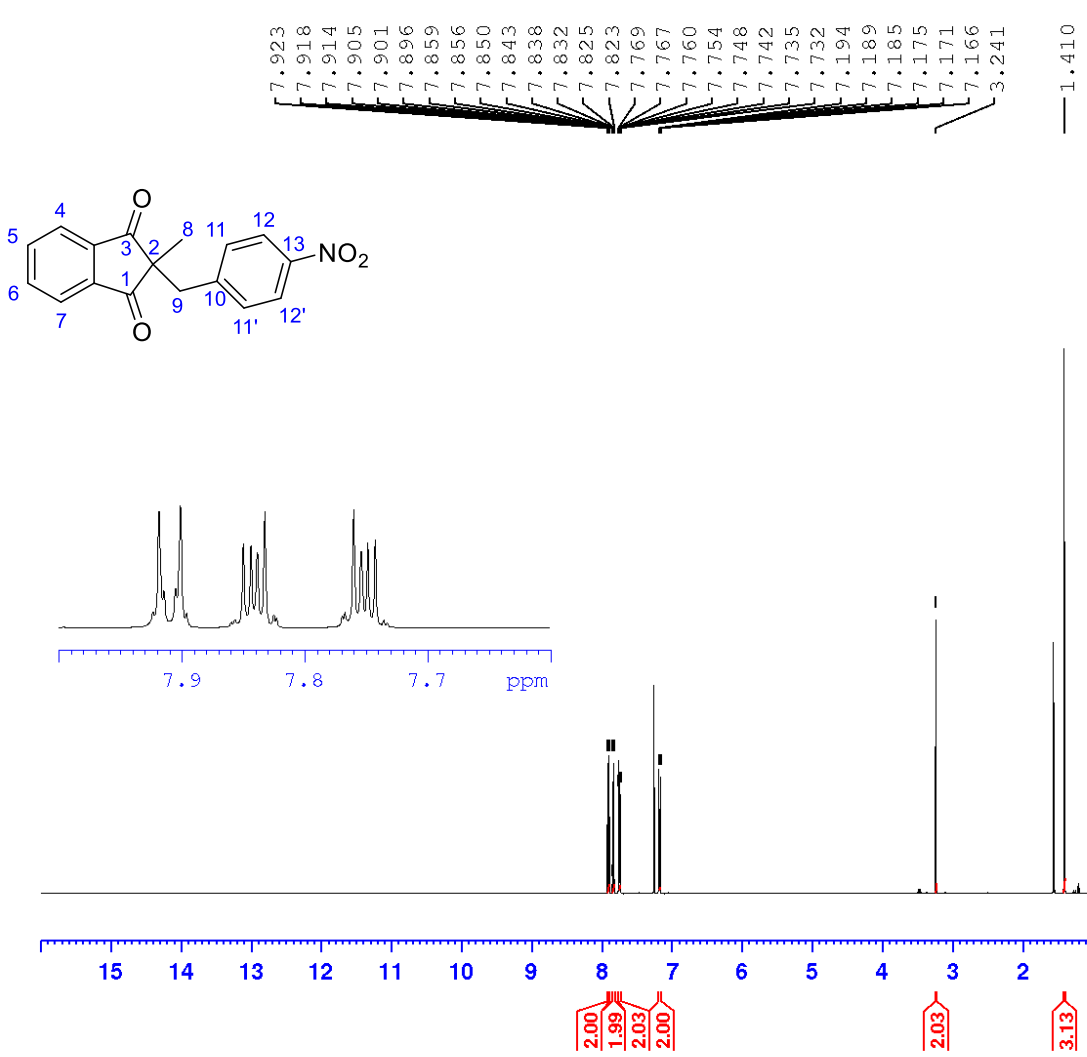
F2 - Acquisition Parameters
Date_           20160427
Time               9.26
INSTRUM          avc500
PROBHD   5 mm CPDUL 13C
PULPROG          zgpg30
TD                65536
SOLVENT           CDCl3
NS                 3072
DS                    2
SWH           31250.000 Hz
FIDRES         0.476837 Hz
AQ            1.0485760 sec
RG                  912
DW               16.000 usec
DE               18.00 usec
TE               298.0 K
D1            2.00000000 sec
D11           0.03000000 sec
TD0                   1

======== CHANNEL f1 ========
SFO1         125.8131152 MHz
NUC1                13C
P1                10.00 usec
PLW1         20.18400002 W

======== CHANNEL f2 ========
SFO2         500.3020012 MHz
NUC2                1H
CPDPRG[2         waltz16
PCPD2             80.00 usec
PLW2          7.99830008 W
PLW12         0.28119001 W
PLW13         0.17996000 W

F2 - Processing parameters
SI                 32768
SF           125.8005309 MHz
WDW                  EM
SSB       0
LB                2.00 Hz
GB        0
PC                1.40
```

^{1}H NMR spectrum of 2-Methyl-2-(4-nitrobenzyl)-1H-indene-1,3(2H)-dione (140)



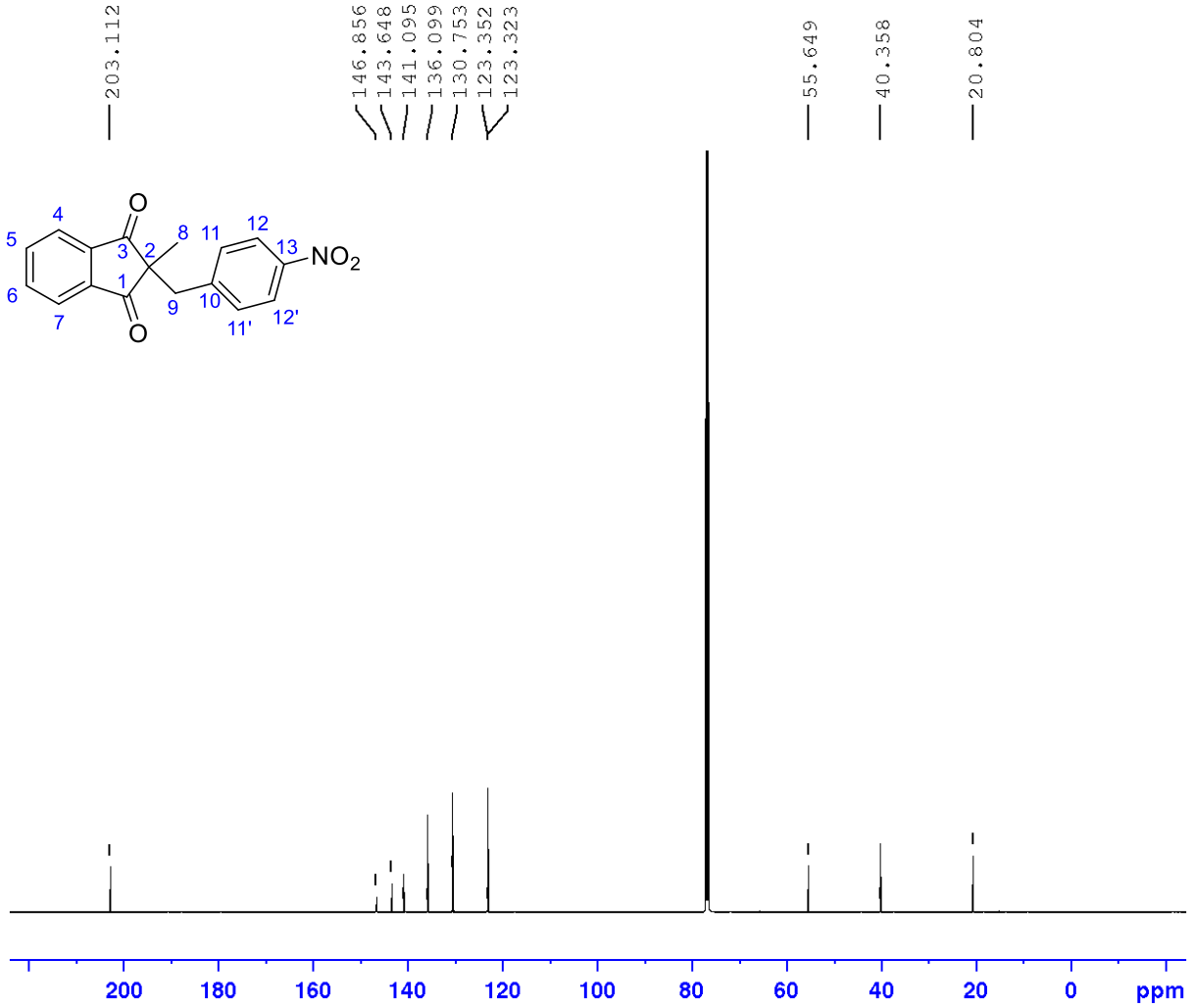

```
Current Data Parameters
NAME      CE057-02_Analysis
EXPNO                    1
PROCNO                   1

F2 - Acquisition Parameters
Date_           20150210
Time               11.55
INSTRUM          avc500
PROBHD   5 mm CPDUL 13C
PULPROG             zg30
TD                 65536
SOLVENT            CDCl3
NS                    16
DS                     4
SWH            10330.578 Hz
FIDRES          0.157632 Hz
AQ             3.1719425 sec
RG                  3.56
DW                48.400 usec
DE                10.00 usec
TE                298.0 K
D1           1.00000000 sec
TD0                    1

======== CHANNEL f1 ========
SFO1         500.3030896 MHz
NUC1                 1H
P1                15.00 usec
PLW1          7.99830008 W

F2 - Processing parameters
SI                 65536
SF           500.3000130 MHz
WDW                  EM
SSB       0
LB                0.30 Hz
GB        0
PC                1.00
```

^{13}C NMR spectrum of 2-Methyl-2-(4-nitrobenzyl)-1H-indene-1,3(2H)-dione (140)




```
Current Data Parameters
NAME      CE057-02_Analysis
EXPNO                    2
PROCNO                   1

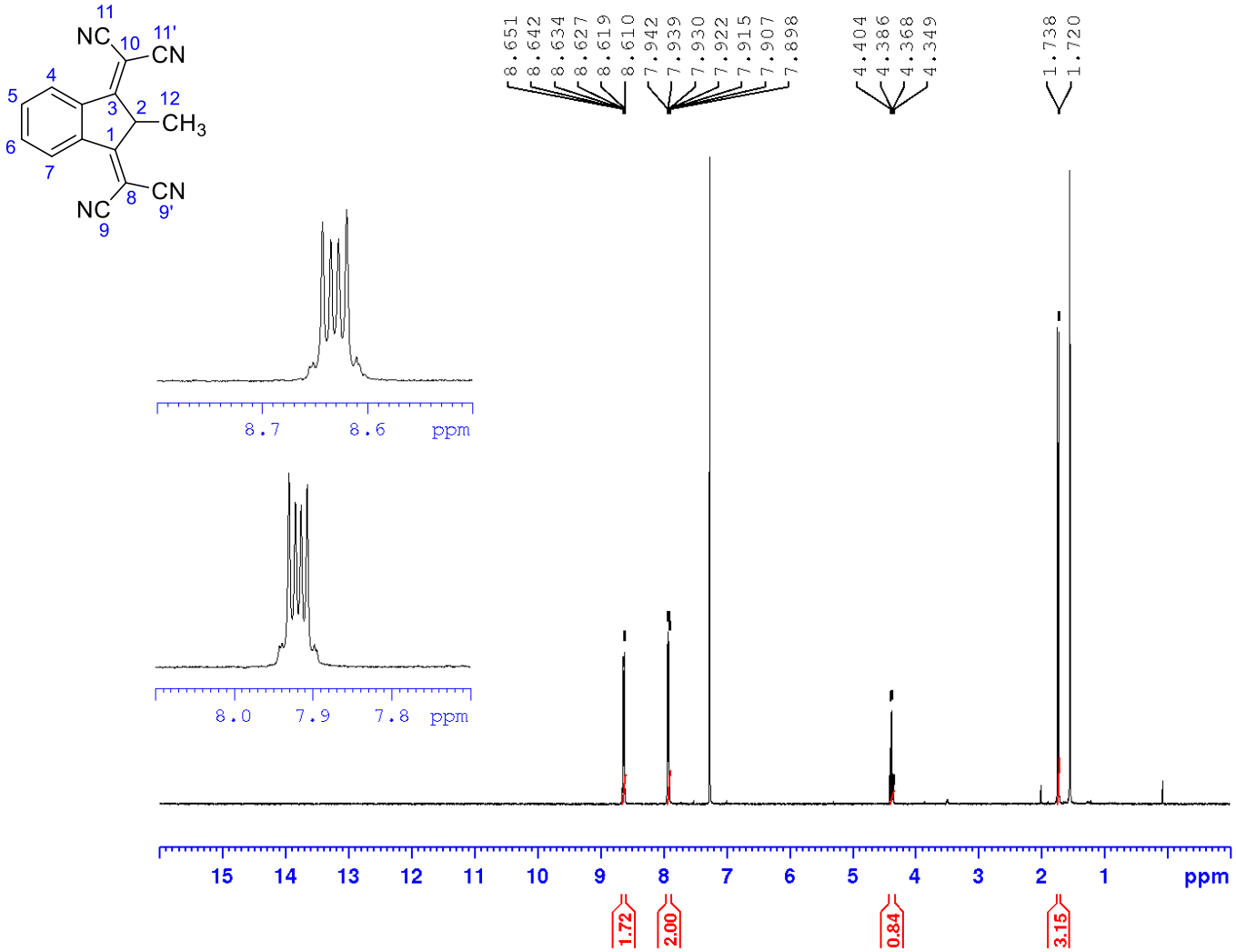
F2 - Acquisition Parameters
Date_           20150210
Time              12.49
INSTRUM           avc500
PROBHD   5 mm CPDUL 13C
PULPROG           zgpg30
TD                65536
SOLVENT           CDCl3
NS                 1024
DS                    2
SWH           31250.000 Hz
FIDRES         0.476837 Hz
AQ            1.0485760 sec
RG                  912
DW               16.000 usec
DE               18.00 usec
TE               298.0 K
D1            2.00000000 sec
D11           0.03000000 sec
TD0                   1

======== CHANNEL f1 ========
SFO1         125.8131152 MHz
NUC1               13C
P1               10.00 usec
PLW1         20.18400002 W

======== CHANNEL f2 ========
SFO2         500.3020012 MHz
NUC2               1H
CPDPRG[2         waltz16
PCPD2             80.00 usec
PLW2          7.99830008 W
PLW12         0.28119001 W
PLW13         0.17996000 W

F2 - Processing parameters
SI                32768
SF           125.8005351 MHz
WDW                EM
SSB       0
LB               1.00 Hz
GB        0
PC               1.40
```

^{1}H NMR spectrum of 2,2'-(2-Methyl-1*H*-indene-1,3(2*H*)-diylidene)dimalononitrile (158)



BRUKER

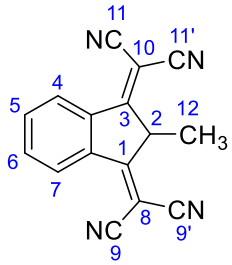
```
Current Data Parameters
NAME        CE102-01_500
EXPNO                  1
PROCNO                 1

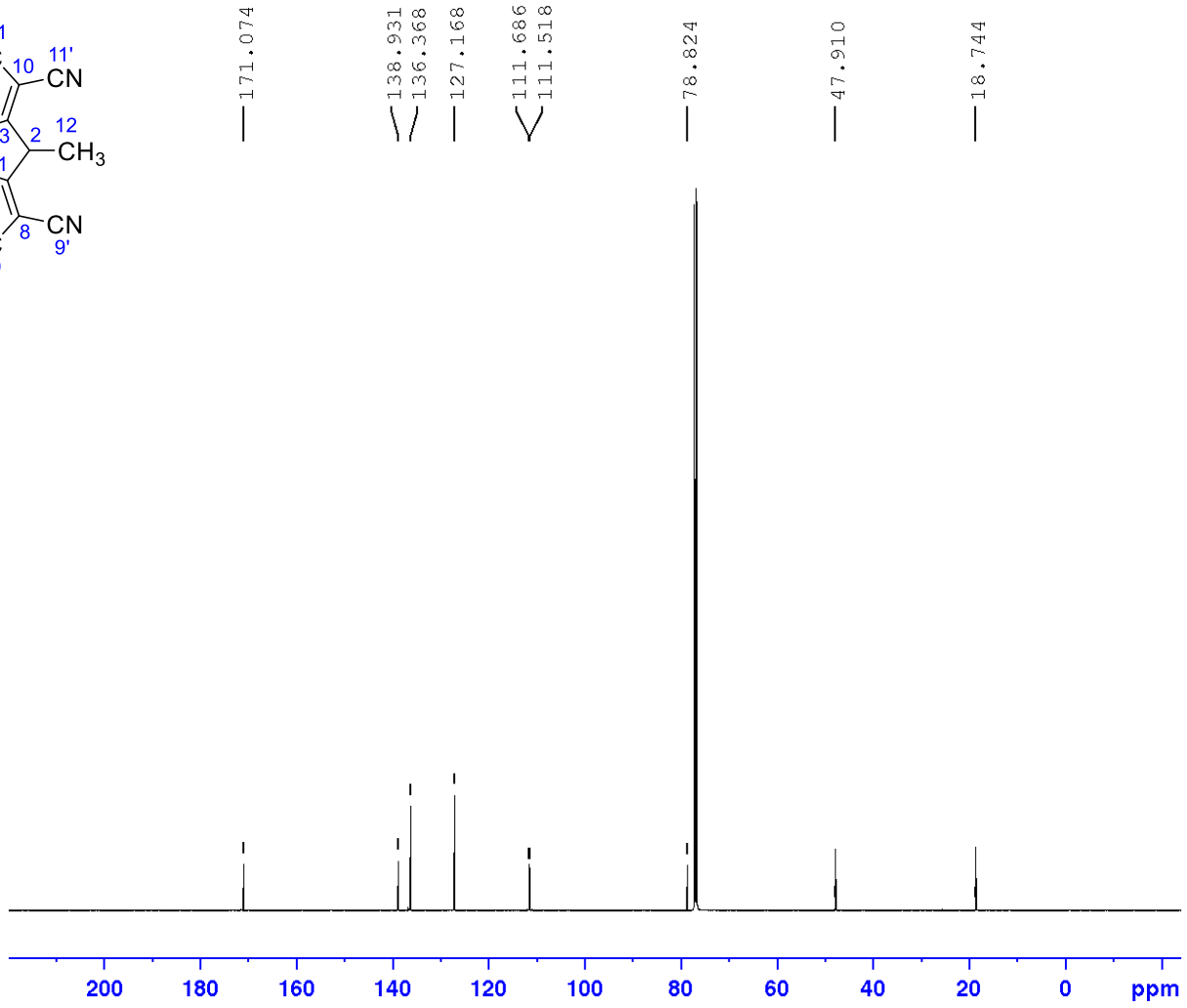
F2 - Acquisition Parameters
Date_           20150504
Time               15.01
INSTRUM          avg400
PROBHD   5 mm PABBO BB/
PULPROG             zg60
TD                 65536
SOLVENT            CDCl3
NS                     8
DS                     2
SWH            10000.000 Hz
FIDRES          0.152588 Hz
AQ             3.2767999 sec
RG                206.87
DW                50.000 usec
DE                 6.50 usec
TE                298.0 K
D1             1.00000000 sec
TD0                    1

======== CHANNEL f1 ========
SFO1         400.2024714 MHz
NUC1                 1H
P1                14.00 usec
PLW1         14.00000000 W

F2 - Processing parameters
SI                 65536
SF           400.2000098 MHz
WDW                  EM
SSB       0
LB                0.30 Hz
GB        0
PC                1.00
```

^{13}C NMR spectrum of 2,2'-(2-Methyl-1*H*-indene-1,3(2*H*)-diylidene)dimalononitrile (158)






```
Current Data Parameters
NAME        CE102-01_500
EXPNO                  4
PROCNO                 1

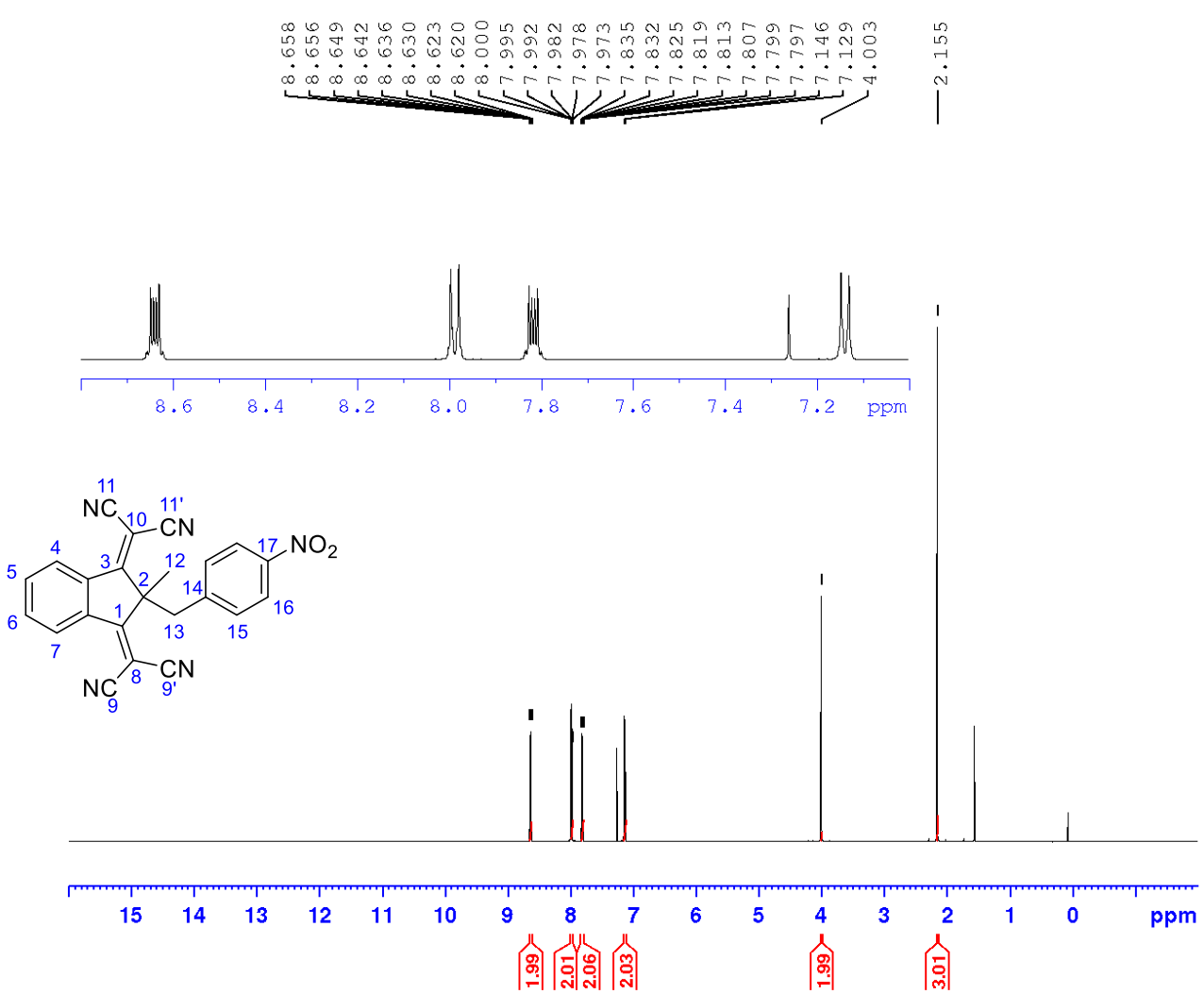
F2 - Acquisition Parameters
Date_           20150509
Time               19.10
INSTRUM          avc500
PROBHD   5 mm CPDUL 13C
PULPROG          zgpg30
TD                65536
SOLVENT           CDCl3
NS                 1024
DS                    2
SWH           31250.000 Hz
FIDRES         0.476837 Hz
AQ            1.0485760 sec
RG                  912
DW               16.000 usec
DE               18.00 usec
TE               298.0 K
D1           2.00000000 sec
D11          0.03000000 sec
TD0                   1

======== CHANNEL f1 ========
SFO1         125.8131152 MHz
NUC1                13C
P1                10.00 usec
PLW1         20.18400002 W

======== CHANNEL f2 ========
SFO2         500.3020012 MHz
NUC2                1H
CPDPRG[2         waltz16
PCPD2             80.00 usec
PLW2          7.99830008 W
PLW12         0.28119001 W
PLW13         0.17996000 W

F2 - Processing parameters
SI                 32768
SF           125.8005351 MHz
WDW                  EM
SSB       0
LB                1.00 Hz
GB        0
PC                1.40
```

^{1}H NMR spectrum of 2,2'-(2-Methyl-2-(4-nitrobenzyl)-1*H*-indene-1,3(2*H*)-diylidene)dimalononitrile (136)



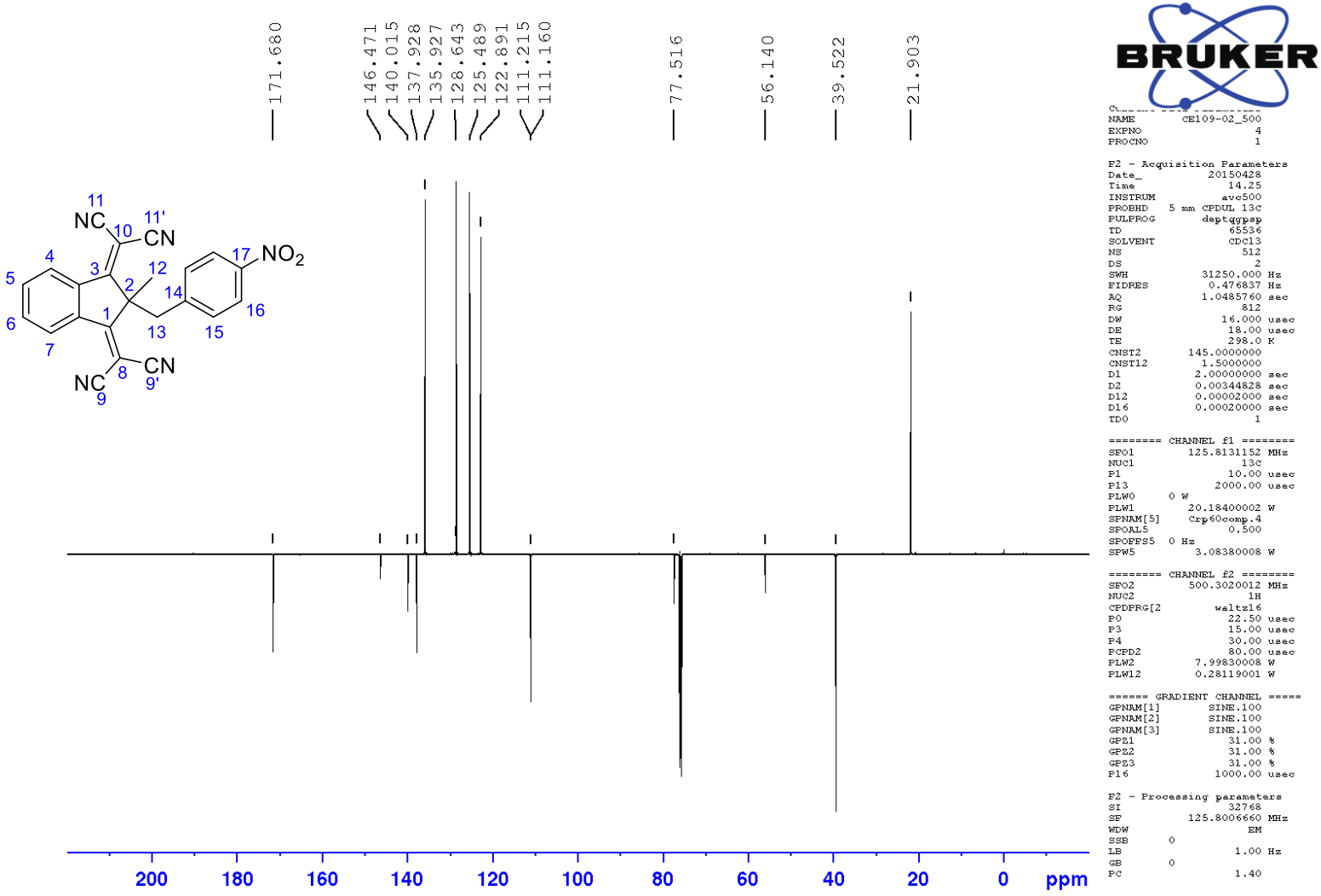

```
Current Data Parameters
NAME        CE109-02_500
EXPNO                  1
PROCNO                 1

F2 - Acquisition Parameters
Date_           20150428
Time               8.17
INSTRUM          avc500
PROBHD   5 mm CPDUL 13C
PULPROG             zg30
TD                 65536
SOLVENT            CDCl3
NS                    16
DS                     4
SWH            10330.578 Hz
FIDRES          0.157632 Hz
AQ             3.1719425 sec
RG                  3.56
DW                48.400 usec
DE                10.00 usec
TE                298.0 K
D1            1.00000000 sec
TD0                    1

======== CHANNEL f1 ========
SFO1         500.3030896 MHz
NUC1                1H
P1                15.00 usec
PLW1          7.99830008 W

F2 - Processing parameters
SI                 65536
SF           500.3000136 MHz
WDW                   EM
SSB       0
LB                 0.30 Hz
GB        0
PC                 1.00
```

^{13}C NMR spectrum of 2,2'-(2-Methyl-2-(4-nitrobenzyl)-1*H*-indene-1,3(2*H*)-diylidene)dimalononitrile (136)




```
NAME            CE109-02_500
EXPNO                      4
PROCNO                     1

F2 - Acquisition Parameters
Date_           20150428
Time                 14.25
INSTRUM              avc500
PROBHD   5 mm CPDUL 13C
PULPROG         deptqgpsp
TD                  65536
SOLVENT             CDCl3
NS                    512
DS                      2
SWH             31250.000 Hz
FIDRES          0.476837 Hz
AQ              1.0485760 sec
RG                    812
DW                16.000 usec
DE                18.00 usec
TE                298.0 K
CNST2         145.0000000
CNST12          1.5000000
D1            2.00000000 sec
D2            0.00344828 sec
D12           0.00002000 sec
D16           0.00020000 sec
TD0                    1

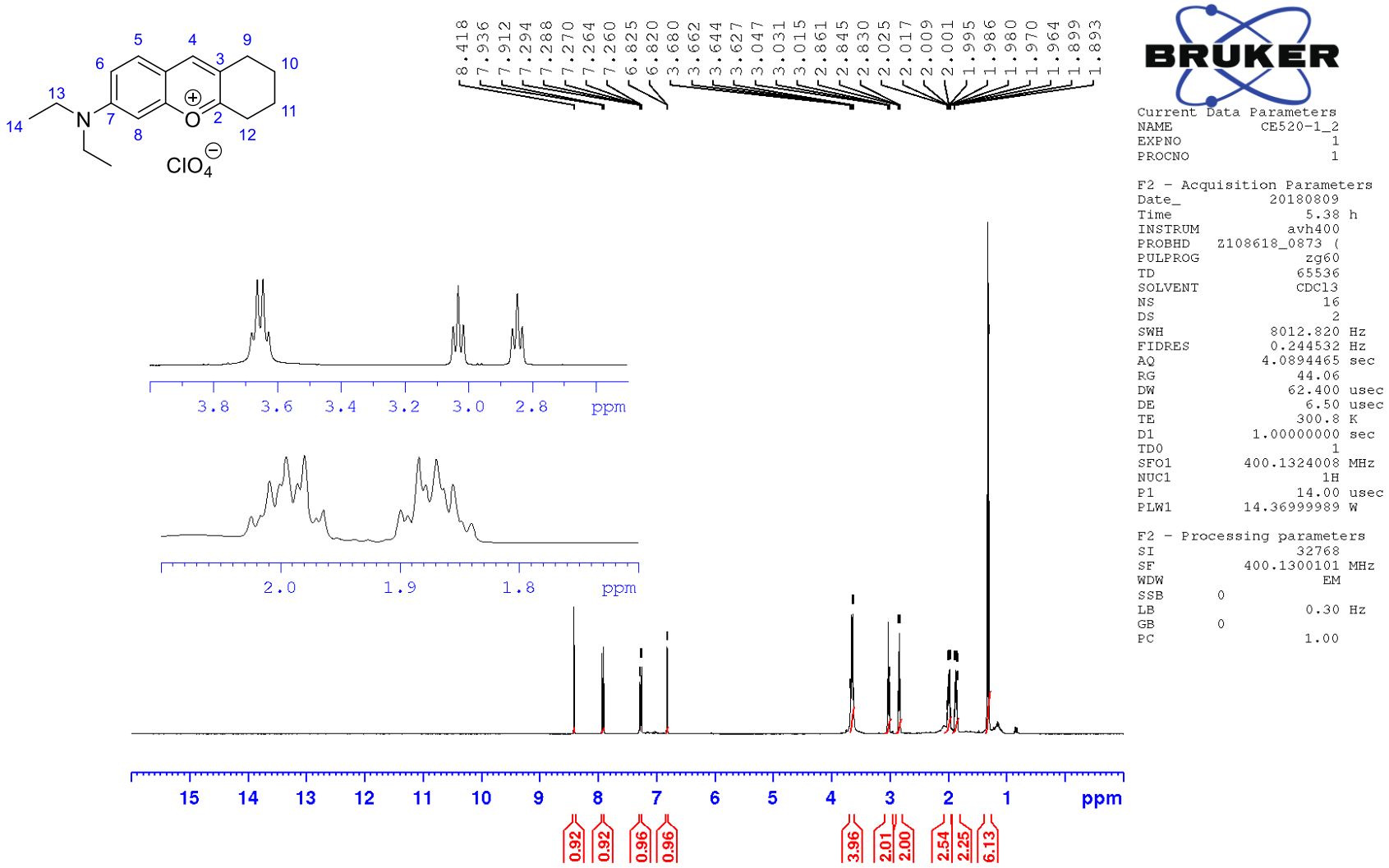
======== CHANNEL f1 ========
SFO1          125.8131152 MHz
NUC1                  13C
P1                 10.00 usec
P13              2000.00 usec
PLW0      0 W
PLW1         20.18400002 W
SPNAM[5]     Crp60comp.4
SPOAL5             0.500
SPOFFS5   0 Hz
SPW5          3.08380008 W

======== CHANNEL f2 ========
SFO2          500.3020012 MHz
NUC2                  1H
CPDPRG[2          waltz16
P0                 22.50 usec
P3                 15.00 usec
P4                 30.00 usec
PCPD2              80.00 usec
PLW2          7.99830008 W
PLW12         0.28119001 W

====== GRADIENT CHANNEL =====
GPNAM[1]         SINE.100
GPNAM[2]         SINE.100
GPNAM[3]         SINE.100
GPZ1                31.00 %
GPZ2                31.00 %
GPZ3                31.00 %
P16               1000.00 usec

F2 - Processing parameters
SI                    32768
SF            125.8006660 MHz
WDW                     EM
SSB       0
LB                   1.00 Hz
GB        0
PC                   1.40
```

^{1}H NMR spectrum of 6-(Diethylamino)-1,2,3,4-tetrahydroxanthylium perchlorate (169)

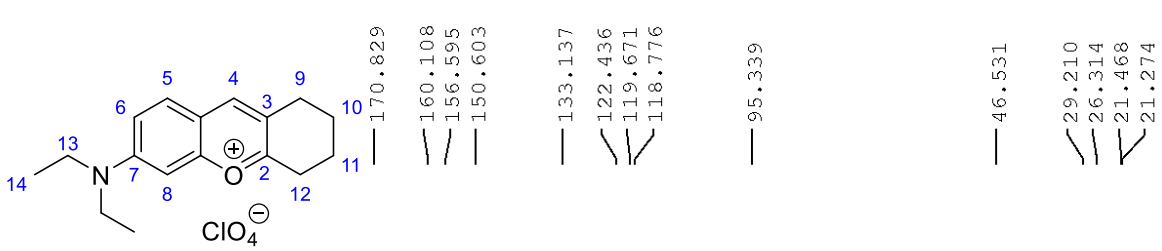


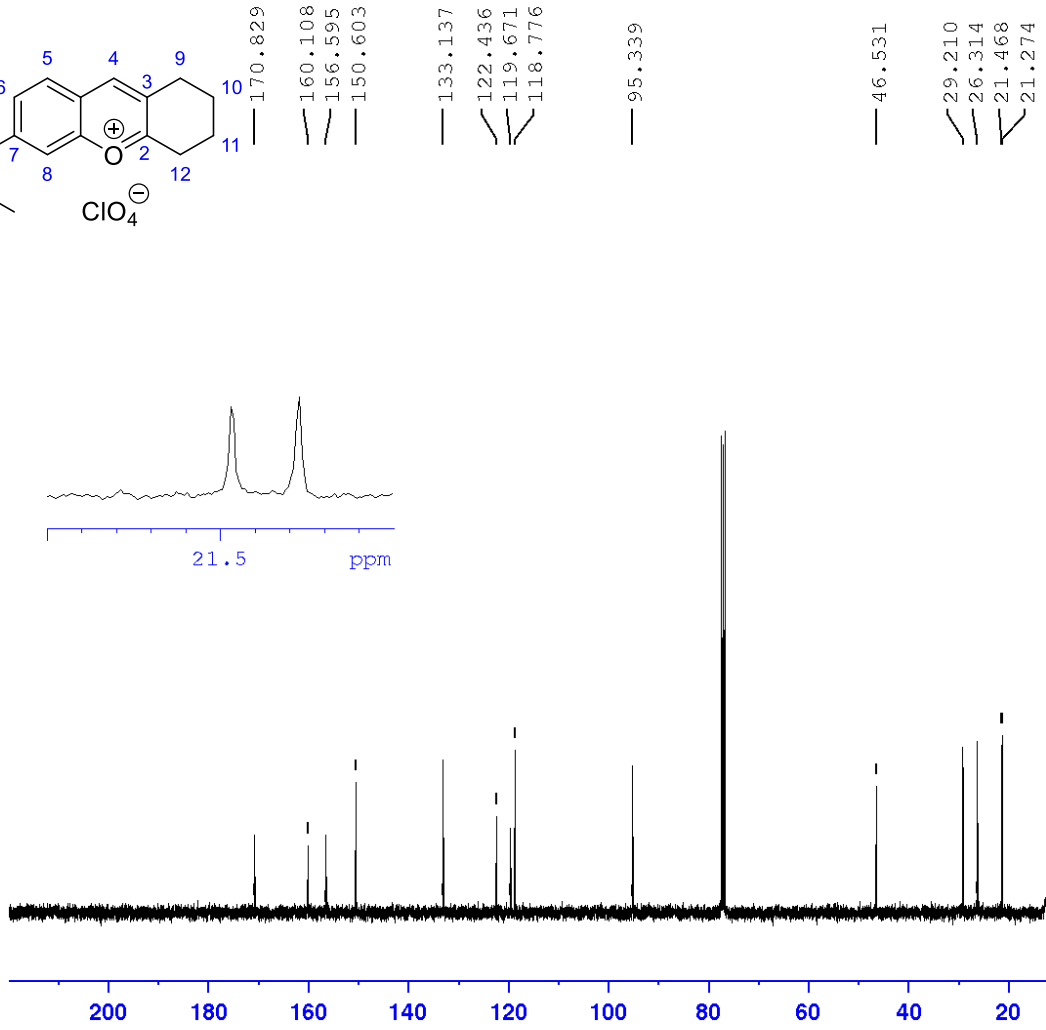

```
Current Data Parameters
NAME                  CE520-1_2
EXPNO                         1
PROCNO                        1

F2 - Acquisition Parameters
Date_                  20180809
Time                       5.38 h
INSTRUM                  avh400
PROBHD    Z108618_0873 (
PULPROG                   zg60
TD                       65536
SOLVENT                  CDCl3
NS                          16
DS                           2
SWH                   8012.820 Hz
FIDRES                0.244532 Hz
AQ                    4.0894465 sec
RG                        44.06
DW                       62.400 usec
DE                        6.50 usec
TE                       300.8 K
D1                    1.00000000 sec
TD0                           1
SFO1                400.1324008 MHz
NUC1                        1H
P1                       14.00 usec
PLW1                14.36999989 W

F2 - Processing parameters
SI                        32768
SF                  400.1300101 MHz
WDW                         EM
SSB                0
LB                        0.30 Hz
GB                 0
PC                        1.00
```

^{13}C NMR spectrum of 6-(Diethylamino)-1,2,3,4-tetrahydroxanthylium perchlorate (169)



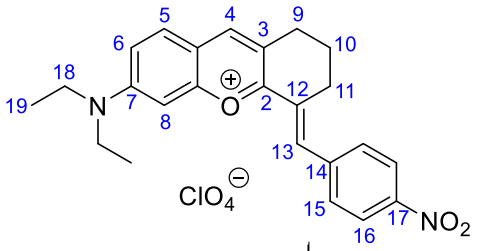


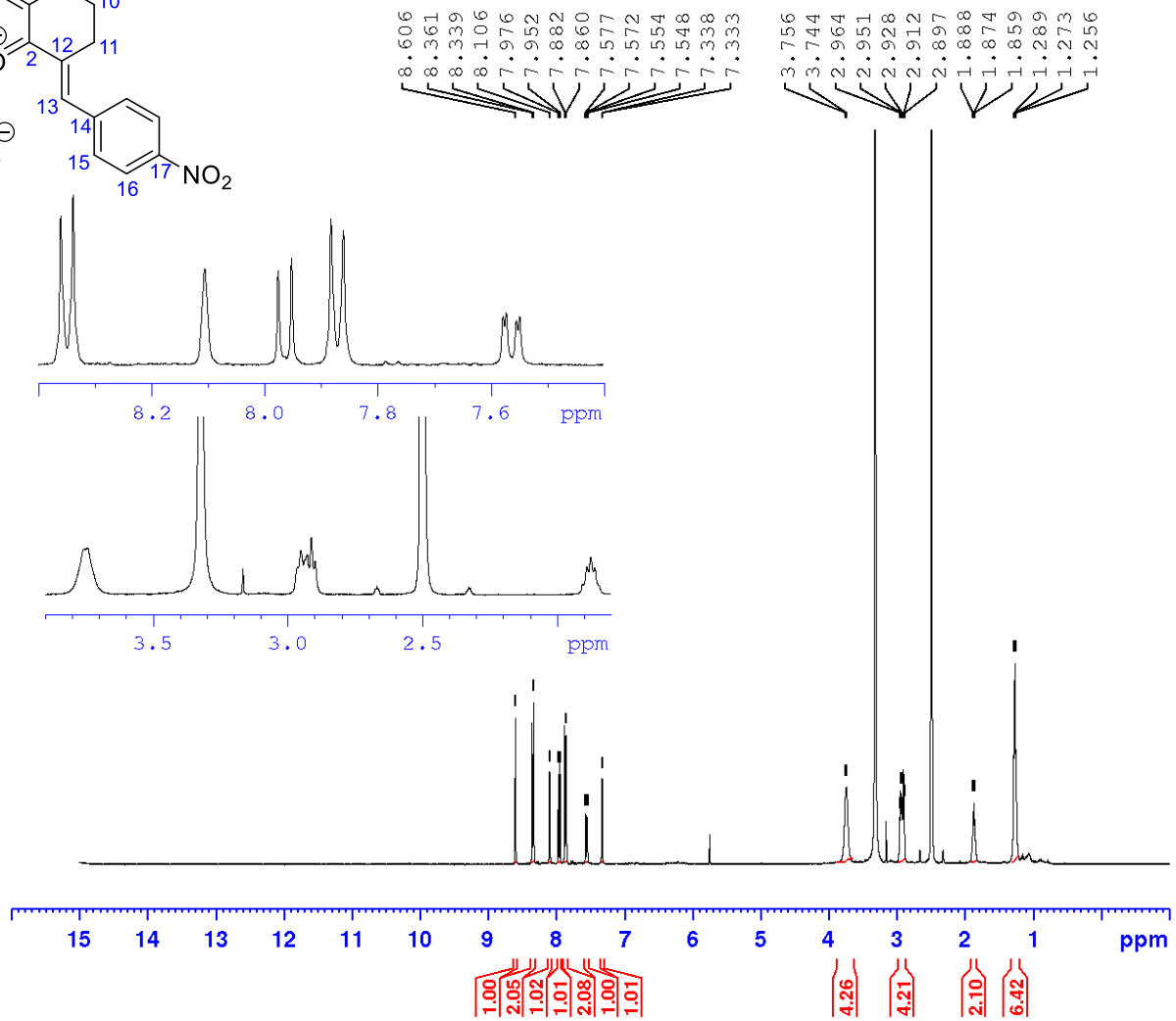

```
Current Data Parameters
NAME              CE520-1_2
EXPNO                     2
PROCNO                    1

F2 - Acquisition Parameters
Date_              20180809
Time                   5.47 h
INSTRUM              avh400
PROBHD    Z108618_0873 (
PULPROG              zgpg30
TD                    32768
SOLVENT               CDCl3
NS                      256
DS                        4
SWH               26041.666 Hz
FIDRES             1.589457 Hz
AQ                0.6291456 sec
RG                   197.18
DW                   19.200 usec
DE                    6.50 usec
TE                   301.7 K
D1             1.00000000 sec
D11            0.03000000 sec
TD0                       1
SFO1          100.6228298 MHz
NUC1                   13C
P1                   10.00 usec
PLW1          47.86100006 W
SFO2          400.1316005 MHz
NUC2                   1H
CPDPRG[2           waltz16
PCPD2                90.00 usec
PLW2          14.36999989 W
PLW12          0.34660661 W
PLW13          0.17371930 W

F2 - Processing parameters
SI                    32768
SF            100.6127617 MHz
WDW                     EM
SSB       0
LB                    1.00 Hz
GB        0
PC                    1.40
```

^{1}H NMR spectrum of (*E*)-6-(Diethylamino)-4-(4-nitrobenzylidene)-1,2,3,4-tetrahydroxanthylium (166)



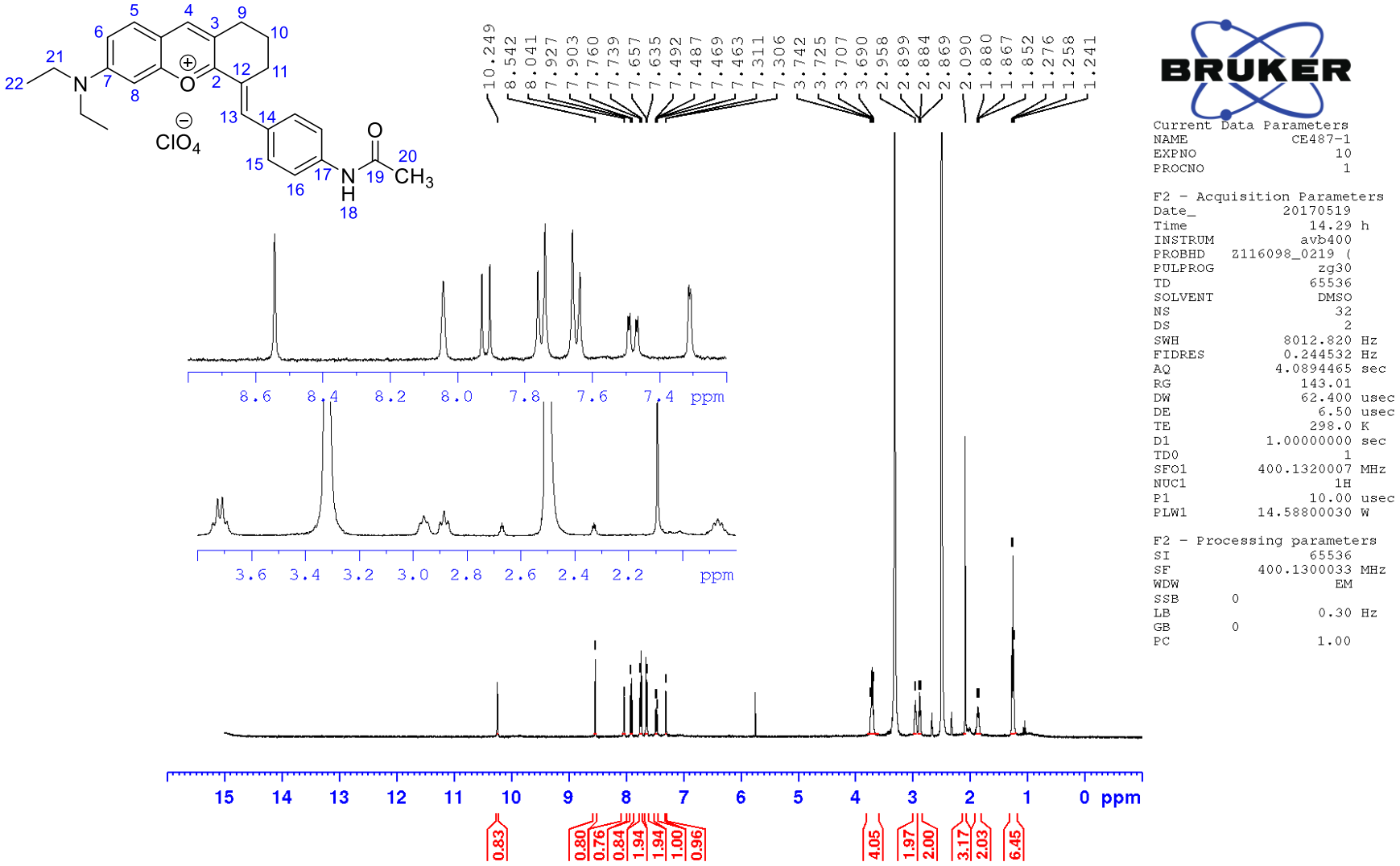



```
Current Data Parameters
NAME                  CE483-1
EXPNO                      10
PROCNO                      1

F2 - Acquisition Parameters
Date_              20170519
Time                  14.50 h
INSTRUM               avb400
PROBHD    Z116098_0219 (
PULPROG                zg30
TD                    65536
SOLVENT                DMSO
NS                       32
DS                        2
SWH                8012.820 Hz
FIDRES            0.244532 Hz
AQ                4.0894465 sec
RG                   143.01
DW                   62.400 usec
DE                    6.50 usec
TE                   298.0 K
D1              1.00000000 sec
TD0                       1
SFO1           400.1320007 MHz
NUC1                    1H
P1                   10.00 usec
PLW1           14.58800030 W

F2 - Processing parameters
SI                    65536
SF             400.1300034 MHz
WDW                     EM
SSB         0
LB                    0.30 Hz
GB          0
PC                    1.00
```

^{1}H NMR spectrum of (*E*)-4-(4-Acetamidobenzylidene)-6-(diethylamino)-1,2,3,4-tetrahydroxanthylium perchlorate (170)

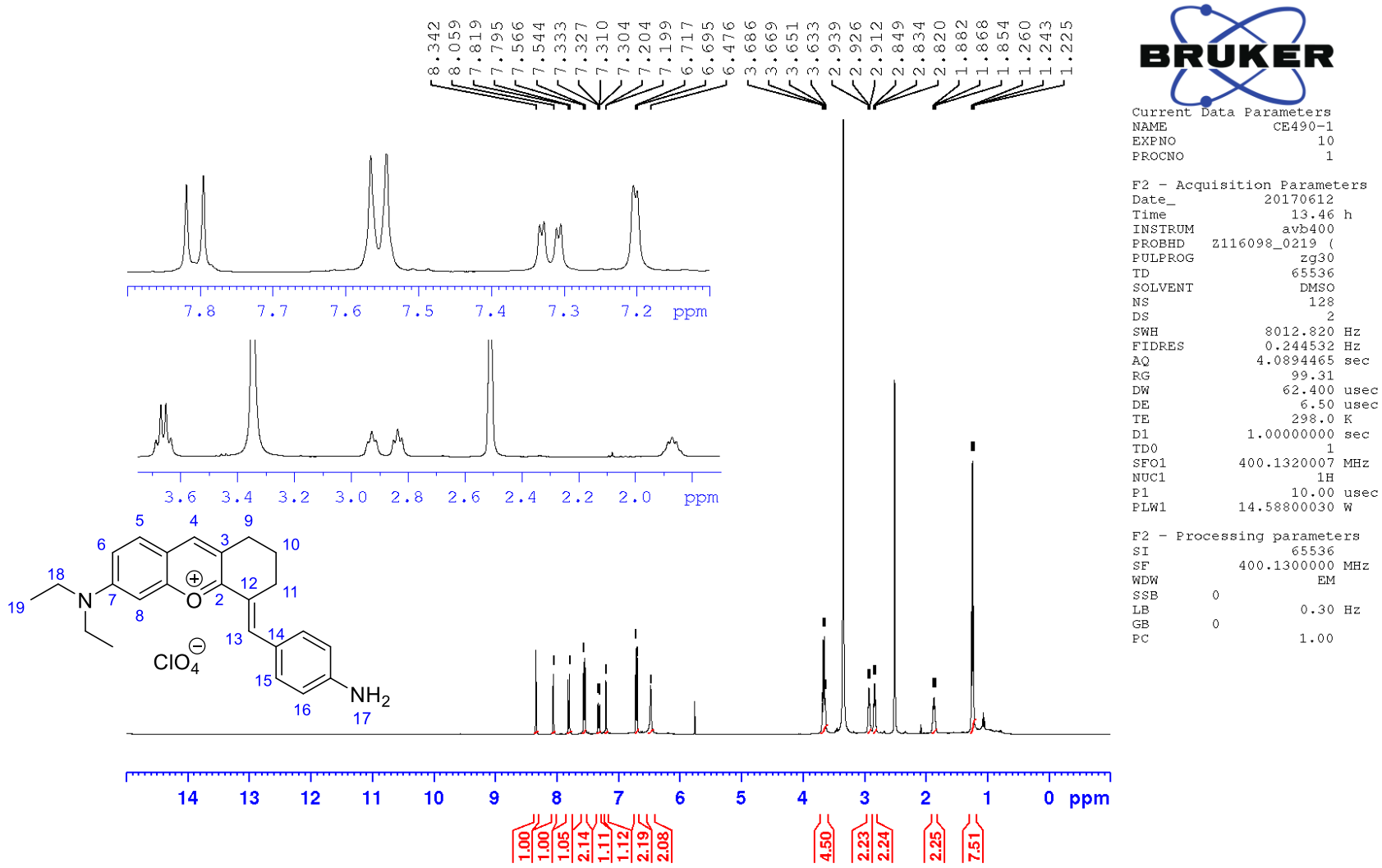



```
Current Data Parameters
NAME                  CE487-1
EXPNO                      10
PROCNO                      1

F2 - Acquisition Parameters
Date_              20170519
Time                  14.29 h
INSTRUM              avb400
PROBHD    Z116098_0219 (
PULPROG                zg30
TD                    65536
SOLVENT                DMSO
NS                       32
DS                        2
SWH                8012.820 Hz
FIDRES            0.244532 Hz
AQ                4.0894465 sec
RG                   143.01
DW                   62.400 usec
DE                    6.50 usec
TE                   298.0 K
D1              1.00000000 sec
TD0                       1
SFO1           400.1320007 MHz
NUC1                    1H
P1                   10.00 usec
PLW1           14.58800030 W

F2 - Processing parameters
SI                    65536
SF             400.1300033 MHz
WDW                     EM
SSB         0
LB                    0.30 Hz
GB          0
PC                    1.00
```

^{1}H NMR spectrum of (*E*)-4-(4-Aminobenzylidene)-6-(diethylamino)-1,2,3,4-tetrahydroxanthylium perchlorate (163)

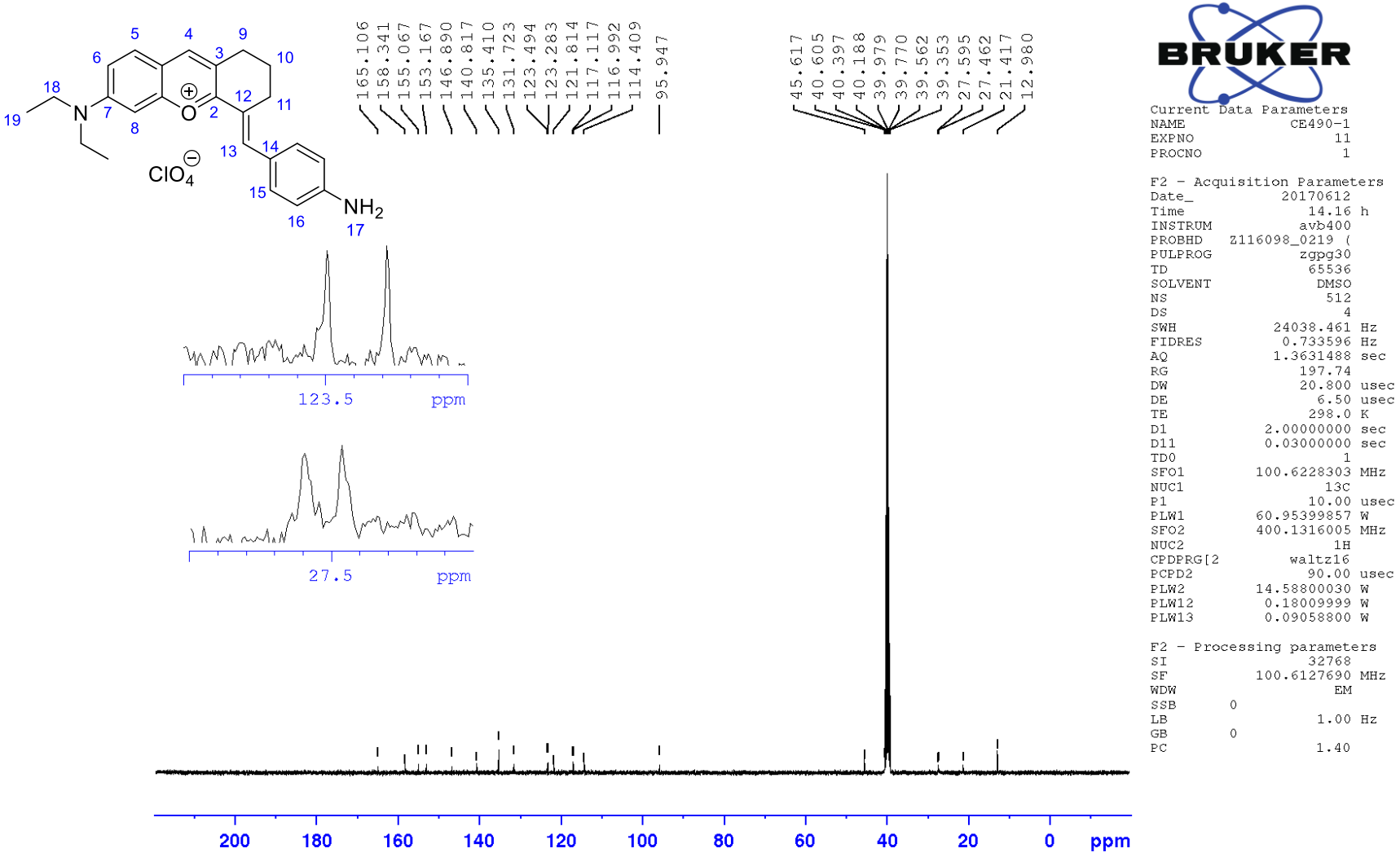



```
Current Data Parameters
NAME                  CE490-1
EXPNO                      10
PROCNO                      1

F2 - Acquisition Parameters
Date_               20170612
Time                   13.46 h
INSTRUM                avb400
PROBHD    Z116098_0219 (
PULPROG                 zg30
TD                     65536
SOLVENT                 DMSO
NS                       128
DS                         2
SWH                 8012.820 Hz
FIDRES              0.244532 Hz
AQ                  4.0894465 sec
RG                      99.31
DW                     62.400 usec
DE                      6.50 usec
TE                     298.0 K
D1                1.00000000 sec
TD0                        1
SFO1             400.1320007 MHz
NUC1                      1H
P1                     10.00 usec
PLW1             14.58800030 W

F2 - Processing parameters
SI                     65536
SF               400.1300000 MHz
WDW                       EM
SSB          0
LB                      0.30 Hz
GB           0
PC                      1.00
```

^{13}C NMR spectrum of (*E*)-4-(4-Aminobenzylidene)-6-(diethylamino)-1,2,3,4-tetrahydroxanthylium perchlorate (163)

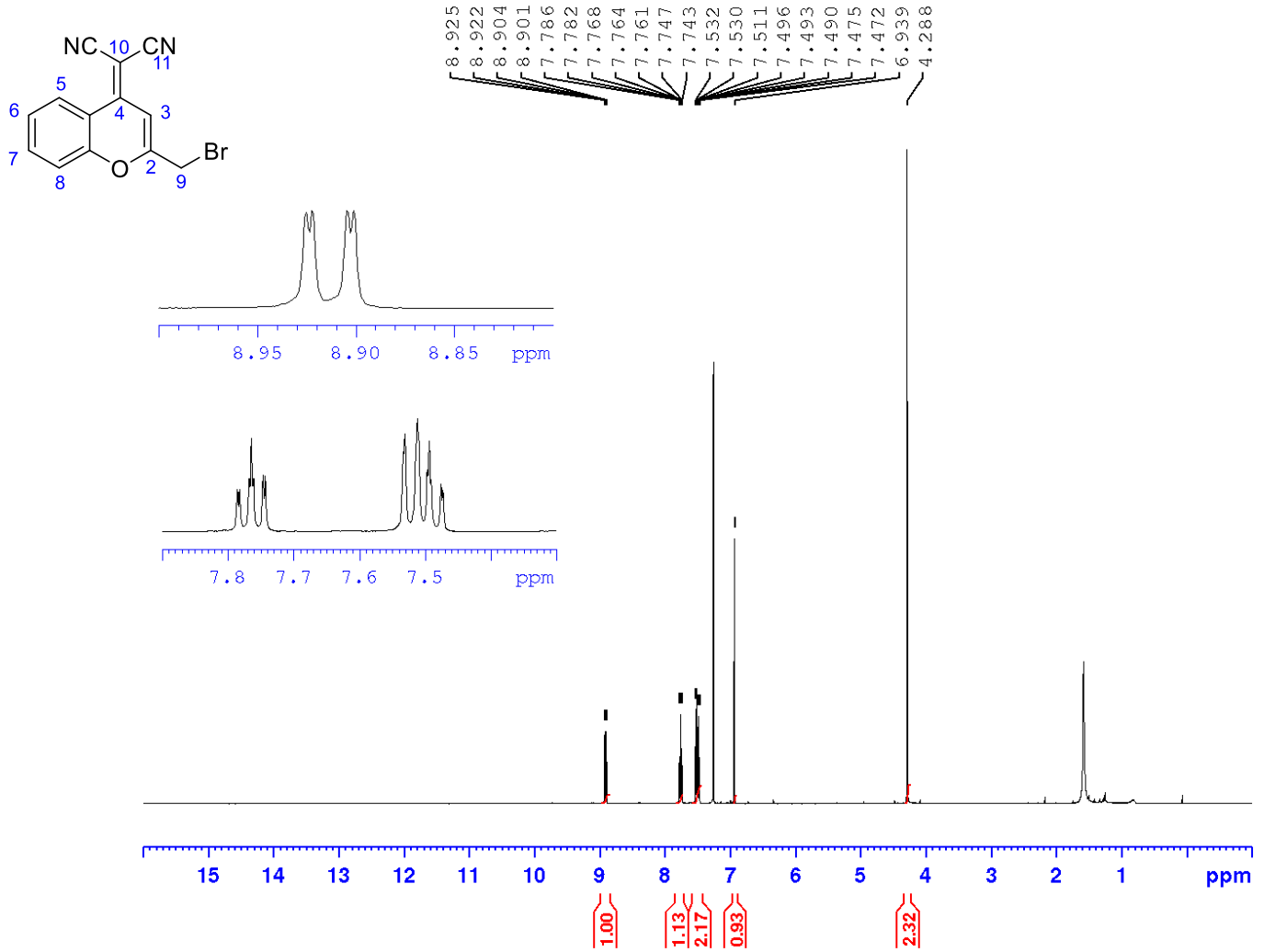



```
Current Data Parameters
NAME                  CE490-1
EXPNO                      11
PROCNO                      1

F2 - Acquisition Parameters
Date_              20170612
Time                  14.16 h
INSTRUM              avb400
PROBHD    Z116098_0219 (
PULPROG              zgpg30
TD                    65536
SOLVENT                DMSO
NS                       512
DS                         4
SWH               24038.461 Hz
FIDRES             0.733596 Hz
AQ                1.3631488 sec
RG                   197.74
DW                   20.800 usec
DE                    6.50 usec
TE                   298.0 K
D1             2.00000000 sec
D11            0.03000000 sec
TD0                        1
SFO1          100.6228303 MHz
NUC1                    13C
P1                   10.00 usec
PLW1          60.95399857 W
SFO2          400.1316005 MHz
NUC2                    1H
CPDPRG[2           waltz16
PCPD2                90.00 usec
PLW2          14.58800030 W
PLW12          0.18009999 W
PLW13          0.09058800 W

F2 - Processing parameters
SI                     32768
SF            100.6127690 MHz
WDW                       EM
SSB       0
LB                    1.00 Hz
GB        0
PC                    1.40
```

^{1}H NMR spectrum of 2-(2-(Bromomethyl)-4*H*-chromen-4-ylidene)malononitrile (188)

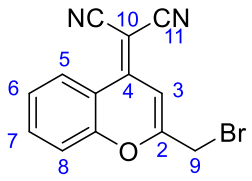


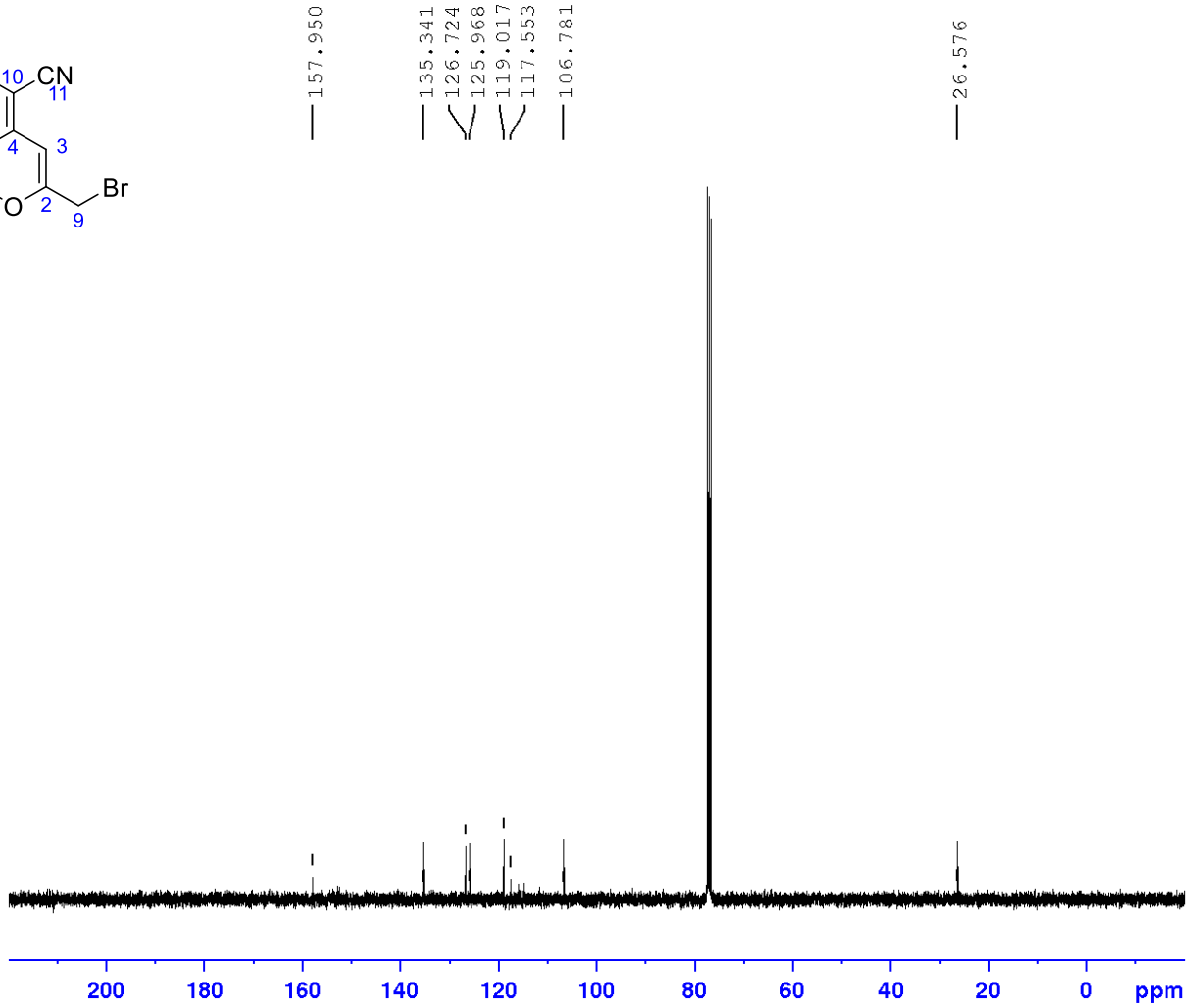

```
Current Data Parameters
NAME       CE436-SPOT2_1
EXPNO                  1
PROCNO                 1

F2 - Acquisition Parameters
Date_           20180830
Time               12.39 h
INSTRUM           avh400
PROBHD   Z108618_0873 (
PULPROG             zg60
TD                 65536
SOLVENT            CDCl3
NS                    16
DS                     2
SWH             8012.820 Hz
FIDRES          0.244532 Hz
AQ              4.0894465 sec
RG                 88.17
DW                62.400 usec
DE                 6.50 usec
TE                298.8 K
D1             1.00000000 sec
TD0                    1
SFO1          400.1324008 MHz
NUC1                  1H
P1                 14.00 usec
PLW1          14.36999989 W

F2 - Processing parameters
SI                 32768
SF            400.1300099 MHz
WDW                   EM
SSB       0
LB                 0.30 Hz
GB        0
PC                 1.00
```

^{13}C NMR spectrum of 2-(2-(Bromomethyl)-4*H*-chromen-4-ylidene)malononitrile (188)



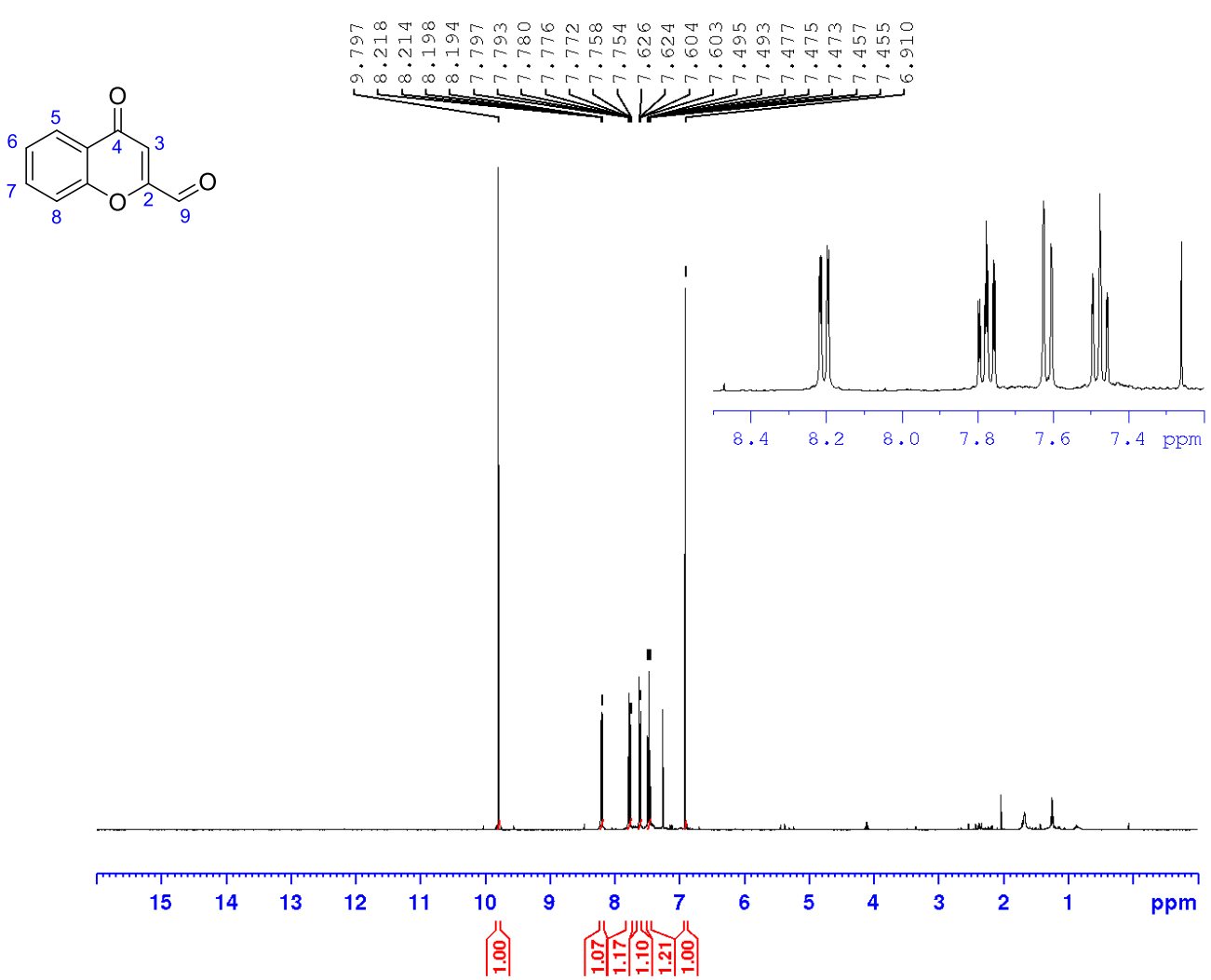



```
Current Data Parameters
NAME       CE436-SPOT2_1
EXPNO                  2
PROCNO                 1

F2 - Acquisition Parameters
Date_           20180830
Time              16.34 h
INSTRUM           avh400
PROBHD   Z108618_0873 (
PULPROG           zgpg30
TD                32768
SOLVENT           CDCl3
NS                  512
DS                    4
SWH           26041.666 Hz
FIDRES         1.589457 Hz
AQ            0.6291456 sec
RG               197.18
DW               19.200 usec
DE                6.50 usec
TE               300.4 K
D1           1.00000000 sec
D11          0.03000000 sec
TD0                   1
SFO1        100.6228298 MHz
NUC1                13C
P1                10.00 usec
PLW1        47.86100006 W
SFO2        400.1316005 MHz
NUC2                1H
CPDPRG[2         waltz16
PCPD2             90.00 usec
PLW2        14.36999989 W
PLW12        0.34660661 W
PLW13        0.17371930 W

F2 - Processing parameters
SI                32768
SF          100.6127543 MHz
WDW                 EM
SSB       0
LB                1.00 Hz
GB        0
PC                1.40
```

^{1}H NMR spectrum of 4-Oxo-4*H*-chromene-2-carbaldehyde (198)

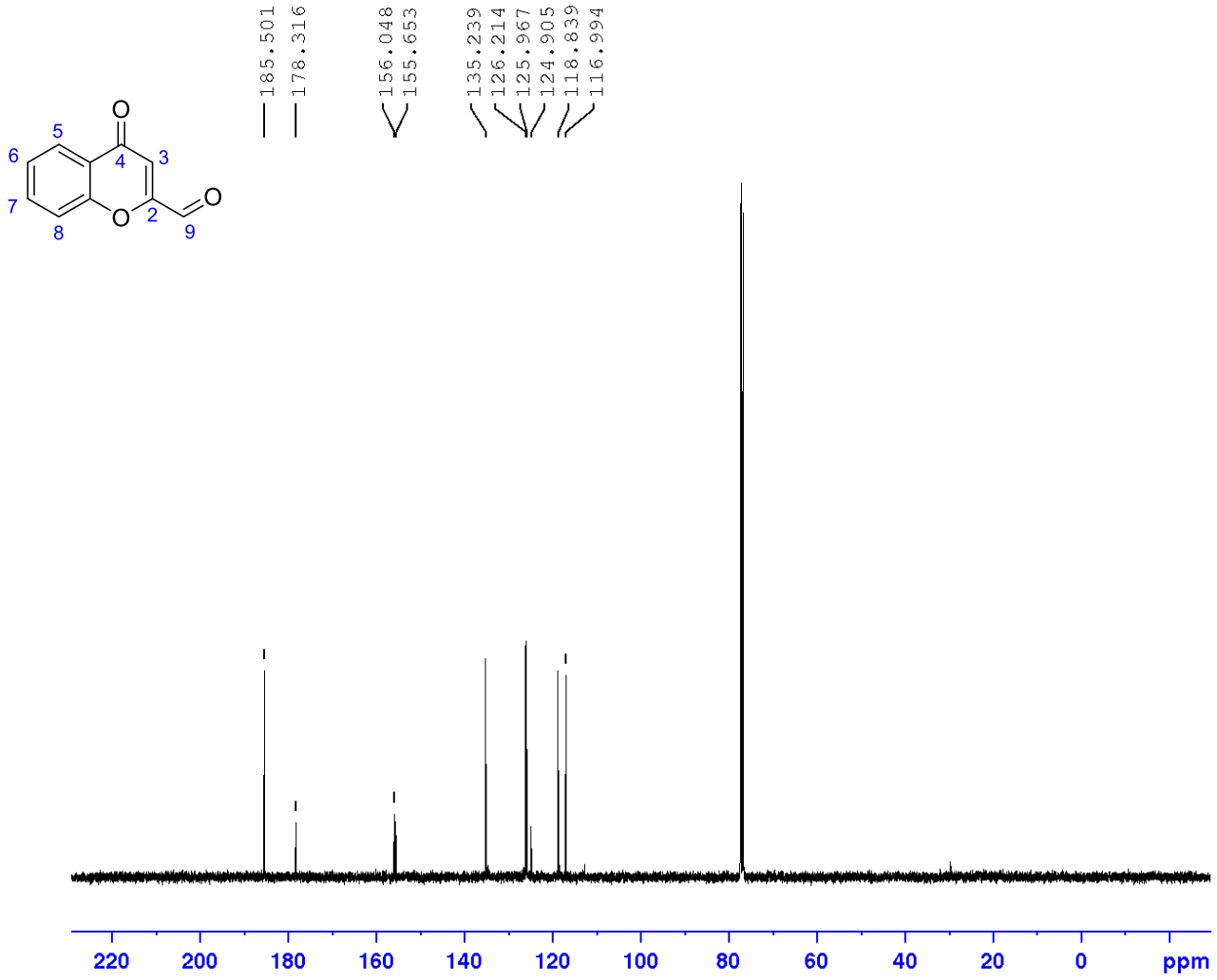



```
Current Data Parameters
NAME       CE457-FR12-30
EXPNO                 1
PROCNO                1

F2 - Acquisition Parameters
Date_           20170407
Time              10.49 h
INSTRUM           avg400
PROBHD   Z108618_0816 (
PULPROG            zg60
TD                65536
SOLVENT           CDCl3
NS                   16
DS                    2
SWH            8012.820 Hz
FIDRES         0.244532 Hz
AQ             4.0894465 sec
RG                91.39
DW                62.400 usec
DE                 6.50 usec
TE                293.3 K
D1           1.00000000 sec
TD0                   1
SFO1         400.2024012 MHz
NUC1                 1H
P1                14.00 usec
PLW1         14.00000000 W

F2 - Processing parameters
SI                32768
SF           400.2000100 MHz
WDW                  EM
SSB       0
LB                0.30 Hz
GB        0
PC                1.00
```

^{13}C NMR spectrum of 4-Oxo-4*H*-chromene-2-carbaldehyde (198)

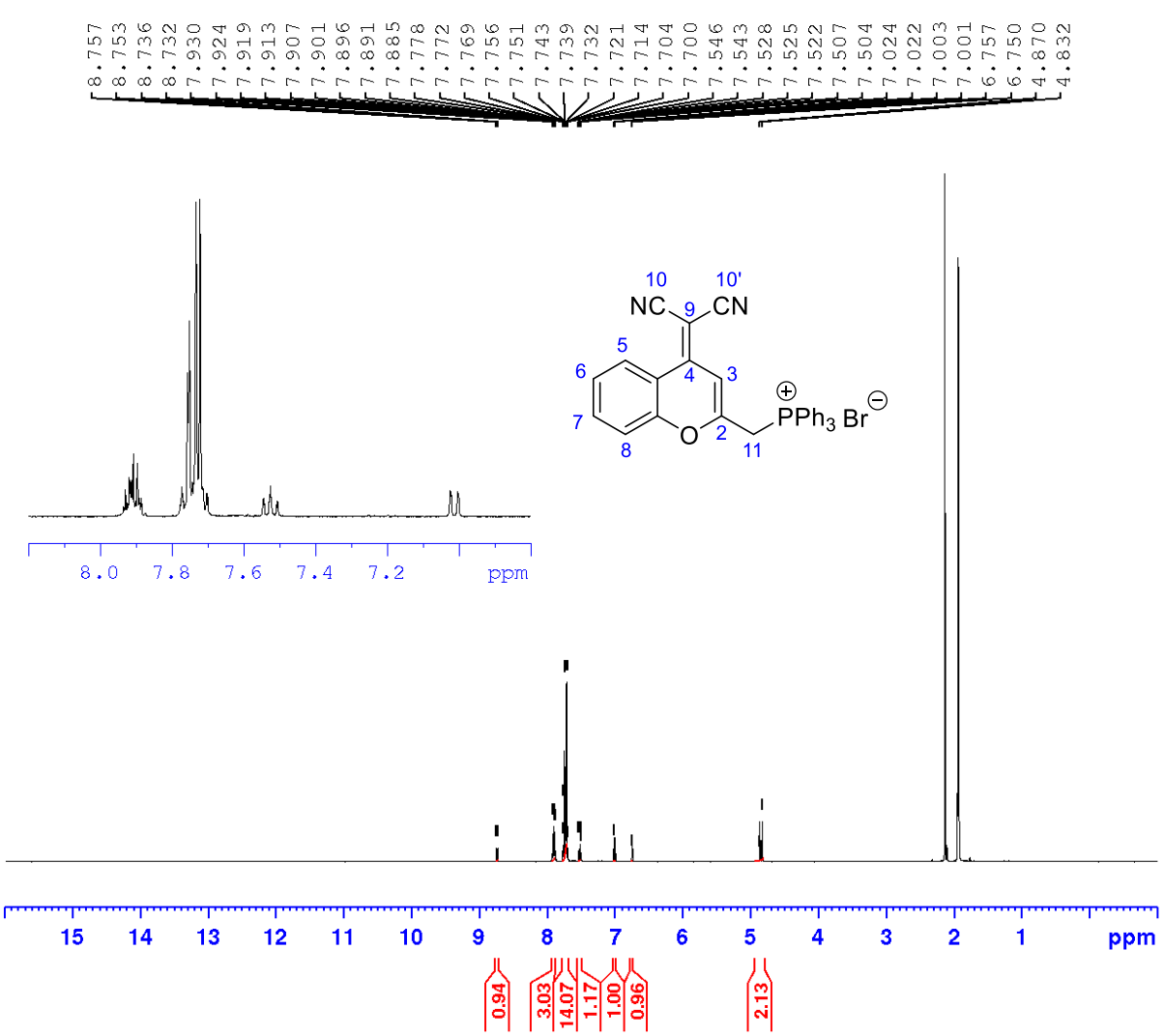



```
Current Data Parameters
NAME                  CE478-1_1
EXPNO                         2
PROCNO                        1

F2 - Acquisition Parameters
Date_                 20180830
Time                      20.28 h
INSTRUM                  avh400
PROBHD    Z108618_0873 (
PULPROG                 zgpg30
TD                       32768
SOLVENT                  CDCl3
NS                         512
DS                           4
SWH                  26041.666 Hz
FIDRES                1.589457 Hz
AQ                    0.6291456 sec
RG                       197.18
DW                       19.200 usec
DE                         6.50 usec
TE                        300.7 K
D1                   1.00000000 sec
D11                  0.03000000 sec
TD0                          1
SFO1                100.6228298 MHz
NUC1                        13C
P1                       10.00 usec
PLW1                47.86100006 W
SFO2                400.1316005 MHz
NUC2                        1H
CPDPRG[2                waltz16
PCPD2                    90.00 usec
PLW2                14.36999989 W
PLW12                0.34660661 W
PLW13                0.17371930 W

F2 - Processing parameters
SI                       32768
SF                  100.6127685 MHz
WDW                         EM
SSB          0
LB                        1.00 Hz
GB           0
PC                        1.40
```

^{1}H NMR spectrum of ((4-(Dicyanomethylene)-4*H*-chromen-2-yl)methyl)triphenylphosphonium bromide (190)

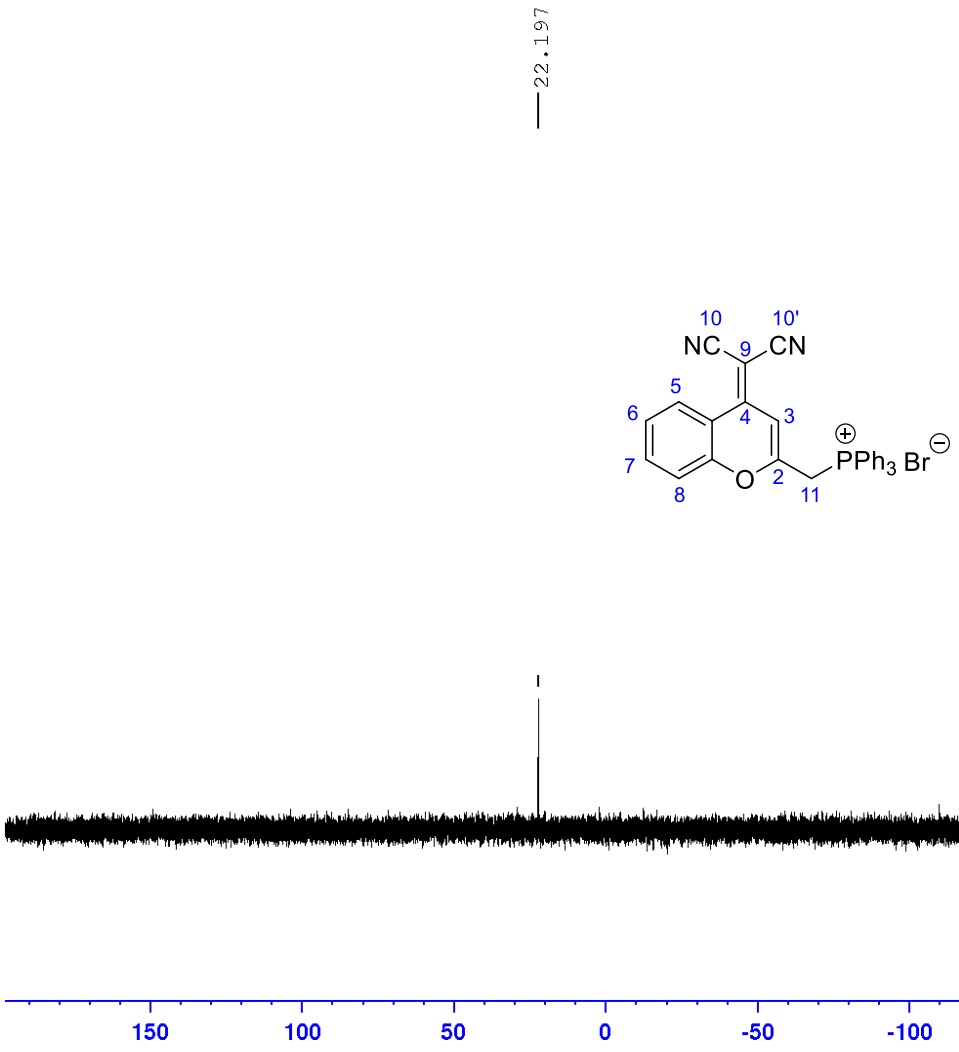



```
Current Data Parameters
NAME      CE459-PPT_MeCN
EXPNO                  1
PROCNO                 1

F2 - Acquisition Parameters
Date_           20170410
Time              10.11 h
INSTRUM           avh400
PROBHD   Z108618_0873 (
PULPROG            zg60
TD                65536
SOLVENT           CD3CN
NS                   16
DS                    2
SWH            8012.820 Hz
FIDRES         0.244532 Hz
AQ             4.0894465 sec
RG                197.18
DW                62.400 usec
DE                 6.50 usec
TE                295.4 K
D1           1.00000000 sec
TD0                   1
SFO1         400.1324008 MHz
NUC1                 1H
P1                14.00 usec
PLW1         14.36999989 W

F2 - Processing parameters
SI                32768
SF           400.1300115 MHz
WDW                  EM
SSB       0
LB                0.30 Hz
GB        0
PC                1.00
```

^{31}P NMR spectrum of ((4-(Dicyanomethylene)-4*H*-chromen-2-yl)methyl)triphenylphosphonium bromide (190)

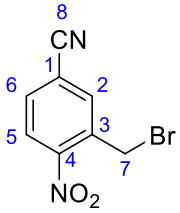


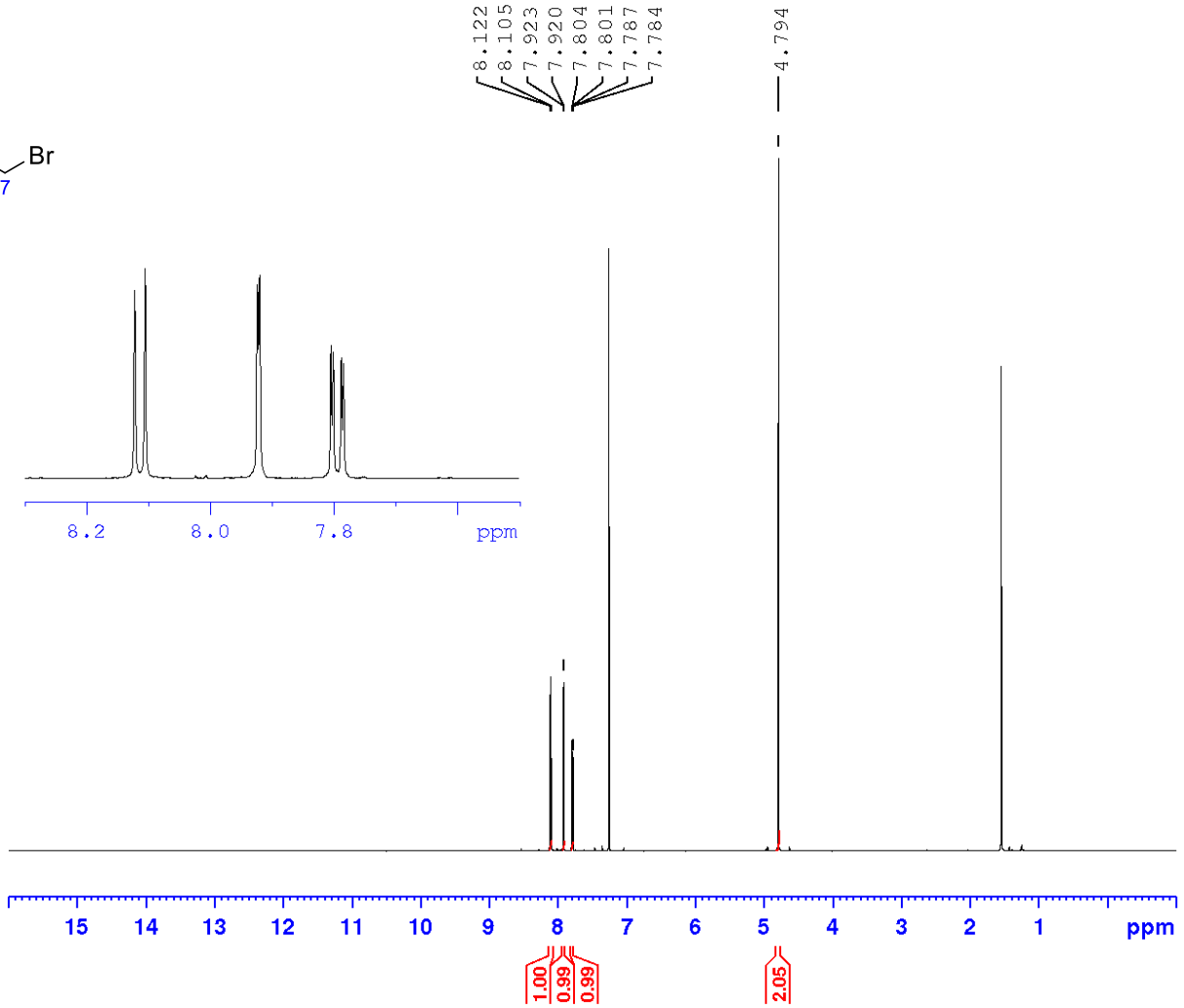

```
Current Data Parameters
NAME      CE459-PPT_MeCN
EXPNO                  2
PROCNO                 1

F2 - Acquisition Parameters
Date_           20170410
Time              10.14 h
INSTRUM           avh400
PROBHD   Z108618_0873 (
PULPROG           zgpg30
TD                131072
SOLVENT            CD3CN
NS                    16
DS                     4
SWH            64102.563 Hz
FIDRES          0.978127 Hz
AQ             1.0223616 sec
RG                197.18
DW                 7.800 usec
DE                 6.50 usec
TE                295.9 K
D1           2.00000000 sec
D11          0.03000000 sec
TD0                    1
SFO1         161.9755930 MHz
NUC1                31P
P1                15.00 usec
PLW1         13.93799973 W
SFO2         400.1316005 MHz
NUC2                1H
CPDPRG[2         waltz16
PCPD2             90.00 usec
PLW2         14.36999989 W
PLW12         0.34660661 W
PLW13         0.17371930 W

F2 - Processing parameters
SI                 65536
SF           161.9755930 MHz
WDW                  EM
SSB       0
LB                 1.00 Hz
GB        0
PC                 1.40
```

^{1}H NMR spectrum of 3-(Bromomethyl)-4-nitrobenzonitrile (215)





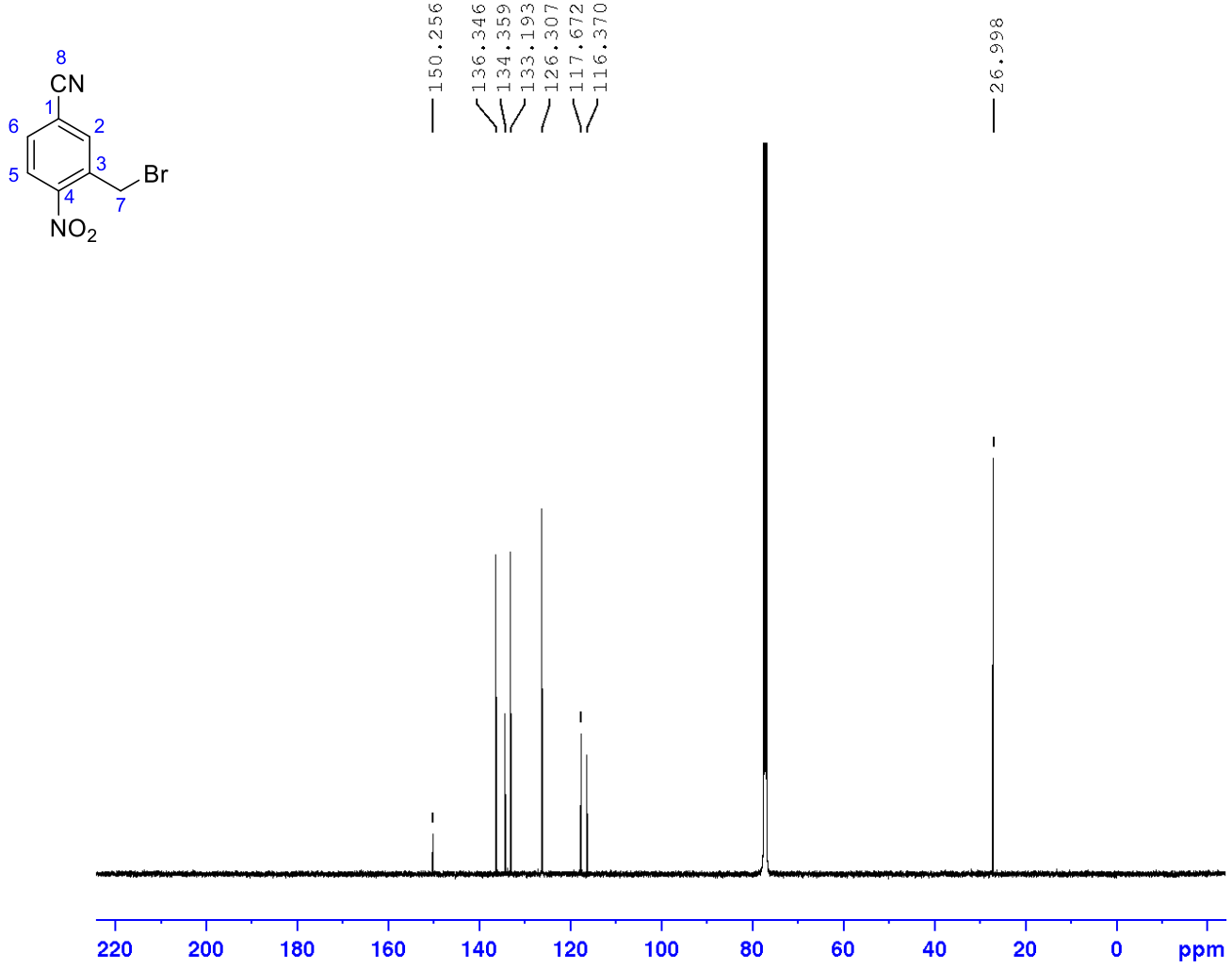

```
Current Data Parameters
NAME      CE550-monobromo_500
EXPNO                   1
PROCNO                  1

F2 - Acquisition Parameters
Date_           20171204
Time                9.55
INSTRUM          avc500
PROBHD   5 mm CPDUL 13C
PULPROG             zg30
TD                 65536
SOLVENT            CDCl3
NS                    16
DS                     4
SWH            10330.578 Hz
FIDRES          0.157632 Hz
AQ             3.1719425 sec
RG                     2
DW                48.400 usec
DE                10.00 usec
TE                298.0 K
D1            1.00000000 sec
TD0                    1

======== CHANNEL f1 ========
SFO1         500.3030896 MHz
NUC1                1H
P1                15.00 usec
PLW1          7.99830008 W

F2 - Processing parameters
SI                 65536
SF           500.3000138 MHz
WDW                   EM
SSB       0
LB                 0.30 Hz
GB        0
PC                 1.00
```

^{13}C NMR spectrum of 3-(Bromomethyl)-4-nitrobenzonitrile (215)




```
Current Data Parameters
NAME      CE550-monobromo_500
EXPNO                       4
PROCNO                      1

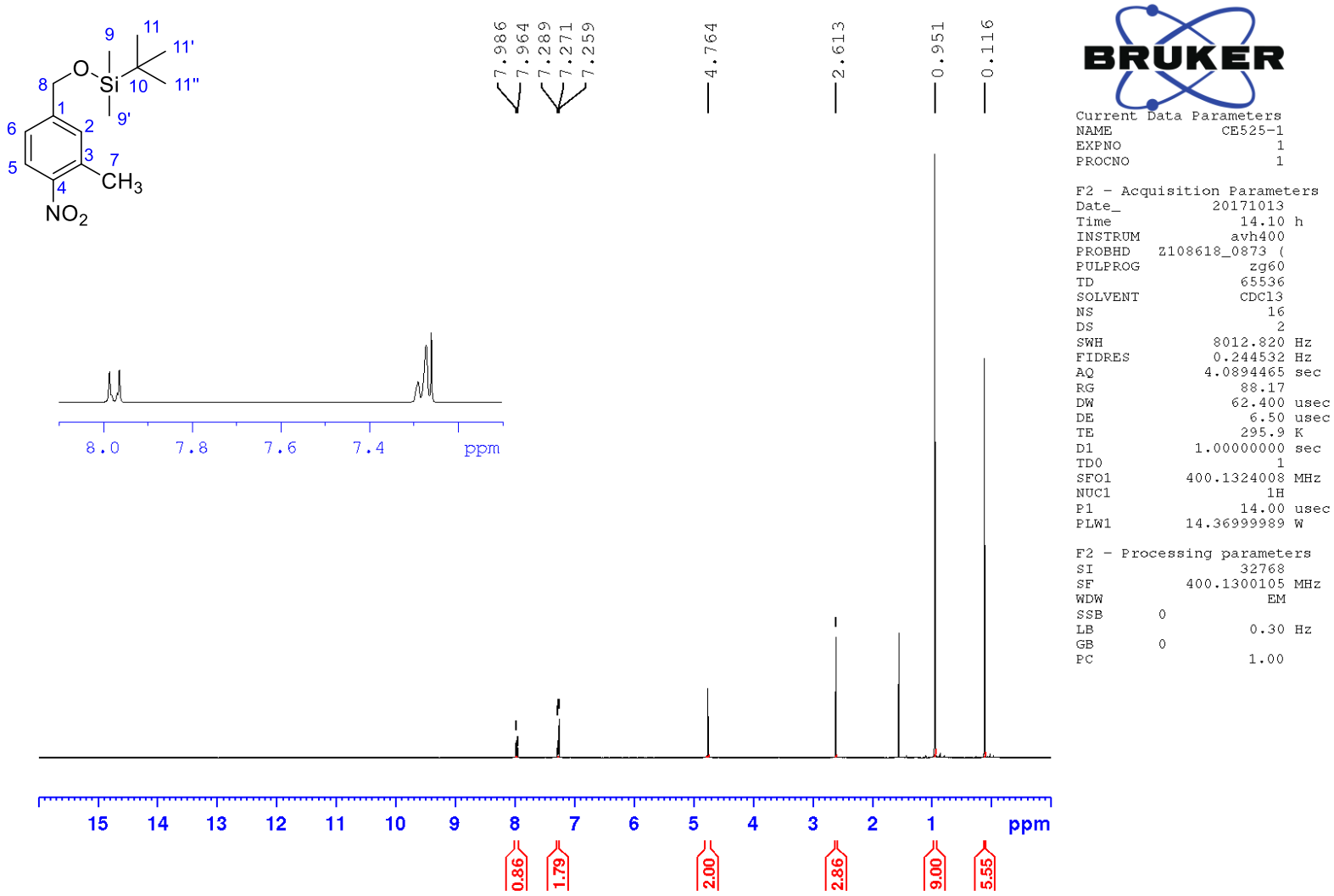
F2 - Acquisition Parameters
Date_           20171204
Time              10.41
INSTRUM           avc500
PROBHD   5 mm CPDUL 13C
PULPROG           zgpg30
TD                65536
SOLVENT           CDCl3
NS                 1024
DS                    2
SWH           31250.000 Hz
FIDRES         0.476837 Hz
AQ            1.0485760 sec
RG                  912
DW               16.000 usec
DE               18.00 usec
TE               298.0 K
D1            2.00000000 sec
D11           0.03000000 sec
TD0                   1

======== CHANNEL f1 ========
SFO1         125.8131152 MHz
NUC1               13C
P1               10.00 usec
PLW1         20.18400002 W

======== CHANNEL f2 ========
SFO2         500.3020012 MHz
NUC2               1H
CPDPRG[2         waltz16
PCPD2             80.00 usec
PLW2          7.99830008 W
PLW12         0.28119001 W
PLW13         0.17996000 W

F2 - Processing parameters
SI                32768
SF           125.8005191 MHz
WDW                EM
SSB       0
LB               1.00 Hz
GB        0
PC               1.40
```

^{1}H NMR spectrum of *t*-Butyldimethyl((3-methyl-4-nitrobenzyl)oxy)silane (212)

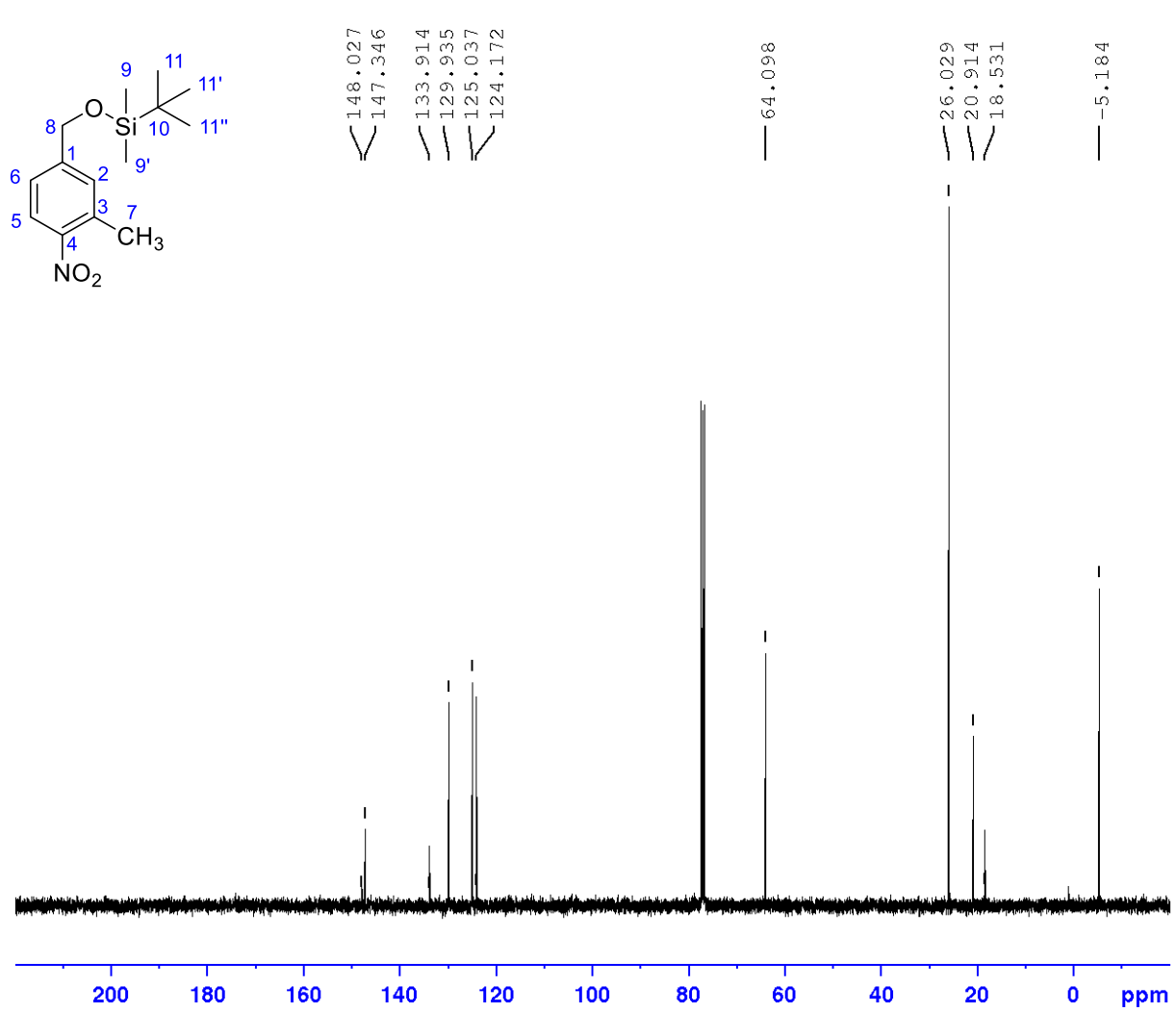



```
Current Data Parameters
NAME                  CE525-1
EXPNO                       1
PROCNO                      1

F2 - Acquisition Parameters
Date_              20171013
Time                  14.10 h
INSTRUM              avh400
PROBHD    Z108618_0873 (
PULPROG                zg60
TD                    65536
SOLVENT               CDCl3
NS                       16
DS                        2
SWH                8012.820 Hz
FIDRES            0.244532 Hz
AQ                4.0894465 sec
RG                    88.17
DW                   62.400 usec
DE                    6.50 usec
TE                   295.9 K
D1              1.00000000 sec
TD0                       1
SFO1           400.1324008 MHz
NUC1                    1H
P1                   14.00 usec
PLW1           14.36999989 W

F2 - Processing parameters
SI                    32768
SF               400.1300105 MHz
WDW                     EM
SSB          0
LB                    0.30 Hz
GB           0
PC                    1.00
```

^{13}C NMR spectrum of *t*-Butyldimethyl((3-methyl-4-nitrobenzyl)oxy)silane (212)

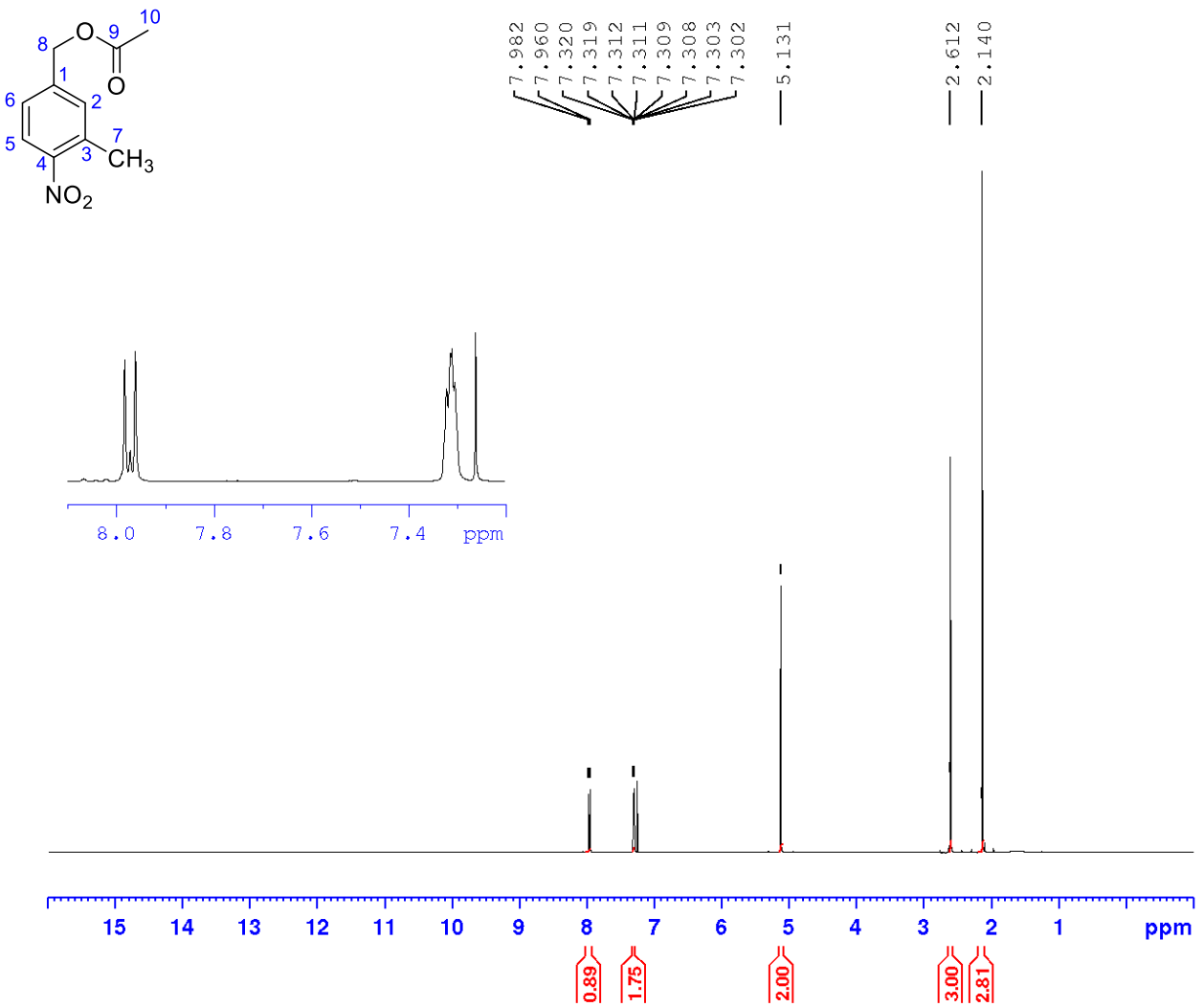



```
Current Data Parameters
NAME                  CE525-1_2
EXPNO                         2
PROCNO                        1

F2 - Acquisition Parameters
Date_                  20180808
Time                       5.09 h
INSTRUM                  avg400
PROBHD    Z108618_0816 (
PULPROG                  zgpg30
TD                        32768
SOLVENT                   CDCl3
NS                          256
DS                            4
SWH                   26041.666 Hz
FIDRES                 1.589457 Hz
AQ                    0.6291456 sec
RG                       206.87
DW                       19.200 usec
DE                         6.50 usec
TE                        301.4 K
D1                   1.00000000 sec
D11                  0.03000000 sec
TD0                           1
SFO1                100.6404331 MHz
NUC1                        13C
P1                        10.00 usec
PLW1                56.00000000 W
SFO2                400.2016008 MHz
NUC2                        1H
CPDPRG[2                waltz16
PCPD2                     90.00 usec
PLW2                14.00000000 W
PLW12                0.33877000 W
PLW13                0.17039999 W

F2 - Processing parameters
SI                        32768
SF                  100.6303553 MHz
WDW                         EM
SSB          0
LB                        1.00 Hz
GB           0
PC                        1.40
```

^{1}H NMR spectrum of 3-Methyl-4-nitrobenzyl acetate (213)



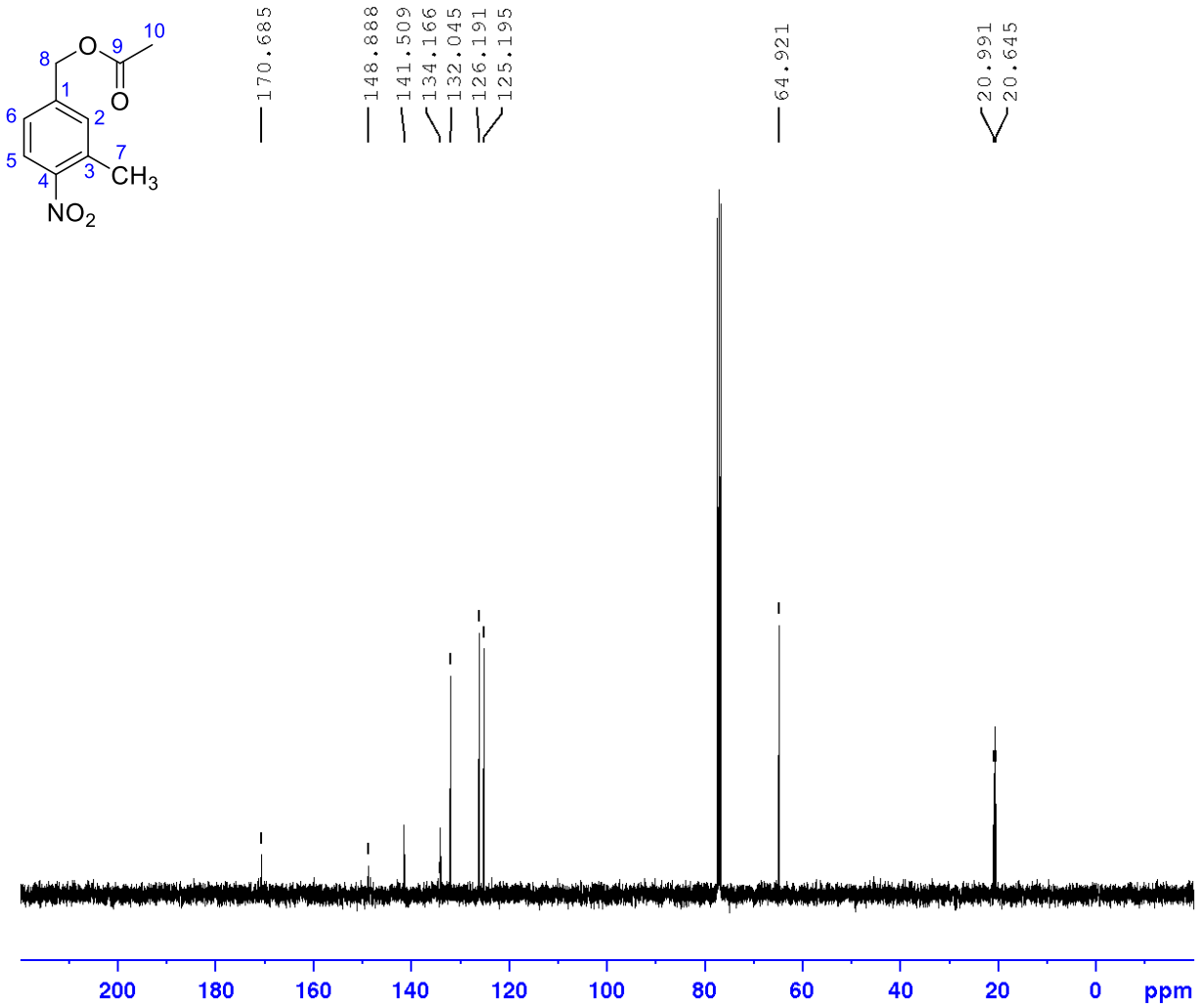
BRUKER

```
Current Data Parameters
NAME            CE529-1_2
EXPNO                   1
PROCNO                  1

F2 - Acquisition Parameters
Date_           20180808
Time                4.48 h
INSTRUM           avg400
PROBHD   Z108618_0816 (
PULPROG             zg60
TD                 65536
SOLVENT            CDCl3
NS                    16
DS                     2
SWH             8012.820 Hz
FIDRES          0.244532 Hz
AQ              4.0894465 sec
RG                 91.39
DW                62.400 usec
DE                 6.50 usec
TE                300.4 K
D1             1.00000000 sec
TD0                    1
SFO1          400.2024012 MHz
NUC1                  1H
P1                14.00 usec
PLW1          14.00000000 W

F2 - Processing parameters
SI                 32768
SF            400.2000100 MHz
WDW                   EM
SSB       0
LB                 0.30 Hz
GB        0
PC                 1.00
```

^{13}C NMR spectrum of 3-Methyl-4-nitrobenzyl acetate (213)

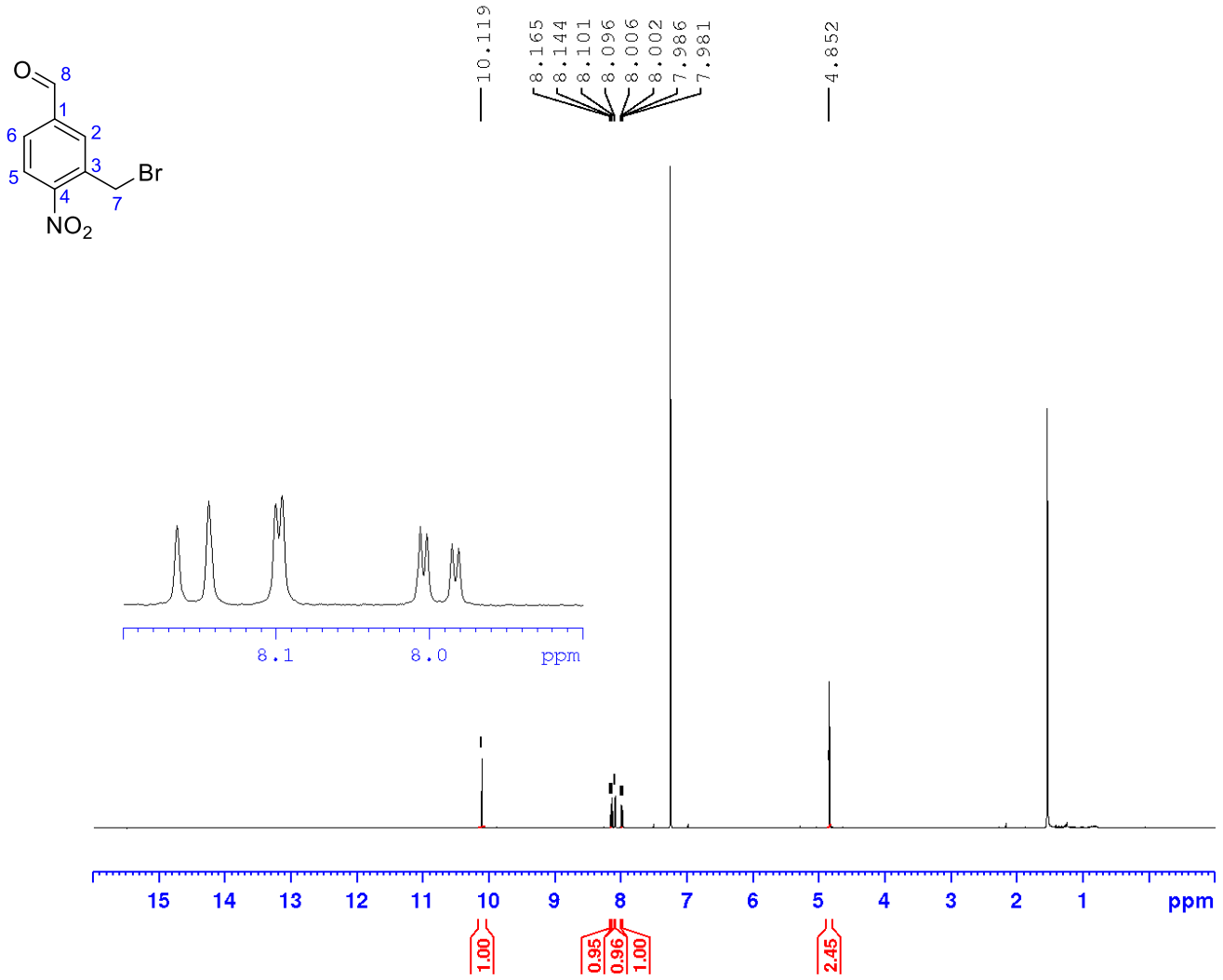



```
Current Data Parameters
NAME            CE529-1_2
EXPNO                   2
PROCNO                  1

F2 - Acquisition Parameters
Date_            20180808
Time                4.56 h
INSTRUM           avg400
PROBHD    Z108618_0816 (
PULPROG           zgpg30
TD                32768
SOLVENT           CDCl3
NS                  256
DS                    4
SWH           26041.666 Hz
FIDRES         1.589457 Hz
AQ            0.6291456 sec
RG               206.87
DW               19.200 usec
DE                6.50 usec
TE               301.3 K
D1           1.00000000 sec
D11          0.03000000 sec
TD0                   1
SFO1        100.6404331 MHz
NUC1                13C
P1                10.00 usec
PLW1        56.00000000 W
SFO2        400.2016008 MHz
NUC2                1H
CPDPRG[2         waltz16
PCPD2             90.00 usec
PLW2        14.00000000 W
PLW12        0.33877000 W
PLW13        0.17039999 W

F2 - Processing parameters
SI                32768
SF          100.6303559 MHz
WDW                 EM
SSB       0
LB                1.00 Hz
GB        0
PC                1.40
```

^{1}H NMR spectrum of 3-(Bromomethyl)-4-nitrobenzaldehyde (216)

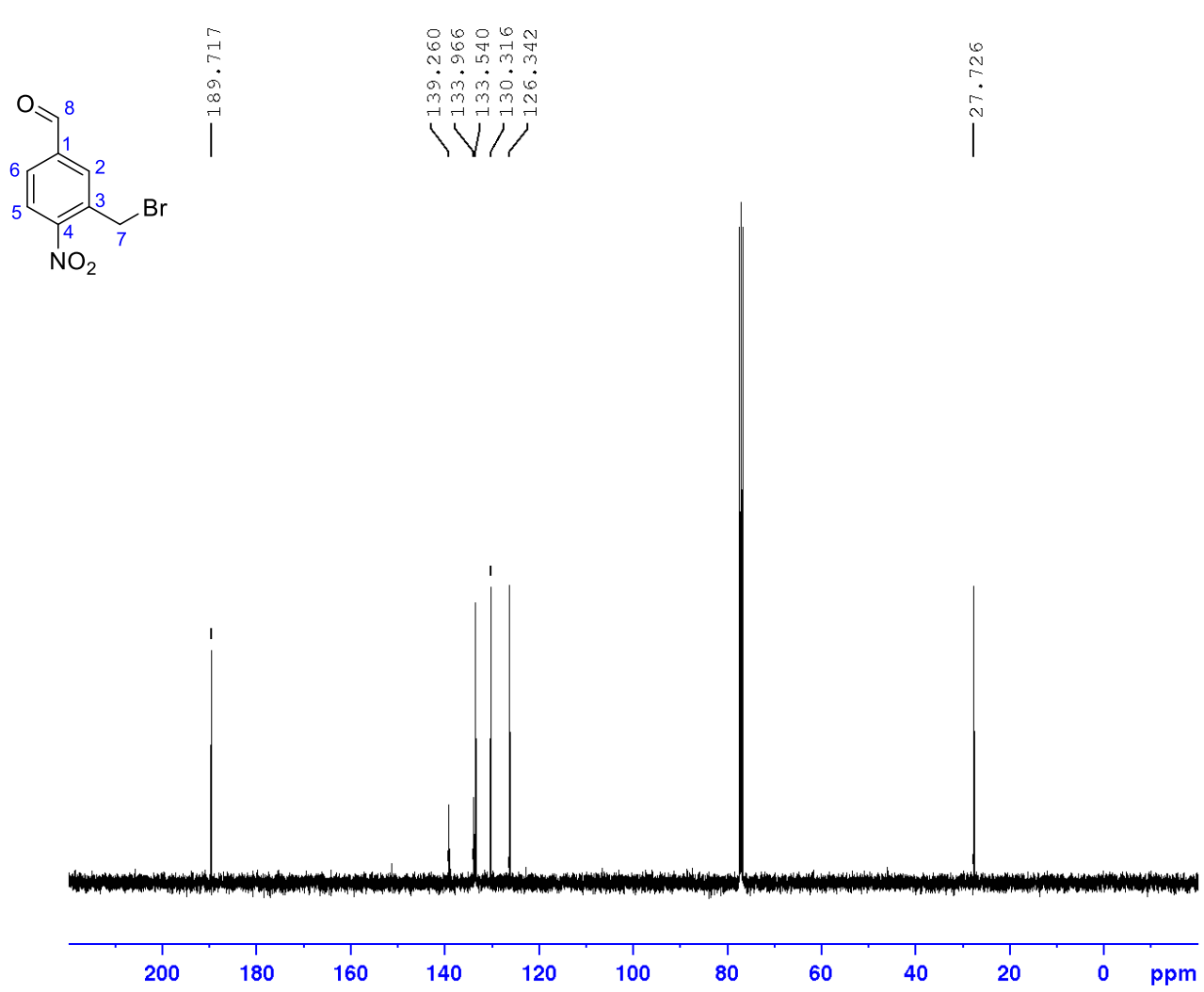



```
Current Data Parameters
NAME            CE543-1_1
EXPNO                   1
PROCNO                  1

F2 - Acquisition Parameters
Date_           20171117
Time               15.54 h
INSTRUM           avg400
PROBHD   Z108618_0816 (
PULPROG             zg60
TD                 65536
SOLVENT            CDCl3
NS                    16
DS                     2
SWH             8012.820 Hz
FIDRES          0.244532 Hz
AQ              4.0894465 sec
RG                 206.87
DW                 62.400 usec
DE                   6.50 usec
TE                  295.5 K
D1            1.00000000 sec
TD0                    1
SFO1          400.2024012 MHz
NUC1                  1H
P1                 14.00 usec
PLW1          14.00000000 W

F2 - Processing parameters
SI                 32768
SF            400.2000100 MHz
WDW                   EM
SSB       0
LB                  0.30 Hz
GB        0
PC                  1.00
```

^{13}C NMR spectrum of 3-(Bromomethyl)-4-nitrobenzaldehyde (216)

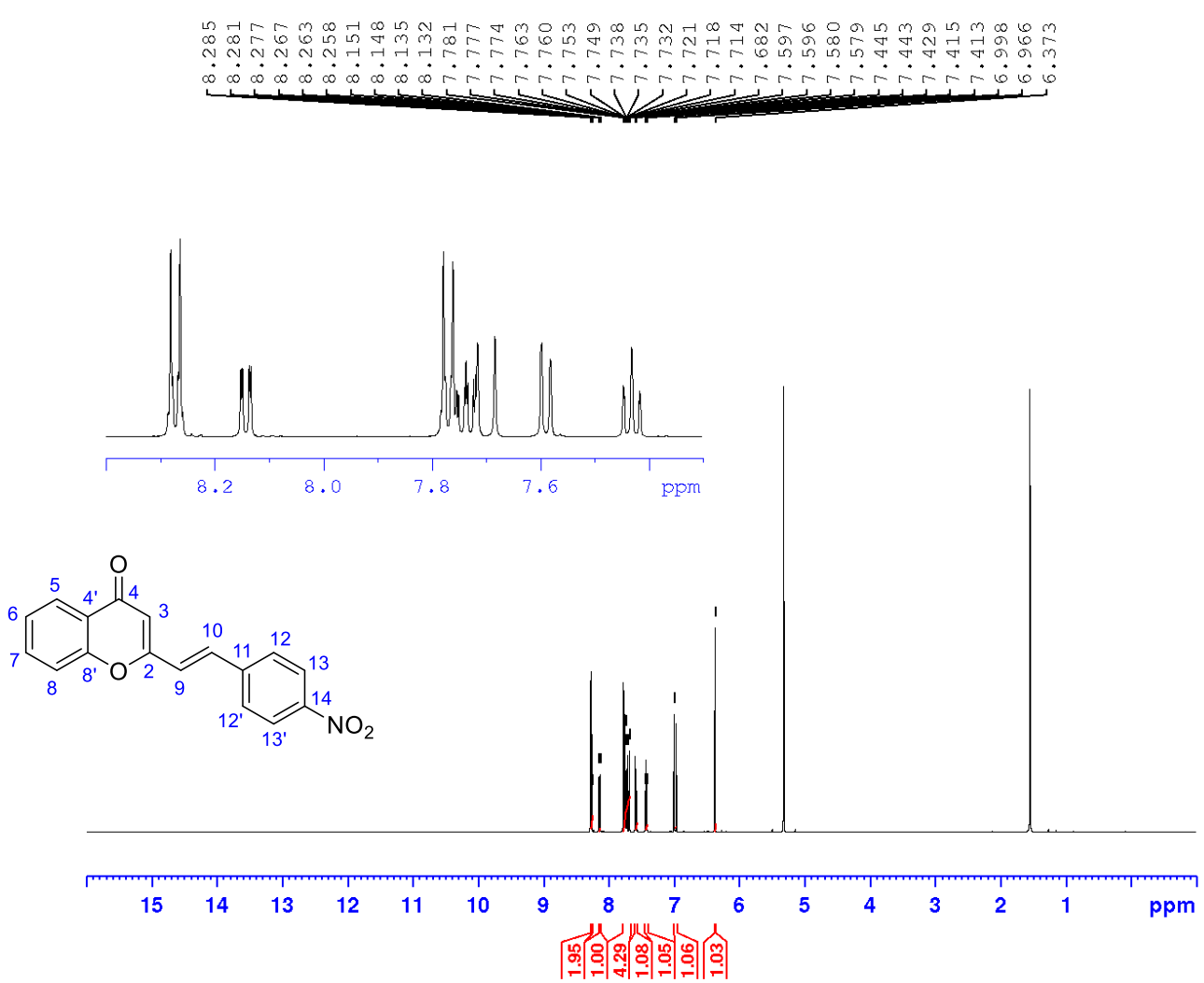



```
Current Data Parameters
NAME            CE543-1_2
EXPNO                   2
PROCNO                  1

F2 - Acquisition Parameters
Date_            20180809
Time                5.33 h
INSTRUM           avh400
PROBHD    Z108618_0873 (
PULPROG           zgpg30
TD                32768
SOLVENT           CDCl3
NS                  256
DS                    4
SWH           26041.666 Hz
FIDRES         1.589457 Hz
AQ            0.6291456 sec
RG               197.18
DW               19.200 usec
DE                6.50 usec
TE               301.6 K
D1           1.00000000 sec
D11          0.03000000 sec
TD0                   1
SFO1        100.6228298 MHz
NUC1                13C
P1                10.00 usec
PLW1        47.86100006 W
SFO2        400.1316005 MHz
NUC2                1H
CPDPRG[2         waltz16
PCPD2             90.00 usec
PLW2        14.36999989 W
PLW12        0.34660661 W
PLW13        0.17371930 W

F2 - Processing parameters
SI                32768
SF          100.6127555 MHz
WDW                 EM
SSB       0
LB                1.00 Hz
GB        0
PC                1.40
```

^{1}H NMR spectrum of (*E*)-2-(4-Nitrostyryl)-4*H*-chromen-4-one (181)



BRUKER

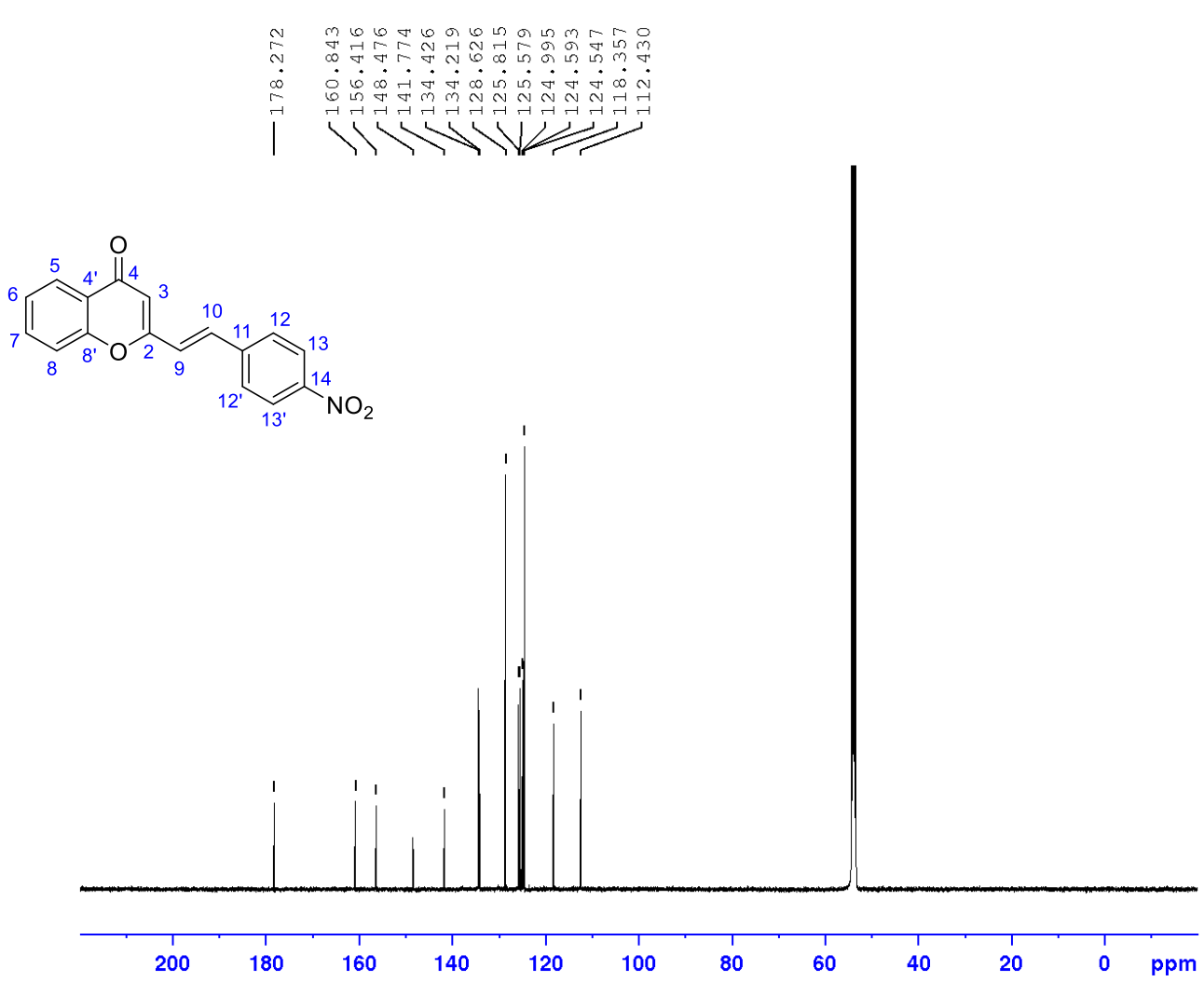
```
Current Data Parameters
NAME         CE536-2_500
EXPNO                  1
PROCNO                 1

F2 - Acquisition Parameters
Date_           20171107
Time               15.06
INSTRUM          avc500
PROBHD   5 mm CPDUL 13C
PULPROG             zg30
TD                 65536
SOLVENT          CD2Cl2
NS                   16
DS                    4
SWH           10330.578 Hz
FIDRES         0.157632 Hz
AQ            3.1719425 sec
RG                  3.56
DW                 48.400 usec
DE                 10.00 usec
TE                 298.0 K
D1            1.00000000 sec
TD0                    1

======== CHANNEL f1 ========
SFO1         500.3030896 MHz
NUC1                 1H
P1                15.00 usec
PLW1          7.99830008 W

F2 - Processing parameters
SI                 65536
SF           500.3000206 MHz
WDW                  EM
SSB       0
LB                 0.30 Hz
GB        0
PC                 1.00
```

^{13}C NMR spectrum of (*E*)-2-(4-Nitrostyryl)-4*H*-chromen-4-one (181)



BRUKER

```
Current Data Parameters
NAME         CE536-2_500
EXPNO                  4
PROCNO                 1

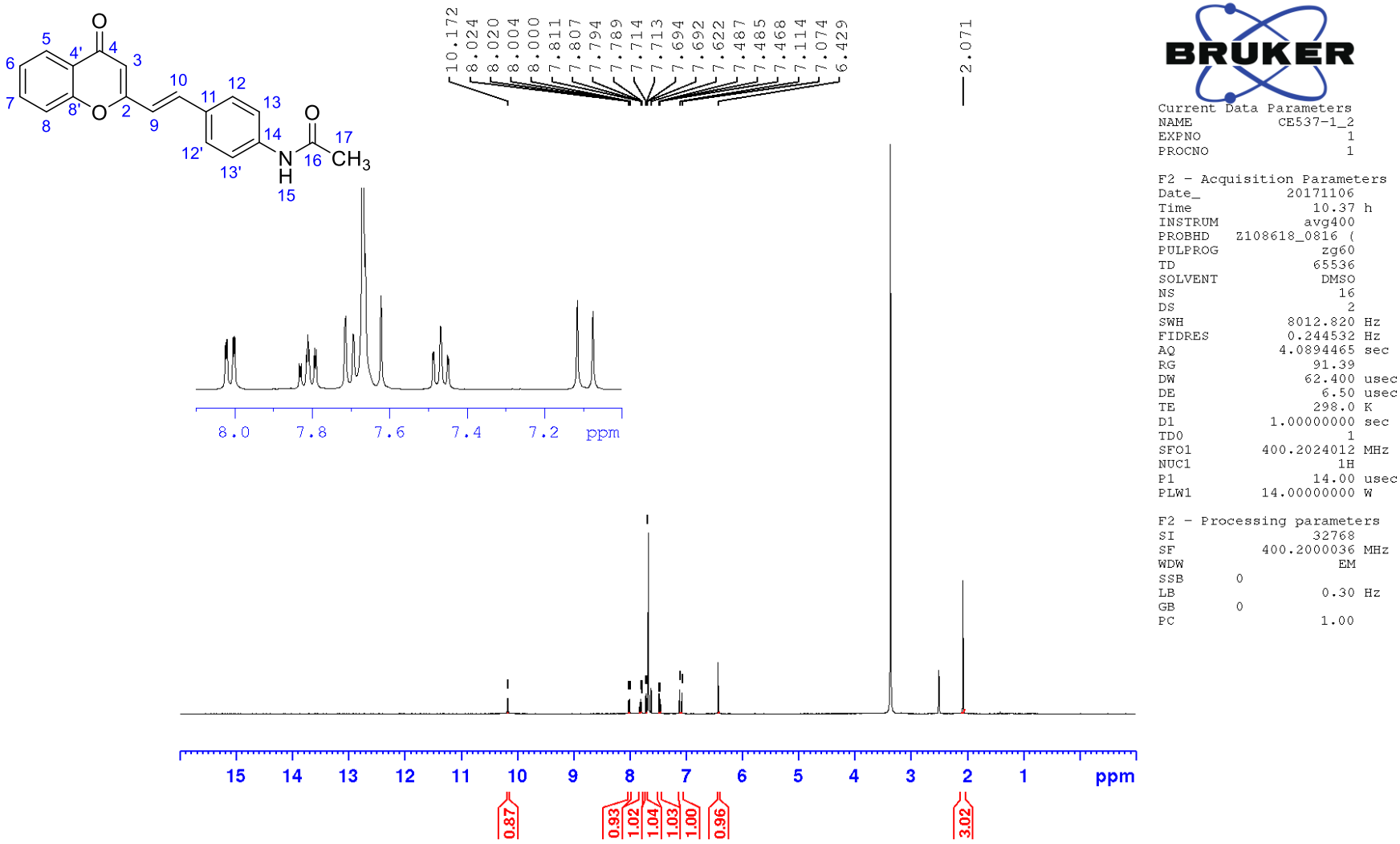
F2 - Acquisition Parameters
Date_           20171107
Time               18.05
INSTRUM          avc500
PROBHD   5 mm CPDUL 13C
PULPROG          zgpg30
TD                65536
SOLVENT          CD2Cl2
NS                 2048
DS                    2
SWH           31250.000 Hz
FIDRES         0.476837 Hz
AQ            1.0485760 sec
RG                  912
DW               16.000 usec
DE               18.00 usec
TE               298.0 K
D1            2.00000000 sec
D11           0.03000000 sec
TD0                   1

======== CHANNEL f1 ========
SFO1         125.8131152 MHz
NUC1                13C
P1                10.00 usec
PLW1         20.18400002 W

======== CHANNEL f2 ========
SFO2         500.3020012 MHz
NUC2                1H
CPDPRG[2         waltz16
PCPD2             80.00 usec
PLW2          7.99830008 W
PLW12         0.28119001 W
PLW13         0.17996000 W

F2 - Processing parameters
SI                 32768
SF           125.8004850 MHz
WDW                EM
SSB       0
LB                1.00 Hz
GB        0
PC                1.40
```

^{1}H NMR spectrum of (*E*)-*N*-(4-(2-(4-Oxo-4*H*-chromen-2-yl)vinyl)phenyl)acetamide (203)

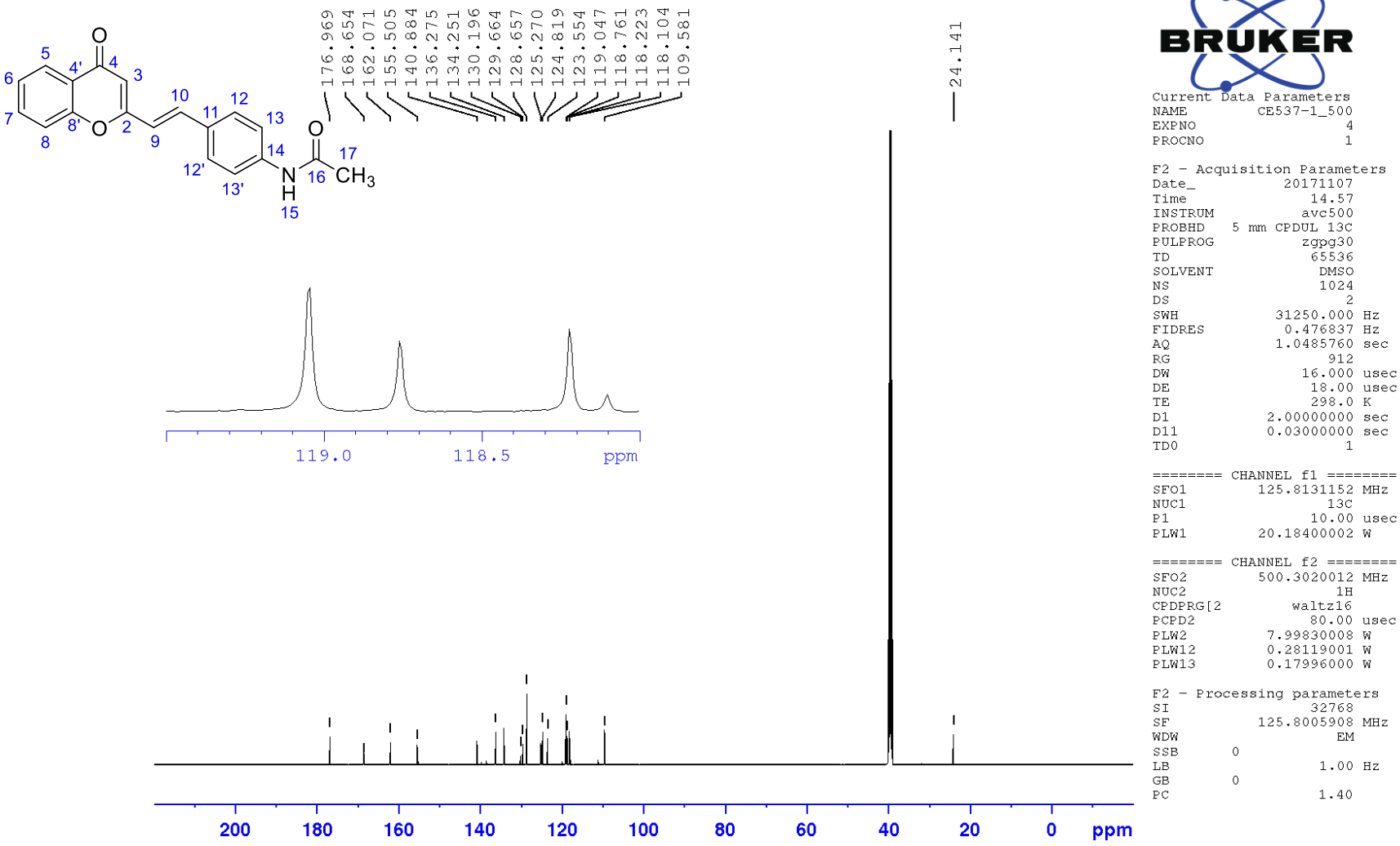



```
Current Data Parameters
NAME          CE537-1_2
EXPNO                 1
PROCNO                1

F2 - Acquisition Parameters
Date_          20171106
Time              10.37 h
INSTRUM          avg400
PROBHD   Z108618_0816 (
PULPROG            zg60
TD                65536
SOLVENT            DMSO
NS                   16
DS                    2
SWH            8012.820 Hz
FIDRES         0.244532 Hz
AQ             4.0894465 sec
RG                91.39
DW                62.400 usec
DE                 6.50 usec
TE                298.0 K
D1            1.00000000 sec
TD0                   1
SFO1         400.2024012 MHz
NUC1                 1H
P1                14.00 usec
PLW1         14.00000000 W

F2 - Processing parameters
SI                32768
SF           400.2000036 MHz
WDW                  EM
SSB       0
LB                0.30 Hz
GB        0
PC                1.00
```

^{13}C NMR spectrum of (*E*)-*N*-(4-(2-(4-Oxo-4*H*-chromen-2-yl)vinyl)phenyl)acetamide (203)




```
Current Data Parameters
NAME          CE537-1_500
EXPNO                   4
PROCNO                  1

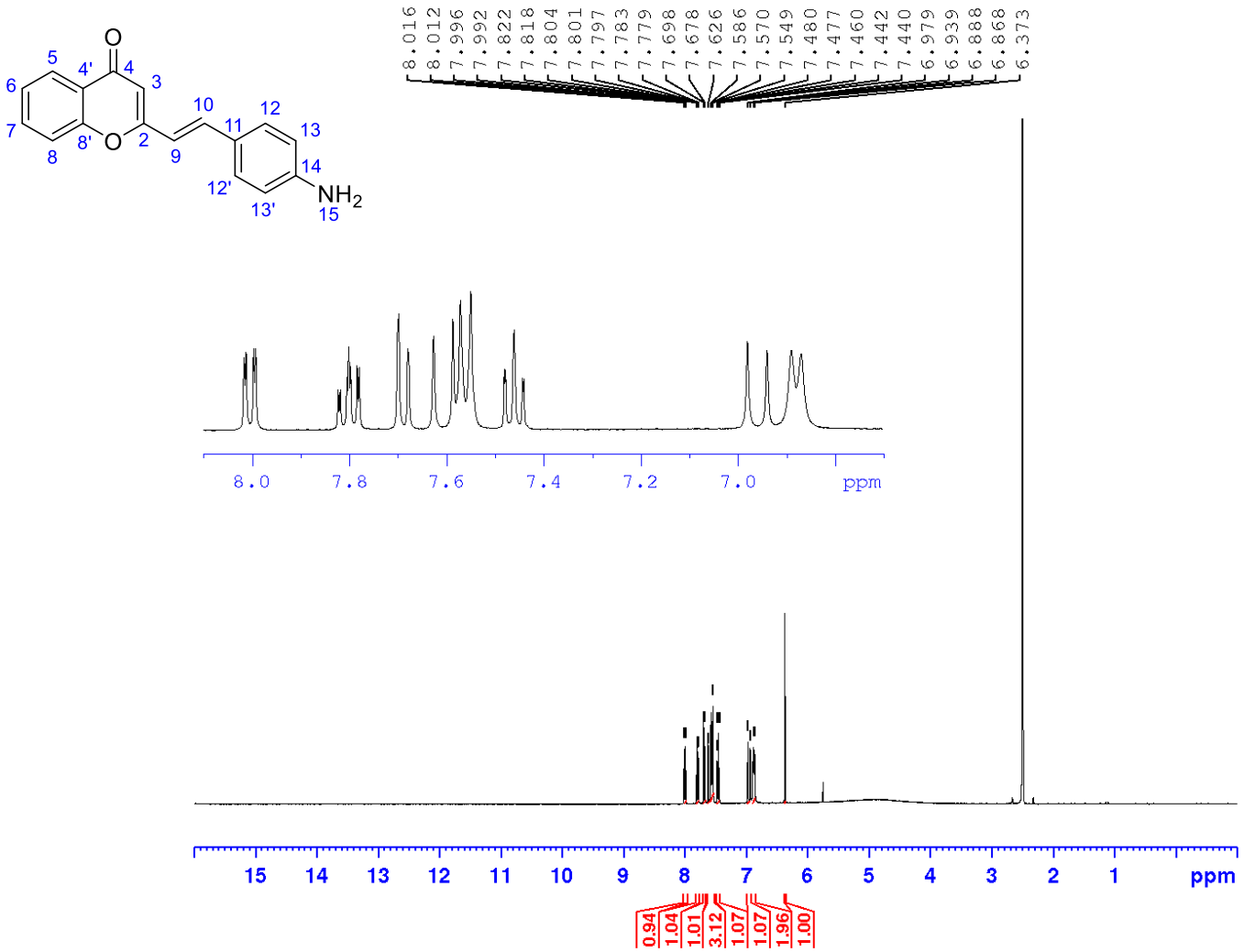
F2 - Acquisition Parameters
Date_           20171107
Time               14.57
INSTRUM          avc500
PROBHD   5 mm CPDUL 13C
PULPROG          zgpg30
TD                65536
SOLVENT             DMSO
NS                  1024
DS                     2
SWH            31250.000 Hz
FIDRES          0.476837 Hz
AQ             1.0485760 sec
RG                   912
DW                16.000 usec
DE                18.00 usec
TE                298.0 K
D1             2.00000000 sec
D11            0.03000000 sec
TD0                    1

======== CHANNEL f1 ========
SFO1         125.8131152 MHz
NUC1                  13C
P1                 10.00 usec
PLW1         20.18400002 W

======== CHANNEL f2 ========
SFO2         500.3020012 MHz
NUC2                  1H
CPDPRG[2         waltz16
PCPD2              80.00 usec
PLW2          7.99830008 W
PLW12         0.28119001 W
PLW13         0.17996000 W

F2 - Processing parameters
SI                 32768
SF           125.8005908 MHz
WDW                   EM
SSB       0
LB                 1.00 Hz
GB        0
PC                 1.40
```

^{1}H NMR spectrum of (*E*)-2-(4-Aminostyryl)-4*H*-chromen-4-one (182)

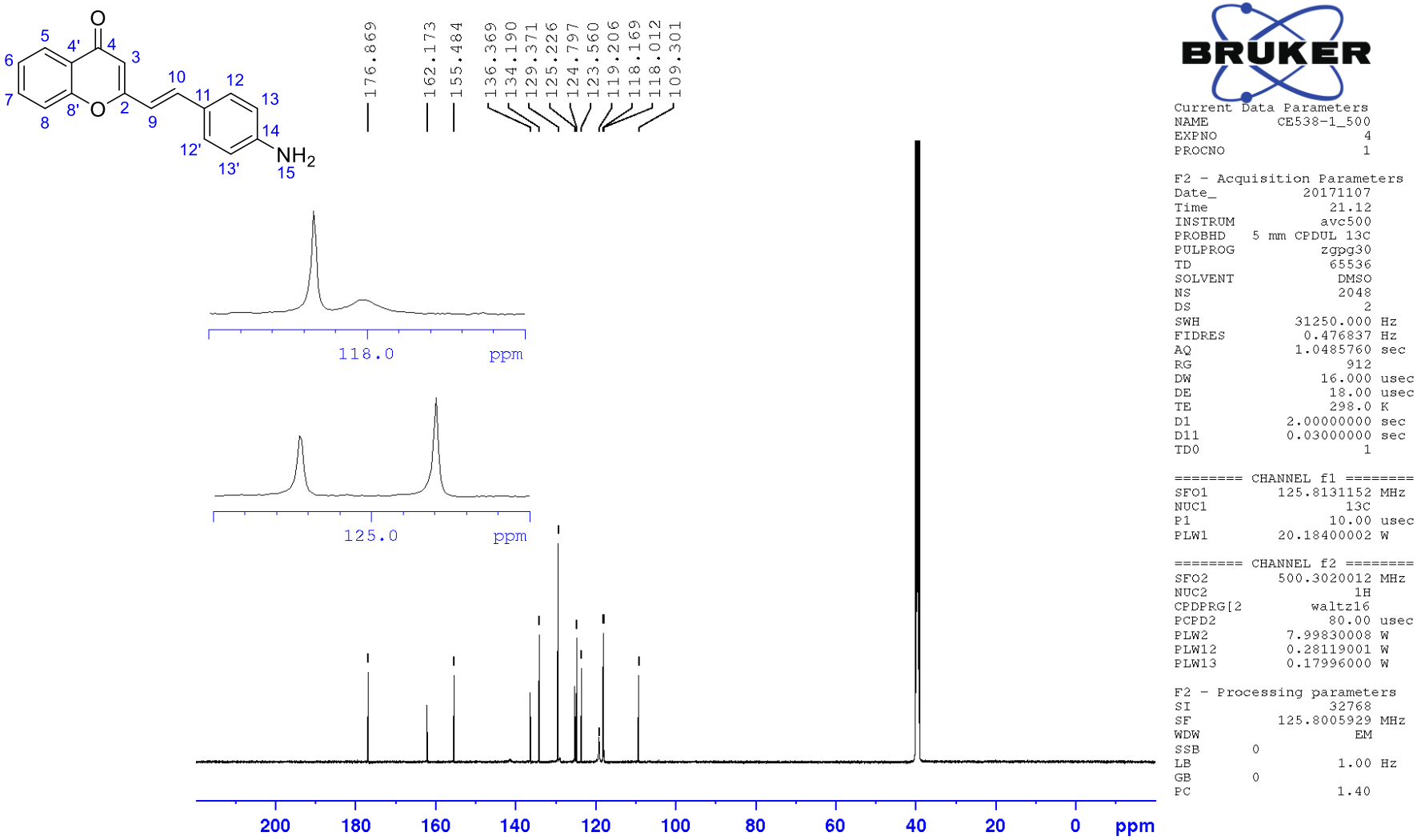



```
Current Data Parameters
NAME          CE538-1_DRY
EXPNO                   1
PROCNO                  1

F2 - Acquisition Parameters
Date_           20171103
Time               15.17 h
INSTRUM           avg400
PROBHD   Z108618_0816 (
PULPROG             zg60
TD                 65536
SOLVENT             DMSO
NS                    16
DS                     2
SWH             8012.820 Hz
FIDRES          0.244532 Hz
AQ             4.0894465 sec
RG                184.19
DW                62.400 usec
DE                 6.50 usec
TE                298.0 K
D1           1.00000000 sec
TD0                    1
SFO1         400.2024012 MHz
NUC1                  1H
P1                14.00 usec
PLW1         14.00000000 W

F2 - Processing parameters
SI                 32768
SF           400.2000036 MHz
WDW                   EM
SSB       0
LB                 0.30 Hz
GB        0
PC                 1.00
```

^{13}C NMR spectrum of (*E*)-2-(4-Aminostyryl)-4*H*-chromen-4-one (182)




```
Current Data Parameters
NAME         CE538-1_500
EXPNO                  4
PROCNO                 1

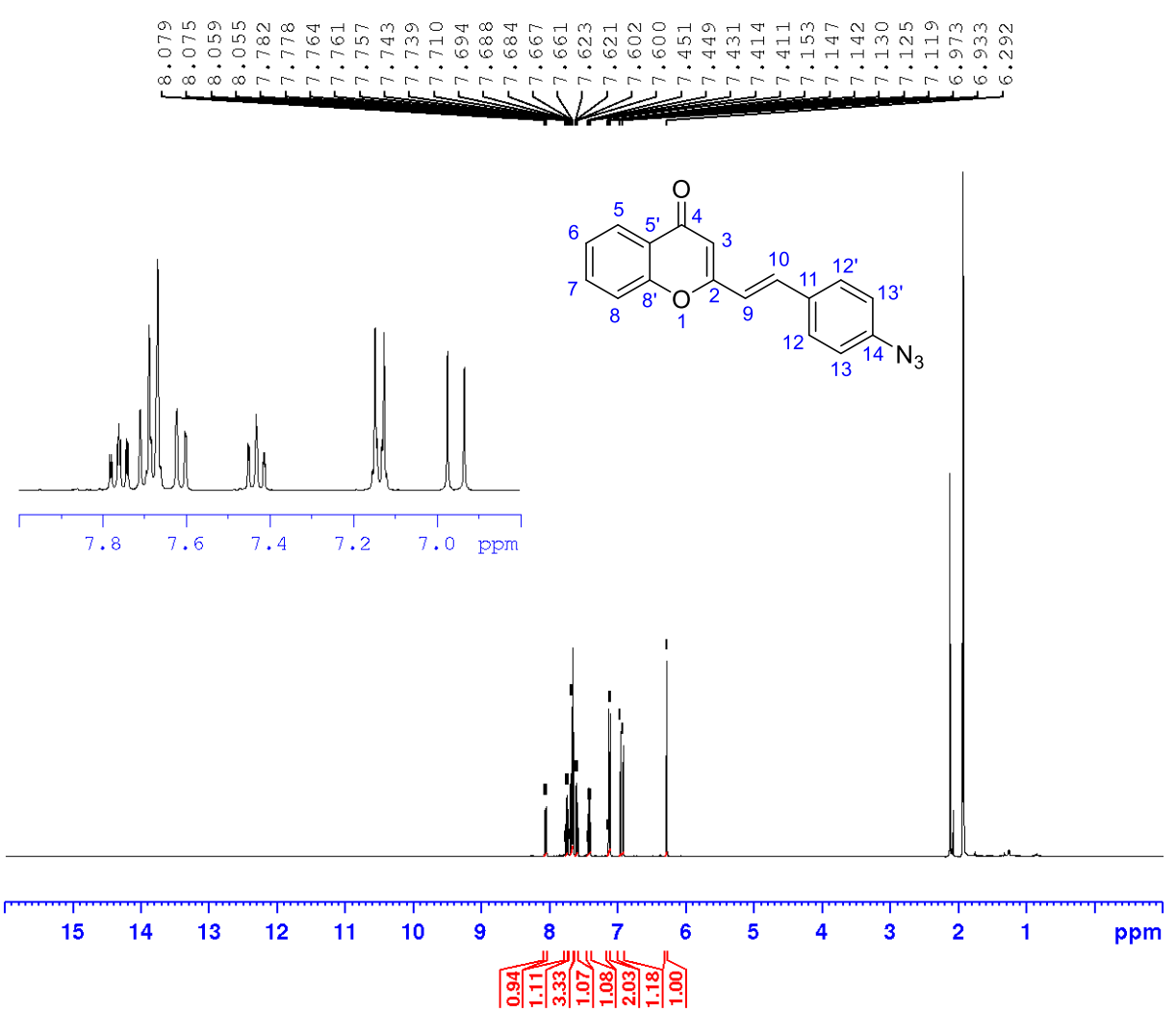
F2 - Acquisition Parameters
Date_           20171107
Time               21.12
INSTRUM          avc500
PROBHD   5 mm CPDUL 13C
PULPROG          zgpg30
TD                65536
SOLVENT             DMSO
NS                  2048
DS                     2
SWH            31250.000 Hz
FIDRES          0.476837 Hz
AQ             1.0485760 sec
RG                   912
DW                16.000 usec
DE                18.00 usec
TE                298.0 K
D1             2.00000000 sec
D11            0.03000000 sec
TD0                    1

======== CHANNEL f1 ========
SFO1         125.8131152 MHz
NUC1                  13C
P1                 10.00 usec
PLW1         20.18400002 W

======== CHANNEL f2 ========
SFO2         500.3020012 MHz
NUC2                  1H
CPDPRG[2         waltz16
PCPD2              80.00 usec
PLW2          7.99830008 W
PLW12         0.28119001 W
PLW13         0.17996000 W

F2 - Processing parameters
SI                 32768
SF           125.8005929 MHz
WDW                   EM
SSB       0
LB                 1.00 Hz
GB        0
PC                 1.40
```

^{1}H NMR spectrum of (*E*)-2-(4-Azidostyryl)-4*H*-chromen-4-one (204)



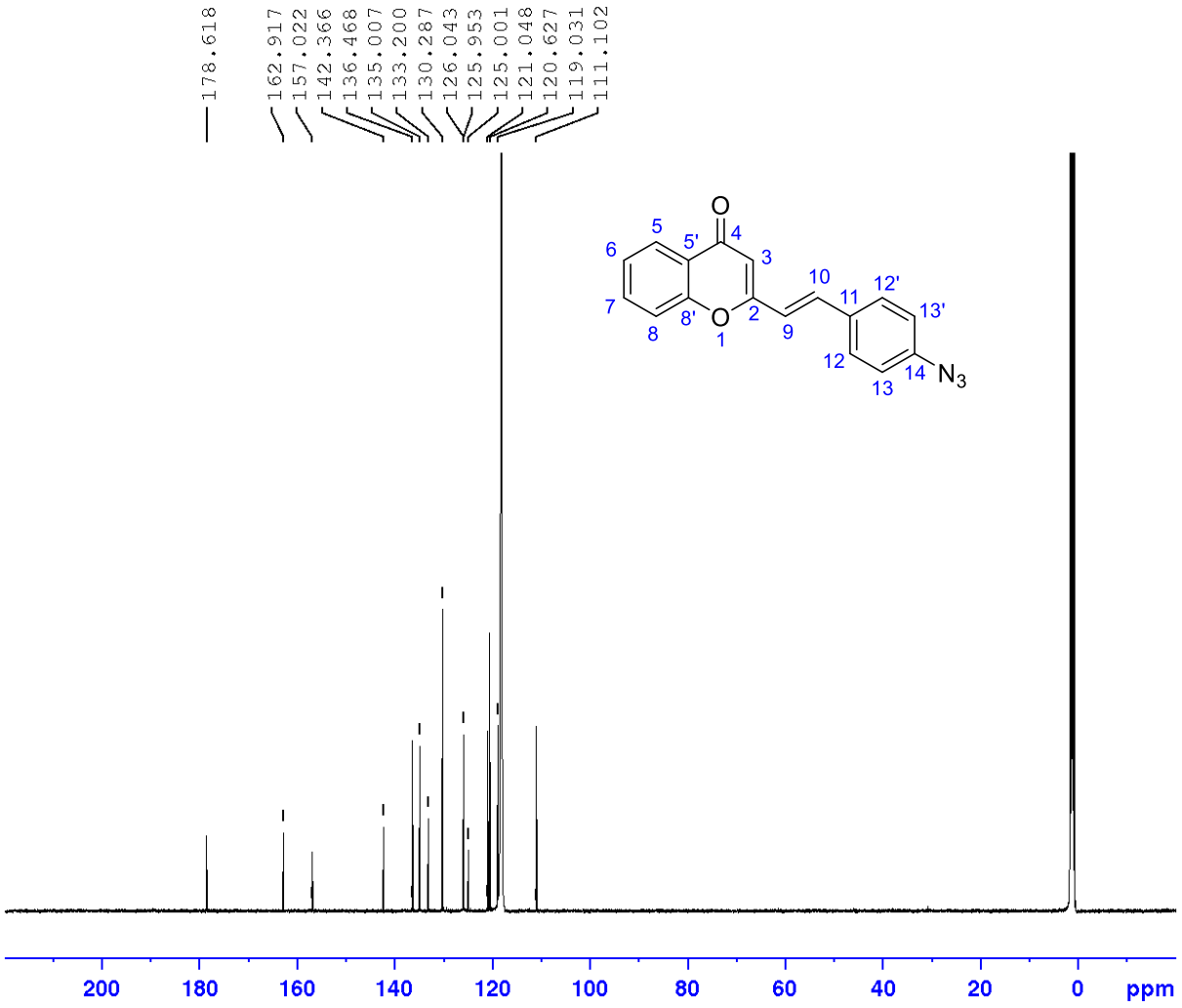
BRUKER

```
Current Data Parameters
NAME        CE549-1_MeCN
EXPNO                  1
PROCNO                 1

F2 - Acquisition Parameters
Date_           20171206
Time               10.20 h
INSTRUM           avh400
PROBHD   Z108618_0873 (
PULPROG            zg60
TD                65536
SOLVENT           CD3CN
NS                   16
DS                    2
SWH            8012.820 Hz
FIDRES         0.244532 Hz
AQ            4.0894465 sec
RG                88.17
DW              62.400 usec
DE               6.50 usec
TE              297.2 K
D1           1.00000000 sec
TD0                   1
SFO1        400.1324008 MHz
NUC1                 1H
P1                14.00 usec
PLW1        14.36999989 W

F2 - Processing parameters
SI                32768
SF          400.1300114 MHz
WDW                  EM
SSB       0
LB                0.30 Hz
GB        0
PC                1.00
```

^{13}C NMR spectrum of (*E*)-2-(4-Azidostyryl)-4*H*-chromen-4-one (204)




```
Current Data Parameters
NAME       CE549-1_500_2
EXPNO                  4
PROCNO                 1

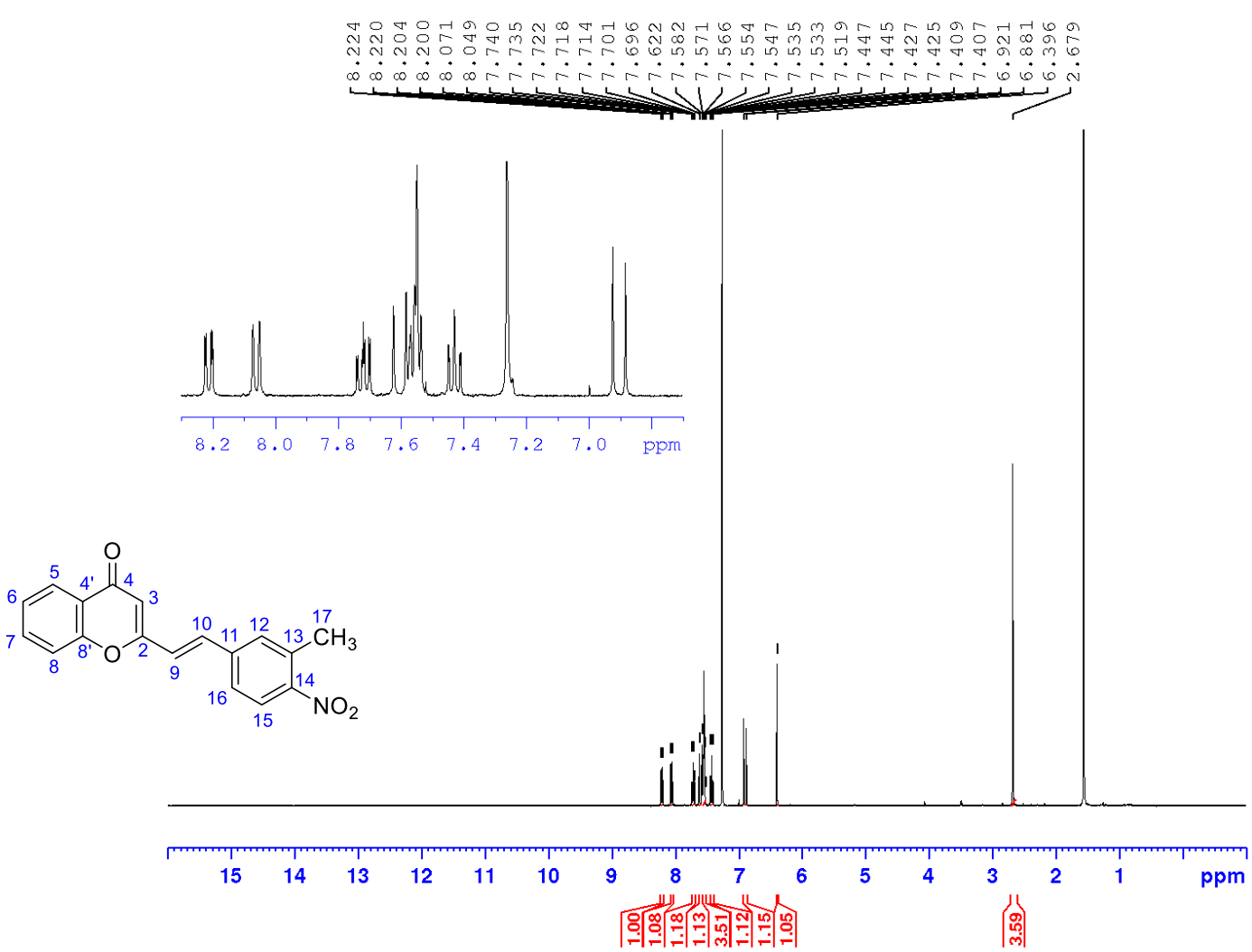
F2 - Acquisition Parameters
Date_           20171215
Time               11.51
INSTRUM          avc500
PROBHD   5 mm CPDUL 13C
PULPROG          zgpg30
TD                65536
SOLVENT           CD3CN
NS                 2048
DS                    2
SWH           31250.000 Hz
FIDRES         0.476837 Hz
AQ            1.0485760 sec
RG                  912
DW               16.000 usec
DE               18.00 usec
TE               298.0 K
D1            2.00000000 sec
D11           0.03000000 sec
TD0                   1

======== CHANNEL f1 ========
SFO1         125.8131152 MHz
NUC1                13C
P1                10.00 usec
PLW1         20.18400002 W

======== CHANNEL f2 ========
SFO2         500.3020012 MHz
NUC2                1H
CPDPRG[2         waltz16
PCPD2             80.00 usec
PLW2          7.99830008 W
PLW12         0.28119001 W
PLW13         0.17996000 W

F2 - Processing parameters
SI                 32768
SF           125.8004121 MHz
WDW                  EM
SSB       0
LB                1.00 Hz
GB        0
PC                1.40
```

^{1}H NMR spectrum of (*E*)-2-(3-Methyl-4-nitrostyryl)-4*H*-chromen-4-one (221)

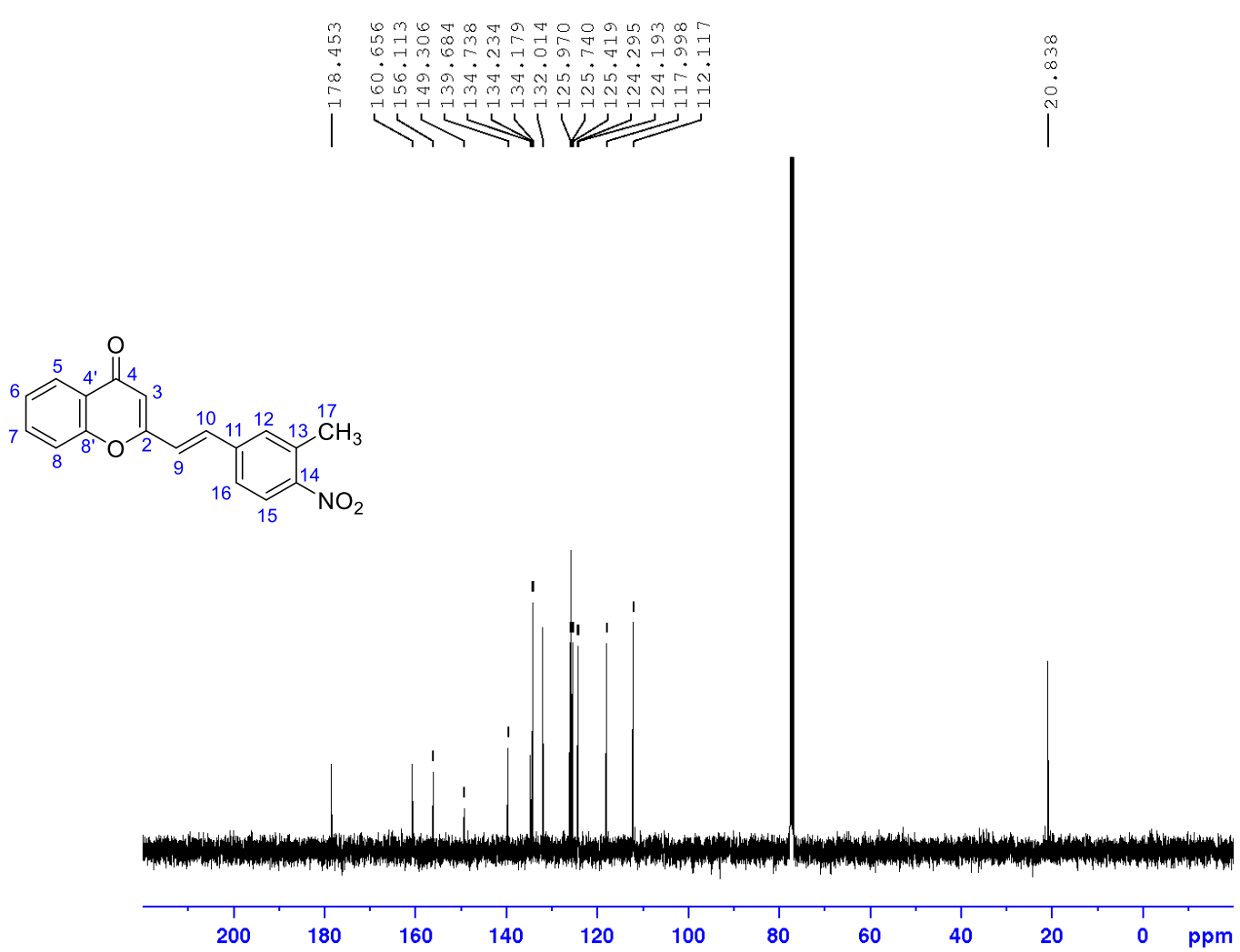



```
Current Data Parameters
NAME                  CE585-1
EXPNO                       1
PROCNO                      1

F2 - Acquisition Parameters
Date_              20180226
Time                  16.48 h
INSTRUM              avg400
PROBHD    Z108618_0816 (
PULPROG                zg60
TD                    65536
SOLVENT               CDCl3
NS                       16
DS                        2
SWH                8012.820 Hz
FIDRES            0.244532 Hz
AQ                4.0894465 sec
RG                   206.87
DW                   62.400 usec
DE                    6.50 usec
TE                   294.1 K
D1              1.00000000 sec
TD0                       1
SFO1           400.2024012 MHz
NUC1                    1H
P1                   14.00 usec
PLW1           14.00000000 W

F2 - Processing parameters
SI                    32768
SF             400.2000094 MHz
WDW                     EM
SSB         0
LB                    0.30 Hz
GB          0
PC                    1.00
```

^{13}C NMR spectrum of (*E*)-2-(3-Methyl-4-nitrostyryl)-4*H*-chromen-4-one (221)

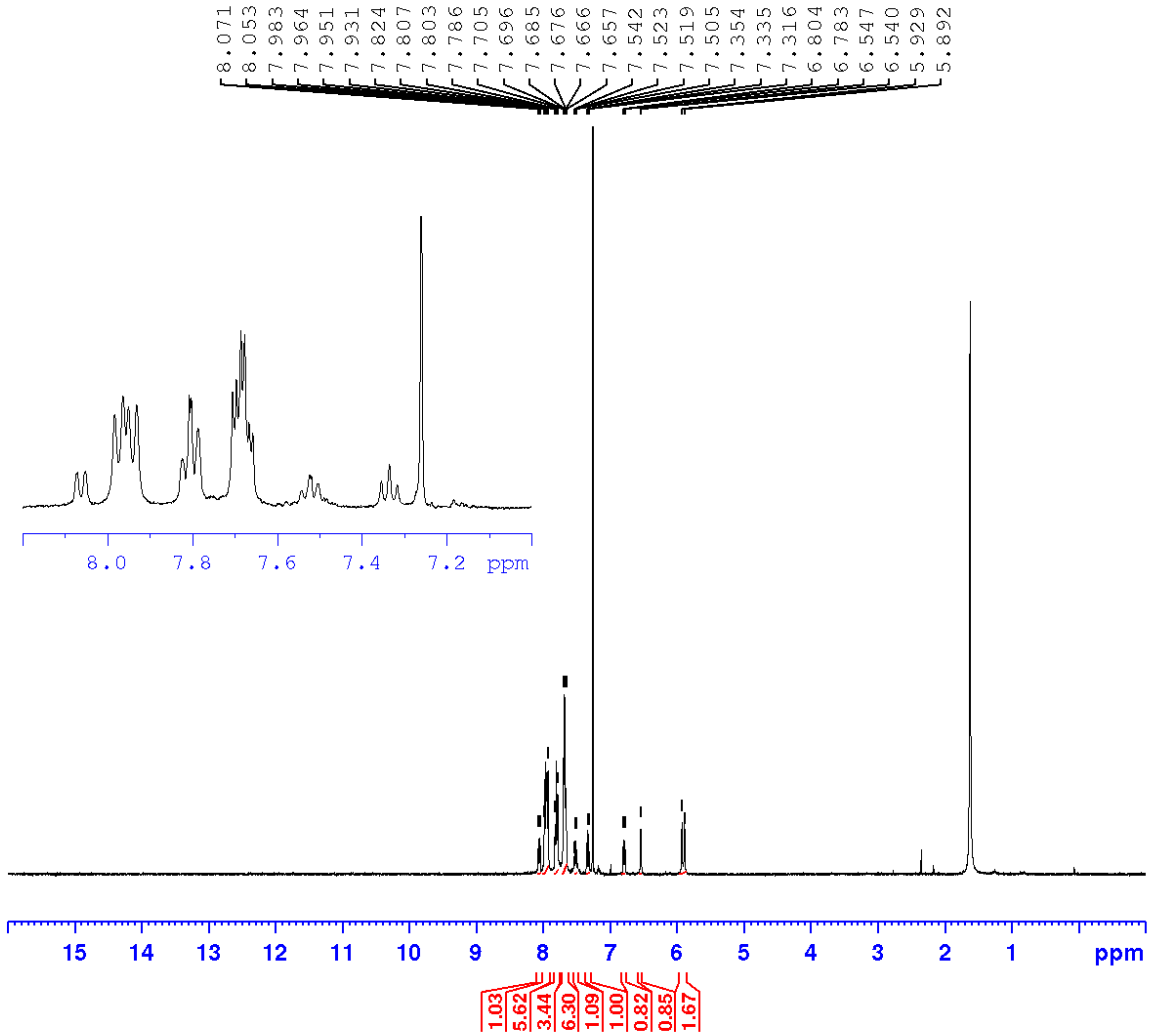



```
Current Data Parameters
NAME                  CE594-1_2
EXPNO                         2
PROCNO                        1

F2 - Acquisition Parameters
Date_                  20180810
Time                      21.43 h
INSTRUM                  avh400
PROBHD    Z108618_0873 (
PULPROG                 zgpg30
TD                       32768
SOLVENT                  CDCl3
NS                         512
DS                           4
SWH                  26041.666 Hz
FIDRES                1.589457 Hz
AQ                    0.6291456 sec
RG                       197.18
DW                       19.200 usec
DE                         6.50 usec
TE                        301.2 K
D1                  1.00000000 sec
D11                 0.03000000 sec
TD0                          1
SFO1               100.6228298 MHz
NUC1                        13C
P1                       10.00 usec
PLW1                47.86100006 W
SFO2                400.1316005 MHz
NUC2                        1H
CPDPRG[2                waltz16
PCPD2                    90.00 usec
PLW2                14.36999989 W
PLW12                0.34660661 W
PLW13                0.17371930 W

F2 - Processing parameters
SI                       32768
SF                 100.6127545 MHz
WDW                         EM
SSB       0
LB                        1.00 Hz
GB        0
PC                        1.40
```

^{1}H NMR spectrum of ((4-Oxo-4*H*-chromen-2-yl)methyl)triphenylphosphonium bromide (220)



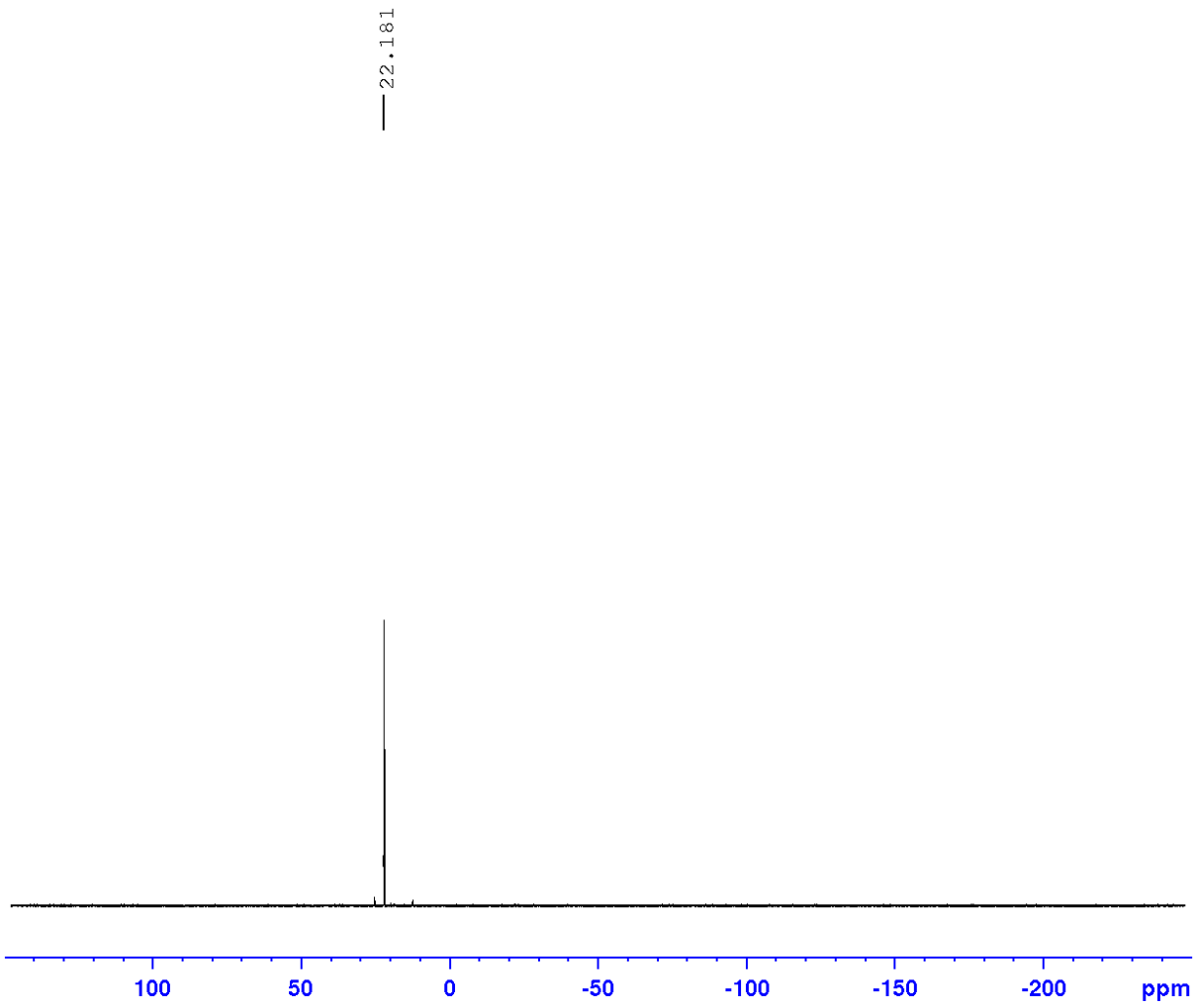
BRUKER

```
Current Data Parameters
NAME                  CE581-PPT
EXPNO                         1
PROCNO                        1

F2 - Acquisition Parameters
Date_                  20180220
Time                      11.38 h
INSTRUM                  avh400
PROBHD    Z108618_0873 (
PULPROG                   zg60
TD                       65536
SOLVENT                  CDCl3
NS                          16
DS                           2
SWH                    8012.820 Hz
FIDRES                 0.244532 Hz
AQ                     4.0894465 sec
RG                        197.18
DW                        62.400 usec
DE                         6.50 usec
TE                        295.6 K
D1                  1.00000000 sec
TD0                           1
SFO1                400.1324008 MHz
NUC1                        1H
P1                        14.00 usec
PLW1                14.36999989 W

F2 - Processing parameters
SI                        32768
SF                  400.1300101 MHz
WDW                          EM
SSB                0
LB                        0.30 Hz
GB                 0
PC                        1.00
```

^{31}P NMR spectrum of ((4-Oxo-4*H*-chromen-2-yl)methyl)triphenylphosphonium bromide (220)

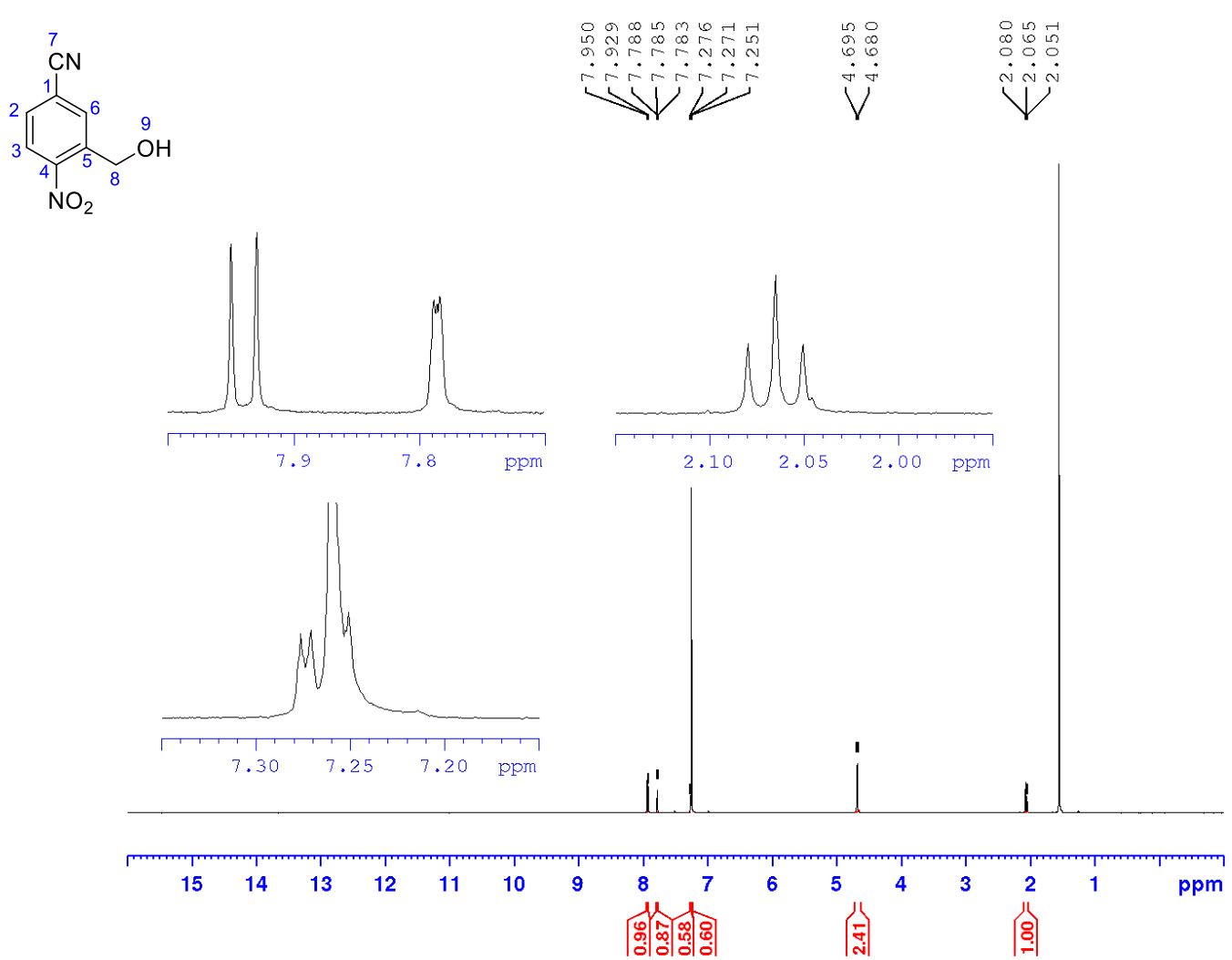



```
Current Data Parameters
NAME                  CE581-1
EXPNO                      10
PROCNO                      1

F2 - Acquisition Parameters
Date_               20180609
Time                   14.54 h
INSTRUM                avb400
PROBHD    Z116098_0219 (
PULPROG                zgpg30
TD                     65536
SOLVENT                  DMSO
NS                         64
DS                          4
SWH                64102.563 Hz
FIDRES              1.956255 Hz
AQ                  0.5111808 sec
RG                     197.74
DW                      7.800 usec
DE                      6.50 usec
TE                     298.0 K
D1                 2.00000000 sec
D11                0.03000000 sec
TD0                         1
SFO1             161.9674942 MHz
NUC1                     31P
P1                      8.00 usec
PLW1              54.00000000 W
SFO2              400.1316005 MHz
NUC2                     1H
CPDPRG[2              waltz16
PCPD2                  90.00 usec
PLW2              14.58800030 W
PLW12              0.24654000 W
PLW13              0.12401000 W

F2 - Processing parameters
SI                      32768
SF               161.9755930 MHz
WDW                       EM
SSB       0
LB                      1.00 Hz
GB        0
PC                      1.40
```

^{1}H NMR spectrum of 3-(Hydroxymethyl)-4-nitrobenzonitrile (227)



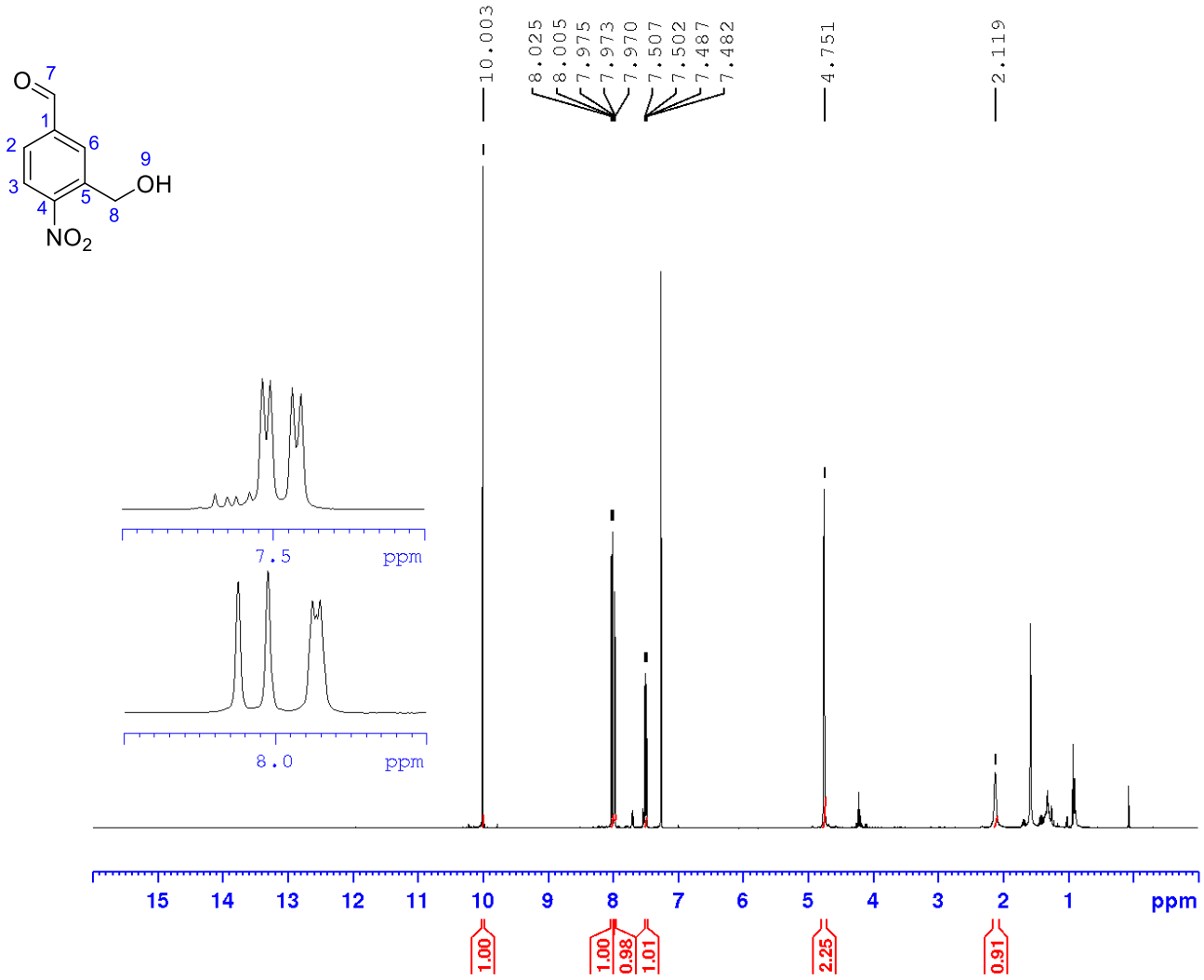
BRUKER

```
Current Data Parameters
NAME                  CE596-2
EXPNO                       1
PROCNO                      1

F2 - Acquisition Parameters
Date_              20180312
Time                  18.38 h
INSTRUM              avg400
PROBHD    Z108618_0816 (
PULPROG               zg60
TD                   65536
SOLVENT              CDCl3
NS                      16
DS                       2
SWH               8012.820 Hz
FIDRES               0.244532 Hz
AQ                4.0894465 sec
RG                    206.87
DW                    62.400 usec
DE                     6.50 usec
TE                    293.9 K
D1             1.00000000 sec
TD0                         1
SFO1           400.2024012 MHz
NUC1                     1H
P1                    14.00 usec
PLW1           14.00000000 W

F2 - Processing parameters
SI                      32768
SF             400.2000094 MHz
WDW                       EM
SSB          0
LB                     0.30 Hz
GB           0
PC                     1.00
```

^{1}H NMR spectrum of 3-(Hydroxymethyl)-4-nitrobenzaldehyde (228)

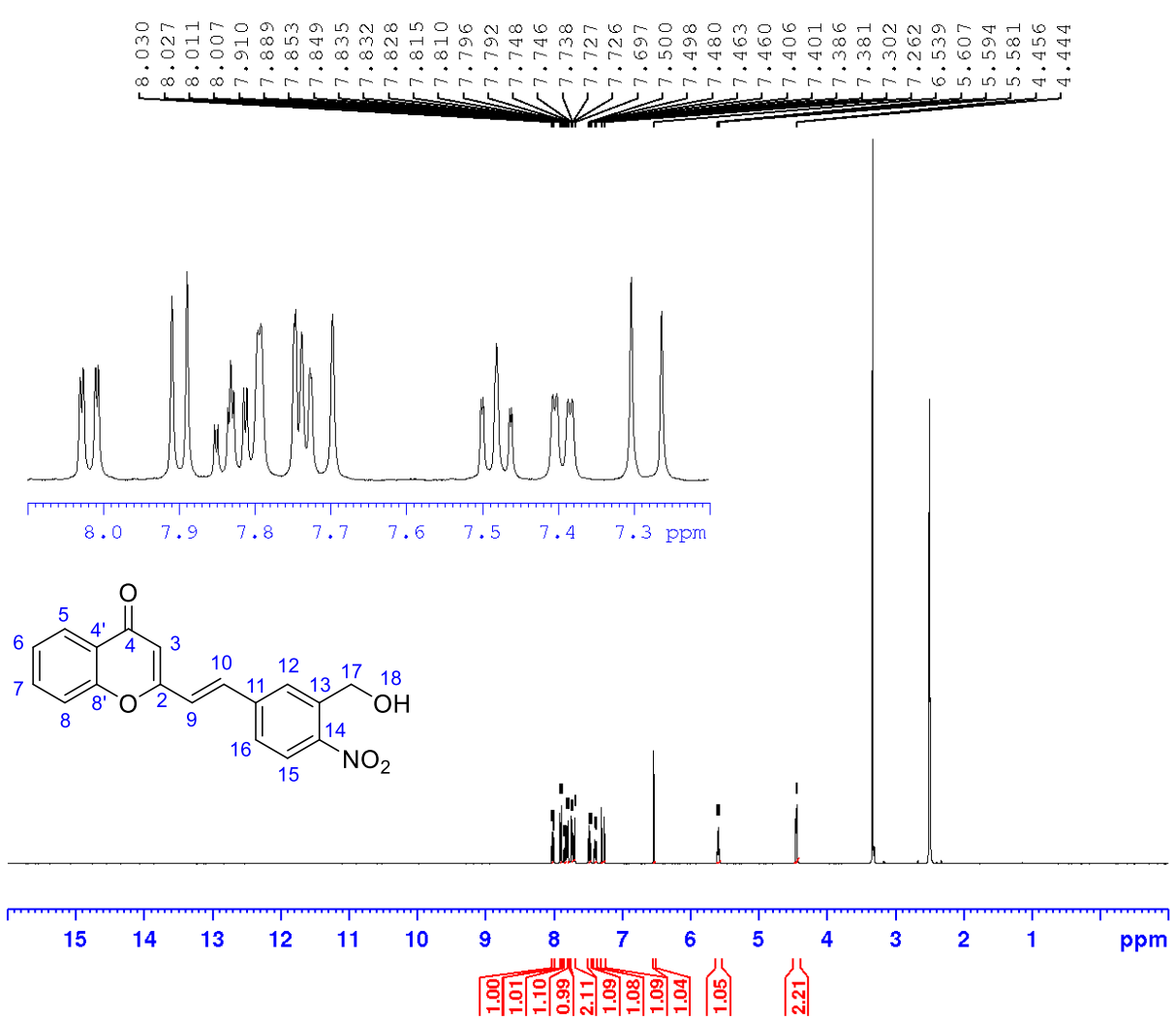



```
Current Data Parameters
NAME                  CE598-1
EXPNO                       1
PROCNO                      1

F2 - Acquisition Parameters
Date_              20180320
Time                    9.26 h
INSTRUM               avh400
PROBHD    Z108618_0873 (
PULPROG                zg60
TD                    65536
SOLVENT               CDCl3
NS                       16
DS                        2
SWH                8012.820 Hz
FIDRES            0.244532 Hz
AQ                4.0894465 sec
RG                     88.17
DW                   62.400 usec
DE                    6.50 usec
TE                   295.9 K
D1              1.00000000 sec
TD0                       1
SFO1           400.1324008 MHz
NUC1                    1H
P1                   14.00 usec
PLW1           14.36999989 W

F2 - Processing parameters
SI                    32768
SF             400.1300100 MHz
WDW                     EM
SSB         0
LB                    0.30 Hz
GB          0
PC                    1.00
```

^{1}H NMR spectrum of (*E*)-2-(3-(Hydroxymethyl)-4-nitrostyryl)-4*H*-chromen-4-one (229)



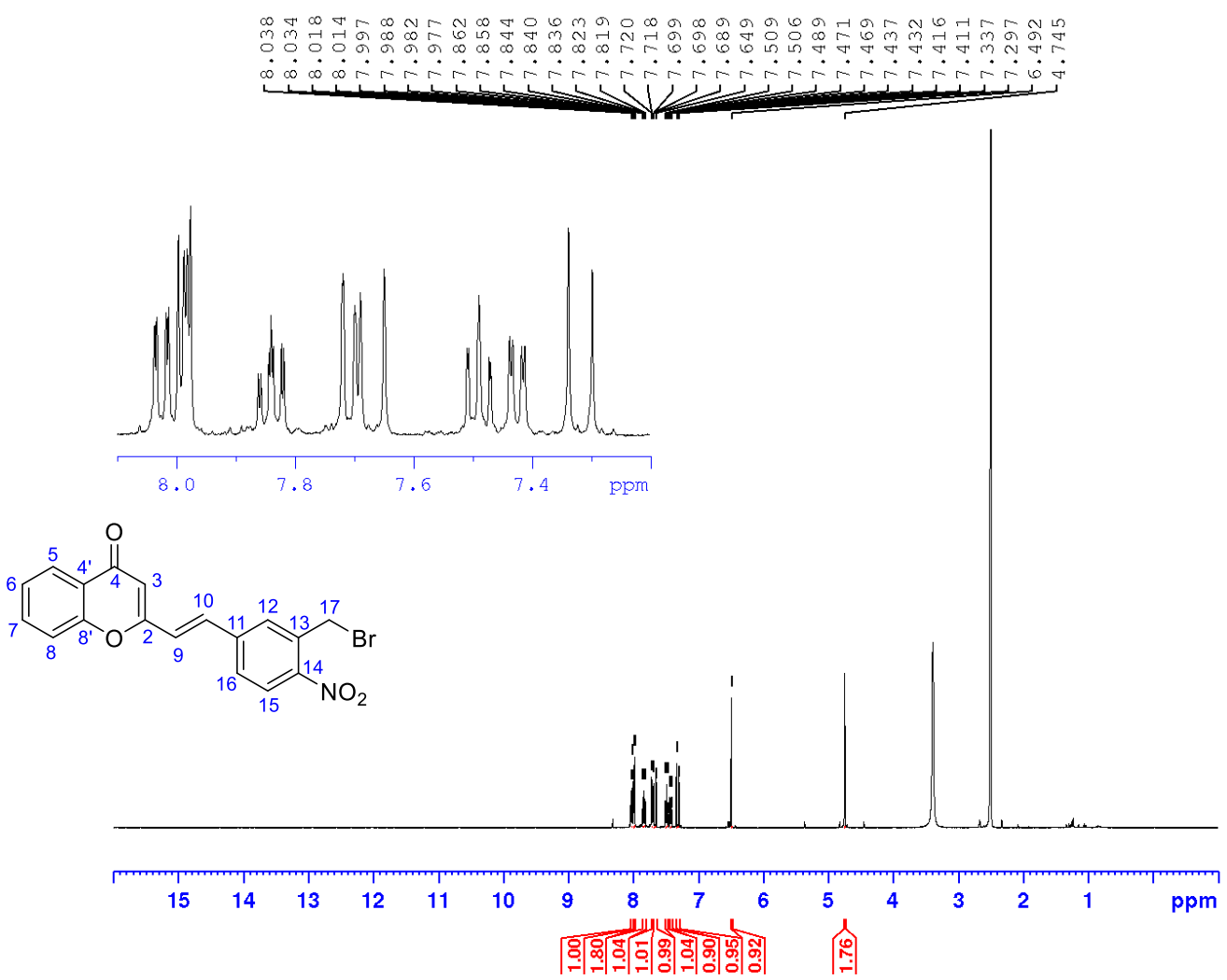



```
Current Data Parameters
NAME                  CE600-1
EXPNO                       1
PROCNO                      1

F2 - Acquisition Parameters
Date_              20180321
Time                   8.48 h
INSTRUM              avg400
PROBHD    Z108618_0816 (
PULPROG                zg60
TD                    65536
SOLVENT                DMSO
NS                       16
DS                        2
SWH                8012.820 Hz
FIDRES             0.244532 Hz
AQ                 4.0894465 sec
RG                    162.47
DW                    62.400 usec
DE                     6.50 usec
TE                    294.4 K
D1              1.00000000 sec
TD0                       1
SFO1           400.2024012 MHz
NUC1                    1H
P1                    14.00 usec
PLW1           14.00000000 W

F2 - Processing parameters
SI                    32768
SF             400.2000031 MHz
WDW                     EM
SSB         0
LB                     0.30 Hz
GB          0
PC                     1.00
```

^{1}H NMR spectrum of (*E*)-2-(3-(Bromomethyl)-4-nitrostyryl)-4*H*-chromen-4-one (224)

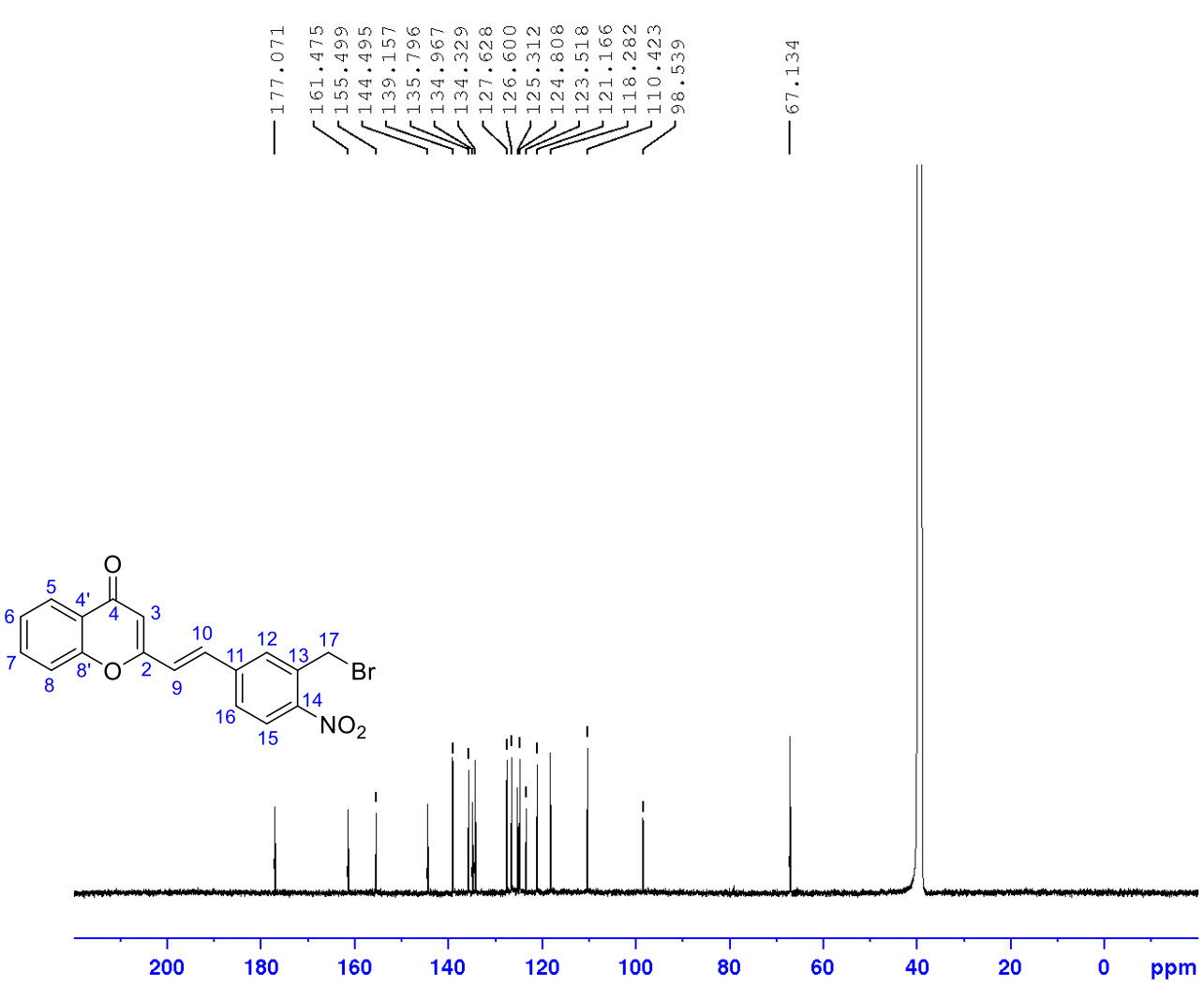



```
Current Data Parameters
NAME        CE608-1_DMSO
EXPNO                  1
PROCNO                 1

F2 - Acquisition Parameters
Date_           20180404
Time              10.43 h
INSTRUM           avh400
PROBHD   Z108618_0873 (
PULPROG            zg60
TD                65536
SOLVENT            DMSO
NS                   16
DS                    2
SWH            8012.820 Hz
FIDRES        0.244532 Hz
AQ            4.0894465 sec
RG                88.17
DW              62.400 usec
DE               6.50 usec
TE              295.6 K
D1           1.00000000 sec
TD0                   1
SFO1        400.1324008 MHz
NUC1                1H
P1               14.00 usec
PLW1        14.36999989 W

F2 - Processing parameters
SI                32768
SF          400.1300032 MHz
WDW                EM
SSB       0
LB              0.30 Hz
GB        0
PC              1.00
```

^{13}C NMR spectrum of (*E*)-2-(3-(Bromomethyl)-4-nitrostyryl)-4*H*-chromen-4-one (224)




```
Current Data Parameters
NAME      CE611-1_500_13C
EXPNO                   4
PROCNO                  1

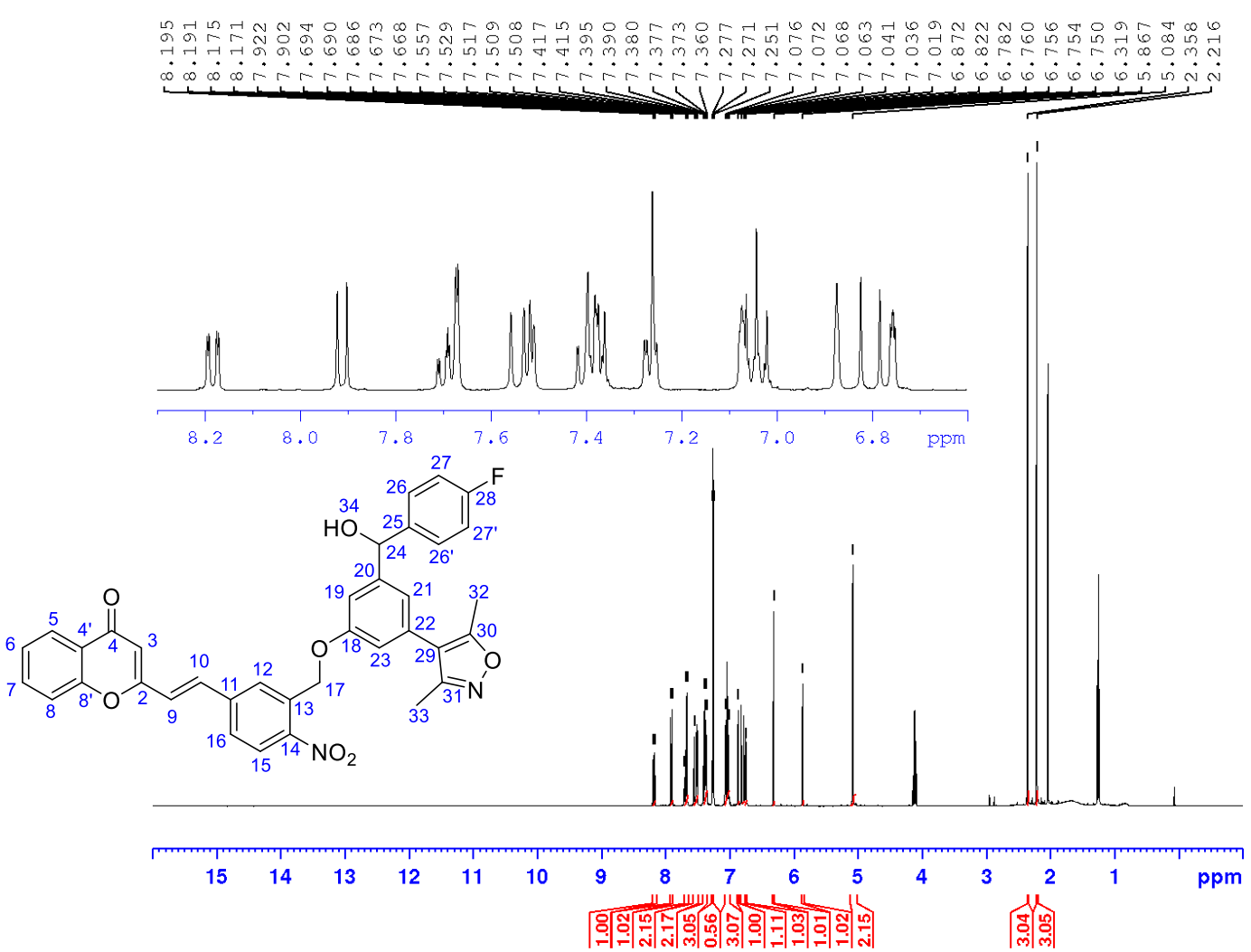
F2 - Acquisition Parameters
Date_           20180831
Time               12.11
INSTRUM          avc500
PROBHD   5 mm CPDUL 13C
PULPROG          zgpg30
TD                65536
SOLVENT             DMSO
NS                  4096
DS                     2
SWH            31250.000 Hz
FIDRES          0.476837 Hz
AQ             1.0485760 sec
RG                   912
DW                16.000 usec
DE                18.00 usec
TE                298.0 K
D1           2.00000000 sec
D11          0.03000000 sec
TD0                    1

======== CHANNEL f1 ========
SFO1         125.8131152 MHz
NUC1                  13C
P1                 10.00 usec
PLW1         20.18400002 W

======== CHANNEL f2 ========
SFO2         500.3020012 MHz
NUC2                  1H
CPDPRG[2         waltz16
PCPD2              80.00 usec
PLW2          7.99830008 W
PLW12         0.60487002 W
PLW13         0.38712001 W

F2 - Processing parameters
SI                 32768
SF           125.8005951 MHz
WDW                   EM
SSB       0
LB                 2.00 Hz
GB        0
PC                 1.40
```

^{1}H NMR spectrum of (*E*)-2-(3-((3-(3,5-Dimethylisoxazol-4-yl)-5-((4-fluorophenyl)(hydroxy)methyl)phenoxy)methyl)-4-nitrostyryl)-4*H*-chromen-4-one (231)



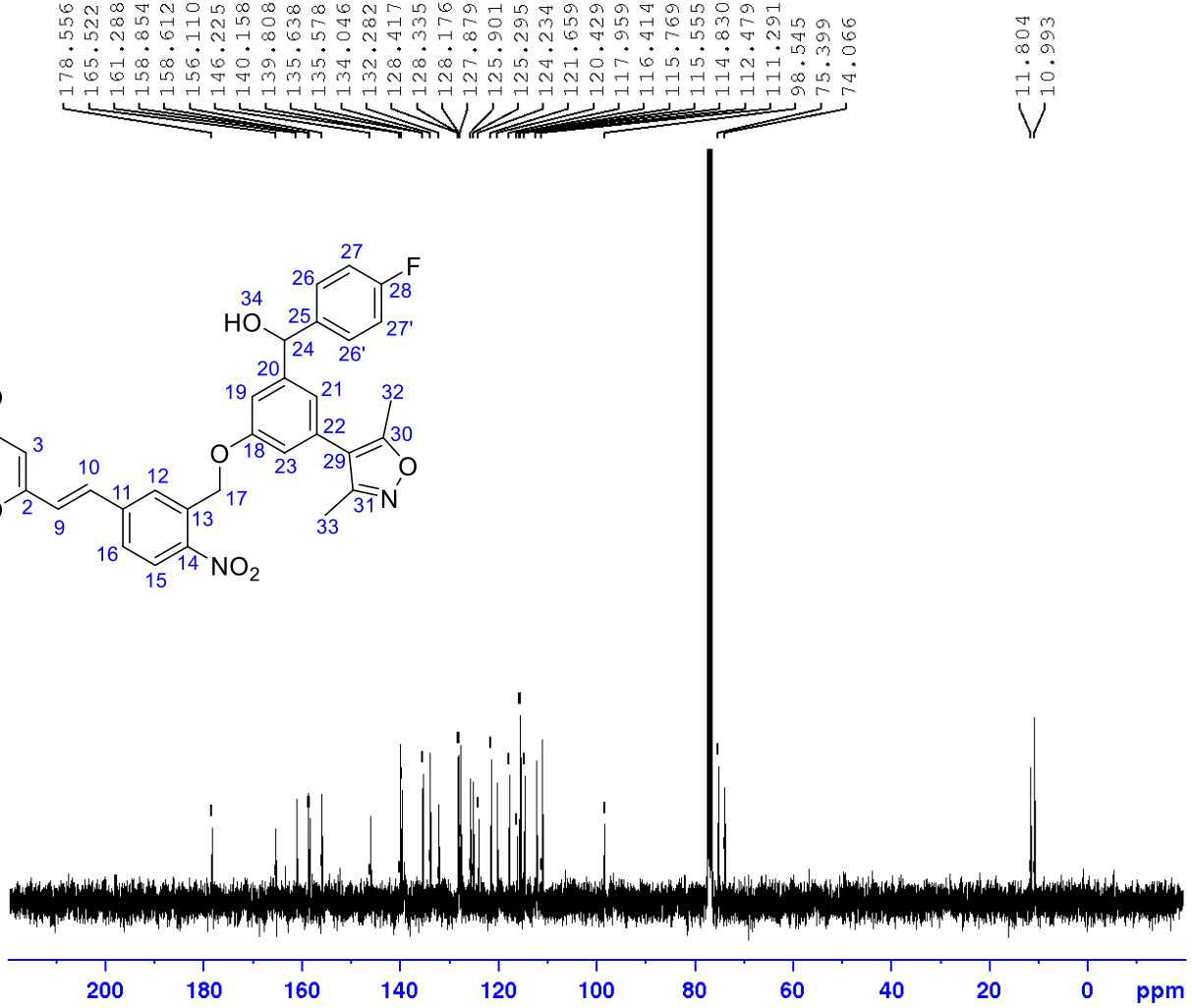
BRUKER

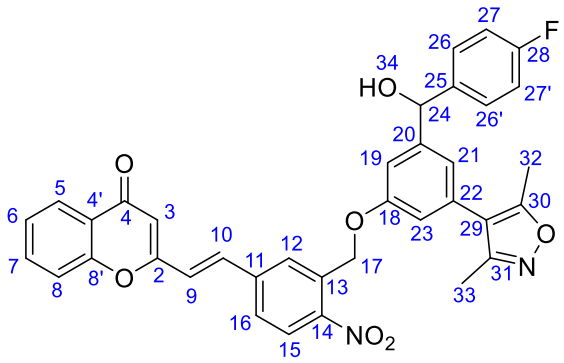
```
Current Data Parameters
NAME                  CE610-1
EXPNO                       1
PROCNO                      1

F2 - Acquisition Parameters
Date_              20180406
Time                  16.42 h
INSTRUM              avh400
PROBHD    Z108618_0873 (
PULPROG                zg60
TD                    65536
SOLVENT               CDCl3
NS                       16
DS                        2
SWH                8012.820 Hz
FIDRES            0.244532 Hz
AQ                4.0894465 sec
RG                    88.17
DW                   62.400 usec
DE                    6.50 usec
TE                   295.8 K
D1              1.00000000 sec
TD0                       1
SFO1           400.1324008 MHz
NUC1                    1H
P1                   14.00 usec
PLW1           14.36999989 W

F2 - Processing parameters
SI                    32768
SF             400.1300100 MHz
WDW                     EM
SSB         0
LB                    0.30 Hz
GB          0
PC                    1.00
```

^{13}C NMR spectrum of (*E*)-2-(3-((3-(3,5-Dimethylisoxazol-4-yl)-5-((4-fluorophenyl)(hydroxy)methyl)phenoxy)methyl)-4-nitrostyryl)-4*H*-chromen-4-one (231)





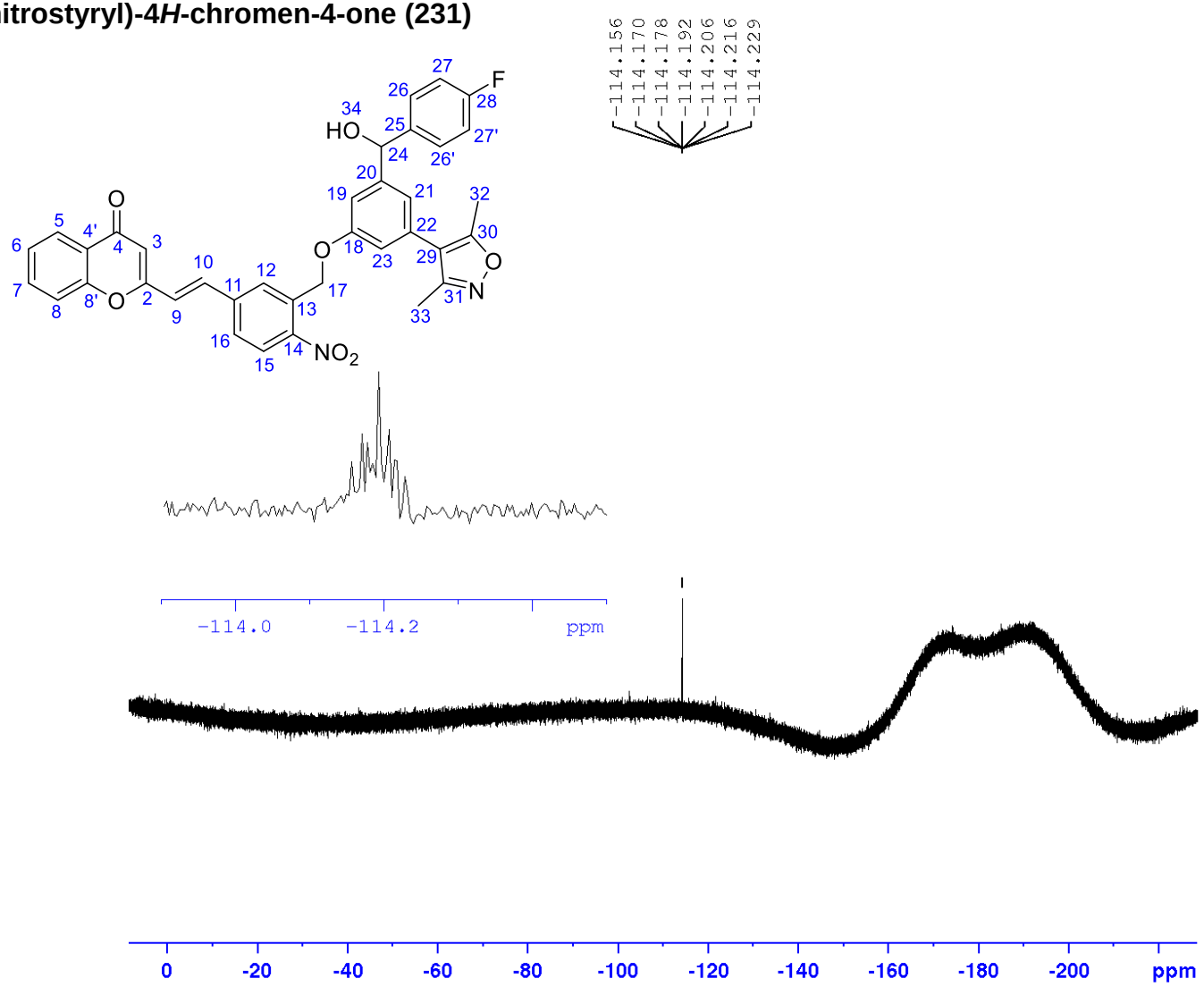



```
Current Data Parameters
NAME      CE610-1_AVB400
EXPNO                 11
PROCNO                 1

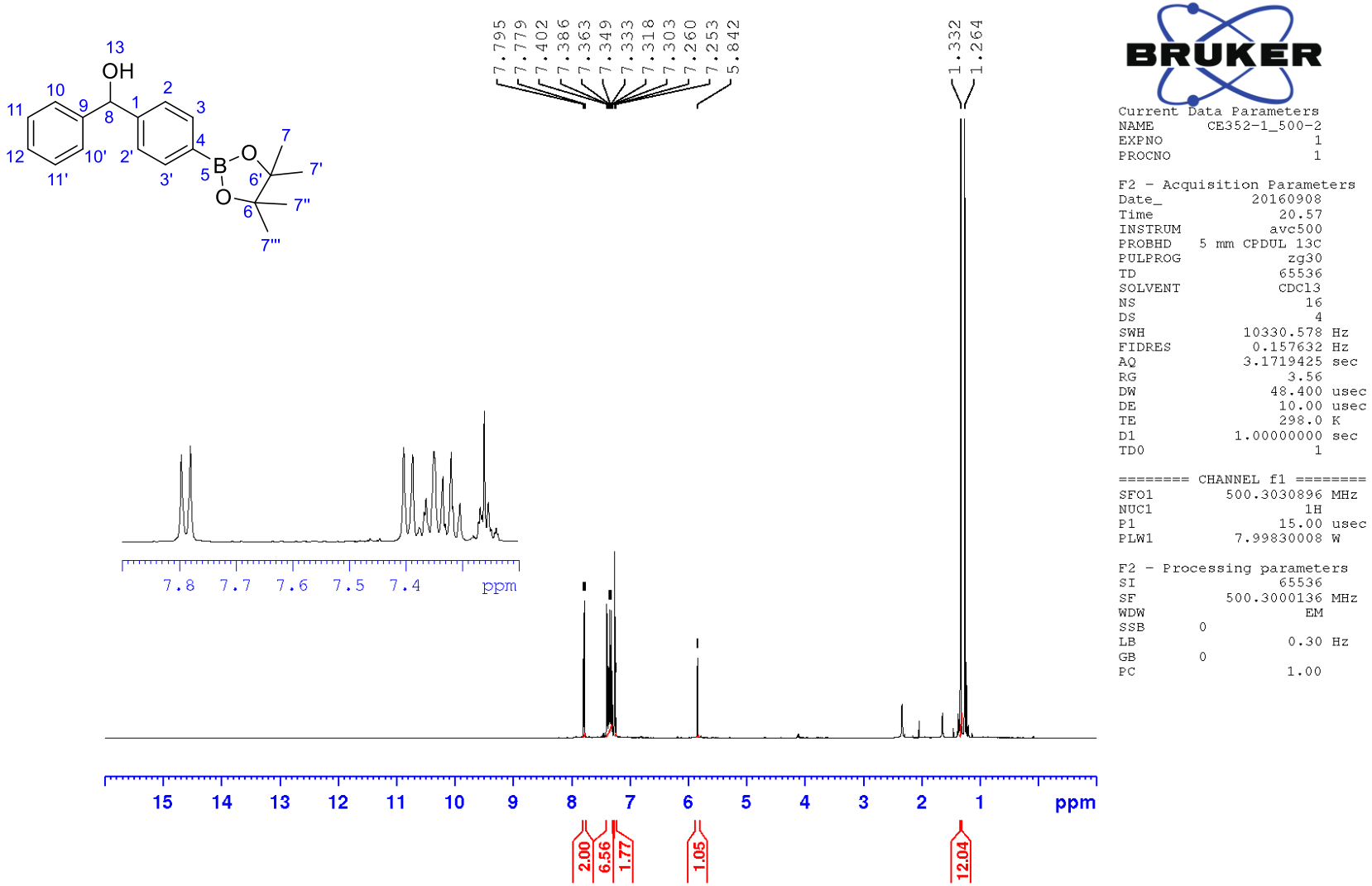
F2 - Acquisition Parameters
Date_           20180409
Time              13.00 h
INSTRUM           avb400
PROBHD   Z116098_0219 (
PULPROG           zgpg30
TD                65536
SOLVENT           CDCl3
NS                  256
DS                    4
SWH           24038.461 Hz
FIDRES         0.733596 Hz
AQ             1.3631488 sec
RG                197.74
DW                20.800 usec
DE                 6.50 usec
TE                298.0 K
D1            2.00000000 sec
D11           0.03000000 sec
TD0                   1
SFO1         100.6228303 MHz
NUC1                13C
P1                10.00 usec
PLW1         60.95399857 W
SFO2         400.1316005 MHz
NUC2                1H
CPDPRG[2         waltz16
PCPD2             90.00 usec
PLW2         14.58800030 W
PLW12         0.24654000 W
PLW13         0.12401000 W

F2 - Processing parameters
SI                32768
SF           100.6127557 MHz
WDW                 EM
SSB       0
LB                 1.00 Hz
GB        0
PC                 1.40
```

^{19}F NMR spectrum of (*E*)-2-(3-((3-(3,5-Dimethylisoxazol-4-yl)-5-((4-fluorophenyl)(hydroxy)methyl)phenoxy)methyl)-4-nitrostyryl)-4*H*-chromen-4-one (231)



^{1}H NMR spectrum of Phenyl(4-(4,4,5,5-tetramethyl-1,3,2-dioxaborolan-2-yl)phenyl)methanol (245)



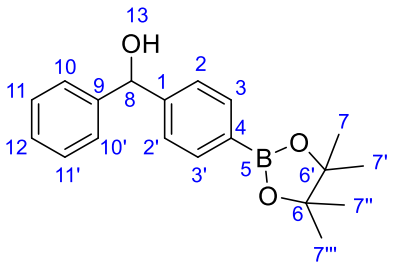

```
Current Data Parameters
NAME       CE352-1_500-2
EXPNO                  1
PROCNO                 1

F2 - Acquisition Parameters
Date_           20160908
Time               20.57
INSTRUM          avc500
PROBHD   5 mm CPDUL 13C
PULPROG             zg30
TD                 65536
SOLVENT            CDCl3
NS                    16
DS                     4
SWH            10330.578 Hz
FIDRES          0.157632 Hz
AQ             3.1719425 sec
RG                  3.56
DW                48.400 usec
DE                10.00 usec
TE                298.0 K
D1            1.00000000 sec
TD0                    1

======== CHANNEL f1 ========
SFO1         500.3030896 MHz
NUC1                   1H
P1                 15.00 usec
PLW1          7.99830008 W

F2 - Processing parameters
SI                 65536
SF           500.3000136 MHz
WDW                   EM
SSB       0
LB                 0.30 Hz
GB        0
PC                 1.00
```

^{11}B NMR spectrum of Phenyl(4-(4,4,5,5-tetramethyl-1,3,2-dioxaborolan-2-yl)phenyl)methanol (245)

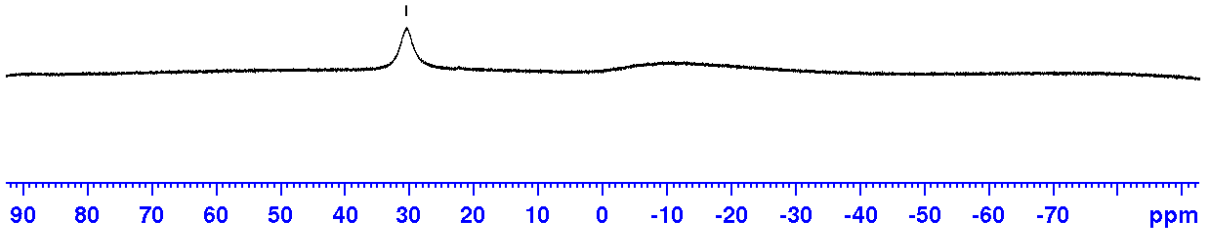


30.580

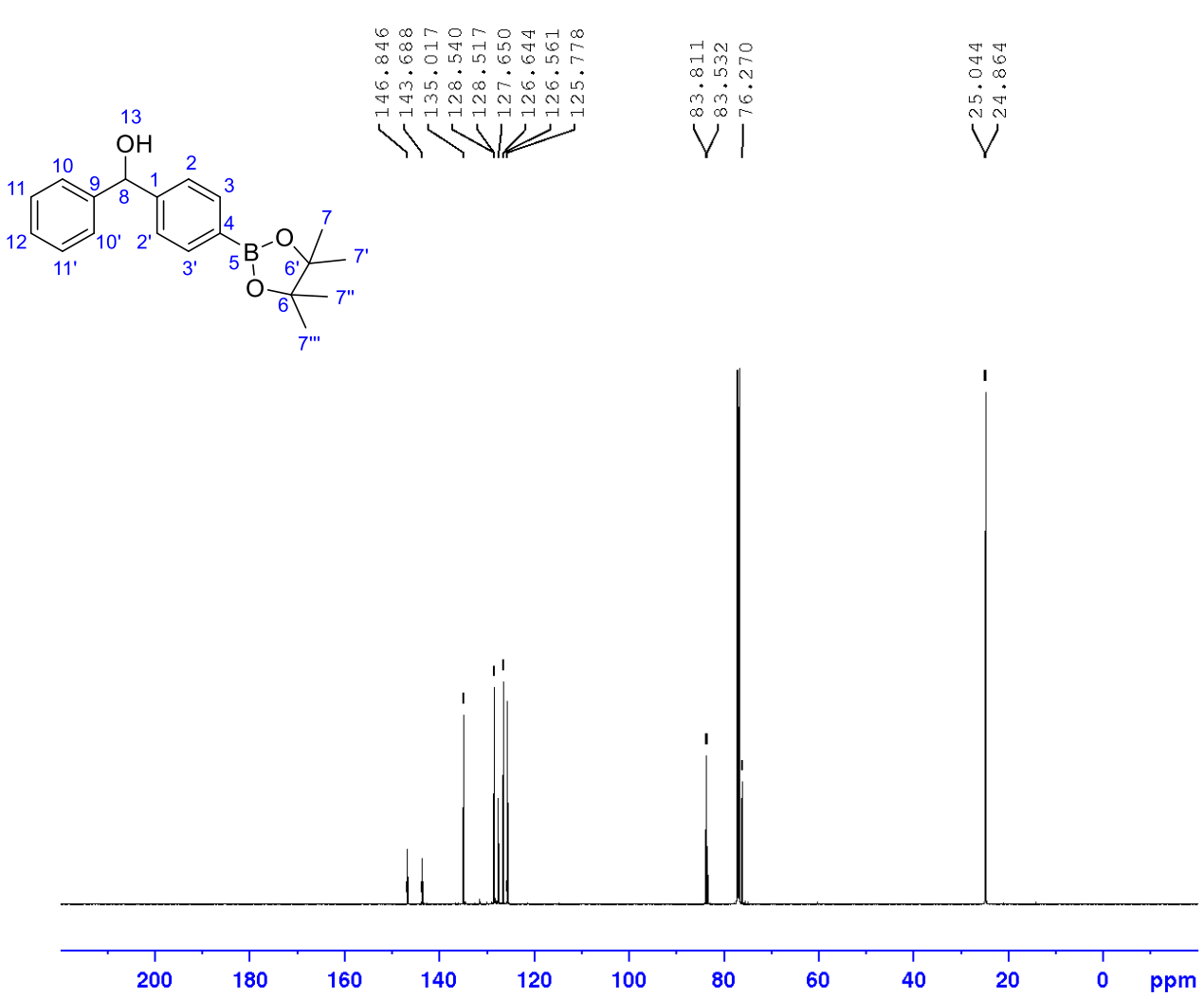
```
Current Data Parameters
NAME          CE352-1_500
EXPNO                   1
PROCNO                  1

F2 - Acquisition Parameters
Date_           20160909
Time                8.13 h
INSTRUM           avx500
PROBHD   Z113652_0208 (
PULPROG                zg
TD                  65536
SOLVENT             CDCl3
NS                     16
DS                      2
SWH            29761.904 Hz
FIDRES          0.908261 Hz
AQ             1.1010048 sec
RG                 191.37
DW                 16.800 usec
DE                  6.50 usec
TE                 298.0 K
D1            1.00000000 sec
TD0                     1
SFO1         160.4615790 MHz
NUC1                11B
P1                 13.00 usec
PLW1         60.00000000 W

F2 - Processing parameters
SI                  32768
SF           160.4615790 MHz
WDW                    EM
SSB       0
LB                  1.00 Hz
GB        0
PC                  1.40
```



^{13}C NMR spectrum of Phenyl(4-(4,4,5,5-tetramethyl-1,3,2-dioxaborolan-2-yl)phenyl)methanol (245)




```
Current Data Parameters
NAME       CE352-1_500-2
EXPNO                  4
PROCNO                 1

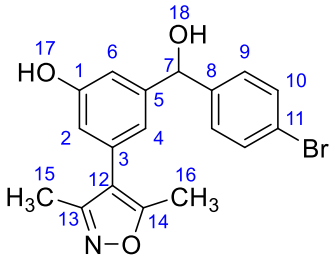
F2 - Acquisition Parameters
Date_           20160908
Time               23.01
INSTRUM          avc500
PROBHD   5 mm CPDUL 13C
PULPROG          zgpg30
TD                65536
SOLVENT           CDCl3
NS                 1024
DS                    2
SWH           31250.000 Hz
FIDRES         0.476837 Hz
AQ            1.0485760 sec
RG                  912
DW               16.000 usec
DE               18.00 usec
TE                298.0 K
D1           2.00000000 sec
D11          0.03000000 sec
TD0                   1

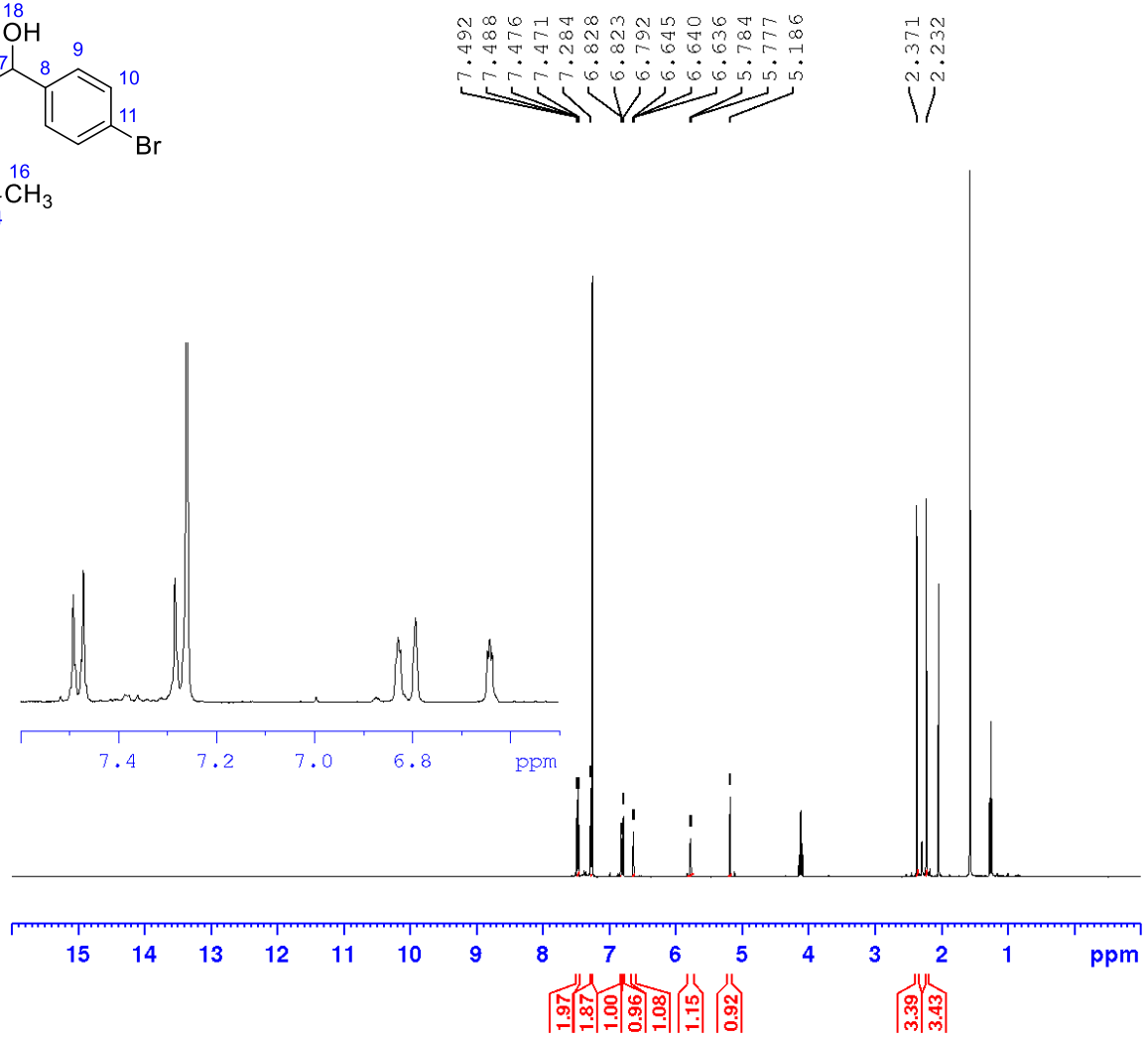
======== CHANNEL f1 ========
SFO1         125.8131152 MHz
NUC1                13C
P1                10.00 usec
PLW1         20.18400002 W

======== CHANNEL f2 ========
SFO2         500.3020012 MHz
NUC2                1H
CPDPRG[2         waltz16
PCPD2             80.00 usec
PLW2          7.99830008 W
PLW12         0.28119001 W
PLW13         0.17996000 W

F2 - Processing parameters
SI                 32768
SF           125.8005351 MHz
WDW                  EM
SSB       0
LB                1.00 Hz
GB        0
PC                1.40
```

^{1}H NMR spectrum of 3-((4-Bromophenyl)(hydroxy)methyl)-5-(3,5-dimethylisoxazol-4-yl)phenol (255)



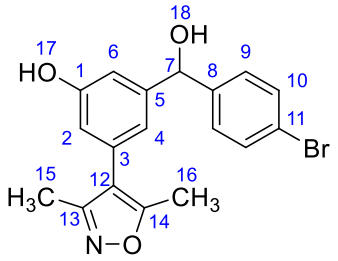


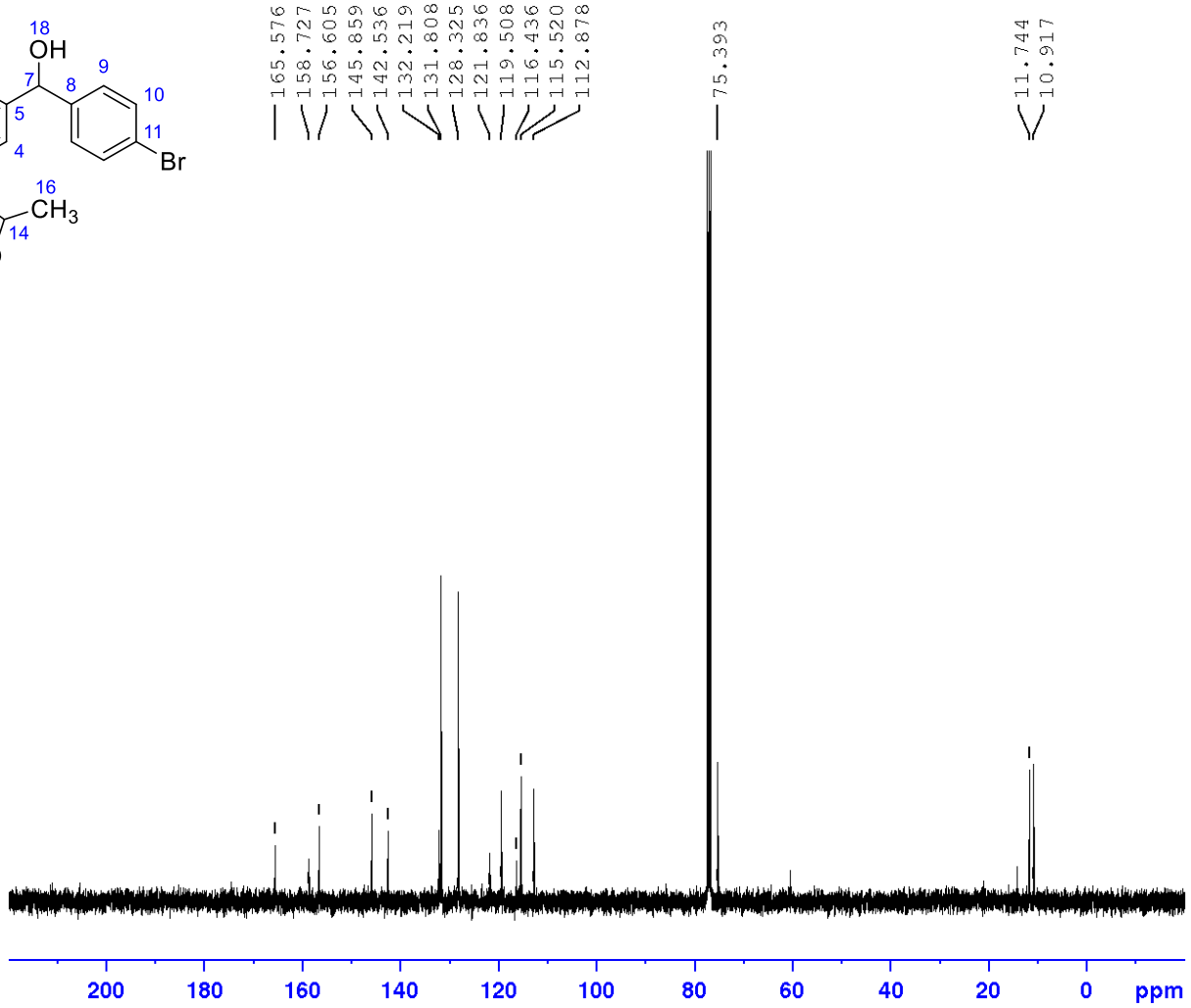

```
Current Data Parameters
NAME                  CE453-1
EXPNO                       1
PROCNO                      1

F2 - Acquisition Parameters
Date_              20170403
Time                  11.16 h
INSTRUM               avh400
PROBHD    Z108618_0873 (
PULPROG                zg60
TD                    65536
SOLVENT               CDCl3
NS                       16
DS                        2
SWH                8012.820 Hz
FIDRES            0.244532 Hz
AQ                4.0894465 sec
RG                   197.18
DW                   62.400 usec
DE                    6.50 usec
TE                   295.0 K
D1              1.00000000 sec
TD0                       1
SFO1           400.1324008 MHz
NUC1                    1H
P1                   14.00 usec
PLW1           14.36999989 W

F2 - Processing parameters
SI                    32768
SF             400.1300102 MHz
WDW                     EM
SSB          0
LB                    0.30 Hz
GB           0
PC                    1.00
```

^{13}C NMR spectrum of 3-((4-Bromophenyl)(hydroxy)methyl)-5-(3,5-dimethylisoxazol-4-yl)phenol (255)



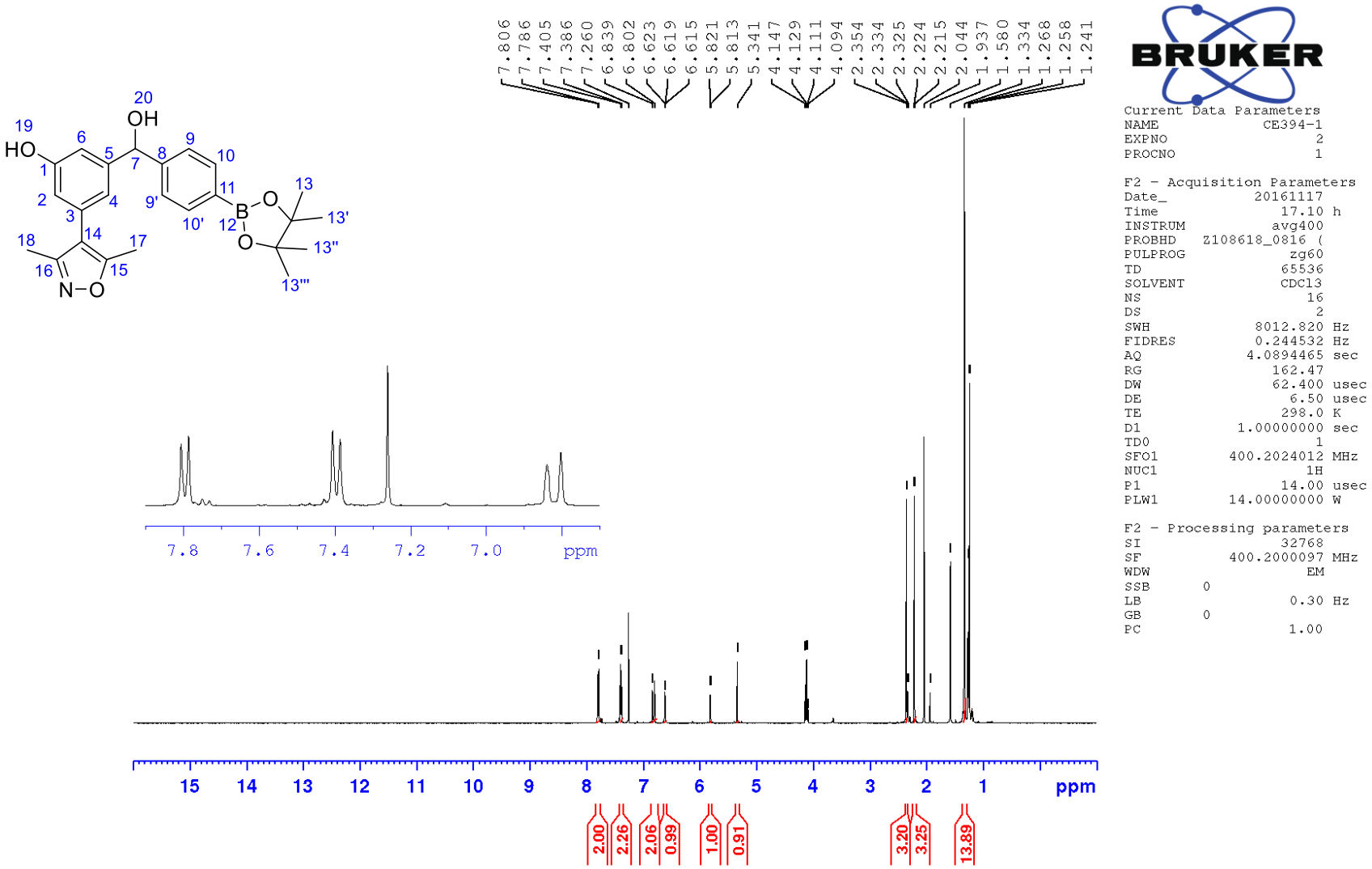



```
Current Data Parameters
NAME                  CE618-1_2
EXPNO                         2
PROCNO                        1

F2 - Acquisition Parameters
Date_                 20180810
Time                     19.14 h
INSTRUM                  avh400
PROBHD    Z108618_0873 (
PULPROG                  zgpg30
TD                        32768
SOLVENT                   CDCl3
NS                          512
DS                            4
SWH                  26041.666 Hz
FIDRES                1.589457 Hz
AQ                   0.6291456 sec
RG                       197.18
DW                       19.200 usec
DE                         6.50 usec
TE                        301.1 K
D1                   1.00000000 sec
D11                  0.03000000 sec
TD0                           1
SFO1               100.6228298 MHz
NUC1                        13C
P1                       10.00 usec
PLW1               47.86100006 W
SFO2               400.1316005 MHz
NUC2                        1H
CPDPRG[2                waltz16
PCPD2                    90.00 usec
PLW2               14.36999989 W
PLW12                0.34660661 W
PLW13                0.17371930 W

F2 - Processing parameters
SI                        32768
SF                 100.6127546 MHz
WDW                         EM
SSB             0
LB                       1.00 Hz
GB              0
PC                       1.40
```

^{1}H NMR spectrum of 3-(3,5-Dimethylisoxazol-4-yl)-5-(hydroxy(4-(4,4,5,5-tetramethyl-1,3,2-dioxaborolan-2-yl)phenyl)methyl)phenol (256)

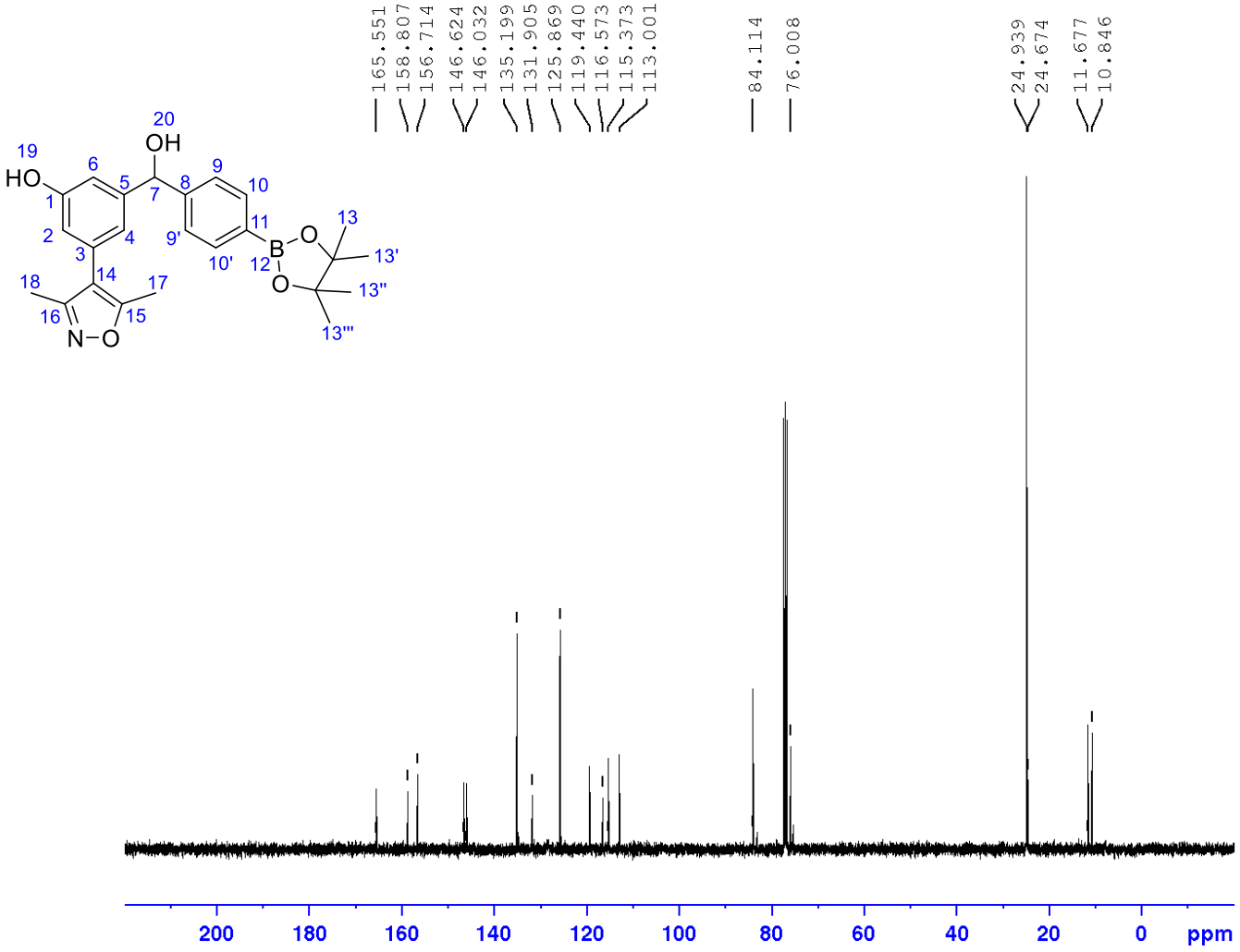



```
Current Data Parameters
NAME                  CE394-1
EXPNO                       2
PROCNO                      1

F2 - Acquisition Parameters
Date_              20161117
Time                  17.10 h
INSTRUM              avg400
PROBHD    Z108618_0816 (
PULPROG                zg60
TD                    65536
SOLVENT               CDCl3
NS                       16
DS                        2
SWH                8012.820 Hz
FIDRES             0.244532 Hz
AQ                 4.0894465 sec
RG                    162.47
DW                    62.400 usec
DE                     6.50 usec
TE                    298.0 K
D1              1.00000000 sec
TD0                       1
SFO1           400.2024012 MHz
NUC1                    1H
P1                    14.00 usec
PLW1           14.00000000 W

F2 - Processing parameters
SI                    32768
SF             400.2000097 MHz
WDW                     EM
SSB         0
LB                     0.30 Hz
GB          0
PC                     1.00
```

^{13}C NMR spectrum of 3-(3,5-Dimethylisoxazol-4-yl)-5-(hydroxy(4-(4,4,5,5-tetramethyl-1,3,2-dioxaborolan-2-yl)phenyl)methyl)phenol (256)

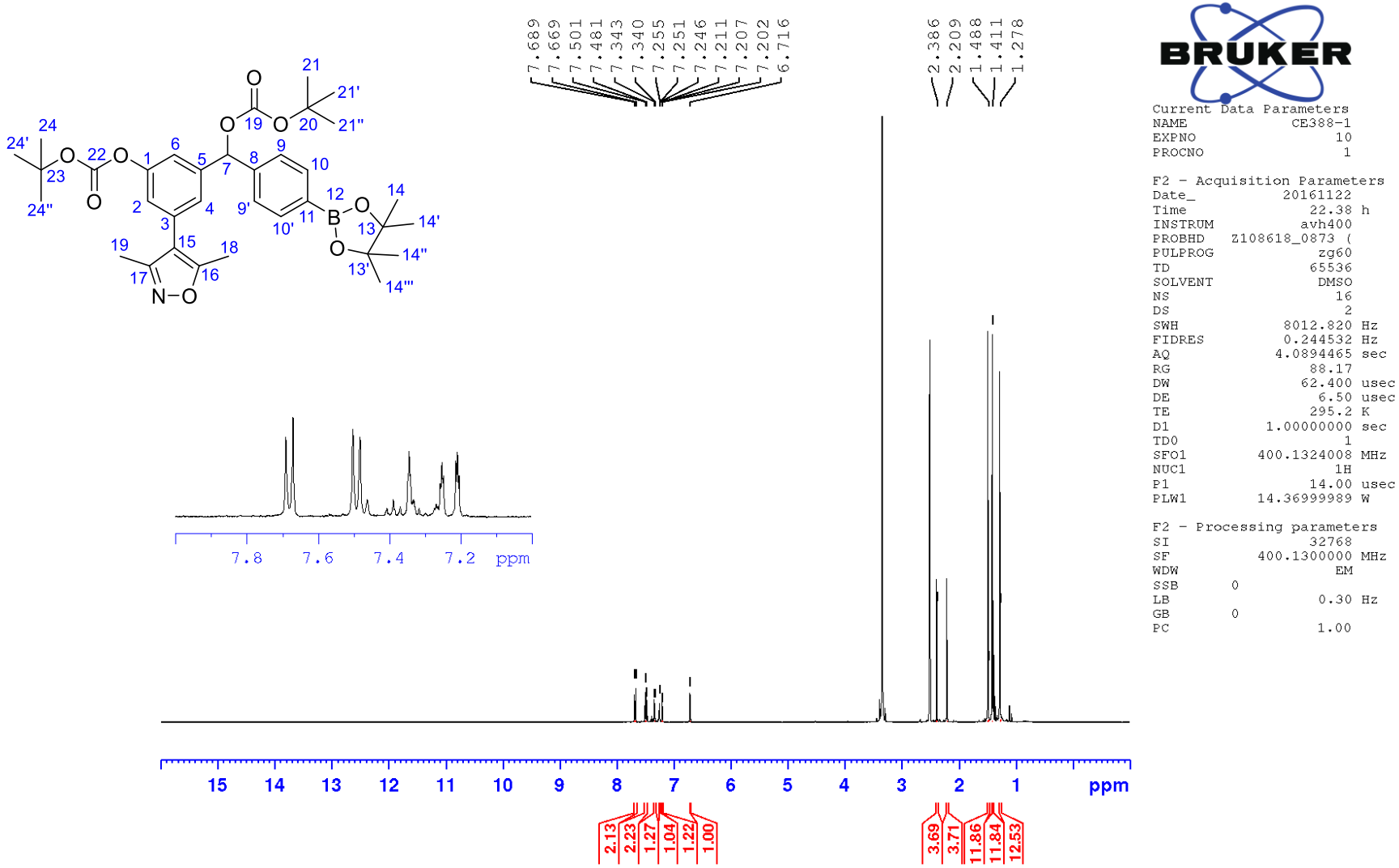



```
Current Data Parameters
NAME            CE394-1_2
EXPNO                   2
PROCNO                  1

F2 - Acquisition Parameters
Date_           20180808
Time                4.43 h
INSTRUM           avg400
PROBHD   Z108618_0816 (
PULPROG           zgpg30
TD                32768
SOLVENT           CDCl3
NS                  256
DS                    4
SWH           26041.666 Hz
FIDRES         1.589457 Hz
AQ            0.6291456 sec
RG               206.87
DW               19.200 usec
DE                6.50 usec
TE               301.3 K
D1           1.00000000 sec
D11          0.03000000 sec
TD0                   1
SFO1        100.6404331 MHz
NUC1               13C
P1                10.00 usec
PLW1        56.00000000 W
SFO2        400.2016008 MHz
NUC2               1H
CPDPRG[2        waltz16
PCPD2             90.00 usec
PLW2        14.00000000 W
PLW12        0.33877000 W
PLW13        0.17039999 W

F2 - Processing parameters
SI                32768
SF          100.6303574 MHz
WDW                EM
SSB       0
LB                1.00 Hz
GB        0
PC                1.40
```

^{1}H NMR spectrum of (3-((*t*-Butoxycarbonyl)oxy)-5-(3,5-dimethylisoxazol-4-yl)phenyl)(4-(4,4,5,5-tetramethyl-1,3,2-dioxaborolan-2-yl)phenyl)methyl *t*-butyl carbonate (257)

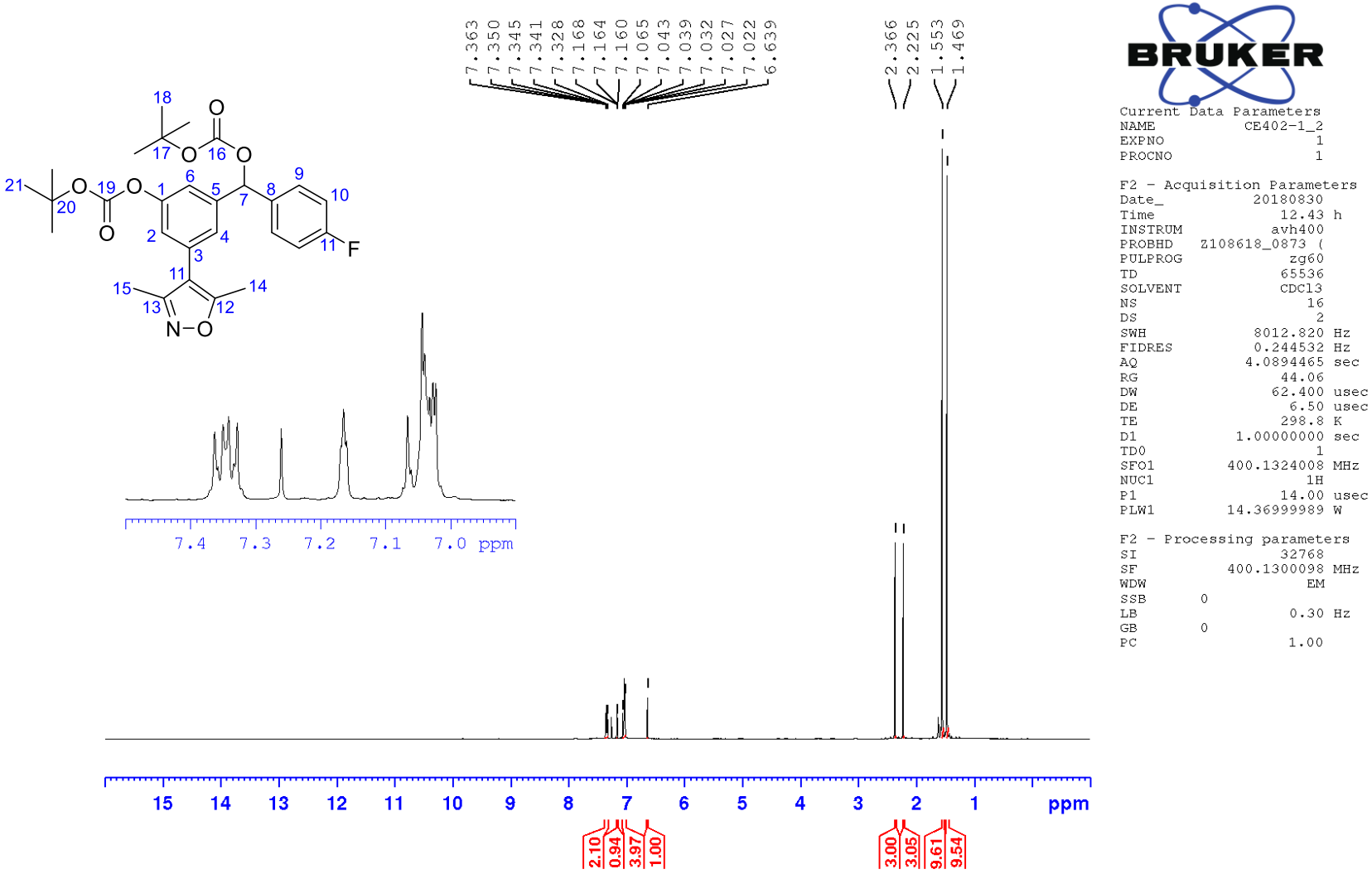



```
Current Data Parameters
NAME                  CE388-1
EXPNO                      10
PROCNO                      1

F2 - Acquisition Parameters
Date_               20161122
Time                   22.38 h
INSTRUM                avh400
PROBHD    Z108618_0873 (
PULPROG                 zg60
TD                     65536
SOLVENT                 DMSO
NS                        16
DS                         2
SWH                 8012.820 Hz
FIDRES              0.244532 Hz
AQ                  4.0894465 sec
RG                     88.17
DW                     62.400 usec
DE                      6.50 usec
TE                     295.2 K
D1                  1.00000000 sec
TD0                        1
SFO1             400.1324008 MHz
NUC1                      1H
P1                     14.00 usec
PLW1            14.36999989 W

F2 - Processing parameters
SI                     32768
SF               400.1300000 MHz
WDW                       EM
SSB          0
LB                      0.30 Hz
GB           0
PC                      1.00
```

^{1}H NMR spectrum of 3-((((*t*-Butoxycarbonyl)oxy)(4-fluorophenyl)methyl)-5-(3,5-dimethylisoxazol-4-yl)phenyl *t*-butyl carbonate (258)

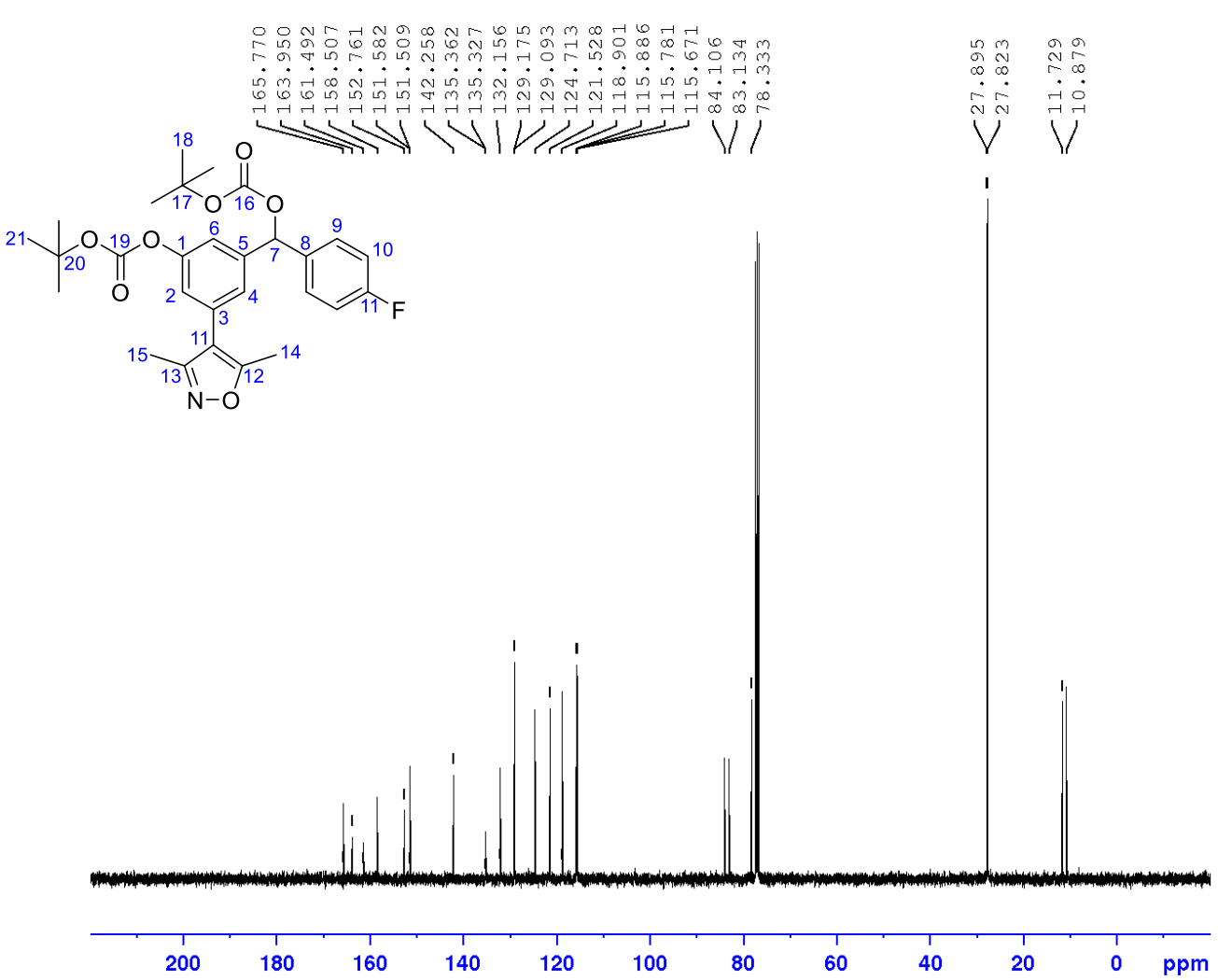



```
Current Data Parameters
NAME            CE402-1_2
EXPNO                   1
PROCNO                  1

F2 - Acquisition Parameters
Date_            20180830
Time                12.43 h
INSTRUM           avh400
PROBHD    Z108618_0873 (
PULPROG             zg60
TD                 65536
SOLVENT            CDCl3
NS                    16
DS                     2
SWH              8012.820 Hz
FIDRES           0.244532 Hz
AQ               4.0894465 sec
RG                  44.06
DW                62.400 usec
DE                 6.50 usec
TE                298.8 K
D1             1.00000000 sec
TD0                    1
SFO1          400.1324008 MHz
NUC1                  1H
P1                 14.00 usec
PLW1          14.36999989 W

F2 - Processing parameters
SI                 32768
SF            400.1300098 MHz
WDW                   EM
SSB       0
LB                 0.30 Hz
GB        0
PC                 1.00
```

^{13}C NMR spectrum of 3-(((*t*-Butoxycarbonyl)oxy)(4-fluorophenyl)methyl)-5-(3,5-dimethylisoxazol-4-yl)phenyl *t*-butyl carbonate (258)

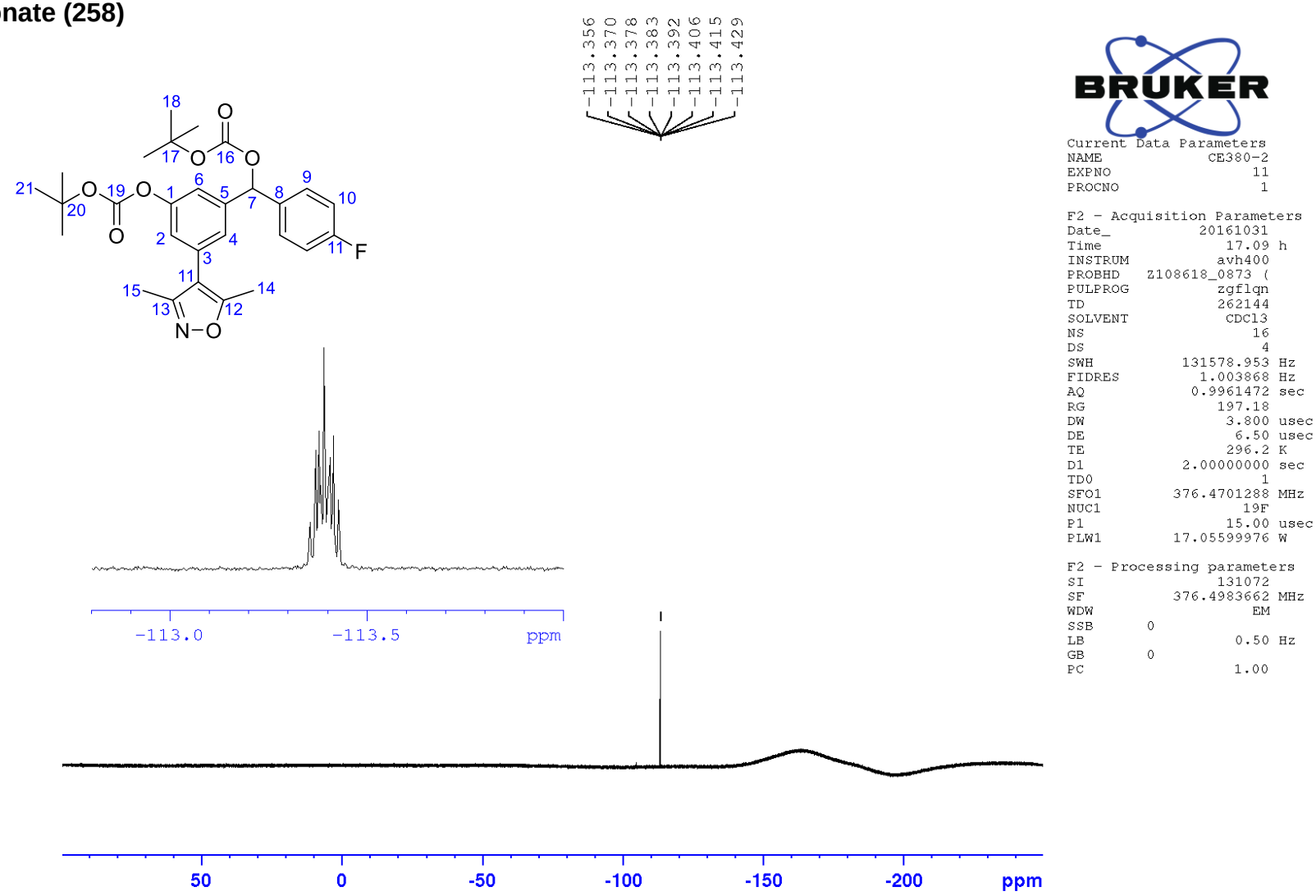



```
Current Data Parameters
NAME            CE402-1_2
EXPNO                   2
PROCNO                  1

F2 - Acquisition Parameters
Date_            20180830
Time                19.12 h
INSTRUM           avh400
PROBHD   Z108618_0873 (
PULPROG           zgpg30
TD                 32768
SOLVENT            CDCl3
NS                   512
DS                     4
SWH            26041.666 Hz
FIDRES          1.589457 Hz
AQ             0.6291456 sec
RG                197.18
DW                19.200 usec
DE                 6.50 usec
TE                300.6 K
D1             1.00000000 sec
D11            0.03000000 sec
TD0                    1
SFO1          100.6228298 MHz
NUC1                  13C
P1                 10.00 usec
PLW1          47.86100006 W
SFO2          400.1316005 MHz
NUC2                  1H
CPDPRG[2          waltz16
PCPD2              90.00 usec
PLW2          14.36999989 W
PLW12          0.34660661 W
PLW13          0.17371930 W

F2 - Processing parameters
SI                 32768
SF            100.6127553 MHz
WDW                   EM
SSB       0
LB                 1.00 Hz
GB        0
PC                 1.40
```

^{19}F NMR spectrum of 3-(((*t*-Butoxycarbonyl)oxy)(4-fluorophenyl)methyl)-5-(3,5-dimethylisoxazol-4-yl)phenyl *t*-butyl carbonate (258)



BRUKER

```
Current Data Parameters
NAME                  CE380-2
EXPNO                      11
PROCNO                      1

F2 - Acquisition Parameters
Date_               20161031
Time                   17.09 h
INSTRUM                avh400
PROBHD    Z108618_0873 (
PULPROG                zgflqn
TD                     262144
SOLVENT                 CDCl3
NS                         16
DS                          4
SWH               131578.953 Hz
FIDRES              1.003868 Hz
AQ                  0.9961472 sec
RG                     197.18
DW                      3.800 usec
DE                      6.50 usec
TE                     296.2 K
D1                2.00000000 sec
TD0                         1
SFO1             376.4701288 MHz
NUC1                     19F
P1                     15.00 usec
PLW1             17.05599976 W

F2 - Processing parameters
SI                     131072
SF               376.4983662 MHz
WDW                       EM
SSB          0
LB                      0.50 Hz
GB           0
PC                      1.00
```